State of the art

Contents

Magnetic surveying instrumentation —a review of recent advances

Peter Hood

Geological Survey of Canada
Ottawa, Canada

Abstract. This paper is a review of recent advances in instrumentation used in ground magnetic and aeromagnetic surveys. A dozen years ago only the fluxgate magnetometer, which has a sensitivity of about 1 gamma, was in use for aeromagnetic mapping surveys. Now there are four basically different airborne magnetometers in field use: the fluxgate, proton precession, aspect-tube and optical absorption magnetometers, all of which measure the total intensity of the earth's magnetic field. The optical absorption magnetometer has a sensitivity nearly two orders of magnitude better than the fluxgate type, and the successful development of these higher-resolution instruments has produced a renaissance in the magnetic prospecting method.

The transistor has made feasible the production of compact, low-power consumption electronic ground magnetometers, and these have now replaced almost completely the more classical magnetic-balance type of instrument. The electronic magnetometers have a number of distinct advantages over the mechanical type. Commercially available electronic ground magnetometers include the fluxgate, proton free-precession, Overhauser and optical absorption magnetometers.

The study of the magnetic properties of rock formations to account for observed anomalies is also receiving increased attention. Thus both the susceptibility and remanent magnetization of a given rock formation should be measured and instruments for this purpose are also commercially available.

Résumé. Cette communication est une revue des récents progrès dans l'appareillage utilisé pour les levés magnétiques terrestres et aériens. Il y a douze ans, on ne se servait essentiellement que d'un seul magnétomètre pour les levés de cartographie aéromagnétique soit le solénoïde à noyau saturable d'une sensibilité d'environ un gamma. Présentement il y a fondamentalement cinq magnétomètres aéroportés différents en usage sur le terrain: le solénoïde à noyau saturable (le fluxmètre), le magnétomètre à protons, l'Overhauser, le déclinomètre (ou variomètre) et le magnétomètre à absorption optique qui, tous, mesurent l'intensité totale du champ magnétique terrestre. Le magnétomètre à absorption optique possède une sensibilité d'environ deux ordres de magnitude de plus que le solénoïde à noyau saturable et la mise au point fructueuse de ces instruments de plus haute résolution a déclenché une renaissance dans la méthode de la prospection magnétique.

L'avènement du transistor a rendu possible la production des magnétomètres électroniques, compacts, à faible consommation d'électricité pour usage au sol, et ces appareils ont maintenant presque complètement remplacé le genre plus classique d'instrument magnétique à balance. Les magnétomètres électroniques possèdent un certain nombre d'avantages distincts sur ceux du genre mécanique.

Les magnétomètres électroniques au sol qu'on peut obtenir dans le commerce sont: le solénoïde à noyau saturable, le magnétomètre à protons, l'Overhauser et le magnétomètre à absorption optique. L'étude des propriétés magnétiques des formations rocheuses dans le but d'expliquer les anomalies observées reçoit également une attention accrue. Ainsi, la susceptibilité magnétique aussi bien que la rémanence d'une formation rocheuse donnée devraient être mesurées et les instruments à cette fin sont également disponibles dans le commerce.

A dozen years ago there was essentially only one magnetometer in standard use for aeromagnetic surveys, the fluxgate type. In 1955 Varian Associates of California introduced the first airborne proton free-precession nuclear magnetometer. There are presently four basically different magnetometers being used, the fluxgate, electron beam, proton precession, and optical absorption magnetometers (see Table I) all of which measure the total intensity (T) of the earth's magnetic field. The first two are vector instruments because the head is orientation sensitive and has to be kept aligned with respect to the earth's field; the rest are scalar magnetometers, that is they are essentially insensitive to orientation. Scalar magnetometers are generally also absolute instruments, whereas vector magnetometers are variometers; thus the former measure the entire ambient magnetic field whereas the latter measure only the variations relative to an arbitrary datum determined by DC current flowing through a buck-out coil wound around the head of the vector magnetometer.

The various types of magnetometers are by no means equivalent because the optical-absorption variety, namely the rubidium, cesium and metastable helium types, have better than an order of magnitude greater sensitivity than the fluxgate. Thus there are now many more magnetometers used in aeromagnetic surveying than there were ten years ago, and these have been summarized in Table I. The electron beam or aspect tube type of magnetometer has been in field use for a decade or so and it will not be further discussed in this paper.

The advent of the transistor has made feasible the production of compact, low power consumption electronic ground magnetometers, and these have now replaced almost completely the more classical magnetic balance type of instrument. The electronic magnetometers have a number of distinct advantages over the mechanical type including a greater ease of operation, and a much higher range of measurement which makes possible a much faster rate of traversing. Commercially available electronic ground magnetometers include the fluxgate, proton free-precession, Overhauser, and optical absorption magnetometers. Table II summarizes the characteristics of commercially available electronic ground instrumentation.

Ground and airborne magnetometers

Fluxgate magnetometers. The first use of a fluxgate element to measure changes in the intensity of the earth's magnetic field appears to have been by the German physicists, Aschenbrenner

Table I. Characteristics of airborne magnetometers used in mineral exploration.

Magnetometer	Principle of Operation	Type	Manufacturer and Model Designation	Field Measured	Readout (A-Analog, D-Digital)	Sensitivity (gammas)	Mount (B-Bird I-Inboard)
Fluxgate (Vector Variometer)	Saturable core	Peak Voltage	Gulf Oil Co. Mark III (USA)	T	All Continuous A	< 1	I
		Second harmonic	McPhar 555 AB (Can)	V	A	50	I
			AN/ASQ-3, 8, 10 (USA)	T	A	< 1	I
			AM-13 (USSR)	T	A	2	B
Electron Beam or Aspect Tube (Vector Variometer)	Deflection of moving electron		Elliott Bros (UK) EMD 13	T	A Continuous	10	I
Proton Precession (Scalar) Absolute)	Free precession of hydrogen proton	Reciprocal	Elliott Bros (UK) EMD 14 & EMD 21	T	D and A Every 0.5 sec	1 to 3	B or I
			Varian Assoc. (USA) V-4914	T	D and A Every 0.6 sec	< 1	B or I
		Direct reading	Barringer (Can) AM-101	T	D, A, and Visual Every 1 sec	1 or 5	B or I
			GSC (Can) TELMAG	T	D and A Every 2 sec	0.1	B or I
			Bureau of Mineral Resources (Australia)	T	A Every 0.5 sec	1	B or I
			Prackla (W. Germany) PM-22 & PM-24	T	D and A Every 1 sec	2	B
			Varian Assoc. (USA) V-4937A	T	D and A Every 1 sec or 0.5 sec	1 or 2	B
			AYaAM-6 (USSR)	T	A Every 1 sec	1	B
	Forced Precession of hydrogen proton	Overhauser	Sud-Aviation (France) MP 121 & MP 122	T	D and A Every 1 sec	0.1	B
Optical Absorption (Scalar Absolute)	Optical pumping	Cesium vapour	CSF/CGG (France)	T	D and A Continuous	0.01	B
		Rubidium vapour	Varian Assoc. (USA) V-4916	T	D and A Continuous	0.05	B
		Metastable helium	Texas Instr. (USA)	T	D and A Continuous	0.05	B

and Goubau (1936) in 1928. However the fluxgate magnetometer was only used in mineral exploration surveys after its successful development during World War II as an airborne submarine detection device. The sensitive element of a saturable-core or fluxgate magnetometer consists of a short length of high-permeability ferromagnetic material, such as Permalloy, having a narrow hysteresis loop. Around this element are wound one or more turns of wire which are connected to AC exciting and indicating circuits. In essence the action of the fluxgate element is that of a magnetic amplifier. There are two basic fluxgate instruments, the peak voltage and second-harmonic types, and for a more complete discussion of the theory of operation the reader is referred to the excellent description by Whitham (1960).

The great advantage of the fluxgate element over the magnetic balance is that the operation of the former is unaffected by motion. For this reason fluxgate magnetometers may be used in a moving vehicle such as an aeroplane, if a suitable orientation technique is used, because the saturable-core element measures the field acting along its axis.

Ground fluxgate magnetometer. Figure 1 shows one of the Canadian-built instruments, the Sharpe MF-1 fluxgate magnetometer, being read at a survey station. Other commercially available instruments, such as the Finnmaster, McPhar M700, and Jalander Type 46-65 and 46-66 are listed in Table III together with their technical specifications as supplied by the manufacturers.

Most of the ground fluxgate magnetometers have the following common characteristics:

1. They are hand-held, with a strap around the operator's neck (see Figure 1).
2. The fluxgate element is mounted in gimbals. For a reading

Table II. Characteristics of commercially-available electronic ground-prospecting magnetometers.

Type of Magnetometer	Principle of Operation	Manufacturer	Model	Field Measured	Readout Device	Max (gammas)	Instrument Mount
Fluxgate	Saturable core	Sharpe Instruments (Canada)	MF-1 MF-1-100 PMF-3	Vertical component	Meter scales	20/div 2/div 100/div	Handheld with carrying strap around operator's neck. All are transistorized.
		McPhar Geophysics (Canada)	M700			20/div	
		Optillinen Tehdas Oy (Finland)	Jalander Type 46-65 Type 46-66			50/div 25/div	
		Levanto Oy (Finland)	Finnmaster	(All instruments except PMF-3 use a vertical freely suspended fluxgate element		20/div	
		Izmiran (USSR)	M-17			10/div	
Proton Precession	Free precession of hydrogen proton	Barringer Research (Canada)	GM102A SM-103	Total field	Counter – 3 sec – 2 sec	10 1	Handheld Transistorized
		Varian Associates (USA)	M49A		Reed Freq. Meter – 6 sec	10	
		Littlemore Scientific Engineering (UK)	Elsec Type 592		Meter – 1 sec	1	
		Izmiran (USSR)	PM-5		Meter	1	
	Overhauser-forced precession of hydrogen proton	Sud-Aviation (France)	MP-102	Total field	Meter	0.1	
Optical Absorption	Optical pumping	Varian Associates (USA)	Model 4920-Cesium	Total field and Vertical Gradient	Continuous and digital	0.1	

the instrument is levelled using a circular bubble. In this position the saturable-core element swings freely in a vertical orientation, and therefore the fluxgate magnetometer measures the vertical component of the earth's magnetic field.

3. The instrument is transistorized and the vertical field in gammas is read directly from a meter.

Sharpe Instruments MF-1 fluxgate ground magnetometer (Figure 2) consists of two thin strips of highly permeable material approximately 4 inches long. A low-frequency field of 1 KHz is applied by the primary coils winding to excite the permeable material strips. The exciting field is sinusoidal, of low distortion and large enough to drive the strips into saturation during each half cycle. As a result, the permeability of the strips is changing at the rate of the second harmonic, that is 2 KHz. The flux produced in the strips by the external ambient field is therefore varied or 'gated' at the second harmonic rate, producing pulses of voltage in the secondary winding. These pulses contain only even harmonics of the exciting frequency. The second harmonic, being the largest, is extracted from the secondary coils and is used as a measure of the external field. The second harmonic signal is filtered by a bandpass filter, then amplified and fed into a phase-sensitive detector where additional filtering takes place as well as detection. A reference signal is obtained by frequency doubling, and is then fed into a phase-shifting network to enable the correct phase adjustment for the phase-sensitive detector. Further conditioning of the reference signal is accomplished through a bandpass filter and then it is amplified before going to the phase-sensitive detector. The DC signal produced in the phase-sensitive detector is directly proportional to the measured field and is further amplified by a DC amplifier and returned in opposition through the meter and feedback winding back to the sensor, effectively returning the sensor to zero ambient field. With sufficient feedback ratio the sensor operates essentially in a zero field, thus assuring excellent linearity over the range of 100,000 gammas. A further advantage of the feedback system is that the variation of the gain of the amplifiers as well as the component value changes are not reflected in the accuracy of the readings. To make possible accurate readings in a high ambient

Contents

Table III. Specifications of commercially available fluxgate magnetometers used in mining surveys.

Manufacturer	Finnmaster	OT Tehdas Oy		McPhar	Sharpe	Sharpe	Sharpe
Country	Finland	Finland	Finland	Canada	Canada	Canada	Canada
Model		Jalander 46-65	Jalander 46-66	M700	MF-1	MF-1-100	PMF-3
Weight (lbs)	5.5	3.2	3.2	9	5.75	5.75	3
Dimensions (inches)	4 diam. x 9	3.16 diam. x 10	3.16 diam. x 10	4 x 7 x 10.5	6.5 x 3.5 x 12.5	6.5 x 3.5 x 12.5	5 x 4 x 8.5
Batteries (number)	11	12	12	2	12	12	2
Total Voltage	16.5	18	18	18	18	18	2.7
Current Consumption (.ma)		25	25		50	50	3
Control Knobs (number)	3	4	4	3	4	4	2
1. ON/OFF Battery Test; Polarity		Separate ON/OFF button	Separate ON/OFF button	Yes	Yes	Yes	Yes Not polarity
2. ± Range (gammas)							
1	1,000	2,500	1,250	1,000	1,000	100	3,000
2	2,500	7,500	2,500	3,000	3,000	300	10,000
3	10,000	25,000	7,500	10,000	10,000	1,000	30,000
4	25,000	75,000	25,000	30,000	30,000	3,000	100,000
5	100,000	250,000	100,000	100,000	100,000	10,000	300,000
6	–	–	–	–	–	30,000	–
7	–	–	–	–	–	100,000	–
					400,000 optional		Same switch for ON/OFF and battery test
Sensitivity in Gammas per Scale Division							
1	20	50	25	20	20	2	100
2	50	150	50	50	50	5	500
3	200	500	150	200	200	20	1,000
4	500	1,500	500	500	500	50	5,000
5	2,000	5,000	2,000	2,000	2,000	200	10,000
6	–	–	–	–	–	500	–
7	–	–	–	–	–	2,000	–
Readability in Gammas on Lowest Scale (1/4 scale division)	5	12.5	6.25	5	5	0.5	50
3. Latitude Adjustments							
(a) Coarse		–	–	–	9 steps	9 steps	–
Gammas/step		–	–	–	8,000	8,000	
Range		–	–	–	72,000	72,000	
(b) Fine		Yes	Yes	Yes	Yes	Yes	Yes
Range (gammas)		± 70,000 with magnets	± 70,000 with magnets	± 100,000	7,000	7,000	75,000
Temperature Stability	15γ from −15°C to +35°C	2γ/°C	2γ/°C	50γ over range −35°C to +55°C	Less than 2γ per °C; 0.5γ/°C optional	Less than 2γ per °C; 0.5γ/°C optional	15γ per °C
Operating Temperature in Field							
Upper Limit	+40°C	+50°C	+50°C	+60°C	+45°C	+45°C	+45°C
Lower Limit	−30°C	−20°C	−20°C	−40°C	−60°C	−60°C	−60°C
Recorder Output	Yes	Optional	Optional	Yes	Optional	Optional	None

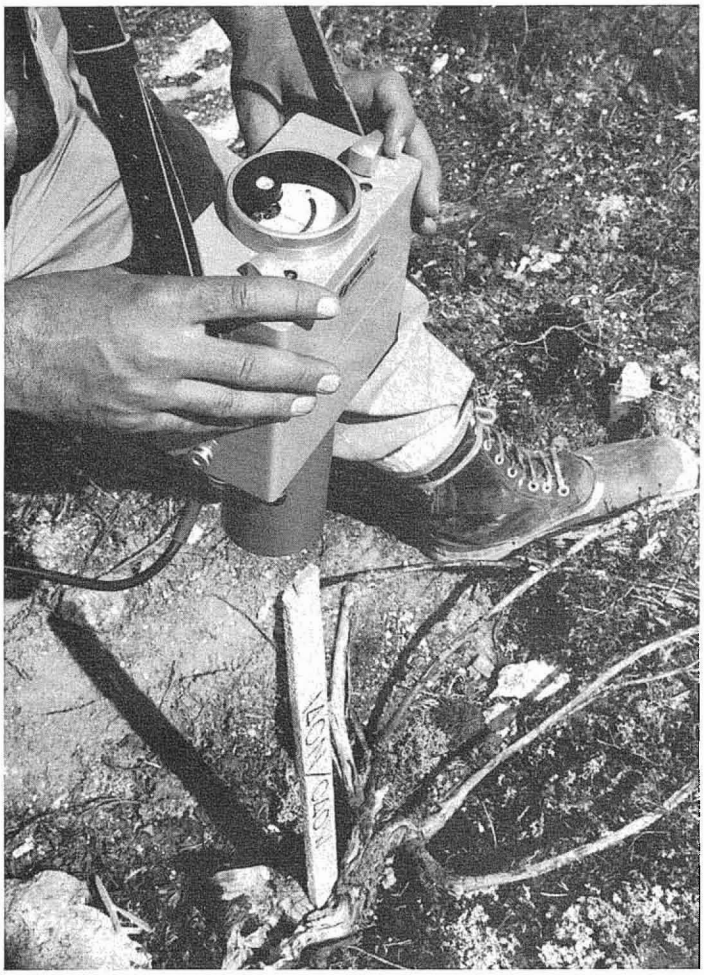


Figure 1. Reading the Sharpe MF-1 fluxgate magnetometer at a survey peg.

field, a well regulated buck-out current is employed. This current is fed into a separate buck-out coil to cancel the major portion of the ambient field and thus permit the reading to be taken on the more sensitive scales.

Use of the fluxgate magnetometer in ground surveys. The field procedure for using the fluxgate magnetometer in ground magnetic surveys is essentially the same as that for other instruments. However it possesses many advantages over tripod-mounted instruments, such as the Schmidt balance, and these are summarized in the following comparison.

1. *Speed.* About one station every 3 minutes with Schmidt balance and every minute with fluxgate for stations 100 feet apart.
2. *Versatility.* Little difficulty with terrain using the fluxgate since it is hand held. Fluxgate can be used in a canoe for waterborne surveys on lakes.
3. *Maintenance.* No electronics to go wrong with the Schmidt balance. No batteries to change.
4. *Price.* About the same.
5. *Sensitivity.* Comparable, but effective sensitivity of the fluxgate can readily be coarsened.
6. *Range.* Fluxgate has much larger (up to ± 400,000 gammas) range compared with Schmidt balance (± 50,000 gammas with an extra large auxiliary magnet). Also range can readily be altered with fluxgate by turning outside control, whereas Schmidt-type must be dismantled to rotate latitude screw. N.B. carrying auxiliary magnets necessitates use of two men.
7. *Personnel.* Traversing by fluxgate is truly a one-man operation. Operator of the Schmidt balance needs more manual dexterity.
8. *Temperature compensation and calibration.* Temperature coefficient can be made negligible (for mining surveys) with both instruments. Calibration curve for both instruments is quite linear, but care should be taken that battery voltage does not change appreciably during traverse using fluxgate since some drift (but not a calibration change) will occur.

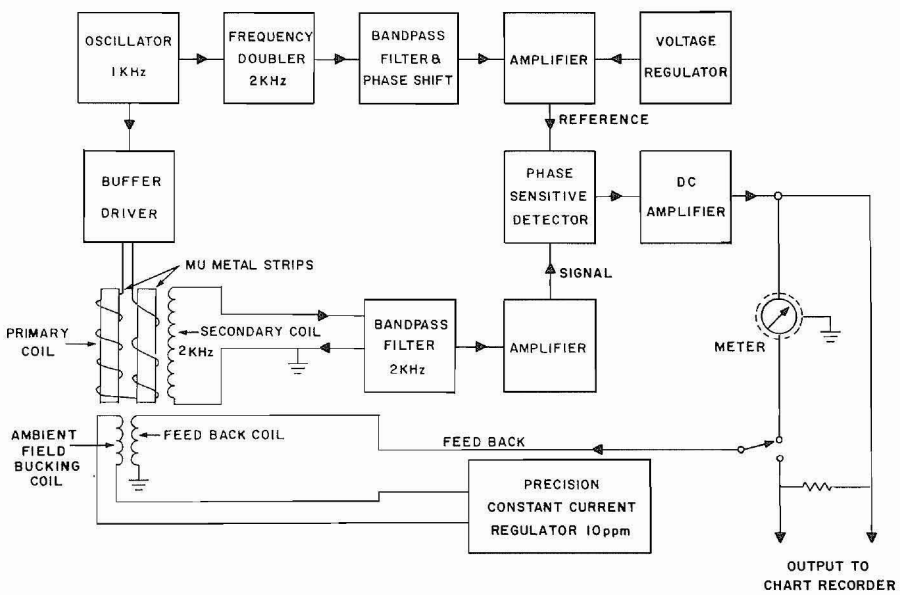


Figure 2. Block diagram of Sharpe MF-1 vertical-force fluxgate ground magnetometer.

Contents

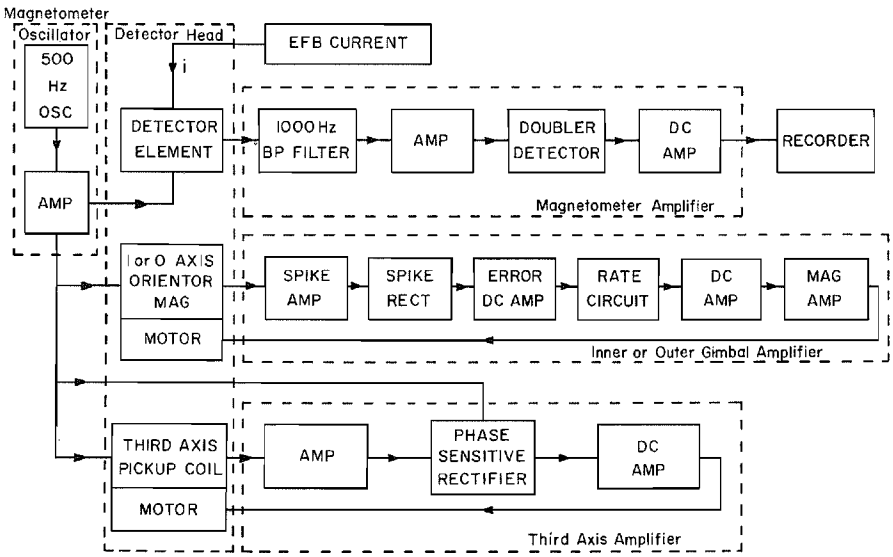


Figure 3. Block diagram of the AN/ASQ-10 second-harmonic fluxgate airborne magnetometer.

9. *Light.* Can work later into the evening with the fluxgate because Schmidt balance requires some light to read scale.

10. *Vertical gradient.* Measurement of the vertical gradient easily made with the fluxgate by taking two readings at different heights at each survey station.

11. *Measurement.* Can read fluxgate directly in gammas. Have to carry out computation with Schmidt-type balance.

Vertical gradient measurements. It is possible to measure the first vertical derivative of the vertical component of the earth's magnetic field using the fluxgate magnetometer (Hood, 1964). This involves the measurement of the magnetic field at two different heights at each survey station, a procedure which does not materially affect the time occupied at a station.

The vertical gradient of the vertical component is defined as

$$\frac{\partial \Delta Z}{\partial h} = \frac{\Delta Z_2 - \Delta Z_1}{h_2 - h_1}$$

The vertical gradient is the magnetic reading (ΔZ_2) at the higher height (h_2) minus the magnetic reading (ΔZ_1) at the lower height (h_1) divided by the distance that the magnetometer is lowered $(h_2 - h_1)$. This will mean in practice that negative gradient values are obtained over the magnetic body being surveyed, but the convention is necessary for mathematical consistency. It is assumed in the formula that the depth of the body is very much greater than the vertical distance between the two readings.

For the fluxgate instrument it is only possible to take a difference in reading over about 2.5 feet since it is necessary to keep the magnetometer oriented while reading it. However, it is possible to read to 5 gammas and even less with the recently developed fluxgate magnetometers. The normal vertical gradient of the earth's magnetic field at high magnetic latitudes is approximately 0.01 gamma per foot.

Aldred (1964) has outlined the circuitry of a second-harmonic fluxgate gradiometer which has been designed for the magnetic location of buried archaeological remains. Two fluxgate elements energized at 1 KHz are mounted 4 feet apart with their axes aligned in a vertical staff which is attached to a horizontal bar. The bar is carried on the shoulders of two operators together with the transistorized electronic unit. Total weight of the equipment is 20 pounds. A centre-zero meter indicates the difference in field between the elements together with the sign of the gradient. A switched gain control gives full-scale ranges of ± 30, ± 100, and ± 300 gammas. The effective sensitivity of the instrument is estimated to be 2 gammas which corresponds to a gradient of 0.5 gamma per foot. This is more than adequate for mining surveys.

Airborne fluxgate magnetometers. In the airborne instrument the fluxgate element must be kept accurately aligned parallel to the earth's field. This is achieved by the use of additional orienting inductors mutually perpendicular and in a plane at right angles to the measuring element. The error signal registered by these inductors when the measuring element becomes misaligned with the magnetic field is applied to servomotors which drive the gimbal-mounted inductor assembly back into alignment.

The airborne fluxgate magnetometers which have had the greatest use in aeromagnetic surveying are the Gulf instrument and the modified military magnetometers of the AN/ASQ series manufactured in the U.S.A. for submarine detection purposes.

The peak-voltage Gulf Mk. III 410Hz fluxgate instrument, which has been widely used for prospecting and geologic mapping has a range of 250,000 gammas, weighs 219 pounds (for inboard installation) and operates from a 28 volt, 360 watt, DC supply. The 10-inch chart-recorder has selectable full scale deflection subranges of 300, 600, 1200, 2400, or 4800 gammas with stepping switches 5/6 of the subrange. Chart speed can be varied from 1 inch to 12 inches per minute or can be driven by Doppler. Instrumental drifts do not exceed 6 gammas per hour (Affleck, private communication).

Earlier MAD equipments used for submarine detection during World War II have been described by Fromm (1952). Later unclassified military magnetometers working on the second-harmonic principle are the 150-pound AN/ASQ-8, and its

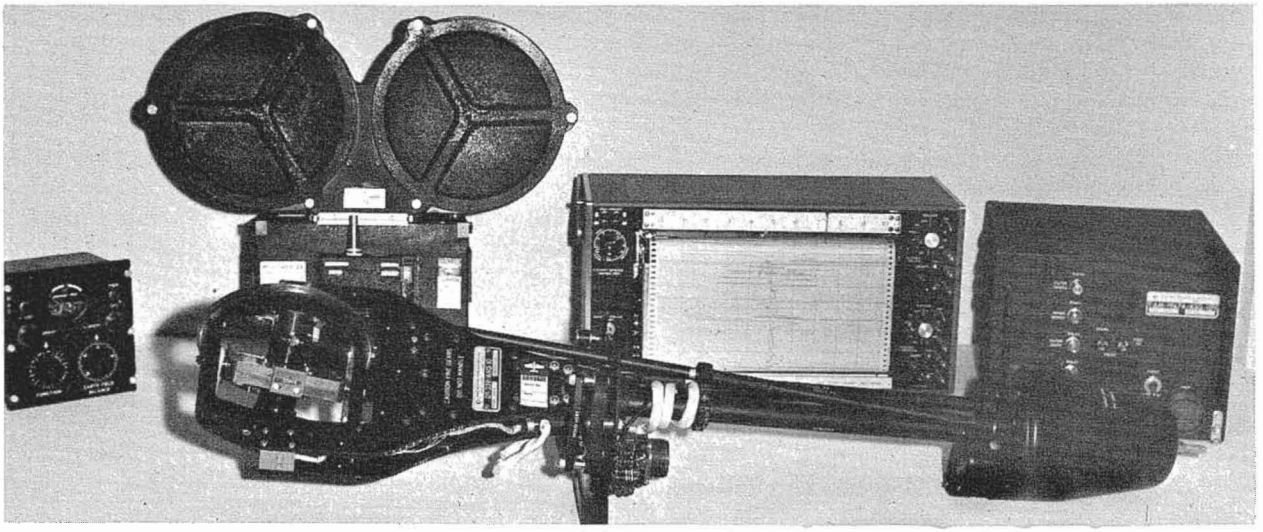


Figure 4. AN/ASQ-10 fluxgate airborne magnetometer and ancillary equipment, consisting of, left to right, detecting set control (C-2548/ASQ-10), Hulcher 35 mm tracking camera, Moseley chart recorder, and amplifier-power supply (AM-1967A/ASQ-10). In the foreground is the detector head (DT-239/ASQ-10). Courtesy Survair Limited, Ottawa.

partially transistorized 36.5-pound replacement, the AN/ASQ-10, which is much lighter and smaller and consumes only one sixth the power (Bureau of Naval Personnel, 1959). The military fluxgate magnetometers cannot be used without modifications because a high pass filter is incorporated to discriminate against low-frequency anomalies such as those produced by the underlying geology.

Figure 3 shows the block diagram of the AN/ASQ-10 magnetometer modified for aeromagnetic survey use (USN, 1964). The magnetometer oscillator supplies a stable 500 Hz drive voltage for the detector magnetometer element and for the orientor sensors in the detector head, whose outputs control the three gimbal systems which maintain the detector magnetometer element parallel to the earth's magnetic field. The detector magnetometer consists of two elements each having a core of eight permalloy strips around which a coil of wire is wound. The eight permalloy strips of each magnetometer are held together by insulating cement to reduce internal eddy currents and thus form a laminated core of approximately square cross section. The magnetometer amplifier selects the second harmonic content of the detector magnetometer by a 1000 Hz bandpass filter whose frequency response is flat over a region around 1000 Hz in case the magnetometer oscillator should shift. The filter has a voltage gain of approximately 16 db at 1000 Hz whereas the attenuation of the fundamental (500 Hz) and all other harmonics is greater than 55 db. The 1000 Hz signal is further amplified, rectified, and the resultant DC output used to drive a recorder. In the unmodified ASQ-10 this DC output is filtered to discriminate against magnetic variations due to the underlying geology and regional variations of the earth's magnetic field and the resultant filtered trace is then applied to the recorder.

The detector head, which can be seen in the foreground of Figure 4, contains the detector magnetometer element and an orienting system to maintain the detector magnetometer element accurately parallel to the earth's total field vector in spite of aircraft manoeuvres. The orientation of the detector element is accomplished by using two accurately controlled perpendicular gimbals, the inner and outer, and a third 'slow-follow' gimbal whose axis is perpendicular to the outer gimbal. The detector head is normally mounted in a stinger installation in the tail of the aircraft, with its long dimension in the direction of flight so that the inner gimbal axis is directed fore and aft and therefore compensates for rolls of the aircraft; the outer gimbal axis is perpendicular to the direction of flight and compensates for aircraft pitches. The brass circular outer axis gear wheel, which is rotated by the outer axis servomotor and therefore rotates the detector magnetometer, is readily seen in Figure 4. The function of the third axis gimbal system is to avoid the possibility of the detector element coming into alignment with the outer axis at one particular heading. When this happens very high gimbal velocities are required to keep the detector element aligned with the total field vector. This occurs, for instance, when the aircraft flies an east or west heading at the magnetic equator. The freedom of movement of the three axes as set by the mechanical construction is ± 65 degrees for the inner axis; ± 130 degrees for the outer axis and ± 90 degrees for the inner axis. The orientation accuracy achieved by this mechanism is approximately ±0.1°, resulting in a possible measuring accuracy of about ± 0.08 gamma in a 50,000 gamma field. Calibration of the compensating circuits can establish the absolute value of the magnetic datum to about ± 0.5 per cent, or approximately ± 250 gammas.

There is an orientor magnetometer pair for both the inner and outer axes. Each orientor magnetometer element consists of one permalloy strip and coil and the two pairs are arranged in the form of a square inside the orientor plate in which the detector magnetometer is mounted at right angles so that all three magnetometer sensors are at right angles to one another. The ends of the orientor strips overlap to minimize magnetic flux leakage around the square and to increase orientor sensitivity. Because the orientor magnetometers normally operate in zero field, there are no net output current pulses from them, so that noise voltages might easily cause unstable servo performance at the null position when signal voltages are small. Unbalancing resistors are therefore shunted across one magnetometer of each pair to produce

alternatively positive and negative signal pulses at a 500 Hz rate. Any rotation of an orientor magnetometer causes the elongation of pulses of one polarity and the shortening of those of the other polarity. These positive and negative spikes are amplified and rectified using push-pull circuitry and the resultant differential DC voltage is amplified and used to drive a servomotor to return the orientor magnetometer to its null position.

The third gimbal system maintains the detector magnetometer near its neutral position, that is midway between the two mechanical stops for the inner gimbal. This is accomplished using error voltages derived from two coils mounted near the detector magnetometer on the outer axis whose axes are perpendicular to the inner axis, and from a coil system mounted at the motor end, one part of which rotates with the third axis which is parallel to the flight direction. The third axis servo system is relatively slow in response. The third axis amplifier (Figure 3) consists of a two-stage 500 Hz voltage amplifier, a phase-sensitive detector which yields DC outputs, a DC amplifier and a magnetic amplifier to drive the third axis servomotor.

The eight electronic unit boxes which comprise the ASQ-8 have been reduced to two in the ASQ-10 (see Figure 4). These are: (a) the detecting set control (C-2548/ASQ-10), seen on the left-hand side of Figure 4, which has the controls necessary for the operation of the magnetometer. The controls include the main power switch, a 12-position function selector switch which combines the functions of meter switch and sensitivity control, an earth field balance rheostat providing a range of 24,000 to 70,000 gammas in 47 steps of 1,000 gammas which controls the buck-out current in the detector head, orienting controls for the inner and outer gimbal systems, and a γ test pushbutton. A meter is provided by which the system voltages may be monitored using the function switch; (b) the amplifier-power supply unit (AM-1967A/ASQ-10) seen on the right side of Figure 4. Apart from the power supplies, five plug-in subassemblies are contained in this unit, which are the magnetometer amplifier, magnetometer oscillator and filament supply regulator, third axis amplifier, inner gimbal amplifier and outer gimbal amplifier.

A second harmonic airborne fluxgate magnetometer, the AM-13 has been developed in the U.S.S.R. Three-orthogonal elements excited at 500 Hz comprise the fluxgate assembly which is gimbal-mounted in a bird but has only two degrees of freedom to maintain the orientation of the fluxgate head. The operating range of the instrument is 11,000 γ, and the sensitivities of the analog recorder chart are 2 γ/mm on the 400 γ subrange, and 10 γ/mm on the 2000 γ subrange. The drift of the system is less than 5 γ per hour.

Proton precession magnetometers. *Free-precession type.* It was observed by Packard and Varian (1954) in 1953 that after a strong magnetic field is removed from a sample of water, an audio-frequency signal may be detected for a second or so. The explanation for this is that the hydrogen proton has a magnetic moment due to its spin so that the magnetic moment vectors will align themselves parallel to an applied magnetic field. When the field is removed and the protons come under the influence of the earth's magnetic field, which will generally have a different orientation to the applied field, the protons precess like gyroscopes. The precession signal will last for several seconds, its amplitude decaying exponentially with time, and during this decay time the precessing protons induce a small alternating voltage at the precession frequency in the polarizing coils. The rate of decrease of amplitude is dependent on the gradient of the ambient field across the sample which causes loss of phase coherence because protons in different parts of the sample precess at slightly different frequencies.

The frequency of precession f is directly proportional to the ambient field T so that we need only ascertain f to calculate T. Thus T gammas = Kf hertz where $K = 23.4874$. Actually $K = 2\pi$/gyromagnetic ratio of the proton so that K is an immutable atomic constant, which means that proton precession magnetometers are absolute instruments. An accurate determination of the gyromagnetic ratio of the proton (γ_p) by Driscoll and Bender (1958) yielded a value of $\gamma_p = 2.67513 \pm 0.00002 \times 10^4$ oersted $^{-1}$ sec $^{-1}$. The result was subsequently confirmed by Vigoureux (1962, 1963).

If the axis of the polarizing/detecting coil is at angle θ to the total field T, the amplitude of the precession signal is proportional to $\sin^2 \theta$. Thus the amplitude for $\theta = 45°$ is only half that for $\theta = 90°$, and it will fall to very low values as θ approaches zero, so that there is a dead zone along the axis of the coil. To avoid this difficulty, two mutually perpendicular coils are commonly used. With this configuration, if the total field T makes an angle θ with the normal to the plane defined by the axes of the coils, then the signal amplitude is proportional to $1/2 (1 + \cos^2 \theta)$ (Whitham, 1960). Thus between $\theta = 0°$ and $\theta = 90°$, the signal amplitude is only reduced by a factor of 2. Alternatively a toroidal coil may be used to avoid the possibility of low precession signal amplitudes; a toroid also picks up less external interference due to nearby electrical systems (Washkurak and Sawatzky, 1966), because it is the electrical equivalent to a single turn with respect to an external source. If the proton head rotates during the count period the precession frequency recorded will be either increased or decreased depending upon the sense of the rotation with respect to the coil system. It is readily apparent from the equation previously given relating the total field to the precession frequency that the precession shift is 23.4874 gammas per rotation per second, i.e., 0.0652 gamma per degree per second.

There are two common ways of determining the proton precession frequencies, which result in the two types of proton magnetometers, namely the reciprocal and direct-reading types.

Reciprocal-type proton free-precession magnetometers. The reciprocal type counts the number of oscillations of a high-frequency oscillator (often 100 KHz) which occur during a given binary number (for example, 1024) of cycles of the proton precession frequency. Thus the higher the proton precession frequency the less will be the total number of high-frequency oscillations counted, which is the reason for the term reciprocal type.

This method is used in the Elsec ground magnetometer manufactured by Littlemore Scientific Engineering Co. in the U.K. A block diagram of the Elsec Type 592 proton magnetometer is shown in Figure 5. The length of the polarizing period is controlled by the timer from 0.6 to 4.5 seconds. The precession signal f is amplified, squared and fed to an 8 to 12 binary chain for frequency division by a factor n. For a ten-stage divider $n = 2^{10} = 1024$, so that the frequency after the tenth stage is around 2 Hz. The signal from this Slow Counter is then applied, via a locking unit, to an electronic gate. The first positive-going edge of

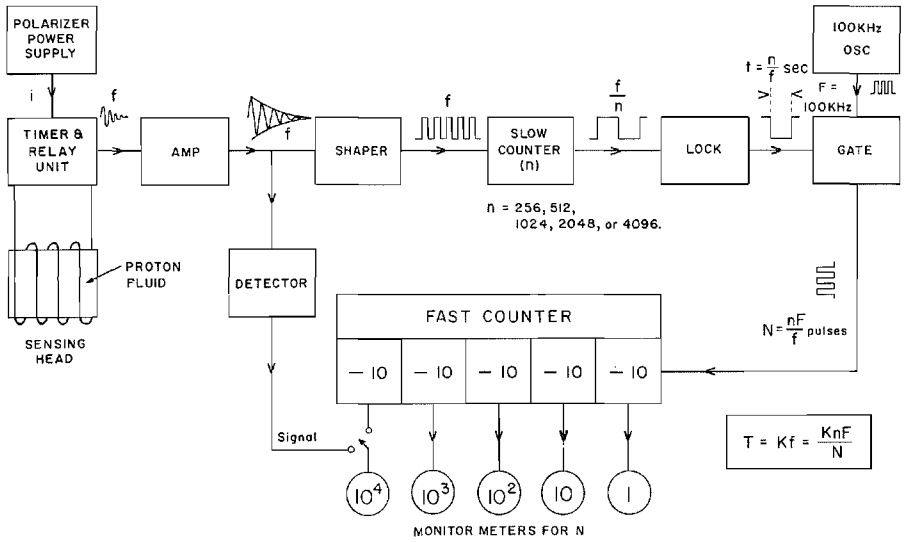


Figure 5. Block diagram of Elsec 592 reciprocal-type proton free-precession ground magnetometer.

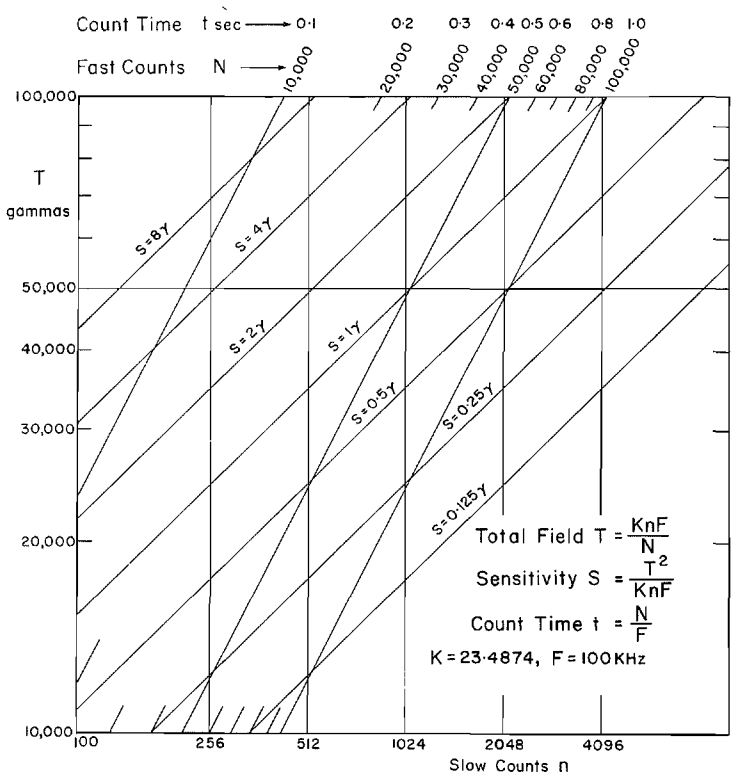


Figure 6. Graph showing the relationship between total field, slow and fast counts, count time, and sensitivity for reciprocal-type proton precession magnetometers using a 100 KHz fast oscillator.

a pulse opens the gate and the next positive-going edge closes the gate which remains closed until the unit is reset. While the gate is open, pulses from the high-frequency oscillator $F = 100$ KHz pass through the gate into the fast counter. The corresponding meter for each decade unit indicates the number of counts in each decade unit, so that the 5-digit number indicated by the five meters gives the number N of 100 KHz pulses which pass through the gate during the time t that it is open. Thus $t = n/f = N/F$ so that $T = Kf = Knf/N$. Thus T is proportional to the reciprocal of N. The sensitivity S of the system is ± 1 count of N which therefore represents T/N gammas. Hence $S = T/N = T^2/Knf$ gammas. Thus the sensitivity is better at the lower values of the

Contents

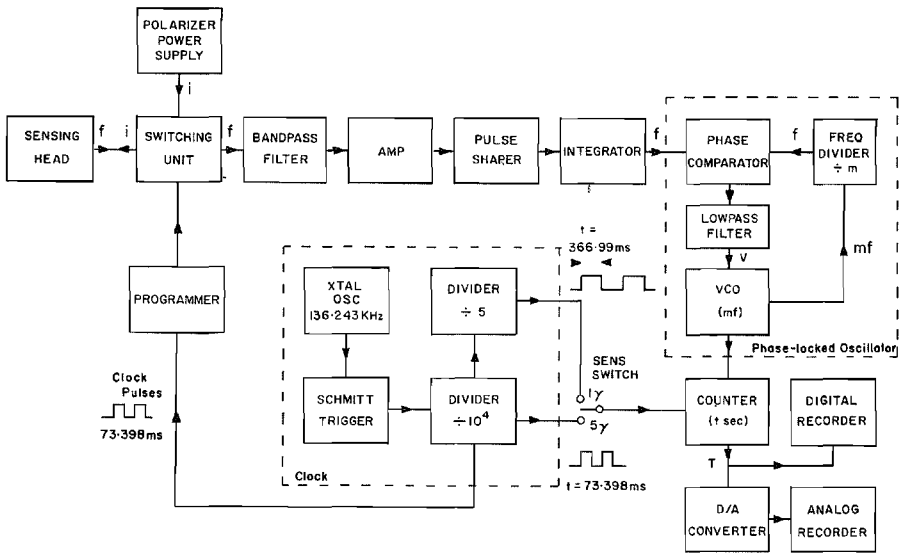


Figure 7. Block diagram of Barringer AM-101 direct-reading proton free-precession airborne magnetometer.

earth's magnetic field. Figure 6 is a graph showing the relationship between T, n and the sensitivity S, and also T, n and N for F= 100 KHz. The count time t has also been shown.

The Elsec Type 592 proton magnetometer weighs 26 1/2 pounds with the standard 12-volt battery pack and detector bottle. The range of the transistorized instrument is 24,000 to 70,000 gammas with a sensitivity of ± 0.5 gamma or better. The accuracy is 1 part in 50,000 over the operating temperature range of −10°C to + 40°C. The Slow Counter may be set for n = 256, 512, 1024, 2048 and 4096 using a front panel switch. Five automatic polarize/count rates are selectable by a front panel switch between about 1 per second and 1 per minute, and there is also a manual position of this switch so that readings may be initiated by push button. The tolerable magnetic gradient quoted for the detector bottle is 200 γ/metre for 0.5-gamma accuracy, 400 γ/metre for 1-gamma accuracy and 800 γ/metre for 2-gamma accuracy.

The Elsec-Wisconsin proton precession airborne magnetometer consists of an Elsec ground instrument, which obtains the basic magnetic field values, and a digital-recording system designed and constructed at the University of Wisconsin (Wold, 1964). The reciprocal magnetic field values and time are outputed in binary coded decimal format on punched paper tape for direct input into a computer. An analog output is also obtained on a suitable recorder.

The PM-1 reciprocal-type proton free-precession magnetometer developed by the Institute of Terrestrial Magnetism, Ionosphere and Radio Wave Propagation (Izmiran) in the U.S.S.R. has been described by Kudrevskiy (1961). Because it is rather bulky for field use it has been replaced by the transistorized reciprocal-type PM-5 instrument (Nalivayko, *et al.*, 1962). This has a 100 KHz fast counter and the slow counter is set to n = 1024. Consideration of Figure 6 shows that the PM-5 has a 1-gamma sensitivity.

Direct-reading proton precession magnetometers. In direct-reading airborne instruments, such as the Barringer AM-101 (Figure 7), the induced signal from the sensing head, which occurs after the polarizing field has been switched off, is amplified, squared and fed to a phase detector. A voltage-controlled oscillator, which is governed by the output of the phase detector, generates a frequency approximately m times the precession frequency f. A portion of this multiplied frequency is fed back to the phase detector through a $1/m$ frequency divider to bring it down to almost f. If a frequency difference exists between the original precession frequency input to the phase detector and the output frequency of the frequency divider, the phase detector will change the output DC voltage to the voltage-controlled oscillator to make the VCO frequency exactly mf. The multiplied frequency mf is then counted for an exact period (t seconds) so that the resultant digital number gives the total field reading directly in gammas. Thus we have the total field.

$$T = Kf = mf\,t \text{ gammas so that } mt = K = 23.4874$$

For a sensitivity S gammas, $S = \dfrac{K}{mt}$

Using a digital-to-analog converter, the output of the counter can be displayed on a strip-chart recorder for monitoring purposes.

Figure 8 shows the three units comprising the Barringer Research AM-101B airborne nuclear magnetometer. From left to right is the bird, the magnetometer console, and the preamplifier for the precession signal from the bird. The instrument is fully transistorized using printed circuitry throughout and a direct readout of the absolute value of the earth's total field is available in 1- or 5-gamma intervals. The magnetic reading may also be read off a Nixie-tube visual display on the front of the unit. A standard single-potentiometer recorder output is provided, and as an option voltages proportional to each of the last three digits of the total field may be supplied for analog recording, or alternatively outputs can be provided for the operation of

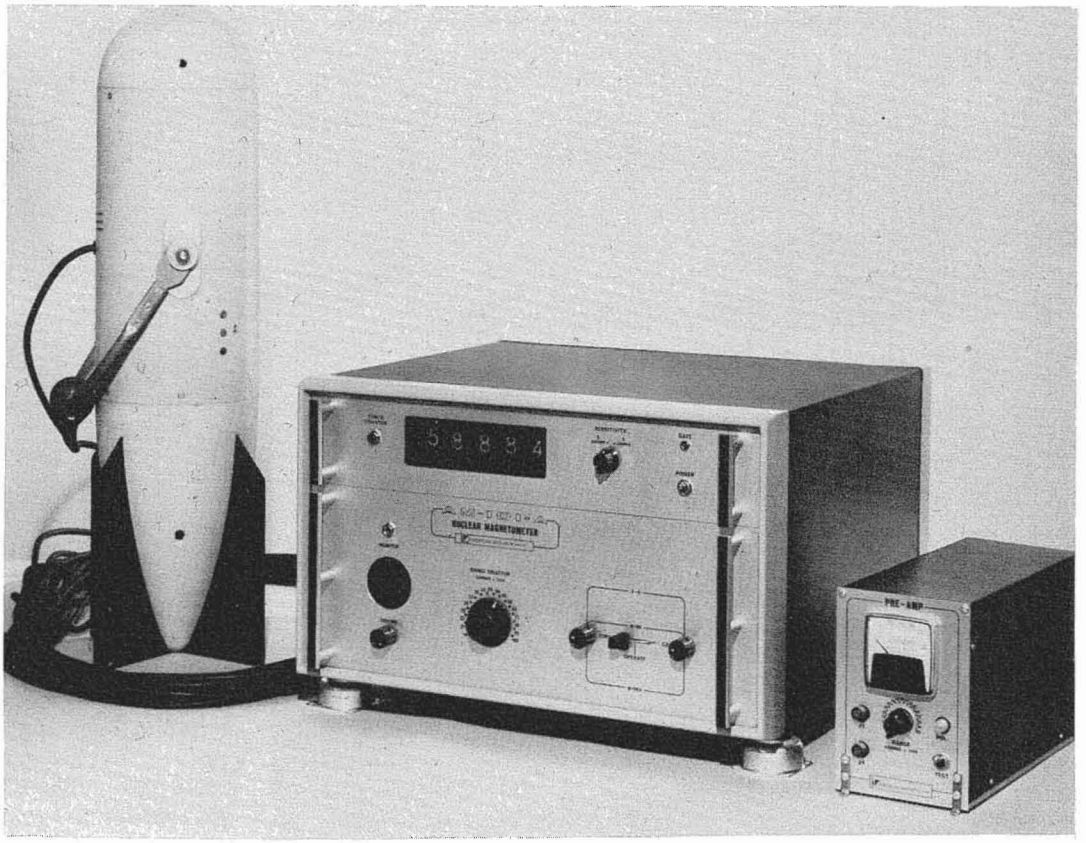


Figure 8. Barringer AM-101B proton free-precession airborne magnetometer. Left to right: bird, magnetometer console, and pre-amplifier.

digital-recording equipment. A further option is the provision of a separate (4-pound) preamplifier unit for use in low signal-to-noise environments which should be mounted as close to the sensing head as possible. The operating range of the 60-pound AM-101B is from 20,000 to 110,000 gammas in eight overlapping ranges of 14,000 gammas selectable by a switch. Automatic tuning of the unit to the precession signal frequency is provided over the complete operating range. The polarize/count time of the instrument for a 1-gamma sensitivity is 1 second, and for a 5-gamma sensitivity is 1/3 second. The count time t is accurately maintained by a crystal-controlled clock (see Figure 7). The output from the 136.243 KHz crystal oscillator is first squared by a Schmidt trigger and then fed to four series-connected decade counters. The output of the fourth decade is used as a source of 73.3983 millisecond clock pulses which are used to control the programmer and the counter so that a 5-gamma sensitivity is obtained using a frequency multiplier m = 64. The sensitivity of the instrument may be increased to 1 gamma by increasing the count time five times to 366.99 milliseconds using the ÷ 5 divider incorporated in the circuit.

Transistorized direct-reading proton precession airborne magnetometers have also been produced by Varian Associates of Palo Alto, California, the V-4937, and by Prakla of Hannover, the PM-22 and PM-24. Development of the DC V-4937 airborne proton magnetometer was begun in 1965 to convert the Varian direct-reading marine proton magnetometer for small aircraft. This instrument offers a ± 1-gamma sensitivity at a 1-second sampling rate, or ± 2-gamma at a 0.5-second sampling rate. The newer version of the Varian direct-reading proton magnetometer, the V-4937A, has several major changes from its predecessor, the V-4937, for instance in the redesign of its circuit boards to operate on a common DC voltage (24-30V) source and to make the V-4937A smaller and lighter (complete airborne version is 105 pounds). The range of this 1-gamma sensitivity instrument is 20,000 to 100,000 gammas, and it requires about 200 watts for operation. Varian Associates also manufacture a portable power pack so that the V-4937A may be operated from 50, 60 or 400 Hz power supplies.

At present, airborne magnetometer surveys must be conducted during periods of relatively undisturbed magnetic diurnal variation, and magnetic control lines must be flown across survey lines at regular intervals to provide the necessary data for the diurnal corrections. In the GSC Telmag (telemetering magnetometer) system (Washkurak and Sawatzky, 1966) a survey aircraft equipped with a proton magnetometer telemeters the total magnetic intensity data to a base station where the magnetic diurnal is continuously and automatically removed. A frequency multiplication factor of 320 with a count time of 0.7340 second is used to obtain total intensity readings with a 0.1-gamma sensitivity.

A direct-reading proton precession airborne magnetometer, the AYaAM-6, has been built in the U.S.S.R. The Larmor precession frequency is multiplied 24 times and counted for 0.97867 second to obtain a 1-gamma sensitivity (Yanovskii, 1963).

Figure 9 shows the relationship between the frequency multiplication factor m, the count time t and the sensitivity S in gammas for direct-reading proton free-precession magnetometers.

Contents

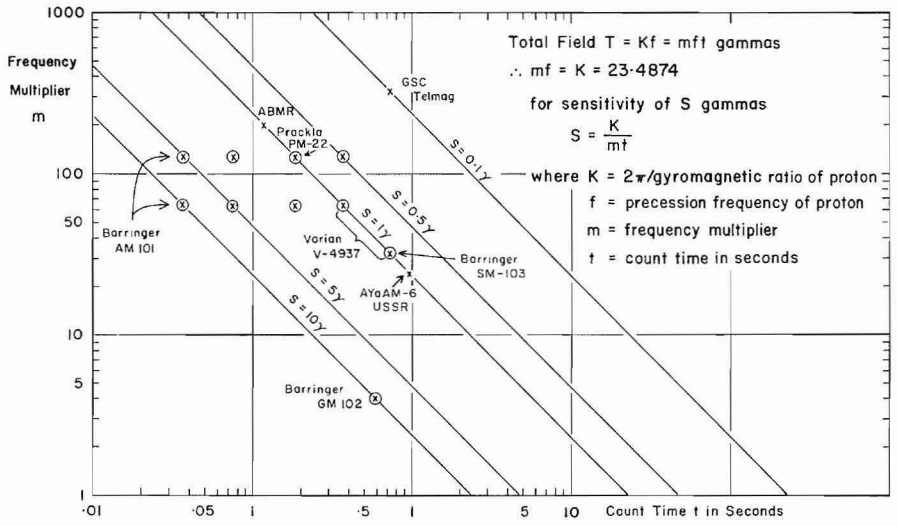


Figure 9. Graph showing the relationship between the frequency multiplication factor, count time, and sensitivity for direct-reading proton precession magnetometers.

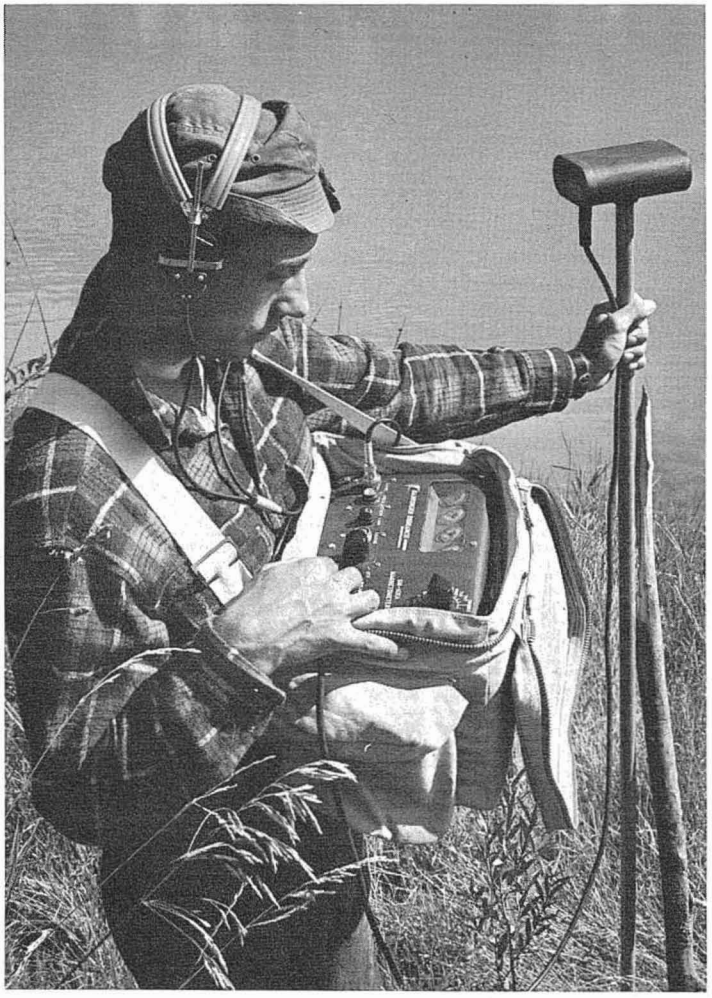


Figure 10. Barringer GM-102A proton free-precession ground magnetometer being operated in the field.

The positions on the graph of a number of actual direct-reading proton precession magnetometers have been indicated.

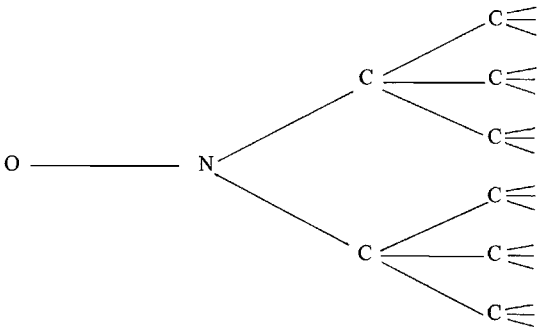
Figure 10 shows the Barringer GM-102A proton free-precession ground magnetometer being used in the field. It is the direct-reading type and the proton precession frequency is multiplied by a factor of 4 and counted for 0.58718 second to give a 10-gamma sensitivity total-intensity reading. A precision tuning-fork oscillator is used to control the count time precisely. The total-intensity reading in gammas is visually displayed using decimal glow-tubes to four decimal places. The range of the 18-pound instrument is 42,300 to 83,000 gammas in 10 ranges selectable by a front panel switch. A headphone set, which is being worn by the magnetometer operator in Figure 10, is used to listen to the decaying proton precession signal and thus to ascertain that the range switch is set to its correct position. When the range switch is set to its correct position the precession signal has an almost musical quality. It is operated from 10 *D* cells which can be the rechargeable NICAD variety. The operating temperature range is $-40°F$ to $+120°F$.

Spin-precession or Overhauser type. In the spin-precession or Overhauser type of magnetometer the liquid sample in the magnetometer sensor contains a parametric substance which possesses the property that the spin energy of its electrons is transferred by coupling to the proton spin of the solvent. This mechanism is called the Overhauser (1953) effect. The spin energy of the electrons is maintained by the application of a suitable high-frequency polarizing field. Thus the polarized protons of the solvent precess continuously at the Larmor frequency which is governed by the ambient magnetic field and which is detected by a suitable pickup coil.

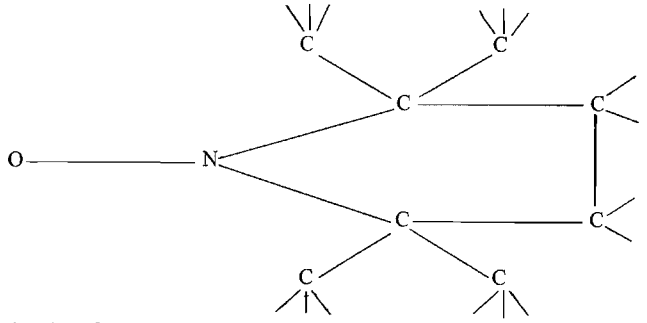
Sud-Aviation of France have developed an airborne magnetometer designated the MP 121 (Thomas, 1965) under licence from the French Atomic Energy Commission. It operates over the range 27,000 to 75,000 gammas. The sampling rate is one reading per second, and a sensitivity of 0.1 gamma is possible with digital recording on punched paper tape. An analog record is also made with a maximum sensitivity of about 0.5 gamma. The analog subranges are 100, 200, 500 and 1000 gammas. Total weight of the airborne installation with towed bird is 280 pounds.

One of the difficulties of Overhauser magnetometers heretofore has been that the precession characteristics of the liquid used in the detector head deteriorated over a relatively short period. However, several semipermanent hydrogenated solvents have been perfected by workers at the Grenoble Laboratory of the French Atomic Energy Commission (Lemaire, *et al.*, 1967). These are a class of organic free radicals consisting of

1. Ditertiarybutylnitroxide ($NO[C(CH_3)_3]_2$) and its derivatives, such as triacetoneamine oxide having the following general formula:

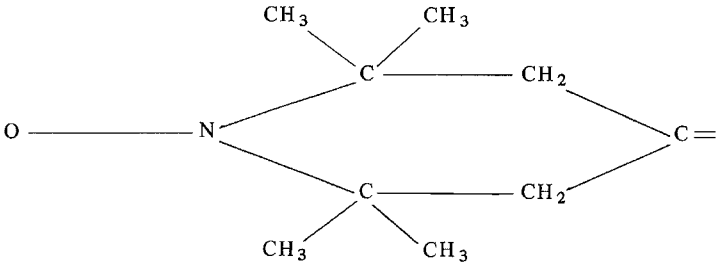


2. Those having a five-numbered heterocyclic ring, the general formula of which is:



Radicals of this group, which have been used as magnetometer samples, have been given the shortened names Tanam-5, Tanane-5, Tanol-5 and Tano-5.

3. Those having a six-membered heterocyclic ring with the following general formula:



Radicals of this group which have been used as magnetometer samples have been given the shortened names Tanol-6, Tanane-6 and Tanoxime-6 by Lemaire, *et al.* (1967). The foregoing organic radicals have electron resonance lines which vary from about 64 MHz to 75 MHz in pure water.

A ground Overhauser magnetometer, the MP 102, has also been developed by Sud-Aviation. It consists of a sensing head and pole, a 10-metre connecting cable, an electronic measuring module and storage batteries. The total weight of the equipment is 51 pounds, and the equipment is designed to operate at temperatures between − 15°C and + 50°C. This continuously reading instrument has a range of 11,100 gammas and a series of plug-in modules allows fields between 20,000 and 81,000 gammas to be measured. Magnetic field variations of 1 gamma can be detected, using the galvanometer on the electronic module, over a working range of 100 gammas. By using a suitable external recorder changes of 0.1 gamma can be detected.

Optical absorption magnetometers. The high-sensitivity atomic-resonance magnetometers are the latest type to be used in airborne geophysical surveys and are currently (1967) under intensive development. Three varieties have been produced, the metastable helium, rubidium and cesium magnetometers. All these magnetometers make use of the optical-pumping technique originally devised by Kastler (1950). The basic physics of these magnetometers is complicated but some idea of the principles involved may be gained from the following simplified explanation which has been modified from the descriptions given by Bloom (1960) and Breiner (1965):

Atoms can emit and absorb electromagnetic radiation ranging from radio waves, whose wavelength is measured in hundreds of metres, through the visible light spectrum to X-rays. Electromagnetic radiation energy is divided into discrete packets or photons and the energy of a photon is directly proportional to its EM frequency. When photons are absorbed or emitted by an atom, the atom gains or loses the energy they contain, changing its physical state in some way. The photons of light, with their comparatively high energy, cause the transition of an electron from one orbit to another. The photons of radio waves merely shift the axes of spinning electrons within an orbit. Since the electrons behave like tiny magnets with fields aligned along their axes, such a shift produces a small change in the magnetic energy of an atom. The transition between energy states, or levels, is reversible: atoms at a higher level tend to fall spontaneously into the lower one; those at the lower level will jump to the higher one if the requisite quanta of energy are available. In jumping up, the atoms extract photons from a transmitted beam of radiation, producing an absorption spectrum; in jumping down, they send out photons, producing an emission, or 'bright line', spectrum.

To understand the principle of optical pumping, consider a simplified atom with only three energy levels, which we shall call *A*, *B* and *C* in increasing order of energy. Levels *A* and *B* are low-lying and very close together; the energy difference between them corresponds to a radio-frequency spectrum line, and initially all the atoms are distributed equally between them. Level *C* is much higher; the transitions *A*-*C* and *B*-*C* correspond to lines in the optical part of the spectrum. Suppose a sample of these atoms is irradiated with a light beam from which the spectral line *BC* has been filtered. The beam contains photons that can excite atoms in level *A* but not in level *B*. Atoms excited out of *A* absorb energy and rise to *C*. They will remain there for a short time and then emit energy, dropping back either to the *A* or *B* state. The proportion going to each state depends on the structure of the atoms, but the important thing is that occasionally an atom drops into *B*. When it does, it can no longer be excited by the incident light. If it returns to *A*, the light will raise it to the *C* state again, and again it will have some probability of

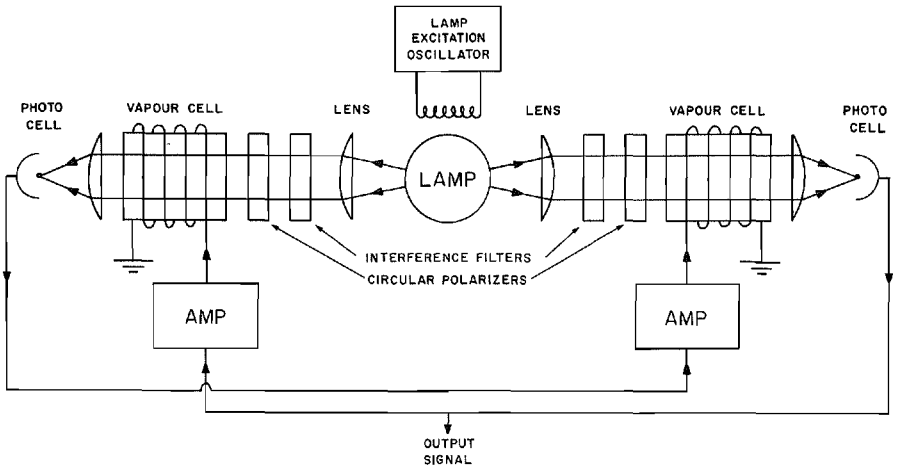


Figure 11. Block diagram of dual-cell self-oscillating optical absorption magnetometer.

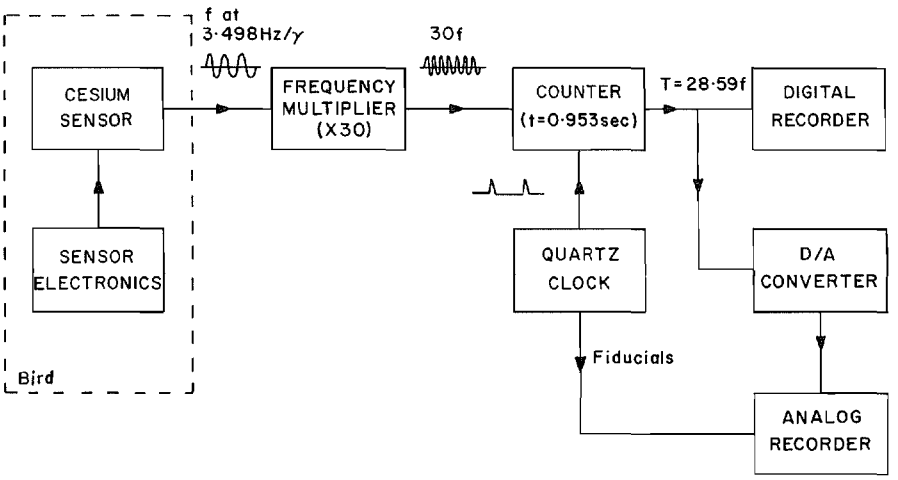


Figure 12. Block diagram of CGTSF/CGG cesium airborne magnetometer.

dropping to *B*. Given enough time, every atom must end up in the *B* state, and the material is then completely 'optically pumped'. Once this condition has been reached the cell becomes transparent, and photons can pass freely through the vapour cell because they are not absorbed. Sweeping the vapour cell with a weak alternating magnetic field disrupts this state and allows pumping to begin again. If one varies the frequency of the applied field and observes the light transmitted through the vapour cell, a sharp absorption is seen to occur when the applied field has a certain frequency, which is the Larmor precession frequency of the electrons. The electrons undergoing the transition between energy sublevels precess about the magnetic field at a Larmor frequency determined by the Zeeman splitting of the levels.

In the actual instrument (see Figure 11) the modulation of the transmitted light is detected by a photocell. The current from the photocell is amplified, shifted in phase by 90°, and used as a feedback signal to drive the alternating magnetic field applied to the vapour cell. This arrangement thus constitutes an oscillator whose frequency is proportional to the total magnetic field intensity at a rate fixed by an atomic constant, 4.667370 ± 0.000035 hertz per gamma for rubidium 85 and 3.498 hertz per gamma in the case of cesium 133. Actually any of the alkaline metals can be used but the vapours of rubidium and cesium possess the correct vapour pressure without an appreciable heating (Giret and Malnar, 1965).

There is a second basic method of monitoring the Larmor frequency by sweeping either the magnetic field or the RF oscillator frequency through resonance using a servo-loop to correct the RF oscillator frequency. Parsons and Wiatr (1962) have described such a swept-field magnetometer.

There is a difference in energy between pairs of Zeeman sublevels proportional to T^2 because of the Back-Goudsmit effect. As the angle between the optical axis and the magnetic field is changed the relative population of the various sublevels changes, producing an appreciable asymmetry in the local pattern when the average line is used for detection. For a typical value of the earth's field of 50,000 gammas, this orientation effect may amount to as much as 20 gammas, under certain conditions, for the rubidium magnetometer. In the case of the cesium magnetometer the Back-Goudsmit effect exists but the orientation effect is negligible (Giret and Malnar, 1965).

Another problem with the single-cell magnetometer is that the correct sign for the phase shift also depends upon the angle between the optical axis and the direction of the total field. Both these problems may be overcome to a great extent by using a dual-cell magnetometer having a common rubidium lamp (see Figure 11). The further disadvantage of the single-cell instrument, which has dead zones, i.e., will not operate when the field is either parallel with or at right angles to the optical axis, may be

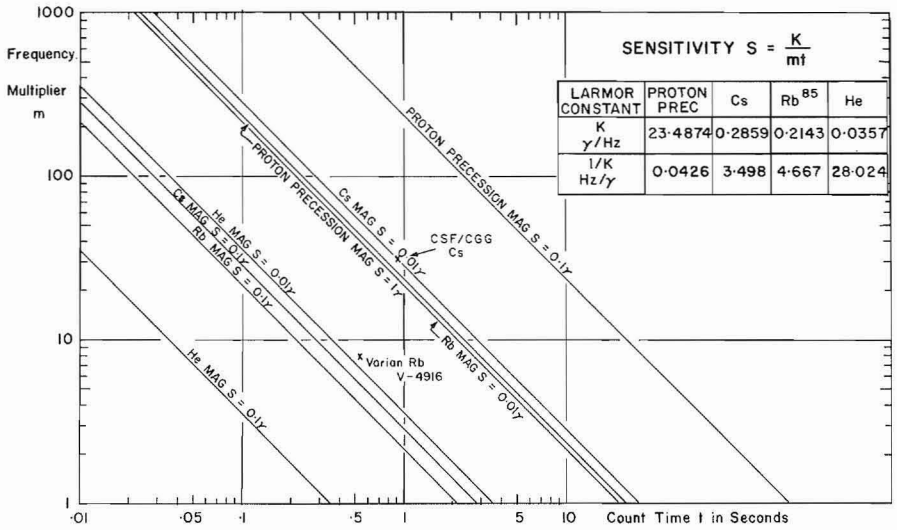


Figure 13. Graph comparing the relationship between the frequency multiplication factor (*m*), count time (*t*), and sensitivity (*s*) for proton precession and optical absorption magnetometers.

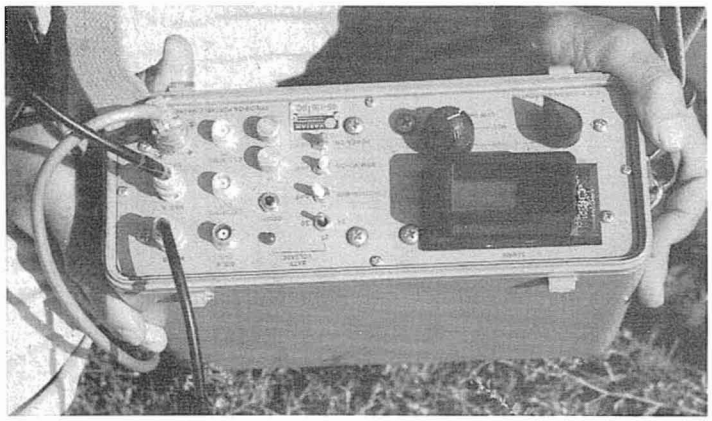


Figure 14. Electronic unit of the Varian Model 4920 cesium ground magnetometer (Courtesy Applied Science Center for Archaeology, University Museum, University of Pennsylvania).

overcome in a dual-cell system by having the optical axes of each half noncoaxial.

Compagnie Générale de Télégraphie sans Fils (CSF) and Compagnie Générale de Géophysique (CGG) have jointly developed a cesium airborne magnetometer (Figure 12) which utilizes the swept-field optical pumping technique (Giret and Malnar, 1965; Giret, 1965). The sensor and associated electronics are contained in a towed bird assembly. In the sensor itself are the light source, the optical system, the cesium cell and the photo-cell detector. The cesium light source is excited by a 60 MHz source, and because the intensity of the light is sensitive to variations in ambient temperature, the source is thermostated. The pyrex vapour cell contains free atoms of cesium in equilibrium with cesium metal. At this pressure, the mean free path of the Cs atoms is large compared to the dimensions of the vapour cell, so that the atoms suffer numerous collisions with the walls, and therefore tend to revert back to a lower energy state. The walls of the vapour cell are therefore coated with paraffin to provide a buffer and improve the relaxation time. The cell is thermostated because the optimum output is obtained at a temperature near 35°C. This makes possible the operation of the magnetometer between −20°C and +45°C. The resultant cesium frequency, which is approximately 175 KHz for a 50,000-gamma field is first multiplied by thirty, and then counted over a 0.953-second period by a frequency meter. The magnetic field values are recorded on a digital magnetic tape recorder at ± 0.01 gamma sensitivity and are also monitored on an analog recorder with a maximum sensitivity of 3.6 gammas per inch. The range of the instrument is 20,000 to 75,000 gammas without adjustment. The optical pumping sensor and associated electronics is towed in a bird from a B-17 aircraft, which is equipped with an Airborne Profile Recorder and a statoscope to provide flight elevation and variations of barometric altitude with an accuracy of 3 feet.

Strome (1964) has described the earlier development of a rubidium airborne magnetometer at the Canadian National Aeronautical Establishment using basic Varian X-4935 dual-cell instruments mounted in a bird and tail boom installations. This high-sensitivity magnetometer has a digital recording system which utilizes both magnetic tape and printer tape, and also has a seven-channel analog monitor system. More recent modifications have enabled the readings from both magnetometers, Decca navigation co-ordinates, and time from a digital clock to be recorded on a single digital magnetic tape by the use of a shift register.

Varian Associates have successfully developed a self-oscillating airborne rubidium magnetometer (Herbert and Langan, 1965; Jensen, 1965) which has been designated the Model V-4916. This transistorized instrument has a sensitivity of 0.05 gamma and consists of four units: the sensor assembly, controller, recorder, and data processor. The sensor assembly contains the coaxial dual-cell rubidium-vapour detector and gimbal assembly for orientation of the thermostated magnetometer head, which provides 360 degrees rotation about the vertical axis, and 180 degrees rotation about the horizontal axis. The controller assembly converts the magnetometer frequency to a DC voltage to drive a Varian chart recorder. This is accomplished using a crystal-controlled oscillator, mixer and discriminator. The controller unit also contains the orientation control system for actuating the gimbal system in the magnetometer head. The rubidium frequency is fed to a phase-lock multiplier which increases the frequency by a factor of eight and this higher

Contents

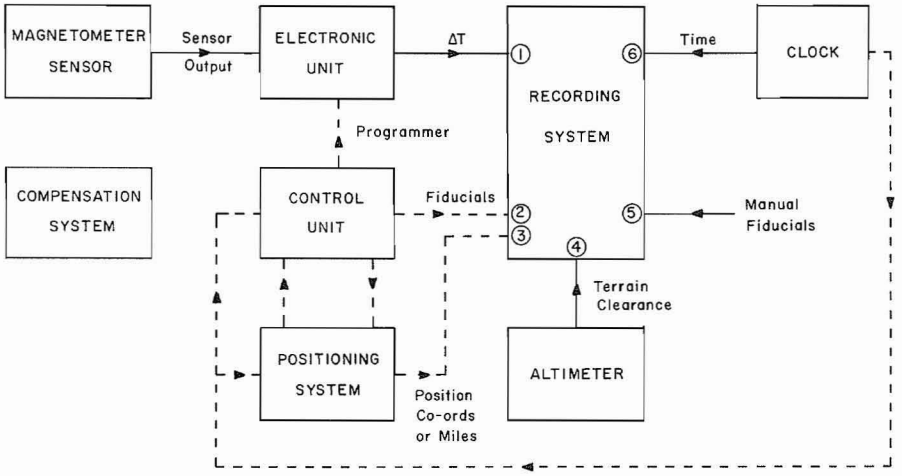


Figure 15. Block diagram of the basic aeromagnetic survey system.



Figure 16. Aero Photo Inc. of Quebec's Aero Commander survey aircraft which is outfitted with a Barringer AM-101 proton free-precession magnetometer. Note magnetometer stinger on the tail of the aircraft.

frequency is then counted for about 0.5 second. Navigational data are provided by a Bendix doppler and Rosemount pressure altimeter. The magnetometer and navigational data together with time is recorded on a single digital magnetic tape by programming through a shift register.

Figure 13 shows the relationship between the frequency multiplication factor, count time, and sensitivity for proton precession and optical absorption magnetometers. It can be seen that the optical absorption magnetometers have a sensitivity approximately two orders of magnitude greater than that achievable with the proton precession type.

The cesium ground magnetometer of Varian Associates of Palo Alto, California, the V4920, is shown in Figure 14. It has a range of 20,000 to 80,000 gammas and has a 0.1-gamma sensitivity. The instrument, which has a digital readout, may be operated either as a magnetometer or as a dual-sensor gradiometer.

Texas Instruments has also built an airborne magnetometer using a metastable helium sensor but to date no details have been released.

Aeromagnetic survey systems

Aircraft installation. The basic aeromagnetic survey system (Figure 15) has not really changed since the first fluxgate survey was flown using a modified ASQ-1 in the northern United States in 1944 (Jensen, 1961). The heart of any airborne magnetometer is the sensing element (or sensor) which detects the small variations in the earth's magnetic field as the aircraft flies along. The various magnetometer sensors which are presently being used for aeromagnetic surveying purposes have been described in the preceding sections. Nowadays the magnetometer head is usually mounted in an inboard installation in the tail of the aircraft (see Figure 16). Inboard installations have been made possible by the improvement in the magnetic compensation of aircraft, and either an active or passive compensation system may be used.

The output of the magnetometer sensor is electronically processed in some way to give a signal, usually a voltage, which is directly proportional to the spatial total field variations (ΔT) measured by the sensor. These are recorded in analog and/or digital form on a suitable recorder. The ΔT variations have to be related to geographic co-ordinates so that a positioning system is required. This is commonly a tracking camera and/or Doppler for surveys over land. It is standard practice to maintain either a constant terrain clearance or a constant elevation above mean sea level so an altimeter is an essential part of the aeromagnetic surveying system and its output is often recorded simultaneously with ΔT. To be able to relate the ΔT variations to the output of the positioning system in the aeromagnetic map compilation process, a control unit is used to provide fiducial marks to the recorder or the positioning system. The control unit may also program the magnetometer to acquire ΔT readings. There are various possibilities all of which have been indicated by the dotted lines on Figure 15. To relate the airborne record to the magnetic diurnal variation recorded on the ground, time must also appear in some fashion in the aeromagnetic survey data.

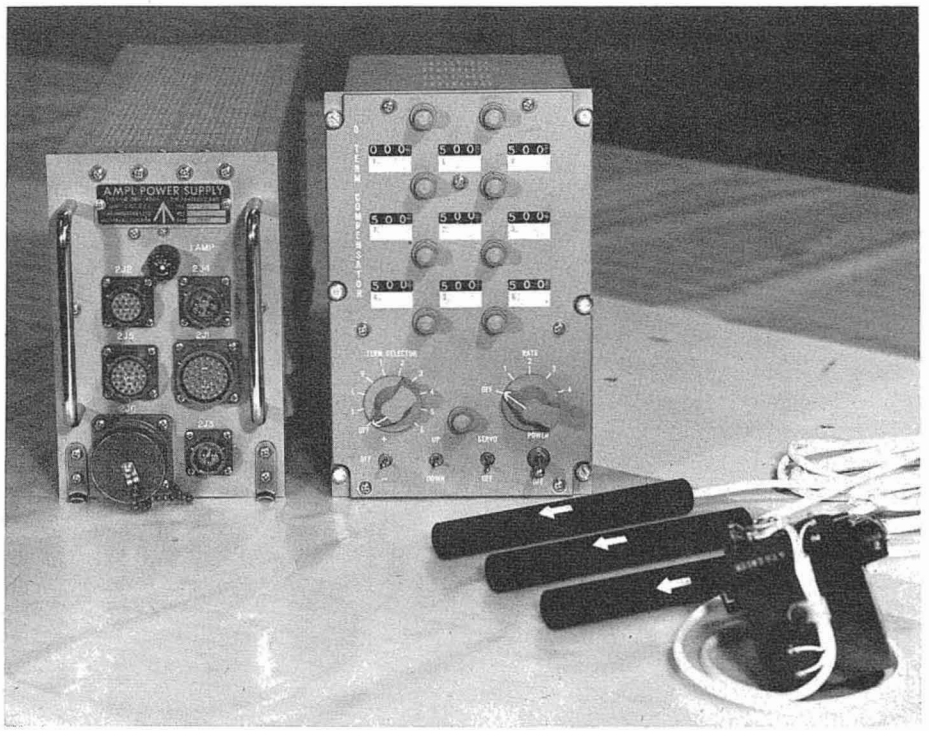


Figure 17. Nine-term compensator for magnetic survey aircraft, Canadian Aviation Electronics Industries Limited.

Many types of aircraft have been used in aeromagnetic surveys since the end of World War II. However since about 1960 there has been a trend to the use of light twin-engined aeroplanes such as the Aero Commander (Figure 16), Beechcraft Queenair, Cessna 310, and Piper Aztec in aeromagnetic surveys because of their economy of operation.

Aside from the development of more sensitive magnetometers, there is a pronounced trend towards the digital recording of aeromagnetic survey data so that the compilation of the final maps might be automated as much as possible. One of the main difficulties to complete automation is the fact that the cheapest method of recovering the track of the survey aircraft is to use 35 mm vertical photography with or without the aid of a Doppler navigation system, so that this will probably remain the basic track location method for some years to come.

The various types of hardware which are essential in an aeromagnetic survey system will be discussed under the following headings: Magnetic compensation of aircraft; Aircraft track recovery; and Radio and radar altimeters.

Magnetic compensation of aircraft. There are three different sources of magnetic interference for inboard installations due to the aircraft itself. The first is the permanent magnetism of the various components made of steel, such as the engines, whose direction remains fixed with respect to the aircraft. The second source is the induced field due to the magnetic susceptibility of these same components and the earth's field. Its polarity and magnitude depend upon the orientation of the aircraft with respect to the earth's magnetic field. The third source of interference is that due to the magnetic effect of eddy currents generated in the skin and other conducting parts of the aircraft by their motion in the earth's magnetic field. In passive compensation systems, the permanent magnetism is eliminated by the use of a set of three-orthogonal compensating coils mounted near the magnetometer head on the roll axis of the aircraft (Bureau of Naval Personnel, 1959) through which the appropriate DC currents may be passed. The induced components are eliminated by the use of Permalloy strips, and the eddy currents are compensated by coils of wire mounted in close proximity to the sensitive element. It is necessary to carry out a set of pitches and rolls of the aircraft in low gradient areas to separate the effects of the various components (Leliak, 1961). The excellence of compensation of a given aircraft is measured by its 'figure of merit'. This index is obtained by summing, without regard to sign, the amplitudes of the 12 magnetic anomalies recorded when the aircraft carries out 20° rolls, 10° pitches and 10° yaws peak-to-peak on north, east, south and west headings.

With the advent of high-sensitivity magnetometers, there was a partial reversion to the use of towed bird systems in aeromagnetic surveying. The reason for this apparent step backwards was that the magnetic compensation of aircraft was not, in general, good enough to cause manoeuvre noise to be unimportant. However active 9- and 16-term magnetic compensation systems have been developed by Canadian Aviation Electronics (CAE) Industries Ltd. of Montreal for use in inboard installations. They drastically cut down the time required for aircraft compensation, and improve the 'figure of merit' of aircraft considerably. Figure 17 shows CAE's 9-term compensator which consists of three saturable-core magnetometer probes, an amplifier-power supply, and the main electronic unit containing the control circuitry. The compensation coils which are mounted near the magnetometer head are shown at the bottom of Figure 17. The compensator can be used in any aircraft with any magnetometer at any magnetic latitude. It provides active and semiautomatic compensation for the permanent, induced and eddy-current aircraft interfering fields. To compensate for these fields at the magnetometer detector, synthetic fields are gen-

erated which simulate and oppose those due to the aircraft. A permanent field component is simulated by sending a constant current through the appropriate compensation coil. An induced field component is simulated by passing a current proportional to the output of a compensation vector magnetometer into the appropriate compensation coil to produce a field proportional to the earth's field component along the compensation magnetometer axis. The eddy-current field component is synthesized by sending a current which is proportional to the differentiated output signal from a compensation magnetometer into the appropriate compensation coil.

Aircraft track recovery. The most widely used method of recovering the aircraft track is still by the use of 35 mm cameras, either continuous strip or the more usual single frame (every two seconds) variety. In areas where the base maps are poor or nonexistent, Doppler navigation has been used. Over water, electronic positioning systems, such as Decca, Shoran and its derivatives Hiran and Shiran, and Raydist (Laurila, 1960) must be used. For reconnaissance surveys the World War II Loran A (USAF 1959/60; Sonnenberg, 1963) system has also been employed, and the more accurate Loran C system is now available for navigational use in many areas.

Tracking cameras. One of the most popular tracking cameras used by Canadian survey companies is the Canadian Applied Research Ltd. Type T232 35 mm camera. It is a self-contained, electrically operated (28 V DC) unit with separate circuits for operating the shutter and actuating the film transport. The screw-in lens mount accepts any type of lens having a standard Leica thread, although adapter rings may be used to accept other types of lenses. The 14-pound camera is fitted with a rotating-disc type, focal-plane shutter having a minimum exposure time of 1/100 second and uses a 25 mm wide × 18 mm long frame format. A 100-foot film magazine is standard but 400-foot magazines are available and these are readily detachable from the main part of the camera using a quick-release lever.

Another much used tracking camera is the electrically operated (28 V DC) Vinten 35 mm camera which is made in the U.K. The 58-pound camera can be remotely controlled from a separate control unit which also produces the fiducial pulses for a chart recorder. The preferred lens for use at heights below 1000 feet is an 18.5 mm Angenieaux. The shutter is a compound type using rotating sectors, the shutter speed being fixed at 1/250 second. The exposure is adjusted by changing the lens aperture. The camera uses standard 35 mm perforated film with a frame format of 24 mm wide × 18 mm long. The magazine holds a 400-foot roll of film which with the 18 mm format gives about 6500 frames per magazine. The magazines are readily changeable in the air. The time interval between vertical photographs is selected by an eight-position switch giving intervals between 0.5 and 6 seconds.

Decca Navigation System. The Decca Navigation System (Decca Navigator Co. Ltd., 1958; Laurila, 1960; Sonnenberg,1963) is an electronic positioning system which uses a master and two or three slave ground transmitting stations, usually referred to as a Decca chain, to radiate phase-locked unmodulated radio waves using frequencies between 70 and 130 KHz. Because the airborne Decca receivers must distinguish between the ground transmitters, each transmitter broadcasts on a separate frequency which is some multiple of the basic frequency 14.16 KHz. In the airborne receiver the CW received from a master and a slave are brought to a common frequency and the phase difference between the two is displayed on a phase meter which is called a decometer. Thus there is a decometer in the Decca receiver for each master-slave pair and these are labelled red, green and purple. The locus of points of equal phase on the earth's surface are hyperbolae with the ground transmitters located at the foci of the hyperbolae. Thus a given decometer reading will indicate a hyperbolic line of position (LOP) on which the aircraft is located, so that two decometer readings are required to establish two LOPs, and the aircraft location is at the intersection of these.

The slave stations are positioned with respect to one another and the master station so that the angles at which the families of hyperbolae, e.g., red and green, cross is as orthogonal as possible, so that a given position fix may be most accurately made. Charts showing the families of hyperbolae are issued by the Decca Navigator Company Ltd. for the various Decca chains which have been permanently established in eastern Canada, western Europe, the Persian Gulf, India, etc. The Decca lattice has also been overprinted on hydrographic charts issued by government agencies. The areas between the lines of zero phase printed on a Decca chart are usually referred to as Decca lanes, and the number of Decca lanes for a given master-slave pair will be dependent on the distance between them. One of the difficulties of a phase-measuring radio location system is the problem of being sure which Decca lane for a given master-slave pair the aircraft is in, because there is a position in every Decca lane in which the phase difference between the master and slave CW transmissions is the same. This problem is overcome using a Lane Identification System in which the normal transmissions are interrupted at periodic intervals from two of the slave stations, the remaining slave station and the master station transmit on a different multiple of 14.16 KHz and by suitable phase comparison of the frequencies the Decca lane for the master-slave pair is displayed on a lane identification meter. The lane identification signals are transmitted once every minute cyclically for the red, green and purple decometers. The useful range of the Decca navigation system is around 240 miles.

One common technique in aeromagnetic surveys over water- or ice-covered areas is to actually fly along the Decca lines of a given master-slave pair. The appropriate decometer is mounted in the cockpit of the aircraft so that the pilot can use it as a left-right indicator. This simplifies the navigational procedure considerably but it means that a constant flight line separation is not maintained because of the hyperbolic shape of the Decca lines.

Shoran navigation system. The Shoran navigation system (Grant, *et al.*, 1955; Laurila, 1960; Newman, 1960), which has often been used in airborne geophysical surveys, is of the pulse transponder type. The transmitter is carried in the aircraft and sends pulses alternately on frequencies of 230 and 250 MHz to two ground stations which transpond on a common 300 MHz frequency. The transit time of the pulses is measured by suitable electronic equipment in the aircraft. Thus, the range distances between the aircraft and each of the two ground stations may be calculated using the established figure for the velocity of light.

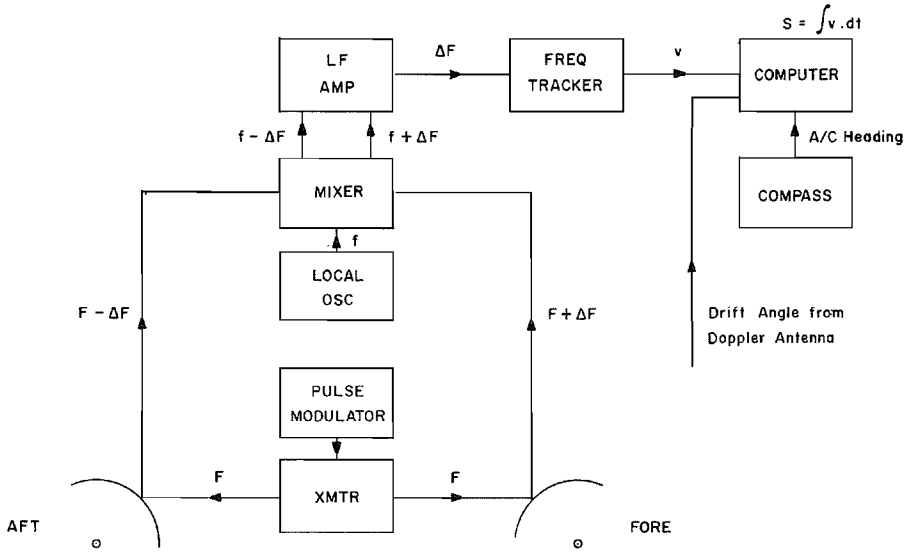


Figure 18. Block diagram of basic Doppler navigation system.

The position of the aircraft may then be fixed by trilateration if the distance between the ground stations is known. This may be done by flying the aircraft between the ground stations and determining the minimum sum of the two range distances. Because of the UHF frequencies used, Shoran is for practical purposes a line-of-sight system.

Doppler navigation system. The Doppler effect was discovered by the German Christian Johann Doppler in 1842 and applies to all wave motion, i.e., both sound and electromagnetic energy. Stated simply, the Doppler effect is the apparent change of frequency of radiant energy when there is relative motion between the transmitter and receiver, the apparent change in frequency being directly proportional to the velocity between the transmitter and receiver. An airborne Doppler system transmits narrow beams of electromagnetic energy of frequency F to the earth's surface, receives a portion of the backscattered energy and measures the frequency shift (ΔF) between the transmitted and received energy. The operative equation is

$$\Delta F = 2 \frac{v}{c} F \cos a \qquad \text{(Tull, 1957)}$$

where v and c are the velocity of the aircraft and light, respectively, and a is the angle of the Doppler beam below the horizontal. Thus the velocity of the aircraft is obtainable directly using the Doppler equation. The drift angle of the aircraft is also measured by Doppler systems using port and starboard beams which are sent out forward and/or aft of the aircraft and comparing the Doppler shifts of the reflected beams. The Doppler shifts will only be the same if the aircraft track accurately bisects the line joining the areas on the ground from which the Doppler beams are reflected. On the more sophisticated airborne equipments, the difference in Doppler frequencies between the port and starboard beams is used to control a servo system which maintains the Doppler antenna in the direction of motion (Wilson and English, 1959). Thus the angle between the antenna and the fore-and-aft line of the aircraft is the drift angle or yaw of the aircraft. Figure 18 is a simplified block diagram of a basic Doppler navigation system. The transmitter supplies a pulsed frequency F in the X-band which is transmitted fore and aft of the aircraft. The reflected frequencies received differ from that transmitted by the Doppler shift ΔF which is extracted, converted to velocity and fed to a computer along with the drift angle from the Doppler antenna and the compass heading.

These three parameters are the only information required to plot the track of the aircraft, and the computer may display this information either as geographical co-ordinates or distance along and across track. The cumulative errors on most Doppler systems are usually between 1 and 2% of distance gone.

Jensen (1965) has considered the stringent flight-path restrictions necessary in the conduct of high-sensitivity aeromagnetic surveys. He concludes that all high-resolution magnetic surveying should be under the control of Doppler navigation, precision pressure altimeters and modern autopilots.

Radio and radar altimeters. These are active systems which utilize electromagnetic energy reflected from the ground. The radio altimeter most commonly used in earlier airborne geophysical surveys was the AN/APN-1, which was developed during World War II. The components of the 28-pound AN/APN-1 are the transmitter-receiver electronic unit, an altitude indicator, altitude limit switch, and two antenna assemblies (USAF, 1959/60). The 28 V DC transmitter-receiver transmits a 400 MHz frequency-modulated signal from the transmitting antenna which is reflected from the earth's surface and detected by the receiving antenna. The transmitter and receiver signals are mixed and the difference frequency obtained which is proportional to the transit time and therefore to the terrain clearance. The altitude indicator is a meter operated by the difference frequency and calibrated in feet of altitude for two ranges, 0–400 feet and 0–4000 feet. The meter current can be readily monitored on a suitable recorder to provide a permanent record of the terrain clearance of the aircraft during survey operations.

The AN/APN-22 radar altimeter (USAF, 1959/60) was designed to eliminate the necessity of having antennas externally mounted on the aircraft. The components of this system are a transmitter-receiver, an electronic control amplifier and the altitude indicator meter. The AN/APN-22 operates in the 4200 to 4400 MHz region and also uses a frequency-modulated signal to obtain terrain clearance.

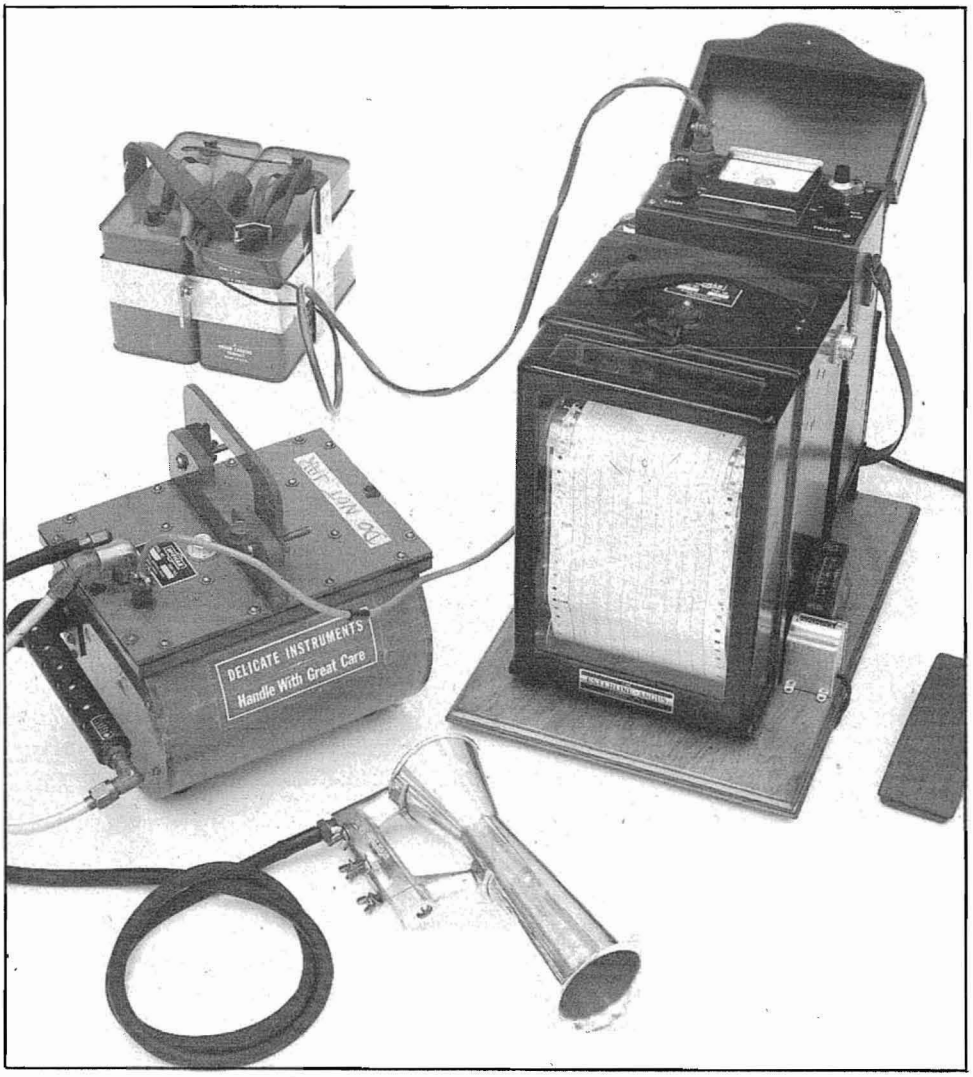


Figure 19. McPhar Model 555AB vertical-force fluxgate magnetometer for airborne prospecting surveys.

Button-on aeromagnetic survey systems. There seems to be a definite place in geophysical prospecting operations for simple, light-weight 'button-on' aeromagnetic survey systems that can be easily installed and removed from a light aircraft, and can carry out aeromagnetic 'prospecting' surveys at an extremely reasonable line-mileage cost.

McPhar Geophysics Ltd. has produced a button-on airborne version (Model 555 AB) of their vertical-force ground fluxgate magnetometer (Figure 19). An air-driven gyro-stabilized sensing head is used to maintain the sensitive element pointing vertically downwards in spite of aeroplane manoeuvres. The gyro may be either powered from the aircraft vacuum system or a simple venturi tube mounted on the side of the aircraft. A suitable recorder is connected to the plug provided on the console so that a permanent record may be obtained. The unit is designed for installation in an uncompensated light fixed-wing aircraft, or helicopter, to carry out inexpensive aeromagnetic surveys with an accuracy of ± 50 gammas. A fiducial foot switch, seen on the right-hand side of Figure 19, is used for the correlation of the magnetic data and the aircraft position.

Barringer Research Ltd. of Toronto have recently introduced a 1-gamma direct-reading proton free-precession magnetometer, designated model SM-103, which has an operating range of 20,000 to 100,000 gammas in 16 overlapping ranges (Figure 20). The tuning of the unit to the precession signal is automatically maintained within a preset range of 5000 gammas. The magnetometer has two outlets so that the output may be recorded in analog form (0–99 gammas in 1-gamma steps and 0–900 gammas in 100-gamma steps) on a suitable chart recorder. There is also a digital output in binary coded decimal 1-2-4-8 format. The unit has an automatic 2-second cycling rate. It may also be manually operated or, for airborne surveys, controlled by an external programmer. The electronic unit weighs only 12 1/2 pounds and operates from a 22- to 28-volt DC power supply. Actually this versatile instrument may be used as either an airborne magnetometer, a station instrument, or a ground survey instrument.

Aeromagnetic gradiometers. The recent development of highly sensitive magnetometers, such as the optical-pumping varieties, has also made feasible the measurement of the first-vertical derivative of the total field in aeromagnetic surveys (Hood, 1965; Langan, 1966; Slack, *et al.*, 1967). This is accomplished by using two sensitive magnetometer heads separated by a constant vertical distance and recording the difference in outputs. The



Figure 20. Barringer SM-103 direct-reading proton free-precession magnetometer.

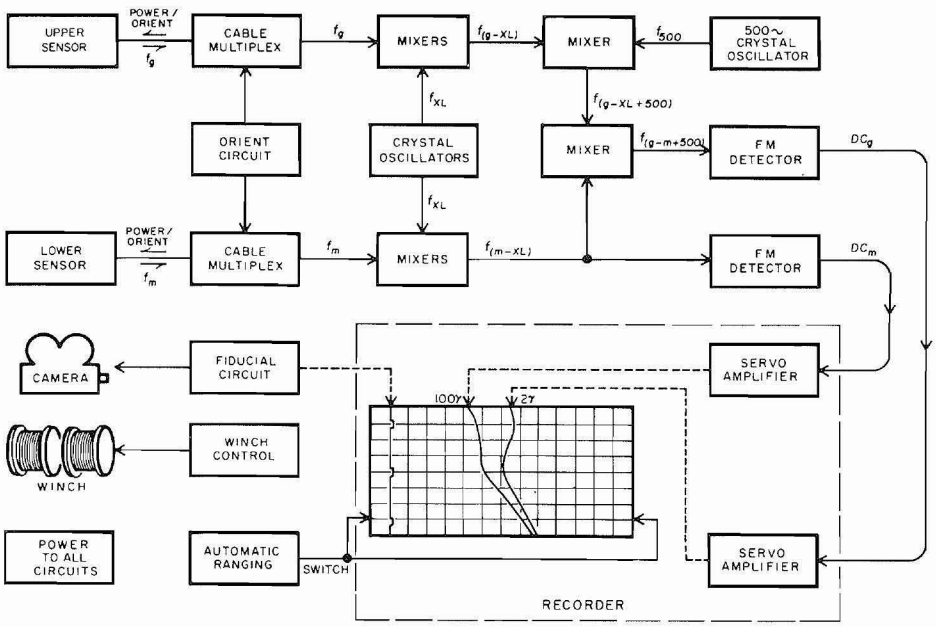


Figure 21. Schematic of Varian/Union Oil Company aeromagnetic gradiometer system (from Slack, *et al.*, 1967).

effect of diurnal is thus eliminated in the resultant differential output, and this is an especially desirable feature in northern Canada where the diurnal variation is usually much greater than is found in more southerly magnetic latitudes.

Figure 21 is a block diagram of the helicopter aeromagnetic gradiometer system built by Varian Associates of California for Pure Oil Co. (now Union Oil Co.) (Slack, *et al.*, 1967). The dual-cell rubidium sensors and associated electronics are flown in two birds which are vertically separated by 100 feet. The birds are raised and lowered using the winch which has a hydraulic brake to allow the cable to reel off slowly should a winch failure occur. In an emergency, the cable may be cut either electrically or manually using a guillotine system. The sensor electronics are powered by 28 V DC flowing down the tow cable together with the sensor orient signal, and the rubidium frequencies (f_g and f_m) are returned along the same conductors. These frequencies are beat with that from a crystal oscillator (f_{xL}) to produce the difference frequencies f_{g-xL} and f_{m-xL}. The latter (lower sensor) frequency is converted to an analog voltage (DC_m) suitable for presentation on the recorder. The signal passing through the upper sensor channel is increased by a bias frequency of 500 Hz to avoid polarity changes and then mixed with the lower sensor frequency. The resultant difference frequency ($f_{g-m+500}$) is then converted to analog form and this gradiometer signal is also displayed on the strip chart recorder using either a 2- or 10-gamma full-scale sensitivity. A camera mounted on the side of the helicopter is operated at eight-second intervals and a fiducial mark is made on the strip chart with each frame for data reduction purposes.

Figure 22 shows the Varian aeromagnetic gradiometer system

Contents



Figure 22. Varian twin-bird aeromagnetic gradiometer system being towed from Aero Service Corp's DC-3 aircraft.

being towed by an Aero Service DC-3 aircraft. The sensor separation is again 100 feet, and a fixed wing aircraft increases the possible line mileage rate by a factor of two or so over the helicopter because not only has the speed of the platform been increased but the range has also been augmented.

The data reduction necessary to produce a vertical-gradient map is much simpler than with the total-field case because no datum levelling is necessary. As the aircraft track will be available from the main compilation it is only necessary to plot the resultant vertical gradient values on the track map and contour. Thus two maps will be obtained for little more than the cost for one but with a greatly increased gain in geophysical information concerning the geometry of the causative bodies. With further improvements in the sensitivity of optical absorption magnetometers it may prove feasible to measure the second vertical derivative directly in aeromagnetic surveys.

Other ground magnetic survey instrumentation

Pocket magnetometers. Several small lightweight hand-held torsion magnetometers have appeared during the past several years which have a similar function to dip needles, that is they are for reconnaissance magnetic prospecting surveys and may be carried on one's person. They have the advantage that they measure the vertical force of the earth's magnetic field instead of a 'dip' angle which for the dip needle is dependent on both the vertical force anomaly and the horizontal component of the earth's magnetic field.

The Arvela vertical-force magnetometer, which is made by Levanto Oy in Finland, weighs only 9 ounces and its dimensions are 1 X 2 3/8 X 3 1/2 inches. Observations by the Arvela are generally made in hand operation being levelled by means of a built-in circular level and the instrument is orientation insensitive. It has two ranges of ± 12,000 and ± 60,000 gammas with scale divisions of 500 and 2500 gammas, respectively. The zero level of the instrument can be readily adjusted to the regional value of the main earth's field.

Craelius Company of Sweden is also manufacturing a lightweight null-type torsion magnetometer (Figure 23) (Model NGU 59A) called the Minimag which was designed by the Geological Survey of Norway. The following description of the instrument has been supplied by the manufacturers:

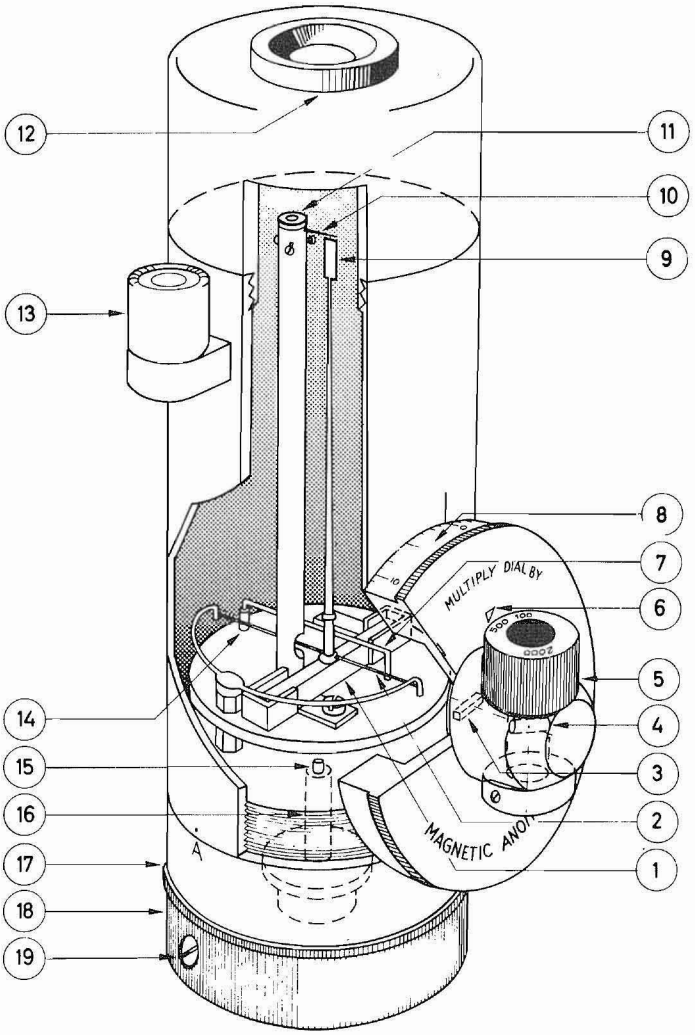


Figure 23. Craelius Minimag Model NGU 59A vertical-force pocket magnetometer. 1. Magnetic needle. 2. Suspension wire. 3. Anomaly compensation magnet. 4. Range compensation magnet. 5. Range selector. 6. Range indicator. 7. Clamping arm. 8. Anomaly scale. 9. Moving index. 10. Fixed index. 11. Internal level. 12. x10 ocular. 13. External level. 14. Clamping button. 15. Fixed magnet. 16. Fixed magnet holder. 17. Clamping ring. 18. Base. 19. Zero adjust screw.

A magnetic needle (1) is suspended on a fine horizontal torsion wire (2) and is free to turn about the wire's axis in the vertical plane. A clamping arm (7) locks the magnet system. Rotating the milled ring section (17) clockwise presses up the clamping lever (14) and frees the system. When clamped, letter *A* on the ring section is against the index mark on the housing. In a given survey area the downward force exerted on the magnetic needle by the vertical component of the earth's magnetic field is compensated by a fixed magnet (15). The local variations that occur in the vertical component are compensated by two moveable compensation magnets (3) and (4) attached to a graduated scale (8). The scale has 50 divisions from + 25 to − 25, and gives the magnetic field directly in gammas. When the internal and opposing force created by the compensation magnets is equal to the deflecting force, the moving index (9) will coincide with the fixed index (10). Increased coincidence accuracy is obtained by observing the index lines through a X10 magnifying ocular (12). The Minimag is levelled with the help of an external bubble level (13). An internal level (11) is seen through the ocular. Bubble levels are adjusted so that the magnetic needle and the suspension wire are both horizontal when the bubble is inside the ring and when the index lines coincide. In this condition the horizontal component of the earth's magnetic field does not influence readings. For normal surveys the Minimag does not need to be oriented to the magnetic meridian. The milled base (18) acts as a tripod fitting and is centre threaded to receive the tripod top screw. The base may be unscrewed and withdrawn, so that the unclamping section with the milled ring (17) may be removed. This gives access to the unclamping button, an extension of the clamping lever (14), in the base of the magnetometer. Depressing this springloaded button unclamps the magnetic needle. The Minimag measuring range is altered by turning the range selector. The operation is easiest understood in the special case when the moveable scale (8) is set to zero. The magnetic axis of the needle (1) and the magnetic axis of the compensation magnets (3) and (4) then lie in the same plane. The compensation magnets will then exert no force on the magnetic needle. If the range compensation magnet (4) is turned by turning the range selector the deflecting force will still be zero. On the other hand, if the scale reading is not zero, the force exerted on the needle by the range compensation magnet (4) will be varied when the range selector is turned. The three different range selector positions, 100, 500 and 2000, correspond to three different ranges with scale values 100γ, 500γ and 2000γ per scale division. This gives measuring ranges of ± 2500γ ±12,500γ and ±50,000γ, respectively. Selected range is shown against the index mark (6) on the scale drum.

Measuring accuracy depends on a number of factors. Greatest accuracy is obtained when the Minimag is oriented so that the magnetic axis of the needle is at right angles to the magnetic meridian. A slight tilt of the magnetometer in easterly or westerly directions does not significantly affect measuring accuracy since the suspension wire passes through the centre of gravity of the needle. A levelling error of about 1/10° in the plane of the magnetic meridian causes an error of about 50γ. This is the average error that occurs when taking measurements without using the tripod. Tripod measurements give increased accuracy. If the Minimag is tripod-levelled using the external level, levelling errors are insignificant and the setting may be made with an accuracy of around 10–15γ. A reading accuracy of one tenth of a scale division is easily achieved; this is equivalent to 10 γ on the most sensitive range. Accuracy is therefore about ± 20γ, when the magnetometer is tripod mounted, when it is levelled with the external bubble and when readings are taken on the most sensitive range. The magnetometer is temperature compensated; the coefficient being ± 2γ/° C. Under normal survey conditions no allowance for temperature drift need be made. The horizontal component may be measured by means of a special angle attachment screwed onto the tripod. The effect of azimuth is small and the orientation of the instrument is not critical.

Measurement of the magnetic properties of rocks. The amplitude of a given magnetic anomaly is directly proportional to the intensity of magnetization of the underlying rock formations.

Contents



Figure 24. Sharpe SM-4 *in situ* susceptibility meter in operation on magnetite iron-formation.

Susceptibility meters. Hand specimens collected from a given rock unit often show a wide range of magnetic susceptibility values, and it is therefore preferable to measure as large a volume of a given rock unit as possible in making a susceptibility measurement. For this reason *in situ* susceptibility meters should be the preferred instrument.

Sharpe Instruments are manufacturing a 1000 Hz transistorized susceptibility meter, the SM-4, which is based on the Carey Foster (1887) mutual inductance bridge. Figure 24 shows it being used in the *in situ* mode which enables susceptibility measurements to be obtained on the rock outcrop; a circuit diagram of the bridge itself is shown in Figure 25. The Carey Foster bridge measures the mutual inductance (M) between coils a,b and c which comprise the coaxial coil system which can readily be seen in Figure 24 lying on the outcrop. The bridge is balanced by adjusting the values of the resistances R_1 and R_3 for minimum sound in the headphones. Before use the susceptibility meter is first balanced with the coil system well away from anything magnetic. The difference ΔR_3 between this base station value and the survey station value of R_3 is related to the susceptibility k of the underlying rock formations by the following formula (Hood and Sangster, 1967):

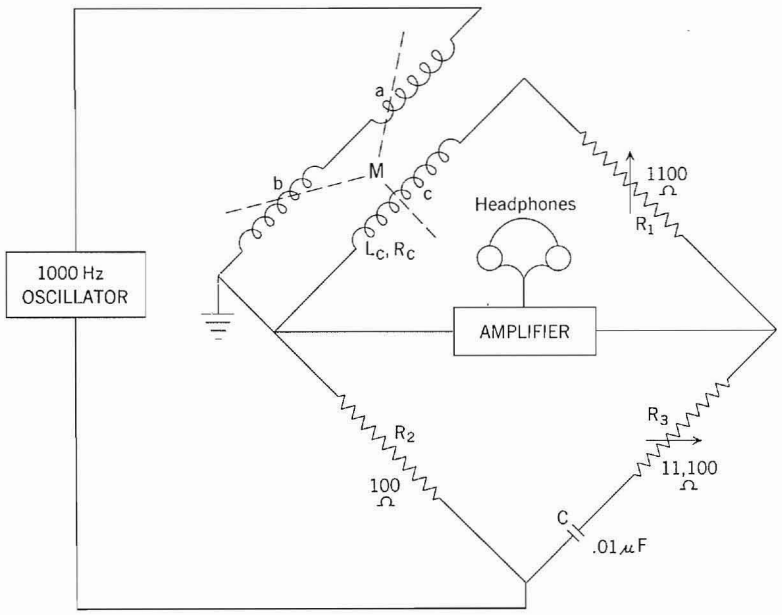


Figure 25. Circuit diagram of Carey Foster mutual-inductance bridge for susceptibility measurements.

The intensity of magnetization of a given rock formation itself is due to the induced magnetization produced by the earth's magnetic field and a remanent (or permanent) magnetization whose amplitude and direction is dependent on the geological history of the rock unit. In rock formations of great geological age, such as the Precambrian rocks of the Canadian Shield, it is usually found that the remanent magnetization is of much less importance than the induced magnetization component. In weak magnetic fields such as that due to the Earth, the intensity of induced magnetization is directly proportional to the applied field, and the constant of proportionality is called the magnetic susceptibility.

$$\Delta R_3 = \frac{(R_2 + R_3)\,[R_2 G_2 - G_1(R_2 + R_3)]}{[L_c R_2\,(1/k + 2\pi) + G_1(R_2 + R_3)]}$$

where G_1 and G_2 are mathematical functions involving the parameters of the coil system. The range of the instrument is from approximately 15 to 100,000 $\times$ 10^{-6} emu/cc, and the absolute accuracy is 5% although the relative accuracy is 1% or better. A susceptibility meter of this type has also been described by Mooney (1952) and was subsequently used in a study of rock outcrops in Minnesota (Mooney and Bleifuss, 1953). Alternatively a set of laboratory coils of 1.5-inch internal diameter may be employed to measure the susceptibility of crushed rock samples or drill core.

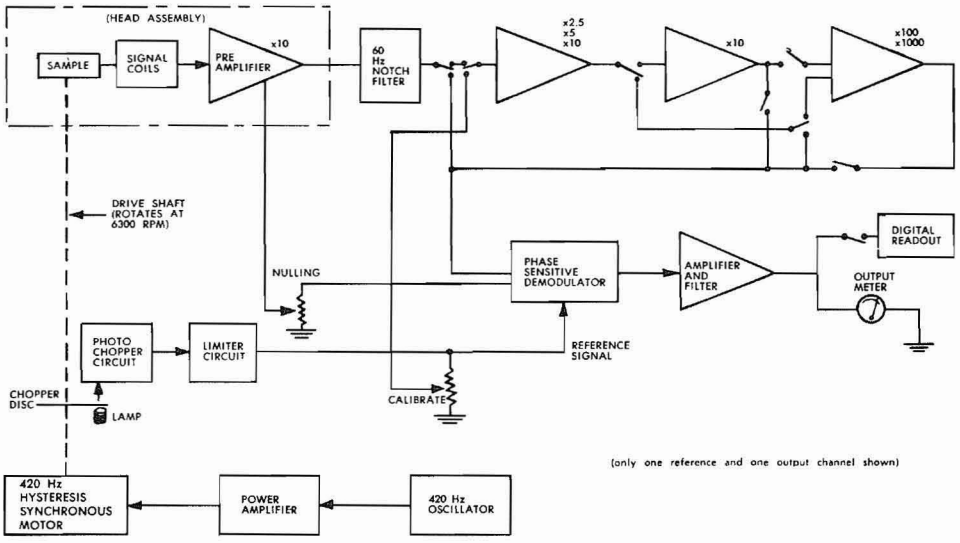


Figure 26. Block diagram of Princeton Applied Research SM-1 spinner-type remanent magnetometer.

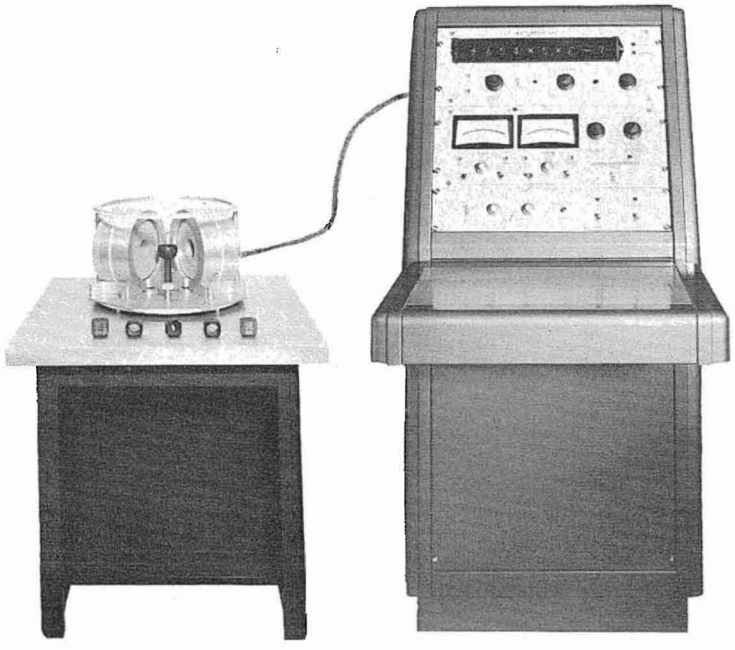


Figure 27. Princeton Applied Research SM-1 spinner-type remanent magnetometer.

Soiltest Inc. of Evanston, Illinois also manufacture a susceptibility meter which utilizes the Carey Foster mutual inductance bridge. The transistorized MS-3 1000 Hz instrument has a range from about 2 to 40,000 $\times 10^{-6}$ emu/cc with a relative accuracy of 1%. The sample holder takes AX(1 3/16 inch) core or smaller, but an external sample holder for BX(1 5/8 inch) core is also available. The rms magnetic field intensity at the sample position is about 2 oersteds. Soiltest Inc. also manufacture a more sensitive version of the MS-3 instrument, the MS-4. The range of the MS-4 is from 3000 $\times 10^{-6}$ emu/cc down to 3 $\times 10^{-6}$ emu/cc, and it can be used for accurately determining trace ferrous ion concentrations and the volume susceptibilities of sedimentary rocks which are usually quite low.

Remanent magnetometers. The first commercially available spinner magnetometers, Models SM-1 and SM-2, for the measurement of the remanent magnetism and anisotropic susceptibility of rock samples have been produced by Princeton Applied Research Corporation of New Jersey. A block diagram of the SM-1 instrument is shown in Figure 26, and a photograph of the system in Figure 27.

The following description of operation has been supplied by the manufacturers:

In operation, the 1-inch sample is first inserted into the plastic sample holder and oriented with respect to an index mark on the sample holder. Friable samples may also be used by employing encapsulation techniques. The sample holder is inserted into the shielded spinner head where it is spun with the spin axis parallel to two series-connected pick-up coils. The signal from the pick-up coils is amplified and synchronously detected with respect to two orthogonal reference signals generated by two photo-choppers, mounted 90° apart with respect to known faces of the sample cup. The demodulated outputs of the synchronous detectors represent the orthogonal components of the magnetic moment of the sample and define its magnitude and direction in the plane normal to the spin axis. The remanent magnetization vector of the sample is completely defined by reorienting (as necessary) the sample in the holder and repeating the measurement procedure. Each demodulated signal is continuously displayed on a front panel meter. When automatic digital readout is incorporated into the system (see Figure 26) either output signal may be continuously or alternately displayed. Generally, the minimum detectable signal is limited by the inherent system noise level. A major contributor to the over-all system noise is the phenomenon known as flicker (or 1/F) noise which first becomes noticeable at approximately 100 Hz and increases in intensity at the rate of 6 db/octave with decreasing frequency. It is clear then that to achieve the highest sensitivity, a spin frequency as high as possible (consistent with mechanical considerations) should be used in order to minimize the effects of flicker noise. The choice of a high spin frequency is further dictated by the fact that the magnitude of the signal generated by rotating the sample within the pick-up coils is directly proportional to the spin frequency. An additional advantage of a high operating frequency is the

avoidance of long overload recovery times in the system electronics.

A relatively high spin frequency of 105 Hz was selected for the Models SM-1 and SM-2 according to these considerations to maximize signal-to-noise ratio. For sample investigations in which sample characteristics dictate a slower spin frequency, the Model SM-2 offers the choice of operation at 15 Hz in addition to the standard 105 Hz. To present an output indication independent of the choice of spin frequency for a given sample, additional amplification is automatically inserted when 15 Hz operation is selected. A synchronous motor was selected for the drive system because of the inherent frequency stability of this method. Since the spin frequency is known and constant, the signal developed in the pick-up coils (which is proportional to frequency) remains constant and no correction due to frequency drift is required.

To measure anisotropic susceptibility, the sample is spun at 52.5 Hz in a uniform magnetic field produced by one pair of Helmholtz coils. In this arrangement the signal is generated by the induced magnetization, which reverses with respect to the sample axes twice in each revolution of the sample. Consequently, the signal frequency is twice the rotational frequency, or 105 Hz. The 52.5 Hz signal resulting from the remanent magnetism is electronically rejected and has no effect on the measurement. The magnetic field used in the anisotropy measurement is so weak that it does not cause a permanent change in the remanent magnetism. Two pairs of Helmholtz coils permit cancellation of the earth's field so that the sample may be spun in field-free space. The large Helmholtz pair develops a field parallel to the shaft's rotation. A second Helmholtz pair on the eddy current shield in the spinner head develops a field along the signal coil axis for magnetic anisotropic susceptibility measurements or for earth field cancellation.

The system will detect changes in magnetic moments as small as 7×10^{-9} emu/cc. There are 21 ranges calibrated in total moment from 0.5×10^{-6} to 5 emu/cc in a 1, 2, 5 ascending sequence, and filter time constants of 1, 3, 10, 30, 100 and 300 seconds are selectable. The calibration accuracy is 1% for magnitude and $\pm$ 0.5° for a remanent magnetism direction measurement.

Actually many remanent magnetometers of both the spinner and the astatic type have been built by various organizations, usually universities, throughout the world during the past 15 years. An up-to-date review of instrumentation is contained in *Methods in Palaeomagnetism* by Collinson, *et al.*, (1967).

Several of the fluxgate magnetometers may be fitted with external fluxgate probes. These have a variety of uses but probably the most useful application concerns the determination of the magnetic properties of rock specimens. In the past the possible contribution of remanent magnetism in producing magnetic anomalies has usually been ignored (Hood, 1963), and the following discussion attempts to show how this contribution may be assessed in the field. It is common experience to find anomalous magnetic lows on aeromagnetic maps. Most of these are the concomitant low usually found north of the magnetic high. However, in a few cases the low stands by itself. The most obvious explanation is that the underlying rock formations have a strong reversed remanent magnetization which overrides the induced component because of the earth's magnetic field. If for some reason it is felt important to demonstrate this experimentally, the following procedure may be carried out.

Unweathered samples should be collected from the outcropping formations with the tops and north directions marked on the samples with chalk, crayon, or preferably with something more permanent. If a Brunton, or better, a sun compass, is available, an oriented sample may be collected (Morgan, 1943) by drawing a horizontal line on the exposed surface, and by marking and measuring the (down) dip angle at right angles to this strike line, whose azimuth is also measured. This would enable the remanent magnetism vector to be more accurately measured at a later date with a remanent magnetometer. If a Brunton compass is used, care should be taken to see that the needle is not appreciably affected by the magnetism of the underlying rock formations.

The next step is to set up the magnetometer in a low gradient area such that the external fluxgate probe is aligned at right angles to the earth's magnetic field (see Figure 28). This is most easily accomplished using the Brunton compass and a levelling bubble. The probe is first made horizontal using the bubble and then the system is rotated until the probe is aligned along the magnetic east-west direction. Because the sensitive element in the probe itself is magnetic, care should be taken that it does not

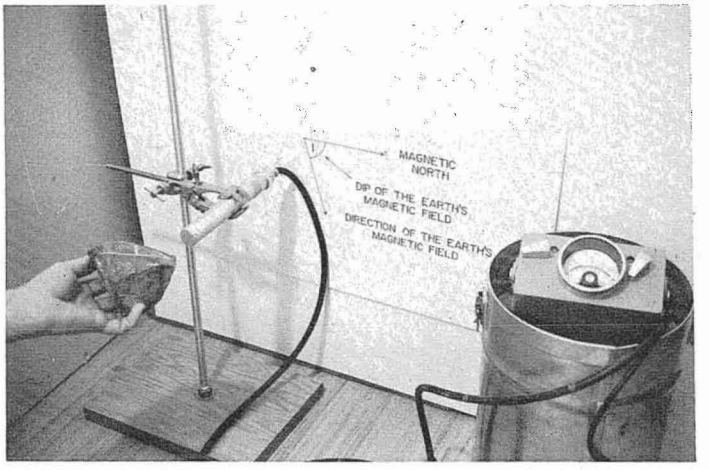


Figure 28. Fluxgate magnetometer set-up using external probe for remanent magnetism determinations.

affect the compass reading. In this orientation the effect of the induced component of magnetization in the rock specimen on the magnetometer element will be reduced to a minimum, because the induced component is parallel to the earth's magnetic field. However the direction of the remanent component is fixed in the rock, and may therefore be made to give a maximum deflection on the magnetometer by aligning it parallel to the axis of the external probe. This is accomplished by rotating the specimen for a maximum or minimum reading on the magnetometer.

If the fluxgate magnetometer has been adjusted to obtain survey readings in the area, the magnetometer will now give a reading which is lower than say the survey base station value by the value of the vertical component (Z) of the earth's magnetic field in the area. For Canada, this will be something in excess of 50,000 gammas. It is therefore necessary to alter the latitude controls until the magnetometer again records on its most sensitive scale.

At this point, a polarity check should be made on the external probe using a bar magnet or a compass. In the northern hemisphere the earth's magnetic field induces a magnetization in rock masses such that the top of the body has south-seeking polarity. This result follows from the fact that the North Magnetic Pole has south-seeking polarity! Now the foregoing statement may appear confusing to the reader but he should recall one of the elementary laws in magnetism, namely that magnetic poles of opposite sign attract one another. A north-seeking compass needle therefore points to the Pole having south-seeking polarity, i.e., the North Magnetic Pole. To ascertain the polarity of rock masses in the earth's crust, it is only necessary to consider the earth as having a giant bar magnet at its centre aligned between the magnetic poles, and geometrically project this direction to the point under consideration at the earth's surface; the polarities remain the same. Each end of the bar magnet is brought up to the end of the external probe and the direction of deflection is noted on the magnetometer meter. The south-seeking end of the magnet should give a positive deflection.

For the actual polarity determination, each rock sample in turn is brought up to the end of the fluxgate probe (see Figure 28) and rotated in line with the axis of the probe first for a maximum and then for a minimum reading. The point on the sample opposite the end of the probe may be marked with an *S* when a maximum is obtained, and similarly with an *N* for the minimum. It may be found that if the sample has projecting corners these may have a pronounced effect; it is therefore best to trim the sample to make it as equidimensional as possible.

The sample should then be reoriented to its *in situ* position using the strike and dip markings. Now consider the line joining the *N* and *S* on the rock sample, and the direction of the total field vector of the earth's magnetism. For Canada the total field vector dips between 73° and 90° in the magnetic north direction. If the projection of the *N*–*S* line in the sample on the total field direction is such that the *S* is down dip from the *N* end, then the rock sample has a reversed remanent magnetization. Moreover the approximate direction of the remanent magnetization may also be ascertained.

Drill-hole magnetometers. During recent years much research and field work has been carried out in Scandinavia in the development of reliable instrumentation for drill-hole magnetic surveying. The outcome of the work carried out in Sweden by the Swedish Geological Survey and the Swedish Mining Association was the Hetona HBM2 fluxgate drill-hole magnetometer, which using transistorized construction and plug-in printed circuits not only made it possible to measure 3 orthogonal components of the magnetic field in a drill hole as small as 36 mm (EX), but also gave an accurate measurement dip of the hole at each observation point. This additional piece of information makes possible a more accurate and reliable interpretation of the survey results, thereby helping to reduce exploration costs. The HBM2 has now been superseded by the HBM3 which incorporates the field experience gained with the earlier HBM2 model. The HBM3 is manufactured by AB HETONA under licence from the Swedish Geological Survey and is sold and distributed throughout the world by Craelius, Stockholm, Sweden. The HBM3 consists basically of a probe and a control box together with a length of cable, cable drum and 12 volt lead-acid batteries for power. The 8-pound probe has a length of 127 cm (4 feet 2 inches) and a maximum diameter of 32 mm (1 17/64 inches). It may therefore be inserted in the smallest diameter standard drill hole (36 mm, EX). The probe contains all the electronic components, such as oscillator, filter, amplifier, the servomotor for change of measuring mode, the dip meter and the 3 fluxgate elements. Up to 1200 metres (3900 feet) of cable may be connected to the standard probe. To eliminate risk of damage during transport to and from the measuring site the fluxgate element section can be unscrewed from the end of the probe and carried separately. To ensure that the probe does not jam when inserted in irregular drill holes, safety collars are fitted. If these become stuck, the probe will come free leaving only the collars jammed in the hole. Collars for 36 mm (1 1/2 inch) and 46 mm (1 3/4 inch) holes are supplied as standard equipment. These collars give a 2–3 mm (1/10 inch) clearance between hole wall and collar periphery. The electronic section makes use of transistors and has interchangeable plug-in printed circuits. The 17.5 pound waterproof control box, contains the stabilizing unit for the compensation current and all the controls and scales necessary to make the magnetic and dip measurements. The control box is fitted with a rechargeable desiccator for additional protection against moisture and all components are protected against corrosion. The control box is also designed for connection to an automatic recording system that is presently under development. The high degree of automation utilized in the HBM3 makes for quick and accurate observation of field strength and dip angle, and the control box is simple to operate. The HBM3 measures:

a) magnetic field component (*X*) in the direction along the line of the drill hole;
b) magnetic field component (*Y*) in a direction at right angles to the line of the drill hole;

Table IV. Specifications of commercially available fluxgate magnetometers used in mineral exploration.

Manufacturer	Model Designation	Field Measured	Readout Device	Range (gammas)	Sensitivity (gammas)	Cable Length (feet)	Drill-hole size (inches)	Weight (lb)	Electronics and Power Supply
Craelius (Sweden)	HETONA HBM-3	*X*, *Y*, *Z*, Dip of hole	Meter	± 100,000 ± 300,000	50 150	3900	> 1.27	283	Transistors 12V batteries
METEX (Finland)	OKI-3D	*X*, *Y*, *Z*	Meter	± 100,000	1000	1200 (Standard)	> 1.26	220	Tubes Dry Cells
Sharpe (Canada)	DHM-1	Component along hole	Digital Counter	± 40,000	25	4000	> 1.05 diameter	15 (Electronics)	Transistors 24V battery

c) magnetic field component (Z) in a direction at right angles to the line of the drill hole and perpendicular to the Y component; and

d) the dip of the drill hole from the vertical.

The accuracy of the instruments are for the magnetic measurements 50 γ on the ± 100,000 γ range, 150 γ on the ± 300,000 γ range, and for the dip measurements 0.5° within the range +90° to −40°.

Actually, there appear to be three fluxgate drill-hole magnetometers on the market at the present time (1968), the ABEM Hetona HBM3, the Metex Oki-3D and the Sharpe DHM-1. The characteristics of these various instruments have been summarized in Table IV. As might be expected with these instruments because the fluxgate element is close to the rock formation, a relatively coarse sensitivity is used. Applications of drill-hole magnetometers have been described by Levanto (1959, 1063), Paarma and Levanto (1960), Zuber (1962), Bergdahl (1963), and Ponomarev and Bakhvalov (1964).

Acknowledgments

The author of this article wishes to thank the following for kindly supplying information used in this review: Aero Service Corporation of Philadelphia, Barringer Research Limited of Toronto, Canadian Aviation Electronics Industries Limited of Montreal, Compagnie Générale de Géophysique of Paris, Craelius of Stockholm, Geoterrex Limited of Ottawa, L.A. Levanto Oy of Helsinki, Littlemore Scientific Engineering Company of Oxford (U.K.), McPhar Geophysics Limited of Toronto, Optillinen Tehdas Oy of Helsinki, Princeton Applied Research Corporation of Princeton (N.J.), Scintrex Limited of Toronto, Howard Slack, Survair Limited of Ottawa, Union Oil Company of California, and Varian Associates of Palo Alto (California).

References

Aldred, J.C., 1964. A fluxgate gradiometer for archaeological surveying. *Archaeometry*. 7: 14-19.

Aschenbrenner, H., and G. Goubau, 1936. Eine Anordnung zur Registrierung Rascher magnetischer Störungen. *Hochfrequenztechnik und Electroakustik*. 47: 177-181.

Bergdahl, S.G., 1963. The drill hole magnetometer and its use for magnetic prospecting. *Colorado Sch. Min. Quart.* 58: 253-258.

Bloom, A., 1960. Optical pumping. *Sci. Amer.* 203: 72-80.

Breiner, S., 1965. The rubidium magnetometer in archeological exploration. *Science*. 150: 185-193.

Bureau of Naval Personnel, 1959. Aviation electronics technician 3 & 2. *Navpers 10317-A*, Washington, D.C., Supt. of Documents.

Collinson, D.W., K.M. Creer, and S.K. Runcorn, 1967. *Methods in Palaeomagnetism*. New York, Elsevier Publishing Co.

Decca Navigator Co. Ltd., 1958. *The Decca navigator system as an aid to survey*. London, Decca Navigator Co. Ltd.

Driscoll, R.L., and P.L. Bender, 1958. Proton gyromagnetic ratio. *Phys. Rev. Lett.* 1: 413-414.

Foster, G.C., 1887. Note on a method of determining coefficients of mutual inductance. *Phys. Soc. Proc.* 8: 137-146.

Fromm, W.E., 1952. The magnetic airborne detector. *Adv. in Electronics*. 4: 257-299.

Giret, R.I., 1965. Some results of aeromagnetic surveying with a digital cesium-vapor magnetometer. *Geophysics*. 30: 883-890.

Giret, R.I., and L. Malnar, 1965. Un nouveau magnétomètre aérien: le magnétomètre à vapeur de caesium. *Geophys. Prosp.* 13: 225-239.

Grant, A.S.G., A.C. Hamilton, S.A. Yaskowich, and C.D. McLellan, 1955. Geodetic application of Shoran. *Geodetic Surv. of Canada*, Publ. 78, 195 p.

Herbert, R. and L. Langan, 1965. The airborne rubidium magnetometer. Varian Assoc., *Geophys. Tech. Mem. 19*, 6 p.

Hood, P.J., 1963. Remanent magnetism – a neglected factor in aeromagnetic interpretation. *Can. Min. J.* 84: 76-79.

Hood, P., 1964. The ground fluxgate magnetometer – a new versatile prospecting tool. *Can. Min. J.* 85: 59-64.

Hood, P., 1965. Gradient measurements in aeromagnetic surveying. *Geophysics*. 30: 891-902.

Hood, P., and D.F. Sangster, 1967. The Carey Foster *in situ* susceptibility meter. *Geol. Surv. Canada*. Paper 65-22, 17 p.

Jensen, H., 1961. The airborne magnetometer. *Sci. Amer.* 204: 151-162.

Jensen, H., 1965. Instrument details and applications of a new airborne magnetometer. *Geophysics*. 30: 875-882.

Kastler, A., 1950. Quelques suggestions concernant la production optique et la détection optique d'une inégalité de population des niveaux de quantification spatiale des atomes. *J. de Phys. et le Rad.* 11: 255-263.

Kudrevskiy, A.I., 1961. The mass production PM-1 magnetometer. *Geomag. and Aeron.* (in translation). 1: 390-393.

Langan, L., 1966. A survey of high resolution geomagnetics. *Geophys. Prosp.* 14: 487-503.

Laurila, S., 1960. *Electronic surveying and mapping*. Columbus, Ohio State Univ. Press.

Leliak, P., 1961. Identification and evaluation of magnetic field sources of magnetic airborne detector equipped aircraft. *IRE Trans. of Aerospace and Nav. Elect.*, p. 95-105.

Lemaire, H., A. Rassat, R. Brière, R.M. Dupeyre, and A. Salvi, 1967. Magnetometers for measuring the earth's magnetic field and its variations. Can. Patent 764, 597. 40 p.

Levanto, A.E., 1959. A three-component magnetometer for small drill holes and its use in ore prospecting. *Geophys. Prosp.* 7: 183-195.

Levanto, A.E., 1963. On magnetic measurements in drill holes. *Geoexploration*. 2: 8-20.

Mooney, H.M., 1952. Magnetic susceptibility measurements in Minnesota. Part 1: Technique of measurement. *Geophysics*. 17: 531-543.

Mooney, H.M., and R. Bleifuss, 1953. Magnetic susceptibility measurements in Minnesota. Part 2: Analysis of field results. *Geophysics*. 18: 383-393.

Morgan, R.E., 1943. A method for collecting oriented mineral specimens. *Econ. Geol.* 38: 603-608.

Nalivayko, V.I., A.V. Tyurmin, and U.V. Fastovskiy, 1962. PM-5 proton field magnetometer. *Geomag. and Aeron.* (in translation). 2: 288-292.

Newman, J.K., 1960. Instrumentation for airborne geophysical surveys with DC-3 aircraft. UN, *Min. Res. Devel. Series 12*, p. 142-146.

Overhauser, A.W., 1953. Paramagnetic relaxation in metals. *Phys. Rev.* 89: 689-700.

Paarma, H., and A. Levanto, 1960. On the use of magnetic measurements in ore prospecting. *21st Internat. Geol. Congr., Copenhagen*, Part 2, p. 98-110.

Packard, M., and R. Varian, 1954. Free nuclear induction in the earth's magnetic field. *Phys. Rev.* 93: 941.

Parsons, L.W., and Z.M. Wiatr, 1962. Rubidium vapour magnetometer. *J. Sci. Inst.* 39: 292-300.

Ponomarev, V.N., and A.N. Bakhvalov, 1964. Determination of the altitude of a thin bed from internal magnetic field measurements. *Bull. Izv., Acad. Sci. USSR* (in translation). 3: 214-219.

Slack, H.A., V.M. Lynch, and L. Langan, 1967. The geomagnetic gradiometer. *Geophysics*. 32: 877-892.

Sonnenberg, G.J., 1963. *Radar and electronic navigation*. London, George Newnes Ltd.

Strome, W.M., 1964. Magnetometer installation in a North Star aircraft. Nat. Res. Council, Canada, *DME/NAE Quart. Bull.* 1963 (4): p. 23-30.

Thomas, J., 1965. Le magnétomètre aéroporte MP 121 Sud-Aviation. *Geophys. Prosp.* 13: 22-36.

Tull, W.J., 1957. Doppler navigation. *Elect. and Comm.* 5: 33 *et seq.*

USAF, 1959/60. Air Navigation. *Manual 51-40*, 3 volumes.

USN, 1964. Magnetic detecting set AN/ASQ-10. *Navweps 16-30 ASQ 10-502*.

Vigoureux, P., 1962. A determination of the gyromagnetic ratio of the proton. *Proc. Roy, Soc.* Ser. A, 270: 72-89.

Vigoureux, P., 1963. Gyromagnetic ratio of the proton. *Nature*. 198: 1188.

Washkurak, S., and P. Sawatzky, 1966. The Serson direct-reading proton free precession magnetometer. Part 2. Airborne use with telemetering

and automatic diurnal correction. *Geol. Surv. Canada,* Paper 65-31: 33-75.

Whitham, K., 1960. *Measurement of the geomagnetic elements: Methods and techniques in geophysics.* London, Interscience Publishers Ltd., p. 104-167.

Wilson, R.A.R., and J.E. English, 1959. New instruments in the airborne search for oil; the Doppler navigation system. *Pet. Times.* 63: 427-428.

Wold, R.J., 1964. The Elsec Wisconsin digital recording proton precession magnetometer system. Geophys. and Polar Res. Centre, U. of Wisconsin, *Res. Rept. Ser. 64-4,* 83 p.

Yanovskii, B.M., 1963. *Earth's magnetism.* Leningrad University, 461 p.

Zuber, J.A., 1962. Magnetische Bohrlochmessungen als Hilfsmittel bei der Erzprospektierung. *Berg-und Huttenmännische Monatshefte.* 107: 299-306.

Semiautomatic methods of interpretation of magnetic data

B.K. Bhattacharyya

Geological Survey of Canada
Ottawa, Canada

Abstract. Most of the methods for quantitative interpretation of aeromagnetic data utilize digitized values at uniformly spaced points. The sources of error inherent in the process of digitizing published aeromagnetic maps at uniform intervals could be eliminated by recording magnetic field values digitally only along flight lines. The irregularly distributed data thus obtained can be treated effectively and accurately for interpolation at grid points located at the intersections of a rectangular grid system.

The available techniques for quantitative treatment of data normally determine some or all of the following: (i) continuation fields, (ii) second vertical derivatives, (iii) fields reduced to the pole and (iv) filtered anomaly fields. These transformations of the total-field anomaly are carried out for depicting some or all of the unknowns regarding the causative body in a diagnostic way. For example, second vertical derivatives and downward continuation fields increase the resolution and sharpness in the observed magnetic anomalies and tend to outline the surface traces of causative bodies with a reasonable amount of success.

In the final stage of interpretation of magnetic data individual anomalies in the residual map are analysed by different methods in order to extract information about the geometry of causative bodies.

Examples of application of various techniques to actual magnetic data have been chosen to cover both mineral exploration work and geological mapping.

Résumé. L'auteur présente un exposé des méthodes faisant appel à la science de l'ordination et utilisées présentement pour l'interprétation de sommes considérables de données magnétiques, particulièrement aéromagnétiques. La plupart de ces méthodes se servent de données recueillies en des points uniformément distants. Il est nécessaire de choisir avec soin l'espacement pour la traduction en numérique des valeurs du champ total tirées des cartes aéromagnétiques. Les sources d'erreur inhérentes au procédé de traduction en numérique à des intervalles uniformes pourraient être éliminées par l'enregistrement en numérique des valeurs du champ magnétique seulement en suivant les lignes de vol. Les données à espacement non-uniforme ainsi obtenues pourraient être traitées efficacement et avec précision par quelques-unes des méthodes numériques mises au point récemment.

Les techniques disponibles pour le traitement quantitif des données déterminent normalement une partie ou la totalité des transformations suivantes: (i) champ de prolongement, (ii) dérivées verticales secondes, (iii) champs réduits au pôle, et (iv) champ d'anomalies filtrées. Ces transformations des anomalies du champ mondial sont effectuées dans le but de décrire d'une façon diagnostique une partie ou l'ensemble des inconnues relatives à la source magnétisée. Par exemple les dérivées verticales secondes et les champs de prolongement vers le bas accroissent le pouvoir de résolution et la netteté des anomalies magnétiques observées et tendent à délimiter les traces superficielles des masses qui sont la cause de ces anomalies avec un succès raisonnable.

A la dernière étape de l'interprétation, des données magnétiques, les anomalies individuelles qui paraissent sur la carte des irrégularités résiduelles sont analysées par différentes méthodes afin d'en extraire des renseignements sur les dimensions, la forme et l'orientation des masses qui causent les anomalies magnétiques.

Des exemples de l'application de diverses techniques à des données magnétiques réelles ont été choisis pour les domaines des travaux d'exploration minérale et de la cartographie géologique.

The value of aeromagnetic maps in mineral exploration work and geological mapping is widely recognised now. This becomes abundantly evident in the number of available publications devoted to the development of methods for treatment and interpretation of aeromagnetic data. Instead of making a review of the various methods, this paper discusses the application of some computer-oriented methods to actual magnetic data. The objective of this paper is not to compare the efficiencies of different methods, but to present examples of some commonly used transformations of the total-field anomaly with a view to depicting some or all of the unknowns regarding the causative body in a diagnostic way.

First, a method for effective and accurate interpolation with irregularly spaced data is discussed. Then, transformations of the total-field anomaly are considered for showing the maps of the following: (i) continuation fields, (ii) second vertical derivatives, (iii) fields reduced to the pole and (iv) filtered anomaly fields. Finally, a discussion is made of the available methods for analysing individual anomalies for determining the dimensions of causative bodies.

Interpolation with nonequispaced data

The total-field aeromagnetic data is usually available in the form of a contoured map. For quantitative treatment, the data in the map is normally digitized according to a rectangular grid with prescribed station-spacings in two orthogonal directions. The individual spacing along one of these directions need not be equal to that along the other. Spacing for digitizing can be somewhere between 1/4 and 1/2 mile for detailed work and about 2 miles for crustal work. The choice of station-spacing is dependent on the size of the anomalies to be studied and the flight-line spacing of the original data.

The process of digitizing is not only time-consuming but also subject to random error. This error mainly originates from interpolation of observed data by human operators, first, in the preparation of the contoured map and second, in obtaining the grid-point data from the map.

The interpolation error could be eliminated if digitizing were done only along flight lines. In such a case, spacing is nonuniform and total field values have to be read along curved flight lines. Under these circumstances there is a need to devise a method

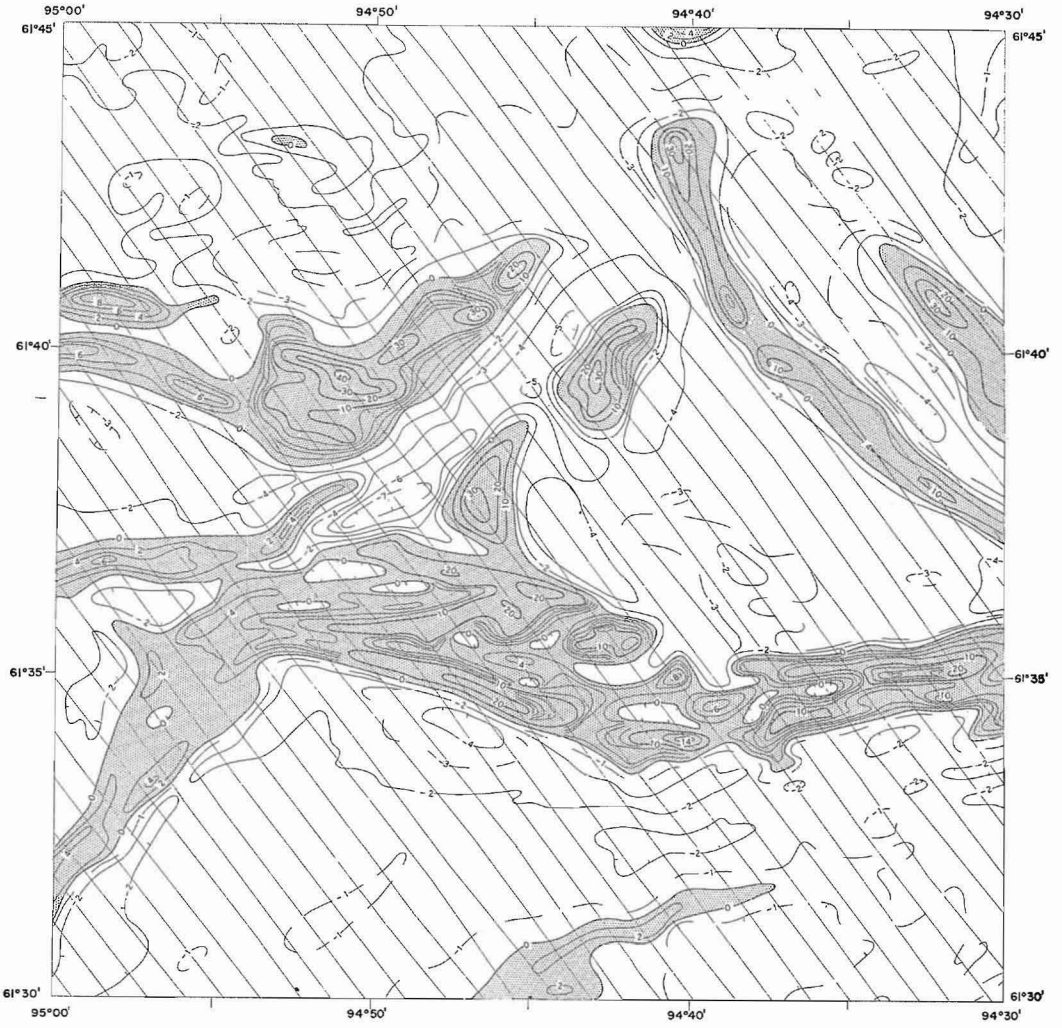


Figure 1. An aeromagnetic map from the Canadian Northwest Territories, contoured in units of 500 gammas.

which will use the irregularly distributed data to compute values of the observed variable at points spaced fixed distances apart in any particular direction. This necessity arises because most of the accurate and reliable methods available for quantitative analysis are suitable only for regularly spaced data.

The method that has been found reliable for accurate interpolation of irregularly distributed data uses least squares fitting of the data with orthogonal polynomials generated by the Gram-Schmidt procedure (Crain and Bhattacharyya, 1967). A brief account of this method will be presented here.

Let the observed variable G_i be known at N locations (x_i, y_i), $i = 1, \ldots N$. Let us assume that a known set of linearly independent functions $\psi_1(x, y)$, $\psi_2(x, y)$, ... be given. Then it is possible to generate a new set of functions $P_1(x, y)$, $P_2(x, y)$, ..., mutually orthogonal, with respect to a weighting factor w, over the group of observed points. In mathematical terms, this orthogonality property may be expressed as

$$\sum_{i=1}^{N} w_i P_k(x_i, y_i)\ P_L(x_i, y_i) = 0, K \neq L. \qquad 1$$

With the above definition, the generation of the polynomials proceeds as follows:

$$\begin{aligned} P_1 &= C_{11}\ \psi_1 \\ P_2 &= C_{12}\ P_1 + C_{22}\ \psi_2 \\ P_3 &= C_{13}\ P_1 + C_{23}\ P_2 + C_{33}\ \psi_3 \end{aligned} \qquad 2$$

$$P_M = C_{1M} P_1 + C_{2M} P_2 + \ldots + C_{M-1,M} P_{M-1} + C_{M,M}\ \psi_M$$

The coefficients C_{1k}, $K = 1, 2, \ldots M$, are assumed to be equal to unity and the remaining coefficients are determined by using Equations 1 and 2. Thus we obtain

$$C_{R,R} = -\frac{\sum_{i=1}^{N} w_i P_1^2 (x_i, y_i)}{\sum_{i=1}^{N} w_i P_1 (x_i, y_i)\ \psi_R(x_i, y_i)} \qquad 3$$

$$C_{k,R} = -\frac{\sum_{i=1}^{N} w_i P_k (x_i, y_i)\ \psi_R(x_i, y_i)}{\sum_{i=1}^{N} w_i P_k^2 (x_i, y_i)}\ C_{R,R} \qquad 4$$

$$k = 2, 3, \ldots, R-1$$

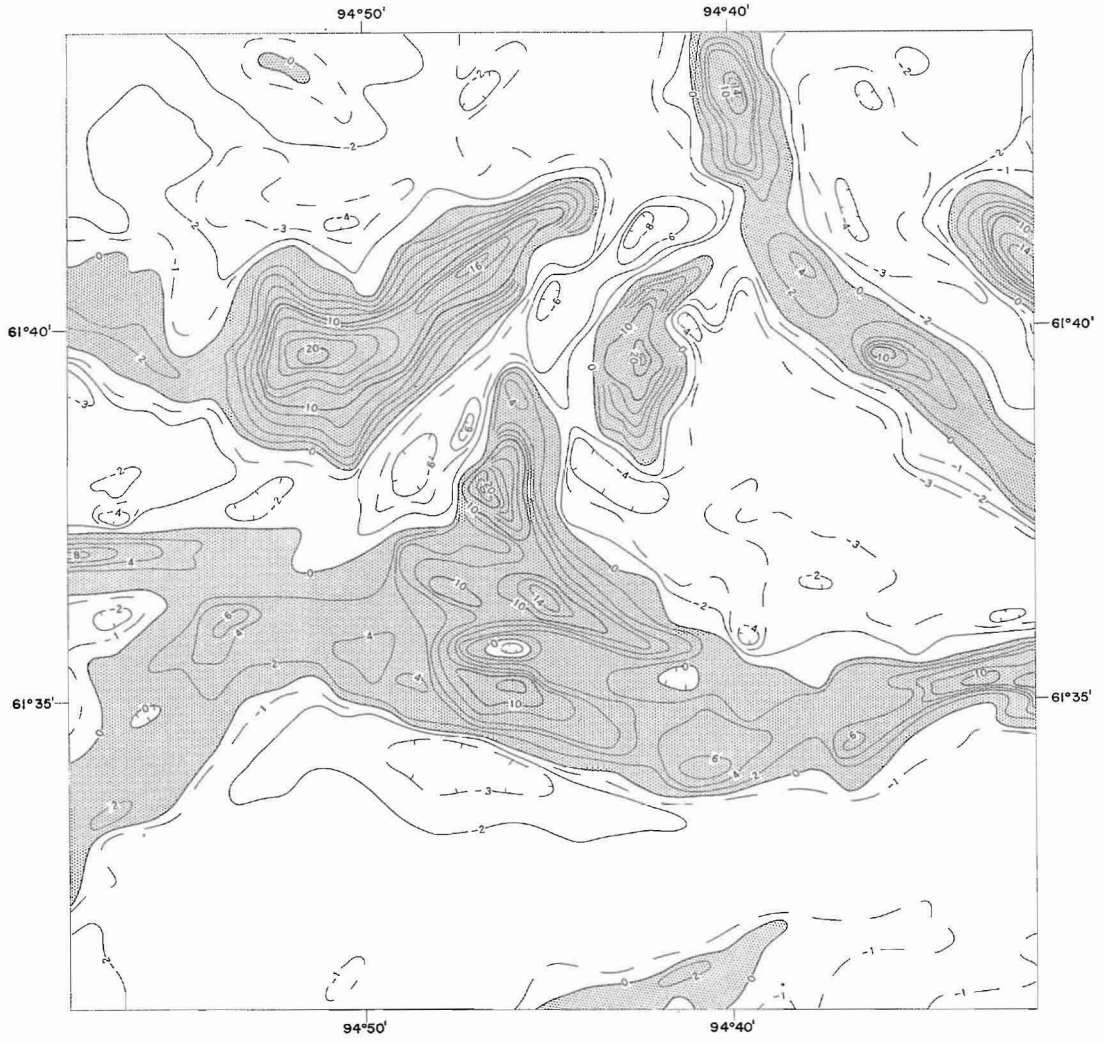


Figure 2. Interpolated map using least squares fit of an orthogonal polynomial surface generated by the Gram-Schmidt method. Contours are labelled in units of 500 gammas.

The data points are represented by a function of the form given below:

$$f_M(x, y) = \sum_{j=1}^{M} a_j P_j(x, y) \qquad 5$$

The coefficients a_j are determined using the least squares method. They are given by

$$a_j = \frac{\sum_{i=1}^{N} w_i G_i P_k(x_i, y_i)}{\sum_{i=1}^{N} w_i P_k^2(x_i, y_i)} \qquad 6$$

In all the above equations, the weighting factors w_i have been included for the sake of generality. It is, therefore, possible to reduce the influence of unreliable observations on interpolation by making the corresponding weighting functions relatively small. However, in cases of all data points being equally reliable and important, the weighting factors should be equal to unity.

As noted before, the ψ-functions in Equation 2 should be linearly independent and defined for all (x_i, y_i), $i = 1, 2, \ldots, N$. For convenience in computation, the ψ-functions are chosen as

$$\psi_1 = 1, \psi_2 = x, \psi_3 = y, \psi_4 = x^2, \psi_5 = xy, \psi_6 = y^2, \ldots.$$

There are various advantages in the use of orthogonal polynomials in problems of interpolation. First, no matrix inversion is necessary in computing the coefficients a_j. Second, any coefficient a_r depends only on the polynomials P_r and the observations G_i and it is independent of previously calculated coefficients. It is, therefore, possible to estimate the statistical significance of each term added to Equation 5, without repeating any previous calculation. Thus in many cases a test procedure can be set up to determine what order of polynomial is appropriate for a given set of data points.

To illustrate the efficiency of the above method, a published aeromagnetic map in the scale of 1 inch to a mile was chosen for analysis. A redrafted version of the map at a smaller scale is shown in Figure 1. The flight lines indicated by thin lines in the figure are spaced about one half mile apart. This particular

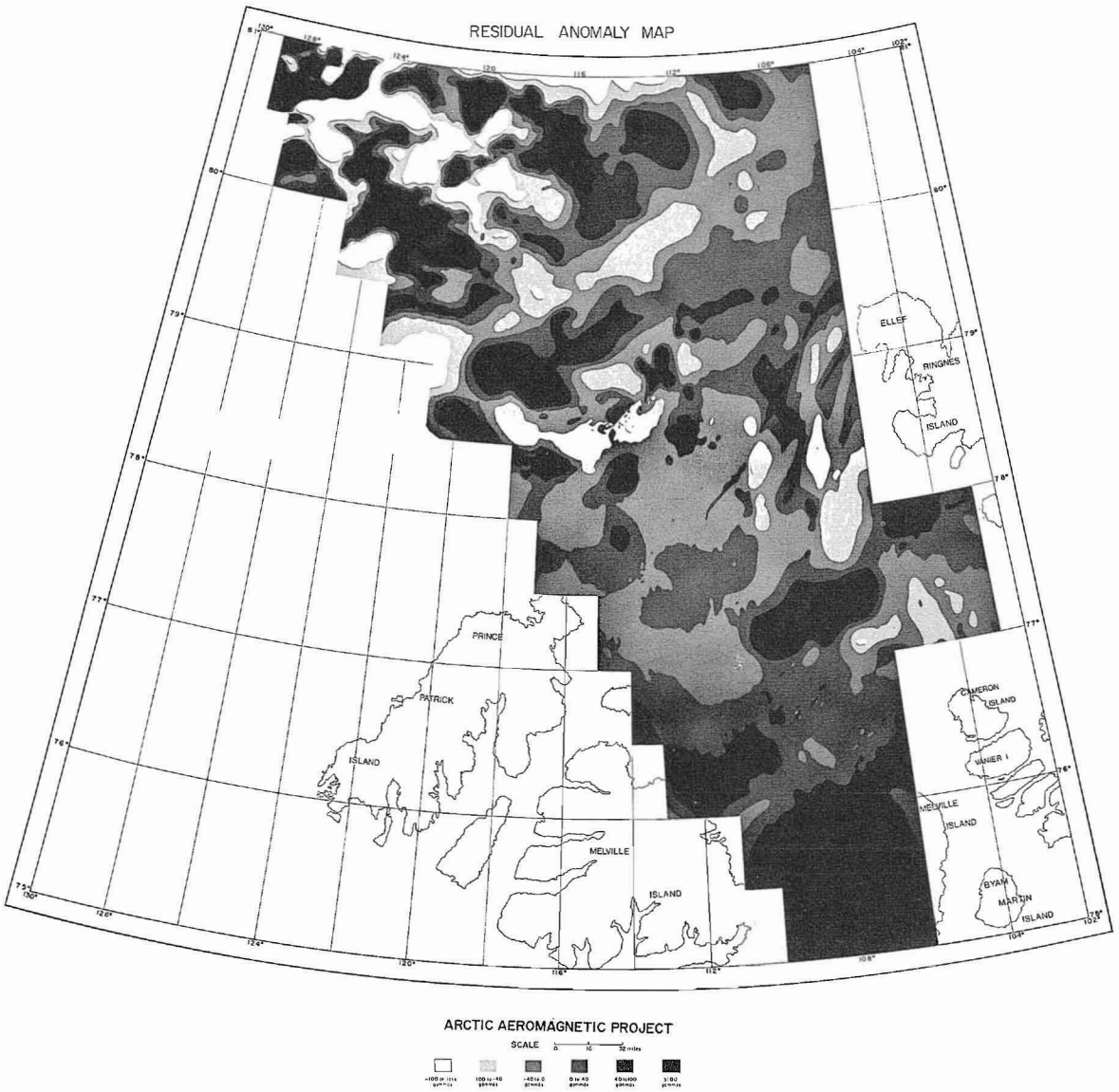


Figure 3. Residual aeromagnetic map of a section of the Canadian Arctic.

aeromagnetic map is fairly complicated with presence of steep gradients at several places.

The data in this map was digitized only along flight lines with the aid of an Electronic Co-ordinatograph. It is obvious from the figure that the flight lines are not equispaced and none of them is perfectly straight.

A single interpolating function for the entire volume of data over a large area normally utilizes polynomials of such a high order as to require considerable computer storage. Moreover, in majority cases a single function does not work satisfactorily over the whole area. This problem can be solved by considering only the data points lying within a small area surrounding a particular grid point. Interpolation within the small area could then be done rapidly and accurately using low-order surfaces.

The most convenient shape of the small areas is the rectangle, large enough to include information from at least two flight lines. In this study, elementary rectangles of width 1.8 miles along N-S axis and 2.0 miles along E-W axis were employed. The grid-point spacing was chosen to be one-half mile along both axes. Thus there was considerable overlap of the rectangles. The dimensions of the rectangles were adjusted to contain 21 points for consideration of polynomials up to 21st order. All the weighting functions were assumed to be unity.

Figure 2 displays a map contoured on the basis of grid-point values obtained by interpolation of the irregularly distributed data by Gram-Schmidt method. The resolution in this figure is fairly high as shown by the separation of the anomalies and good representation of small features such as the elongated anomaly trending northeast in the southern portion of the map. One important feature is that the gradients present in the map correspond very well with the original map. This feature is particularly desirable when quantitative interpretation of the data is performed. The shapes of the anomalies are well maintained. The magnitudes of very high peaks have been slightly smoothed.

Contents

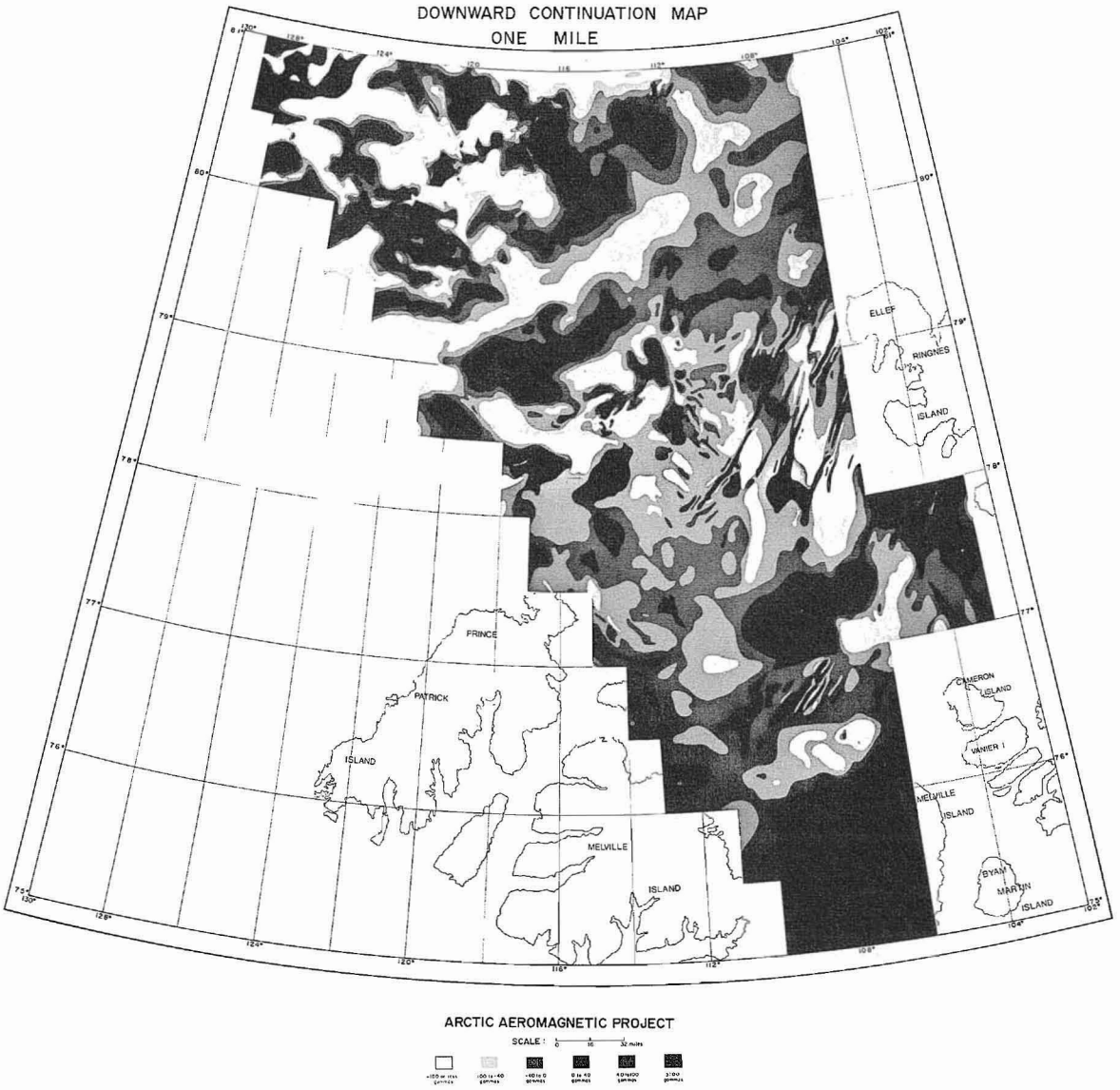


Figure 4. Residual map continued downward to a level of 1.6 km below flight elevation.

Some of this smoothing may be attributed to the one-half mile grid spacing. The method appears to yield equally good results in both low and high gradient areas.

Treatment of aeromagnetic data

The total magnetic field measured in the direction of the geomagnetic field contains the combined effect of all the magnetic sources present at and below the earth's surface. The variation of this field from point to point is caused not only by magnetized crustal bodies but also by the sources producing geomagnetic field variations. The crustal bodies normally produce high-intensity anomalies of relatively small horizontal extent. Amongst them are occasionally found bodies of immediate economic importance for mining and exploration. The rest of the sources in the interior of the earth generally produce anomalies of vast horizontal extent because of their great depths and sometimes because of their large dimensions. These anomalies are normally characterized by broad and smooth variations over relatively small areas. In such cases, it is often possible to represent them to a reasonably satisfactory degree by two-dimensional quadratic surfaces fitted to the total field values by the principle of least squares. The undesirable effects of these anomalies are that they somewhat distort the local anomalies and also tend to mask anomalies due to weak but shallow sources. After removal of these effects, the remaining total field is called the 'residual'.

The 'residual' magnetic data is subjected to a number of varying treatments for evaluation of various transformed fields, as mentioned before (Peters, 1949; Henderson and Zietz, 1949; Elkins, 1951; Rosenbach, 1953; Henderson, 1960; Danes, 1962; Danes and Oncley, 1962). There are various approximate methods available for performing these transformations. In this paper an analytic expression in the form of two-dimensional

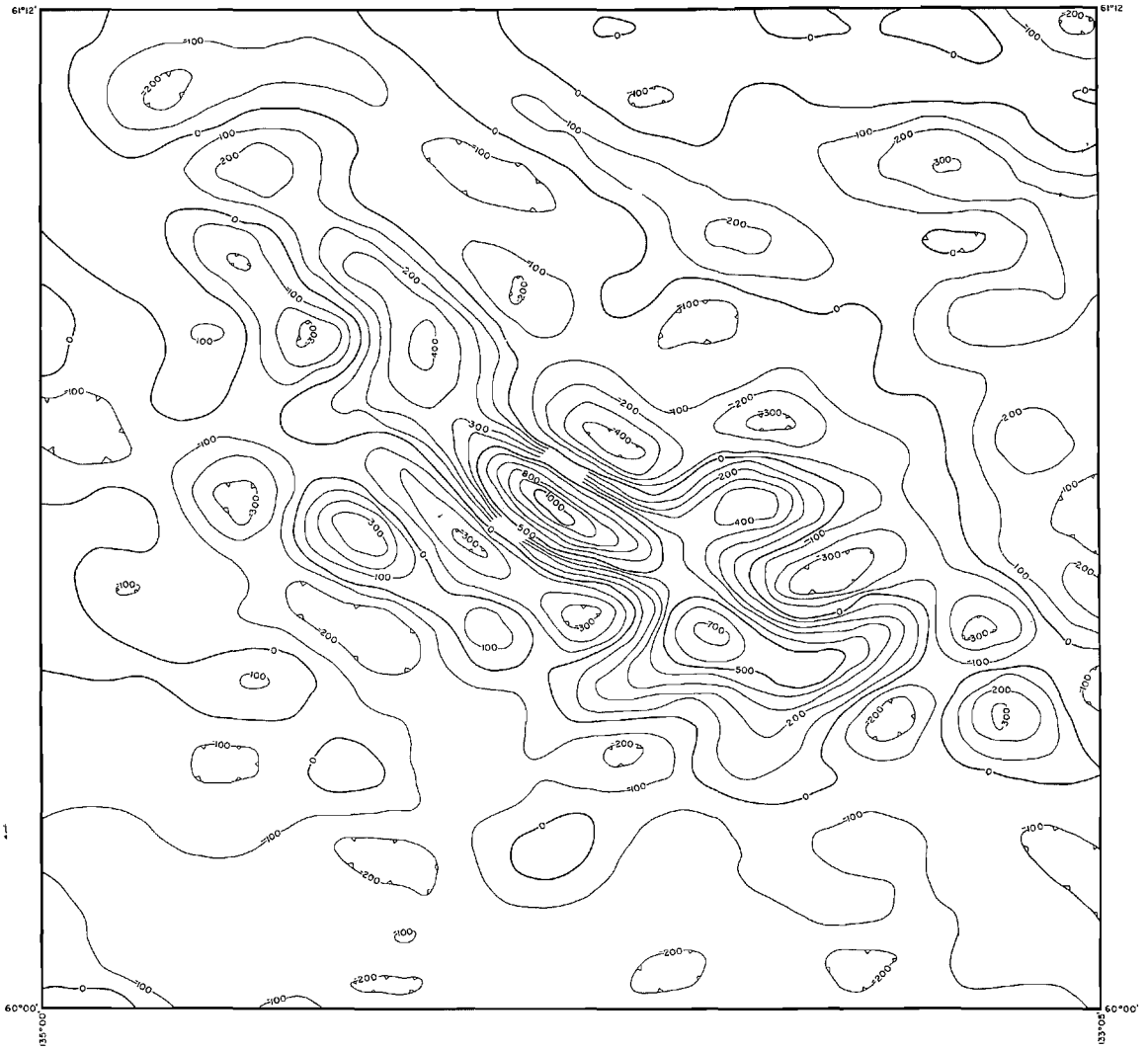


Figure 5. Filtered aeromagnetic map of a part of south-central Yukon.

Fourier series (Bhattacharyya, 1965) representing the residual data was used for calculating most of the transformed fields.

Continuation fields. The residual field is continued above or below the level of observation in order to either reduce or accentuate the effects of bodies close to the earth's surface. The downward continuation of the field provides more resolution and sharpness on the magnetic map than the original field does. On the other hand, upward continuation is approximately equivalent to stripping the magnetic data of the effects of shallow sources and thereby making the magnetic map anomalies broader and smoother. Downward continuation can normally be done down to a level which is about two-thirds the depth to the top of the body from the level of observation. Any further continuation causes the magnetic field to fluctuate violently from positive to negative values within a short horizontal distance. This happens because of practically exponential amplification of any error inherent either in the original data or in the process of computation or in both.

Figure 3 shows the residual aeromagnetic map of a section of the Canadian Arctic. The anomalies in the residual map are conspicuous by their low gradients and broad, flat characteristics, indicating great depths to the basement. Figure 4 presents the continuation field to a depth of 1 mile below the level of observation. In the process of downward continuation, erroneous results were first encountered due to the strong influence of short wavelength components produced by very tight spacing chosen initially for digitizing the data. Hence it was decided to remove all wavelengths shorter than 3.2 km (2 miles). This process of filtering got rid of all unwanted oscillations and provided reliable and accurate values for the continued field.

In contrast to the residual map, the trend and orientation of the anomaly bands in the continuation map are much better defined and are more apparent. The anomalies are much more accentuated. One prominent feature which is worth mentioning here is the string of prominent magnetic lineaments (Figure 3) trending north-northeast in the area adjoining the northeastern part of the Sverdrup Basin. They cut across a group of magnetic lows which are probably due to deep linear structural troughs coincident with a tertiary fold axis. The magnetic lineaments in the downward continuation map (Figure 4) are very prominent and seem to have intruded the Mesozoic sediments of the basin.

In Figure 4 undesirable, fictitious oscillations can also be

Contents

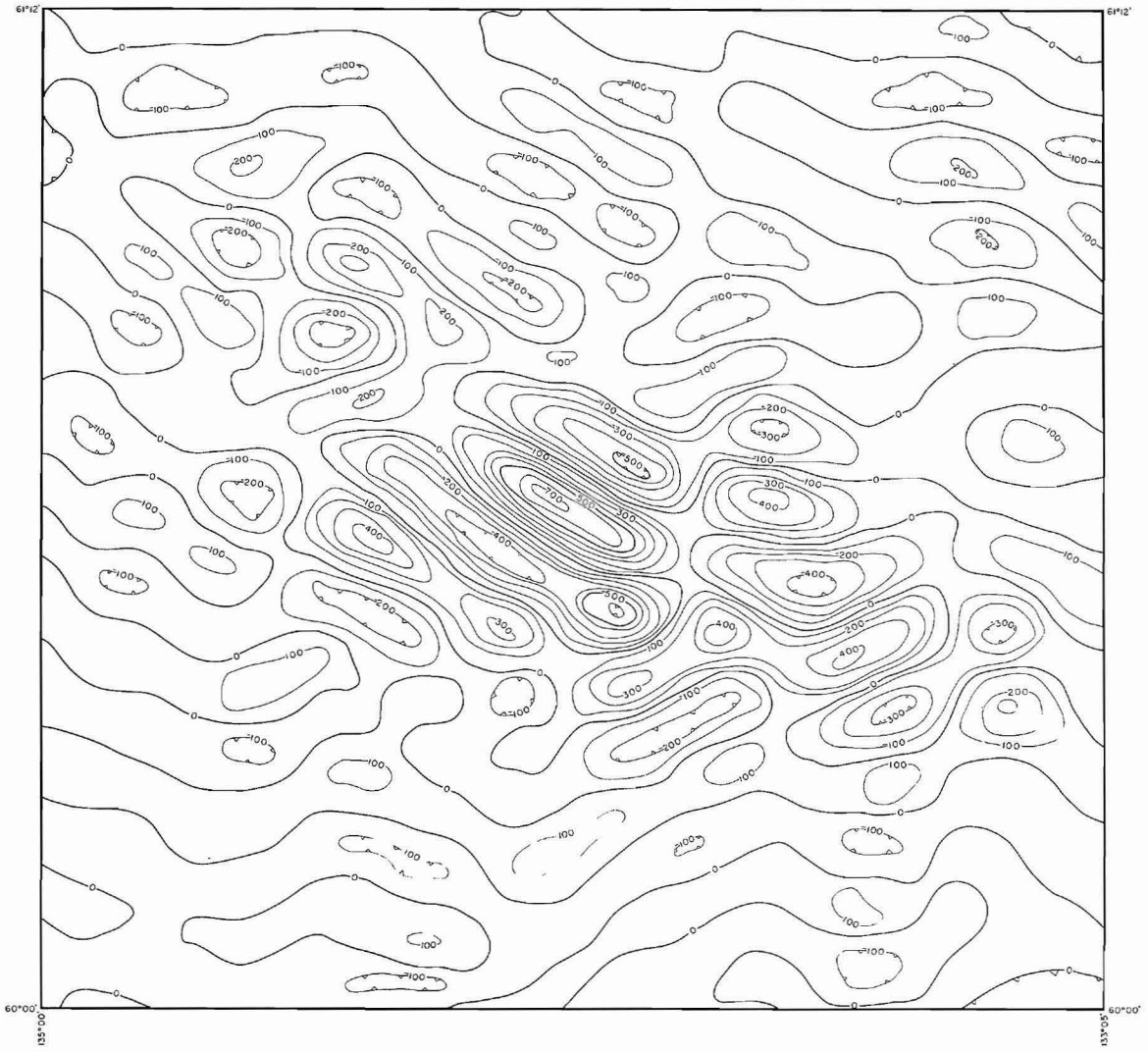


Figure 6. Second vertical derivative map of the total-field values over south-central Yukon.

observed in cases of local anomalies in the Sverdrup Basin. These anomalies are attributable to tabular magnetic bodies and to horizontal sills and volcanic rocks locally folded, faulted and intruded by gypsum in piercement structures (Gregory, *et al.*, 1961).

Second vertical derivatives. Second vertical derivative method is firmly based on the relative emphasis of local anomalies and de-emphasis of regional anomalies. The second vertical derivative is the negative of the sum of the two horizontal second derivatives. Hence it is a measure of the changes of magnetic gradient and the derivative anomalies are coincident with the nonlinear part of the observed total field map.

Another interesting feature of the derivative maps is the manner in which they tend to delineate magnetized geological formations. The zero contour of these maps has been found to be very effective in outlining the horizontal boundaries of the causative bodies. This is why this method has been used for approximating the contact between geologically different bodies (Vacquier, *et al.*, 1951).

Figure 5 presents a filtered aeromagnetic map of a part of south-central Yukon adjoining British Columbia. This area constitutes geologically and physiographically a section of the northern Canadian Cordillera. In the figure the extreme south-western corner occupied by a granitic intrusive is a part of the Coast Range crystalline zone – the Coast Geanticline. The zone is formed of a complex of plutonic masses with subordinate metamorphic rocks. Northeast of the Geanticline lies a belt of primarily Mesozoic volcanic and sedimentary rocks intruded by numerous granitic plutons. These Mesozoic rocks constitute a part of the Whitehorse Trough – a long basin of Mesozoic sedimentation running through the median axis of the Cordillera. The Whitehorse Trough is interrupted by a large upthrown block – the Atlin horst – of Paleozoic rocks (chiefly Permian) intruded by granitic plutons.

A critical examination of the geology and magnetics of the area makes it clear that the strong positive anomaly belts are, in most cases, related to the distribution of ultrabasic rocks and basic volcanics and intrusives. It also seems reasonable to

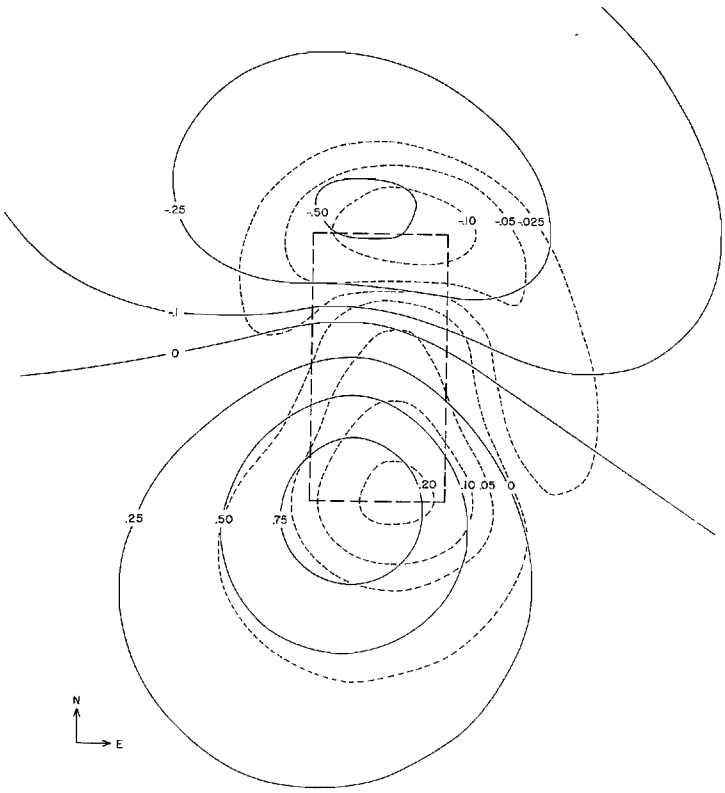


Figure 7. The total field and its vertical second derivative caused by a prism-shaped body shown by thick dashed lines at the centre. The solid lines indicate the total field and the dashed lines, the second derivative.

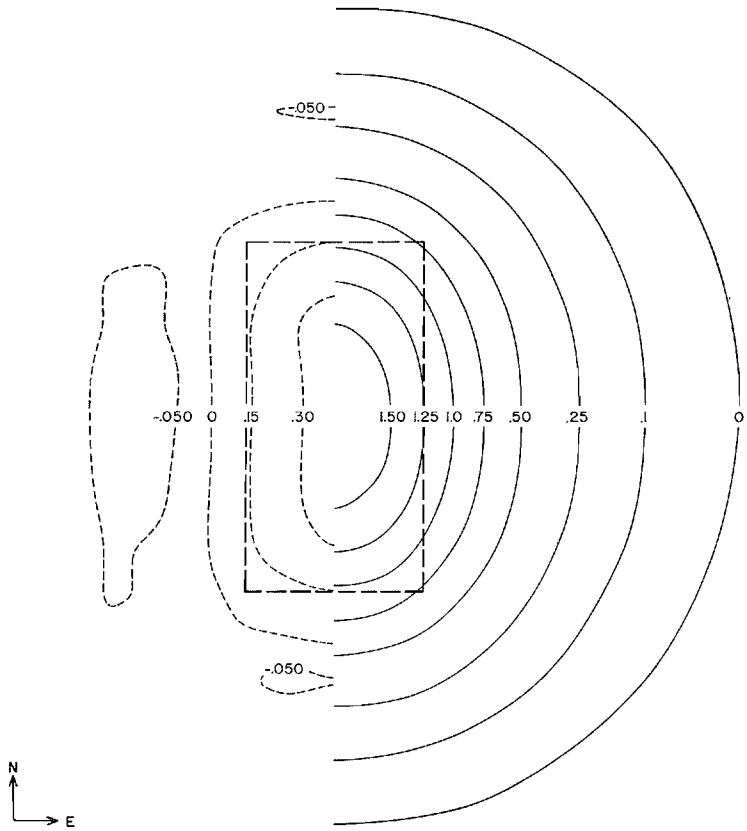


Figure 8. The total field of Figure 7 reduced to the pole and its second derivative. The solid lines indicate the total field and the dashed lines, the second derivative.

conclude from evidences just outside the area in Figure 5 that though the volcanic rocks make partial contribution to the intensity, they are not primarily responsible for the high intensity zones. It appears that the high positive magnetic anomalies in this area are caused mostly by ultrabasic bodies. The nature of the anomalies also suggests that ultrabasic rocks exist in depth in much more continuous and extensive bands than is suggested by their outcrops at the present erosion level.

The filtered data presented in Figure 5 are fitted with bicubic spline functions in order to calculate the second vertical derivative values. The derivative map is shown in Figure 6. It is apparent that the anomaly closures in Figure 5 extending beyond the contacts of the sources have been reduced considerably in Figure 6. The dimensions of the anomalies in the second derivative map are more likely to be representative of those of the causative bodies. Thus, the horizontal extents of the blocks of ultrabasic rocks in the area can be more accurately estimated.

It may be mentioned here that faulting in the northwest-southeast direction has been recognized from surface geological work along a very narrow section west of 134° W longitude and close to 60° 30′N latitude. This section has been found to coincide with the zero contour separating the positive 400 gamma per 1.5 mile squared anomaly from the associated negative anomaly of the same magnitude. It is suggested that the nearly straight line segment of the zero contour indicates the extension of the NW-SE trending fault.

A study of Figures 5 and 6 proves the effectiveness of the second derivative maps as an aid to magnetic interpretation. Caution should be exercised, however, in calculating the second derivative values because of possible erroneous results arising out of unavoidable and sometimes excessive amplification of high frequencies in the data.

Reduction to the pole. As noted before, the geomagnetic vector at the place of observation and the magnetization vector associated with the causative body are very important parameters in determining the size and shape of the anomaly. For reliability and accuracy in magnetic interpretation it would be highly desirable to evaluate a hypothetical anomaly from the observed anomaly when the causative body is physically moved to the north pole and the magnetization vector is made vertical by transformation (Baranov, 1957; Baranov and Naudy, 1964; Bhattacharyya, 1965). Such a hypothetical anomaly can indeed be evaluated with great accuracy with the help of the two-dimensional harmonic expansion of the total field values. The resulting anomaly would look practically like a gravity anomaly and hence it was originally called the 'pseudo-gravity' anomaly. However, because the meaning of this term can sometimes be misunderstood, Baranov and Naudy (1964) referred to it as the anomaly 'reduced to the pole'.

Calculation of the parameters of a magnetized body becomes simpler and more accurate when the total field values reduced to the pole rather than the original field values are used. This is apparent from a comparison of Figures 7 and 8 which show

Contents



Figure 9. Residual aeromagnetic data in the Moose River aeromagnetic belt in Ontario.

respectively the original and reduced anomalies. In these figures the solid lines indicate the total field and the dashed lines the second derivative. The anomaly illustrated in Figure 7 is produced by a rectangular prismatic body having horizontal dimensions of 8 and 4 units along north and east directions, respectively. The body is at a depth of 3 units and infinitely extended in the vertical direction. For the calculations it is assumed that the geomagnetic vector is defined by an inclination I of 60° N and declination D of 0° and that the magnetization vector has an inclination I_0 of 20°N and a declination D_0 of 45°E.

The positive anomalies of the total field and the second derivative are located appreciably in a southerly direction from the centre of the causative body. The negative anomalies to the north of the body, when compared to the positive ones, are of considerable magnitude. The anomalies are unsymmetrical with respect to the body. The zero contour of the second derivative does not seem to be influenced at all by the outline of the body.

On the other hand, the reduced total field and second derivative anomalies (Figure 8) are symmetrical with respect to the body; they are centred around the midpoint of the body. The negative anomalies of the total field have practically disappeared and those of the second derivative are very much reduced in magnitude. The zero contour of the second derivative follows the boundary of the disturbing body extremely well. A study of these figures reveals the effectiveness of the method of reduction to the pole as an aid to magnetic interpretation.

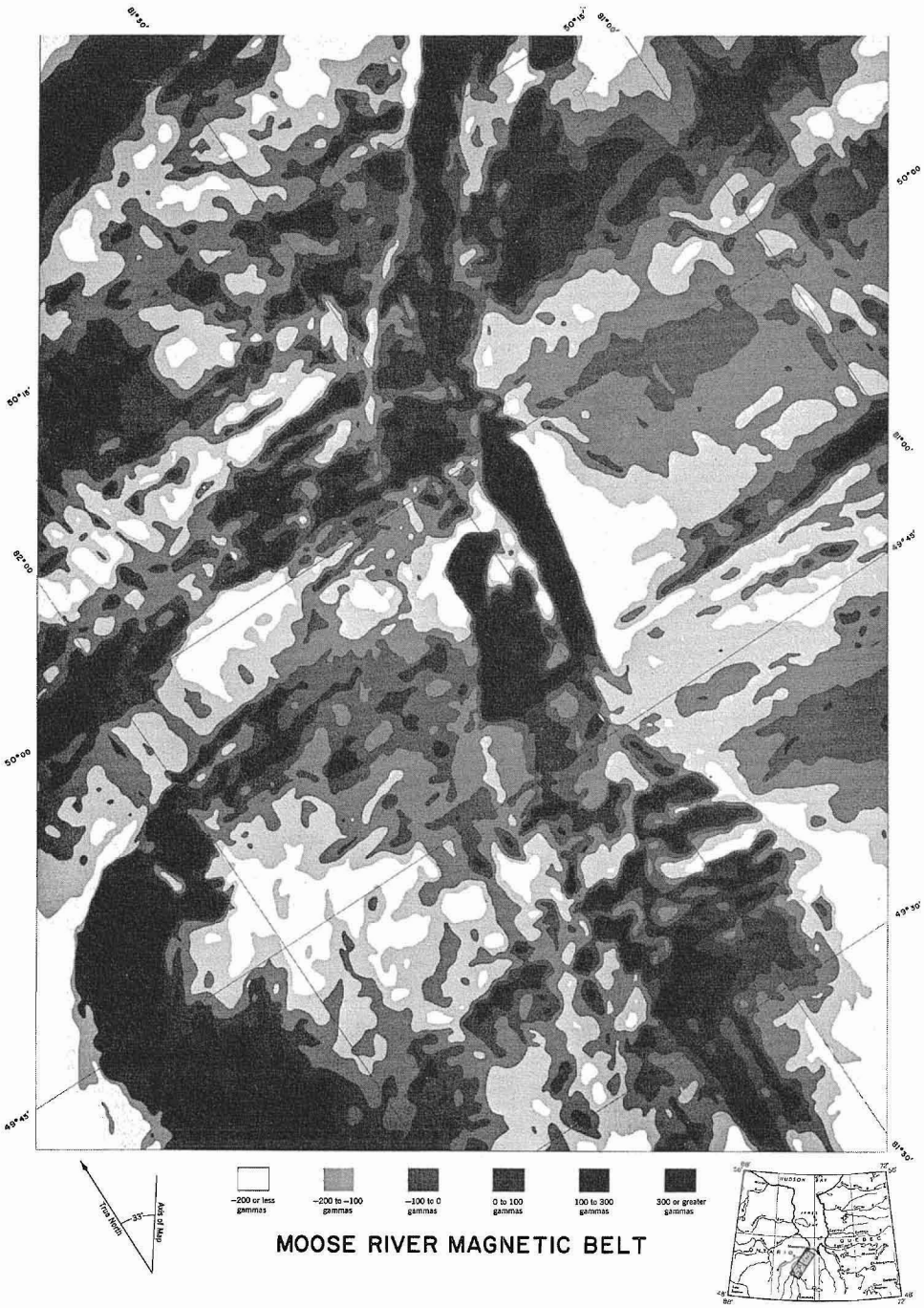


Figure 10. Moose River residual aeromagnetic data reduced to the pole.

For reduction of the total field to the pole, magnetization of the rock mass is often assumed to be due to induction alone because of the unknown magnetization vector. In some cases this assumption may lead to erroneous results. In the majority of cases, however, the reduced maps are found to yield a better approximation to more consistent results than do the original maps.

The original and reduced total fields are illustrated in Figures 9 and 10 for actual aeromagnetic data in the Moose River aeromagnetic belt in Ontario. Magnetization of the rock mass is assumed to be due to induction of the present earth's field. The geomagnetic inclination and declination are, on the average, 78° 5′N and 10° 30′W respectively.

The locations of the major anomalies in the residual map have not been very much affected by the process of reduction to the pole because of high geomagnetic latitude of the area. Nevertheless, the detailed shapes of the anomalies are somewhat different in the two maps and in some cases, the centres of anomalies have been shifted to the north by about one quarter mile. For further investigation regarding the geometry of the causative bodies, the detailed shapes of the reduced anomalies are found important.

Filtered anomaly fields. An aeromagnetic map usually contains a number of features which are superposed on each other. These features may be composed of regional, local, deep and micro-anomalies. The aim of an interpretation of such maps is to extract

Contents

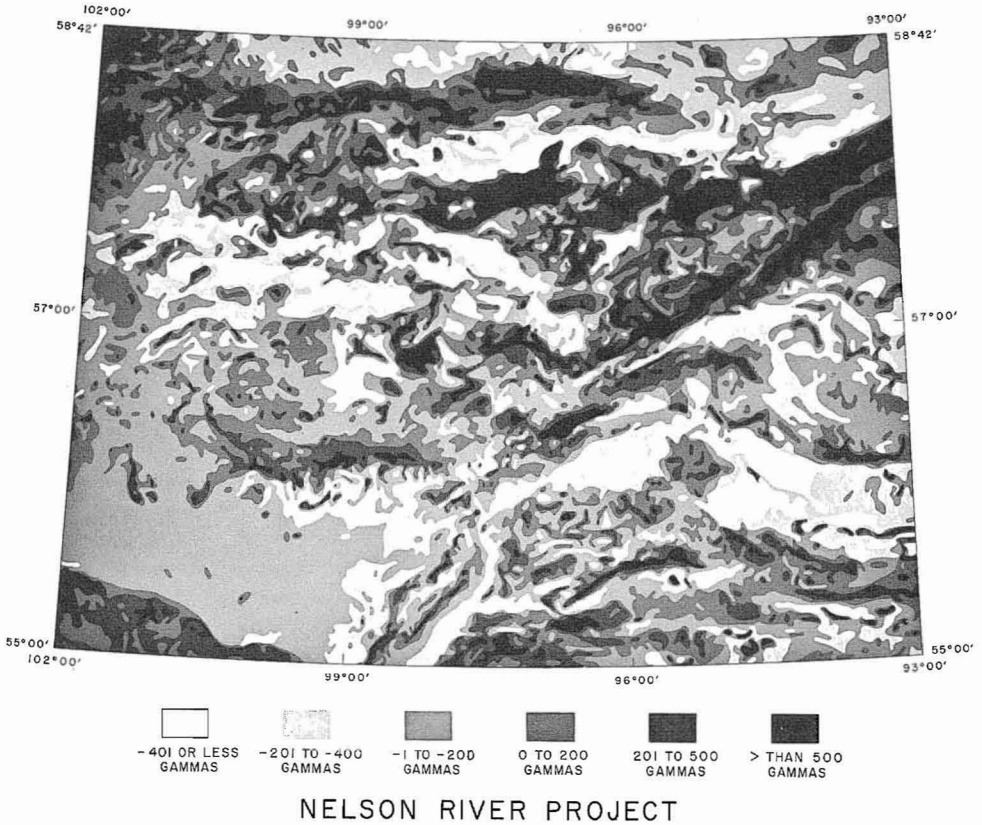
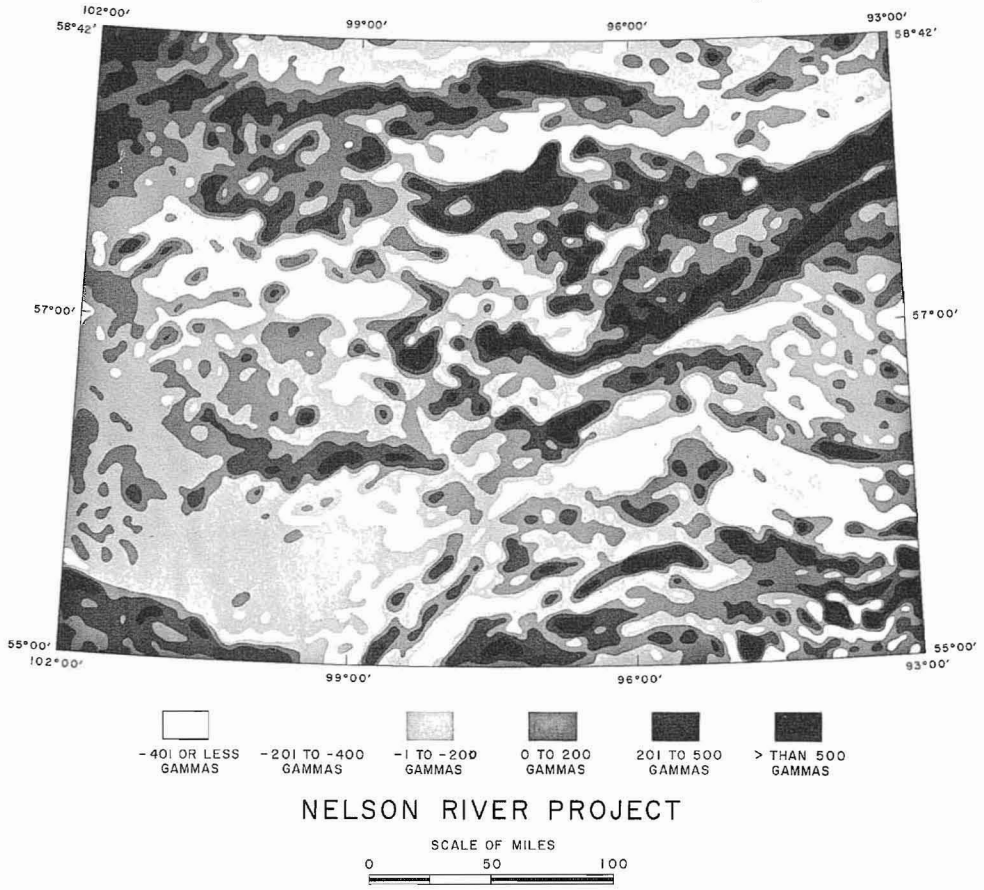


Figure 11. Residual aeromagnetic map of northern Manitoba.

Figure 12. Filtered aeromagnetic map with cut-off wavelength of 10 miles.



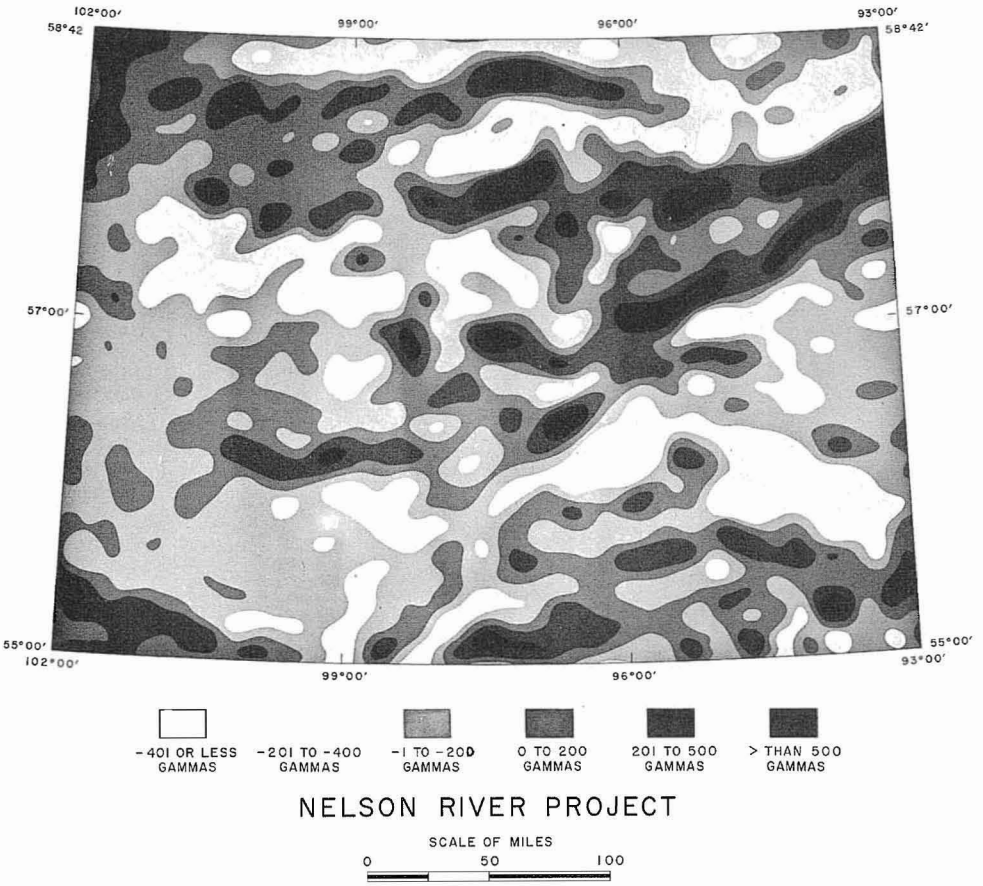


Figure 13. Filtered aeromagnetic map with cut-off wavelength of 20 miles.

as much useful information as possible from the data. Since often one type of anomaly masks another one, there is a need to separate the various features from each other.

The anomalies produced by shallow bodies are normally characterized by their sharpness and high intensity. They are the small-wavelength anomalies in the magnetic map. On the other hand, the deep-seated magnetized masses give rise to large-wavelength, low-intensity anomalies. It is, therefore, recognized that under suitable conditions spectral energy of anomalies may be concentrated in separate bands of wavelengths for shallow and deep causative bodies. This fact provides the foundation for the application of frequency filtering techniques to the relative emphasis and de-emphasis of certain features in the magnetic data.

Figure 11 presents the residual aeromagnetic map of northern Manitoba, bounded by latitudes 55°N and 58°43′20″N and longitudes 93°W and 102°W. This map contains the effects of all magnetized bodies in the crust. The residual map brings out the major geological trends of the entire area in a very noticeable way. These trends are superimposed on the small-wavelength and high-intensity anomalies produced by sources at shallow depths and of local character. It would be highly desirable to separate the effects of shallow sources confined within narrow horizontal limits from those of the major trends and deep-seated crustal bodies.

The residual data presented in Figure 11 was represented by a two-dimensional Fourier series. With the help of this expression, all wavelengths shorter than 10 miles (Figure 12) and 20 miles (Figure 13) were removed from the over-all spectrum. The filtered anomaly maps thus obtained show the regional trends and crustal anomalies very clearly. It should be mentioned here that by retaining only the short wavelengths and filtering out the large wavelengths, the effects of shallow sources could have been clearly presented.

Analysis of anomalies

In the analysis of anomalies the objective is to determine all the parameters associated with the causative body as accurately as possible. As noted before, these parameters are the size, shape and orientation of the body as well as the polarization vector associated with it. A large number of methods have been proposed in the geophysical literature for determining these parameters. Some of these methods will now be briefly mentioned.

As indicated before, the second vertical derivative maps (Vacquier, *et al.*, 1951; Henderson and Zietz, 1949; Bhattacharyya, 1965) can often be successfully used for estimating the dimensions of the horizontal sides of a body. Figure 14 presents the total field and its second derivative for a prismatic body. While the total field map (solid lines) gives wrong estimates about the location of the origin and the horizontal dimensions, the zero contour of the second derivative (broken lines) follows the edges of the body very closely. This contour has an inflection point along every side of the body. If these points for parallel sides are joined together by straight lines, the point of intersection of the two lines defines fairly accurately the centre of the body. The two lines may be taken as the axes of the body. The lengths of the lines between inflection points are good measures of the horizontal dimensions.

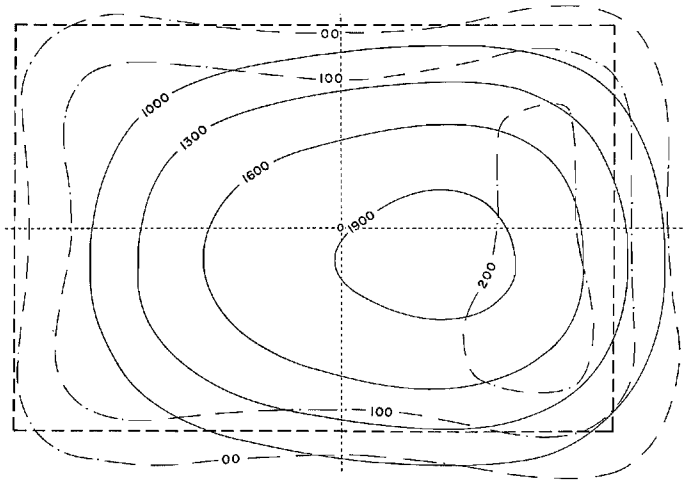


Figure 14. The total field and its second derivative of a prismatic body with dimensions 8 and 12 units respectively. The depth to the top is 3 units and the depth to the bottom 8 units. The solid lines indicate the total field and the dashed lines, the second derivative.

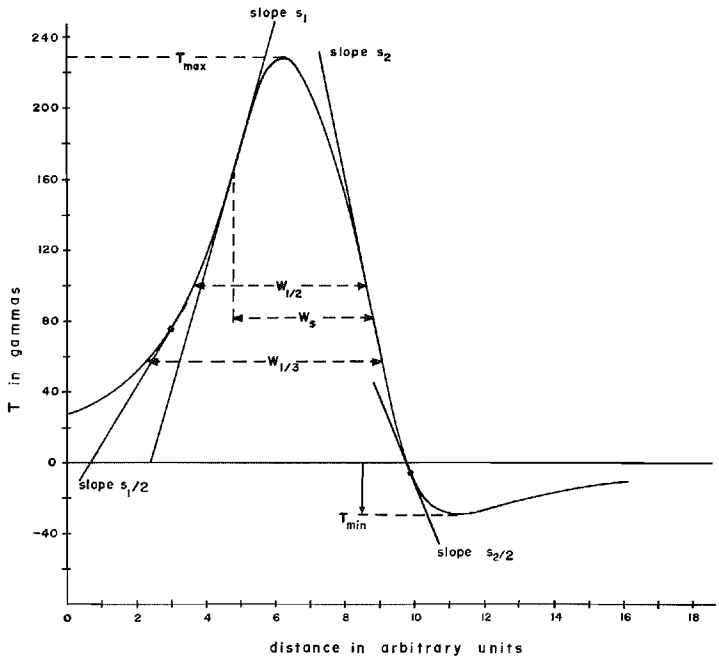


Figure 15. Characteristic parameters of a profile.

Many methods based on different models (Henderson and Zietz, 1948; Peters, 1949; Vacquier, *et al.*, 1951; Smellie, 1956; Grant and West, 1965) are available to calculate the depth to the top of a causative body from the plane of observation. In most cases the depth is estimated with the help of various characteristic parameters of a carefully chosen profile (Figure 15). Some of these parameters are given below:

(i) T_{max} and T_{min}, the maximum and minimum values in the profile;
(ii) w_s, horizontal distance between the points of inflection;
(iii) $w_{1/2}$, $w_{1/3}$, widths of the profile half-way and one-third of the way up from the minimum to the maximum value;
(iv) S_1, S_2, maximum horizontal gradients of the profile; and
(v) $S^1_{1/2}$, $S^2_{1/2}$, one half of the maximum horizontal gradients.

Most of the available methods make the assumption that magnetization of the rock mass is caused by induction of the present geomagnetic field alone. However, remanent magnetization, positive and negative, is normally present in the rocks of the earth's crust. The combination of remanent and induced magnetization may orient the total magnetization vector in an arbitrary direction. In some of the recent papers, the determination of the direction of this vector has been the subject of study for specific model sources, e.g., infinitely long dikes (Hutchison, 1958); point dipole and line of dipoles (Sutton and Mumme, 1957); a point dipole, a horizontal line of dipoles, a thin, dipping sheet, a thick, dipping sheet, and a sloping step (Hall, 1959). Some of these papers have determined particular characteristics of profiles which are indicators of the direction of magnetization.

The methods mentioned so far have been developed for the analysis of single profiles. The estimation of the depth to the top of a body with these methods may be subject to gross errors because of many simplifying assumptions (Agocs, 1958). First, the magnetic trends are assumed to be at right angles to the direction of the profile. Second, the magnetic anomalies are taken to be due to sharp discontinuities in the magnetization of rocks. Third, it is assumed that the bodies are dipping vertically. Fourth, the values at the edges of a profile are often the combined effects of different magnetized bodies located close to each other, rather than the effects of a single causative body.

Because of the limitations of the methods using profiles for analysis, it would be very desirable to have a method that would utilize the two-dimensional characteristics in the central portion of the anomaly. This portion contains the magnetic effects of the causative body and is least adulterated by those from other bodies in its neighbourhood. Based on the characteristics of the anomaly near the centre, an iterative method (Bhattacharyya, 1966) has recently been developed to calculate, with the help of digital computers, the total magnetization vector, depth and the horizontal and vertical dimensions of rectangular block-shaped bodies. The reason for using this model is that the magnetic effects of a number of closely spaced bodies blend together to such an extent when viewed from a large distance that they appear as a single anomaly pattern. The rectangular block model serves to outline the volumes of rock within which magnetic minerals are found in greatest concentration.

This method uses the expressions for the total field and all its first derivatives at the origin, which is directly over the centre of the body. The latter quantities can be obtained from the total field values of the anomaly. Now, by the use of Taylor's expansion it can be shown that the total-field values in the vicinity of the origin can be expressed, to a first degree of approximation, in terms of the total field and its first derivatives at the origin. Hence the parameters of the body calculated with the proposed method automatically explain, to a limited extent,

the two-dimensional features of the anomaly in its central portion.

Concluding remarks

This paper has dealt with some of the techniques available now for facilitating the work of quantitative interpretation of aeromagnetic data. A few years ago before the development of modern data processing equipment most of these methods could not be used because of the staggering amount of calculation required. The advent of the digital computer with all its accessories has opened up possibilities undreamed of before. New processes and techniques have evolved to squeeze out information from aeromagnetic data with a great amount of efficiency. In this fast-changing process, the cost of quantitative interpretation, instead of increasing, has really been reduced in terms of the available information. The results are becoming more accurate and are being presented in a more readily understandable form than before.

References

Agocs, W.B., 1958. Results of airborne magnetometer profile from Brownsville, Texas to Guatemala city. *Geophysics.* 23: 726-737.

Baranov, V., 1957. A new method for interpretation of aeromagnetic maps: pseudo-gravimetric anomalies. *Geophysics.* 22: 359-383.

Baranov, V., and H. Naudy, 1964. Numerical calculation of the formula of reduction to the magnetic pole. *Geophysics.* 29: 67-79.

Bhattacharyya, B.K., 1965. Two-dimensional harmonic analysis as a tool for magnetic interpretation. *Geophysics.* 30: 829-857.

Bhattacharyya, B.K., 1966. A method for computing the total magnetization vector and the dimensions of a rectangular block-shaped body from magnetic anomalies. *Geophysics.* 31: 74-96.

Crain, I.K., and B.K. Bhattacharyya, 1967. Treatment of non-equispaced two-dimensional data with a digital computer. *Geoexploration.* 5: 173-194.

Danes, Z.F., 1962. Structural calculation from gravity data and density logs. *Mining Transactions.* 223: 23-29.

Danes, Z.F., and L.A. Oncley, 1962. An analysis of some second derivative methods. *Geophysics.* 27: 611-615.

Elkins, T.A., 1951. The second derivative method of gravity interpretation. *Geophysics.* 16: 29-50.

Grant, F.S., and G.F. West, 1965. *Interpretation theory in applied geophysics.* New York, McGraw-Hill.

Gregory, A.F., M.E. Bower, and L.W. Morley, 1961. Geological interpretation of aerial magnetic and radioactivity profiles. *Geol. Surv. Can.,* Bull. 73.

Hall, D.H., 1959. Direction of polarization determined from magnetic anomalies. *J. Geophys. Research.* 64: 1945-49.

Henderson, R.G., and I. Zietz, 1948. Analysis of total magnetic intensity anomalies produced by point and line sources. *Geophysics.* 13: 428-436.

Henderson, R.G. and I. Zietz, 1949. The computation of second vertical derivatives of geomagnetic fields. *Geophysics.* 14: 508-516.

Henderson, R.G., 1960. A comprehensive system of automatic computation in magnetic and gravity interpretation. *Geophysics.* 25: 569-585.

Hutchison, R.D., 1958. Magnetic analysis by logarithmic curves. *Geophysics.* 23: 749-769.

Peters, L.J., 1949. The direct approach to magnetic interpretation and its practical application. *Geophysics.* 14: 290-320.

Rosenbach, O., 1953. A contribution to the computation of the "second derivative" from the gravity data. *Geophysics.* 18: 894-912.

Smellie, D.W., 1956. Elementary approximation in aeromagnetic interpretation. *Geophysics.* 21: 1021-1040.

Sutton, D.J., and W.G. Mumme, 1957. The effect of remanent magnetization on aeromagnetic interpretation. *Austral. J. Phys.* 10: 547-557.

Vacquier, V., N.C. Steenland, R.G. Henderson, and I. Zietz, 1951. Interpretation of aeromagnetic maps. *Geol. Soc. Am.,* Mem. 47: 151.

The use of gravimeter measurements in mining and groundwater exploration

W.E. Strange

Geonautics, Inc.
Washington, U.S.A.

Abstract. Improvements in the portability, range, calibration, accuracy and drift characteristics of modern land gravimeters provide data of increased accuracy in conjunction with a decrease in time, effort and cost for a survey. The new instruments also make possible the execution of special work such as gravity-gradient surveys, three-dimensional mine surveys and offshore gravity surveys. A more difficult problem has been the development of gravimeters for use on moving platforms. Much progress has been made on gravimeters for shipboard use but airborne systems are still in the experimental stage. The borehole gradiometer offers real promise for providing porosity estimates in groundwater studies and density estimates in mining work.

Computerized field data handling permits rapid data plotting and contouring as well as swift and accurate reductions including the terrain correction, and, in the case of moving platform systems, processing of information from other sensors.

Computerized data handling can be conveniently grouped in two categories: separation of local and regional anomalies and the fitting of density models to explain the observed gravity field. A number of techniques for resolving these problems are available and many others are still under consideration.

Résumé. Les améliorations en portabilité, gamme, et précision ont résulté en une hausse de rendement des opérations avec des appareils conventionnels. Ces instruments permettent également des travaux spéciaux comme mesures du gradient, mesure "à trois dimensions" dans des mines, et des mesures sous-marines. La mise au point d'appareillages pour des mesures mobiles pose toujours des problèmes techniques. La plupart du progrès dans ce domaine est rapporté sur des installations à bord des bateaux. La gravimétrie aéroportée étant au stade purement expérimental. Le gravimètre destiné aux mesures dans les forages rend possible l'estimation de la porosité dans les puits d'eau et de la densité dans les forages miniers.

Le traitement digital des levées résulte en une très grande amélioration de la rapidité et précision dans la préparation des cartes de l'anomalie Bouguer. Toutes les corrections, y compris la correction du terrain peuvent être appliquées d'une façon automatique. Dans le cas des mesures mobiles les indications des appareils complémentaires peuvent être apportées à la réduction des données gravimétriques.

L'analyse des données tombe dans deux catégories. La première traite le problème de la séparation des anomalies locales et régionales. La deuxième contient le problème de la construction des modèles qui servent à l'explication des anomalies observées. Il existe de nombreuses méthodes pour le traitement de ces deux problèmes. Des autres méthodes sont toujours au stage de perfectionnement.

The task assigned to this author was the preparation of a paper describing the state of the art in gravimetry as it is applied to mining and groundwater exploration. Two approaches existed. One was to consider all the literature concerning specific applications of gravimetry to particular mining and groundwater problems. A second approach was to delineate those recent advances in instrumentation, data handling and methods of analysis which have opened the way to new and improved utilization of gravity data whatever the problem to which it is being applied.

The second approach was taken for a number of reasons, not the least of which was that the bulk of the gravimetric work is not being carried out to support mining and groundwater exploration. Of some 300 to 350 gravimeters in use in the exploration industry perhaps 10 to 15 percent are involved in mining and groundwater applications. It is therefore not surprising that the major advances in gravimetric instrumentation and analysis have arisen from the application of gravimetry in such fields as geodesy, scientific investigations of earth structure and oil exploration. As a corollary to the approach taken here the size of the reference list has been kept to a minimum, with only the most recent and most important papers cited. The interested reader can easily follow the chain of literature beginning with these articles by using their bibliographies.

The paper has been broken into three broad sections. Under instrumentation, the accuracies and capabilities of existing gravimeters are covered. The important advances in the areas of increased accuracy and ease of use of land gravimeters and the development of numerous specialized gravimeters which have greatly extended the range of application of gravimetry is discussed. In the field of data handling, the impact of computers on data-handling procedures is considered as the most important subject. Under the heading of data analysis the most modern methods of regional-residual separation, density model construction and total anomalous mass computation are covered.

Instrumentation

Conventional gravimeters. At present some 300 gravimeters are in use in the exploration industry of which perhaps 10 to 15 percent are involved in mining and groundwater applications. This includes both modern gravimeters and older models.

Only three types of highly portable modern land gravimeters are now being actively constructed in significant quantities. These are the LaCoste-Romberg gravimeters, the Worden gravimeter and the Canadian gravimeter. The LaCoste-Romberg gravimeter employs a metal-sensing element while the Worden and Canadian gravimeters have quartz-sensing elements. The LaCoste-Romberg meter must be maintained at constant temperature. The other instruments have temperature compensation effected by means of bimetallic strips and in theory do not require maintenance of constant temperature. However, in practice the quartz-element gravimeters should also be maintained at constant temperature if best performance in terms of low and linear drift rate is to be maintained.

The best of the modern gravimeters are a vast improvement over the older gravimeters. These improvements, which have

taken place primarily in response to the demands and requirements of geodetic gravimetry, can be summarized as follows: (1) decrease in weight and volume, (2) improved calibration, (3) elimination of need for reset, and (4) decrease in magnitude and increase in linearity of drift.

The modern gravimeter is a truly portable instrument. The LaCoste gravimeter, with power supply, weighs approximately 25 pounds. The Worden gravimeter, with power supply, weighs approximately 15 pounds. The Canadian meter is similarly portable. These gravimeters are also extremely compact and with all necessary equipment can be fitted into carrying cases having no linear dimension greater than 24 inches. This decrease in size and volume has been brought about primarily by decrease in the size of the sensing elements, miniaturization of the electronics and use of the nickel-cadmium battery to provide power for temperature control.

Modern gravimeters are capable of providing local surveys, such as are common in mining and groundwater applications, which have a precision of the order of ±0.02 milligal. This precision is achievable with a minimum of effort in the field because of the linearity of the measuring system, the accuracy of the calibration constants and the low and linear drift rate. The LaCoste-Romberg gravimeter appears to be somewhat superior to other gravimeters in these respects. It has a reading system accurate to better than one part in 50,000 and can be calibrated to a relative accuracy of ±0.015 milligal over an equator-to-pole gravity range. Normally the LaCoste-Romberg gravimeter has a linear drift rate of less than 1 milligal per month if care is taken to avoid excessive vibration (Hamilton and Brulé, 1967). Relative calibration constants for the LaCoste-Romberg gravimeter can be obtained at the factory with only a single precisely known gravity interval required to set scale.

With the modern gravimeter, the most difficult, time-consuming and expensive part of a gravity survey is the determination of vertical control. This must be accurate to one or two tenths of a foot to make full use of the instrument accuracy.

The accuracy of modern gravimeters has made possible the use of determinations of horizontal gradients of gravity in certain cases to overcome the elevation determination problem (Thyssen-Bornemisza, 1965, and references therein).

Modified land gravimeters. Turning from conventional land gravimeters we will consider a number of groups of specialized gravity-sensing instruments which have greatly extended the horizontal and vertical domain over which useful gravity data can be obtained. The first of these groups of specialized instruments is the modified land gravimeter.

The specialized gravimeter representing the smallest change from conventional instruments is the gravimeter developed for and used on floating sea ice. This instrument is simply a conventional gravimeter whose sensing element has been adjusted to provide infinite sensitivity and whose readout system has been slightly altered. It is capable of measurement accuracies of the order of ±.2 milligal when used on floating ice and is highly portable (R.M. Iverson, pers. comm.). Such instruments are extremely useful for near-shore oceanic and lake reconnaissance surveys in polar areas.

As exploration has moved offshore, so has gravity measurement. This problem was first attacked by placing a man in a diving bell with a gravimeter and lowering him to the bottom (Frowe, 1946). Following this came the LaCoste-Romberg underwater meter, a self-leveling instrument, which could be lowered to the bottom and read remotely. A description of this gravimeter is given in LaCoste (1967). The basic modifications consisted of (1) the development of a servocontrolled elevator and (2) overdamping of the sensing element so that the velocity of the beam rather than its displacement was proportional to gravity. These modifications were necessary to accommodate the seismic motion of the ocean bottom due to waves, etc.

The bottom gravimeters have proven capable of accuracies of ±0.02 to ±0.10 milligal, depending on bottom conditions and weather, when used in water depths of 500 feet or less as has commonly been the case. To make full use of the level of accuracy provided by these meters precise measurements of water depth and electronic ship-positioning systems are necessary. Beyer, *et al.* (1966) have made additional modifications to a LaCoste-Romberg underwater meter and obtained measurements in water as deep as 900 meters with accuracies of about ±0.5 milligal.

An application of underwater gravimeters of special interest to the mining industry is the regional survey of the Great Lakes which is now being carried out by the U.S. Army Map Service and the University of Wisconsin. The regional survey of Lake Superior has been completed and should provide a better understanding of the structure of this important area.

The underwater gravimeter is also useful in other applications where unstable conditions cause vibrations or where automatic remote readout and leveling are needed. It can be used on ice (although it is less portable than the ice gravimeter mentioned previously, it is more accurate) or in marshy and swampy areas.

An interesting application of the underwater meter has been in conjunction with a helicopter. This interesting approach was developed by the U.S. Geological Survey and is now being used commercially in exploration applications. In this method a hovering helicopter lowers a LaCoste-Romberg underwater gravimeter to the ground while three remote angle/ranging stations determine the helicopter's vertical and horizontal position. By this positioning method the helicopter can be located horizontally with an accuracy of one part in 40,000 and vertically to ±1 foot at a distance of 15 miles. This system is the most economic procedure under certain terrain and vegetation conditions.

Borehole gravimeters. Before discussing instruments on moving platforms, let us turn to an important recent development in gravimeters fixed with respect to the earth. This development is in gravity instruments capable of making measurements in boreholes. A general discussion of borehole gravimeters can be found in McCulloh, *et al.* (1967). Two borehole meters are presently available for operational use, the Esso borehole meter and the LaCoste-Romberg borehole meter.

The Esso borehole meter, now under license to Scintrex Ltd., is a vibrating string instrument (Howell, *et al.*, 1965; Henderson, 1967). The string operates in the fundamental mode and an individual reading requires about 20 minutes. The meter is currently being improved to shorten the reading time as well as provide for a higher accuracy in determining vertical position of the sensing element and for more compact electronics. The instrument at present fits into a sonde with an outside diameter of 4 inches.

The LaCoste-Romberg borehole meter, developed by that company in conjunction with the U.S. Geological Survey, is an astatized spring mass gravimeter mounted on gimbals for leveling (McCulloh, *et al.*, 1967). The instrument is capable of leveling itself automatically in holes deviating by up to 6.5 degrees from the horizontal. An individual reading requires 5 minutes. The meter fits into a sonde with an outside diameter of between 6 and 7 inches.

Both meters are capable of ±.01-mgl rms reading accuracy and of withstanding widely varying borehole environment conditions, particularly with respect to temperature.

A wide variety of applications for borehole meters exists. For example, the average total porosity over a 50-foot interval can be measured with an accuracy of about 2 percent. This capability is potentially of great use in groundwater applications.

Promising possible applications for the borehole meter exist in the mining industry in such applications as tracing orebodies in faulted areas and providing means of estimating the magnitude and vertical location of orebodies in the near vicinity of test holes. For maximum utilization in mining applications, the outside diameter of the sonde must be reduced to allow its use in smaller holes. This is entirely feasible since the majority of applications of interest to the mining industry are at shallow depths. The diameter of the sonde for oil applications is in part controlled by the need to provide insulation against the very high temperatures often encountered in the deep wells of the oil industry.

Shipboard gravimeters. Although shipboard gravimeters capable of providing useful regional gravity information were developed during the 1950s, it has only been during the last few years that exploration accuracies have been attainable. This increase in accuracy has come about through both improvement in instrumentation and recognition of and accounting for horizontal acceleration and cross-coupling errors either through real time analog or later digital correction.

Instruments currently of interest to the exploration industry are of two types: spring mass systems and modified accelerometers. The LaCoste-Romberg and the Graf-Askania gravimeters are modified spring mass gravimeters mounted on inertial stable platforms. Information on the characteristics of the LaCoste-Romberg shipboard gravimeter may be found in LaCoste, *et al.* (1967), and LaCoste (1967). Information on the Graf-Askania gravimeter may be found in Schulze, *et al.* (1964), Hayes, *et al.* (1962), Bower (1966), and Wall, *et al.* (1966).

A recent addition to the gravimeter field is the Bell Aerosystems shipboard gravimeter, also mounted on a stable platform. The sensing element of this gravimeter is a single-axis, pendulous, force rebalance accelerometer. The development of this instrument for the U.S. Navy Oceanographic Office and U.S. Coast and Geodetic Survey represented a successful modification of missile technology to the gravity problem. Descriptions of this instrument may be found in Henderson (1967), and Henderson and Iverson (1967).

The LaCoste-Romberg shipboard gravimeter is presently being used in offshore oil surveys. A discussion of the accuracies of the system and operational and data reduction requirements are given by LaFehr and Nettleton (1967a). Comparisons of line crossings with bottom gravimeter measurements indicated that average accuracies of ±0.5 to 0.7 milligal were being obtained. The Bell Aerosystems shipboard gravimeter was first tested in June 1966 and has not yet been used in oil or mineral explorations. A discussion of these initial tests has been given by Coons and Smalet (1967). These tests indicated an accuracy of ±0.3 milligal was attainable with this instrument.

Accuracies achievable by shipboard gravimeters are heavily dependent upon two factors, sea state and navigational accuracy. To obtain accuracies such as reported above requires relatively calm seas and an accurate electronic surveying system such as Lorac, Decca, or Raydist. Moreover the data reduction procedures used to remove effects of horizontal and vertical accelerations and of the velocity of the ship relative to the earth are extremely critical. The best methods of accomplishing this are still being discussed (Coons and Smalet, 1967; LaFehr and Nettleton, 1967b).

Airborne gravimeters. A final subject to be considered is the use of gravity instruments on aircraft. Experimental measurements of gravity on fixed-wing aircraft have been carried out since about 1960. An early test supported by the U.S. Army Map Service and using a LaCoste-Romberg shipboard gimbal-mounted gravimeter showed that, with sufficiently accurate navigation, accuracies of about ±5 mgl were achievable for averages over several minutes of flight time (Coons, *et al.*, 1962). Despite considerable subsequent effort at the Air Force Cambridge Research Laboratory, no significant improvements in accuracy have been achieved over the past 5 years. Thus, fixed-wing aircraft measurements offer little promise for the mining or groundwater industries in the foreseeable future.

Because of their ability to hover and move at slow speeds, the use of helicopters as platforms for gravity measurements is of greater promise. In 1965 the U.S. Naval Oceanographic Office began tests on gravimeters mounted in helicopters (Gumert, 1966). The U.S. Army Map Service has continued testing using a LaCoste-Romberg stable platform meter and has achieved accuracies of about .5 milligal while the helicopter was hovering. The results with the helicopter underway were much less satisfactory, with the accuracies of measurements being around ±5 mgl. The use of the helicopter, at least in the hover mode, seems to represent a possible useful technique in the near future for mining and groundwater applications.

Data handling

The state-of-the-art in data handling is the state-of-the-art in computerization. Computerization has affected data handling in a number of ways.

For routine data reduction the advantage of the computer is one of accuracy coupled with the ability to freely modify the Bouguer factor in anomaly computation. Once the data have been computerized, permanent files can be kept on tape or disk for later processing. The files can be augmented as new data are obtained. A discussion of this type of application in the mining industry may be found in Morris and Sultzbach (1966).

Present computer methods allow considerably more sophistication to be used in terrain corrections if it is desired. Normal terrain corrections are handled quickly and efficiently by the computer (Kane, 1962; Bott, 1959). The computer can also account for *a priori* knowledge of density of terrain or carry out various mathematical and statistical checks to detect possible variations in density of the terrain (Grant, 1965). The major

limitation to computerized terrain corrections remains the fact that the topographic information must still be digitized by hand to provide computer input.

Automatic digitalization of topographic data is still in the experimental stage. Spectra Physics and Aero Service have jointly developed an airborne laser profiler which, when coupled with stereo photography, may allow rapid digitalization of topography. However, such a procedure is not technically or economically feasible at the present time.

Perhaps the greatest advantage of computers in data handling lies in the ability to carry out rapid and accurate plotting and contouring of data. This can be done in two ways, either by using an analog plotter controlled by computer output or by using the printer as a plotter and contourer. For a final output the analog plotter is generally favored. However, for many purposes such as intermediate analyses, printer plotting and contouring is preferable because of the speed with which it can be accomplished. For example, a modern digital computer can provide a plot of Bouguer anomaly, station number, etc., for 1000 randomly located stations in less than one minute, using the high-speed printer. These maps can be plotted on any scale of map projection desired. Such a capability encourages the analyst to look at many different possibilities.

For shipboard (and helicopter) gravimetric measurements, computers provide the means to combine the information from the sensing element with information from the stable platform and ship locational information and carry out the digital filtering necessary during data reduction rapidly and efficiently (Coons and Smalet, 1967). With shipboard gravimeters, an efficient computerized reduction program is essential to successful operations.

Data analysis

The literature on gravity data analysis is exceedingly voluminous. However, the papers can conveniently be placed in a rather small number of categories. These categories are: (1) papers describing methods of enhancing the detection of the gravity effects of interest, (2) papers describing methods of constructing density models which will account for observed gravity effects, and (3) papers concerning methods of estimating the total mass causing a given anomaly. With borehole gravimeters, an additional aim may be porosity estimates for groundwater studies.

One of the oldest problems in gravity analysis is to extract from the observations that part of the gravity field caused by the density distributions of interest. Because one is normally interested in low-amplitude anomalies of limited horizontal extent the problem is often described as regional-residual separation. In any case, all procedures assume a difference in wavelength between the anomalous effect of interest and those not of interest. The techniques in use today consist of second-derivative and ring residual methods, wavelength filter methods, and least squares function fitting methods.

The second-derivative and ring residual methods have been in use the longest as a means for regional-residual separation. Their advantages and disadvantages have been discussed by many authors, Rosenbach (1953), Nettleton (1954), and Roy (1961), to name a few. The primary problems have arisen from the tendency of these procedures to magnify errors and for the need to interpolate to obtain the evenly spaced data grid required for their application. Recently, through the work of Swartz (1954), Dean (1958), and Meskó (1966), among others, the derivative and ring residual procedures have come to be understood as representing numerical filters. With this understanding there have been developments of wavelength filters which are designed to pass certain wavelengths (Dean, 1958; Fraser, *et al.*, 1966; Zurflueh, 1967). These have overcome many of the problems attendant with the older ring filters and represent a promising means of data analysis.

A second means of regional-residual separation consists of using functions, giving the value of gravity in terms of x, y position, whose constants have been determined by least squares fitting to the available data. Residuals may be obtained using this procedure either in the form of differences between functions of differing complexity which have been fitted to the data or in the form of differences between a fitted function and the observed data. Since the advent of computers which have made possible the solution of the large number of linear equations involved, least squares function fitting has been increasingly used, not only in gravity analysis, but in other forms of geophysical data analysis and in geological data analyses where it is usually referred to as trend surface analysis.

The most commonly used fitting functions are power series in x and y. These originated with fitting of a simple plane and have advanced to the point where functions containing powers of x and y in excess of ten are used (Coons, *et al.*, 1964). As a practical matter this method has proven exceedingly useful for exploration applications and has allowed anomalies of the order of 0.1 mgl or less in amplitude to be recovered from the background noise. These methods also have disadvantages, however. In general only the central two thirds of an area being analyzed can be used, and if a large area is to be analyzed in parts very large overlaps are necessary. This is readily understandable if one considers a power series polynomial to be the sum of several Chebyshev polynomials. These polynomials have a variable wavelength characteristic across the area being analyzed, with the wavelengths becoming increasingly shorter away from the center of an area.

For this reason the use of trigonometric series might well be desirable. Thus far, attempts along this line have considered using a Fourier series (Odegard and Berg, 1965). More sophisticated types of trigonometric function sets are needed.

Allison and Coons (1966) have demonstrated that the filtering procedure and the power series fitting procedures often give strikingly similar results.

A second type of analysis consists of the construction of density models which will explain the observed gravity field. Computerized methods of computing the gravity effect of two-dimensional (Talwani, *et al.*, 1959) and three-dimensional (Talwani and Ewing, 1960) density models exist. There is no limit to the complexity of the density models which may be chosen provided one is willing to pay the cost in computer time. Usually the lack of sufficient supplementary data to remove the basic indeterminacy of the gravity problem makes rather simple models adequate to extract all the information content of the data.

If some density information and information on the geometry of formation contacts exists, the problem may be made determinant and an iterative solution used to solve for the remaining

unknown density-geometry information (Danés, 1960; Healy and Press, 1964; Corbato, 1965). As commonly used the method consists of defining all parameters except one density interface and solving for it.

Although the geometry of the bodies of anomalous mass causing any given gravity effect are in general indeterminate the total anomalous mass is not.

The determination of total anomalous mass is of special importance in mining and, because one is dealing with bodies of relatively small dimensions, is simpler than in other types of applications. The method depends upon the application of Green's theorem and has been most recently discussed by LaFehr and Nettleton (1967 a and b). The accuracy of the method depends upon the accuracy with which the gravity effect of the body under study can be separated from the remainder of the gravity field.

Acknowledgment

The author would like to express his thanks to Mr. R.M. Iverson for providing much of the information used in preparing the section on instrumentation.

References

Allison, W.E., and R.L. Coons, 1966. Computers in gravity interpretation. Preprint, Annual Meeting, Society of Exploration Geophysicists; Houston, Texas.

Beyer, L.A., R.E. VonHuene, T.H. McCulloh, and J.R. Lovett, 1966. Measuring gravity on the sea floor in deep water. *J. Geophys. Res.* 71 (8): 2091-2100.

Bott, M.H.P., 1959. The use of electronic digital computers for the evaluation of gravimetric terrain corrections. *Geophys. Prospecting.* 8: 45-54.

Bower, D.R., 1966. The determination of cross-coupling errors in the measurement of gravity at sea. *J. Geophys. Res.* 71: 487-493.

Coons, R.L., J.W. Mack, and W. Strange, 1964. Least-square polynomial fitting of gravity data and case histories. In *Computers in the Mineral Industries.* G.A. Parks, Ed., Stanford University Press, 498-519.

Coons, R., W. Strange, and G.P. Woollard, 1962. Evaluation and study of airborne gravimeter operational test. Reference 62-2, Geophysics and Polar Research Center, Dept. of Geology, University of Wisconsin, Madison, Wisconsin.

Coons, R.L., and M. Smalet, 1967. Surface ship gravity in oil exploration. Preprint, XXXVIIth Annual International Meeting, Society of Exploration Geophysicists; Tulsa, Oklahoma.

Corbato, C.E., 1965. A least-squares procedure for gravity interpretation. *Geophysics.* 30 (2): 228-233.

Danés, Z.F., 1960. On a successive approximation method for interpreting gravity anomalies. *Geophysics.* 25: 1215-1228.

Deans, W.C., 1958. Frequency analysis for gravity and magnetic interpretation. *Geophysics.* 23 (1): 97-127.

Fraser, D.C., B.D. Fuller, and S.H. Ward, 1966. Some numerical techniques for application in mining exploration. *Geophysics.* 31 (6): 1066-1077.

Frowe, E.W., 1946. A diving bell for underwater gravimeter operation. *Geophysics.* 12 (1): 1-12.

Gumert, W.R., 1966. Helicopter gravity surveying system. Preprint, XXXVIth Annual International Meeting, Society of Exploration Geophysicists; Houston, Texas.

Hamilton, A.C., and B.G. Brulé, 1967. Vibration-induced drift in LaCoste and Romberg geodetic gravimeters. *J. Geophys. Res.* 72: 2187-2197.

Hayes, D.E., J.L. Worzel, and H. Karnick, 1962. Tests on the 1962 model of the Anschutz Gyrotable. *J. Geophys. Res.* 69: 749-757.

Healy, J.H., and F. Press, 1964. Geophysical studies of basin structures along the eastern front of the Sierra Nevada, California. *Geophysics.* 29: 337-359.

Henderson, G., 1967. A gravimeter for marine, airborne and lunar surface measurements. Preprint, XIVth General Assembly, International Union of Geodesy and Geophysics; Lucerne, Switzerland.

Henderson, G., and R. Iverson, 1967. An earth-referenced lunar gravimeter. Preprint, 1967 International Symposium, American Astronautical Society; Huntsville, Alabama.

Howell, L.G., K.O. Heintz, and A. Barry, 1965. The development and use of a high-precision downhole gravity meter. Paper presented, XXXVth Annual International Meeting, Society of Exploration Geophysicists; Dallas, Texas.

Kane, M.F., 1962. A comprehensive system of terrain corrections using a digital computer. *Geophysics.* 27: 455-462.

LaCoste, L.J.B., 1967. Measurement of gravity at sea and in the air. *Reviews of Geophysics.* 5 (4): 477-526.

LaCoste, L., N. Clarkson, and G. Hamilton, 1967. LaCoste and Romberg stabilized platform shipboard gravity meter. *Geophysics.* 32 (1): 99-109.

LaFehr, T.R., and L.L. Nettleton, 1967a. Quantitative evaluation of a stabilized platform shipboard gravity meter. *Geophysics.* 32 (1): 110-119.

LaFehr, T.R., and L.L. Nettleton, 1967b. Data reduction, signal analysis, and accuracy of shipboard gravity meter operations. XXXVIIth Annual International Meeting, Society of Exploration Geophysicists; Tulsa, Oklahoma.

McCulloh, T.H., L.J.B. LaCoste, J.E. Schoellhamer, and E.H. Pampeyan, 1967. The U.S. Geological Survey-LaCoste and Romberg precise borehole gravimeter system-instrumentation and support equipment. USGS Professional Paper 575-D, p. D92-D100.

Meskó, A., 1965. Frequency analysis for gravity interpretation. *Geophys. Prospecting.* 13 (3): 475-488.

Meskó, C.A., 1966. Two-dimensional filtering and the second derivative method. *Geophysics.* 31 (3): 606-617.

Morris, D.B., and R.A. Sultzbach, 1966. Gravity data reduction and interpretation using a digital computer; a case history. Preprint, 1966 Symposium and Short Course on Computers and Operations Research in Mineral Industries, Pennsylvania State University.

Nettleton, L.L., 1954. Regionals, residuals, and structure. *Geophysics.* 19 (1): 1-22.

Odegard, M.E., and J.W. Berg, 1965. Gravity interpretation using the Fourier integral. *Geophysics.* 30 (3): 424-438.

Rosenbach, Otto, 1953. A contribution to the calculation of the 'Second derivative' from gravity data. *Geophysics.* 18 (4): 894-912.

Roy, A., 1961. On some properties of residuals and derivatives. *J. Geophys. Res.* 66: 543-548.

Schulze, R.E., E. Brede, and E. Thebis, 1964. German Patent 1 165 290.

Swartz, C.A., 1954. Some geometrical properties of residual maps. *Geophysics.* 19 (1): 46-70.

Talwani, M., and M. Ewing, 1960. Rapid computation of gravitational attraction of three-dimensional bodies of arbitrary shape. *Geophysics.* 25: 203-225.

Talwani, M., J.L. Worzel, and M. Landisman, 1959. Rapid gravity computations for two-dimensional bodies with application to the Mendocino submarine fracture zone. *J. Geophys. Res.* 64: 49-59.

Thyssen-Bornemisza, S., 1965. Reconnaissance survey using average horizontal gradients of gravity. *Geophysics.* 30 (4): 661-664.

Wall, R.E., M. Talwani, and J.L. Worzel, 1966. Cross-coupling and off-leveling errors in gravity measurements at sea. *J. Geophys. Res.* 71: 465-485.

Zurflueh, E.G., 1967. Applications of two-dimensional linear wavelength filtering. *Geophysics.* 32 (6): 1015-1035.

Application of resistivity methods in mineral and groundwater exploration programs

George V. Keller

Colorado School of Mines
Golden, Colorado

Abstract. The 'direct-current' resistivity methods have been used for about a half century and have reached a certain degree of maturity. In many respects, particularly in design of field equipment and approach to interpretation of field data, little has changed in the past twenty to thirty years. In other respects, including the design of field programs and the evaluation of resistivity measurements in geologically meaningful terms, rapid advances are currently being made. During the past decade, the electrode arrays used in field surveys have changed, and now, one may select an array which is best suited for a specific problem. For example, the Schlumberger array provides the greatest depth of penetration for a given amount of work, while the dipole array provides the greatest safety in working in areas where there is a great deal of culture.

Studies of the relationship between resistivity and other rock characteristics, such as porosity, texture, salinity of groundwater and content of ore minerals, have provided a basis for evaluating resistivities once they are measured, as well as a basis for predicting the probable success of resistivity surveys for specific exploration problems.

Résumé. Les méthodes de résistivité à 'courant continu' sont utilisées depuis environ un demi-siècle et elles ont atteint un certain degré d'efficacité. Dans plusieurs domaines et surtout dans la conception de l'équipement et l'interprétation des données recueillies, peu de changements ont été apportés au cours des 20 ou 30 dernières années. Dans d'autres domaines, y compris l'élaboration des programmes de travaux sur le terrain et l'évaluation des mesures de résistivité du point de vue géologique, les progrès sont très rapides. Au cours des dix dernières années, l'arrangement des électrodes utilisé dans des travaux sur le terrain a été modifié et l'on peut maintenant choisir une disposition qui convient le mieux à un problème particulier. Ainsi, la disposition Schlumberger permet le maximum de pénétration pour une somme de travail déterminée, tandis que la disposition en dipôle offre la meilleure sûreté dans les régions fortement marquées par la main de l'homme.

Les études de la relation qui existe entre la résistivité et les autres caractéristiques de la roche, comme la porosité, la texture, la salinité des eaux souterraines et la teneur en minerais ont fourni une base d'évaluation des résistivités après qu'elles ont été mesurées de même qu'un fondement à la prédiction du succès des relevés par résistivité appliqués à des problèmes précis d'exploration.

Direct-current methods for measuring earth resistivity have been in use continuously for the past half century, with early development stemming from the work of investigators in different parts of the world, primarily Wenner (1915), Schlumberger (1920) and Rogozin (1903). Over the years, the basic approach to earth resistivity surveys has changed surprisingly little, though there have been advances in instrumentation which have allowed progressively deeper and deeper investigations.

The resistivity of the earth can be measured as readily using alternating electric fields as static fields, but geophysical practice has led to the use of the term 'resistivity survey' in the restrictive sense to methods in which direct-current theory can be applied. In direct-current surveys, the current supplied to the ground has a sufficiently low-frequency spectrum that the theory for current flow can be developed on the basis of direct-current behavior. This leads to mathematical analyses involving the solution of LaPlace's equation with appropriate boundary conditions, whereas the use of higher frequency or AC fields leads to the solution of Maxwell's equations or a wave equation, a mathematical procedure which may be considerably more difficult.

Interpretation has changed little over the past thirty years, being based largely on the comparison of field measurements with curves computed theoretically for various models. Computation of such reference curves was a very tedious process until high-speed computers became available. Today, there is an abundance of such reference curves, as given in recent publications by Orellano and Mooney (1966), Al'pin, *et al.* (1966), van Dam (1967) and others. The use of curve comparison techniques limits the resolution which may be obtained in interpretation, the limit being related to the scales with which data may be plotted for comparison. This limitation has been at least as restrictive in the development of accurate interpretation of electrical surveys as has been the limit imposed by imprecision in field surveys. Over the years, it has been suggested in the literature that it should be possible to interpret resistivity surveys more directly, but no great success with such direct methods of interpretation has yet been described.

Notable progress is being made in evaluating resistivities in terms of other, more interesting rock properties in recent years. If it can be assumed that field surveys can be converted into meaningful values for rock resistivity, the problem remains of explaining the significance of these values, inasmuch as the rock resistivity is rarely the ultimate object in an electrical survey. More commonly, one conducts an electrical survey to determine if sulfide minerals are present in a rock, and if so, to what extent, or to find the amount and salinity of groundwater. Only with the increased confidence in our ability to interpret field measurements which has been built up over the years has this problem of evaluating resistivities become important.

Another topic which has become important in recent years is the proper selection of an electrode array for making resistivity surveys. For many years, resistivity surveys were done with the Wenner array in the English-speaking world or with the Schlumberger array in other parts of the world. Other arrays were used experimentally or for special applications, but it has been within the past decade that other electrode arrays have substantially displayed the older, conventional arrays in routine work. These newer arrays are generally of the dipole-dipole type (Cantwell, *et al.*, 1964) or of the pure dipole type (Al'pin, *et al.*, 1966), and there is a great diversity in the electrode arrangements which can be used. Therefore, the relative characteristics of the various arrays, such as power required, signal-to-noise ratio

Contents

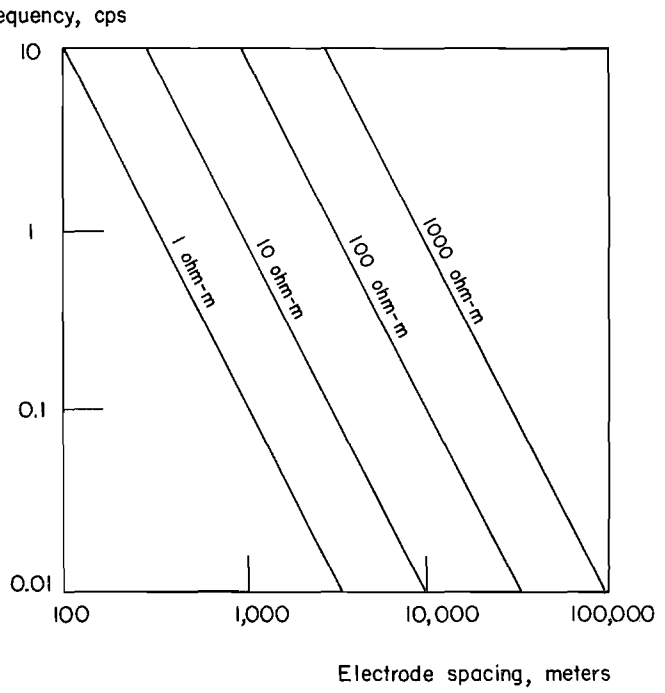


Figure 1. Maximum frequencies which may be used in 'direct-current' resistivity sounding, as a function of resistivity and array spacing.

provided, and depth of investigation or sensitivity to lateral contrasts in resistivity, should be quite important in deciding which array is most appropriate for a given exploration problem.

In this review, I will cover a few aspects of recent developments in instrumentation, the properties of electrode arrays and the evaluation of resistivities once they have been determined from a survey. For a more comprehensive review of the present state of the art in resistivity surveying, particularly with respect to interpretation, I will refer you to several excellent books which have been published quite recently, and which cover the material much more thoroughly than is possible in a review paper. These include a very complete review of resistivity methods by Van Nostrand and Cook (1966), a treatment of vertical soundings with the Schlumberger method (Kunetz, 1966) and a discussion of dipole methods by Al'pin, *et al.* (1966).

Instrumentation

In recent years, notable advances in instrumentation have included the development and application of solid-state power supplies, operational amplifiers and other solid-state circuitry. These have resulted in lower weight per unit power capability in source equipment and greater sensitivity in receiving equipment. The lower weight per power capability has been somewhat of an illusion, inasmuch as the use of dipole arrays, which require relatively high power for penetration, and the desire to penetrate to greater and greater depths have increased the requirement for power capacity faster than the unit weight of power supplies has been decreased. The primary result of increased sensitivity in receiving equipment through the use of operational amplifiers has been that now sensitivity is limited by electrical noise in the ground, originating either in industrial currents or natural earth currents, rather than being limited by the insensitivity of meters used in early field equipment. To some extent, the detrimental effect of electrical noise in the earth has been reduced by the use of synchronous detection systems, in which the transmitter current and the receiver polarity are switched periodically in synchronism. Noise which is asynchronous with the switching frequency is then averaged out, if averaging can be performed over a long enough time interval. However, it should be remembered that synchronous switching is not a new technique, but the essence of the Gish-Rooney (1925) system for differentiating resistivity signals from self-potential which has been in use for forty years.

Shallow resistivity surveys – to depths of a few hundred feet or less – have not required any real advances in instrumentation other than those which reduce the weight of equipment or make its use more convenient. Development of equipment has been associated largely with the desire to map resistivity at greater depths; for example, in mapping intermontane basins for groundwater reserves, penetrations of 1000 to 10,000 feet are commonly desired. It is obvious that greater penetration might be obtained in either of two ways: by increasing the current supplied to the ground so that detectable signals may be seen at greater electrode spacings, or by increasing the sensitivity of the receiving equipment, so that the smaller signals at larger spacings may be seen. The latter approach appears to be favored because of the inherent difficulties in providing enough power to the ground to compensate for the increase of spacings to miles, as is required in deep-penetration surveys. Currents ranging from tens to thousands of amperes are required to provide a signal which will override noise at spacings measured in miles. Providing such currents would require the use of 10 to 100 kilowatts of power, operating at voltages of 500 to 5000. The weight of such primary power supplies is very great, and the risk in using voltages in excess of 1000 is worrisome. Although the use of primary power as great as a megawatt in deep-penetration resistivity surveys has been described (Jackson, 1966), most development of deep-probing methods seems to be centered on the receiving equipment.

For penetrations of thousands of feet, frequencies less than 1 cps must be used to assure direct-current behavior, with lower frequencies being required for deeper penetration, or penetration in more conductive rocks. The maximum frequency which may be used in direct-current surveys is given graphically in Figure 1 as a function of the depth of investigation and the average resistivity of the rock being penetrated. In the frequency range required for deep surveys, the primary contribution to noise is from micropulsations in the earth's magnetic field (Bleil, 1964). The power density spectrum for such noise shows an almost linear inverse relation to frequency, with sharp peaks superimposed, as shown in Figure 2. Noise varies markedly with time, showing diurnal and longer period periodicities in amplitude. Micropulsation noise varies with latitude, being considerably stronger at auroral latitudes than at midlatitudes. Micropulsation noise also varies in amplitude with local resistivity, the amplitude being proportional to the square root of local resistivity, all other things being equal. All of these factors must be taken into consideration in designing sensitive receiving equipment to operate at frequencies lower than 1 cps.

A straightforward approach to discriminating between signal and noise at these low frequencies is the use of a graphic recorder,

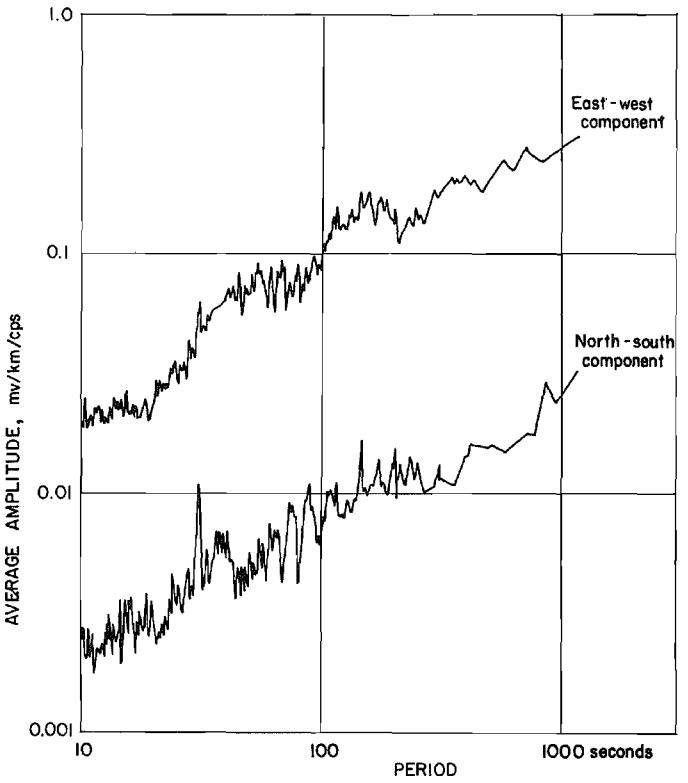


Figure 2. Typical spectra of low-frequency noise, averaged over an interval of 24 hours. Original data were recorded at China Lake, California.

The use of broadband recording is limited ultimately by the dynamic range of graphic recorders – the ratio of the largest signal which may be recorded onscale to the least signal which may be detected. The dynamic range of graphic recorders is about 46 db (the threshhold level of detection being about 1/200 the maximum onscale range) if the recorded signals must lie within one recorder span to as much as 66 db (2000:1) for recorders in which offscale deflections are automatically stepped back by one chart width. A requirement that signal levels be measured with an uncertainty of no more than 5 percent is equivalent to requiring that the minimum signal level must be at least 20 times as large as the threshhold level for detection on the recorder, so that 26 db of dynamic range is not available. Thus, with graphic recording, signal amplitudes may be lower by 20 to 40 db than the maximum noise amplitudes in a wideband recording system.

The dynamic range of a recording system may be increased by going to digital recording, rather than using graphic recording. Such a system has been in use at the Colorado School of Mines for deep resistivity soundings for several years. The voltage from the measuring electrodes is introduced to a linear voltage-controlled oscillator which has a frequency of 100 kcps for zero voltage input, and a rate of change of frequency with input voltage of 1 cps per microvolt. The output of the oscillator is fed to a counter with a precisely-controlled gate with a duration of 1 second. The number of oscillations in a second is counted and punched on paper tape. The gate resets, and counting starts for the next digital sample. The sampling rate is slightly less than one per second, so that the highest frequency which may be seen is somewhat less than 1/2 cps. The input voltage is averaged over the gate period of 1 second, providing antialiasing for higher frequency noise.

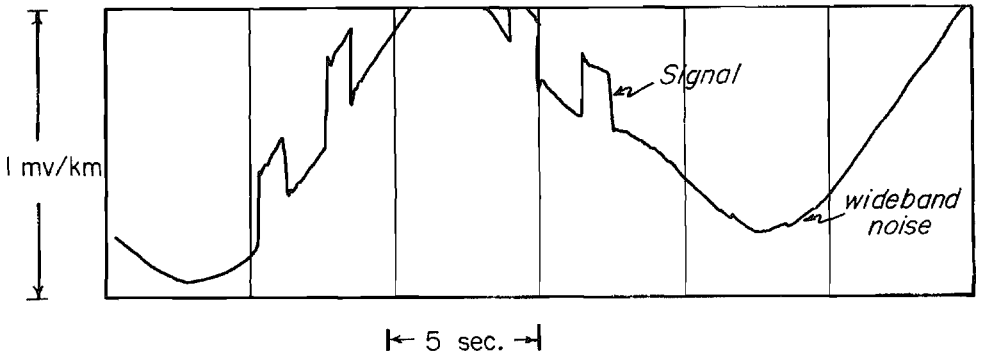


Figure 3. Typical graphical recording of electric field detected with measuring electrodes in deep soundings.

such as an oscillograph or a recording potentiometer, which records the voltage at the receiving electrodes 'wideband'; that is, all frequencies up to about 1 cps are recorded with no attempt at filtering the micropulsation noise in this frequency range. With such recordings, it is usually possible to identify and scale the amplitude of signals from transmitted current pulses even when the amplitude of the signal is only a few percent of the maximum noise level in the recorded frequency band. An example of such a wideband recording is shown in Figure 3.

With the simple technique of graphic wideband recording, the signal level which may be measured with reasonable accuracy is lower by a factor of about 1000 than that which can be detected with simple nongraphic means such as are used in shallow-penetration equipment.

Punching of five significant figures provides a dynamic range of 100 db, and with a requirement for a signal accuracy of 26 db, this means that signals with amplitudes 76 db below maximum noise amplitude should be measurable. Extraction of signals under such conditions is done by convolution filtering using a high-speed computer. Although the approach has been found to work as expected, there are several serious drawbacks to digital recording of electrical survey data which must be overcome before this approach is practical. One serious difficulty is that a signal so deeply buried in noise cannot be seen on a graphic recorder which may be used as a monitor. No quality control of measurements can be applied in the field: it is not known whether a usable signal has been recorded until after computer processing. Then, it may not be feasible to go back and repeat recordings.

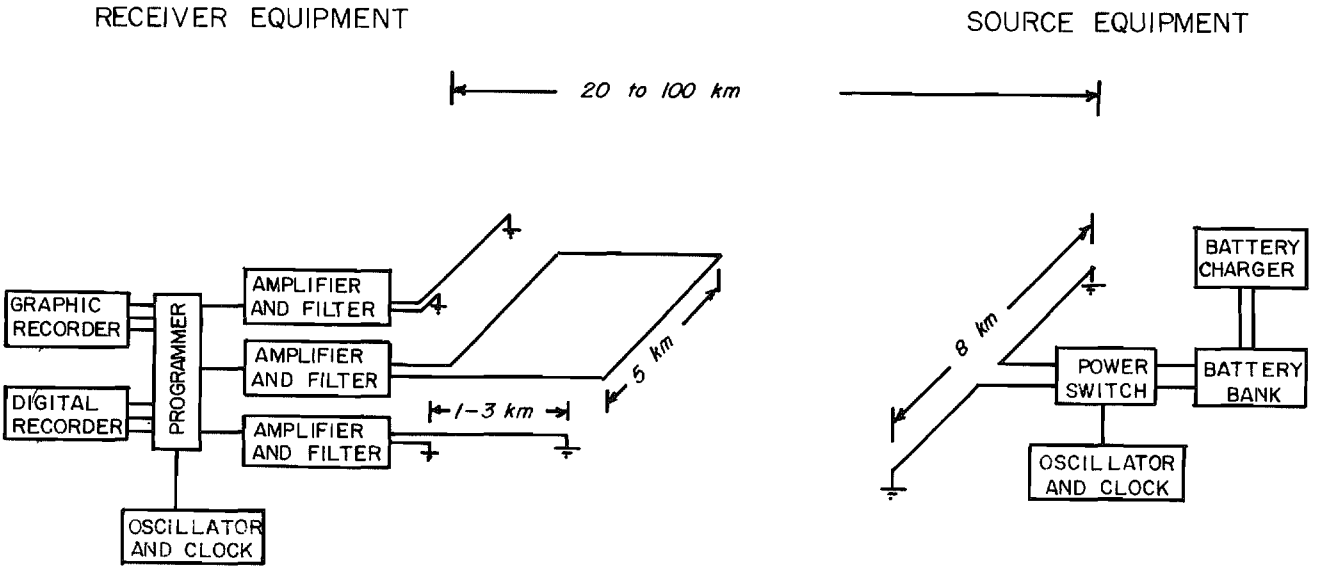


Figure 4. Block diagram of equipment being used at the Colorado School of Mines for deep resistivity surveys.

This difficulty may be reduced by doing sufficient processing in the field so that the quality of a signal may be assessed, with refinements in processing being done later. Synchronous detection provides one method of processing which is practical in the field. In synchronous detection, the polarity of the receiving electrodes is alternated at the same frequency as the source current. In terms of modern digital filter theory, this can be viewed as convolution of the received signal with a filter which has precisely the same spectrum as the transmitted signal. According to Burg (1964), if signal and noise are uncorrelated, as they are in resistivity surveying, the frequency response of an optimum filter is given by:

$$H = \frac{\Phi_s(\omega)}{\Phi_s(\omega) + \Phi_n(\omega)} \qquad 1$$

where $\Phi_s(\omega)$ is the power density spectrum for the signal and $\Phi_n(\omega)$ is the power density spectrum for the noise. If the signal power density is lower than the noise power density, and if the noise power density is a constant (so-called white noise), the optimum filter is merely a constant times the signal power density spectrum. Therefore, synchronous detection can be viewed as optimum filtering under these restrictions. The noise spectrum is not white (see Figure 2) but convolution filtering is commutative, so that additional filtering to render the noise spectrum white may be done prior to synchronous detection, as in the case of rejection of specific noise frequencies such as 60 cps, or after the fact, with a filter being designed on the basis of noise as recorded.

A variety of equipment for synchronous detection is available. The system now being field tested at the Colorado School of Mines is based on the Nuclear-Chicago data retrieval computer, model 7100. Power is supplied to the ground with a silicon controlled-rectifier system which converts power from a 20-kw, 220V 60 cps source to direct-current pulses of up to 60 amperes. The on-off cycles of current are triggered from signals generated by a precision oscillator, operating at 1 mcps with an accuracy of 1 part in 10^8 per week, but counted down so that pulse repetition rates of a tenth or hundredth of a cycle per second may be used. At the receiving end, the voltage is amplified and whitened by appropriate filtering, and then sampled at intervals triggered by an oscillator identical to the one at the transmitter. The voltage is sampled for a duration of 39 microseconds, with 400 time-spaced samples being stored in memory. On successive cycles of operation, the new samples are added to the old. A block diagram of the equipment is shown in Figure 4.

Comparison of arrays used in measuring resistivity

A great many techniques have been used in measuring earth resistivity, variations being primarily in the way the various electrodes are placed relative to one another. High power, and accordingly, heavy equipment, is required in making deep penetration resistivity surveys, so both efficiency and safety are factors to be considered more seriously than in the case of normal shallow penetration surveys. A factor in planning deep penetration surveys is consideration of the advantages and disadvantages of the various electrode arrays.

Let us consider three basic arrays: the Wenner, the Schlumberger, and the polar dipole arrays (see Figure 5). In the Wenner array, four equally-spaced colinear electrodes are used, with the outer two normally being current electrodes and the inner two, measuring points. The array spacing is expanded about the array midpoint in making an electrical sounding, but all four electrodes are spaced at equal distances at all times.

In the Schlumberger array, four colinear electrodes are used also, with the outer two being current electrodes and the inner two, measuring points. The inner two are located at the center of the array, and their separation is small compared to the total array length, usually less than one fifth of the total length. With this short separation between measuring points, the measured voltage divided by the separation is approximately equal to the voltage gradient at the midpoint of the array. In making a depth sounding, the separation between the outer two electrodes is increased in steps. The spacing between the inner two electrodes

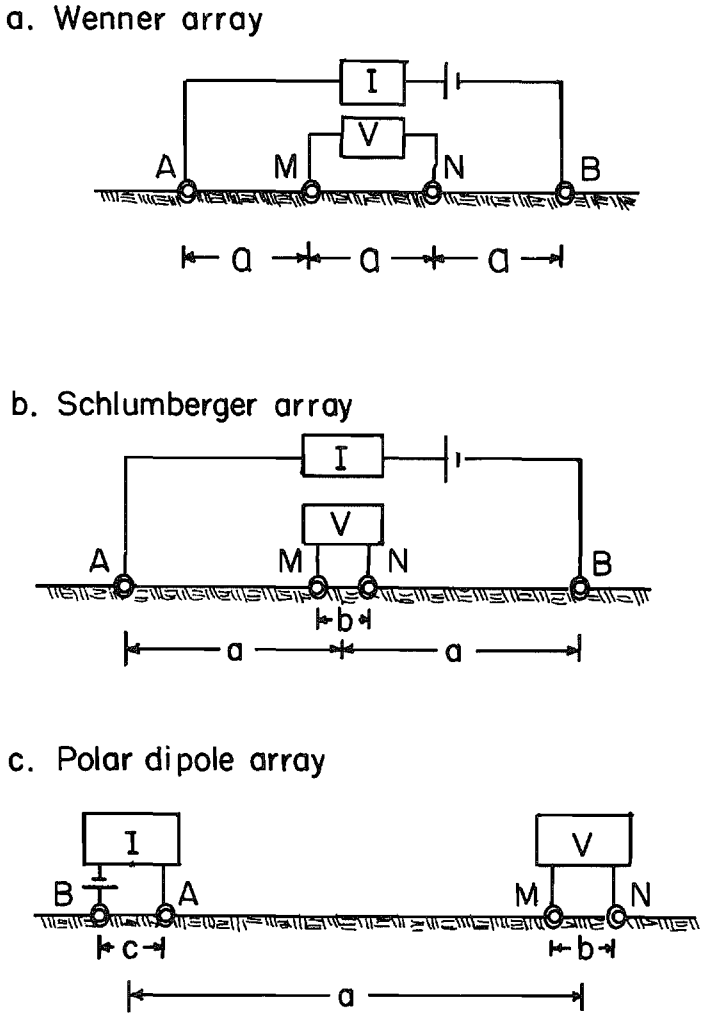


Figure 5. Electrode arrays commonly used in measuring resistivity.

is not changed so long as the voltage level is high enough to record.

With a dipole array, four electrodes are used, but these do not necessarily occupy positions along a common line. With a dipole array, the distance between the center of the current pair and the center of the measuring pair is large compared with the spacing within either pair. The orientations of the current and measuring pairs (or dipoles) relative to the line between their centers are arbitrary. Of the various orientations of dipole pairs which might be used, we will restrict our attention to the 'polar' dipole arrangement for brevity. In the polar array (Figure 5c), the dipoles are placed along a common line, and in sounding, the measuring dipole is moved away from the current dipole along the polar axis of the current dipole.

In comparing various arrays, comparable conditions must be established for each. If high-sensitivity recording equipment is used so that the apparent noise level at the input contributed by the recording equipment is a microvolt or less with the filtering used, the lowest signal level which can be detected will be limited by the level of telluric noise between the measuring electrodes, rather than by the insensitivity of the recording equipment. The telluric noise level varies widely with time, location and local resistivity, but these factors will be common for all electrode arrays. The telluric field developed in the earth will contribute a voltage at the measuring electrodes which is proportional to their separation. This noise voltage is

$$V_n = \overline{MN}\, E_T \qquad 2$$

where E_T is the telluric electric field, in volts per meter, and $\overline{MN}$ is the spacing between measuring electrodes.

The voltage we wish to compare with these noise voltages is the signal voltage between the measuring electrodes generated by the current supplied to the ground. For the Wenner array, the measured signal is

$$V_{s,W} = \frac{I\rho}{2\pi a_W} \qquad 3$$

where I is the current supplied to the ground, ρ is the resistivity of the ground and a_W is the spacing between any two adjacent electrodes. For the Schlumberger array, the measured signal is

$$V_{s,S} = \frac{bI\rho}{\pi a_S^2} \qquad 4$$

where b is the spacing between measuring electrodes and a_S is half the distance between current electrodes (the standard measure of spacing for the Schlumberger array). For the polar dipole array, the measured signal is

$$V_{s,P} = \frac{bcI\rho}{\pi a_P^3} \qquad 5$$

The amount of current supplied to the ground I is limited by two factors: (1) the maximum weight of cable W_c and the weight of the power source W_p which one wishes to transport; and (2) the maximum safe voltage V_B at which one chooses to operate. The weight W_c is proportional to the cable length and cross section:

$$W_c = \sigma_c L A \qquad 6$$

where L is the length, A is the cross section and σ_c is the density of the material from which the cable is fabricated. On the other hand, the cable resistance is inversely proportional to the cross section:

$$R_c = \rho_c L/A \qquad 7$$

where ρ_c is the resistivity of the cable material. The current which can be supplied to the ground is determined by the combined resistance of the power source, the cable and the ground:

$$I = \frac{V_B}{R_c + R_i + R_g} \qquad 8$$

where R_i is the internal resistance of the power source and R_g is the contact resistance of the current electrodes.

Let us now compare the maximum spacing which can be obtained with given equipment parameters for each of the three

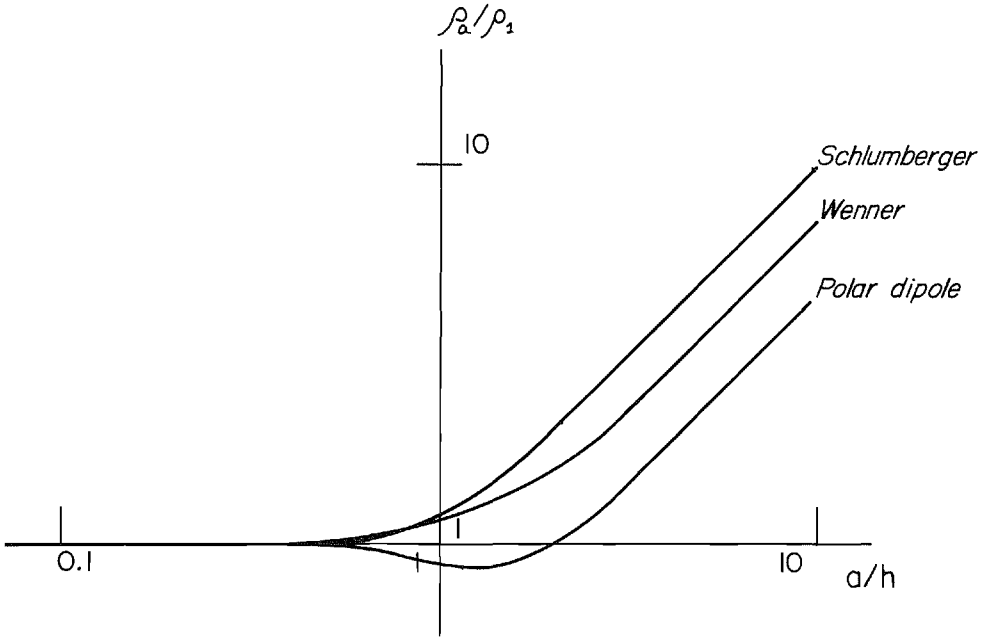


Figure 6. Apparent resistivity ρ_a measured with various arrays for the case of a layer with resistivity ρ_1 and thickness h resting on an insulating substratum.

arrays, with the maximum spacing being defined as the spacing at which the signal voltage will be equal to the noise voltage given in Equation 2. Solving Equations 3, 4 and 5 for this maximum spacing, we get:

for the Wenner array,

$$a_{W,max} = \left[\frac{V_B \rho^{1/2}}{2\pi k_T (R_c + R_i + R_g)}\right]^{1/2} \qquad 9$$

where the telluric electric field E_T has been taken proportional to the square root of resistivity, $E_T = k_T \rho^{1/2}$;

for the Schlumberger array,

$$a_{S,max} = \left[\frac{V_B \rho^{1/2}}{\pi k_T (R_c + R_i + R_g)}\right]^{1/2} \qquad 10$$

and for the polar dipole array,

$$a_{P,max} = \left[\frac{V_B c \rho^{1/2}}{\pi k_T (R_c + R_i + R_g)}\right]^{1/3} \qquad 11$$

In comparing arrays, we might compare the maximum spacings that can be used with each for given equipment limitations, but it is more reasonable to compare effective probing depths – the depths at which a boundary may be detected with a given array spacing. Effective probing depth is difficult to define in a general way, but one useful approach is to consider a simple model of a uniform layer underlain by an insulating basement (Keller, 1966). Consider the apparent resistivity which is observed with a Schlumberger array under such circumstances. For array spacings considerably less than the thickness of the layer, the observed resistivity is nearly equal to the actual resistivity of the layer, while for spacings larger than several times the layer thickness, the observed resistivity is directly proportional to the array spacing. This proportionality may be derived by considering a point source of current at the surface of the layer. Inasmuch as no current can leave the layer through either the upper or lower surfaces, the current must spread outward uniformly. The total current supplied at the source can be used in calculating the current density at distances from the source which are large compared to the thickness of the layer:

$$j = \frac{I}{2\pi r h} \qquad 12$$

where j is the current density, r is the distance from the current source where the current density is being observed and h is the thickness of the layer. The electric field intensity may be determined by applying Ohm's law:

$$E = \frac{I}{2\pi r S} \qquad 13$$

where S is the conductance of the layer h/ρ, ρ being the resistivity.

The apparent resistivity measured with the Schlumberger array is defined in terms of electric field intensity. With two current electrodes as are used in the conventional Schlumberger array, the apparent resistivity will be

$$\rho_S = \pi r^2 \frac{E}{I} = \frac{r}{S} \qquad 14$$

The observed resistivity ρ_S is proportional to spacing, the constant of proportionality being $1/S$. The complete apparent resistivity curve as a function of spacing is shown graphically in Figure 6.

We may define the effective probing depth for the Schlumberger array as d_S, half the current-electrode separation at which the horizontal asymptote for resistivities measured with small spacings intersects a line representing the linear relation

given in Equation 14. The existence of the insulating basement is little apparent for measurements made with spacings smaller than the layer thickness h, while the presence of the insulating basement exerts a pronounced effect on measurements made with larger spacings.

The effective probing depths for other arrays may be defined similarly. The resistivity vs. spacing curves for a buried insulator are shown on Figure 6 for the Wenner and polar dipole arrays as well as for the Schlumberger array. With the Wenner array, the equation for the linearly rising segment of the curve is

$$\rho_W = \frac{2\ ln\ 2}{S} a_W \qquad 15$$

and the effective probing depth d_W is therefore $(2\ ln 2)a_W$. With the polar dipole array, the equation for the linearly rising segment is

$$\rho_P = \frac{1}{2S} a_D \qquad 16$$

and the effective probing depth is $a_D/2$.

These definitions may now be used with Equations 9, 10 and 11 to determine the maximum depth of penetration which may be obtained with these three electrode arrays with a given set of parameters for the equipment. For the Wenner array

$$d_{W,max} = \left[\frac{V_B \rho}{2\pi k_T (R_c + R_i + R_g)}\right]^{1/2} 2\ ln\ 2 \qquad 17$$

For the Schlumberger, the maximum depth of penetration is the same as the maximum spacing given in Equation 10, while for the polar dipole array, the maximum depth of penetration is half the value for maximum spacing given by Equation 11.

The Wenner and Schlumberger arrays apparently require very nearly the same current electrode spacing to see a layer at a given depth, so it may be assumed that the equipment parameters V_B, R_c and R_i are essentially the same for the two methods, and if the same field technique is used with each, the grounding resistance should be the same. The ratio of the maximum depths of penetration obtainable with each is then simply

$$\frac{d_{S,max}}{d_{W,max}} = \frac{2^{1/2}}{2\ ln\ 2} = 1.02 \qquad 18$$

The reach of the Schlumberger system is about 2 percent greater than that of the Wenner system, when both are used under comparable conditions.

Comparison of the Schlumberger and polar dipole arrays is somewhat more difficult because the equipment parameters need not be the same in the two cases. The ratio of maximum attainable depths is

$$\frac{d_{S,max}}{d_{P,max}} = 2\left[\frac{\rho^{1/2}}{\pi k_T} \cdot \frac{V_{B,S}^3}{V_{B,P}^2} \cdot \frac{1}{c^2} \cdot \frac{(R_c + R_i + R_g)_{P2}}{(R_c + R_i + R_g)_{S2}}\right]^{1/6} \qquad 19$$

where the subscripts P and S are used to indicate equipment parameters for the polar dipole and Schlumberger systems, respectively. With the dipole system, in view of the shorter spacing between current electrodes, higher operating voltages may be used, the cable resistance R_c lowered, and other changes made. Evaluation of Equation 19 for the case in which the same operating voltage is used and the cable resistance is decreased in proportion to the square of the length, as would be the case if a cable with the same weight were used with the two methods, provides the result that the dipole method can reach only about one-third as deep as the Schlumberger method. However, in view of the large number of parameters contained in Equation 19, it should be evaluated for specific operating conditions to determine what penalty, if any, in penetration is paid in using the dipole method. The primary advantage of the dipole method, of course, is the logistic simplicity in that great lengths of cable do not need to be laid out to obtain deep penetration, as is the case with the Wenner and Schlumberger arrays.

Another factor to be considered in comparing arrays is the relative sensitivity to resistivity contrasts in different locations with respect to the electrode array. For example, the dipole arrays are considerably more sensitive to lateral changes in resistivity than is the Schlumberger or Wenner array. Unfortunately, this aspect of array comparison has not yet been treated comprehensively.

Resistivity of water-bearing rocks. Evaluation or resistivities in terms of rock properties should be distinguished from the more usual discussion of interpretation of resistivity surveys, which consists mostly of trying to guess what the rock resistivity is, having made a set of measurements of voltage, current and electrode separation, such as comprise an electrical resistivity survey. Water, sometimes carrying a large amount of salt in solution, is the rock component which is most important in determining bulk resistivity, for rocks which occur within the first few miles of the earth's surface; only rarely do conductive minerals such as sulfides occur in sufficient abundance to determine the resistivity of a rock.

Depositional environment controls the properties of groundwater to some extent; marine sedimentary rocks generally have a higher concentration of salt in solution than do continental

Table I. Average resistivities of groundwater (from Chebotarev, 1955).

Rocks From Which Water Samples Were Taken	Number of Samples	Resistivity at 20° C, ohm-m	
		Median	Range
Igneous rocks, Europe	314	7.6	3 – 40
Igneous rocks, South Africa	175	11.0	0.5 – 80
Metamorphic rocks, South Africa	88	7.6	0.8 – 80
Metamorphic rocks, Precambrian of Australia	31	3.6	1.5 – 8.6
Pleistocene to recent continental sediments, Europe	610	3.9	1 – 27
Pleistocene to recent sediments, Australia	323	3.2	0.4 – 80
Tertiary sedimentary rock, Europe	993	1.4	0.7 – 3.5
Tertiary sedimentary rock, Australia	240	3.2	1.35 – 10
Mesozoic sedimentary rock, Europe	105	2.5	0.31 – 47
Paleozoic sedimentary rock, Europe	161	0.93	0.29 – 7.1
Chloride waters from oil fields	967	0.16	0.049 – 0.95
Sulfate waters from oil fields	256	1.2	0.43 – 5.0
Bicarbonate waters from oil fields	630	0.98	0.24 – 10

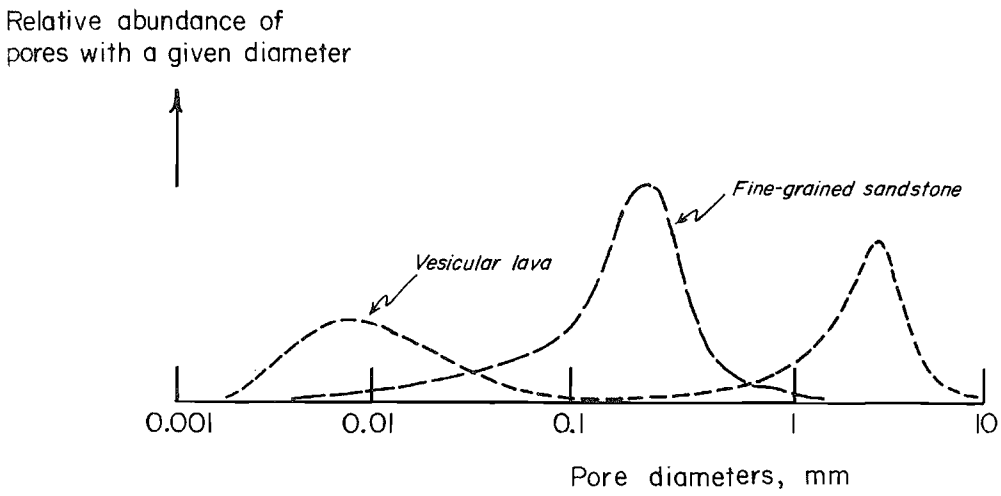


Figure 7. Typical distribution curves (schematic) for pore sizes in a granular rock such as sandstone and in a vesicular rock such as lava.

sedimentary rocks. Commonly, Paleozoic rocks are saturated with saltier water than more recent rocks, the higher salinity being a result of the loss of water on compaction and the addition of salts by solution of mineral grains. The salinity of water in fine-grained rocks tends to be higher than the salinity in coarse-grained rocks because of the greater adsorptive capacity of rocks with large internal surface area.

Chebotarev (1955) has given a summary of a great number of groundwater analyses (see Table I). Various classes of water apparently differ widely in normal salinity; bicarbonate waters have a median salinity of only about 400 parts per million, while sulfate waters have a median salinity of about 5000 parts per million and chloride waters have salinities in excess of 10,000 parts per million. For comparison, present-day ocean water is of the chloride type with a total salinity of 33,000 to 35,000 parts per million.

In rocks very near the surface, water undergoes a continuous exchange with the atmosphere. Water produced from underground for human or industrial consumption or irrigation is usually water which has been underground a relatively short period of time, geologically. This water usually contains a low concentration of dissolved solids. In areas of heavy rainfall, water in surface rocks may have a very low salinity because over long periods of time, circulating water will leach all the soluble ions from the rocks, leaving behind only ions which are not readily soluble. In arid climates, the amount of evaporation may be greater than the recharge from rainfall, with extra water migrating laterally or upward from the permanent water table. Evaporation of these migrating waters results in an increase in salinity of near-surface waters, and in extreme cases, in the formation of caliche zones. In arid areas, surface groundwaters may be moderately saline.

The resistivity of a water-bearing rock is a function of the amount of water in the rock, its salinity and the manner in which the water is distributed through the rock. The amount of water in a rock is usually determined by the porosity of the rock – the amount of void space in a rock which may be filled with water. The manner of distribution of the water in a rock is usually determined by the texture – a description of the size and shape of the void spaces.

In some rocks, particularly consolidated sediments, porosity is intergranular in origin, being the space left over between grains when the rock was formed. In other rocks, and particularly in igneous rocks, porosity occurs primarily in the form of joints. A third form of porosity, which may be found in limestones and volcanic rocks, is vesicular or vuggy porosity, consisting of large, irregular cavities formed either by solution, as in limestones, or by large gas bubbles, as in volcanic rocks.

Pore spaces must be interconnected and filled with water for a rock to conduct electricity. Pore volumes may consist of two parts; larger voids which serve as storage pores, and finer connecting pores. Most of the resistance to current flow is provided in the connecting pores because of their smaller cross sections. A rock with a high ratio of storage pore volume to connecting pore volume, such as a rock with vesicular porosity, will have a higher resistivity for a given porosity than a rock in which the ratio is low.

The very simplest relation between resistivity and water content which might exist in a rock would be

$$\rho_t = \rho_w \phi^{-1} \qquad 20$$

where ρ_t is the bulk resistivity, ρ_w is the resistivity of the water contained in the rock and Φ is the fractional porosity filled with water. This equation would describe the resistivity of a bundle of smooth tubes oriented in the direction of applied voltage.

The resistivity actually observed for a real rock will almost always be larger than the value predicted by Equation 20. The greater resistivity may be attributed to two effects: that of a parameter G which reflects the variability in cross section of the pore structure, and that of a tortuosity parameter T which reflects the increased distance over straight-line distance required for current to travel through the rock:

$$\rho_t = TG\rho_w \phi^{-1} \qquad 21$$

The significance of the structural parameter G is indicated by the probability distribution curves (or histograms) for the distribution of pore cross sections in a rock shown in Figure 7. Two examples are shown: one for intergranular porosity, in which pore cross sections group about a single average value, and one for vesicular porosity, in which pore cross sections group about two principal values, one for the vesicles and the other for the connecting pores. The effect of pore size distribution on

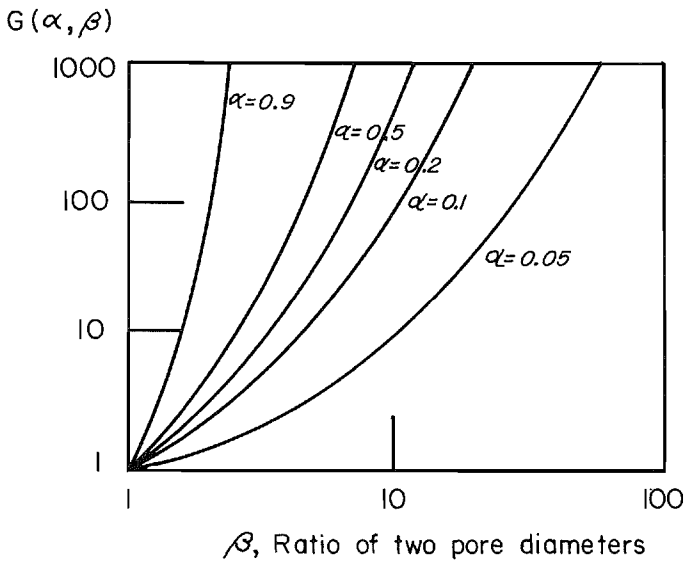


Figure 8. Increase in resistivity G caused by having pores of two diameters with a ratio β. The ratio of pore volume in large pores to pore volume in small pores is α.

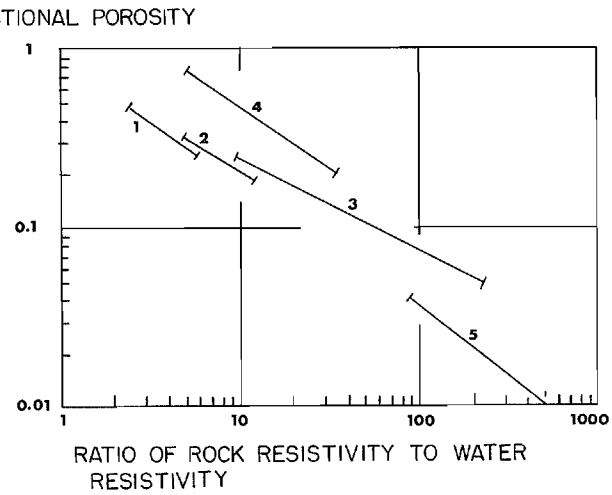


Figure 9. Graphical representations of the various expressions for Archie's law given in Table II.

resistivity may be evaluated approximately by constructing a single linear pore with a cross section varying according to the distribution of pore sizes. The more nearly uniform the pore sizes, the closer will be the resistance of the pore structure to the value predicted in Equation 20.

As an example, consider a pore structure made up of pores of two diameters only, with the ratio of the two diameters being β, with α being the fraction of the total porosity which is made up of pores with the larger diameter. The parameter G is

$$G = 1 + \beta^3 \frac{\alpha}{1-\alpha} \qquad 22$$

The variation of the parameter G with the ratio of pore diameters and with the distribution of pore diameters is shown in Figure 8. It is apparent that G is very large when pore diameters differ markedly.

In addition to the increase in resistance caused by variations in pore size, the length of the path along which current flows relative to linear distance also increases the resistance measured in a rock sample over the resistance for a bundle of smooth tubes. The tortuosity factor is usually about 1.3 to 2.0, so that tortuosity of current flow is less important in determining the resistivity of a rock than variability in pore size.

The parameters T and G are difficult to measure separately. However, data indicate that the effect of texture is not independent of porosity, and so porosity can be considered as the principal independent variable in discussing the effect of rock texture on bulk resistivity. Much experimental work has been done in the petroleum industry in correlating bulk resistivities with other rock properties. It has heen observed that rocks with primarily intergranular porosity have resistivities which vary approximately as the inverse square of the porosity when the rock is fully saturated with water. This relation has become known as Archie's law:

$$\rho_t = a\rho_w \phi^{-m} \qquad 23$$

where a and m are parameters whose values are assigned arbitrarily to make the equation fit a particular group of measurements. The parameter m is sometimes called the 'cementation factor' because its value appears to vary with the degree of cementation of a granular rock.

The parameters a and m correlate well with the lithology and texture of a rock. The value for the parameter a varies from slightly less than 1 in clastic detrital rocks to as large as 3.5 in vesicular or tuffaceous rocks. The parameter m varies from values as small as 1.3 in packed sand to values as large as 2.3 in tightly-cemented clastic rocks. Typical expressions for Archie's law applicable to various types of rocks are listed in Table II. The same expressions are shown graphically in Figure 9.

Table II. Typical forms of Archie's law for various rocks.

1. Weakly cemented detrital rocks, such as sand, sandstone and some limestones, with a porosity range from 25 to 45 percent, usually Tertiary in age
$$\rho_t/\rho_w = 0.88\ \phi^{-1.37}$$
2. Moderately well cemented sedimentary rocks, including sandstones and limestones, with a porosity range from 18 to 25 percent, usually Mesozoic in age
$$\rho_t/\rho_w = 0.62\ \phi^{-1.72}$$
3. Well cemented sedimentary rocks with a porosity range from 5 to 25 percent, usually Paleozoic in age
$$\rho_t/\rho_w = 0.62\ \phi^{-1.95}$$
4. Highly porous volcanic rocks, such as tuff, aa and pahoehoe, with porosity in the range from 20 to 80 percent
$$\rho_t/\rho_w = 3.5\ \phi^{-1.44}$$
5. Rocks with less than 4 percent porosity, including dense igneous rocks and metamorphosed sedimentary rocks.
$$\rho_t/\rho_w = 1.4\ \phi^{-1.58}$$

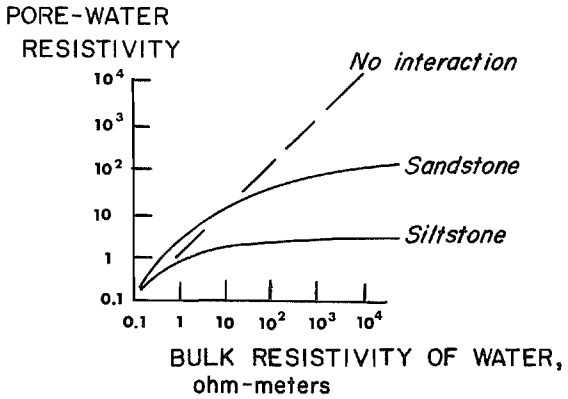
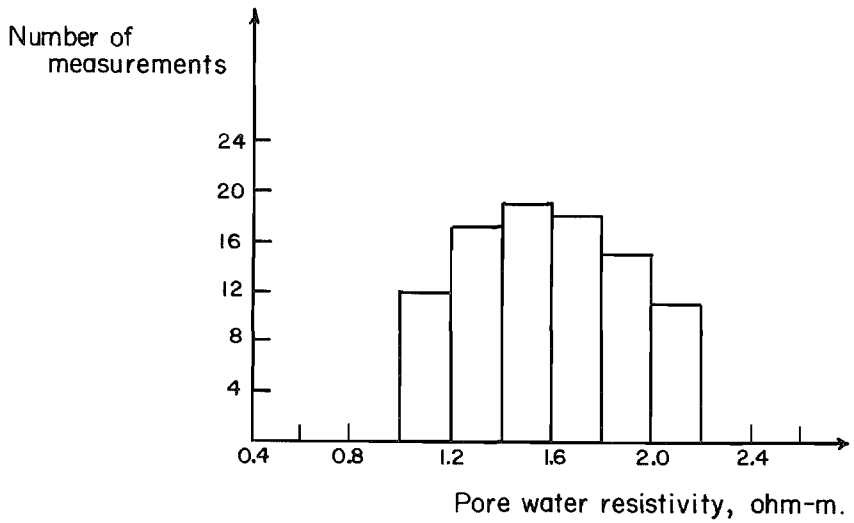


Figure 10. Relation between bulk and in-place resistivities of water when interaction between the water and solid minerals in a rock contributes to conduction.

These ions render the water in a pore structure conductive, even when the water extracted from the rock has no salinity. All rocks possess some exchange capacity, and so, the conductivity of an electrolyte in a pore structure will always be increased by ions supplied by desorption. Even in rocks with very low exchange capacities, pore water resistivity rarely exceeds 10 ohm-meters. In fine-grained rocks such as shale, pore water resistivities are always lower than would be expected on the basis of chemical analyses of water extracted from the rock. The added salinity may be relatively unimportant if the normal salinity of the water is high, but if the pore water is dilute, it is practically impossible to predict the resistivity of the water in the pores unless the ion exchange capacity of the rock is known.

The nature of surface conduction is less well known. When water is in contact with a typical silicate surface, several layers of water molecules collect in an adsorbed layer at that surface. The adsorbed water layer is under high pressure, with viscosity being greater than that of free water. As a result, ion mobility in the

Figure 11. Apparent groundwater resistivities determined from resistivity measurements made first on natural state samples, and then on samples resaturated with a saline electrolyte. Samples were volcanic tuff from the Oak Spring formation, Nye County, Nevada.



In using Archie's law (Equation 23), it has been observed that the appropriate value for water resistivity within the pore structure is not always the same as that which may be measured on a sample extracted from a rock. According to Equation 23, the resistivity of a rock should increase in direct proportion to the resistivity of the pore water. However, it is commonly observed that resaturation of rocks with waters which have less salt in solution leads to lower values of bulk resistivity than predicted by Archie's law. This may be explained by considering that the conductivity of the water distributed through the pore space is increased by two processes; ionization of clay minerals and surface conductance.

Clay minerals such as kaolinite, halloysite, montmorillonite, vermiculite, illite, chlorite and others have the property of absorbing certain ions in an exchangeable state (Dallavalle, 1948). When clay is mixed with water, the exchangeable ions may separate from the clay mineral in a process resembling ionization. adsorbed layer is much reduced, and the conductivity is reduced. If the water is relatively pure, conductivity may be increased in the adsorbed layer by proton transfer between neighbouring water molecules.

As a result of the reactions which may take place between an electrolyte and the minerals comprising a rock, the conductivity of an electrolyte is usually affected as shown in Figure 10. The dotted curve is the case in which the conductivity of the solution in the pore structure is the same as the conductivity of the solution in bulk. The solid curve is the more likely relation between rock resistivity and water resistivity when interaction takes place between the water and the minerals: at high salinities (low resistivity), the resistivity of the electrolyte in the pores is increased slightly because of the increase in viscosity of the adsorbed water; at low salinities (high resistivities), the resistivity of the pore water approaches a maximum value, rather than increasing without limit. The resistivity of the pore water will not

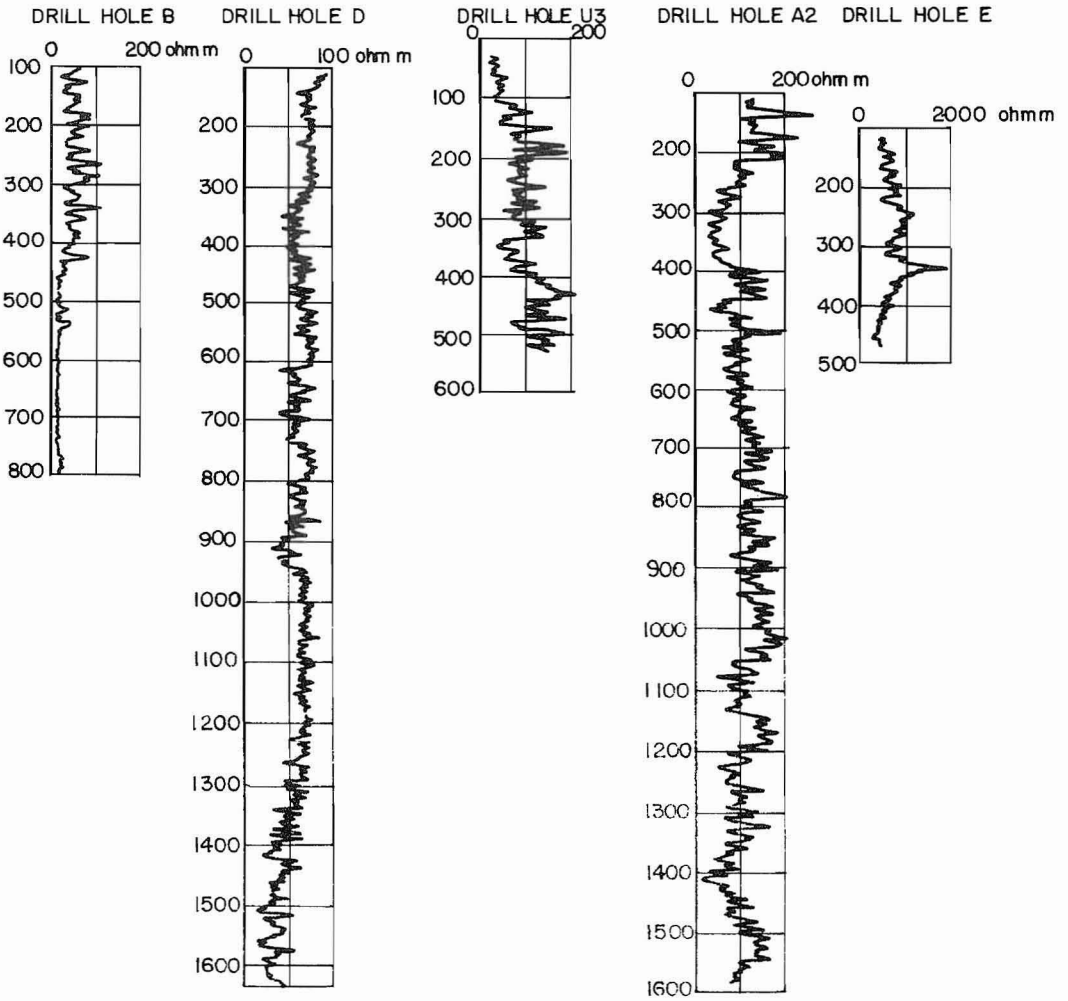


Figure 12. Resistivity logs from holes in alluvium in Yucca Valley, Nevada.

exceed some limiting value determined by the amount of interaction. Both the increase in resistivities at high salinities and the decrease in resistivities at low salinities are more pronounced in fine-grained rocks than in coarse-grained rocks.

The effect of interaction can be determined experimentally by measuring the resistivity or rock samples saturated both with a highly saline water and with distilled water. Interaction is negligible in the case of saline water saturation, while in the case of distilled water saturation, conduction is only by salinity added through interaction. The empirical parameters a and m for Archie's law may be determined from resistivities measured on the samples saturated from saline water; then, Archie's equation may be used to solve for the effective salinity of the pore water when the sample is resaturated with distilled water. Values for groundwater resistivity in samples of Oak Spring tuff from Nye County, Nevada (Keller, 1962) are shown in the histogram in Figure 11. The median groundwater resistivity is about 1.6 ohm-meters, while samples of natural water extracted from the same rocks have resistivities ranging from 50 to 150 ohm-meters.

The pore space in a rock need not necessarily be filled with an electrolyte; in near-surface rocks, part of the pore space may be filled with air. The resistivity of a rock only partially saturated with water will generally be less than the resistivity of the same rock fully saturated with water. Studies of the effect of desaturation on the resistivity of various types of oil reservoir rocks containing saline water has led to the recognition of an empirical expression resembling Archie's law:

$$\rho_t = \rho_{100} S_w^{-n} \qquad 24$$

where ρ_t is the bulk resistivity of the partially desaturated rock, ρ_{100} is the bulk resistivity of the same rock when 100 percent saturated with water of the same salinity, S_w is the fraction of the pore volume occupied by water and n is an empirical parameter which usually has a value of approximately 2. Equation 24 indicates that the resistivity increases as the square of the reduction in water content, suggesting that resistivity measurements would be effective in determining whether or not a rock were water saturated. Several difficulties are found when this approach is applied to rocks which produce potable water. If the water content in a rock is reduced by evaporation, the residual water is enriched in salts and solution, and it is found that the resistivity of the pore water decreases almost in direct

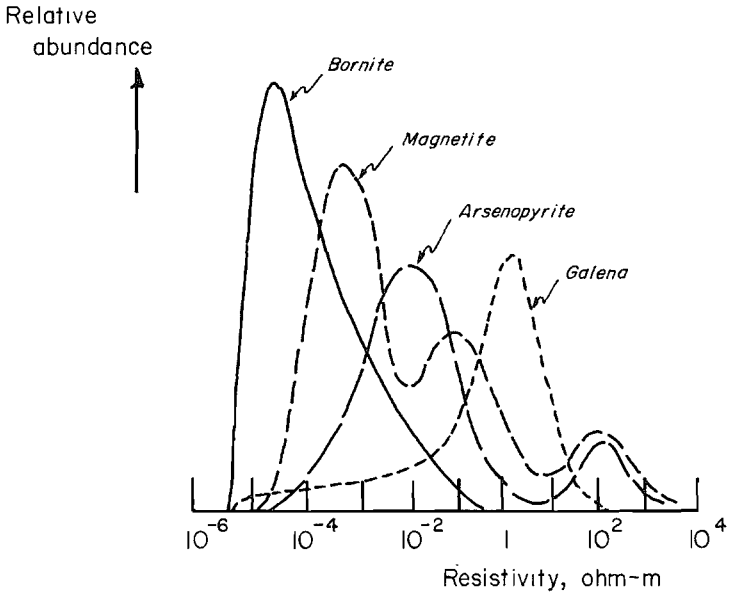


Figure 13. Relative abundances of measured values for the resistivity of several common ore minerals.

proportion to the decrease in saturation, diminishing the effect of desaturation on resistivity. Moreover, if a rock is saturated with fresh water, most of the conduction is contributed by salinity added by clay ionization, which takes place in the finer pores preferentially. Dehydration takes place preferentially in the larger pore structures, so it is not uncommon to find rock sequences in which the resistivity is nearly independent of saturation for rather large variations in saturation.

An example of such an effect is given by resistivity surveys run in drill holes in an alluvial valley in Nevada (Figure 12). These logs were obtained from a series of water wells drilled in Yucca Valley, Nye County, Nevada. The valley-fill material is a typical assemblage of interfingering and lenticular beds of unconsolidated detrital material. The alluvium ranges from clay size to cobbles and boulders. The alluvial fill is as much as several thousand feet thick in the center of the valley, and produces considerable quantities of potable water under favorable conditions. All five logs shown in Figure 12 penetrate well below the water table. All five show generally the same character from the top to the bottom, except for drill hole B. Resistivities on the individual logs vary over a range generally of about 2 to 1, even though the wells penetrate rocks with water saturations ranging from 10 or 15 percent to 100 percent. The low resistivity zone in drill hole B represents fine-grained alluvium that retains a large amount of water by capillarity, and the top of the conductive zone should not be confused with the water table.

Resistivity of ore-bearing rocks. Few rocks contain large enough concentrations of conductive minerals such as the various sulfides, magnetite, graphite or carbon to render them conductive without any contribution from water filling the pore spaces. Although such rocks might be considered to be volumetrically insignificant, their value as ores for various metals makes them quite important. Several extensive studies of the electrical properties of these conducting minerals have been reported in the literature over the years (Harvey, 1928; Semenov, 1948; Parasnis, 1956; Parkhomenko, 1967).

The reported values for resistivity of these semiconducting minerals generally show very wide ranges even for a single mineral. Variability in resistivity is to be expected in semiconductors inasmuch as the electrical properties are determined primarily by small amounts of impurities and by imperfections, rather than by the bulk composition of the material. Some minerals have relatively narrow ranges in values reported for resistivity, and these should be viewed with suspicion, inasmuch as the lack of scatter is due more likely to a limited number of measurements than to a uniformity of character for the mineral. It is better to treat the resistivities for conducting minerals statistically, as Semenov (1948) and Parkhomenko (1967) do. Typical distribution curves for several of the more common conductive minerals are shown in Figure 13. These distribution curves exhibit patterns which reflect factors contributing to the variability of resistivity values reported for specific minerals. Three different types of distribution curve are apparent:

1. A distribution curve with a well defined maximum value, with the distribution skewed towards high values of resistivity, such as the curve for bornite in Figure 13. Bornite is mineralogically simple, and so may have a characteristic value for resistivity given by the peak of the distribution. The skewing of the distribution may represent experimental errors, which would tend to be in the direction of high values, or to the effect of impurities, which would tend to interfere with conduction more frequently than to assist.

2. A distribution curve with several well defined maximums, such as the curve for magnetite. Several maximums in the distribution curve suggest that the mineral has several different types of internal structure, insofar as electrical conduction is concerned. Magnetite is not a well defined mineral, as bornite is, but is a mixture of ferric and ferrous oxides. Commonly, when conduction is determined by impurities in a mineral, the individual maximum values in the distribution will correlate with the source of the samples: samples from different sources may have different types of impurities.

3. A distribution curve with a well defined maximum value, with the distribution skewed towards low values of resistivity, such as the curve for galena in Figure 13. This behavior is observed in minerals which are normally more resistant than the majority of ore minerals. In such cases, conduction is controlled by the addition of the proper impurities. Impurities cause some samples to have considerably lower resistivities than the purer forms of the same chemical compound.

Consideration of the distribution curves in Figure 13 leads to the conclusion that electrical resistivity is not a diagnostic property for specific ore minerals. Low resistivity is a diagnostic property for the class of ore minerals, inasmuch as virtually all of them have resistivities less than the lowest values found for other types of minerals. This lack of diagnosticity is unfortunate, but has no great effect on the way electrical prospecting methods are applied in the search for ores. Commonly, ore deposits contain a wide variety of conductive minerals, and the commonest may not be the one which makes the orebody economic. For example, pyrite is a ubiquitous mineral in ore deposits, occurring in a great many orebodies in combination with other, more valuable sulfides. In considering the probable resistivity of an ore deposit, we need only worry about the total complex of ore minerals.

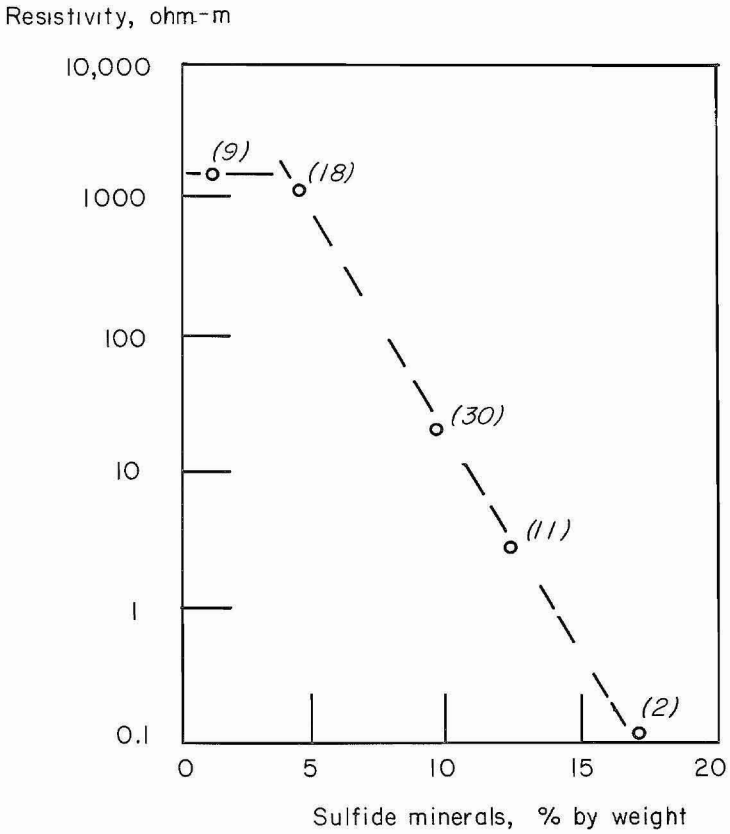


Figure 14. Variation of resistivity with the content of pyrrhotite and other sulfide minerals in gabbro (from Anderson, 1962).

Conductive minerals must be present in sufficient quantities to render a rock as a whole conductive. The habit of a mineral (the geometric form in which it habitually occurs) is as important as the amount in determining the effect on the bulk resistivity of a rock. Minerals which contribute most to rock conductivity occur in dendritic forms, so that a small amount will decrease the bulk resistivity of the rock tremendously. Other conducting minerals may occur only as isolated grains, or may be enveloped in a coating of an insulating mineral such as calcite or quartz.

An example of how the amount of conducting mineral affects the over-all conductivity of a rock is shown in the data in Figure 14. In this example, the rock is pyrrhotite-bearing gabbro from Maine (Anderson, 1962). To minimize scatter of the plotted data, each plotted point is an average for several measurements, the number being indicated in parentheses. Pyrrhotite concentrations of up to 4 or 5 percent (by volume) have little effect on bulk conductivity, but 8 percent pyrrhotite reduces the bulk resistivity by three orders of magnitude. Zablocki (1966) points out that this threshhold content for conducting minerals is sensitive to the texture of these minerals, even when only one species of mineral is being considered. For example, in the Lake Superior iron district, 8 percent magnetite content is enough to reduce the resistivity of chert from several thousand ohm-meters to less than 1 ohm-meter, primarily because magnetite grains are overgrown by needle-like crystals of hematite which form a conducting network. On the other hand, in a replacement-type magnetite deposit in California where there are no such hematite overgrowths, 25 percent magnetite by volume is required to reach the threshhold for conduction.

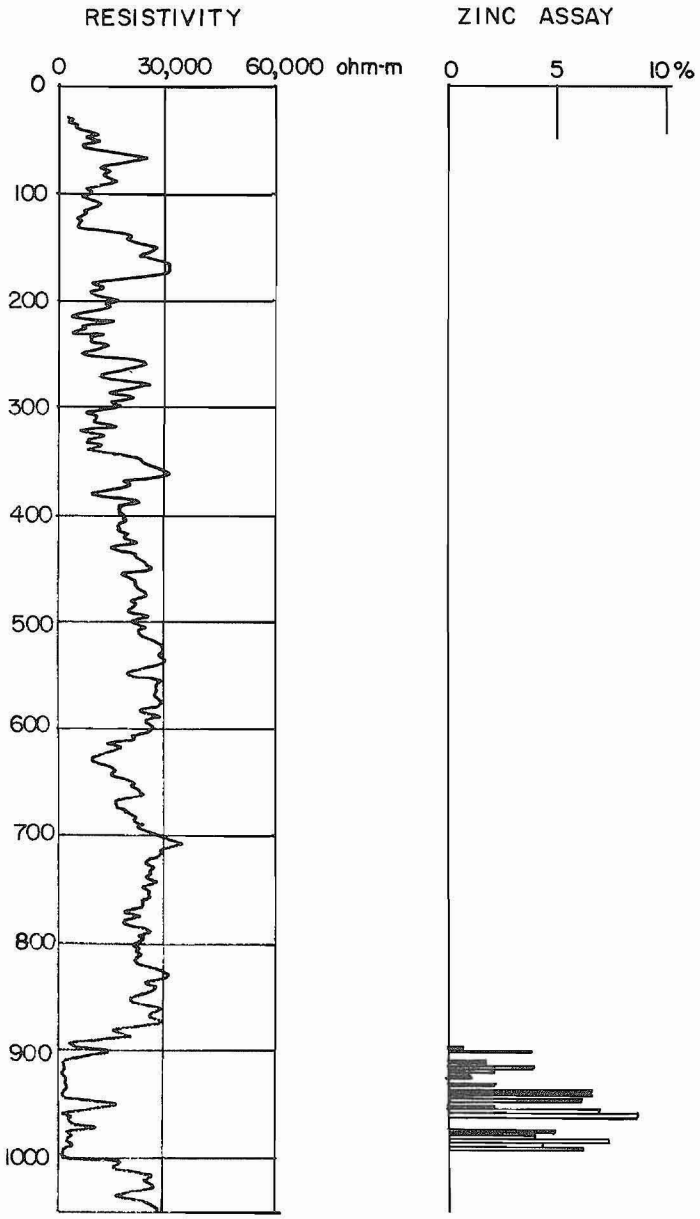


Figure 15. Resistivity log of an exploratory hole penetrating zinc mineralization in the Mascot-Jefferson City district of Tennessee.

In considering the electrical properties of orebodies, care should be taken that the electrical anomaly associated with an orebody is actually caused by the ore minerals. Parkhomenko (1967) has pointed out the peculiar fact that while many orebodies are much more conductive than the host rock in which they are located, the conductivity is not nearly as high as one might expect from sample measurements. An example of a conductive orebody in which the conductivity is not associated directly with the ore minerals is shown by the electric log in Figure 15. This is a log of an exploratory drill hole in the Mascot-Jefferson City zinc district (Keller, 1960). The sequence penetrated by the drill hole consists of Paleozoic limestones and

Contents

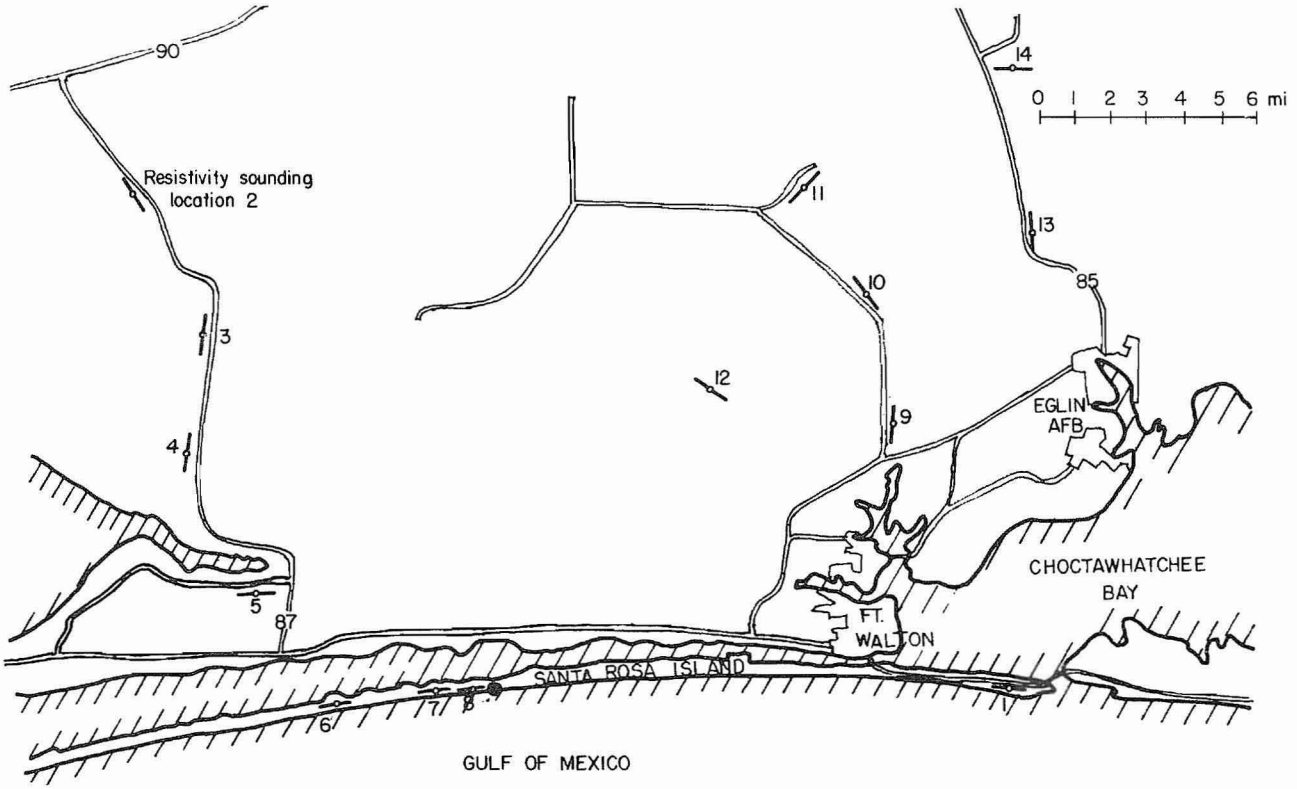


Figure 16. Map of the area around Fort Walton, Florida, showing locations of resistivity soundings.

dolomites with very high resistivity. Mineralization in the form of iron-free sphalerite is found in a brecciated zone between 900 and 1000-foot depth, in an interval where the resistivity is lowered by a factor of approximately 50, to several hundred ohm-meters. Sphalerite is one of the few sulfide minerals that is not an excellent conductor, and so, the moderate resistivity might be attributed to conduction of the sphalerite. In fact, the moderate resistivity is due entirely to porosity developed by brecciation, and the ore is only indirectly associated with the reduction in resistivity. It is likely that many orebodies are characterized by resistivity anomalies of this sort. Mineralizing solutions will tend to follow the more permeable, more porous sections of rock, which are also more conductive because of their high water content. If alteration minerals are of the sericite-chlorite family, interaction effects may cause the resistivity to be further reduced. If gangue minerals such as calcite and quartz are abundant, the orebody may have a higher resistivity than the surrounding rock. Thus, it is not unusual to find resistivity anomalies associated with ore deposits, but these anomalies may not be direct indicators of mineralization.

Application of resistivity surveys

Direct-current resistivity surveys have been applied extensively in exploration for groundwater, less extensively in the search for mineral deposits. There is an abundant literature on the application of resistivity surveys to specific exploration problems, and the bibliography in the Professional Paper of Van Nostrand and Cook (1967) provides a guide to this literature.

Resistivity methods can be highly effective in evaluating groundwater reserves under some conditions, although rock resistivity is insensitive to changes in salinity such as may be associated with the difference between potable and brackish water. One particular case is found along coastal areas and on islands, where a lens of fresh water essentially floats on sea water, depressing the salt-water level below sea level. The contact between fresh-water and salt-water saturated rocks is easily detected because of the high conductivity of the salt-water saturated section. According to the Ghyben-Herzberg principle, the water table rises about 2 feet above sea level for every 80 feet the salt-water level is depressed. This ratio is changed if the fresh water is moving from land to sea, or if there are permeability barriers, but in coastal areas, the mapping of a fresh-water diagonal salt-water contact is most helpful in mapping water reserves.

An example of a survey in such an area is one done in the vicinity of Fort Walton, Florida. (See Figure 16 for a map of the area with locations of resistivity soundings.) In this area, groundwater is produced from surficial sand and gravel beds. Along the coastal areas, water wells are drilled below sea level, and if water is drawn off too rapidly, the salt water encroaches into areas supplying fresh water.

Fifteen electrical soundings were made at locations indicated on Figure 16, using the Schlumberger array. Several typical sounding curves are shown in Figure 17. The surficial sands and gravels have a very high resistivity where they are saturated with fresh water because they have almost no clay content to add ions

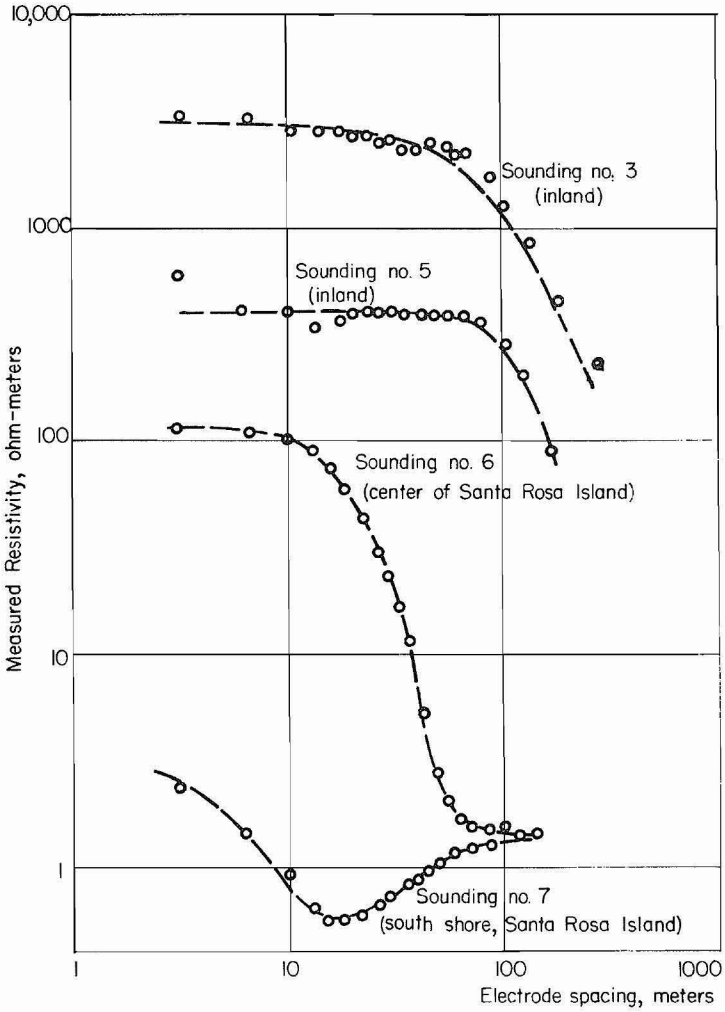


Figure 17. Resistivity sounding curves from the vicinity of Fort Walton, Florida.

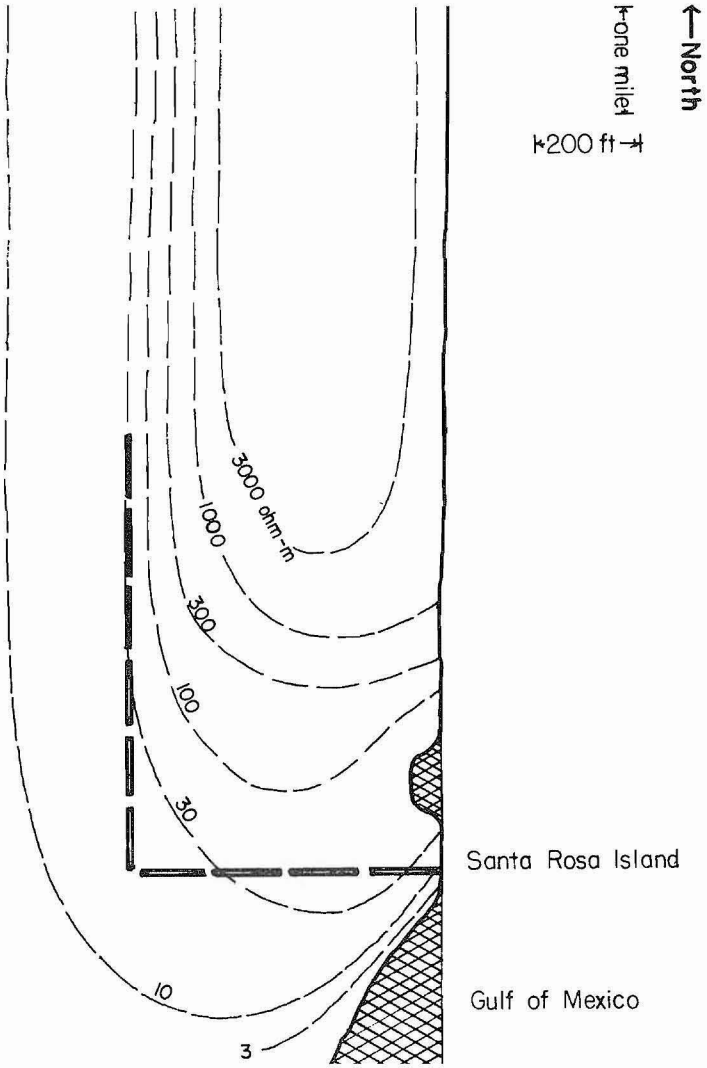


Figure 18. Interpreted resistivity cross section along a north-south line in the vicinity of Fort Walton, Florida.

to pore water. The resistivity of the same material saturated with sea water is only slightly higher than 1 ohm-meter. The transition from surface material with a resistivity of hundreds or thousands of ohm-meters to material saturated with salt water is striking. The survey was used to construct the resistivity cross section shown in Figure 18, which clearly indicates the depth to salt water, the flow of fresh water under the ocean, and the slight increase in salinity of the fresh water as it migrates under Santa Rosa Island.

In the western United States, resistivity surveys are used in hydrologic studies, primarily in mapping rock units which control groundwater flow. A typical example is the use of resistivity surveys to map the configuration of intermontane basins which are filled with detrital sediments. As seen in Figure 12, it is difficult to locate the water table in such rocks with resistivity surveys because the resistivity does not usually change markedly at the water table. However, groundwater movement is frequently related to the topography of the bottom of such filled valleys, and this can be mapped with resistivity quite well because there is usually a large contrast in resistivity between the alluvial fill and the basement rock.

Many other specific examples of the use of resistivity either directly or indirectly to locate water resources are available. An important point to be noted is that an understanding of the way in which rock resistivity varies with water content is especially helpful in the intelligent application of resistivity methods.

References

Al'pin, L.M., M.N. Berdichevskii, G.A. Vedrintsev, and A.M. Zagarmistr, 1966. *Dipole methods for measuring earth conductivity.* New York, Consultants Bureau, 302 p.

Anderson, L.A., 1962. Electrical properties of sulfide ores in igneous and metamorphic rocks near East Union, Maine; in *Short Papers in the Geological Sciences,* U.S.G.S. Prof. Paper 400B, p. B125-B128.

Bleil, D.F., 1964. *Natural electromagnetic phenomena below 30 kc/s.* New York, Plenum Press, 470 p.

Burg, John P., 1964. Three-dimensional filtering with an array of seismometers. *Geophysics.* 29 (5): 693.

Cantwell, T., J.N. Galbraith, Jr., and P. Nelson, 1964. Deep resistivity results from New York and Virginia. *J. Geophys. Res.* 69 (20): 4367-4376.

Chebotarev, I.I., 1955. Metamorphism of natural waters in the crust of weathering. *Geochimica et Cosmochimica Acta.* 8: 22-48, 137-170, 198-212.

Dallavalle, J.M., 1948. *Micromeritics.* New York, Pitman, 555 p.

Gish, O.H., and W.J. Rooney, 1925. Measurement of resistivity of large masses of undisturbed earth. *Terr. Magn. Atmos. Elec.* 30: 161-188.

Harvey, R.D., 1928. Electrical conductivity and polished mineral surfaces. *Econ. Geol.* 23: 778-803.

Jackson, D.B., 1966. Deep resistivity probes in the southwestern United States. *Geophysics.* 31 (6): 1123-1144.

Keller, G.V., 1960. Electrical properties of zinc-bearing rocks in Jefferson County, Tennessee; in *Short Papers in the Geological Sciences,* U.S.G.S Prof. Paper 400B, p. B128-B132.

Keller, G.V., 1962. Electrical resistivity of rocks in the area 12 tunnels, Nevada Test Site, Nye County, Nevada. *Geophysics.* 27 (2): 242-252.

Keller, G.V., 1966. Dipole method for deep resistivity studies. *Geophysics.* 31 (6): 1088-1104.

Kunetz, Geza, 1966. *Principles of direct current resistivity prospecting.* Berlin, Gebruder Borntraeger, 103 p.

Orellano, Ernesto, and Harold M. Mooney, 1966. *Master tables and curves for vertical electrical sounding over layered structures.* Madrid, Interciencia.

Parasnis, D.S., 1956. The electrical resistivity of some sulfide and oxide minerals and their ores. *Geophys. Prosp.* 4: 249-278.

Parkhomenko, E.I., 1967. *Electrical properties of rocks.* New York, Plenum Press, 314 p.

Rogozin, E.I., 1903. *The use of electricity in investigations of orebodies* (in Russian). St. Petersburg.

Schlumberger, Conrad, 1920. Essais de prospection électrique du sous-sol. *Acad. Sci. Comptes Rendus,* 170 (9): 519-521.

Semenov, A.S., 1948. Resistivity of minerals with high conductivities (in Russian). *Geofizika.* Vol. 13 (VSEGEI), Leningrad.

Van Dam, J.C., 1967. Mathematical denotation of standard graphs for resistivity prospecting in view of their calculation by means of a digital computer. *Geophys. Prosp.* 15 (1): 57-70.

Van Nostrand, Robert G., and Kenneth L. Cook, 1966. *Interpretation of resistivity data.* U.S.G.S. Prof. Paper 499.

Wenner, Frank, 1915. A method of measuring earth resistivity. *U.S. Bur. Standards Bull.* 12, Paper 258: 469-478.

Zablocki, C.J., 1966. Electrical properties of some iron formations and adjacent rocks in the Lake Superior region. In *Mining Geophysics.* 1: 465-492. Publ. by Soc. Expl. Geophys.

Ground electromagnetic methods

Robbert A. Bosschart

Scintrex Ltd.
Downsview, Ont., Canada

Abstract. The basic methods of ground electromagnetic prospecting have undergone little change during the last three decades and only a few truly novel procedures have been added during this period. Major advances have, however, been made in instrumentation as well as in the interpretation of field data. As a result the effectiveness of electromagnetic prospecting has markedly improved over the years.

The most widely used contemporary methods are briefly described. The effect on the response of frequency, coil configuration and other relevant characteristics determining the range of applicability of the respective systems is discussed and the effectiveness in different geological environments is compared.

Résumé. Les méthodes électromagnétiques fondamentales au sol sont demeurées à peu près les mêmes au cours des derniers trente ans et peu de modifications y ont été apportées. Les instruments, cependant, ont été améliorés et des progrès importants ont été enregistrés dans l'interprétation des données recueillies sur le terrain. Il en est résulté une efficacité grandement améliorée de la prospection à l'aide des méthodes électromagnétiques.

L'auteur décrit les méthodes modernes les plus répandues, et étudie l'effet exercé sur la réponse de la fréquence, la configuration de la bobine et autres caractéristiques qui déterminent le champ d'applicabilité des divers systèmes et leur efficacité dans les divers milieux géologiques.

Because of the many alternative ways the ground can be energized and the resulting magnetic field distribution investigated, ground electromagnetic methods comprise many prospecting systems of greatly varying viability. This review deals only with methods that are now in use, including those that have survived and prospered in the competitive climate of practical mining exploration, as well as some new but mostly unproved techniques.

Most present-day electromagnetic surveys are carried out with a few versatile, time-tested methods, generally known as the tilt angle or vertical loop methods, the Slingram or horizontal loop method, and the Turam method.* These standard methods are all continuous wave systems with operating frequencies in the middle audio spectrum (200 to 5000 Hz) and are representative of the following three groups: orientation measuring systems; moving source compensation systems; and fixed source compensation systems.

Besides the standard methods some other prospecting techniques are employed on a more limited scale. These special methods are usually optimized to perform under a specific combination of conditions, with a resulting loss of versatility.

All methods included in the present review are relatively well known and have been described in detail in many articles and in textbooks on applied geophysics (Grant and West, 1965; Keller and Frischknecht, 1966; Parasnis, 1962 and 1966). By their very nature, however, these descriptions tend to stress positive aspects only. For the practising geophysicist faced with economic realities, it is often difficult to obtain a balanced view of a prospecting system, recognizing weakness as well as strength, failure as well as success.

Therefore within the limited scope of the present review, an objective evaluation and comparison of electromagnetic methods will be attempted against the background of their natural environment. Descriptions of methods will be as brief and general as possible.

*A systematic terminology is lacking. Brand names as well as arbitrary names to indicate field techniques are used. Many different names refer to the same basic method.

Standard methods

The tilt-angle or vertical loop method. In tilt-angle, dip-angle or vertical loop EM systems (Grant and West, 1965; Keller and Frischknecht, 1966; Ward, 1959; West, 1960), an alternating magnetic field is established and the direction of the total magnetic field due to the transmitter and to eddy currents induced in the ground is measured. A number of different transmitter-receiver configurations are employed, which have in common that during the measurements the transmitting coil is held stationary in a selected orientation and the receiver coil is used as a 'null' measuring device, i.e., rotated around a selected axis until it is in a position of minimum induction. In the latter position the plane of the receiver coil contains the total field vector, or, when secondary fields are present, the major axis of the polarization ellipse. For most surveys the vertical transmitter and horizontal receiver configuration is used. Initially the transmitters were large and not easily manoeuvrable and therefore were kept stationary until all lines within their range were traversed by the receiver ('fixed transmitter' technique, Figure 1). With the advent of light, mobile, solid-state instruments faster 'broadside' or 'parallel line' techniques have come into use (Figure 2), whereby transmitter and receiver are moved in unison on two parallel grid lines, and the rate of coverage has been further increased with the introduction of double transceiver systems. These latter systems also have made possible improved in-line techniques, such as the 'shoot-back' method (Grant and West, 1965), which overcomes some of the terrain problems inherent in common in-line measurements.

Detailed measurements are usually conducted with the previously mentioned fixed transmitter configuration. The transmitting coil is kept on the anomaly axis and the receiver is traversed perpendicular to the strike. The results thus obtained often allow a somewhat better evaluation of the conductor location and its depth of burial.

Many forms of instrumentation for tilt-angle methods exist, varying from systems using large triangular, mast-mounted motor generator driven transmitting loops to light solid-state equipment using air-cored or iron-cored coils and battery-powered oscillators. Some modern instruments are of the transceiver type and

Contents

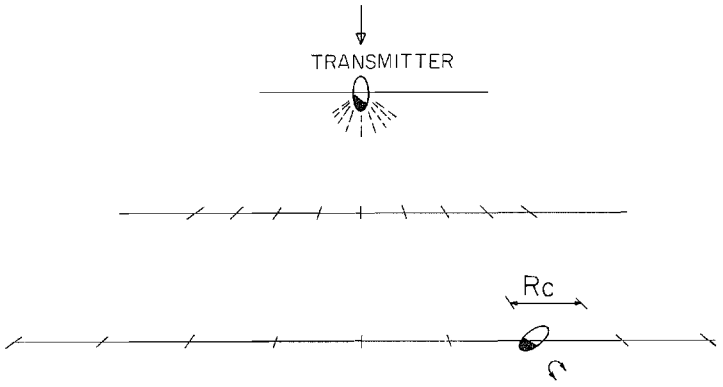


Figure 1. Vertical loop EM fixed transmitter method.

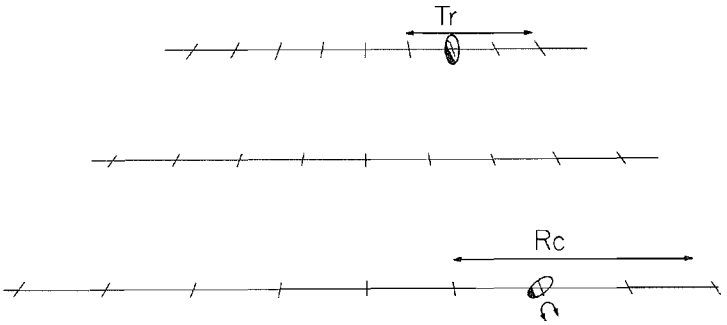


Figure 2. Vertical loop EM parallel-line or broadside method.

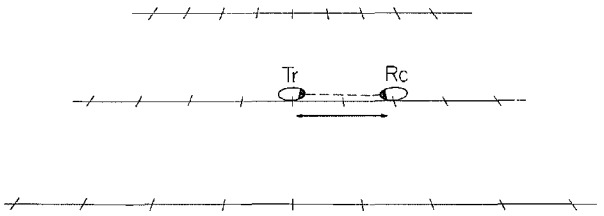


Figure 3. Slingram or horizontal loop method.

some double as moving source compensation systems. Operating frequencies vary from 400 to 5000 Hz and many two-frequency versions are available.

The larger, powerful transportable systems permit transmitter-receiver separations up to 750 m. The spacing of the lighter, portable systems is limited to 200 to 300 m.

The results of directional surveys are usually presented as profiles showing the angular deviation from the free-air null position in the plane of measurement. The approximate horizontal location of the conductor axis is indicated by the crossover point for single, steeply dipping conductors, or by the inflections of the curve, for multiple conductors. Depth of burial, conductivity, size and geometry are reflected in the curve shapes and amplitudes, but they are usually difficult to distinguish. Ambiguity can often be removed by using two, well separated frequencies.

The Slingram or horizontal loop method. Moving-source compensation systems are known under a variety of names, of which Slingram or horizontal loop are the most widely used (Grant and West, 1965; Keller and Frischknecht, 1966; Parasnis, 1962). All have in common that two light coils, one transmitting, one receiving, are moved in line, in a constant configuration over the terrain (Figure 3). The resultant field at the receiver is measured in complex components, expressed in per cent of the free-air primary field. A reference signal is passed from the transmitter to the compensator by a cable. The coils are usually held horizontal and coplanar. Frequencies vary between 500 and 4000 Hz and coil separations between 30 and 150 m.

Many different versions of this system exist, the differences generally being rather superficial. All present systems require an interconnection cable between transmitter and receiver and all are similarly sensitive to separation and orientation variations. Air-cored as well as iron-cored coils are used. Most instruments are calibrated for a number of standard separations, e.g., 30, 60 and 100 m, multifrequency versions are available and some instruments can also be used as tilt-angle systems.

The results are usually presented as profiles showing the variation of real (in-phase) and imaginary (out-of-phase, or quadrature) components of the secondary field plotted at the midpoint between the coils. The system is symmetrical and the positions of transmitter and receiver are interchangeable.

The horizontal location of the conductor is indicated by the minimum real component deflection and peak negative imaginary deflection. More accurately, for steeply dipping bodies the conductor edges are exactly half the coil separation from the point where the curves go through zero, the distance between these edges giving the over-all width of the conducting zone, which may include several separate bands (Bosschart, 1961).

For a single sheetlike conductor the dip can be estimated from the asymmetry of the curves.

In most cases the conductor properties σ (conductivity) and t (thickness) are directly related to the real and imaginary components of the anomaly amplitude, and Argand diagrams are often employed to determine σt from field data. Most commonly the Argand diagram representing the response of a vertical half plane is used as a basis for interpreting field anomalies (see Figure 10). When it can be safely assumed that the conductor approximates these conditions the depth to the top edge of the conductor can be estimated as well. With flatter dips the absolute values of the component amplitudes increase, not the amplitude ratio. σt determination would not be much affected but depth estimates would be too small.

The assumption of infinite extension is, by approximation, justified for bodies with a strike length at least three times the *T-R* separation. With the standard 60 m coil separation most target conductors will fall in this category. With larger *T-R* separations some may appear as finite bodies and the Argand diagram will no longer apply without a separate size correction.

The Turam method. The Turam method is the most commonly employed fixed source system and in its inductive application the only one that can be considered a standard method (Bosschart, 1964; Bosschart and Seigel, 1966; Hedstrom, 1937). The general layout and typical results are shown in Figure 4. Field strength ratios and phase differences are measured between successive observation points by two receiving coils connected to a compensator bridge. Usually the ratio of vertical components is measured; more rarely the ratios between horizontal components

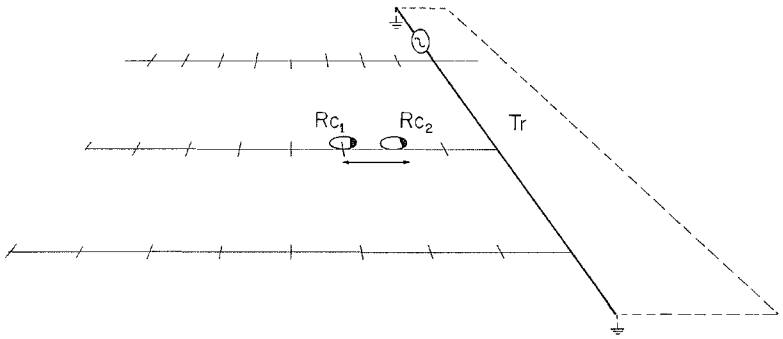


Figure 4. Turam method.

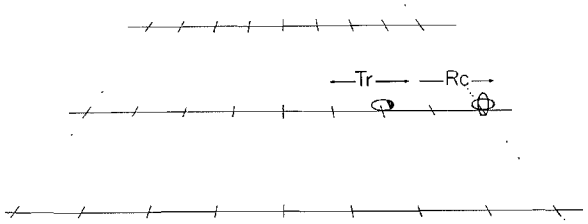


Figure 5. Cross-ring method.

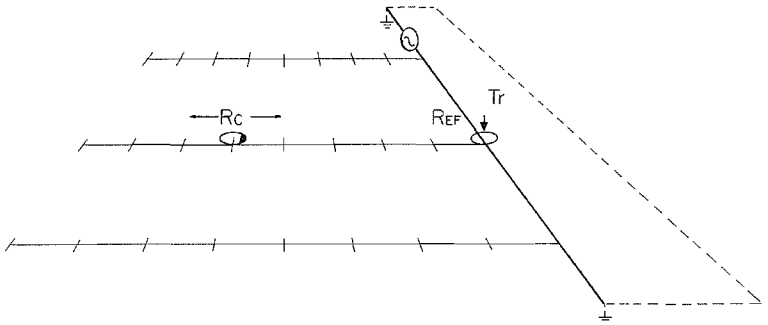


Figure 6. Compensator method.

or between vertical and horizontal components are determined. The observations are normalized by calculated free-space primary field values at the respective measuring points.

Rectangular wire loops of dimensions varying between 5000 X 3000 m and 200 X 200 m are mainly used as inductive sources. It is common practice to take measurements outside these loops, although it is also possible, of course, to measure on the inside. For galvanic-inductive surveys the ground is energized by means of long, straight, grounded wires. The return flow of current between the grounding points is then superimposed upon the induced current pattern.

A limited number of versions of the Turam system are commercially available.

Operating frequencies vary between 100 and 1000 Hz and two or three frequencies are usually provided. Iron-cored as well as air-cored coils are used. The transmitting equipment varies somewhat with the preferred field technique, since grounded layouts require higher power to overcome contact resistance.

Purely inductive energization is preferred for systematic surveys because the results are amenable to quantitative interpretation, which gives the method a degree of selectivity not obtainable with grounded layouts. The addition of conductive current does not as a rule render the method more sensitive. With grounded primary layouts the number and strength of anomalies is usually much greater, and this may be mistaken as evidence of increased sensitivity. But the increased emphasis is in most cases on undesirable conductors. The long primary layouts tend to induce relatively stronger eddy currents in the larger conductors. Size will replace conductivity as the predominant factor in the response, an undesirable effect in base-metal prospecting, where the ore conductors are generally the smallest conducting bodies.

The galvanic portion of the primary field will have an even stronger preference for the larger conductors; moreover it will mainly affect the in-phase part of the response and thereby invalidate all deductions based on complex relations.

The normalized results are usually presented in the form of profiles showing the variations of field strength ratios and phase differences. Because of the constant coupling between the source and conductors the curves permit accurate determinations to be made of the horizontal location and the depth of the current axis. The value of σt can be determined from the amplitude relations with the aid of Argand diagrams, as for moving-source methods. The difference is that in this configuration the majority of conductors have to be considered as bodies of finite size, and additional size corrections have to be made (Bosschart, 1964).

Special methods

Cross-ring method. Many of the special methods are variations of the standard procedures. A modified moving source system is the cross-ring method (Braekken, 1964; Frischknecht, 1959), which employs two perpendicular receiving coils and requires no cable connection between transmitter and receiver (Figure 5). Operating frequencies are in the 3000 to 4000 Hz range. The measured quantity is the complex ratio between the two receiving coils. The system is not distance sensitive, but with one pair of coils in a zero coupling configuration it is even more orientation sensitive than the horizontal loop system and requires a clear line of sight. It is a versatile tool for some types of detailed surveying, but less suitable for normal systematic surveying. Other things being equal it is subject to the same penetration limiting conditions as the horizontal loop method.

Compensator and radio-reference methods. The compensator (or Sundberg method) and radio-reference methods employ large

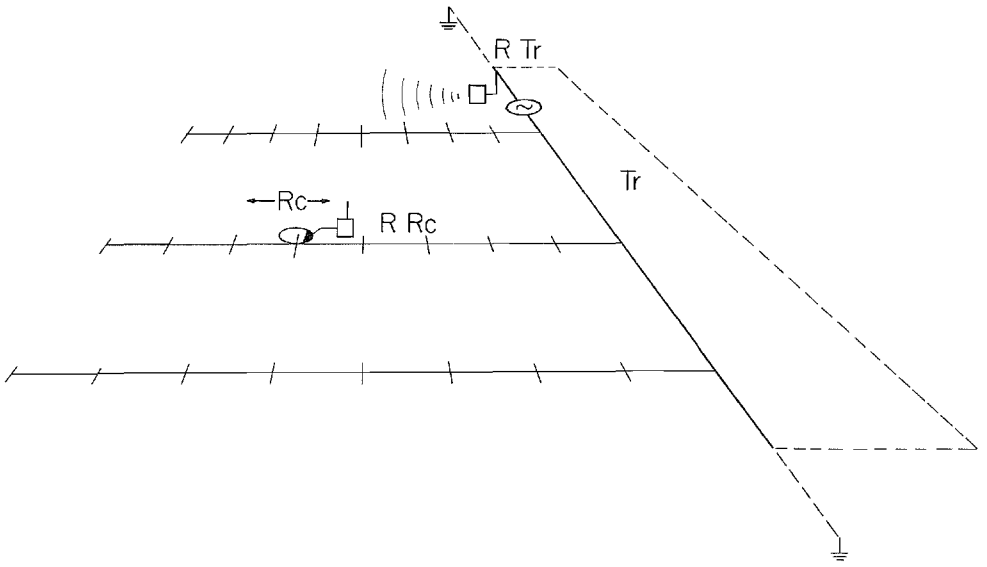


Figure 7. Radio-reference method.

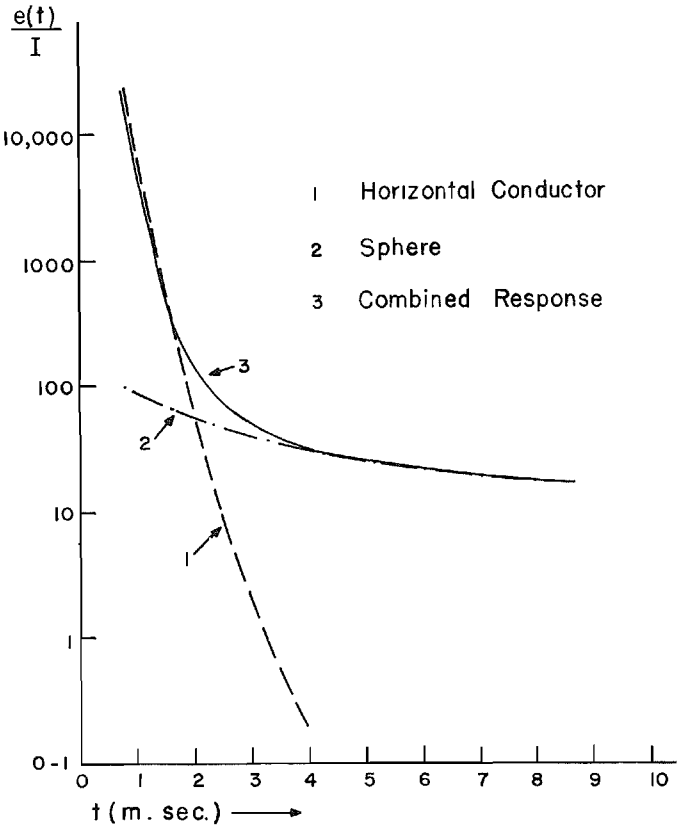


Figure 8. Response of a sphere under a horizontal conductor in a time-domain system (after Velikin and Bulgakov, 1967).

fixed layouts like the Turam method, and one moving receiver measuring the resulting electromagnetic field in complex components. In the compensator method a reference voltage from a small coil, coupled inductively to the primary field, is transmitted by wire to the receiver (Figure 6); in the radio-reference method a radio link is used to transmit a phase reference (Figure 7). Low frequencies between 10 and 300 Hz are employed in both methods, which have their main application in investigating problems where mobility is not an important requirement, such as mapping local structure, or flatly dipping mineral deposits.

Galvanic-inductive Turam method. The Turam method with galvanic-inductive energization, i.e., with a grounded primary source, may be particularly useful when the target conductors are bodies in which significant eddy currents are difficult to induce, for instance elongated cylindrical bodies. Such targets may be energized sufficiently by the galvanic current flow to become detectable.

Mise à la masse method. The direct contact to orebody (mise à la masse) technique, which has been successfully employed in potential surveys, is sometimes used in ground cable EM surveys, to try and enhance the response of the deeper extensions of a body and thus its detectability in depth. The success of this technique depends on whether the main part of the galvanic current will indeed flow through the mineralization rather than prefer a return path through the overburden and mask the desired response. This, to understate the case, cannot be taken for granted.

Radiofrequency methods. Radiofrequency methods have their own limited field of application. The only method presently finding appreciable use for surface prospecting makes use of the worldwide network of military VLF (18 - 22 kc) radio transmitters. A light, portable receiver is tuned in to the station most suitably located relative to the survey area and the tilt angle of the field as well as a measure for the imaginary component are obtained.

Radio wave methods using still higher frequencies are at the present time employed mainly in subsurface applications.

Time-domain methods. In time-domain or transient methods the ground is energized by current pulses and the resultant transient field is examined after the termination of a current pulse. The current pulses may have a duration of 1.5 to 100 milliseconds and wave forms varying from half sine to step waves with zero or

finite rise times (ramp step waves) may be used. The resultant transient response is sampled at discrete time intervals or integrated over predetermined time periods. Since the response on the transient decay curve with increasing time corresponds to the response at decreasing applied frequency, a differentiation between conductors can be achieved on a time basis. The high-frequency responses, arising mainly from poor conductors, such as overburden, occur in the early stages of the transient. The low-frequency responses from good conductors are of much longer duration and become detectable in the later stages. Figure 8 shows the scale-model response of a sphere of good conductivity and 50 m radius under a horizontal layer representing a 100 m deep overburden cover of medium conductivity (curve 3), as well as the individual response of the overburden (curve 1) and the sphere (curve 2). Under these conditions sampling after a 2-millisecond delay would effectively remove the overburden response.

As this example suggests, time-domain methods would particularly have an application in areas of heavy and conductive cover.

Two different, recently developed, time-domain systems are in use*. One method employs loops of dimensions varying from 200 × 200 m to 10 × 10 m for transmission as well as reception. Step wave excitation is used and the ratio of transient over primary current is measured at delay times between 1 and 15 milliseconds. These delay times can be adjusted to match local geoelectrical conditions, i.e., to emphasize desirable and suppress undesirable conductive responses. A relatively light power source can be used, but the entire loop layout has to be relocated for each subsequent observation (Velikin and Bulgakov, 1967).

A second method uses ramp step wave energization (step wave with a finite rise time) to obtain the greatest energy concentration in the low-frequency part of the spectrum (5 to 50 Hz). Selected portions of the decay curve, covering a time span of 0 to 100 milliseconds, are integrated over several measuring cycles (Dolan and McLaughlin, 1966).

The combination of time-separated transmission and measuring cycles with independent transmission and receiving coils results in low noise levels and considerable geometrical flexibility (Dolan and McLaughlin, 1966; McLaughlin, 1967).

Drill-hole methods. Drill-hole versions of all standard methods are, or have been in use.

In orientation-measuring systems the receiver coil, with its axis parallel to the direction of the hole, is lowered in successive steps while a large transmitting coil at the surface is tilted until a minimum voltage is obtained from the receiving coil (Keller and Frischknecht, 1966).

At least one method employs a moving-source configuration whereby transmitter and receiver, at a fixed separation, are both lowered in the hole. Complex components are measured as in the horizontal loop method (McLaughlin, 1967).

In fixed-source compensation applications a transmitting loop is laid out on the surface. Either complex field components are measured down the hole by a single coil, or field gradients are measured by two receiving coils which are kept at a constant separation.

*The most successful time-domain system, the INPUT system (Boniwell, 1967) has been employed mainly as an airborne system. It appears to lend itself less well to ground applications.

Instrumentation for these methods is generally similar to the one used in surface applications, but higher frequencies can advantageously be used, because the effect of a conducting unconsolidated cover can largely be left out of consideration.

Detection capabilities

The foregoing synopsis, even though it is confined to the most commonly employed methods, presents a large variety of alternatives. How are we to decide which method will best suit a particular purpose?

The topographic and geologic environment as well as the object of the survey have a bearing on the effectiveness of different prospecting systems and they have to be defined. The requirements of a system for mapping near-surface resistivities, for depth sounding, or for locating buried ore conductors obviously vary. The presence of other than target conductors, the conductivity contrasts, the dimensional and geometrical relations as well as the topographic relief, all are factors affecting the problems a method may be faced with.

The relative merits of individual prospecting methods in a specific exploration problem will be determined by: (1) potential depth of investigation; (2) ability to detect, resolve and locate all significant conductors; (3) ability to discriminate between different types of conductors, specifically between desirable and undesirable conductors; and (4) efficiency, i.e., flexibility, ease of operation, rate of coverage, cost, etc.

These matters are usually interrelated and their relative importance may vary. The potential depth of investigation is controlled by the signal-to-noise ratio in the measuring results; signal being the response of target conductors, noise including the sum of instrumental noise, operational distortion, the response of undesirable geological conductors, and interference from external fields. Thus the penetration depends, among other things, on what is defined as a target conductor. What in one type of survey is a target may in another type of survey have only nuisance value.

Instrumental noise is no longer a very significant factor in modern instruments, but operational noise is the major limiting factor in many ground methods. It arises from discrepancies in coil separation, alignment and orientation and from observation inaccuracies. It is affected by topographic relief and by visibility, and it includes a significant human element.

Geological noise is the aggregate of the responses of undesirable geological conductors. In base-metal prospecting these may, for instance, include overburden, fault and shear zones, serpentinized formations, or carbonaceous sediments. In depth sounding the roles of signal and noise could, at least partly, be reversed.

External noise from natural sources is generally insignificant, but fields from man-made sources such as power lines may locally cause high noise levels.

Operational noise varies greatly between methods and also between operators. Other things being equal it can be held to insignificant levels in orientation-measuring systems when the topography is reasonably level, and it usually does not affect the signal-to-noise ratio. In moving-source methods it is of major importance and the determining factor controlling the potential investigation depth. Fixed-source methods, particularly methods measuring the ratio of two components, are least subject to operational noise, even under conditions of severe topographic relief.

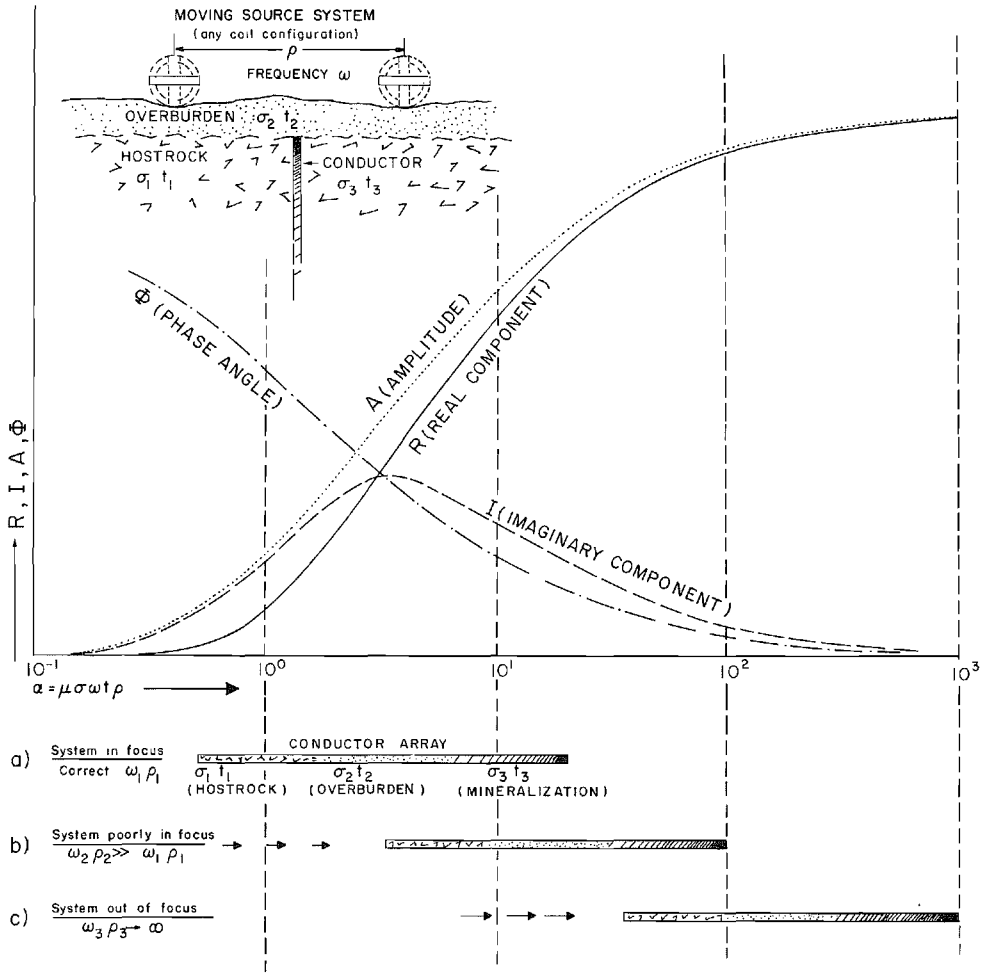


Figure 9. Thin tabular conductor and typical geological environment in a moving-source configuration. General response diagram and conductor array.

The definition of geological noise and signal are relative. The two can be distinguished when the causative bodies have measurably contrasting conductivities or when their dimensions or geometry relative to the prospecting configuration show characteristic differences.

For instance, a problem of base-metal prospecting could be visualized in a simplified manner, as mapping steeply dipping tabular bodies of relatively high conductivity and limited strike length under a horizontal cover of medium to poor conductivity. Then either a system highly favouring the response of vertically over horizontally oriented conductors, or a system capable of separating the relevant conductivity ranges could be employed effectively. The limited length of the target anomalies could be used as a criterion, or even the depth of the current axis, if the cover thickness were known.

However, the geometry of the average search problem is rarely sufficiently known, or consistent enough, to furnish reliable criteria for a separation of signal from geological noise. In the majority of problems the essential criterion is whether a prospecting system can differentiate between conductors on the basis of conductivity.

The general aspects of the response of ground electromagnetic profiling methods can be studied with the aid of response diagrams of the type shown in Figure 9, picturing the variations of real and imaginary components of the peak anomaly from a two-loop electromagnetic system over a conducting half plane with the induction parameter $\alpha=\mu\sigma\omega t\rho$, wherein ω = frequency, ρ the T-R separation, σ the conductivity, μ the permeability and t the thickness (Grant and West, 1965; Ward, 1959). The range of conductors present in a particular investigation area, including the sources of geological noise as well as the target conductors, can be pictured by a horizontal bar ('conductor array'), covering, for example, 1 1/2 decades of induction parameter values, the low values representing, for instance, overburden and faults, medium and high values disseminated and concentrated sulphide mineralization, respectively.

By the operating parameters ω and ρ the conductor array can be moved to the right, where the response approaches the inductive limit, or to the left, resistive limit, where the response will disappear in the noise level. Obviously the best rejection of geological noise is obtained when the left side of the conductor array is kept in the insensitive part, and the best differentiation between significant conductors when the centre and right portion of the conductor array coincide with the two decades of the response variation where the complex components have their most characteristic rate of change. For larger values of $\omega\rho$ the curves flatten and all elements of the conductor array give rise to a similar response; near the limit of induction the factors embodied in the induction parameter cease to affect the response and conversely cannot be derived from the results for the purpose of interpretation.

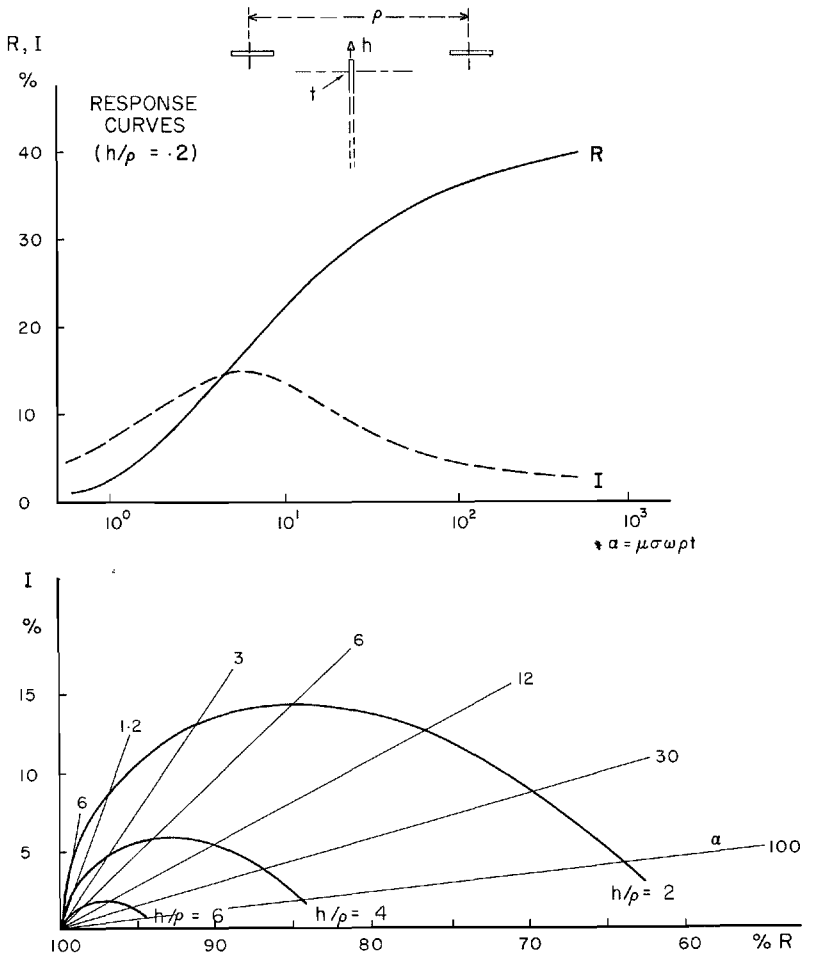


Figure 10. Half plane in a moving-source configuration. Response curves and related Argand vector diagram.

The effect of factors not embodied in this presentation further emphasize the need to properly focus the prospecting system. The intensity of anomalies observed in the field is also controlled by dimensional and geometric factors such as depth, strike and dip, and in some cases strike length. Near the inductive limit these factors dominate the response. In ore prospecting, where the target conductors are generally the smallest bodies in the conductor array, and often occur in the least favourable orientation, this is obviously most undesirable. Such targets can be found only by stressing conductivity and diminishing the influence of all other factors on the response.

The same geometrical factors may throughout the full variation of the response function cause geological noise to have greater amplitudes and mask anomalies arising from target conductors of higher conductivity. In such cases $\omega\rho$ has to be reduced until the target response becomes detectable above the noise level.

When the proper range of the response corresponds with the conductor array, the product of the conductor properties σ and t can be determined from the complex amplitude ratios. For moving source methods this is usually done with the aid of Argand diagrams of the type shown in Figure 10 (Grant and West, 1965; Hedstrom and Parasnis, 1958; Keller and Frischknecht, 1966).

Because the geometry affects the absolute amplitudes, only the amplitude ratios are relevant in determining σt. Size can normally be neglected; as long as the strike length of the conductor is not less than three times the coil separation the half plane approximation is close enough for all practical purposes (Bosschart, 1961; Parasnis, 1962; West, 1960). When this ratio becomes smaller the body appears in the measuring configuration as finite and the derivation of σt becomes more complicated. This is one disadvantage of using large coil separations.

σ and t can rarely be determined separately but the chances of confusing narrow zones of high conductivity with wide zones of poor conductivity are limited, and σt is a rather consistent means to differentiate geological conductors, because the effect of t on the response is confined to the range $0-\left(\frac{1}{\mu\omega\sigma}\right)^{1/2}$ (Keller and Frischknecht, 1966).

The scale of fixed-source methods is different, because the *T-R* spacing is generally smaller than the mean diameter of the transmitting loop, and has no influence on the response. Instead, the response is affected by the dimensional relation between loop and conductor. If the conductor is a steeply dipping tabular body it will respond as a half plane when the strike length is more than approximately three times the main energizing leg of the primary layout. When the strike length is smaller, the response will become that of a finite tabular conductor. The variation of the

Contents

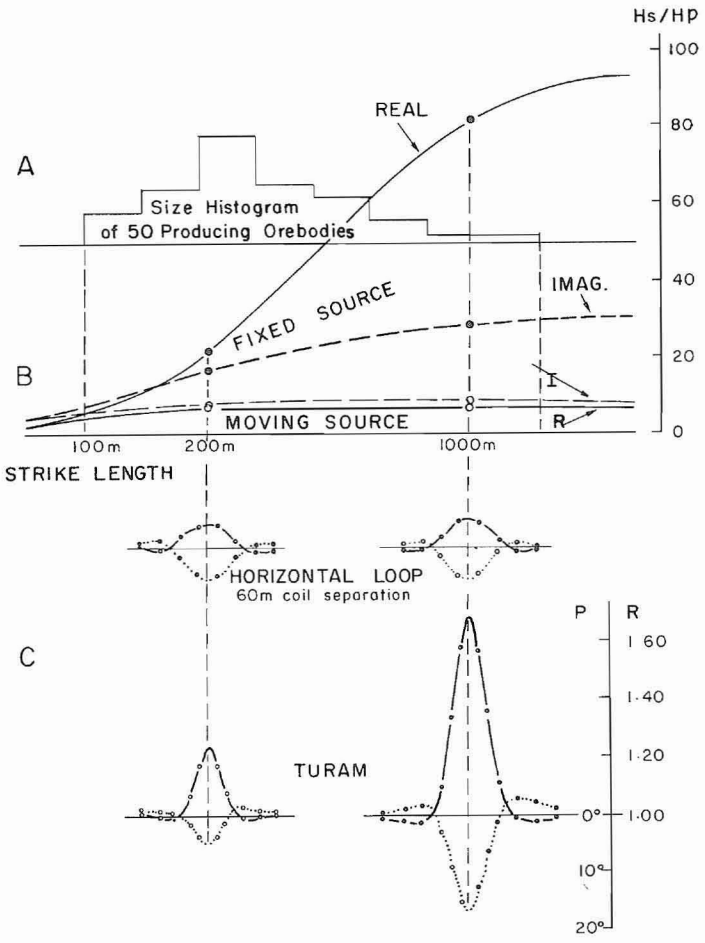


Figure 11. The effect of size variation in moving-source and fixed-source configurations.

Figure 12. Composite Argand diagram incorporating size variation in fixed-source systems.

response from finite sheet to half plane is illustrated in Figure 11. It differs from variation of the induction parameter mainly in the behaviour of the imaginary component, which instead of declining after reaching a maximum value, increases with larger size, to asymptotically reach the half plane response (Bosschart, 1964).

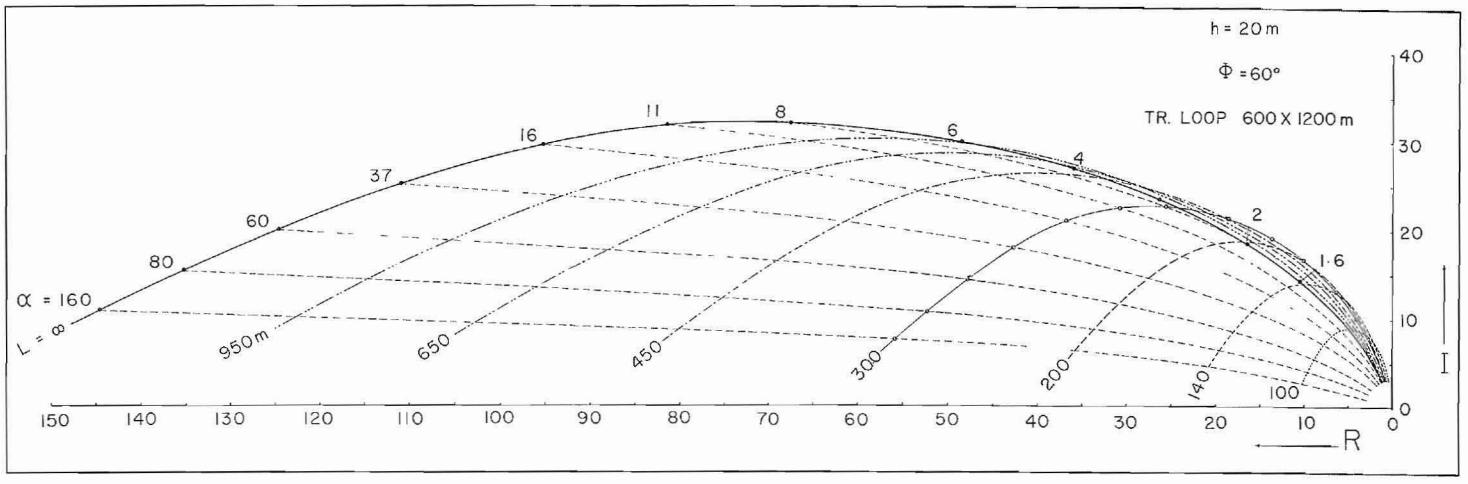
Varying the energizing loop size, though somewhat more cumbersome than varying the *T-R* separation in a moving source system, is a technique which may be effectively used in fixed-source surveys to enhance the signal-to-noise ratio in the presence of conductive overburden.

The derivation of σt is complicated because sulphide deposits in the usual fixed-source configuration almost invariably appear as finite bodies and the resulting variable size factor cannot simply be incorporated in the response parameter, but requires a separate reduction treatment. The single Argand diagram for a half plane response is inadequate. Composite diagrams, built up from individual diagrams for a series of finite sizes, can be used instead (Bosschart, 1964) (Figure 12).

The results obtained with orientation measuring systems are represented in Figure 9 by the amplitude curve. When a single frequency and constant separation are employed the results are dependent on σ and t as well as on size and geometric factors. Only by employing a second, well separated frequency (1:4 at least) can the effects of size and geometry be eliminated and an estimate of σt made. Varying ρ should achieve similar results, but in practice this is not possible without simultaneously varying a number of other factors, because measurements are taken along the strike extension rather than at right angles. It is generally more difficult to obtain quantitative information from orientation measuring data, also because measurements in the most diagnostic part of the curves are less accurate because of the presence of field ellipticity.

In time-domain measurements the full response of the total conductor array is essentially available and the system can be focussed on any part of it simply by selecting the right time intervals to sample, or the right periods to integrate the transient response (Dolan and McLaughlin, 1966; McLaughlin, 1967; Velikin and Bulgakov, 1967).

The conductor characteristics are separated on the basis of elapsed time, which corresponds to decreasing frequency. A basis for interpretation can be obtained from model experiments or



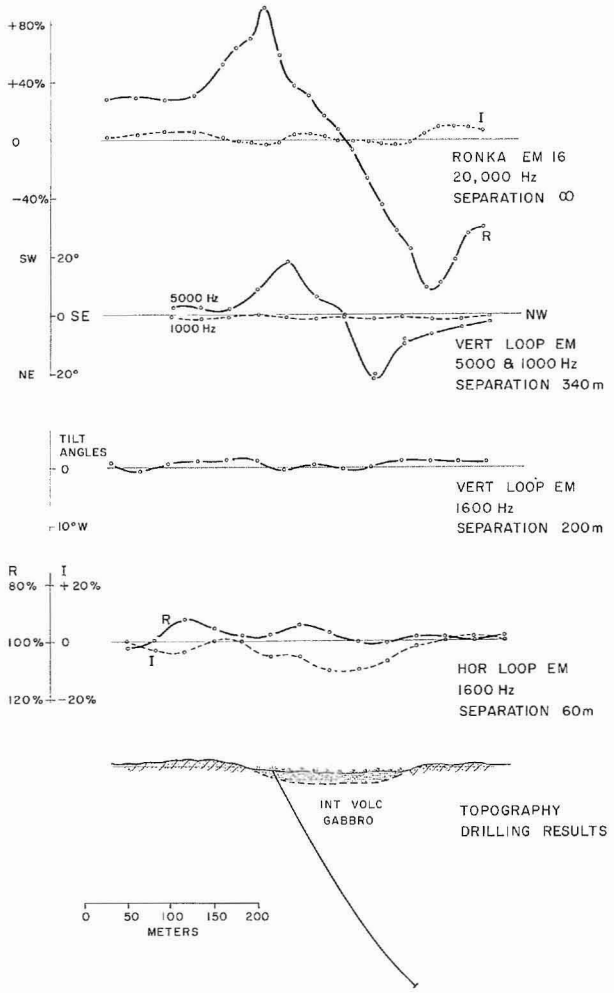


Figure 13. Operating parameter $\omega\rho$ and geological noise.

calculated from the harmonic response of equivalent systems by the Fourier transform. Since measurements are taken in zero primary field no coupling problems between transmitter and receiver need be considered. The coil separation ρ has nevertheless sufficient effect on the response to distinguish between near-surface and deep conductors. By varying ρ the response of the former will change as a result of the scale changes, while the response of the deeper conductors will remain relatively unaffected (Dolan and McLaughlin, 1966).

Evaluation and comparison

Ground electromagnetic methods can be evaluated objectively on their potential capabilities only. Unlike passive geophysical methods which measure a permanent field distribution, human judgment in the approach to the search problem determines to a large extent the end result of electromagnetic surveys. Case history therefore forms an inadequate and sometimes misleading basis for a comparison between methods.

Most frequently a choice will have to be made among the standard methods. Cases where any of the special methods are applicable will be fewer and easier to assess.

Standard methods

Orientation measuring systems. The technique employed in orientation systems, i.e., measuring the direction of the total field or its components by means of a null configuration, combines major advantages in operational efficiency with limited capabilities. The latter partly result from the insufficiency of null configurations to measure in elliptically polarized fields. The plane of the receiving coil, when it is in a position of minimum induction, contains the total field vector, or, when phase shifted secondary fields are present, the major axis of the polarization ellipse (Grant and West, 1965). With increasing ellipticity the null position widens and the measurements begin to lose definition. Accurate observations require a σt separation of signal and noise of two orders of magnitude or more, as well as proper matching between the conductor array and the operating parameter ω and ρ so that the geological noise is kept in an area of low amplitude and the signal in an area of reduced phase angle, to avoid elliptical polarization (Figure 9). The same conditions, of course, also result in the best potential depth penetration. Extending $\omega\rho$ above its optimum value results in increased geological noise, arising from the poorly conducting portion of the conductor array, while field ellipticity may remain quite noticeable. With a further increase of $\omega\rho$ the intensity (curve A) will increase to saturation, but the field ellipticity will decrease and disappear (curve φ). This happens where the response of the total conductor array approaches the inductive limit. It is one of the main, but least recognized problems in the application of tilt-angle methods, and the cause of many disappointing results, that so many surveys are unknowingly carried out with too large $\omega\rho$ values. The sensitivity of the null configuration receivers, particularly when high frequencies are used, permits large separations, and large separations are generally assumed to result in great penetration. The lack of field ellipticity gives the operator a deceptive feeling of security and for the unaware there is no indication that the survey is out of focus. This problem is illustrated in Figure 13, which shows a series of four electromagnetic profiles, three with a tilt-angle system, representing the same traverse. From top to bottom $\omega\rho$ decreases from infinity to 1×10^5. The anomaly, very pronounced above $\omega\rho \approx 10^6$, begins to disappear at lower values. The horizontal loop data finally confirm the presence of a flat-lying poor conductor ($\sigma t \approx 2$). The bottom profile presents the topographic section and a 300 m barren hole drilled in the mistaken belief that the strong anomalies obtained in the two top traverses were the result of deeper penetration.

Significant results and large penetration can be obtained with large $\omega\rho$ values only if the cover is virtually non-conducting, which may well be considered the exception. An example is shown in Figure 14, where $\omega\rho$ varies from .5 to 2.5×10^6 and a penetration of 100 m was obtained. The cover is glacier ice.

As stated earlier, qualitative interpretation is generally ambiguous and rules of thumb have to be applied with restraint. They are often employed in determining depth, and Figure 15 is an example of the ambiguity that can at times be expected. Both profiles were obtained from bodies under the same thickness of overburden: in 15(b) a wide zone of massive sulphides, in 15(a) a zone of disseminated mineralization of the same width. The curve shapes mainly reflect conductivity. The distance between maxima would give a good approximation of the depth in Figure 15(b) but almost twice the true depth in 15(a).

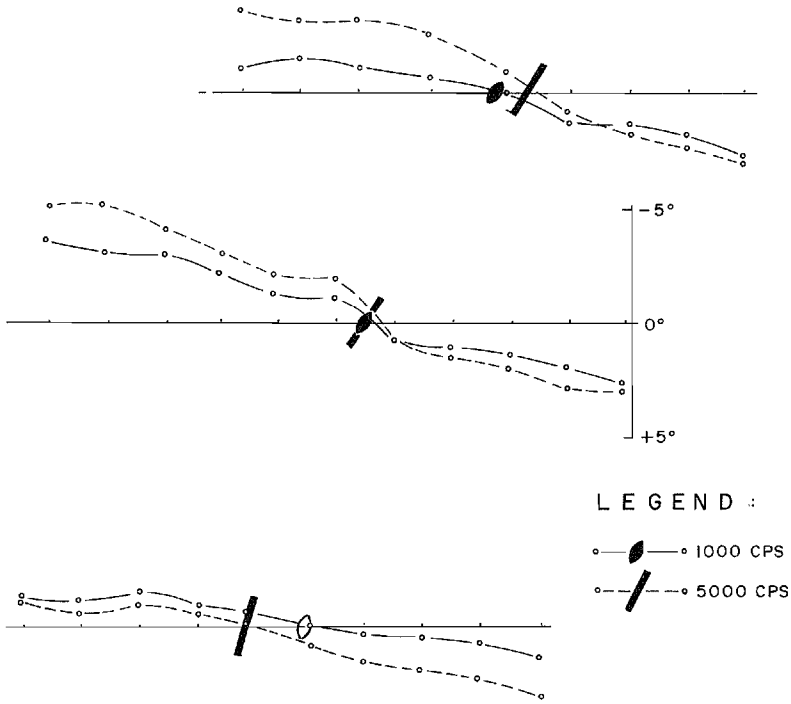


Figure 14. Two-frequency vertical loop response of a massive sulphide body under 100 m glacier ice.

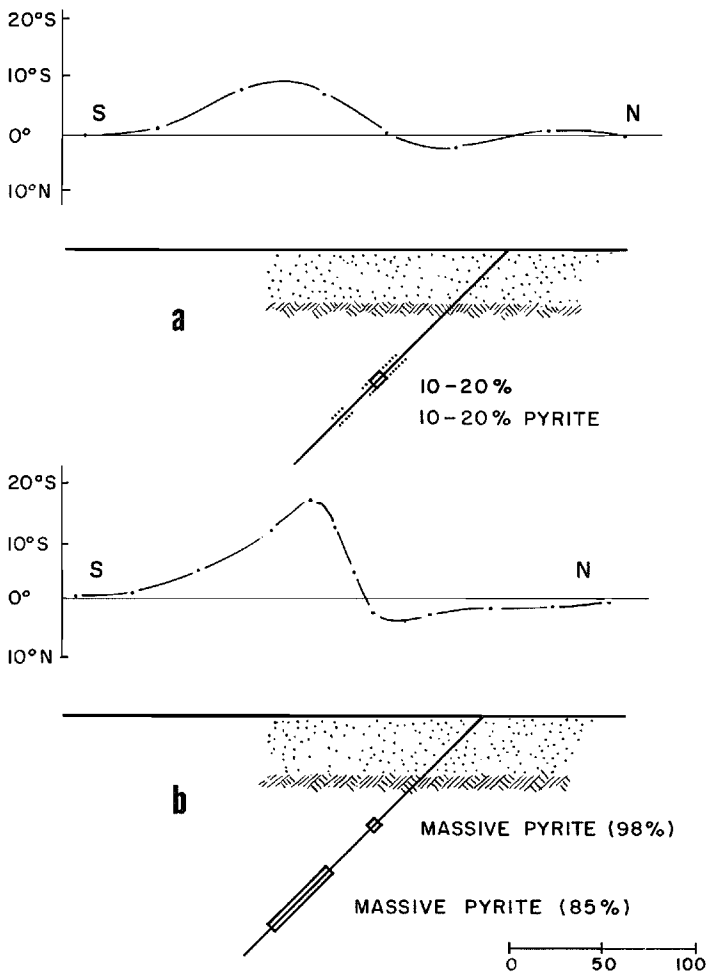
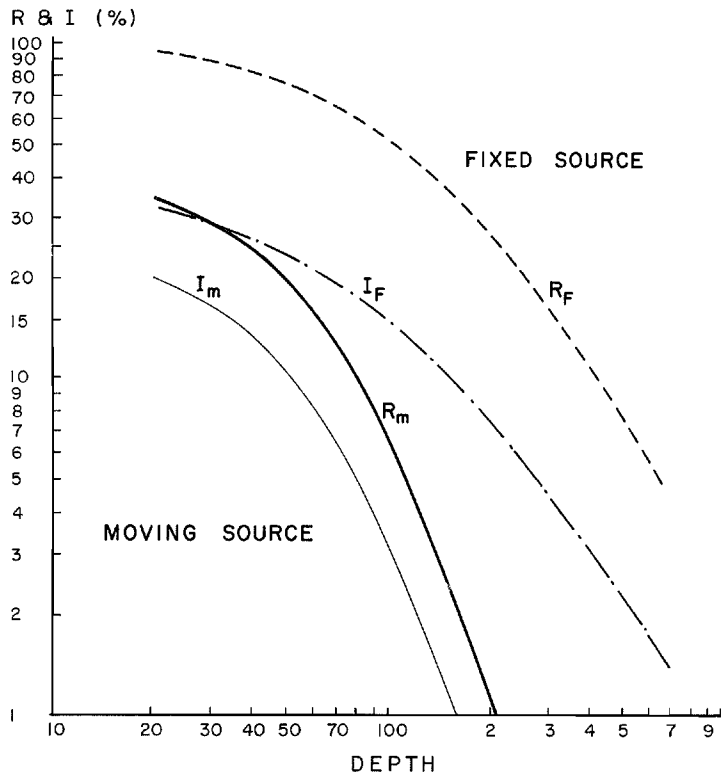


Figure 15. Effect of conductivity on vertical loop response.

Figure 16. Variation of the response with depth of a thin tabular conductor in a moving-source and in a fixed-source configuration.



In the proper application of tilt-angle methods the emphasis should be an operational efficiency. The cutting of grid lines in dense vegetation is time consuming and the cost is often as high as the cost of the subsequent geophysical survey. Particularly in following up airborne surveys, where the main problem is to determine the location of conductors whose relative significance has already been assessed in the interpretation of the airborne data, orientation measuring methods are preferred electromagnetic tools.

Moving-source methods. In many respects, moving-source, compensation methods present the best approach in the search for ore deposits. Profiling perpendicular to the strike of the formations with horizontal coils assures efficient coverage as well as good coupling with bodies in any probable geometrical relation. Transmitter and receiver positions are interchangeable and the scale of the configuration can easily be varied. Although the standard configuration, with coils horizontal, would not seem the best geometry for ore prospecting because of the high coupling with near-surface horizontal conductors, this drawback can at least partly be overcome by a judicious choice of $\omega\rho$. Moreover, the standard coil separations of 60 to 100 m generally result in the most favourable relation between the dimensions of measuring configuration, average target conductors and sources of geological noise. The major limiting factor in ground applications is the practical difficulty of maintaining a constant distance and coil configuration. Under average conditions operational noise limits the potential penetration to little more than half the coil separation. Topographic relief rapidly reduces the signal-to-noise ratio to the point of entirely vitiating the effectiveness of these prospecting systems.

The freedom of varying ω and ρ is restricted. Separations larger than 100 m are possible but hardly practical in average terrain because of the long connecting cable. To keep $\omega\rho$ at reasonable values the frequency has to be reduced in proportion to any separation increase. This means increasing the transmitting power with approximately the 4th power of the separation, and therefore increasing weight. Increasing the separation while keeping $\omega\rho$ constant will result in more penetration, but also in a concurrent loss in resolution. Which is more important depends on the individual search problem. Present instrumentation seems to cover the useful range of $\omega\rho$ variation adequately and the useful application of moving-source compensation methods in their present form, i.e., with their inherent dependency on coil distance and orientation, is restricted to relatively shallow investigation in areas of moderate topographic relief. Properly focussed, these methods yield easily interpretable results of excellent diagnostic quality (Bosschart, 1961; Grant and West, 1965; Parasnis, 1962).

Cut and chained grid lines are a necessity. Otherwise the rate of coverage is high and the operational efficiency can be considered good.

Fixed-source methods. The use of large fixed sources is a burden necessitated by conditions which cannot be negotiated with moving-source techniques. Some of the more obvious inconveniences are additional weight, extra fieldwork, restriction of mobility, directional energization, complication of data reduction and interpretation.

These disadvantages are nevertheless in many cases outweighed by two factors: greater potential depth penetration and independence of topographic relief.

The greater penetration of fixed-source methods is related to the different scale; measurements are taken in an area where the rate of fall-off of the primary and secondary fields varies between the inverse first and second powers.* Combined with the inherent size sensitivity and low instrumental and operational noise levels this may give, for example, the Turam method a potential penetration well over 200 m under average conditions. Figure 16 shows a comparison between the rate of fall-off of a moving source system (horizontal loop, 60 m separation) and a Turam system over a steeply dipping tabular conductor of $\alpha = 18$ and a strike length of 300 m.

The rate of fall-off of peak anomaly amplitude with depth for the fixed-source configuration is less than 2nd power to a depth of 200 m and the in-phase response at that depth is about 6%, clearly detectable above the normal noise level, which, other things being equal, is considerably lower than for the moving-source system. The rate of fall-off for the latter configuration increases from the 3rd to the 5th power between 30 and 60 m depth, while the in-phase response falls from 6% to 1% over the same range. With a 2% assumed noise level the anomaly is detectable to 36 m.

The significance of size sensitivity is illustrated by Figure 11. Between a strike length increase from 150 to 1000 m, which covers most of the range of base-metal target conductors, the moving-source response does not change appreciably, whereas the fixed-source response increases some five times. In other words, in the average search problem, target size has a negligible effect on the detectability in a standard moving-source configuration, but contributes materially to detectability in a fixed-source system. The larger the body, the greater the depth at which it will be detectable.

The observations are virtually independent of topographic relief because they are made in a constant field distribution. Particularly with gradient measurements the precise location of the coils and their separation have little effect on the results, except in very steep gradients, for instance close to the source. If required, corrections can easily be made. Figure 17 is an example of Turam field results obtained under conditions of severe topographic relief in corrected and uncorrected form. The discrepancies between the two sets of data are insignificant.

For a number of reasons, for instance the directionality of the energization, resolution and data quality depend more than in other methods upon the astuteness of the geophysicist and the interpretation is complicated by the necessity to treat more target conductors as finite bodies. Focussing has to be accomplished mainly by means of the frequency. An accurate determination of σt can be derived from the results (if obtained with purely inductive energization) as well as unambiguous determinations of current concentration depths, which are not obtainable with directional or moving source methods.

As to operational efficiency, cut and chained grids are a necessity and the rate of coverage per man day is lower than for the other standard methods.

*It should be noted here that the penetration is, contrary to often expressed beliefs, not related to the T-R separation, i.e., it is not appreciably different whether close to, or far away from the transmitting loop, within the range normally covered in these surveys (Bosschart, 1964).

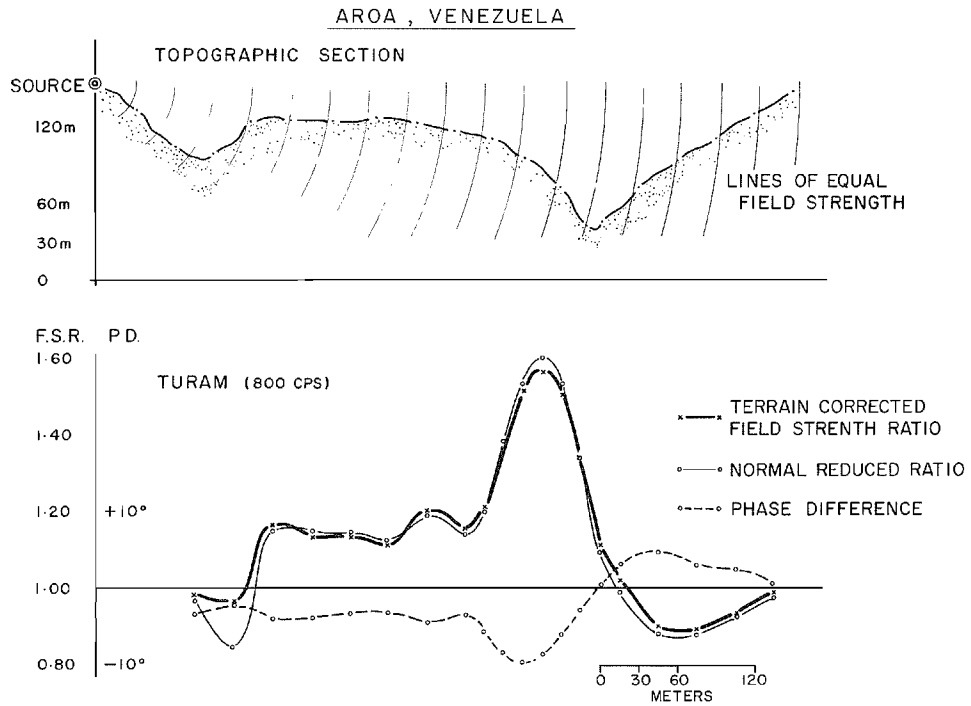


Figure 17. Effect of topographic relief on Turam measurements.

The comparison of the standard methods can be summarized in very general terms as follows:

1. The tilt-angle method is most suitable in reconnaissance and ground follow-up surveys where a minimum of quantitative information is required (e.g., when the targets have been screened on the basis of the airborne response) and mobility and efficiency are of the essence. It is less suitable for systematic coverage, where the lack of selectivity and of quantitative information are more of a disadvantage.

2. The horizontal loop method is particularly well suited for systematic surveys in areas of shallow overburden and low topographic relief where a high degree of selectivity is required.

3. The Turam method has to be resorted to for systematic investigations where conditions of heavy overburden or severe topographic relief prevail.

Special methods. The specific purpose of the different special methods is usually sufficiently clear to leave no doubt when or where they are to be used. The compensator and radio-reference methods, as well as time-domain methods have been successfully employed in problems beyond the capabilities of the standard methods, for instance where overburdens of high conductivity and great thickness covered the target conductors. Where the geometry precluded the induction of sufficiently strong eddy currents in the target conductors, methods using galvanic energization have proved useful. Usually these special methods have a low operational efficiency.

On the other side of the scale the VLF radiofrequency methods have a narrow area of special usefulness. In the rare areas where the ratio of target conductors to sources of geological noise is very high these methods have advantages over other methods because of their ability to detect mineralization of almost any concentration (as long as there is some conductivity the response is otherwise virtually independent of it) and because of their high operational efficiency. Since $\omega\rho$ is infinite, this applies only in a truly neutral geoelectrical environment (Pritchett, 1952), which, of course, requires exceptional geological conditions. Under average conditions these methods see little else than geological noise because the response is near saturation and the system far out of focus for mineral prospecting. A typical example of the results that may be obtained in a Precambrian environment is shown in Figure 13.

Cases have been encountered where the presence of a steeply dipping sulphide conductor under conducting overburden apparently gave rise to distortion in the imaginary component, and this has been proposed as evidence that the system would produce a characteristic and diagnostic response over mineralized bodies. This observation could be explained as follows: The induced current in the steeply dipping conductor will be in phase with the transmitted field, independent of the conductivity σ, because the response is governed by an infinite $\omega\rho$. However the path from the secondary source to the receiver is comparatively short; here ρ becomes very small and as a result, the response may move far enough in the direction of the resistive limit to become appreciably phase-shifted (Figure 9). Thus, any phase shift observed from the surface would then relate to the cover, and not to the underlying conductor, i.e., all it would take is any secondary current source somewhere under a slightly conducting cover to produce an imaginary component. Other things being equal, the latter will be the same, independent of whether the source is a good or a poor conductor. Traditionally, however, proponents of radiofrequency exploration methods favour rather esoteric explanations over interpretation based on extrapolated hard theory. (Pritchett, 1952, and discussions).

Drill-hole methods. Very similar considerations to those applied to surface methods relate to drill-hole methods. One important difference is that the unconsolidated cover can be neglected.

Tilt-angle methods will generally provide the least diagnostic information, moving-source methods the best resolution and most diagnostic information combined with the least penetration and no directionality. Fixed-source compensation methods will in most cases be the best compromise. All suffer equally from the presence of conductive material, even the smallest stringers, in or near the hole. The close proximity of the receiver to such minor conductors will give rise to high noise levels. All drill-hole methods yield the best results in barren holes. Because overburden masking is not a factor, higher $\omega\rho$ values can be used. Nevertheless, very high values, such as are characteristic in radio-reference methods, drastically lower the diagnostic value of the results.

In general, information obtained from electromagnetic drill-hole methods tends to be more ambiguous than the results of comparable surface methods.

Conclusion

Few basic changes or additions have been made to ground electromagnetic methods during the last three decades. Instrumental improvements, in step with electronic developments, have mainly resulted in improved reliability and portability. The most significant advances have been made in the interpretation of field data and in the understanding of the abilities and limitations of the different systems. Mostly for these latter reasons the effectiveness of ground electromagnetic surveys has materially improved in recent years.

One might well ask whether any substantial improvements or changes can be expected in the future. To extend the variation of the operational parameters beyond the ranges we can now cover does not seem to represent a substantial improvement. The presently attainable ranges are adequate to optimize the different systems for most search problems. Only a further lowering of the $\omega\rho$ range would help in some cases.

No truly valuable improvements in directional systems are envisaged. Neither do major improvements in fixed-source methods seem likely. Some further gain in portability may be made by sacrificing primary field strength and increasing receiver sensitivity. However, this process tends to render a system more vulnerable to external noise and unfortunately the latter increases with advancing civilization.

Perhaps the most immediate contribution to our present prospecting capabilities would be the lowering of the noise level of moving-source ground methods by reducing their dependency on coil separation and orientation. In this direction a significant gain in penetration could be achieved without losing resolution and without having to resort to unwieldy large coil separations.

Time-domain methods probably have the best potential for improving ground surveying in the future, because of the much greater range of information that can be obtained and because the taking of measurements in the absence of the exciting field permits greater geometric flexibility and is conducive to lower noise levels. At their present state of development these methods have a rather low operational efficiency and are economically unattractive.

Far-reaching improvements in frequency-domain methods can be expected from recent advances in electronic technology, which could bring the information obtainable with these methods at least on par with time-domain results. New techniques such as digital filtering and phase locking, as well as the feasibility to include elaborate computer circuitry in small packages, are creating entirely new means to separate signal and noise and record multiple channels of information. These techniques may enable us to monitor the response of the entire conductor array and select from it whatever information will be relevant to a specific prospecting problem.

To what extent these new developments will ultimately be incorporated in ground systems seems uncertain. The role of the latter is changing. Light airborne methods are increasingly replacing ground methods in the larger systematic surveys.

For the time being local detailed investigations and follow-up surveys on airborne anomalies may remain the exclusive domain of the hand-carried instrument and warrant its further sophistication.

Increased accuracy in the location of targets from the air may soon render it possible to entirely forego the geophysical ground phase in large-scale surveys and leave electromagnetic ground methods exclusively as tools for the investigation of local problems. A considerable shift in emphasis away from our present standard methods and toward special methods could result from such a development.

References

Barringer, A.R., 1963. The use of audio- and radiofrequency pulses for terrain sensing. The University of Michigan, Ann Arbor, *Proc. Second Symp. on Remote Sensing of Environment,* p. 201 - 214.

Boniwell, J.B., 1967. Some recent results with the INPUT airborne EM system. *Trans. CIMM.* 52: 60 - 67.

Bosschart, R.A., 1961. On the occurrence of low-resistivity geological conductors. *Geophys. Pros.* 9 (2): 203 - 212.

Bosschart, R.A., 1964. Analytical interpretation of fixed source electromagnetic prospecting data. Thesis, U. of Delft, 102 pp.

Bosschart, R.A., and H.O. Seigel, 1966. Some aspects of the Turam electromagnetic method. *Trans. CIMM.* LXIX: 156 - 161.

Braekken, H., 1964. The cross-ring system. *Geoexploration.* 2 (1): 36 - 50.

Brant, A.A., W.M. Dolan, and C.L. Elliot, 1966. Coplanar and coaxial EM tests in Bathurst area, New Brunswick, Canada, 1956. *Mining Geophysics.* I, Tulsa, Society of Exploration Geophysicists.

Dolan, W.M., and G.H. McLaughlin, 1966. Time-domain electromagnetic induction method and apparatus for detection of massive sulphide orebodies. Canadian Patent No. 748,548, Dec. 13, 1966.

Frischknecht, F.C., 1959. Scandinavian electromagnetic prospecting. *Trans. AIME.* 214.

Grant, F.S., and G.F. West, 1965. *Interpretation theory in applied geophysics.* New York, McGraw-Hill Book Co., 583 pp.

Hedstrom, E.H., 1937. Phase measurements in electrical prospecting. AIME Techn. publ. 827.

Hedstrom, E.H., and D.S. Parasnis, 1958. Some model experiments relating to electromagnetic prospecting with special reference to airborne work. *Geophys. Prosp.* 6 (4): 322 - 341.

Keller, G.V., and F.C. Frischknecht, 1966. *Electrical methods in geophysical prospecting.* New York, Pergamon Press, 517 pp.

McLaughlin, G.H., 1967. Developments in EM instrumentation. UNO Seminar, Moscow.

Parasnis, D.S., 1962. *Principles of applied geophysics.* London, Methuen; New York, Wiley, 176 pp.

Parasnis, D.S., 1966. *Mining geophysics,* Amsterdam, Elsevier, 356 pp.

Parasnis, D.S., 1966. Electromagnetic Prospecting C-W Techniques. *Geoexploration.* 4 (4): 177 - 208.

Pritchett, W.C., 1952. Attenuation of radiofrequency waves through the Earth. *Geophysics.* 17(2): 193 - 217.

Sundberg, K., 1931. Principles of the Swedish geo-electrical methods. *Erganzungshefte angew. Geophys.* I.

Sundberg, K., and E.H. Hedstrom, 1933. Structural investigations by electromagnetic methods. World Petroleum Congress.

Tornquist, G., and R.A. Bosschart, 1958. Some recent results of geoelectrical prospecting in Sweden. *Geoph. Surv. in Min., Hydr. and Eng. Proj.* The Hague: 20 - 31.

Velikin, A.B., and Ju.I. Bulgakov, 1967. Transient method of electrical prospecting (one-loop version). UNO Seminar, Moscow.

Wait, J.R., 1954. Mutual coupling of loops lying on the ground. *Geophysics.* 19 (2): 290 - 296.

Wait, J.R., 1960. Some solutions for electromagnetic problems involving spheroidal, spherical and cylindrical bodies. *J. Res. Natl. Bur. Standards.* B64: 15 - 32.

Ward, S.H., 1959. Unique determination of conductivity, susceptibility, size and depth in multifrequency electromagnetic exploration. *Geophysics.* 24: 531 - 546.

Ward, S.H., 1967. The electromagnetic method. *Mining Geophysics.* II, Tulsa, Society of Exploration Geophysicists: 224 - 372.

Werner, S., 1958. Geophysical history of a deep-seated pyritic orebody in northern Sweden. *Geophysical Surveys in Mining, Hydrological and Engineering Projects.* European Assoc. Exploration Geophysicists. The Hague: 3 - 19.

West, G.F., 1960. Quantitative interpretation of electromagnetic prospecting measurements. Ph.D. thesis, University of Toronto.

Airborne electromagnetic methods

Stanley H. Ward

University of California
Berkeley, California, U.S.A.

Abstract. Many different airborne electromagnetic systems for operation from both fixed-wing aircraft and from helicopters have been developed in the last twenty years. The physical basis of all such systems is described in detail. Eighteen systems are classified on the basis of coil configuration and method of operation. A listing of factors in the design of AEM systems is amplified by a detailed discussion of system noise, geologic noise, and the separation of message from noise. The presentation of interpretational schemes and short catalogues of type curves for frequency-domain and time-domain systems facilitate a rigorous discussion of the relative merits of many AEM systems according to seven criteria.

Anticipated future developments include: (1) multicomponent, multifrequency, and multiphase systems, (2) digital data acquisition, (3) automatic interpretation via computer, extension of the frequency range, and finally the inductive measurement of induced electrical polarization.

Résumé. De nombreux systèmes électromagnétiques aéroportés, utilisables tant à bord d'avions que d'hélicoptères, ont vu le jour au cours de ces vingt dernières années. L'auteur fournit ici la description détaillée de la base physique de tout ces systèmes. Leur classification d'après la configuration du bobinage et le mode opératoire permet d'en dénombrer dix-huit. Une étude détaillée du bruit du système, du bruit géologique, et de la séparation du signal et du bruit, vient s'ajouter à l'énumération des facteurs dont dépend la configuration des appareils pour MEA. La présentation de schémas d'interprétation et de catalogues de courbes types pour les systèmes dont le principe est basé sur la fréquence ou sur le temps, facilite une étude rigoureuse des mérites relatifs d'un grand nombre de ces systèmes en fonction de sept critères.

Le développement qu'il est possible de prévoir comprend: (1) la mise au point de systèmes à composantes multiples, fréquences multiples et phases multiples; (2) L'enregistrement de données numériques; (3) l'interprétation automatique au moyen d'ordinateurs, l'élargissement de la gamme des fréquences, enfin, la mesure inductive de la polarisation électrique provoquée.

The objective of this paper is to review modern airborne electromagnetic techniques as applied to mining and groundwater exploration. Since many different airborne electromagnetic (AEM) techniques have arisen since their introduction in 1950, it is expedient to set down the general basis of inductive AEM systems, to discuss the problems arising in their design, to classify and compare the known operating systems, to illustrate the procedures for interpretation of the resulting data, and finally to indicate the areas in which improvements of AEM systems are being or can be made.

For previous general surveys of AEM systems the reader is referred to articles by Pemberton (1962); Grant and West (1965); Keller and Frischknecht (1966); Parasnis (1966); and Ward (1967). Many articles illustrating specific systems have also appeared in the literature, including those by Slichter (1955); Ward (1957); Hedstrom and Parasnis (1958); Tornquist (1958); Ward and Barker (1958); Cheriton (1959); Hedstrom and Parasnis (1959); Paterson (1959); Tikhonov and Dmitriev (1959a,b); Ward (1959a,b); Fleming and Brooks (1960); Joklik (1960); MacKay and Paterson (1960); Mizyuk (1960); Ward (1960); Boyd and Roberts (1961); Khomenyuk (1961); Paterson (1961a,b); Pemberton (1961a,b); Schaub (1961a,b); Rattew (1962); Schaub (1962a,b,c); Wieduwilt (1962); Barringer (1963); Guar (1963); Geleynse and Barringer (1964); Collett (1966); Brant, *et al.* (1966); Paterson (1966); Podolsky (1966); Schaub (1966a,b); Ward, *et al.* (1966); White (1966); Boniwell (1967); and Ward, *et al.* (1968a).

Active electromagnetic techniques may be classified as inductive if current is induced in the subsurface by a transmitter consisting of an energized coil of wire, or as conductive if current is transferred to the ground by a long energized cable grounded at both ends. The discussion in this paper will be restricted to inductive methods since practically all modern AEM systems are of this type. AFMAG is the only passive AEM system currently in use and it should be classed with the active inductive systems.

The first successful inductive AEM system was placed in operation in 1950, but intensive and extensive use of such devices by more than one company was delayed until mid-1955 (Pemberton, 1962). These developments were pioneered by McPhar Engineering Co. of Canada Ltd. who, with the technical staff of The International Nickel Company of Canada Ltd., developed the first system. Dozens of systems have appeared since 1950 and indications forecast a completely new era of development of such systems.

Until 1965, the use of AEM systems was confined largely to the search for base-metal ore deposits. However, progress has been made in applying one system to the delineation of aquifers in unconsolidated sediments (Collett, 1966; Boniwell, 1967). For mining or hydrological purposes we can state that the primary application of AEM systems is the rapid mapping of shallow conductors of electricity such as graphitic schists, carbonaceous sediments, fault and shear zones, swamps, clay or clayey gravel overburden, and sulphide mineralization. The possibility exists for AEM mapping of dielectric constant and magnetic permeability as well as electrical conductivity but these objectives have not yet been exploited. AEM systems are used both in direct search for metallic ores and in the indirect search for various ore through the mapping of structure. Normally an AEM system is not designed to respond to rock type as in airborne magnetic surveys. Rather, it is designed to produce discrete anomalies over such conductive media as listed above. It is only when a structure contains anomalously conductive materials that the structure may be mapped because of this association. Reference will be made later to the desirability of generalizing this design concept.

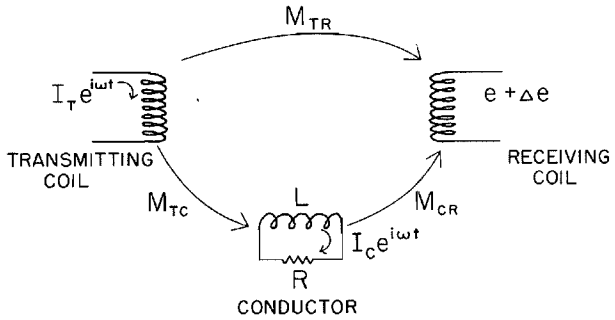


Figure 1. Schematic representation of energy transfer paths and elements of an AEM system in the presence of a conductor.

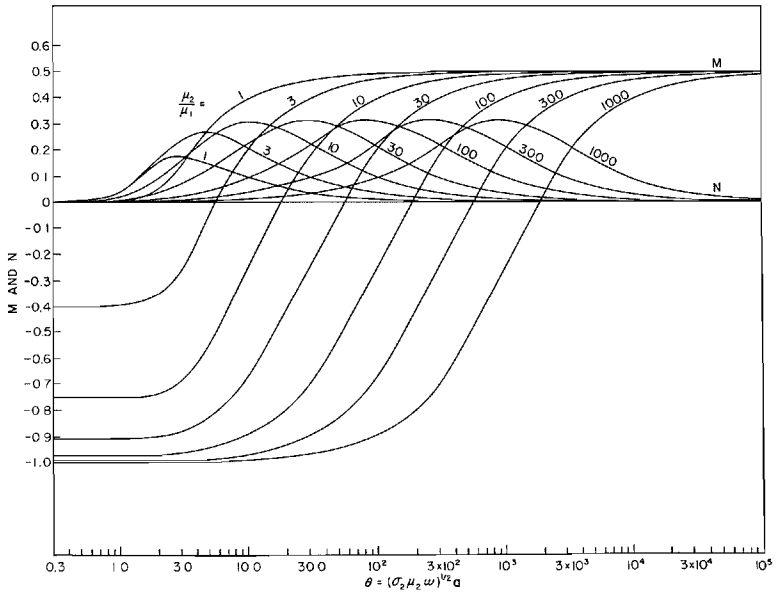


Figure 2. The real M and imaginary N components of the reflection coefficient of a sphere in a uniform alternating magnetic field as functions of the induction number $\theta = (\sigma\mu\omega)^{1/2}\, a$.

The basis of inductive AEM systems

The basic principle of active inductive AEM systems is measurement of the change of the mutual impedance between a pair of wire loops or coils, as this pair is moved relative to a subsurface conductor of electricity. Let us imagine that we can simulate this conductor by a closed circuit containing inductance L and resistance R. Then, referring to Figure 1, energy is transferred from the transmitting coil to the receiving coil via a direct path M_{TR} and indirectly via the subsurface conductor $M_{TC} \rightarrow M_{CR}$. Faraday's law of induction informs us that the voltage e induced directly in the receiving coil by a current $Ie^{i\omega t}$ in the transmitting coil is

$$e = -N_R \frac{d\phi_T}{dt} = -\mu A_R N_R \frac{d\vec{H}_T}{dt} \qquad 1$$

where A_R and N_R are the area and turns, respectively, of the receiving coil, μ is the permeability of the medium in which the coil is placed, ω is the angular frequency and H_T is the intensity of the transmitted alternating magnetic field. Beyond a distance of ten transmitting coil radii, H_T will be dipolar and hence is described by

$$\vec{H}_T = \frac{N_T A_T I_T}{4\pi} \left[\frac{(2x^2 - y^2 - z^2)\vec{i} + 3xy\vec{j} + 3xz\vec{k}}{\rho^5} \right] \qquad 2$$

where $\rho^2 = x^2 + y^2 + z^2$; $\vec{i}$, $\vec{j}$, $\vec{k}$ are unit vectors in the x, y, z directions; and N_T, A_T, I_T are the turns, area, and current of the transmitting coil. The axis of the dipole is in the x direction according to Equation 2. Let us call the quantity in brackets GF since it merely describes the geometry of the field. Then the voltage e induced in the receiving coil is

$$e = -\frac{i\mu\omega}{4\pi} N_T A_T I_T N_R A_R (GF)_{TR} e^{i\omega t} \qquad 3$$

where the subscript TR has been added to GF to indicate that the origin for x, y, z is at the transmitter and that for Equation 3, the values of x, y, z inserted in GF are the coordinates of the receiving coil.

Similarly, a voltage will be induced in the subsurface conductor of Figure 1, here represented in its simplest form by a loop with inductance and resistance. The incremental voltage transferred to the subsurface loop is

$$e^* = -\frac{i\mu\omega}{4\pi} N_T A_T I_T N_C A_C (GF)_{TC} e^{i\omega t} \qquad 4$$

This voltage will cause a current to flow, in the subsurface conductor, the amplitude and phase of which are determined as follows. The voltage drop across the equivalent inductance and resistance of the conductor is

$$e^+ = -RIe^{i\omega t} - L\frac{d}{dt}(Ie^{i\omega t}) = -I(R + i\omega L)e^{i\omega t} \qquad 5$$

and since $e^* + e^+ = 0$, we find

$$I_C = \frac{-i\mu\omega}{4\pi} N_T A_T I_T N_C A_C \frac{(GF)_{TC}}{R + i\omega L} \qquad 6$$

The current I_C causes an incremental voltage to be developed in the receiving coil

$$\Delta e = \frac{-i\mu\omega}{4\pi} N_C A_C I_C N_R A_R (GF)_{CR} e^{i\omega t} \qquad 7$$

Then this incremental voltage, expressed as a fraction of the primary voltage e is

$$\frac{\Delta e}{e} = \frac{1}{4\pi}\left(\frac{-i\mu\omega}{R + i\omega L}\right) N_C^2 A_C^2 \frac{(GF)_{CR}(GF)_{TC}}{(GF)_{TR}} \qquad 8$$

The phase of this ratio then is controlled by the ratio of the equivalent R and L in the subsurface, its amplitude is controlled by the frequency, by the magnitudes of R and L, by the square of the equivalent NA product of the conductor, and by the transmitter-conductor-receiver configuration. The more resistive

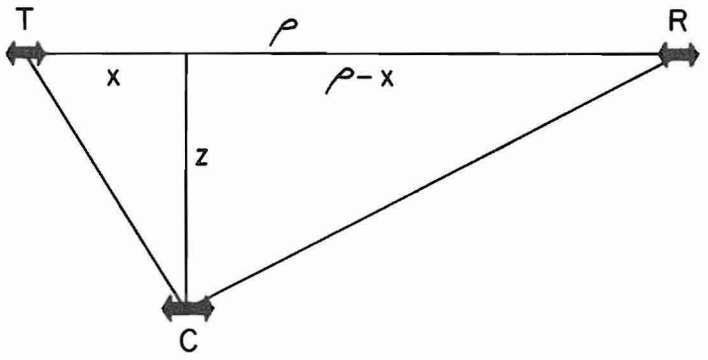


Figure 3. Geometry for a coaxial double dipole system above a small loop whose axis is parallel to the axis of the double dipole system.

the subsurface body, the greater will be the quadrature component; while the larger the conductor, the larger the amplitude of the response.

This small-coil representation of a buried conductor provides the necessary insight into the main factors controlling the response of the conductor to a double dipole prospecting system. For further illustration, the response of a sphere in a uniform alternating magnetic field may be set down as

$$\Delta\vec{H} = H_0\, a^3\,(M + iN)\left[\frac{(2x^2 - y^2 - z^2)\vec{i} + 3xy\vec{j} + 3xz\vec{k}}{\rho^5}\right] \quad 9$$

where H_0 is the amplitude of an inducing field directed along $\vec{i}$; a, σ and μ are the radius, conductivity, and permeability of the sphere; while M and N are the real and imaginary parts of the reflection coefficient of the sphere and each is a function of $\theta = (\sigma\mu\omega)^{1/2}a$. Sketches of M and N are shown as functions of θ in Figure 2. An analogy between the sphere and the small coil of Equation 8 leads to the associations

$$N \longleftrightarrow \frac{-R\omega}{R^2 + \omega^2 L^2} \quad 10$$

$$M \longleftrightarrow \frac{-\omega^2 L}{R^2 + \omega^2 L^2} \quad 11$$

Referring to Figure 3, where we have represented the subsurface conductor by a dipole or small coil of wire, and the transmitting and receiving coils as coaxial dipoles, the geometrical factors appearing in Equation 8 are

$$(GF)_{TR} = \frac{2\vec{i}}{\rho^3} \quad 12$$

$$(GF)_{TC} = \frac{(2x^2 - z^2)\vec{i} + 3xz\vec{k}}{(z^2 + x^2)^{5/2}} \quad 13$$

$$(GF)_{CR} = \frac{[2(\rho - x)^2 - z^2]\,\vec{i} - 3xz\vec{k}}{[z^2 + (\rho - x)^2]^{5/2}} \quad 14$$

Only the x components of Equations 13 and 14 induce voltages in the conductor and receiver, respectively.

From the above discussion we can conclude that measurement of the in-phase and quadrature parts of the normalized incremental voltage, $\Delta e/e$, can provide information on the location, depth, and induction number of the buried conductor.

The mutual impedance between the transmitting and receiving coils in the absence of a subsurface conductor is

$$Z = \frac{e}{I_T} \quad 15$$

while the change in mutual impedance brought about by the conductor is

$$\Delta Z = \frac{\Delta e}{I_T} \quad 16$$

and the normalized change in mutual impedance is then

$$\frac{\Delta Z}{Z} = \frac{\Delta e}{e} \quad 17$$

The quantities given by Equation 17 are dimensionless and hence are measured in parts per million (ppm).

The above formulation has been developed in the frequency domain so that the complex voltage ratio $f(\omega) = \Delta e(\omega)/e(\omega)$ is a function of angular frequency ω. Measurement of the real or imaginary parts of $f(\omega)$ is made continuously at one or more frequencies.

If measurements are to be made in the time domain, a repetitive impulsive source of current is applied to the transmitter and measurements of a function $g^1(t) = \Delta e(t)$ are made during intervals when the transmitter current is off. This function may be normalized by the voltage induced in the receiving coil when the transmitter current is on, i.e., $g(t) = \Delta e(t)/e(t)$ and then a quantity comparable to $f(\omega)$ is obtained with which to study the system. In fact, through Fourier transformation we may extract frequency-domain information from time-domain measurements or vice versa. The transform pair

$$g(t) = \int_{-\infty}^{\infty} g(\omega)\, e^{i\omega t} d\omega \quad 18$$

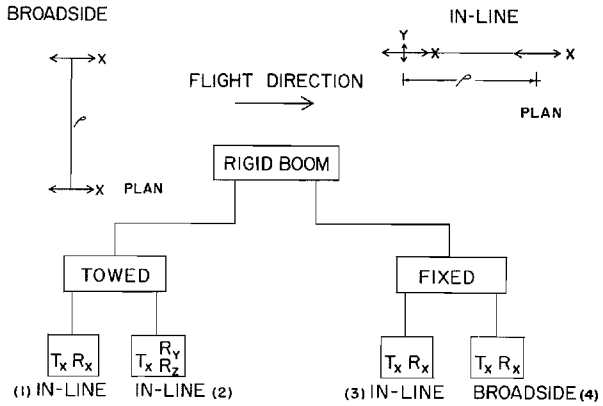
$$g(\omega) = \frac{1}{2\pi}\int_{-\infty}^{\infty} g(t) e^{-i\omega t}\, dt \quad 19$$

permits us to compute the spectrum $g(\omega)$ of the impulsive function $g(t)$.

Factors in the design of AEM systems

The factors which must be considered in the design of an AEM system include: (a) enhancement of message-to-noise ratio, (b) the operating frequency or frequencies in the frequency domain or the times, numbers, and intervals of samples in the time domain, (c) coil configuration, (d) the number of transmitting and receiving coils, (e) measurement of in-phase or quadrature components in frequency-domain systems, (f) the efficiency of search and depth of exploration of the system, (g) the response of the system to the various shapes and orientations of the conductors to be mapped by the system, (h) the geological and topographical environment in which the system is to be used, and (i) the cost of design, engineering, and operation of the system. No one system can be optimal in all respects, and hence any

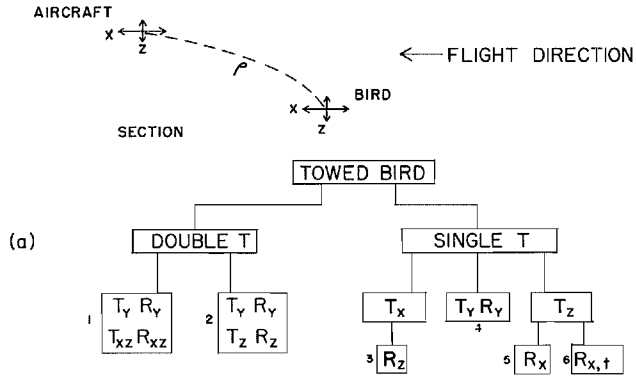
Contents



(b)

TYPE	SYSTEM	AIRCRAFT	COMP	f (Hz)	ρ (Ft / M)	n (PPM)	n_e (PPM)
1	NuCOM	H	I,Q	1000	20/6.1	10	156
	LOCKWOOD	H	I,Q	4000	30/9.1	10	46E
	SCINTREX HEM 701	H	I,Q	1600	30/9.1	3	14
	BARRINGER #1	H	I,Q	400	30/9.1	3	14
	SANDER	H	I,Q	1050	23/7.0	10	97
2	BARRINGER #2	H	I,Q	400	30/9.1	3	14
3	VARIAN-T.G.S	H	I,Q	400	50/15.2	10	10
	NEWMONT-AERO	H	I,Q	390	60/18.3	40	23E
	AERO CANSO	F	I,Q	390	83/25.3	20?	5?
4	AERO OTTER	F	I,Q	320	62/18.9	20	10
	BOLIDEN	F	I,Q	3200	52/15.9	20	18
	SCINTREX / AIRESOURCE	F	I,Q	320	62/18.9	20	10

Figure 4. The classification and characteristics of rigid boom airborne electro-magnetic systems.



(b)

TYPE	SYSTEM	AIRCRAFT	COMP	f (Hz)	ρ (Ft /M)	n(PPM)	n_e(PPM)
1	INCO	F	A/Ø	1800/2000*	500/152	1500	1500
2	ABEM (2 PLANE)	F	A/Ø	880	800/245	3000	1500
3	McPHAR F-400	F	Q	340/1070	400/122	250	500
4	AEROPHYSICS	F	Q	140	500/152	4500	4500E
5	HUNTING (NOW LOCKWOOD)	F	Q	400/2300	500/152	850	850
6	INPUT	F	6 t		500/152	?	<700E

*NOMINAL

Figure 5. The classification and characteristics of towed bird airborne electromagnetic systems.

practical system represents a compromise of the optima for each of the above constraints and others. In subsequent paragraphs we shall attempt to present an evaluation of the above factors as they relate to current and future AEM systems.

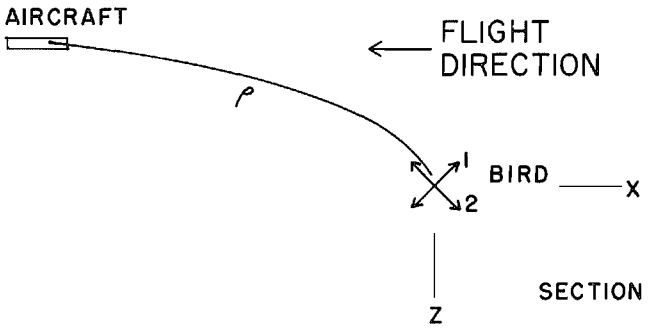
The classification of AEM systems

A basic division of active AEM systems can be made into those in which both the transmitting and receiving coils are rigidly mounted on the airframe, on some structure attached to the airframe, or on a structure towed from the aircraft; and those in which the transmitting coil is fixed to the airframe while the receiving coil is mounted in a 'bird' beneath and behind the aircraft. We shall label these *rigid boom* and *towed bird* systems. Each of these divisions may be further subdivided according to the configurations of transmitting and receiving coils employed. In Figure 4, one possible subdivision of the rigid boom types is given. The letters T and R refer to transmitting coil and receiving coil while the subscripts X, Y, Z refer to the orientation of the axis of the coil; X is the direction of flight and Z is vertical. Rigid boom coil arrays have always been *towed* with the axis of the system parallel to the direction of flight (in-line) but they have been fixed to the airframe with the axis of the system parallel (in-line) or perpendicular (broadside) to the direction of flight. Only two broadside arrays have appeared on the market and in each of these the coils are mounted on special wing tips on a fixed wing (F) aircraft. The in-line arrays have been mounted on fixed-wing aircraft F, mounted on fixed-wing F or helicopter H or towed from a helicopter H.

Also appearing in Figure 4 are the operating frequency f, the coil separation ρ, the published or estimated (E) noise level n, and the noise level reduced to its equivalent for a 50-foot separation n_e on the basis of the requirement for an inverse cube decrease in noise level with reduction in coil separation. An equivalent noise level of order 10 ppm evidently is attainable with rigid boom systems today.

All of the rigid boom systems listed in Figure 4 record both the real and imaginary part of the change in mutual impedance between the transmitting and receiving coils.

A subdivision of towed bird systems is portrayed in Figure 5. At present, towed bird AEM systems employ either one or two transmitting coils. Those which employ two transmitting coils do so to minimize noise and employ matched receiving coils. All three orientations of transmitting coils have been used, usually with a single receiving coil, although one system now employs three receiving coils. Figure 5(b) provides information on the operating frequency f, the coil separation ρ, the noise level n quoted by the manufacturer or estimated (E) by the author, and the equivalent noise level reduced to a 500-foot separation n_e. An equivalent noise level of order 1000 ppm evidently is available for towed bird systems with current technology. The frequency domain systems record either amplitude A, phase ϕ, or quadrature component Q. The only time domain system, INPUT, samples the secondary decay field at 6 times after the termination of the primary field. Figure 5(b) indicates what component or components is recorded by each system.



	AIR CRAFT	COMP	f (Hz)	ρ (Ft/M)	n
AFMAG	F,H	$A(e_1/e_2)$	150/510	200/61	1°

Figure 6. The configuration and characteristics of airborne AFMAG.

In Figure 6 we have indicated the basis of measurement with airborne AFMAG, the only passive inductive AEM system. The fields monitored by this system arise in world-wide atmospheric discharges (sferics) primarily arising in lightning strokes. Two receiving coils are used, each of which is confined to the *X-Z* plane, and the amplitude of the ratio of the voltages in the two coils is monitored at each of two frequencies simultaneously (Ward, *et al.*, 1966; Ward, *et al.*, 1968a).

Descriptions of operating AEM systems

To some extent, Figures 4, 5 and 6 provide descriptions of AEM systems which have been made operational. More detailed information on some systems is contained in a recent article by Ward (1967). The systems described in the latter article are Inco, Hunting Canso, Abem rotary field, Input, Aerophysics Anson, Hunting helicopter, Nucom helicopter, Newmont/Aero helicopter, Varian-TGS, Canadian Aero Canso, Canadian Aero Otter, and AFMAG.

There seems little point in repeating these instrumental descriptions in a review paper of this type in which emphasis is on the fundamentals rather than all of the details of airborne electromagnetic methods.

Sources of noise in AEM systems

The *signal* recorded by an AEM system is the sum, with due regard to phase and amplitude, of *message* and *noise*. Message may be defined as the summation of anomalies due to the targets sought while noise is any other part of the signal. The depth of exploration obtainable with any electromagnetic method is governed by the *message-to-noise* ratio at the receiver. For this purpose we define noise to include:

Instrument noise (a)

1. Thermal agitation noise in the detection coils.
2. Thermal agitation noise in the input circuit of the first amplifier.
3. Noise mechanically induced in the detecting coils. This may include magnetostriction in iron-cored coils, microphonic vibrations and oscillations of the coils in the earth's main magnetic field, oscillations of nearby ferrous or conductive objects in the earth's main field, relative motion between the receiving coil and the airframe, boom, wings, etc., in which eddy currents have been induced by the transmitter, and changes in the effective area of the transmitting or receiving coils.
4. Aircraft engine, electrical, or machinery noise.
5. Thermal drift of the parameters of the transmitting or receiving coils or associated electronics.
6. Mutual impedance changes due to relative rotation between transmitting and receiving coils.
7. Mutual impedance changes due to change in separation between transmitting and receiving coils.

Disturbance field noise (b)

1. Alternating magnetic fields resulting from artificial sources such as power lines, or radio transmission.
2. Alternating magnetic fields resulting from natural sources such as thunderstorms.

Geologic noise (c). The background of minor anomalies of no significance, upon which the significant anomalies are superimposed.

The combination of instrument noise and disturbance field noise is often referred to as the *system* noise since it is the noise which remains if the system is flown at a sufficiently high altitude to be out of the influence of geologic noise. Noise sources (a)1 through (a)4 plus (b)2 must have spectral overlap within the passband, or harmonics of the passband, of the receiver before they will contribute. Noise sources (a)5 through (a)7 plus (c) must have rise times within the rise-time interval of the receiver before they will contribute. To illustrate this last point, the following two examples are given: (a) The thermal drift of an AEM system often is a slowly varying function of time which may be removed by high pass filtering the DC output of the receiver rectifier circuit. (b) Relative motion between transmitting and receiving coils is usually caused by air turbulence and the step-like rise time of this noise source may be minimized by low pass filtering of the DC output of the receiver circuit. Any filtering of the output of the system may destroy some message as well as reduce the noise.

Disturbance field noise is a function of time, space and instrument passband and is beyond the control of the designer. Sufficient power in the transmitter will always provide a message which overrides this noise source, but seldom do we have the freedom to tolerate the weight of equipment to permit this solution. The minimizing of all of the sources of system noise is not easy. Coherent detection devices and active notch filters have permitted a substantial reduction of noise in recent years. Receiving coils are usually parallel tuned because this multiplies any voltage induced in the coil by $Q = \omega L/R$; in this fashion noise sources (a)1 and (a)2 are practically eliminated.

Any maximum-coupled coil system mounted on a rigid boom is effectively free of noise due to relative rotation between the transmitting and receiving coils, since this noise is only proportional to the cosine of the angle of rotation. On the other hand, variation in the separation for maximum coupled systems produces a change in mutual impedance proportional to $3\Delta\rho/\rho$ and for this quantity to be less than 10 ppm on a 50-foot (15.25 m) boom requires that the length of the boom be constant to less than 0.002 inch (0.005 cm). Once again, only boom length changes having rise times within the rise-time interval of the receiver are of importance.

For minimum coupled systems mounted on a rigid boom, the boom shortening is unimportant but the relative rotation between

Contents

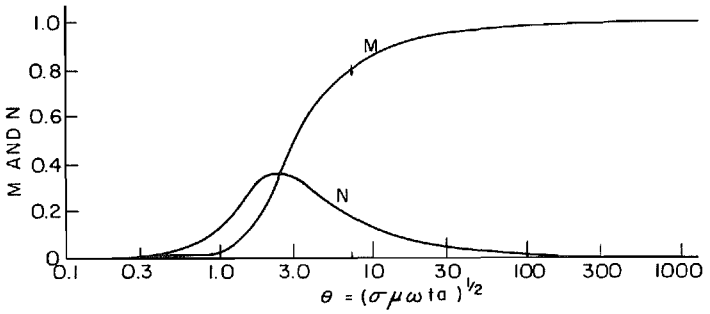


Figure 7. The real M and the imaginary N components of the reflection coefficient of a disk in a normal uniform alternating magnetic field as functions of the induction number $\theta = (\sigma\mu\omega)^{1/2} a$.

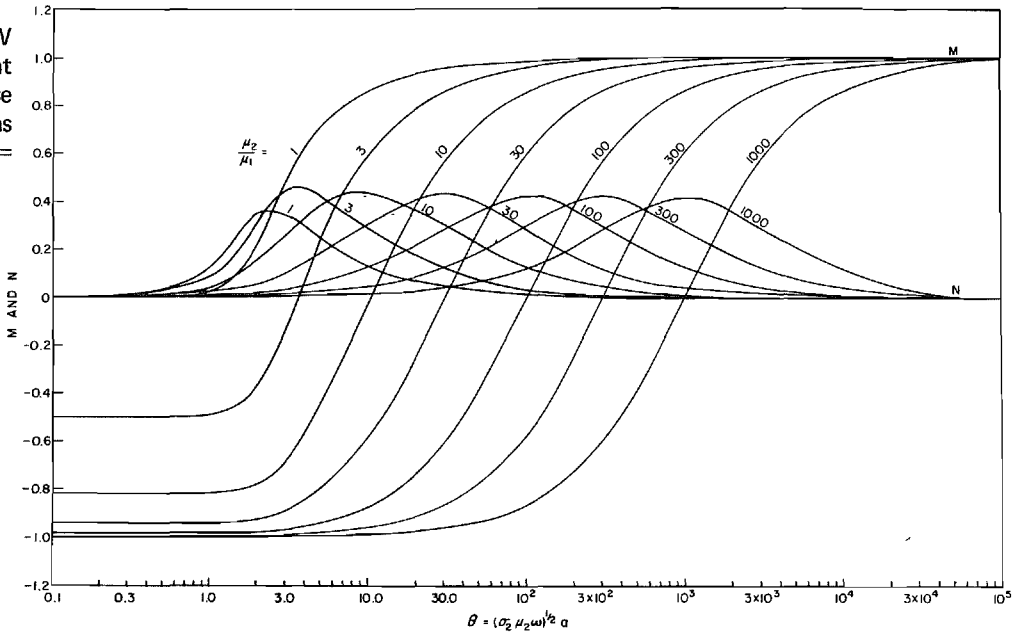
Universal response curves

Figure 2 illustrates the manner in which the real (M) and imaginary (N) parts of the reflection coefficient of a sphere in a uniform field vary with the induction number $[\theta = (\sigma\mu\omega)^{1/2}a]$. Most of the change of the real or imaginary parts of the reflection coefficient occurs for values of θ between 1 and 30, assuming that the permeability of the sphere is equal to that of its surroundings. The induction numbers for various electromagnetic boundary value problems usually may be written in the form

$$\Theta = \sigma\mu\omega L_1 L_2$$

where σ is the electrical conductivity of the model, υ is the magnetic permeability of the model, ω is the angular frequency, while L_1 and L_2 are significant linear dimensions of the problem.

Figure 8. The real M and the imaginary N components of the relection coefficient of a horizontal cylinder in a transverse uniform alternating magnetic field as functions of the induction number $\theta = (\sigma\mu\omega)^{1/2} a$.



the coils now varies as the sine of the angle of rotation. For this noise source to contribute less than 10 ppm, the relative rotation, $\sin\varphi \sim \varphi$, must not be greater than 10^{-5} or 2 seconds of arc with the usual requirements on bandpass.

Geologic noise is a relative term, for what may be message in one search problem may become noise in another. This noise may be of longer or shorter space wavelength than the message, or there may be partial or complete spectral overlap between message and geologic noise. As we shall see subsequently, enhancement of the ratio of message to geologic noise may be effected through judicious choice of the coil separation ρ, the operating frequency f, and the coil configuration employed. Generally, the fixed boom systems produce much less geologic noise than the towed bird systems. While most past systems have been designed with the intent to suppress geologic noise, there is considerable justification for recording all the geologic information and to separate message from geologic noise in the interpretation process. Only the INPUT system has been designed to provide this facility. The use of several sampling times for time domain equipment or of two or more frequencies with frequency domain equipment is essential for separating message from geologic noise in the interpretation process.

The following induction numbers are pertinent in AEM exploration (Ward, 1967):

Sphere, uniform field	$\Theta = \sigma\mu\omega a^2$;	a = radius
Infinite horizontal cylinder, uniform field	$\Theta = \sigma\mu\omega a^2$;	a = radius
Thin disk, uniform field	$\Theta = \sigma\mu\omega ta$;	a = radius t = thickness
AEM systems above a homogeneous earth	$\Theta = \sigma\mu\omega(\rho^2 + h^2)$;	h = height ρ = separation
A half plane or whole plane beneath an AEM system	$\Theta = \sigma\mu\omega t(\rho^2 + h^2)^{1/2}$;	t = thickness ρ = separation h = height

It is convenient to square θ and write the squared quantity as Θ ; the frequency always appears to the first power in the

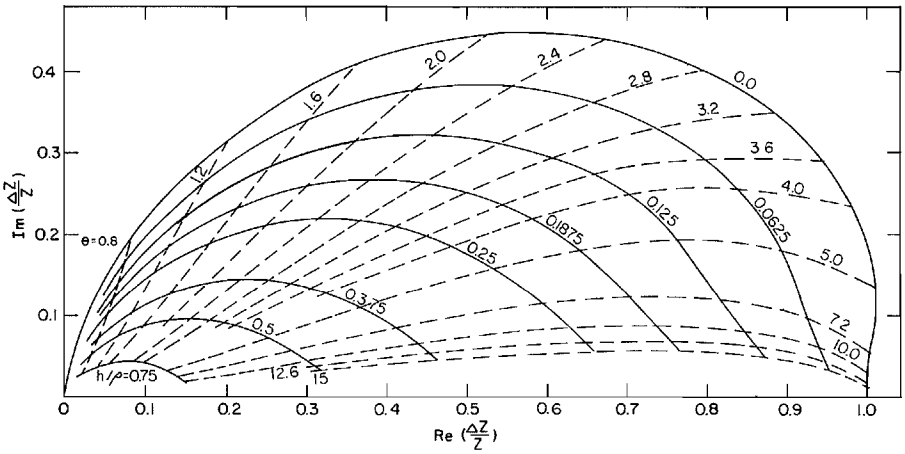


Figure 9. Argand diagram for a vertical coplanar coil system above a homogeneous earth (after Frischknecht, 1967). Z is the free space mutual coupling while ΔZ is the incremental change in this coupling introduced by reflection from the earth.

inductive numbers Θ . The latter two expressions may be rewritten in the convenient forms

$$\sigma\mu\omega\rho^2\left(1+\frac{h^2}{\rho^2}\right) \quad \text{and} \quad \sigma\mu\omega t\rho\left(1+\frac{h^2}{\rho^2}\right)^{1/2}$$

The mutual impedance of a coil pair employed in an AEM system is a nonlinear function of these last two expressions.

We noted above that most of the change of the reflection coefficient for a sphere of $\mu_2/\mu_1 = 1$ occurs for θ values between 1 and 30, i.e., for Θ values between 1 and 1000. The reflection coefficients for disk and cylinder are portrayed, in Figures 7 and 8 respectively, as functions of their respective induction numbers. Evidently, most of the change of these reflection coefficients also takes place for values of Θ between 1 and 1000, provided $\mu_2/\mu_1 = 1$.

For the sphere, disk and cylinder, we would be inclined to conclude that a variation in frequency over a range of 10^3 could cause the reflection coefficients of these bodies to trend from zero real and imaginary parts ($M = 0, N = 0$) through equal real and imaginary parts ($M = N$), and finally to maximum real part and zero imaginary part ($M_{MAX}, N = 0$). Herein lies the basis of all schemes for estimating the induction numbers from AEM survey data (but refer to the limitations of such schemes noted by Bosschart, 1964).

As an example of the mutual coupling of a double-dipole system above a homogeneous earth, Figure 9 (after Frischknecht, 1967) is presented. This figure is an Argand diagram, for a vertical coplanar coil system, based on calculations of the real and imaginary parts of the mutual impedance ratio $\Delta Z/Z$.

For example, we might measure, at one location, one or more magnetic field components at each of two frequencies ω_1 and ω_2. The ratio of the field components from, say, Equation 9 would be

$$\Delta H(\omega_1)/\Delta H(\omega_2) = \frac{M(\omega_1) + iN(\omega_1)}{M(\omega_2) + iN(\omega_2)} \qquad 20$$

and if we measure the ratios of the real and imaginary parts separately, we obtain:

$$\mathrm{Re}\left[\frac{\Delta H(\omega_1)}{\Delta H(\omega_2)}\right] = \frac{M(\omega_1)}{M(\omega_2)} \qquad 21$$

$$\mathrm{Im}\left[\frac{\Delta H(\omega_1)}{\Delta H(\omega_2)}\right] = \frac{N(\omega_1)}{N(\omega_2)} \qquad 22$$

Provided we can interpret the shape of the body from the areal distribution of the field components, then we may refer to figures such as Figures 2, 7, and 8 and determine, uniquely, a value of $\theta(\omega_1)$ which will permit the Ratios 21 and 22 to be satisfied; this will be a unique value of $\theta(\omega_1)$. If, however, we are prepared to assume a value for μ, and since we know ω_1, we can obtain one of the products

σa^2 ; sphere

σa^2 ; horizontal cylinder

$\sigma t a$; disk

Ward (1959b) has demonstrated that it is possible to determine σ and a uniquely for a sphere, and the extension of this result to the cylinder is readily made. It is not, however, easy to obtain t, a, and σ for the disk. For a lamellar body such as a disk, we must usually confine our interpretation to calculation of the σt product. Clearly, if θ achieves high values such that $\theta(\omega_1) \sim\theta(\omega_2)$, then no estimate of θ, nor of σt for a lamellar body, can be made. It is a trivial observation that $\theta(\omega)$ cannot be estimated when $M(\omega)\sim 0$. Since ω is confined to a range of 10^3 for $M = 0$ to $M = M_{MAX}$, then the product σt for lamellar bodies such as disks must be confined to a *measurable* range of 10^3. Of course, the lower limit of σ, t, θ, M, N, or H which can be measured is established by the noise level of the system. The upper limit of $[H(\omega_1) - H(\omega_2)]$ which can be measured is established by the precision and frequency stability of the instrument. We suggest that $[H(\omega_1) - H(\omega_2)]$ cannot, in general, be measured by AEM systems with precision adequate to deduce $\theta(\omega_1)$ when $\theta(\omega_2)$ exceeds 30 or when $\theta_1(\omega)$ is less than unity. In some AEM systems even a three decade range of $\theta(\omega)$ is not measurable as we shall see subsequently. There are several practical means of estimating the σt product of lamellar bodies. One might measure the ratio $N(\omega_1)/N(\omega_2)$ as is done, for example, with the Hunting Canso AEM system, the ratio $N(\omega)/M(\omega)$, as is done for all rigid boom systems, or combine the measurements $A = [M^2(\omega) + N^2(\omega)]$ and $\tan\phi = N(\omega)/M(\omega)$ where ϕ is the phase and A is the amplitude of the mutual impedance (the ABEM and Inco systems). The ratio

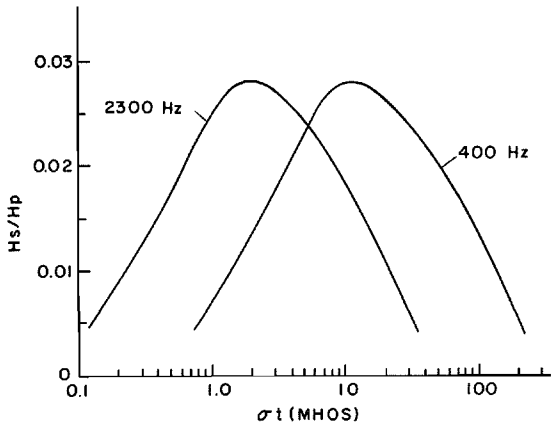


Figure 10. Experimental measurements of the peak quadrature anomaly for a vertical half plane as a function of the product of conductivity σ and width t (after Paterson, 1961a).

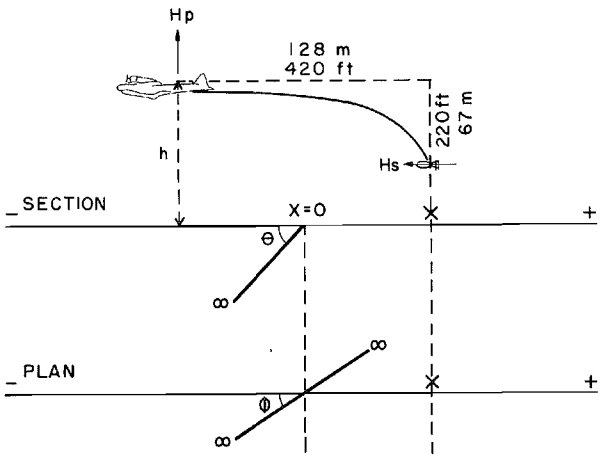


Figure 11. Geometry for Hunting Canso AEM system flying over a half plane; strike of half plane is φ relative to flight direction; dip of half plane is θ; height of aircraft is h (after Paterson, 1961a).

$M(\omega_1)/M(\omega_2)$ is not measured in any currently operating AEM system.

In the time domain we measure $H(t_i)/H(t_j) = \Delta e(t_i)/\Delta e(t_j)$ and relate these quantities to the σt product of lamellar bodies.

It is not surprising, from the foregoing discussion, that Strangway (1966) has noted that the σt product for all massive sulfide bodies falls in the narrow range of 1 to 300 mhos, when σt is estimated from horizontal loop ground electromagnetic survey data. On the other hand, we may deduce from Figure 10 that the measurable range of σt is from 0.5 to 50 mhos with the Hunting Canso AEM system, at 120 m altitude, assuming a noise level of 1000 ppm; for σt in excess of about 50 mhos, the 2300 Hz response is below the noise level, while for σt less than 0.5 mhos, the 400 Hz response is below the noise level. Similarly, from Figure 11, we estimate an acceptable range of σt for the Varian-TGS AEM system flown at 45 m above a conductor to be about 2 to 1000 mhos, as expected. A similar system, the Newmont-Aero helicopter AEM system, because of a higher noise level, has an estimated σt window of about 5 to 800 when the helicopter is flown at 45 m altitude.

The fact that the σt products for massive sulfides often fall within the 'windows' of acceptable σt products for most AEM systems indicates that we have designed our equipment adequately; there should be nothing surprising about this observation.

Paterson (1966) examined 27 AEM anomalies detected by the Hunting Canso system and found that the σt product ranged from 2.2 mhos to 14 mhos; these values lie in the center of our predicted range of 0.5 to 50 mhos for this system. For eleven of these 27 anomalies, the conductivity fell within the range 0.1 mhos per meter to 1.0 mhos per meter according to Paterson. If taken on face value, this range of conductivities confirms the earlier observations by Paterson (1959) and West (1960) that sulfide orebodies exhibit a 'bulk resistivity' which is 100 to 1000 times lower than the typical resistivity of a hand specimen of massive sulfides. Bosschart (1961) argued against this hypothesis and established that for the *horizontal loop ground electromagnetic method,* the range of σt observed for 14 examples was approximately 0.5 to 500 mhos, and that the conductivities derived therefrom were in the range 4 to 500 mhos per meter. Undoubtedly, the discrepancy between the conclusions drawn by Paterson (1959) and those drawn by Bosschart (1961) can be explained partially by the different σt windows accepted by the Hunting airborne and the horizontal loop ground electromagnetic methods. Bosschart (1964) notes that simplified interpretation schemes based on thin sheet models have limited application and that bodies possessing three finite dimensions are best for simulating ore deposits. While we agree in principle with Bosschart, we still believe that the thin sheet half-plane model is adequate for most interpretation of airborne electromagnetic data, but that interpretation of detailed ground electromagnetic data warrants more exact simulation.

There is another facet of σ determination which must be borne in mind and that is the effect of the height of the detecting system above the conductor. This effect is easy to illustrate by reference to the response of a sphere. At altitudes and for systems above the sphere so that the primary or transmitted field is nearly uniform across the conductor (so that $h>a>\rho$) the response is governed by the induction number

$$\Theta_1 = \sigma\mu\omega a^2 \qquad 23$$

while for altitudes and systems above the sphere so that $h\sim\rho<a$, the response of the sphere may be replaced approximately by the response of a half-space, and this response is governed by

$$\Theta_2 = \sigma\mu\omega(\rho^2 + h^2) \qquad 24$$

Thus, in the former instance the ratio of in-phase to quadrature responses of a sphere is essentially independent of h or ρ; this situation pertains to fixed boom AEM systems over deep small targets. By contrast, in the latter instance the ratio of in-phase response to quadrature response of a sphere is essentially independent of the radius of the sphere; this situation pertains to fixed boom AEM systems over shallow, large targets. The range of measurable σ for these two extreme examples might be quite different.

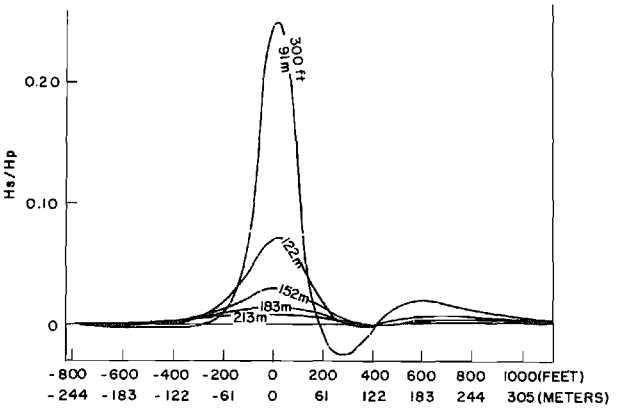


Figure 12. Variation of the in-phase anomaly with height for vertical half plane; theoretical curves applicable to Hunting Canso AEM system; strike and dip both 90°; conductivity of half plane is infinite (after Paterson, 1961a).

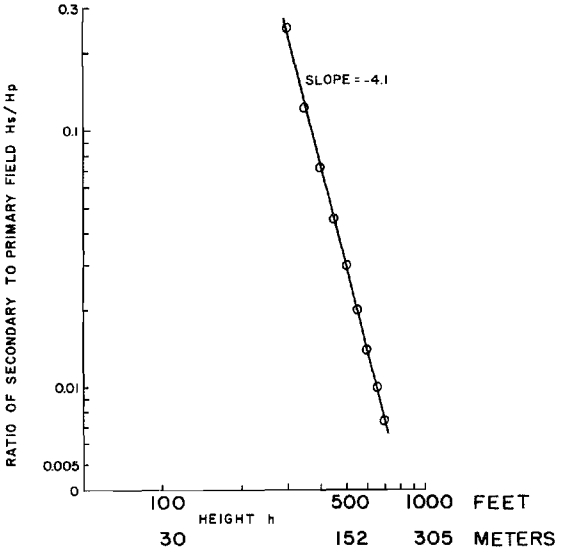


Figure 13. Variation with aircraft height of peak in-phase anomaly obtained with Hunting Canso system over a vertical half plane. Data from Figure 12 (after Paterson, 1961a).

The basis of quantitative interpretation of AEM data

The first step in interpretation of airborne electromagnetic data is that of estimating quantitatively the characteristic parameters of the source, such as dip, depth, depth extent, width and conductivity. The next step usually involves correlation of the deduced parameters with independent estimates based on complementary geophysical data, such as gravity and magnetics. The third step is the most difficult since it is the establishment of geologic credibility for the quantitative interpretations. With good geologic control the latter step may be tractable; however, usually we lack such control and must rely upon inference plus experience gained from previous case histories.

Most quantitative interpretation (step 1) is based on scale model measurements of the magnetic field components about a half-plane conductor. Provided we analyze a profile over the center of a thin body of limited strike length, this is a justifiable procedure. When the depth extent or the strike length are less than about 2000 feet in the full-scale system, the half-plane model is inadequate. Other models must then be introduced. For the sake of simplicity, we shall center our discussion of interpretation on the half-plane model.

We may match a field curve with one or more members of a catalogue of field curves, or we may analyze certain characteristics of the field curves in terms of the variability of these characteristics and their relationship to source parameters as determined in scale model experiments. Usually, we choose the latter procedure.

Examples of model curves pertaining to one towed bird and one rigid boom system will be sufficient to illustrate the principles of interpretation of AEM data.

Interpretation of data from a towed bird AEM system. The availability of a complete interpretation scheme for the Hunting Canso system facilitates use of this system for illustrative purposes. The interpretation scheme referred to is contained in an article by Paterson (1961a). The elements of that scheme are as follows.

Paterson assumed a half plane as the basic model in a series of scale-model experiments and theoretical calculations which contributed information upon which the interpretation scheme is based. The geometry for the model experiments and theoretical calculations is illustrated in Figure 11. The aircraft is assumed to be flying from right to left for all model illustrations and the anomaly is plotted beneath the receiving coil. The experimental and theoretical data were so collected as to illustrate the effects on recorded secondary field profiles of changes in geometry such as depth to the top of the half plane, strike of the half plane, dip of sheets including a half plane, and of such departures from the half-plane model as finite depth extent, finite depth extent and finite strike length, horizontal conductive sheets of finite size, wide conductors, and multiple sheet conductors. The pertinent secondary field profiles for each of these effects are presented in the next paragraphs. All of the results for the half-plane model were obtained by calculation of the in-phase secondary field assuming infinite conductivity. While the quadrature secondary field rather than the in-phase secondary field is measured in the full-scale system, some of the effects of changing the geometry of the models can be investigated by studying profiles of either in-phase or quadrature fields.

a) *Effect of depth.* Figure 12 displays the profiles of the normalized secondary field response Hs/Hp for half-plane depths beneath the aircraft ranging from 90 m to 215 m. From these model curves, the relation of Figure 13 is derived.

b) *Effect of strike.* Figure 14 contains profiles of the normalized secondary field response Hs/Hp for various strikes of the half plane relative to the aircraft flight direction. From this set of model curves, Figure 15 was derived.

c) *Effect of dip.* As the dip of the sheet varies from 0 to 180°, so does the shape of the profile of Hs/Hp according to Figure 16. Data similar to those of Figure 16 were used to plot Figure 17.

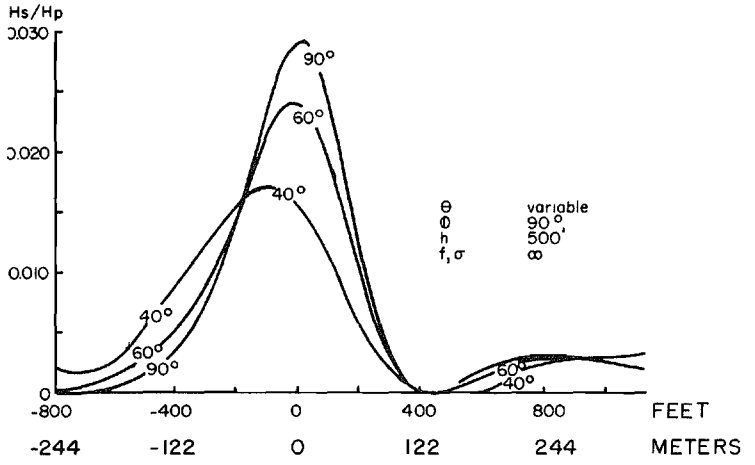


Figure 14. Effect of strike angle on the in-phase anomaly obtained with the Hunting Canso system over a vertical half plane; height 152 m; conductivity of half plane is infinite (after Paterson, 1961a).

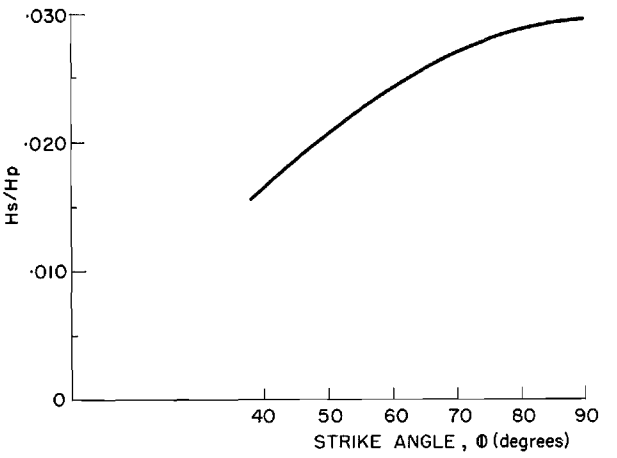


Figure 15. Variation with strike of peak in-phase anomaly obtained with the Hunting Canso system over a vertical half plane. Data from Figure 14 (after Paterson, 1961a).

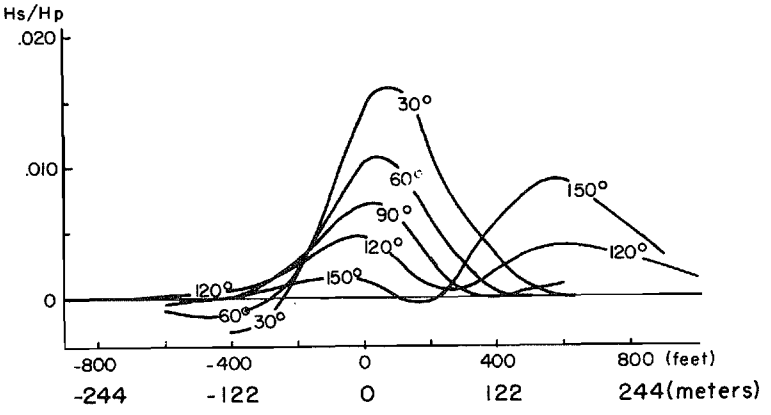


Figure 16. Effect of dip on the quadrature anomaly obtained with a model of the Hunting Canso system over a conductive sheet; height is 152 m; strike is 90°; frequency is 2300 Hz; conductivity is 0.131 mhos/meter; thickness is 30 meters; 122 m depth extent (after Paterson, 1961a).

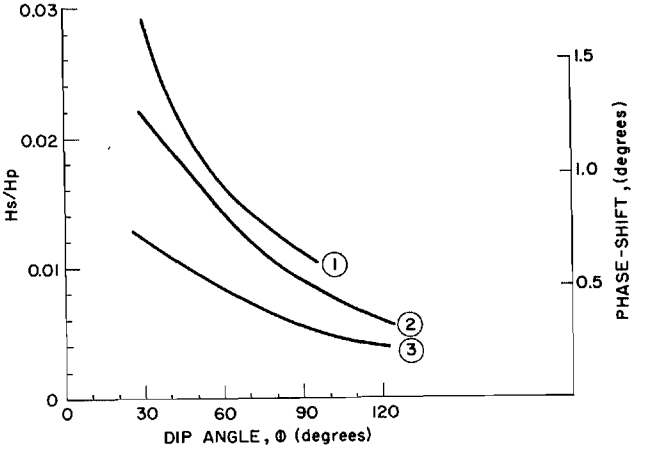


Figure 17. Variation with dip of peak quadrature anomaly obtained with a model of the Hunting Canso system over a sheet of conductivity 0.131 mhos/meter and thickness 30 meters; height is 152 meters; frequency is 2300 Hz; the strike is 90°; (1) half plane, (2) 183 m depth extent, (3) 91 m depth extent (after Paterson, 1961a).

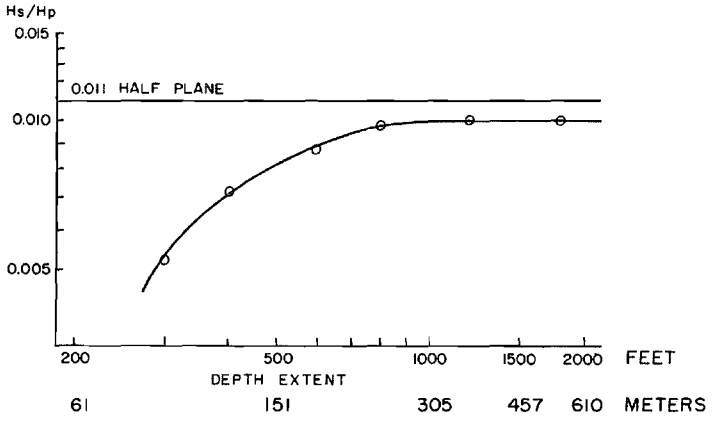


Figure 18. Variation with depth extent on peak quadrature anomaly obtained with the Hunting Canso system over a vertically dipping sheet at 90° strike and 152 m depth; the frequency is 2300 Hz, conductivity 0.131 mhos/meter, and thickness 30 meters (after Paterson, 1961a).

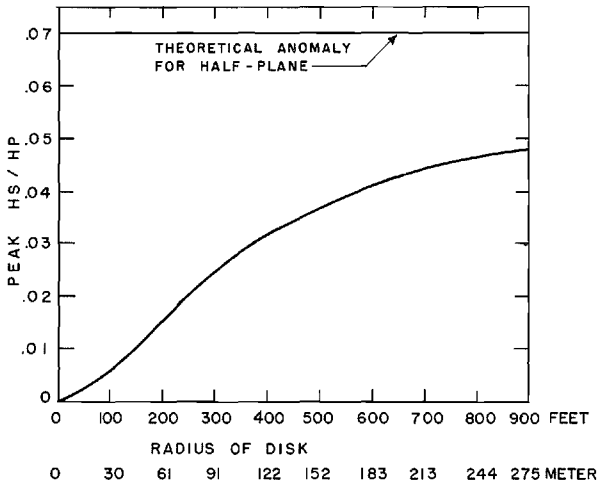


Figure 19. Variation with disk radius of the peak in-phase anomaly obtained with the Hunting Canso system; strike and dip are 90°; height of aircraft 122 m, conductivity of disk is infinite (after Douloff, 1960).

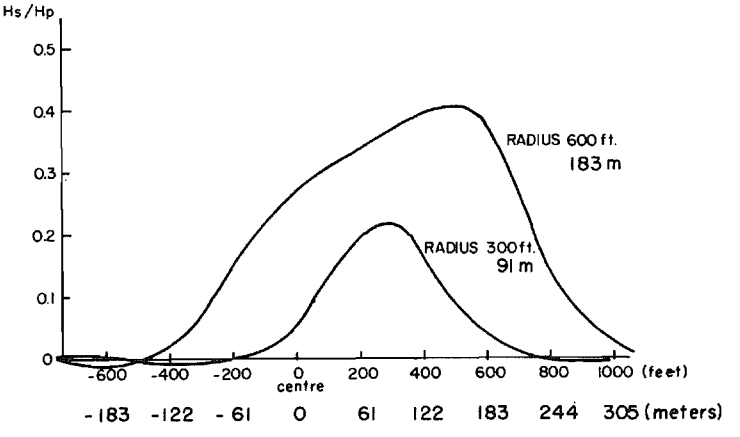


Figure 20. In-phase anomalies due to thin horizontal disks as obtained by scale-model experiments simulating the Hunting Canso system (after Paterson, 1961a).

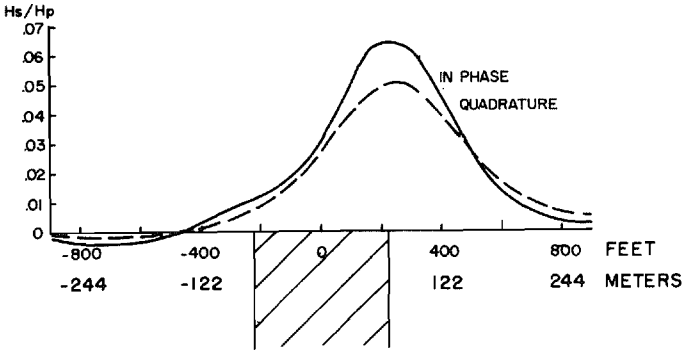


Figure 21. Quadrature and in-phase anomalies obtained with model of Hunting Canso system over broad conductor dipping and striking 90°; frequency 5000 Hz; conductor dimensions 580 X 275 X 137 m; aircraft height 150 m (after Paterson, 1961a).

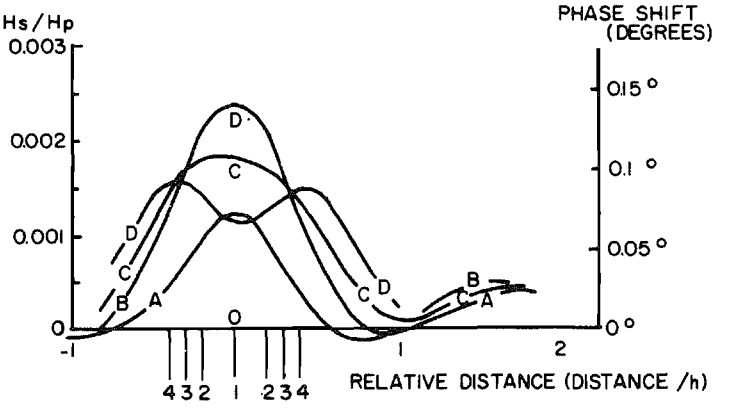


Figure 22. Quadrature anomalies obtained with model of Hunting Canso system over two parallel sheet conductors at separations $A = 0$, $B = 0.345h$, $C = 0.518h$, $D = 0.69h$; the strike and dip are 90°; frequency 2300 Hz; conductivity-thickness product 0.0012 mhos; depth extent, length, and height $0.31h$, h and h, respectively (after Paterson, 1961a).

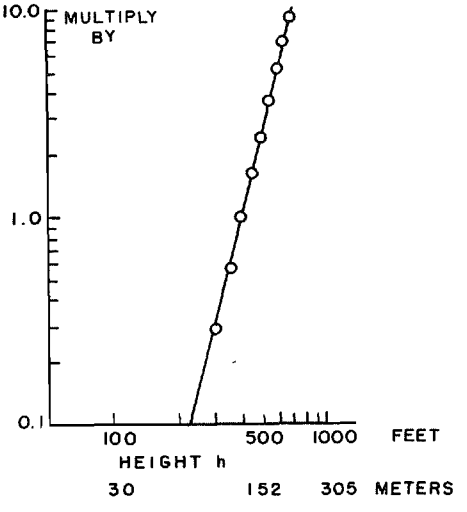


Figure 23. Correction graph used to convert quadrature anomaly obtained at height h to equivalent anomaly at 400 feet (122 m). Hunting Canso system (after Paterson, 1961a).

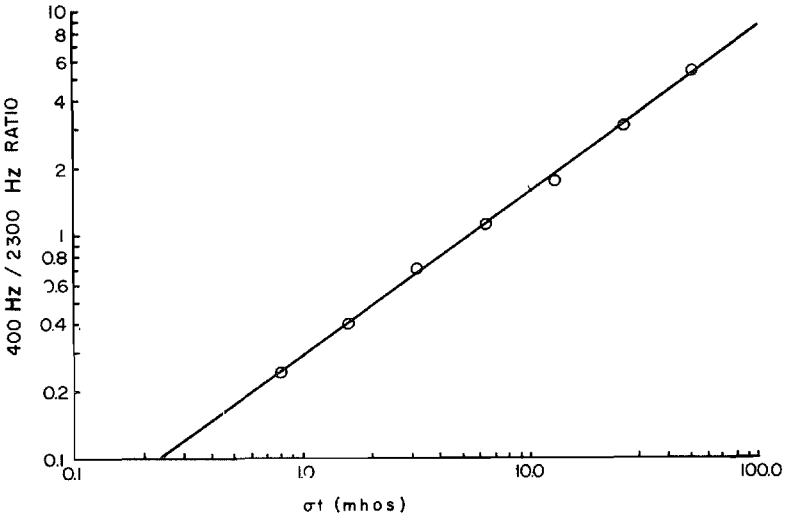


Figure 24. Ratio of 400 Hz quadrature anomaly to 2300 Hz quadrature anomaly versus the conductivity-thickness product for a vertical half plane obtained by a scale model of the Hunting Canso system (after Paterson, 1961a).

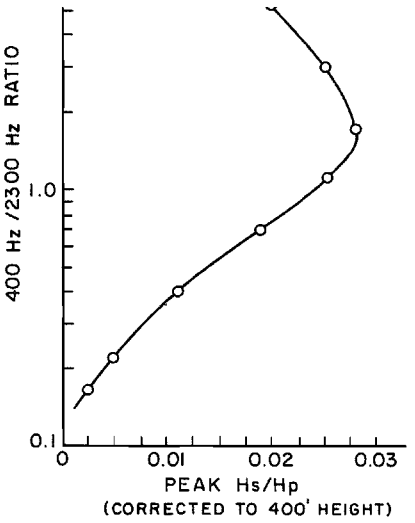


Figure 25. Ratio of 400 Hz quadrature anomaly to 2300 Hz quadrature anomaly versus peak 400 Hz anomaly for vertical half plane at 400 feet (122 m) aircraft height above conductor as obtained by scale model of the Hunting Canso system (after Paterson, 1961a).

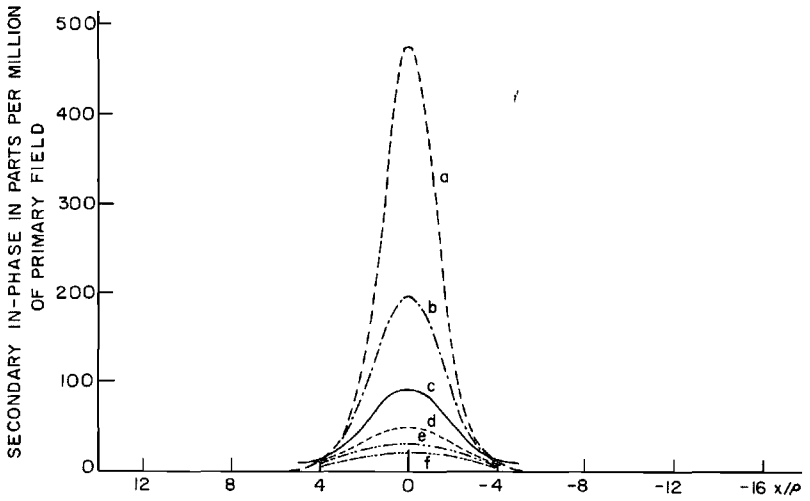


Figure 26. In-phase anomaly, in parts per million of primary field, obtained over a half plane with a model of the Varian-TGS system. Curves *a* through *f* pertain to depths below system of 3ρ, 4ρ, 5ρ, 6ρ, 7ρ, and 8ρ, respectively (after Ward, 1967).

d) *Effect of finite depth extent.* The peak quadrature response was measured in a scale-model experiment wherein the models were long, thin vertical conductive sheets of different depth extents. The theoretical response for a half plane is shown for comparison in Figure 18.

e) *Effect of finite depth extent and finite strike length.* From scale-model profiles over vertical circular disks of various radii, the effect of finite depth extent and finite strike length may be studied. Figure 19 contains a plot of peak values of the ratio Hs/Hp versus disk radius and the theoretical peak anomaly for a half plane is shown for comparison.

f) *Effect of horizontal conductive sheets of finite size.* Horizontal disks of radii 90 m and 180 m were used to model thin, flat conductors of limited horizontal extent. Figure 20 contains the results.

g) *Effect of conductor width.* A model conductor 580 m in length by 275 m in depth extent by 137 m in width was surveyed at 150 m aircraft altitude and the profiles of Figure 21 resulted. The peak response is over the edge nearest the approaching aircraft. The width of the anomaly is large.

h) *Effect of multiple sheet conductors.* Two sheet conductors of length h, depth extent 0.3 h, and conductivity-thickness product 0.0012 mhos were placed as), 0.345 h, 0.578 h, and 0.69 h apart where h is the aircraft height. The quadrature anomalies are shown in Figure 22, from which we observe that resolution is not obtained until the sheets are separated by 0.69 h. Then the anomaly is not unlike that due to a horizontal disk.

Once a catalogue of model curves, similar to those discussed above, is obtained, an interpretational procedure may be developed. Paterson (1961a) has developed a distinctive interpretational procedure for anomalies which arise in sources approximating a half plane. Anomalies with profiles such as those of Figures

21 and 22, are a first indication that the half-plane model is not satisfactory. If the conductor is of finite depth extent, one step in Paterson's interpretation procedure may permit recognition of this fact. The recommended interpretation procedure for anomalies which appear to be satisfied by a vertical half-plane model is as follows:

1. Correct the peak quadrature (400 Hz and 2300 Hz) anomalies for strike deviation from 90 degrees using Figure 15.
2. Correct the peak quadrature 400 Hz and 2300 Hz anomaly for aircraft altitude deviation from 200 feet (122 m) using Figure 23.
3. Estimate the dip of the conductor by comparing the observed profile with the model profiles of Figure 16.
4. Estimate the conductivity-thickness product (σt) from Figure 24. The *ratio* of the 400 Hz to 2300 Hz anomaly is nearly independent of altitude within the range 100 to 250 meters for this particular system.
5. Plot the ratio of the 400 to 2300 Hz anomalies versus the corrected peak 400 Hz anomaly on Figure 25. If the point falls on the model curve shown, the half-plane model is applicable. If the plotted point falls to the left of the curve, it is because the conductor is of finite dimensions or occurs at a depth greater than 400 feet; these are the conditions for the amplitude of the 400 Hz anomaly to be less than that given by the model. If the point falls to the right, the conductor is not vertical or eddy currents in the overburden are contributing; these are the conditions for the amplitude of the 400 Hz anomaly to be greater than that given by the model.
6. If the point falls to the left of the model curve in Figure 25, the 400 Hz anomaly may be multiplied by a factor to bring it on the model curve. This factor, carried over to Figure 24, will permit estimation of the height of the aircraft above the top of the conductor. Since the altitude of the aircraft is measured continuously by radio altimetry, the depth of burial of the conductor may be estimated.
7. Estimate the strike length of the anomaly from a plan map wherein the anomalies on adjacent flight lines are plotted.

Interpretation of data from a fixed boom AEM system. Reference will be made here to a scheme, based upon scale-model data acquired by personnel of the Texas Gulf Sulphur Company, for interpretation of data obtained with the Varian-TGS helicopter AEM system.

The model curves of Figures 26 through 29 illustrate the effects of varying depth, dip, width, and of multiple parallel conductors; all thin sheet conductors employed would approximate a half plane.

The system is relatively insensitive to the direction of flight within 30 degrees of normal to the strike of a conductor and hence strike has not been treated as a variable.

The data from Figure 26 have been used to construct the Argand diagram of Figure 30. Similar diagrams are constructed for dips of 60°, 30°, and 0°. The quantities plotted in these diagrams are the peak in-phase and peak quadrature anomalies obtained from the model data of curves such as those appearing in Figures 26 and 27.

Interpretation of data from the Varian-TGS AEM system then follows the sequence:

1. Estimate the dip of the conductor by comparing the observed profile with the model profiles of Figure 27.
2. Measure the in-phase and quadrature amplitudes of an anomaly to locate a point on the Argand diagram.
3. Estimate the height h of the system above the conductor from the Argand diagram. Deduct the known terrain clearance of the aircraft to obtain a depth of burial of the conductor.
4. Estimate the conductivity-thickness product (σt) from the Argand diagram.
5. Estimate the strike length of the anomaly from a plan map wherein the anomalies on adjacent flight lines are plotted.

This procedure is nearly identical to that employed for the ABEM and Newmont-Aero AEM systems (Hedstrom and Parasnis, 1958; Brant, *et al.*, 1966) and numerous ground electromagnetic systems (e.g., Strangway, 1966).

General. In the above interpretation schemes we have not discussed the effect of magnetic permeability on the anomalies detected by an AEM system. Figures 2 and 8 indicate that the in-phase response for a strongly magnetic body may be of opposite sign to that obtained over a conductive body. Ward (1959b, 1961), Wieduwilt (1962), Bosschart (1964), and Podolsky (1966) have discussed this feature. For a permeable, conductive sphere in a uniform alternating magnetic field, the limiting low- and high-frequency anomalies are given by (Ward, 1959b).

L.F.

$$\Delta\vec{H}_L = H_0\, a^3\, \frac{\mu_2-\mu_1}{\mu_2-2\mu_1}\left[\frac{(2x^2-y^2-z^2)\vec{i}+3xy\vec{j}+3xz\vec{k}}{\rho^5}\right] \qquad 25$$

H.F.

$$\Delta\vec{H}_H = -H_0\,\frac{a^3}{2}\left[\frac{(2x^2-y^2-z^2)\vec{i}+3xy\vec{j}+3xz\vec{k}}{\rho^5}\right] \qquad 26$$

where μ_2 and μ_1 are the permeabilities of the sphere and surroundings, respectively. For $\mu_2 \gg \mu_1$, the values $\Delta\vec{H}_L$ and $\Delta\vec{H}_H$ are of opposite sign. At some intermediate frequency the in-phase eddy current (H.F.) induced dipole moment is equal and opposite to the in-phase *static* magnetic (L.F.) induced dipole moment and the net in-phase dipole moment is zero. The magnitude of the induction number determines the sign of the net dipole moment. Let us assume that a rigid boom system and a towed bird system are above a homogeneous earth at their usual operating altitudes; their induction numbers are:

Towed bird

$$\Theta_T = \sigma\mu\omega(\rho^2+h^2)\ ;\ \begin{matrix}\rho\sim 150\text{m}\\ h\sim 150\text{m}\end{matrix} \qquad 27$$

Rigid boom

$$\Theta_R = \sigma\mu\omega(\rho^2+h^2)\ ;\ \begin{matrix}\rho\sim 15\text{m}\\ h\sim 30\text{m}\end{matrix} \qquad 28$$

Then the ratio Θ_T/Θ_R is of order 40. The rigid boom system is much more apt to record a *static* magnetic dipole moment than a

Contents

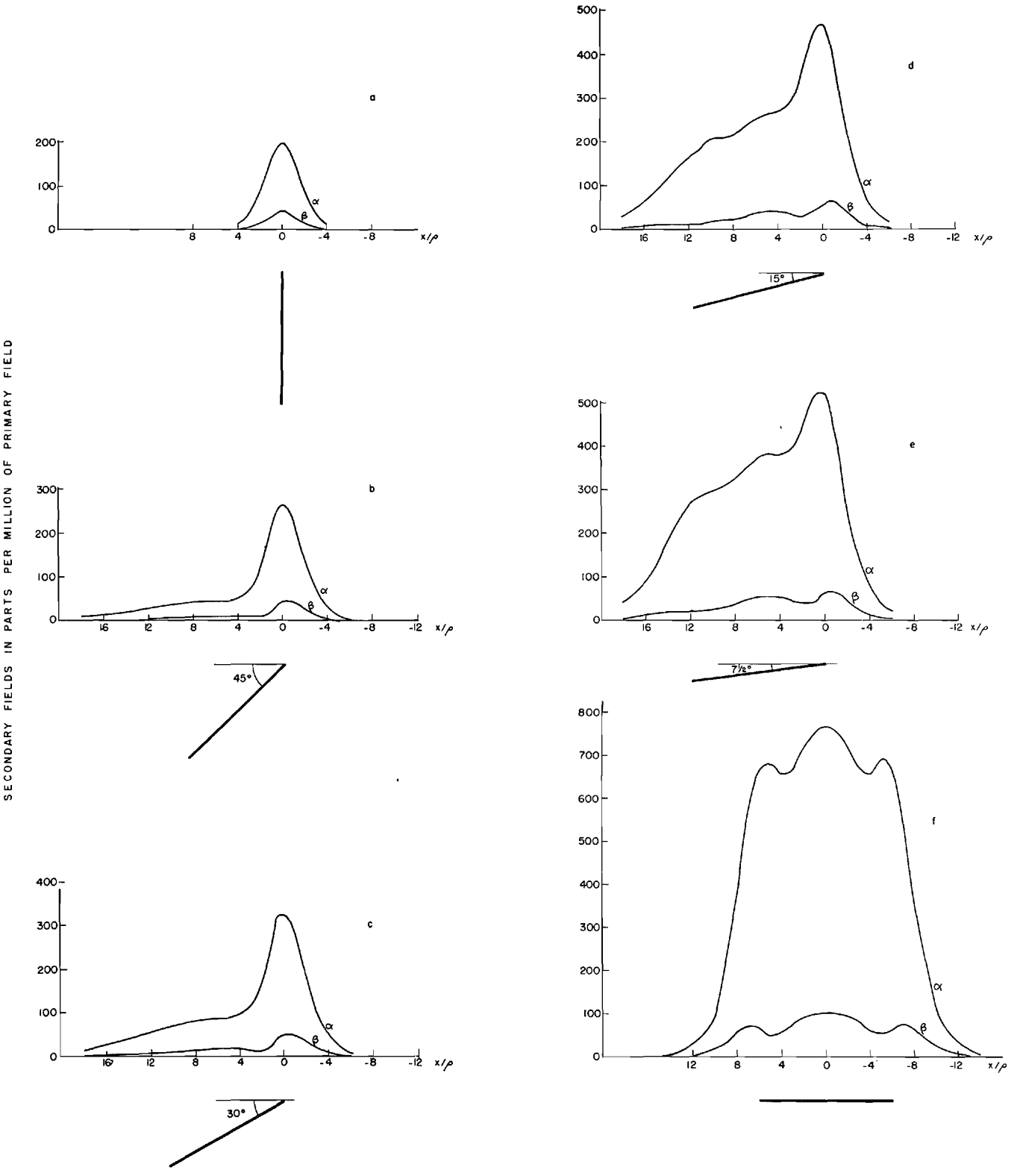


Figure 27. In-phase α and quadrature β anomalies, in parts per million of primary field, obtained over a dipping half plane with a model of the Varian-TGS system. Dips are as shown in the figure (after Ward, 1967).

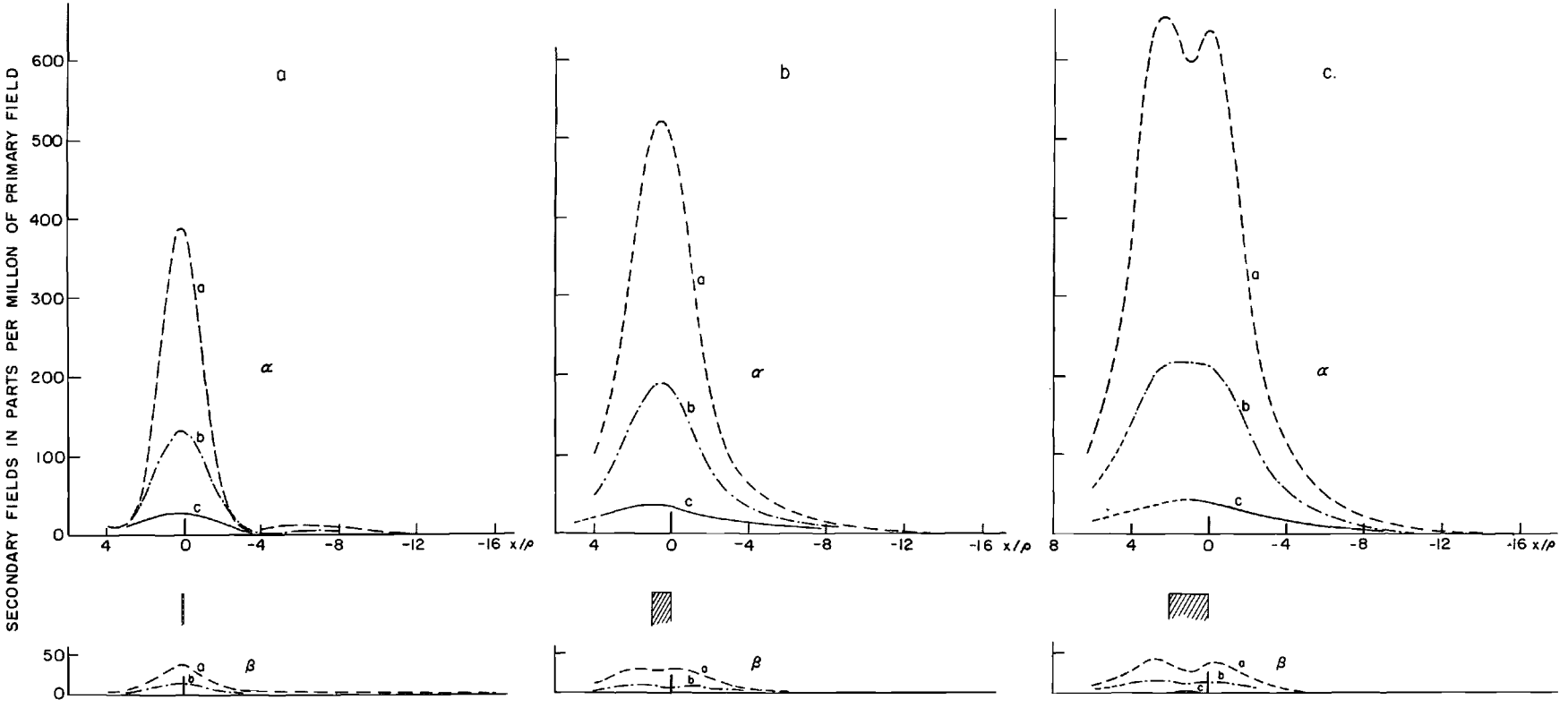


Figure 28. In-phase α and quadrature β anomalies, in parts per million of primary field, obtained over vertical conductors of different widths with a model of the Varian-TGS system. Widths are as shown on the figure (after Ward, 1967).

Contents

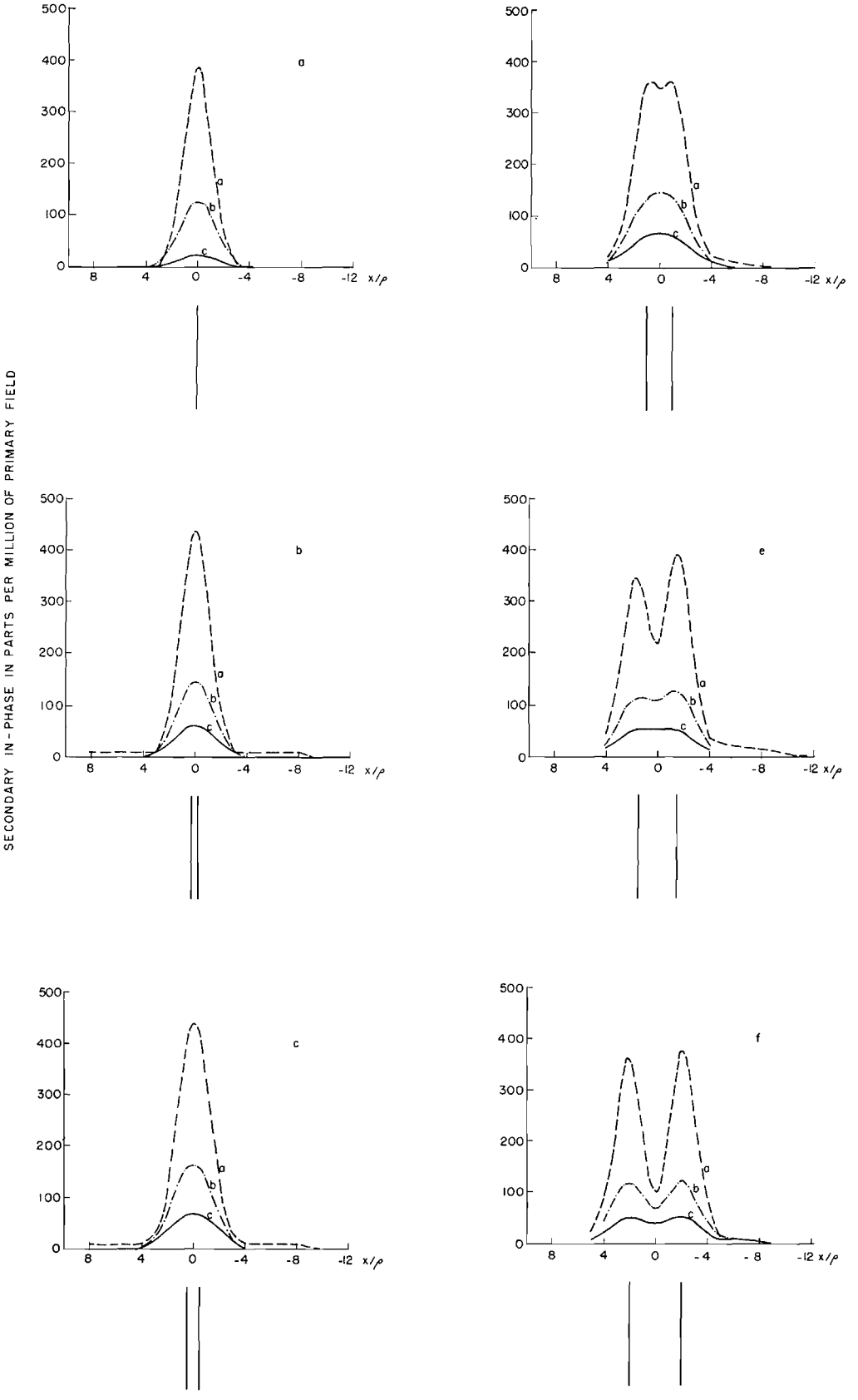


Figure 29. In-phase anomalies, in parts per million of primary field, obtained over two parallel sheet conductors with a model of the Varian-TGS system. The separations between the conductors are as shown on the figure (after Ward, 1967).

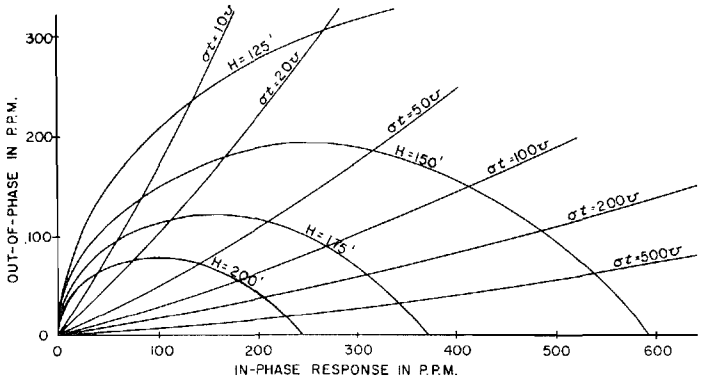


Figure 30. Argand diagram for the Varian-TGS AEM system applicable to the interpretation of data over a vertical half-plane model (after Podolsky, 1966).

towed bird system since the induction number of the former is much less than the induction number for the latter. This observation is borne out in practice; rigid boom systems frequently give rise to a *negative* or *magnetic* response over ultrabasic rock types or over magnetic iron formation. Note also that the *magnetic* response occurs only in the in-phase component and hence should not be recorded by most fixed wing, towed bird systems since they rely solely upon quadrature measurements.

In the analysis for towed bird or rigid boom systems we stopped the interpretation at the σt product rather than proceeding to estimate the width t and, in turn, the conductivity σ. While many interpreters attempt this latter step, it is a dangerous procedure for the typical, inhomogeneous conductor detected by an AEM system. It is usually sufficient to *characterize* the deposit by its σt product (Bosschart, 1961).

Field examples. Figure 31 contains an anomaly profile obtained with the Newmont/Aero helicopter system over the Whistle Mine massive sulphide deposit near Sudbury, Ontario, Canada. Interpreted as a steeply dipping sheet-like conductor, we obtain a σt product of 140 mhos and a depth below aircraft of 35 m using the Argand diagram given by Brant, Dolan, and Elliot (1966). This value of σt is in a range, for the Newmont/Aero system, which is typical of very conductive massive sulphides. The magnetic anomaly in direct association with the electromagnetic anomaly suggests pyrrhotite as the main sulphide mineral and indeed this is the case at the Whistle Mine. The magnetic method, used in direct conjunction with the electromagnetic method, usually permits distinction between magnetic sulphides and nonsulphides and has immeasurably aided the interpretation of airborne electromagnetic data.

As a contrast to the above example, Figure 32 contains profiles over a graphite zone also obtained with the Newmont/Aero system. While at least two parallel conductive bands have been detected, interpretation of the main peak on the basis of a half-plane model yields useful information. We learn, from the appropriate Argand diagram that the σt product is 3.5 mhos and the altitude of the aircraft above the top of the conductor is 20 m. The value of σt so deduced is too low for most massive sulphides and this fact, coupled with the lack of an accompanying magnetic anomaly quickly leads the interpreter to downgrade this anomaly.

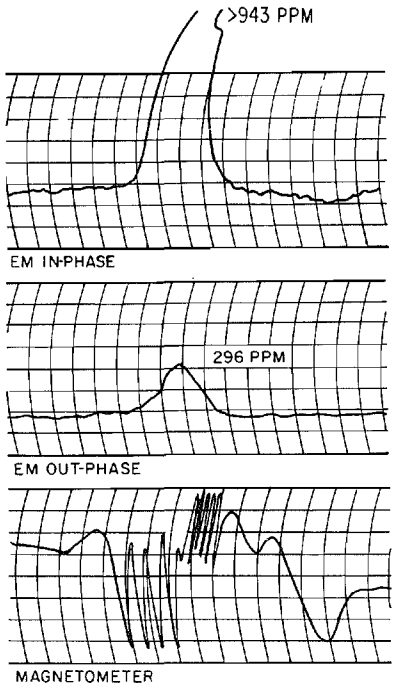
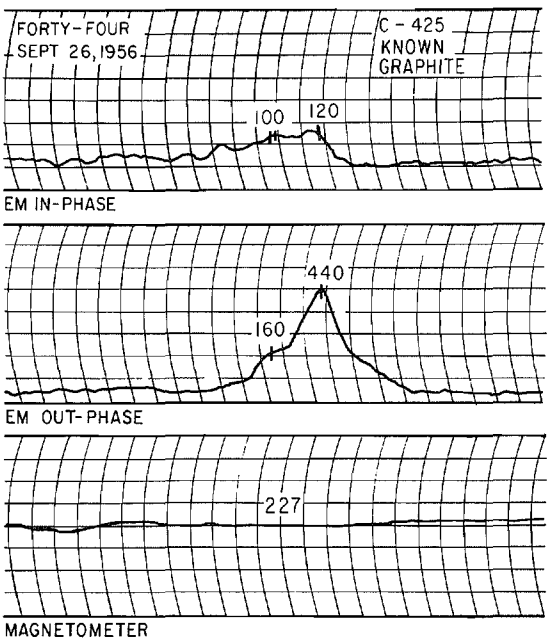


Figure 31. Electromagnetic and magnetic profiles obtained over the Whistle Mine, Sudbury, Ontario, Canada, with the Newmont/Aero helicopter system (courtesy of Canadian Aero Service Ltd.).

Figure 32. Electromagnetic and magnetic profiles obtained over a graphite zone in New Brunswick, Canada, with the Newmont/Aero helicopter system (courtesy of Canadian Aero Service Ltd.).



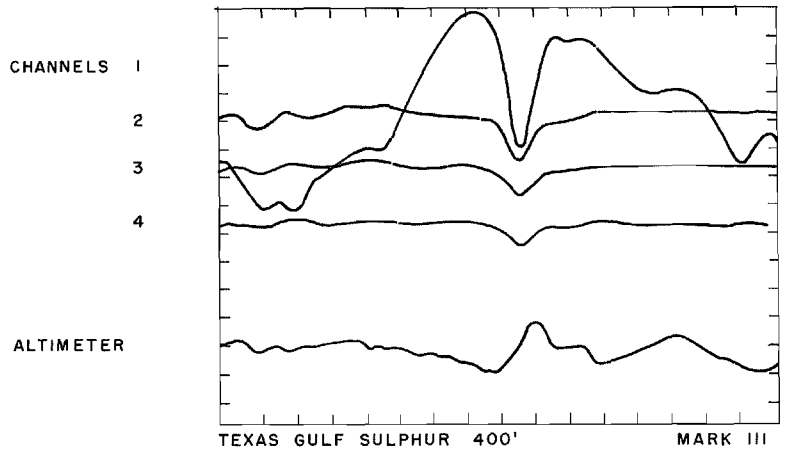


Figure 33. Electromagnetic profiles obtained over the Kidd Creek, Ontario, Canada, deposit of Texas Gulf Sulphur Co., with the Mark III Input system (courtesy of Barringer Research Limited).

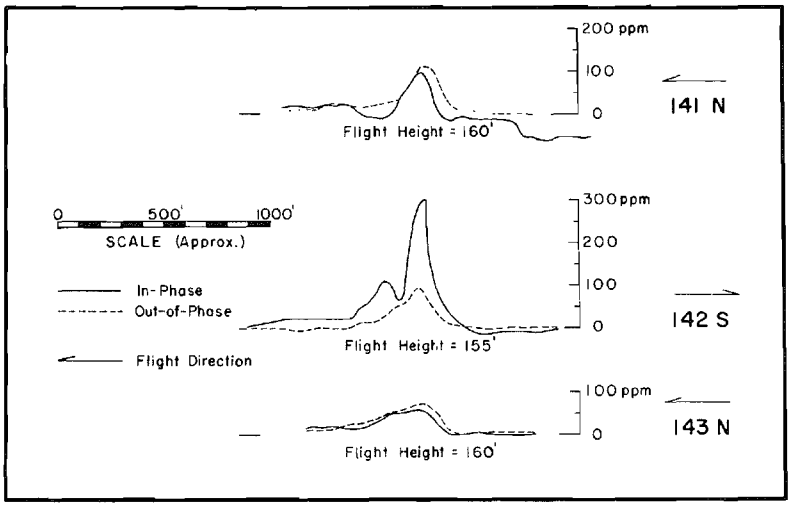


Figure 34. Electromagnetic profiles obtained over a magnetite-sulphide complex body with the Varian-TGS helicopter system (after Podolsky, 1966).

There are, of course, massive sulphide orebodies which produce no distinct magnetic anomaly. Such a situation was found to exist at the Kidd Creek deposit of the Texas Gulf Sulphur Co. The Input responses over this deposit, which occurs beneath a conductive clay overburden, is shown in Figure 33. The first channel reflects both the conductive overburden plus the orebody while the subsequent channels, representing sampling of the pulse decay curve at later intervals, reflect mostly the orebody. The persistence of the orebody response through all four channels is an indication of a high *σt* product although a means for estimating this quantitatively is not available to the writer.

Podolsky (1966) reports upon an anomaly which he attributes to a combination of a *magnetic* response and an *eddy current* response. His example, reproduced in Figure 34, was obtained with the Varian-TGS helicopter system. The in-phase anomaly on line 142S could be interpreted as indicating two conductors about 150 feet apart. However, Podolsky discards this interpretation because the half-peak width of the principal peak is too narrow for an anomaly of this magnitude, and because there is little or no evidence of two parallel conductors in the quadrature anomaly. An alternative interpretation, later substantiated by evidence from diamond drilling, associates a broad, positive anomaly (dotted line) with massive sulphide mineralization and a narrow negative anomaly with a concentration of magnetite. The observed profile is then the combination of these two parts. Wieduwilt (1962) has also presented an example of a negative (magnetic) anomaly obtained with the Newmont/Aero helicopter system.

An example of a plan presentation of data obtained with the Hunting Canso system is presented in Figure 35. The 400 Hz quadrature response has been 'contoured' in the right panel of the figure and the numbers in circles are the ratio of 400 Hz anomaly to 2300 Hz anomaly. Because an anomaly obtained with AEM systems is dependent upon the fourth to sixth power of aircraft height above the conductor, these contours really should be considered as form lines. The area encompassed by the figure is overlain with 10 to 30 m of conductive clay overburden and hence the geologic noise is high. However, the value of 1.3 for the ratio of 400 Hz response to 2300 Hz response and the strong coincident magnetic response drew attention to the anomaly in the center of the figure. This anomaly led directly to the discovery of the orebody of Mattagami Lake Mines in northern Quebec, Canada. Diamond drilling revealed that the strong magnetic anomaly was due to a magnetite concentration associated with sphalerite-chalcopyrite-pyrite orebody.

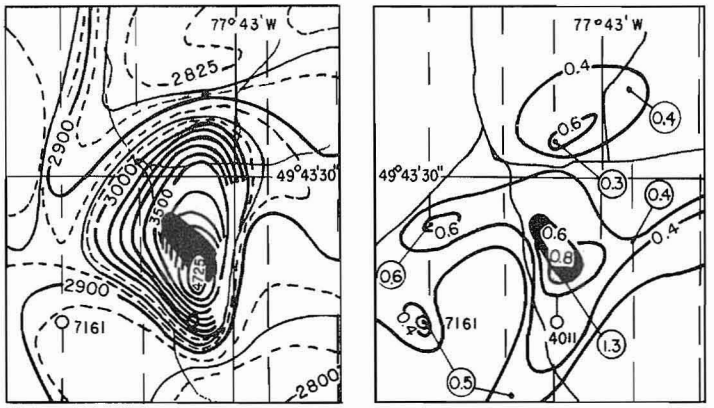


Figure 35. Plan presentation of electromagnetic and magnetic data acquired over Mattagami Lake Mines, Quebec, Canada, by the Hunting Canso AEM system (after Paterson, 1966).

Merit rating of AEM systems

The potential user of an AEM system invariably asks the consulting geophysicist for an opinion on the relative merits of the numerous available systems. It is difficult to remove subjectivity from such opinions, but the following factors offer guidance in the selection of a system for a particular geological problem.

Detection capabilities. Ideally one would like to have available, for each AEM system, scale-model profiles which would permit comparisons of the systems in terms of their responses to the following targets:

1. Sphere – to simulate an ore lens
2. Vertical cylinder – to simulate an ore pipe
3. Horizontal cylinder – to simulate a manto
4. Dipping half plane – to simulate a large vein or slab
5. Dipping disk – to simulate a small vein or slab
6. Horizontal disk – to simulate a limited patch of conductive overburden
7. Horizontal thin sheet – to simulate an extensive cover of conductive overburden.

With the above information the user could make his own objective decision on the sensitivity of each system for each of the types of targets he expects to encounter. Unfortunately, very few of the purveyors of airborne electromagnetic surveys have deemed it necessary to make this information available to potential clients with the result that the selection of an AEM system for a particular application is often made subjectively.

Most systems currently available measure but a single spatial component of the secondary magnetic field and this limits the ability of the interpreter to discriminate between anomalies due to the different source types listed above.

Message-to-noise ratio. As was discussed previously, we wish to distinguish between system noise and geologic noise. The system noise levels listed in Figures 4 and 5 constitute one aspect of the writer's merit rating of known AEM systems; these noise levels are reasonably hard. However, to determine their significance, we need to measure the ratio of peak anomaly to system noise for each of the targets listed in the previous section.

Geological noise is quite another matter. For ore search we usually like to reject the geologic noise due to patches and extensive covers of overburden, lakes, swamps and other surficial features. However, for hydrological purposes, this is not true. For infinite thin sheets of overburden, we can predict on theoretical grounds that the merit rating of AEM systems based on rejection of this type of overburden response is as follows:

1. T_Y - R_Z
2. T_X - R_X
3. T_Y - R_Y
4. T_Z - R_Z
5. T_X - R_Z

where X is along the line joining the transmitter T and receiver R while Z is vertical. Many operating AEM systems are combinations of these basic coil configurations so that special calculations are required to obtain a merit rating for each known system. Frischknecht (1967) provides information which permits ready calculation of the uniform overburden rejection merit rating for all known systems. For finite patches of conductive overburden the relative merit ratings may be quite different and the horizontal disk model becomes pertinent.

We may reduce the response of patches or extensive layers of overburden by reduction of ρ or ω. The response of a highly conductive half space becomes a problem in arid regions and it may be decreased by decreasing the product $\omega\rho^2$. For most rigid boom systems, $\omega\rho^2$ is of order 5×10^5 m^2 sec^{-1} while for most towed bird systems it is about 10^2 larger. Hence it is not surprising that the rigid boom systems are much less responsive to highly conductive overburden or host rock than are the towed bird systems. However, the responses of some desirable targets may be lost in reducing $\omega\rho^2$ so that a figure of merit for geologic noise really depends upon analysis of the geologic problem and environment at hand. For example, if one wishes to map moderately conductive faults and shears as well as highly conductive massive sulphides, then $\omega\rho^2$ needs to be high and one may need to be prepared to accept and recognize a high overburden response as well. If more than one spatial component of secondary field is measured, then discrimination between conductors differently oriented may be possible. Similarly if more than one frequency (or a multitude of time samples in time-domain systems) is employed it is possible to vary $\omega\rho^2$ and so discriminate between the different sources on this basis. For any given geological problem, one needs to decide what is geologic noise and what is message and conduct an AEM survey which provides optimum discrimination between the two. The ability of a system to provide an estimate of σt materially aids the interpreter in this discrimination process.

Resolution. Two adjacent conductors can be resolved better as the flying height h and the coil separation ρ are made smaller. Hence resolution is better with fixed boom systems than with towed bird systems as a comparison of Figures 22 and 29 will attest. The Hunting Canso system will resolve two parallel conductors when they are 95 m apart whereas the Varian-TGS system will resolve them when they are as close as 30 m.

Efficiency. In an airborne electromagnetic survey we are seldom justified in attempting to detect or delineate all of the anomaly sources in the area of search. We shall demonstrate that any attempt to detect *all* elongate conductors in the length range 120 to 560 m is prohibitively costly and that about a 75% probability of detection of randomly oriented targets in this length range is a

Contents

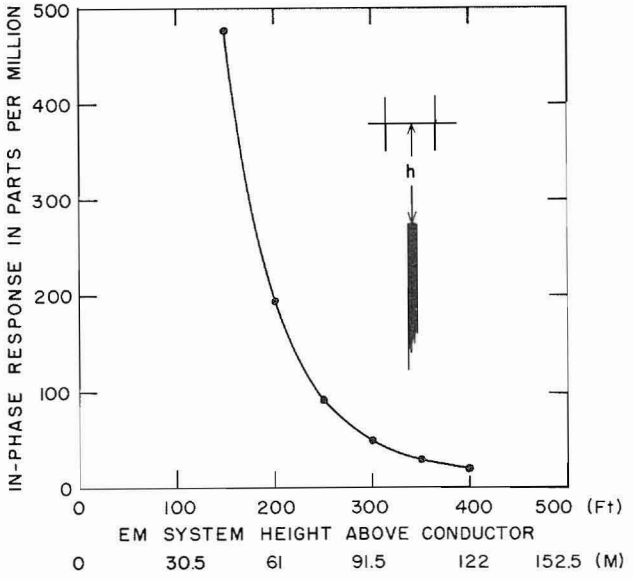


Figure 36. Maximum in-phase response versus height h of Varian-TGS helicopter system above a half-plane conductor (courtesy of Texas Gulf Sulphur Co.).

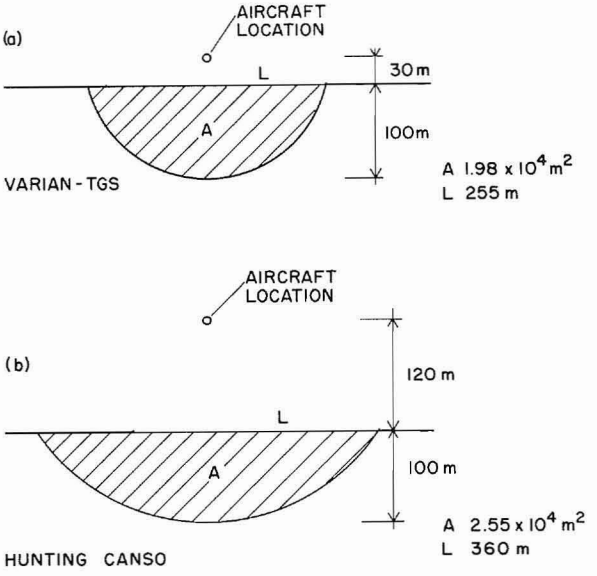


Figure 37. Limits of exploration for (a) Varian-TGS system, and (b) Hunting Canso system in a non-dissipative earth.

SYSTEM	ASSUMED SURVEY ALTITUDE	ESTIMATED DEPTH OF EXPLORATION	A	L	ADAPTABILITY	OPERATION IN RUGGED TERRAIN	ACCOMPANYING INSTRUMENTATION
NUCOM	30 m	35 m		119 m	AH	2	
LOCKWOOD	30 m	58 m		163 m	AH	2	M
SCINTREX HEM 701	30 m	89 m		231 m	AH	2	M
BARRINGER #1	30 m	89 m		231 m	AH	2	M
SANDER	30 m	61 m		163 m	AH	2	?
BARRINGER #2	30 m	89 m		231 m	AH	2	M
VARIAN - TGS	30 m	100 m	$1.98 \times 10^4 m^2$	253 m		1	
NEWMONT-AERO	30 m	76 m		203 m		1	M
AERO CANSO	60 m	?		?		6	M,G
AERO OTTER	45 m	85 m		191 m		3	M
BOLIDEN	45 m	63 m		278 m		3	
INCO	122 m	69 m		296 m		6	M
ABEM	90 m	100 m		340 m	AF	7	
McPHAR F400	122 m	115 m		365 m	AF	5	A, M, G
AEROPHYSICS	122 m	25 m		165 m		6	
HUNTING (LOCKWOOD)	122 m	110 m	$2.55 \times 10^4 m^2$	360 m		6	M,G
INPUT	122 m	>110 m ?		>400m		6	M,G

CODE :
AH ADAPTABLE TO HELICOPTER
AF ADAPTABLE TO FIXED WING AIRCRAFT
M MAGNETOMETER
G γ RAY SPECTROMETER
A AFMAG

Figure 38. Characteristics of available AEM systems.

break point for costs. Slichter (1955), Agocs (1955), and Savinskii (1965) among others have discussed the statistics of search in relation to geophysical surveys.

There are various ways in which one might determine the efficiency of an AEM survey. Schaub (1961a, 1962c) has considered efficiency as defined by that area under the anomaly due to a sphere which lies above the noise level; the area under the anomaly is expressed in units of the noise level. He finds that the relative efficiencies of the various AEM systems change with the terrain clearance.

An alternative means of estimating efficiency is to calculate the area searched beneath the earth's surface by each AEM system, operating at its normal terrain clearance. For example, the Varian-TGS system with a noise level of 10 ppm and a coil separation of 15 m has a depth of exploration for a half plane in an essentially non-dissipative earth of about 100 m assuming a terrain clearance of 30 m. Figure 36 provides the scale-model evidence upon which this conservative estimate is based. If we then draw an arc of radius 130 m with the detection system as center, we find that the intersection with a planar earth is as illustrated in Figure 37a. The area of the segment A is 1.98×10^4 meters squared. For a towed bird system such as the Hunting Canso system we assume a terrain clearance of about 120 m and an arc of radius 220 m as illustrated in Figure 37b. The radius of

such an arc depends on the system noise level and on the response of the system to a half plane. If we accept the noise levels listed in Figures 4 and 5, then the depths of exploration are as shown in Figure 38.

The depth of exploration estimates have been obtained in the following manner:

1. Assume the same amplitude of response to a half plane for all systems within the towed bird class and separately for all systems within the rigid boom class.
2. Assume that the response of the half plane decreases as the fourth power of depth $(D + H)$ below the aircraft for all systems.
3. The depth of exploration D is then

Rigid boom

$$D = \left[\sqrt[4]{\frac{n_e \text{ (System)}}{n_e \text{ (Varian-TGS)}}} \times (D + H)\right] - H$$

where H is the aircraft height.

Towed bird

$$D = \left[\sqrt[4]{\frac{n_e \text{ (System)}}{n_e \text{ (Hunting)}}} \times (D + H)\right] - H$$

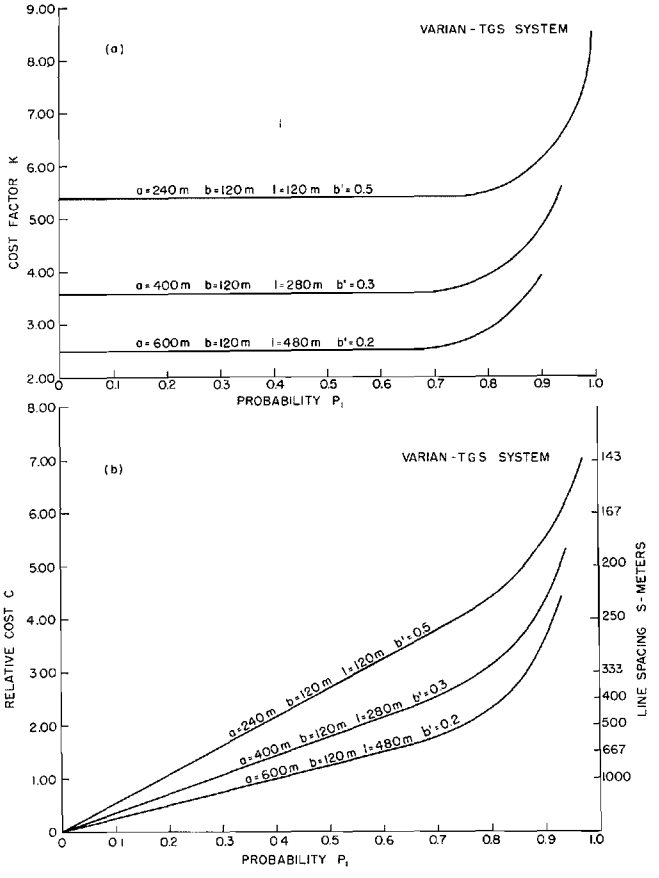


Figure 39. Relative cost C and cost factor $K = C/P_1$ probability P_1 of detection, on one or more lines, of anomalies of various lengths by Varian-TGS system.

The two assumptions stated are both open to question so that the estimated depths of exploration must be considered as approximate only.

Still another measure of efficiency is the length L of the chord formed by the earth's surface and the exploration arc; these lengths L are also tabulated in Figure 38 for all systems.

The final measure of efficiency discussed here is perhaps the most significant. We use Figure 14 to obtain the width of the anomaly, at a noise level of 850 ppm for the Hunting Canso system, of approximately 800 feet or 240 m. Similarly, from Figure 26 the width of the anomaly for a noise level of 10 ppm for the Varian-TGS system is approximately 400 feet or 120 m. If we then add these anomaly widths to the length and thickness of a conductor, we obtain the true anomaly widths and lengths. For example, with the Varian-TGS system a thin sheet conductor 120 m long will produce a measurable anomaly 240 m long by 120 m wide. The anomaly will be roughly elliptical in shape and of major axis $a = 240$ m and minor axis $b = 120$ m; the ratio $b' = b/a$ of these axes is 0.5. We may then use the tables by Savinskii (1965) to obtain the probability P_1 of one or more flight lines passing over a randomly oriented anomaly of given b' in a grid of lines spaced a distance s apart. If then we assume the costs C per square kilometer to be proportional to the kilometers of line flown, we may obtain an expression for the cost factor K as

$$K = \frac{C}{P_1} \qquad 29$$

We have plotted both C and K versus P_1 for each of the Varian-TGS helicopter and Hunting Canso systems in Figures 39 and 40, respectively. From these figures we observe that there is a cost breakpoint at a probability of about 75% for randomly oriented conductors of lengths 120 to 560 m for either rigid boom or towed bird systems. We also observe that the costs for the towed bird system are about half that of the rigid boom system for equal probabilities and assuming the same operating cost per kilometer. In fact, the operating costs for helicopters are considerably higher than fixed-wing aircraft because of lower flying speeds.

On a purely statistical basis, and assuming that operating costs are independent of the kilometers of survey line flown, the cost factor is independent of probability below probabilities of 0.7 (Figures 39a and 40a). We also learn from Figures 39b and 40b that it costs nothing to obtain a zero probability of detecting an anomaly!

Operating costs are roughly proportional to the number of kilometers flown so that the Relation 29 should be modified to

$$K = \frac{aC}{P_1} \qquad 30$$

where a is a fractional cost reduction governed by the number of kilometers flown on any survey. The cost C used in Figures 39 and 40 was obtained from

$$C = \frac{10^3}{s} \qquad 31$$

where s is the line spacing in meters. Thus C may be made a true cost upon multiplication by an appropriate monetary unit.

Contents

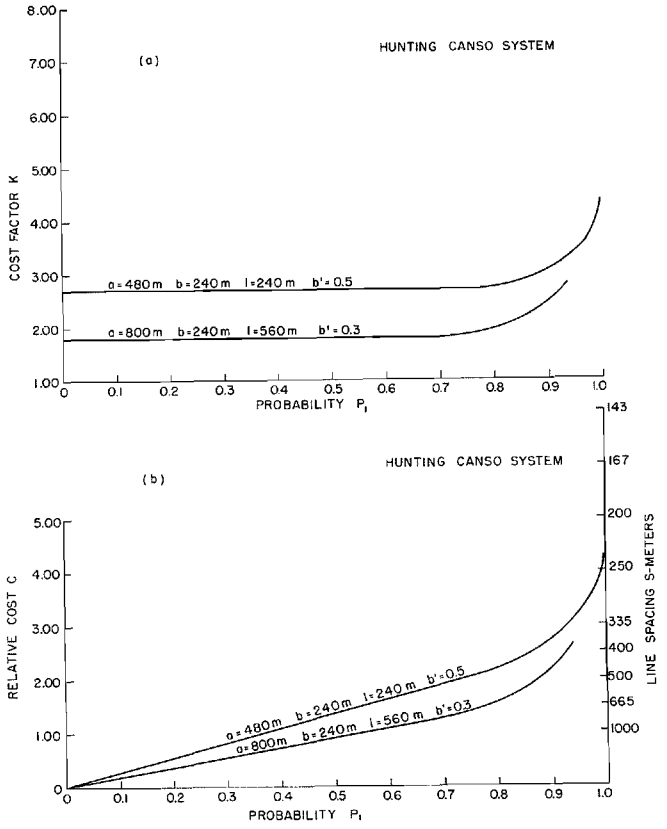


Figure 40. Relative cost C and cost factor $K = C/P_1$ versus probability P_1 of detection, on one or more lines, of anomalies of various lengths by Hunting Canso system.

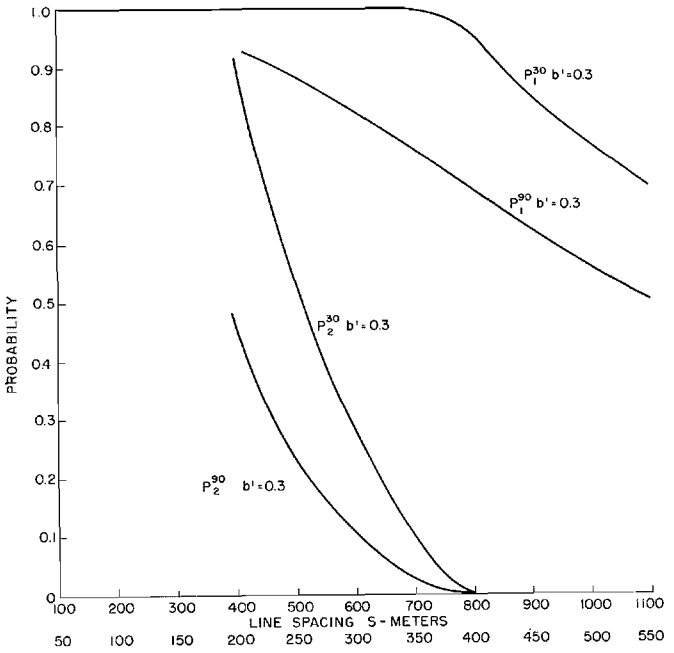


Figure 41. Probability of detection P versus line spacing s. Subscripts 1 and 2 refer to detection by one or more lines, and by two lines, respectively. Superscripts 30 and 90 refer to maximum range of strike from normal to flight lines. Upper s scale pertains to Hunting Canso system while lower s scale pertains to Varian-TGS system.

At a line spacing of 400 m, we observe the following:

Hunting Canso System				*Varian-TGS System*			
conductor length (m)	P_1	C	K	conductor length (m)	P_1	C	K
560	0.930	2.50	2.68	480	0.830	2.50	3.10
240	0.865	2.50	2.89	280	0.698	2.50	3.58
				120	0.465	2.50	5.40

The above figures pertain to constant cost per square kilometer and a preselected line spacing of 400 m. If now we attempt to obtain the same probability for 480 m and 280 m conductors with the Varian-TGS system as for the 560 and 240 m conductors with the Hunting Canso system, the relative line spacings and costs are:

Hunting Canso			*Varian-TGS*		
$l = 560$ m	$s = 400$ m	$c = 2.50$	$l = 480$ m	$s = 230$ m	$c = 4.30$
$l = 240$ m	$s = 400$ m	$c = 2.50$	$l = 280$ m	$s = 265$ m	$c = 3.75$

Evidently the Varian-TGS system should be flown at 250 m line intervals to obtain the same probabilities as the Hunting Canso system when flown at 400 m line intervals; the costs are proportional to the line density.

In the above calculations, the width of anomaly used for both systems is that derived for a vertical half plane. Conductors as short as 240 m will have half widths slightly less than those used but the correction is small. One could carry out similar analyses for all systems and obtain the two general conclusions:

1. For randomly oriented conductors of lengths typical of massive sulphide orebodies it is inefficient to seek probabilities in excess of about 75%.

2. Towed-bird systems are more efficient than rigid boom systems.

If the conductors have a preferred orientation rather than a random orientation, then the probability of detection increases if this preferred orientation is within 30 degrees of normal to the flight lines. In Figure 41 the comparison between the probabilities for random (P^{90}) and preferred (P^{30}) orientations is made. The labels P_1^{30} and P_1^{90} refer to the probability of one or more lines crossing the anomaly while P_2^{30} and P_2^{90} refer to the probabilities of two lines crossing the anomaly; the superscript 30 refers to the preferred orientation and the superscript 90 refers to the random orientation. The curves apply either to conductors 560 m long in an area surveyed with the Hunting Canso system, in which case the upper line spacing scale is employed, or to conductors 280 m long in an area surveyed with the Varian-TGS system, in which case the lower line spacing scale is used.

For these particular conductors, a 75% probability for random orientation becomes nearly 100% for preferred orientation. The anomaly due to 560 m conductors roughly normal to the flight lines will be detected on two flight lines at about 90%

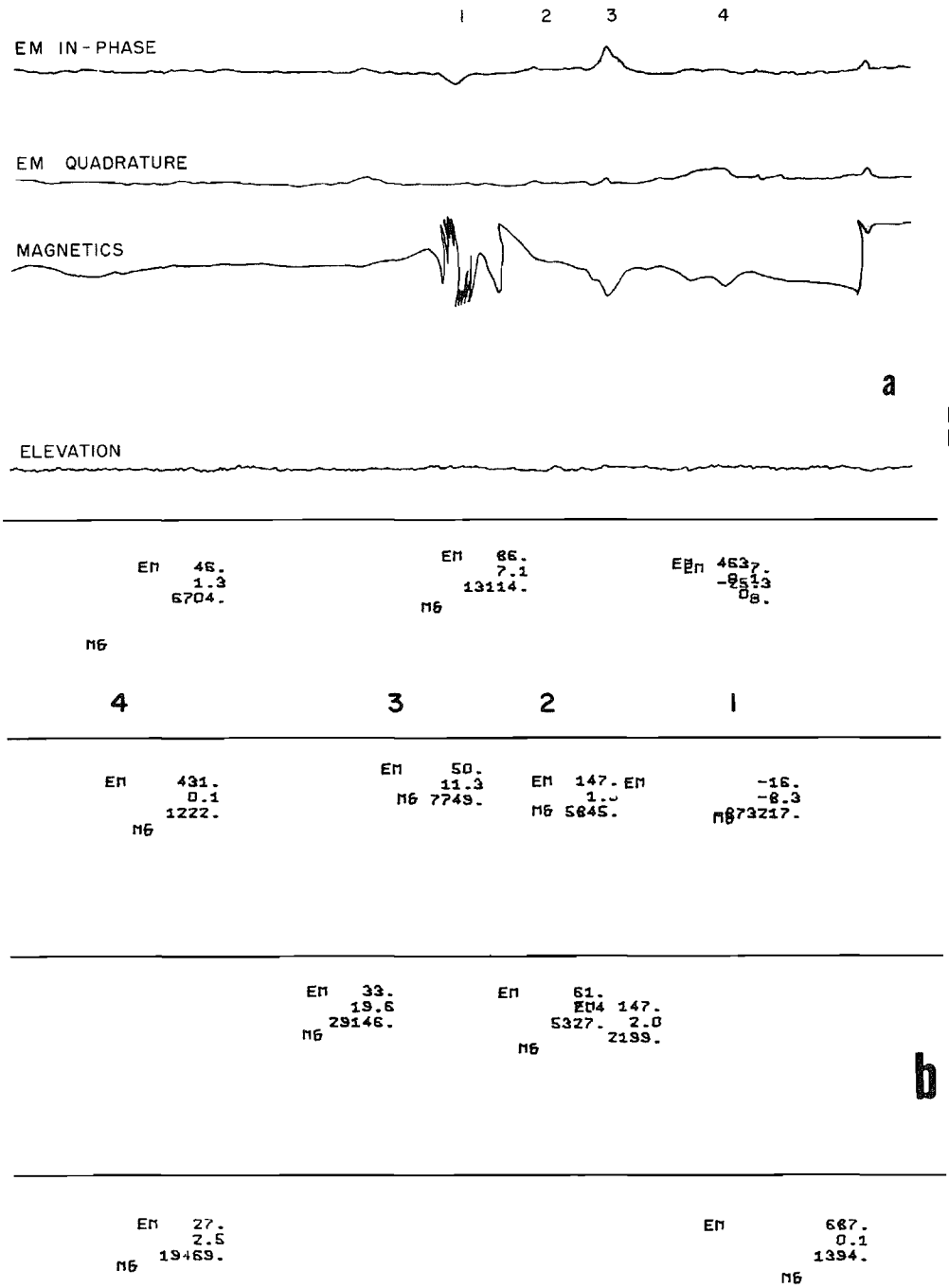


Figure 42. Example of computer interpretation and printout of Newmont/Aero helicopter electromagnetic method.

probability if the spacing is 400 m for the Hunting Canso system but the probability will be only about 45% if the conductors are randomly oriented. It would appear from Figures 40 and 41 that a 400 m spacing is too high for the Hunting Canso system for conductors 240 to 560 m in length and that an efficient spacing is 550 m. On the other hand, the Varian-TGS system is apparently the most efficient for line spacings of about 275 m, assuming conductors in the 120 m to 480 m length range.

The efficiency of any fixed boom system will be decreased relative to the Varian-TGS system if its spread ρ is less than 50 feet and the efficiency will be increased relative to the Varian-TGS system if its spread ρ is greater than 50 feet.

Adaptability to any aircraft. Most airborne electromagnetic systems are designed for use with a specific aircraft. Those which may *readily* be adapted to any helicopter are labelled *AH* in Figure 38 and those which may *readily* be adapted to any fixed wing aircraft are labelled *AF* in the same figure.

Performance in rugged terrain. The most versatile system in rugged terrain unquestionably is a helicopter system where the boom is an integral part of the helicopter. Following this type of system, in order of merit, are: rigid boom towed from helicopter, rigid boom mounted on light aircraft, and finally towed bird systems. While this rating must be somewhat subjective, we believe that the figures for it, as given in Figure 38, are apt to

meet with general approval. Aircraft manoeuverability obviously enters into this rating.

Compatible equipment. Accompanying some active electromagnetic systems are such auxiliary remote sensors as a magnetometer *M*, an AFMAG (*A*) unit, and a gamma-ray spectrometer *G*. If such instruments are known to accompany the electromagnetic system, they are so indicated in Figure 38.

General merit. The general merit of an AEM system greatly depends upon the topographic and geological environment in which the system is to be applied. Perhaps the above discussion will permit the reader to select a system suited to his particular task. General merit ratings must be somewhat subjective since definitive comparisons of the various systems in relation to all of the above criteria are not yet available.

Possible future developments

There is evidence that the following expansions of the concept of an airborne electromagnetic system are being initiated now:

1. Multicomponent receiving coil systems;
2. Two frequencies *and* two phase components;
3. Digital data acquisition; and
4. Automatic interpretation via digital computers.

The first of the expansion steps listed is highly desirable if we are to make a true record of the subsurface conductivity distribution and then to discriminate between the various sources. This discrimination is materially assisted by the use of two or more frequencies and the measurement of both in-phase and quadrature phase components where necessary. It is extremely important that attention be given to acquiring all possible information on the subsurface conductivity distribution and to discriminate only in the interpretation stage. To make this feature possible, it is necessary to acquire the vast amount of electromagnetic, and auxiliary, data on digital magnetic tape and to process and interpret this data automatically.

Figure 42b shows a primitive example of a computer interpretation and print-out of data acquired by the Newmont/Aero helicopter system. In this interpretation the pertinent Argand diagram is stored in the computer, as is a basic magnetic interpretation scheme for dikes. The output then is a display, at the correct location along the flight line, of σ, t, k and d where σ is the conductivity, k is the susceptibility, t is the width, and d is the depth of a thin dike model which fits the observed data.

One flight line of the raw data, upon which the computer interpretation is based, appears in Figure 42a. The anomalies labelled 1, 2, 3 and 4 serve to relate the second flight line in the printout to the raw data. The distances of the centers of the letters *EM* and *MG* from the flight line above them, are the depths deduced from electromagnetic and magnetic data, respectively. The first number below the flight line is the thickness t in feet, the second number is the conductivity in mhos per meter, and the third number is the susceptibility in cgs units. Much more sophisticated interpretation schemes can be developed and all portrayal and location of data may be made automatic. A small computer may be carried on board some aircraft or maintained at a field camp for daily data processing. These are possibilities well within the state of the art.

Beyond the above developments there lie the possibilities of extending the frequency range beyond the narrow 10^2 Hz to 5 X

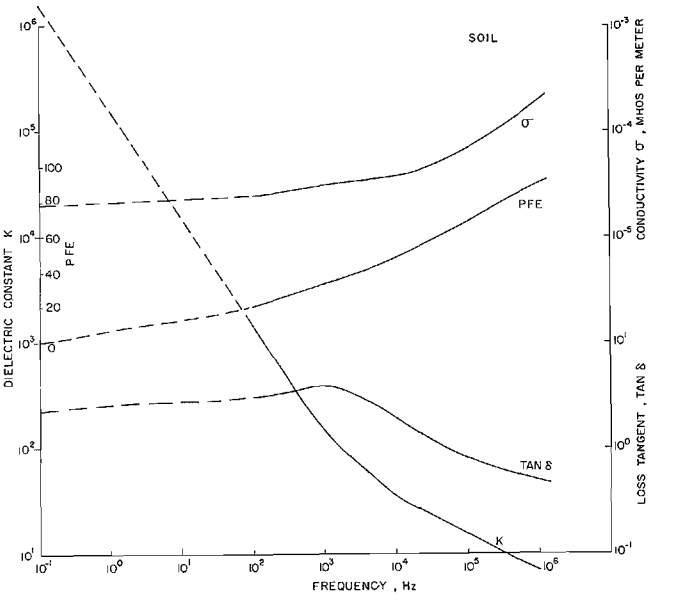


Figure 43. Relaxation spectra for volcanic ash soil with 14% by weight of water (after Jiracek, 1967).

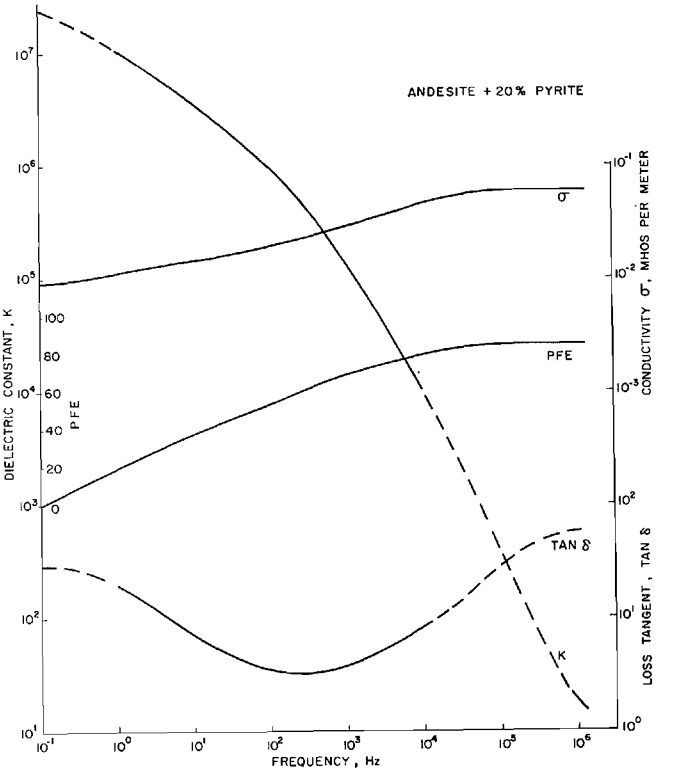


Figure 44. Relaxation spectra of mix of andesite particle plus 20% pyrite particles (after Collett, 1959).

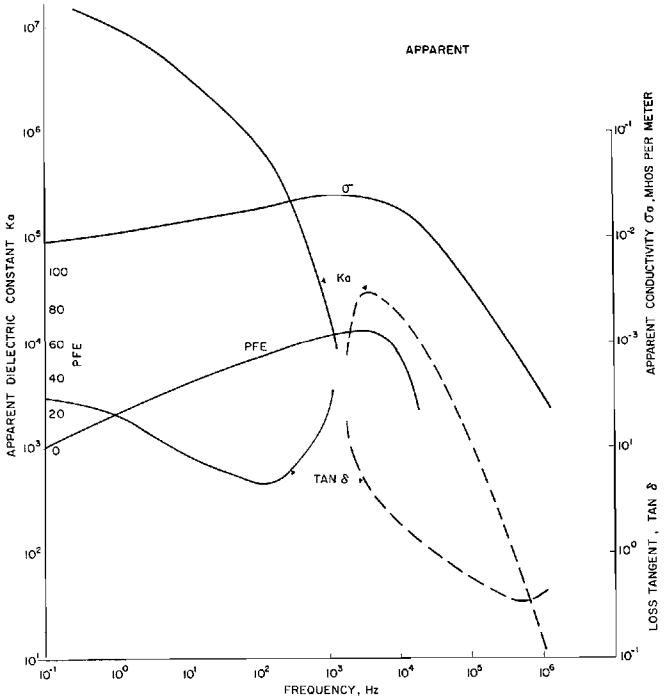


Figure 45. Apparent relaxation spectra for two-layer earth. Material of first and second layers is described by data of Figures 43 and 44, respectively. The depth of the first layer is 10 m.

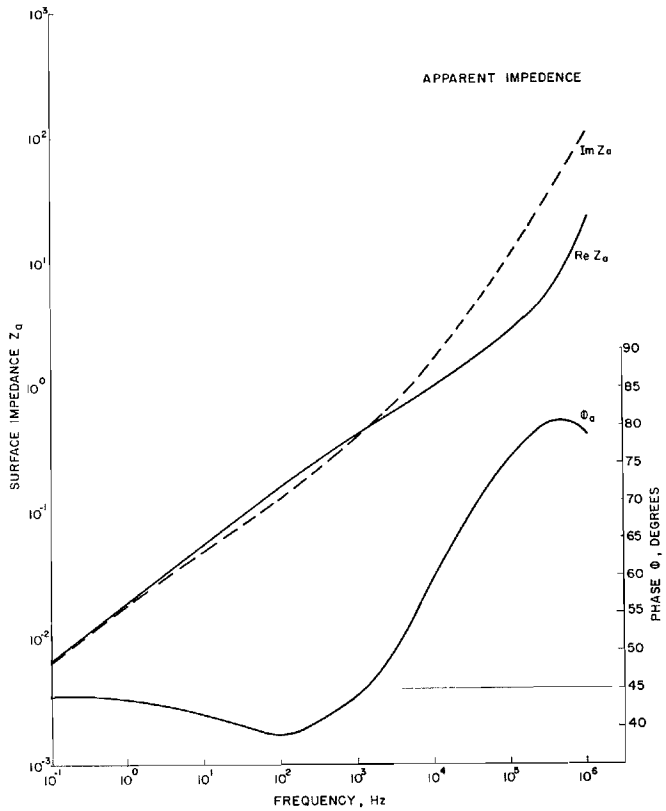


Figure 46. Real and imaginary parts and phase of apparent impedance of the two-layer earth described by Figure 45.

10^3 Hz range currently employed to permit working in geologic environments not hitherto suited to the limited-scope AEM systems available to us. Additionally there is the distinct possibility of measuring the induced polarization phenomena inductively from the air.

To illustrate this latter point, let us assume that the frequency range 10^{-1} Hz to 10^6 Hz could be used for AEM exploration. Then the behaviour of the conductivity and dielectric constant for typical earth materials must be known over this frequency range to predict the electrical parameters which can be measured inductively from a moving aircraft. Figure 43 shows the relaxation spectra for a volcanic ash soil with 14% by weight of water (Jiracek, 1967). Information was only available above 10^2 Hz so that the data is extrapolated below this frequency with obvious gross uncertainty. Figure 44 shows the relaxation spectra for a somewhat synthetic mix of 80% andesite and 20% pyrite particles as described by Wait (1959) and Collett (1959); the dielectric constant and loss tangent are uncertain below 10^0 Hz and above 10^4 Hz. If these two materials constitute a two-layer earth, then the apparent relaxation spectra of the equivalent homogeneous earth are as shown in Figure 45. If we could, in fact, measure these apparent quantities over a broad frequency range then we would be able to deduce the parameters of the two-layer earth structure which give rise to them. The apparent resistivity profile could be caused by a three-layer 'non-polarizable' earth but the rate of change of conductivity with frequency (the PFE or percent frequency effect) is sufficiently large to indicate a strongly polarizable layer, which is in fact present. The apparent dielectric constant is extremely high at low frequencies, again suggesting polarizable material. The discontinuities in apparent dielectric constant and loss tangent just above 10^3 Hz are due to the phase between the electric and magnetic vectors exceeding 45° as illustrated in Figure 46. Later we shall see that this phase of the impedance corresponds to a phase of 90° for the complex conductivity.

The model and the formulation upon which Figures 45 and 46 are based are as follows:

Model	Layer 1	σ_1 , K_1 as Figure 43
		$\mu = \mu_0$, thickness = 10 m
	Layer 2	σ_2 , K_2 as Figure 44
		$\mu = \mu_0$, thickness = ∞

Formulation. The complex plane wave impedance Z, for an $e^{i\omega t}$ time dependence, of a homogeneous nonmagnetic half space is

$$Z = |Z|e^{i\phi} = \frac{i\mu_0\omega}{\gamma} = \frac{\pm E_j}{H_k} \; ; \; j \neq k \qquad 32$$

where ϕ is the phase and Z the modulus of Z, ω is the angular frequency, μ is the magnetic permeability of free space, γ is the

Contents

wave number of the half-space, and where (E_j, H_k) are orthogonal electric and magnetic intensity pairs. The wave number γ may be written for our purposes as

$$\gamma = [i\mu_0\omega(\sigma' + i\epsilon'\omega)]^{1/2} \quad 33$$

in which the dielectric permittivity ϵ', and the conductivity σ' are real functions of frequency. The loss tangent then is defined by

$$\tan\delta = \frac{\sigma'}{\omega\epsilon'} \quad 34$$

The amplitude reflection coefficient for normal incidence is written as

$$r = \frac{Z - Z_0}{Z + Z_0} \quad 35$$

where Z_0 is the plane wave impedance of free space. The amplitude reflection coefficient is, in general, complex since Z is complex. At high frequencies such that $\sigma'/\omega\epsilon' \ll 1$, γ is real so that Z and hence r are real.

We could replace Equation 33 by

$$\gamma^2 = i\mu_0\omega\sigma \quad 36$$

where

$$\sigma = \sigma' + i\epsilon'\omega \quad 37$$

is a complex conductivity which can account for both real conductivity and dielectric constant. This complex conductivity is then, via Equation 32, related to the impedance as follows:

$$\sigma = \frac{i\mu_0\omega}{(Z)^2} = \frac{i\mu_0\omega}{|Z|^2 e^{i2\phi}} \quad 38$$

$$\sigma' = \frac{\mu_0\omega}{|Z|^2}\sin 2\phi \quad 39$$

$$\epsilon' = \frac{\mu_0}{|Z|^2}\cos 2\phi \quad 40$$

The phase ϕ is zero for an electromagnetic wave incident upon a loss-free dielectric half space and is 45 degrees for an electromagnetic wave incident upon a conductor in which dielectric displacement currents are negligible. If the half space is layered and representable by a lossy dielectric, then the phase may range from negative through large positive angles as the frequency is varied. When the phase passes through zero degrees, the conductivity σ' changes sign according to Equation 39, whereas when the phase passes through 45°, the dielectric permittivity ϵ' changes sign according to Equation 40.

For an n-layered structure, we may use the formulation (Ward, 1967):

$$Z_a = Z_1\frac{\hat{Z}_2 + Z_1\tanh\gamma_1 h_1}{Z_1 + \hat{Z}_2\tanh\gamma_1 h_1} \quad 41$$

$$\hat{Z}_2 = Z_2\frac{\hat{Z}_3 + Z_2\tanh\gamma_2 h_2}{Z_2 + \hat{Z}_3\tanh\gamma_2 h_2} \quad 42$$

$$\hat{Z}_n = Z_n\frac{\hat{Z}_{(n+1)} + Z_n\tanh\gamma_n h_n}{Z_n + \hat{Z}_{(n+1)}\tanh\gamma_n h_n} \quad 43$$

where $Z_j = i\mu_0\omega/\gamma_j$ is the characteristic impedance of the jth layer. Z_j is the impedance at the top of the jth layer, and Z_a is the *apparent impedance* of the structure and at any given frequency is equal to the impedance of an equivalent homogeneous half space. The h_j are the thicknesses of the layers in the structure.

Then the amplitude reflection coefficient for an n-layered structure is

$$r = \frac{Z_a - Z_0}{Z_a + Z_0} \quad 44$$

and the complex apparent conductivity, the real apparent conductivity and the real dielectric permittivity are from Equations 38, 39 and 40, respectively:

$$\sigma_a = \frac{i\mu_0\omega}{|Z_a|^2 e^{i2\phi_a}} \quad 45$$

$$\sigma_a' = \frac{\mu_0\omega}{|Z_a|^2}\sin 2\phi_a \quad 46$$

$$\epsilon_a' = \frac{\mu_0}{|Z_a|^2}\cos 2\phi_a \quad 47$$

It is convenient to use dielectric constant rather than permittivity so that Equations 40 and 47 yield

$$K' = \frac{\mu_0}{\epsilon_0}\frac{1}{|Z|^2}\cos 2\phi \quad 48$$

and

$$K_a' = \frac{\mu_0}{\epsilon_0}\frac{1}{|Z_a|^2}\cos 2\phi_a \quad 49$$

where ϵ_0 is the dielectric permittivity of free space.

In the next part of the discussion, formulas are used which have been developed assuming an $e^{-i\omega t}$ time dependence. To relate them to the preceding, the following substitutions are made:

$$\begin{array}{cc} \frac{e^{i\omega t}}{\gamma^2} & \frac{e^{-i\omega t}}{-k^2} \\ \gamma & -ik \\ i & -i \end{array} \quad 50$$

The electric field component in the direction of the axis of an infinitesimal electric dipole grounded to a homogeneous earth is

$$E_x = \left[\frac{Ids}{2\pi\sigma}\right]\left[-\frac{\partial^2}{\partial y^2}\left(\frac{1}{\rho}\right) + \frac{1 - ik\rho}{\rho^3}e^{ik\rho}\right] \quad 51$$

The first term represents the resistive coupling while the second term represents the inductive coupling in the standard conductive method of measuring induced electrical polarization (e.g., frequency dependence of σ^1). We usually select $k\rho$ so that the inductive term is negligible in conductive induced polarization measurements. If we now wish to make these measurements

inductively we might measure the horizontal magnetic component of a coil of vertical axis located on a homogeneous earth

$$H\rho = \frac{-1}{i\mu\omega}\frac{C}{\rho^3}\left[-k^2\rho^2\,(I_1K_1 - I_0K_0) - 4ik\rho\,(I_1K_0 - I_0K_1) + 16\,I_1K_1\right] \qquad 52$$

where C is the dipole moment $\vec{c} = -i\mu\omega I\vec{da}/4\pi$, ρ is the distance of the point of observation from the center of the transmitting coil, k is the wave number, I_0, K_0, I_1, K_1 are modified Bessel functions of first and second kind of orders zero and unity and of argument $(-k\rho/2)$. If we are to find measurable values of *both* in-phase and quadrature parts of $H\rho$, then $k\rho$ must be confined to the range 1 to 30 as discussed earlier. A second constraint on $k\rho$ is that it possess approximately equal real and imaginary parts if both ϵ' and σ' are to be measured with precision. That is,

$$k\rho = \left[\mu\omega(\epsilon'\omega + i\sigma')\right]^{1/2}\rho \qquad 53$$

is to have $\epsilon'\omega$ within one order of magnitude of being equal to σ' in order that displacement currents, represented by $\epsilon'\omega$, are not dominated by conduction currents. The other constraint, that $1<|k\rho|<30$ may be satisfied by selection of ρ. Presumably, if ϵ and σ' were constants, one could choose a frequency ω such that $\epsilon'\omega \sim \sigma'$ and then choose a ρ such that $1<|k\rho|<30$. Such a procedure conceivably could demand a frequency f anywhere from 10^{-1} Hz to 10^6 Hz and might demand some extreme values of ρ. While our knowledge of relaxation spectra for earth materials over a very broad frequency range is meager, it appears that $\sigma'/\omega\epsilon' = \tan\delta$ is within one order of unity for many rocks and soils (see Figures 43 and 44, and articles by Collett, 1959; Von Hippel, 1954; and Keller and Licastro, 1959) regardless of frequency up to about 10^6 Hz. Thus, both ω and ρ may be variables with which to adjust $|k\rho|$. It is essential that ϵ' and σ be measured as functions of frequency within the range 10^{-1} Hz to 10^6 Hz for many earth materials before one can embark upon a program of development of inductive induced electrical polarization.

The concept of apparent dielectric constant as well as apparent conductivity would appear to be important to interpretation of electromagnetic data acquired over a broad frequency band. It is evident from Figures 43, 44 and 45 that all earth materials are polarizable somewhere within the 10^{-1} Hz to 10^6 Hz frequency band so that selection of the operating frequency may need to be governed by the relative response of conventionally 'polarizable' and 'non-polarizable' rock or soil units. Depth of penetration is an additional factor to consider.

Wait (1954), Bhattacharyya (1964), Phillips, *et al.* (1968), Ward, *et al.* (1968b), Morrison, *et al.* (1968), and especially Dias (1968) have presented additional discussions of the possibility of measuring both dielectric constant and electrical conductivity by inductive means.

If operating frequencies of an AEM system can be extended downward towards 1 Hz or lower, then it will also be possible to measure the magnetic permeability and to determine, uniquely, all of the parameters of subsurface permeable conductors in the manner described by Ward (1959b, 1961).

The reduction of system noise and the recognition but not elimination of geological noise are two areas of development to which we may look with some considerable optimism. Each of these developments will lead to a greatly enhanced depth of exploration. To facilitate both of these developments, systems must encompass more frequencies and a broader frequency range, more received components or even more than one transmitting coil, and coherent detection schemes either by analog devices in the aircraft or subsequently by computer. A thorough analysis of the statistical characteristics of message and noise (both geological and system) is required to permit the design of optimum filters to separate assumed message from assumed noise. It is entirely possible that a dynamic filter will be required for this purpose so that if the statistical characteristics of either message or noise change, then the filter will automatically change its characteristics to suit.

Conclusion

While there is a healthy expansion of the concept of an airborne electromagnetic system, there is much need for an optimum system of vastly greater scope and capability. Many of the recent *new* airborne electromagnetic methods are little more than updated modifications of systems developed many years ago.

Acknowledgments

The University of California and the Mobil Oil Co. have provided research funds permitting completion of this review. Some of the material upon which this manuscript is based was obtained while the writer was engaged in research sponsored by the U.S. Office of Naval Research (Contract NONR 222(89)) and the U.S. National Aeronautics and Space Administration. I am indebted to G.R. Jiracek for the computations of relaxation spectra and to B. Fuller and C.E. Johnson for the automatic interpretation scheme presented here; their work was performed at the University of California, Berkeley.

References

Agocs, W.B., 1955. Line spacing effect and determination of optimum spacing illustrated by Marmora, Ontario, magnetic anomaly. *Geophysics,* 20 (4): 871 - 885.

Barringer, A.R., 1963. The use of audio and radio frequency pulses for terrain sensing. The University of Michigan, Ann Arbor, *Proc. Second Symp. on Remote Sensing of Environment,* p. 201 - 214.

Bhattacharyya, B.K., 1964. Electromagnetic fields of a small loop antenna on the surface of a polarizable medium. *Geophysics,* 29 (5): 814 - 831.

Boniwell, J.B., 1967. Some recent results with the INPUT airborne EM system. *Trans. CIM,* LII: 60 - 67.

Bosschart, R.A., 1961. On the occurrence of low resistivity geological conductors. *Geophys. Prosp.,* 9 (2): 203 - 212.

Bosschart, R.A., 1964. Analytical interpretation of fixed source electromagnetic prospecting data. Delft University, Ph.D. thesis, 103 pp.

Boyd, D., and B.C. Roberts, 1961. Model experiments and survey results from a wingtip-mounted electromagnetic prospecting system. *Geophys. Prosp.,* 9 (3): 411 - 420.

Brant, A.A., W.M. Dolan, and C.L. Elliot, 1966. Coplanar and coaxial EM tests in Bathurst area, New Brunswick, Canada, 1956. *Mining Geophysics,* Volume I, Tulsa, Society of Exploration Geophysicists, p. 130 - 141.

Cheriton, C.G., 1959. Anaconda exploration in the Bathurst District of New Brunswick, Canada. *AIME Trans.,* 217: 278 - 284.

Collett, L.S., 1959. Laboratory investigation of overvoltage. In *Overvoltage Research and Geophysical Applications,* Ed. J.R. Wait, New York, Pergamon Press.

Collett, L.S., 1966. Airborne electromagnetic survey over the Winkler Aquifer, Manitoba. G.S.C. Paper 66-2, *Report of Activities November 1965 to April 1966,* Geological Survey of Canada, p. 6 - 9.

Dias, C.A., 1968. Theory for an inductive method of measuring induced electrical polarization (Ph.D. thesis in preparation).

Douloff, A.A., 1960. The response of a disk in a dipole field. *Geophysics,* 26 (4): 452 - 464.

Fleming, H.W., and R.R. Brooks, 1960. Geophysical case history of the Clearwater deposit, Northumberland County, New Brunswick, Canada. *AIME Trans.* 217: 131 - 138.

Frischknecht, F.C., 1967. Fields about an oscillating magnetic dipole over a two-layer earth, and application to ground and airborne electromagnetic surveys. *Quarterly, Colorado School of Mines,* 62 (1).

Gaur, V.K., 1963. Electromagnetic model experiments simulating an airborne method of prospecting. *Bull. Nat'l Geophys. Res. Inst.,* 1: 167 - 174.

Geleynse, M., and A.R. Barringer, 1964. Recent progress in remote sensing with audio- and radiofrequency pulses. The University of Michigan, Ann Arbor, *Proc. Third Symp. on Remote Sensing of Environment,* p. 469 - 494.

Grant, F.S., and G.F. West, 1965. *Interpretation theory in applied geophysics.* New York, McGraw-Hill Book Co.

Hedstrom, E.H., and D.S. Parasnis, 1958. Some model experiments relating to electromagnetic prospecting with special reference to airborne work. *Geophys. Prosp.,* 6 (4): 322 - 341.

Hedstrom, E.H., and D.S. Parasnis, 1959. Reply to comments by N.R. Paterson. *Geophys. Prosp.,* 7 (4): 448 - 470.

Jiracek, G.R., 1967. Feasibility of radio sounding to the groundwater table in Hawaii. Technical Report No. 10, Water Resources Research Center, University of Hawaii, Honolulu, Hawaii,.

Joklik, G.F., 1960. The discovery of a copper-zinc deposit at Garon Lake, Quebec. *Econ. Geol.,* 55: 338 - 353.

Keller, G.V., and F.C. Frischknecht, 1966. *Electrical methods in geophysical prospecting.* New York, Pergamon Press.

Keller, G.V., and P.H. Licastro, 1959. Dielectric constant and electrical resistivity of natural-state cores. U.S.G.S. Bull. 1052-H.

Khomenyuk, Yu. V., 1961. The double rotating field method. *Bull. (Izv.) Acad. Sci. U.S.S.R.,* Geophys. Ser., no. 12, p. 1182 - 1183 (English edition).

MacKay, D.B., and N.R. Paterson, 1960. Geophysical discoveries in the Mattagami District, Quebec. *CIM Bull.,* 53 (581).

Mizyuk, L. Ya., 1960. Methods and apparatus for airborne electrical prospecting. *Bull. (Izv.) Acad. Sci. U.S.S.R.,* Geophys. Ser., no. 6, p. 522 - 528 (English edition).

Morrison, H.F., E. Wombwell, and S.H. Ward, 1968. Electromagnetic response of polarizable permeable spheres and cylinders in a uniform field (in preparation).

Parasnis, D.S., 1966. *Mining Geophysics.* New York, Elsevier Publishing Co.

Paterson, N.R., 1959. Comments on paper by Hedstrom and Parasnis. *Geophys. Prosp.,* 7 (4): 435 - 447.

Paterson, N.R., 1961a. Experimental and field data for the dual-frequency phase-shift method of airborne electromagnetic prospecting. *Geophysics,* 26 (5): 601 - 617.

Paterson, N.R., 1961b. Helicopter EM test, Mobrun orebody, Noranda. *Can. Min. J.,* November.

Paterson, N.R., 1966. Mattagami Lake Mines – a discovery by geophysics. *Mining Geophysics,* Volume I, Tulsa, Society of Exploration Geophysicists.

Pemberton, R.H., 1961a. Combined geophysical prospecting system by helicopter. *Min. Eng.,* January.

Pemberton, R.H., 1961b. Target Mattagami. *Trans. CIM,* LXIV: 16 - 23.

Pemberton, R.H., 1962. Airborne EM in review. *Geophysics,* 27 (5): 691 - 713.

Phillips, R.J., H.F. Morrison, and D.P. O'Brien, 1968. Electromagnetic fields of a horizontal loop above a polarized layered earth (in preparation).

Podolsky, G., 1966. An evaluation of an airborne electromagnetic anomaly in northwestern Quebec. *Mining Geophysics,* Volume I, Tulsa, Society of Exploration Geophysicists.

Rattew, A.R., 1962. Helicopter-borne electromagnetic, magnetic, and radiometric survey, Coronation Mines. *Trans. CIM,* LXV: 143 - 150.

Savinskii, I.D., 1965. *Probability tables for locating elliptical underground masses with a rectangular grid.* New York, Consultants Bureau.

Schaub, Yu. B., 1961a. On a quantitative measure of the information acquired by airborne electromagnetic prospecting methods. *Bull (Izv.) Acad. Sci. U.S.S.R.,* Geophys. Ser., no. 3, p. 232 - 236 (English edition).

Schaub, Yu. B., 1961b. An experimental test of the rotating magnetic field method. *Bull. (Izv.) Acad. Sci. U.S.S.R.,* Geophys. Ser., no. 7, p. 669 - 673 (English edition).

Schaub, Yu. B., 1962a. The influence of the specific resistance of the surrounding medium on the form of anomaly curves obtained in aerial electrical prospecting. *Bull. (Izv). Acad. Sci., U.S.S.R.,* Geophys. Ser., no. 5, p. 423 - 426 (English edition).

Schaub, Yu. B., 1962b. Prospecting by the rotating magnetic field method using LI-2 and AN-2 airplanes. *Bull. (Izv.) Acad. Sci., U.S.S.R.,* Geophys. Ser., no. 7, p. 591 - 595 (English edition).

Schaub, Yu. B., 1962c. Efficiency of electromagnetic prospecting by helicopter. *Bull. (Izv.) Acad. Sci., U.S.S.R.,* Geophys. Ser., no. 8, p. 585 - 588 (English edition).

Schaub, Yu. B., 1966a. Airborne electromagnetic prospecting by the pulse-bunching method over isometric orebodies. *Izvestiya, Acad. Sci. U.S.S.R.,* Physics of the Solid Earth, no. 12, p. 794 - 797 (English edition).

Schaub, Yu. B., 1966b. Resolving power of the pulse-bunching method in mapping rocks. *Izvestiya, Acad. Sci. U.S.S.R.,* Physics of the Solid Earth, no. 12, p. 798 - 800 (English edition).

Slichter, L.B., 1955. Geophysics applied to prospecting for ores. *Econ. Geol.,* Fiftieth Anniversary Volume, p. 885 - 969.

Strangway, D.W., 1966. Electromagnetic parameters of some sulfide ore bodies. *Mining Geophysics,* Volume I, p. 227 - 242, Tulsa, Society of Exploration Geophysicists.

Tikhonov, A.N., and V.I. Dmitriev, 1959a. The influence of interference in the induction method of electrical prospecting from the air. *Bull. (Izv.) Acad. Sci. U.S.S.R.,* Geophys. Ser., no. 9, p. 991 - 992 (English edition).

Tikhonov, A.N., and V.I. Dmitriev, 1959b. On the possibility of using the induction method of electrical prospecting from the air for geological map-making. *Bull. (Izv.) Acad. Sci. U.S.S.R.,* Geophys. Ser., no. 10, p. 1053 - 1055 (English edition).

Tornquist, G., 1958. Some practical results of airborne electromagnetic prospecting in Sweden. *Geophys. Prosp.,* 6 (2): 112 - 126.

Von Hippel, A.R., 1954. *Dielectric Materials and Applications.* Cambridge, Massachusetts, M.I.T. Press.

Wait, J.R., 1954. Mutual coupling of loops lying on the ground. *Geophysics,* 19 (2): 281 - 289.

Wait, J.R., 1959. The variable-frequency method. In *Overvoltage Research and Geophysical Applications,* Ed. J.R. Wait, New York, Pergamon Press.

Ward, S.H., 1957. Airborne electromagnetic surveying. *Methods and Case Histories in Mining Geophysics.* Montreal, Canadian Institute of Mining and Metallurgy, p. 71 - 78.

Ward, S.H., and R.A. Barker, 1958. Case history of the Juniper Prospect. *Trans. AIME,* p. 100 - 104.

Ward, S.H., 1959a. AFMAG – airborne and ground. *Geophysics,* 24 (4): 761 - 789.

Ward, S.H., 1959b. Unique determination of conductivity, susceptibility, size and depth in multifrequency electromagnetic exploration. *Geophysics,* 24: 531 - 546.

Ward, S.H., 1960. AFMAG: a new airborne electromagnetic prospecting method. *Trans. AIME,* 217: 333 - 342.

Ward, S.H., 1961. The electromagnetic response of a magnetic iron ore deposit. *Geophys. Prosp.,* 9 (2): 191 - 202.

Ward, S.H., J. O'Donnell, R. Rivera, G.H. Ware, and D.C. Fraser, 1966. AFMAG – applications and limitations. *Geophysics,* 31 (3): 576 - 605.

Ward, S.H., 1966. Introduction to Chapter III, *Mining Geophysics,* Volume I, Tulsa, Society of Exploration Geophysicists.

Ward, S.H., 1967. The electromagnetic method. *Mining Geophysics,* Volume II. Tulsa, Society of Exploration Geophysicists, p. 224 - 372.

Ward, S.H., D.P. O'Brien, J.R. Parry, and B.K. McKnight, 1968a. AFMAG – interpretation (in press).

Ward, S.H., G.R. Jiracek, and W.I. Linlor, 1968b. Electromagnetic reflection from a plane-layered lunar model. *J. Geophys. Res.,* 73 (4): 1355 - 1372.

West, G.F., 1960. Quantitative interpretation of electromagnetic prospecting measurements. Ph.D. thesis, University of Toronto, Canada.

White, P.S., 1966. Airborne electromagnetic survey and ground follow-up in northwestern Quebec. *Mining Geophysics,* Volume I, Tulsa, Society of Exploration Geophysicists.

Wieduwilt, W.G., 1962. Interpretation techniques for a single-frequency airborne electromagnetic device. *Geophysics,* 27 (4): 493 - 506.

Mining exploration with natural electromagnetic fields

D.W. Strangway

Massachusetts Institute of Technology
Cambridge, Massachusetts

K. Vozoff

Geoscience Incorporated
Cambridge, Massachusetts

Abstract. Natural EM fields, long a source of interference in magnetic and electrical surveys, have become the basis for at least three exploration techniques: AFMAG, tellurics, and magnetotellurics. Difficulties are found when attempting to apply these methods due to the weakness and variability of the fields. Useful results are being obtained, but for maximum effectiveness the true complexity of the relationships between primary magnetic fields and their induced currents must be taken into account. New techniques of interpretation, and improved instrumentation, are permitting more effective use of these methods than has been possible previously. It appears they will be of major use to mining exploration in areas of high background resistivity and deeply buried sulphide bodies.

Résumé. Les champs électromagnétiques naturels, qui ont été longtemps une source d'interférence pour les relevés magnétiques et électriques, sont devenus le fondement d'au moins trois techniques d'exploration: l'AFMAG, la tellurique et la magnétotellurique. Des difficultés se présentent lors d'application de ces méthodes à cause de la faiblesse et de la variabilité de ces champs. On obtient des résultats utiles, mais pour en arriver à un maximum d'efficacité, il faut tenir compte de la grande complexité des relations qui existent entre les champs magnétiques primaires et les courants qu'ils provoquent. De nouvelles techniques d'interprétation et des instruments améliorés permettent maintenant d'utiliser ces méthodes avec plus d'efficacité qu'auparavent. Leur utilisation semble devoir se répandre dans les régions à grande conductivité de fond et qui renferment des gisements sulfurés enfouis à grande profondeur.

Natural electromagnetic fields are well known to the field geophysicist. These fields appear as noise in magnetic surveying, in resistivity and IP surveying, in electrical well-logging, and in EM surveying. However, as our understanding of these fields increased it became apparent that they could be used as bases for new exploration methods. In the past few years natural EM field methods have been applied increasingly to problems in exploration, and in earth sciences generally. These problems range from studies of the interior of the earth (on the large scale) to the search for minerals (on the small scale). By name, the established methods which use these natural fields are the telluric method, the AFMAG method, and the magnetotelluric method. In this paper a discussion of the principles of the methods, their instrumentation, interpretation, and applications will be presented.

Principles

Most of the methods begin by depicting the primary natural field as the sum of many plane EM waves, at many frequencies, travelling vertically downward from the air into the earth. Since, in a plane EM wave, the magnetic field is perpendicular to the direction of travel, this primary magnetic field is horizontal. When it enters the earth it induces currents which, in a uniform or horizontally layered earth, are horizontal and perpendicular to the magnetic vector. As we follow the wave further into the earth the secondary magnetic fields, those due to the induced currents, build up in strength but are opposite in direction to the primary magnetic fields. Consequently the field weakens as it penetrates farther into the earth. This is known as the skin effect. The penetration is a function of the frequency and the conductivity of the medium, and is determined by the quantity called 'skin depth'. For an electrically uniform earth, skin depth δ is

$$\delta = \left(\frac{1}{\pi f \mu \sigma}\right)^{1/2}$$

where δ is skin depth in meters, f is frequency in hertz, σ is conductivity in (ohm-meters)$^{-1}$, and μ is permeability in henry/meter.

For all but very strongly magnetic rocks,

$$\mu \approx \mu_0$$
$$\approx 4\pi \times 10^{-7} \text{ henry/meter}$$

and

$$\delta = S(f\sigma)^{-1/2} \text{ meters}$$
$$S = \left(\frac{10^7}{4\pi^2}\right)^{1/2}$$
$$= 503$$

The familiar plots of skin depth versus frequency are shown in Figure 1, for a range of conductivities and frequencies of interest. Skin depth is small for high frequencies in conductive rocks. It is large for low frequencies in resistive rocks. Consequently, high frequencies are used for shallow, small-scale geologic studies, whereas lower frequencies are used for deeper, larger-scale studies. Typically we use 10^{-5} to .5 hz for tectonic studies, 10^{-4} to 50 hz for petroleum exploration, and 5 to 10^4 hz for mining exploration. The ranges are also indicated in Figure 1. Thus for the same primary field, in a resistive region the magnetic fields and their induced currents will be distributed from the surface to a large depth, whereas in a conductive region they will be concentrated near the surface. Associated with the induced

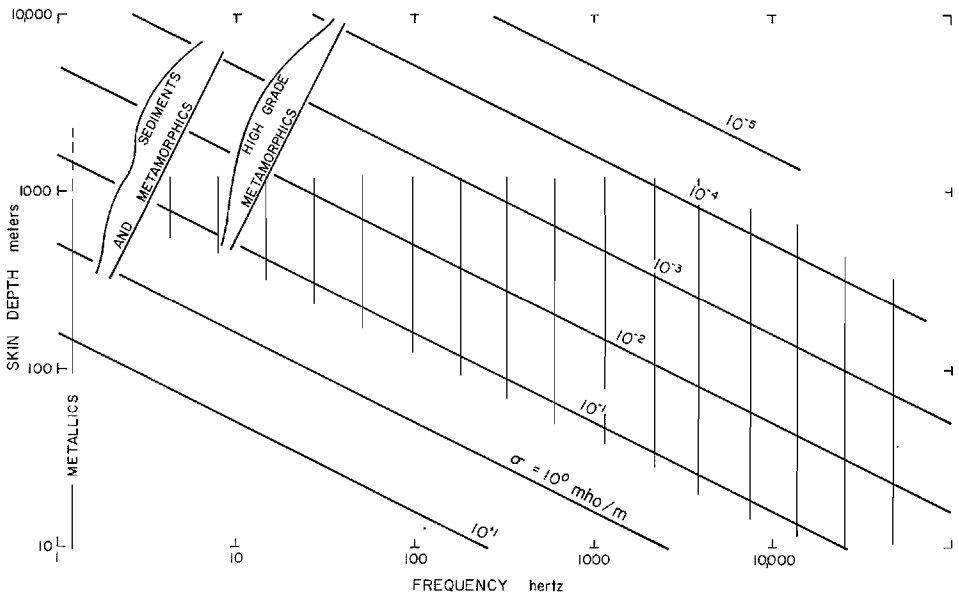


Figure 1. Skin depth chart.

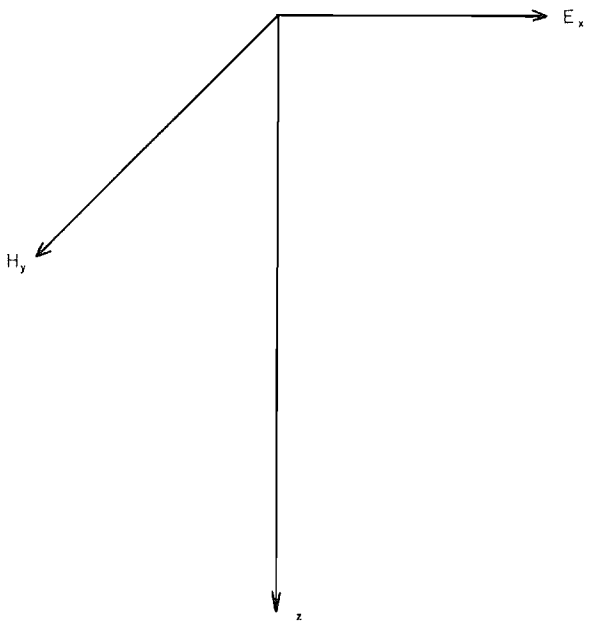


Figure 2. Coordinate system used for discussing magnetotellurics.

currents is an electric field. On the surface of a uniform earth there is a simple relationship between the magnetic field at any frequency (f) in any horizontal direction (y) and the electric field at right angles to it (x). This is

$$E_x = \left\{\frac{5f}{\sigma}\right\}^{1/2} H_y$$

where the common units E in millivolts/kilometers, H in gamma are used. The coordinate system is shown in Figure 2. In this case, the phase of H leads that of E by a constant $\pi/4$ radians (45 degrees) at all frequencies.

When the earth consists of two or more horizontal layers (Figure 3), E and H are still horizontal and perpendicular to one another, but their ratio and their phase difference then depend on

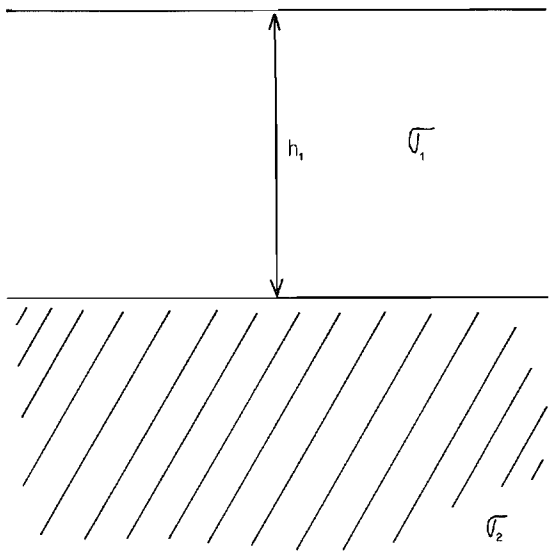


Figure 3. Geometry for the two-layer case.

frequency in a more complex way. For example, if skin depth is much less than h_1 (Figure 3), the ratio depends only on σ_1 while if

$$\delta >> h_1$$

their ratio depends only on σ_2. The technique in which E and H are measured and compared is called the magnetotelluric method. its best description is still that by Cagniard (1953). We usually deal with

$$\rho_a = \frac{1}{5f}\frac{E^2}{H^2}$$

at each frequency, where ρ_a is the apparent resistivity in (ohm-meters), and

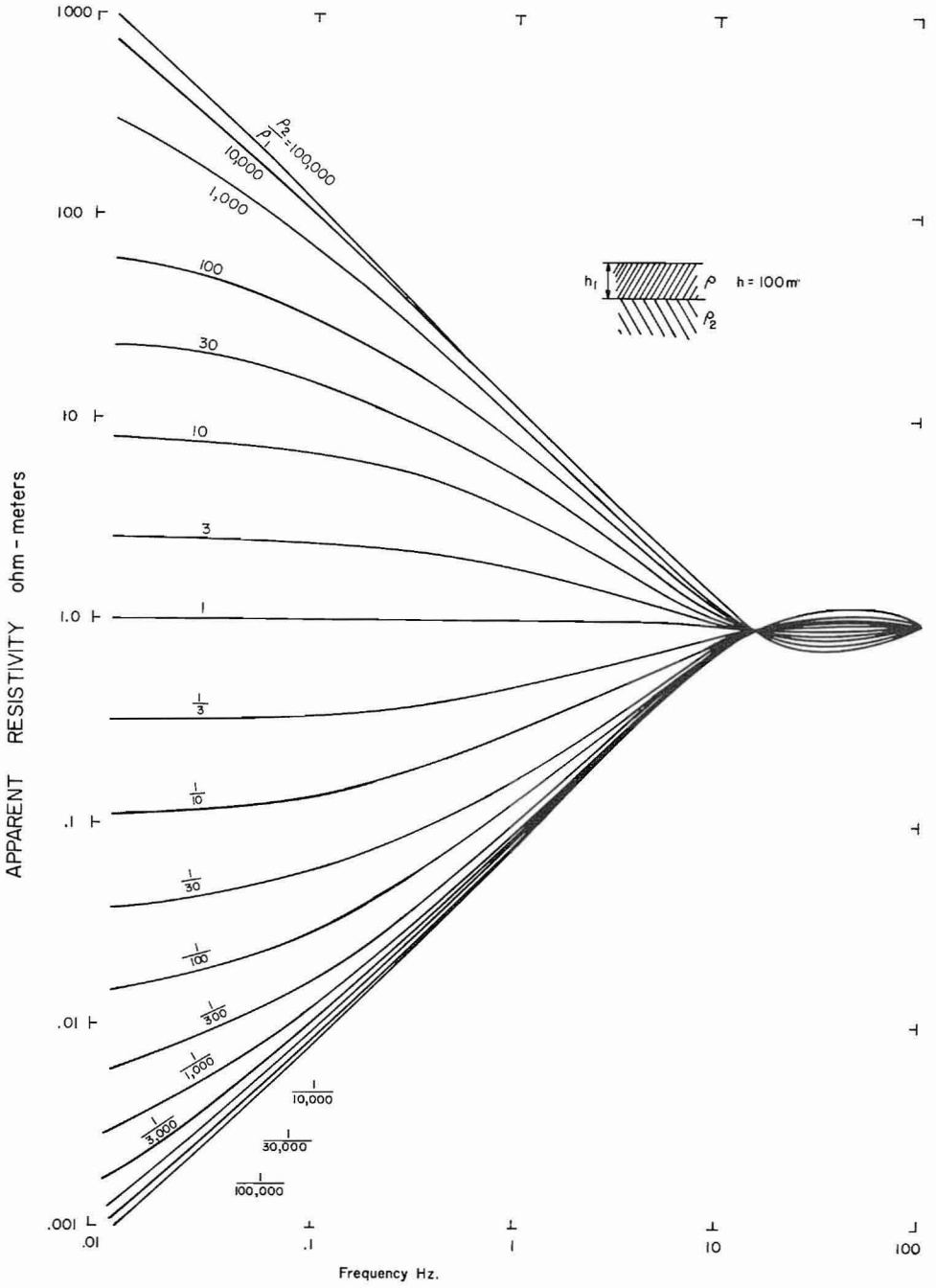


Figure 4. Apparent resistivity plots for the two-layer case.

$$\rho_a \equiv 1/\sigma_a.$$

Apparent resistivity for the two-layer case, for $\rho_1 = 1$ ohm - m and for various values of ρ_2 is shown in Figure 4. Here h_1 is taken to equal 100 meters. A family of three-layer curves is shown in Figures 5a and 5b. In this family ρ_1 and ρ_3 are both equal to 1 ohm-meter, h_1 is a constant 100 meters, and ρ_2 and h_2 are varied.

These curves can be taken to represent a wide variety of situations because the normal scaling relations apply. For example, if we take any curve, multiply all lengths by the factor L and all conductivities by the factor C, the curve is correct if we multiply all frequencies by the factor

$$F = (L^2C)^{-1}$$

In fact, so long as we keep the ratios

$$\rho_2/\rho_1, \rho_3/\rho_1, \text{etc.}$$

and

$$h_2/h_1, h_3/h_1, \text{etc.}$$

Contents

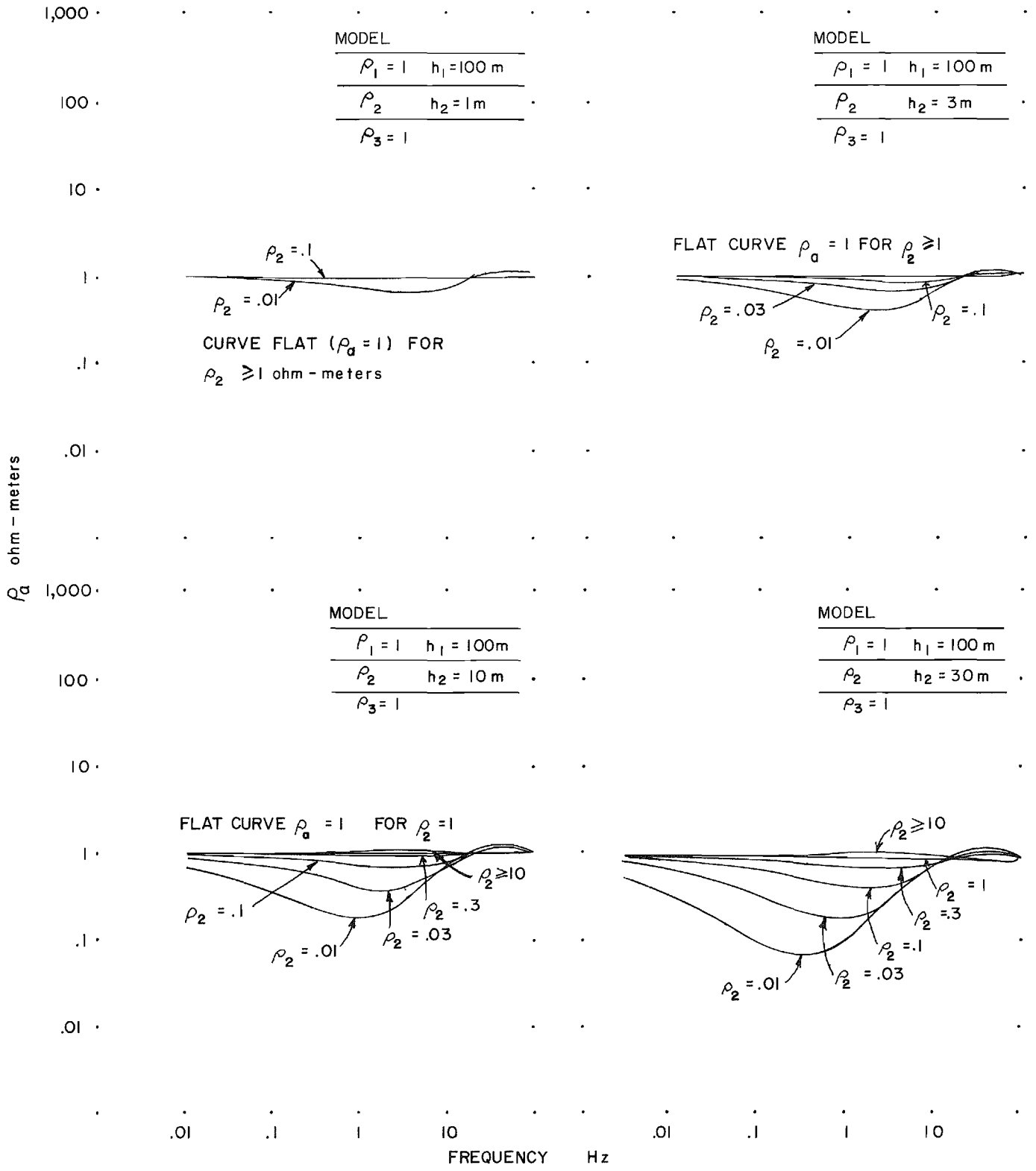
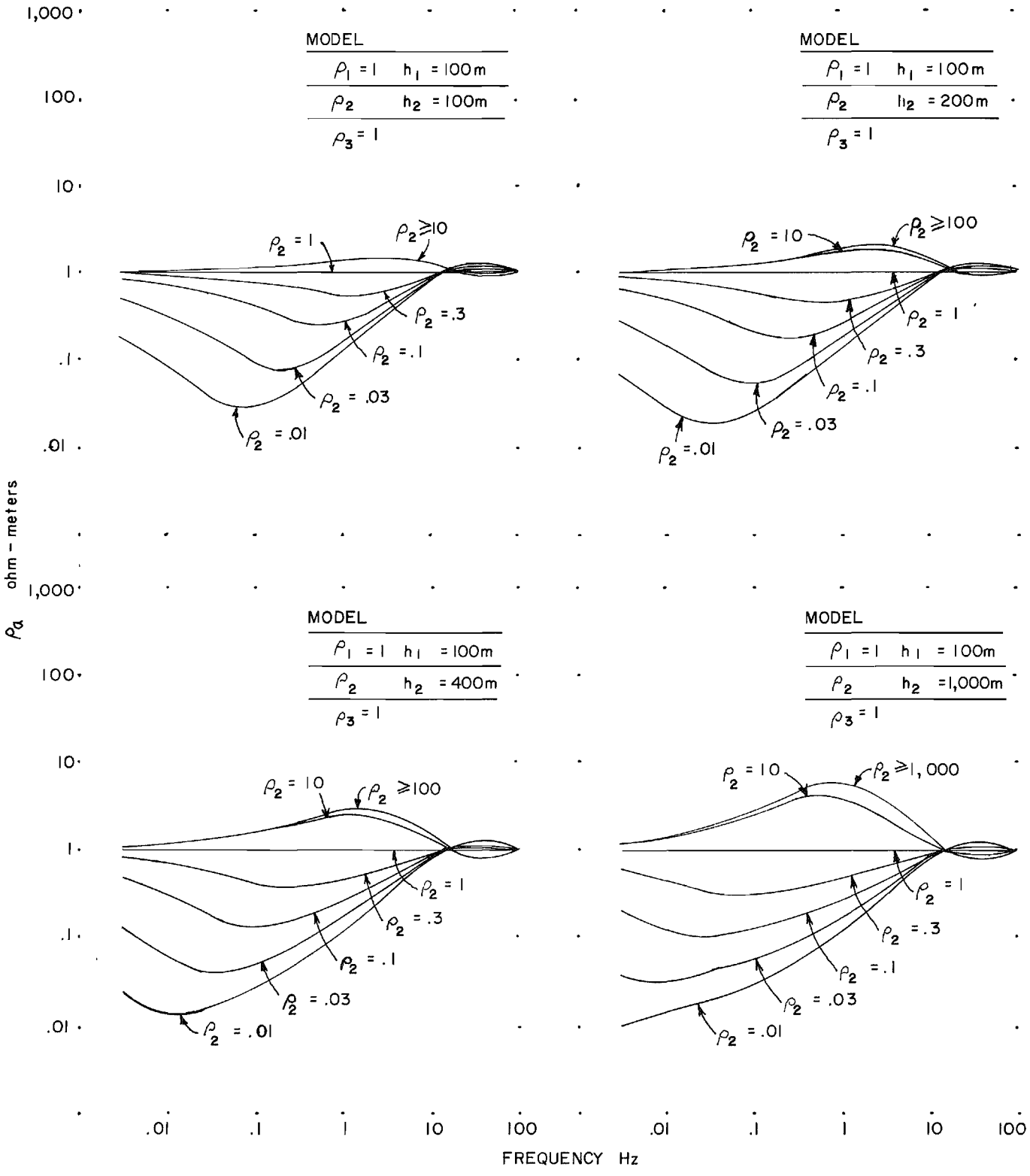


Figure 5. Apparent resistivity plots for the three-layer case.


MODEL
ρ1 = 1 h1 = 100m
ρ2 h2 = 100m
ρ3 = 1
ρ2 = 1
ρ2 ≥10
ρ2 =.3
ρ2 =.1
ρ2 = .03
ρ2 = .01
MODEL
ρ1 = 1 h1 = 100m
ρ2 h2 = 200m
ρ3 = 1
ρ2 = 10
ρ2 ≥100
ρ2 = 1
ρ2 = .3
ρ2 = .1
ρ2 = .03
ρ2 =.01
MODEL
ρ1 = 1 h1 = 100m
ρ2 h2 = 400m
ρ3 = 1
ρ2 = 10
ρ2 ≥100
ρ2 = 1
ρ2 = .3
ρ2 = .1
ρ2 = .03
ρ2 = .01
MODEL
ρ1 = 1 h1 = 100m
ρ2 h2 =1,000m
ρ3 = 1
ρ2 = 10
ρ2 ≥1, 000
ρ2 = 1
ρ2 = .3
ρ2 = .1
ρ2 = .03
ρ2 = .01
ρa ohm - meters
1,000
100
10
1
.1
.01
.01
.1
1
10
100
FREQUENCY Hz

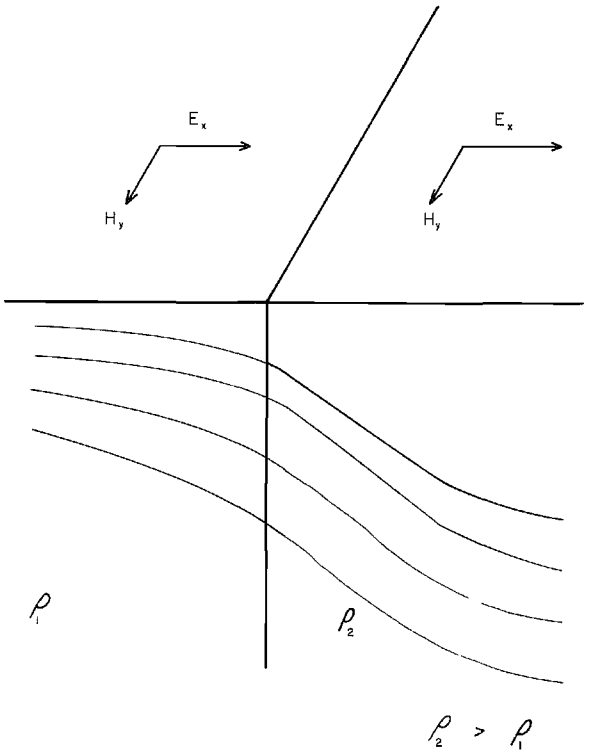


Figure 6. Cross section of vertical contact showing electric field lines.

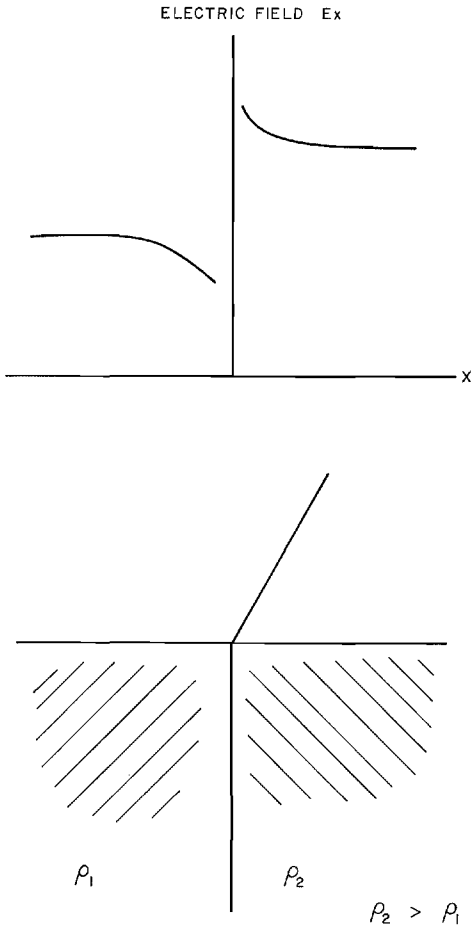


Figure 7. Expected electric field variation across a contact.

constant, we can multiply all conductivities by C, all thicknesses by L, and our curves will be correct if we multiply the frequency scale by F, where

$$F = \frac{1}{L^2 C}$$

and the apparent resistivity scale by $(1/C)$. Thus the curves of Figure 5 would be equally valid for

$$\rho_1 = \rho_3 = 17 \qquad (C = 1/17)$$

and

$$h_1 = 10^3 \qquad (L = 10)$$

if we multiply the frequency scale by

$$F = (L^2 C)^{-1}$$
$$= .17$$

and multiply the ρ_a scale by C^{-1}.

From our point of view this means that we can use one set of curves to cover a wide variety of situations. Changing the thickness of the upper layer has the same effect as changing the frequency or the resistivity. From a study of three-layer curves some interesting features that are peculiar to magnetotellurics become obvious. As an exploration tool the technique is probably of most use in exploring for layers of low relative resistivity since the method is an inductive one. Because high-resistivity layers cause very little attenuation of the signals the method is peculiarly suited to exploration through high-resistivity material, such as volcanics or limestones. At the same time this ability to 'see' through a high-resistivity layer means that the depth resolution is poor. A very thick layer can have a small effect on the electric field so that large depth errors can be present and can accumulate if there is a multiple layer situation. This situation is somewhat analogous to the problem of detecting a low velocity layer in the seismic technique. The curves shown in Figure 5 illustrate this point. The effect of an intermediate layer of varying thickness and resistivity between two media with the same resistivity is illustrated. A second layer of the same thickness as the upper layer is not detectable if it has a resistivity higher than the upper layer. On the other hand a layer only 1/10 of the upper layer thickness is readily detectable, provided the resistivity of the intermediate layer is about 1/30 of the upper layer resistivity.

The above discussion has been limited to the layered situation. In actual field operations, however, the situation is not usually so straight-forward, as there seem to be many more lateral variations in resistivity than one might expect. As soon as we make the problem two-dimensional, rather than one-dimensional, we need to be concerned with the problems of directionality of

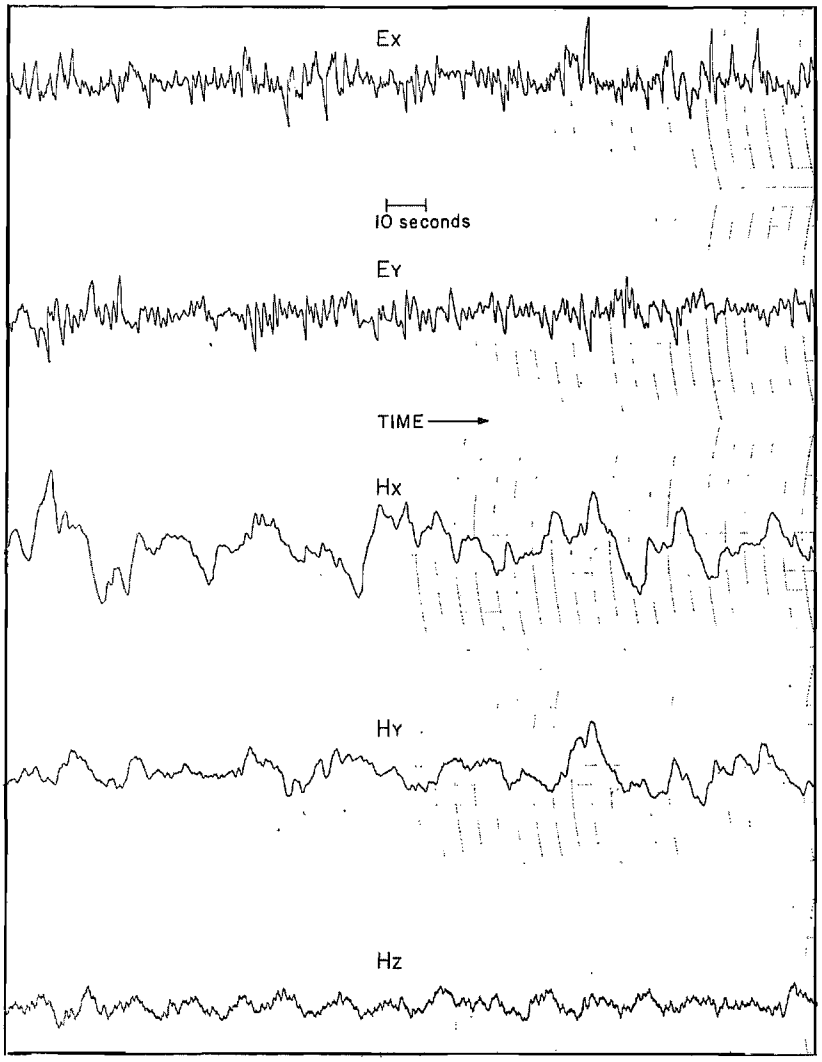


Figure 8. Typical electric field and magnetic field records.

the source field and the lack of orthogonality between the inducing field and the electric fields in the ground. This is a difficult situation to handle analytically and complicates the otherwise beautiful simplicity of the magnetotelluric technique. The practical approach to this problem in magnetotellurics is to get a large amount of data covering the area of interest. With many observations it is usually a trivial problem to determine approximately where the major lateral resistivity contrasts exist. By comparison with models it is possible to extract a great deal of structural information from the field data.

Two of the major natural EM field exploration methods depend completely on the existence of lateral resistivity changes. These are the telluric and the AFMAG methods, which are completely valueless in uniform or layered situations. When pronounced lateral changes exist, however, their surface locations can usually be found more quickly and cheaply by either of these techniques than by magnetotellurics.

Considering the vertical fault of Figure 6, the general primary magnetic field is a combination of an H component perpendicular to the fault and another component parallel to the fault. For the latter component E is induced perpendicular to the fault. The currents must adjust smoothly for skin effects in going from ρ_1 to ρ_2 so that they flow as shown in Figure 6. Evidently E on the conductive side (ρ_1) starts to fall as we approach the contact. Conversely, approaching the contact from the reverse side we find E actually rises. This is the 'overshoot' known from the works of d'Erceville and Kunetz (1962) and Rankin (1962), and plotted in Figure 7. E and ρ_a are actually discontinuous across the contact.

The H component perpendicular to the fault induces currents parallel to the fault. This case cannot be modelled by the analytic techniques of d'Erceville, Kunetz, and Rankin. The condition governing the transition here is that E, and therefore ρ_a, must be continuous. In fact both vary smoothly across the contact. Of more interest in this case is the appearance of a secondary *vertical* H component as we cross the contact. It is this induced field component on which the AFMAG method is based. Measuring the changes in E at the surface is, of course, the telluric method. Models are discussed further in a later section.

Magnetic induction

In a recent study Goldstein and Ward (1966) have considered the problem of distinguishing magnetic anomalies because of remanence from those due to induction. It is well known that, for spherical magnetic bodies of radius R in which $(\omega\mu\sigma)^{1/2}R$ is

Contents

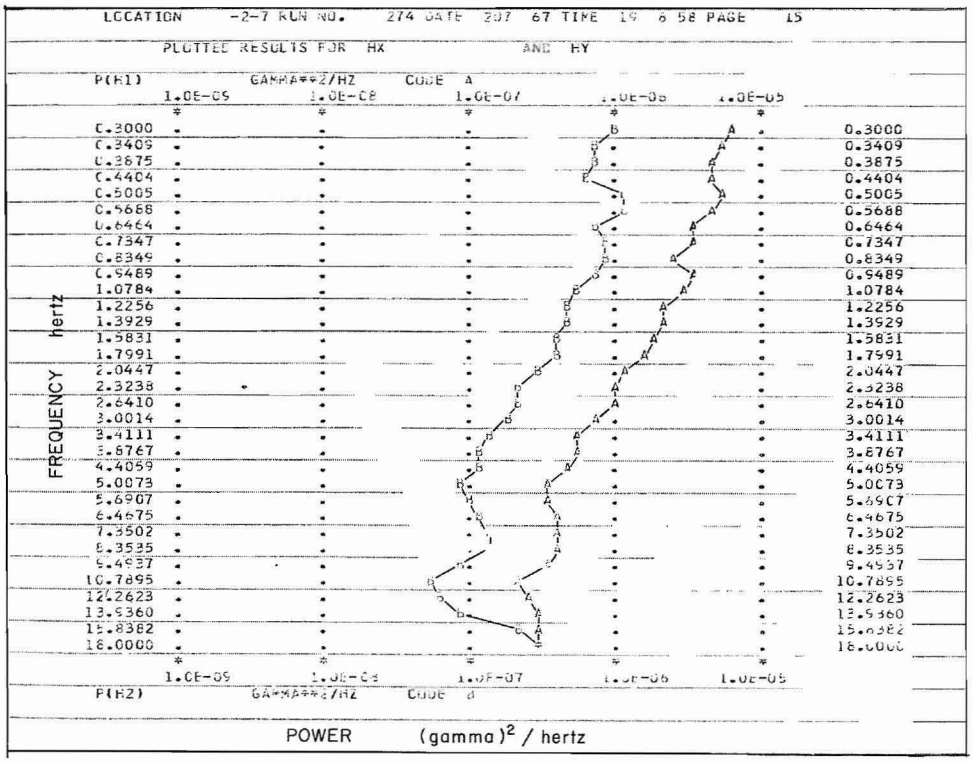


Figure 9. Power spectrum of electric and magnetic field energy.

small, the body responds as a 'soft' magnet rather than as a conductor. The approach of these investigators was to measure low-frequency pulsations at two locations simultaneously, one location being on a magnetic anomaly, the other a kilometer or so away from the anomaly. In the vicinity of strong magnetic anomalies due to known magnetite deposits, the EM fields observed by the two magnetometers differed substantially in amplitude. On the other hand, observations over anomalies in volcanics known to have high remanence showed no observable difference between the two magnetometer records. The requirement for two recording magnetometers leads to a need for equipment which is either expensive or nonstandard, so that this method is not yet easy to apply in the field.

Nature of the source fields

Source fields of many kinds are available, covering the complete range of frequencies of interest. Most recent work has been done using micropulsations in the range of 10 to 10^{-4} hz. However a few investigators, including several Russian workers (Vladimirov, 1960, 1961), personnel of the Geological Survey of Canada, and Watt, *et al.* (1963) have been doing work in the audio frequency range where thunderstorm energy propagates in the earth-ionosphere cavity.

The fields are due to two major sources (Bleil, 1964). Below 1 to 5 hz the fields are primarily due to currents flowing in the ionosphere. Typical fluctuations around a few gammas are quite common in this frequency range and it is these fluctuations which give rise to electromagnetic induction. A typical set of records is shown in Figure 8. Figure 9 is a typical power spectrum showing the distribution of signal with frequency in the band 0.3 to 18 hz. The energy generally falls with increasing frequency to a minimum around 5 hz, beyond which it slowly rises again. In the low-frequency range, mean directional properties at the source are fairly random so that, given sufficient recording time, all source directions are sampled. This is very fortunate since individual observations should then be reproducible even though the electric field does not always flow perpendicular to the source field. At higher frequencies the source fields are not so uniform in direction, depending on the location of thunderstorm centers, and one can get sets of nonrepeatable data depending upon the relative directions of source field and lateral resistivity contrast.

A second problem that is now well recognized is the problem of nonuniformity of the source field in space. If the magnetic field is not uniform, it leads to the conclusion that we cannot assume the field to be a plane wave. In this case the determination of apparent resistivity is not simple and requires that we have a knowledge of the distribution of fields. This would also destroy the inherent simplicity of the magnetotelluric approach. The question has been discussed in detail by several workers (Price, 1962; Wait, 1954; Madden and Nelson, 1964). As a rough approximation it is clear that the measurements present no difficulty as long as the surface field variations occur in distances large compared to the skin depth. The real problem of course is to determine the equivalent skin depth in the case of a layered medium. If high-resistivity material is present, the limitation is much more stringent than in the low-resistivity case where the signals attenuate rapidly and the skin depth is small. Experimental confirmation that the source problem is not severe is provided by the fact that in areas of uniform layered geology, data are quite repeatable. If the source were a problem it should show a time dependency. The problem also becomes less severe as one goes to higher frequencies where the skin depths become very small in relation to the free space wavelengths.

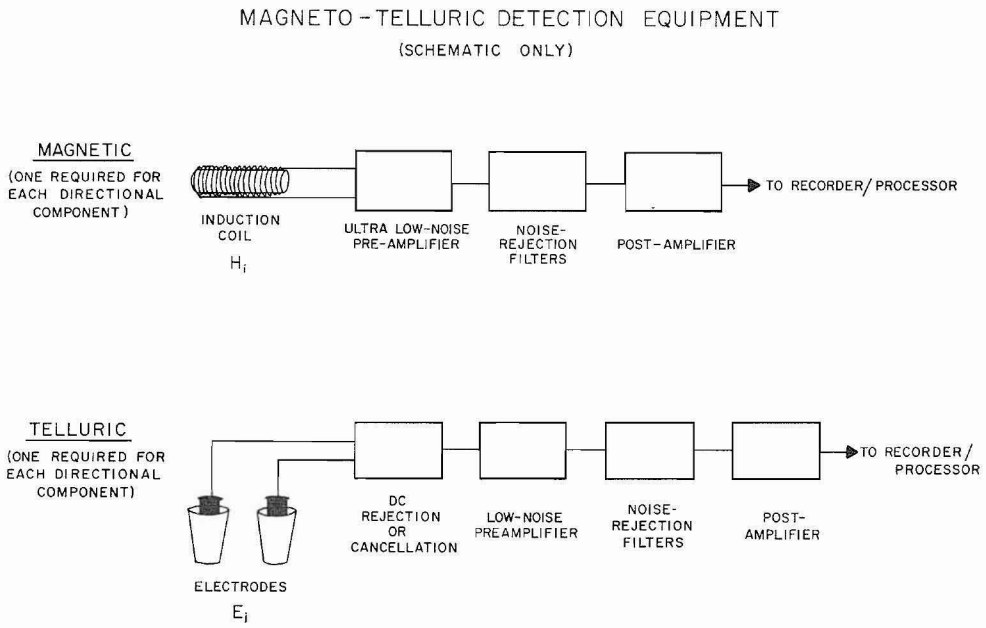


Figure 10. Block diagram of measuring system recording wide band signals.

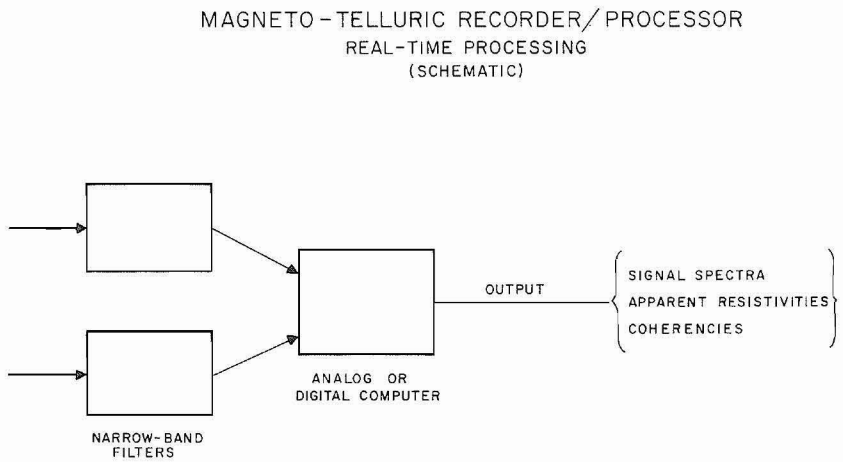


Figure 11. Block diagram of measuring system using narrow band approach.

Instrumentation

The approach used by various workers in the measurement of the magnetic and telluric fields is fairly direct. The measurement of electric fields is conducted using a long cable attached to two electrodes in the ground. These electrodes must be of a low noise nature. Distance between electrodes should be as great as possible to maximize the voltage to be measured. At the same time the line should be short enough to ensure that the structures of interest can be detected. In exploration this means using electrode separations of tens to several hundreds of meters. The voltage is detected by high gain amplifiers and processed by appropriate band pass filters as shown in Figures 10, 11 and 12. In other systems, a series of highly tuned circuits perform the measurement of the electric field directly at discrete frequencies. In the system shown in Figure 10, the electric field is recorded on magnetic tape and the frequency analysis is done later using conventional techniques of spectral analysis as shown in Figure 12.

The common detector used for the magnetic variations is a coil with a highly permeable core. Typical coils have very large numbers of turns, since the magnetic fields to be detected are so small. The magnetic field measurement is the most difficult one to make and is most subject to disturbances such as wind vibrations. Very high-gain, low-noise amplifiers are required to detect and process these signals. These voltages are then put through band-pass filters and also recorded on magnetic tape. It is usual to monitor the signals on a chart recorder and it is illustrated in Figure 12.

In a system where the data are frequency analyzed in the field using a series of parallel feedback filter networks it is possible to derive the ratio E/H directly and then using operational amplifiers to square and multiply by the appropriate factors to obtain the apparent resistivity directly. This real-time system is not in common usage but should prove very useful in the near future. It is not practicable for the ULF band of measurements. Coherencies, phases, and the necessary tensor operations can be done in the field.

In some cases magnetometers are used to detect the magnetic field variations. Plouff (1966), for example, describes a system in which the magnetic detector is a rubidium vapor magnetometer with a sensitivity of 0.01 gamma. To ensure that only the horizontal magnetic field is measured the vertical component of the earth's magnetic field is bucked out using a coil.

Contents

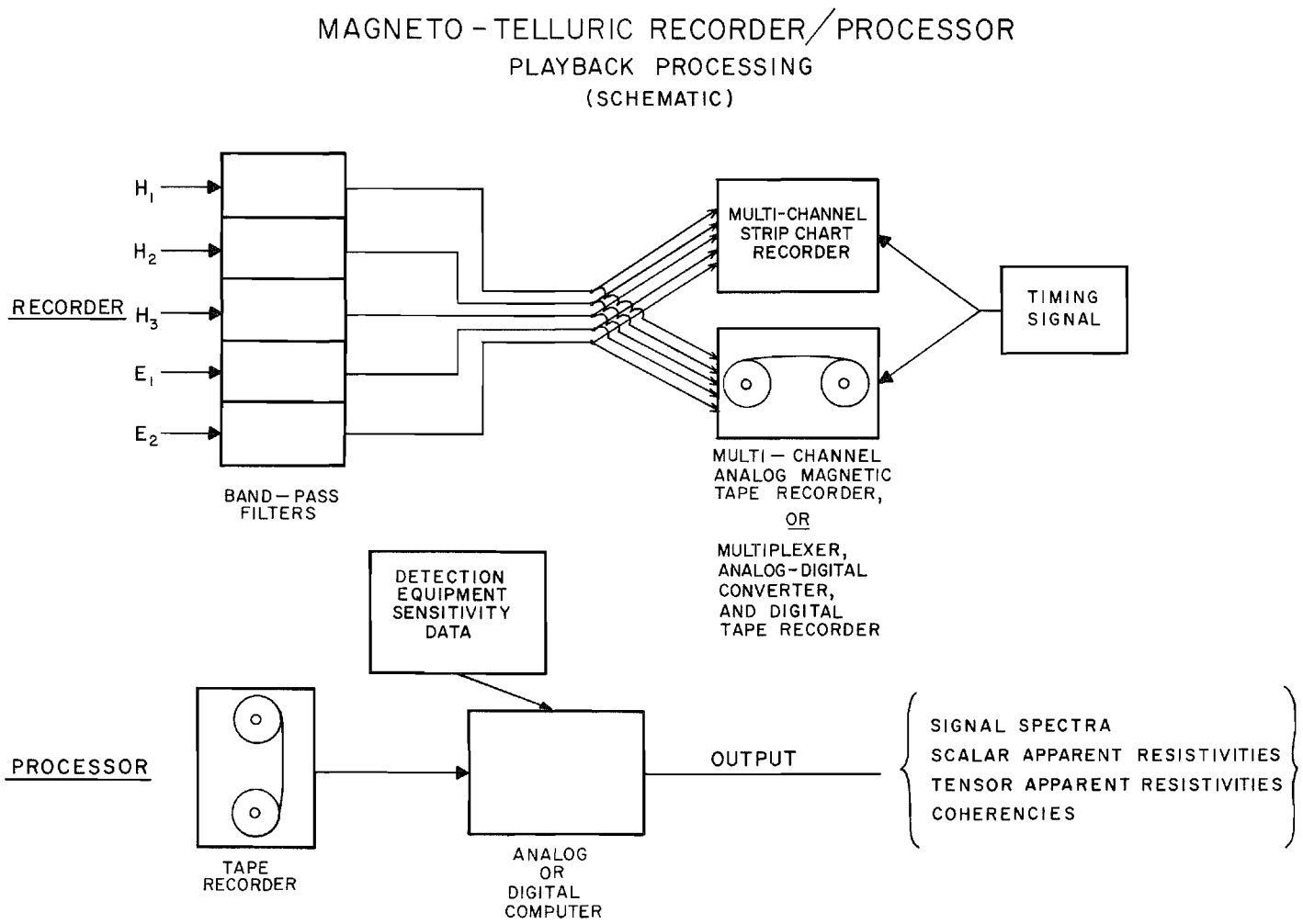


Figure 12. Block diagram of signal processing system.

Yungul (1966) describes a system in which the resistivity is determined at a single site using a normal magnetotelluric survey or some other type of resistivity survey. The rest of a survey is conducted by comparing the voltages in two pairs of electric field lines, one pair at a base station and the other moving to various parts of the area. By this procedure one can eliminate the need for the mobile magnetic pulsation system. This is a considerable advantage in field operations since the magnetic field is the hardest to measure.

Examples

There are ever increasing numbers of examples becoming available. Many of the geologic problems to which this technique has been applied are in areas of uniform, layered geology where it is indeed possible to determine the resistivity structure and then to compare it with known resistivity logs in drill holes, or with resistivity values determined in other ways. Of more interest are the two- and three-dimensional problems.

This technique was applied to a problem in the southwestern United States where the major geologic feature consisted of a vertical contact, where a major Basin and Range fault has caused a large amount of displacement bringing high-resistivity material against low. In Figure 13 the apparent resistivity values at a series of stations are shown. In this case the vertical axis represents period while the horizontal axis is the distance along the traverse. Numbers plotted in this 'cross section' are $\log_{10}\rho_a$. In areas of high resistivity the depths penetrated are large while in low-resistivity areas the depth penetration at the same period is small. The electric field detector in this case was oriented normal to the fault and a remarkable similarity between the known fault and the resistivity pattern is observed. This is one type of problem for which the magnetotelluric method is well suited and more applications of this approach will undoubtedly be seen in the future.

Developments in analysis

As data quality has improved, evidence has grown that the tensor approach to analysis is realistic and worthwhile in many areas, although in the most complex geological situations it is not sufficiently general (Cantwell, 1960). It is also evident that, in practice, the significance of the 'simple Cagniard apparent resistivity' can be elusive. It can never be accepted without first

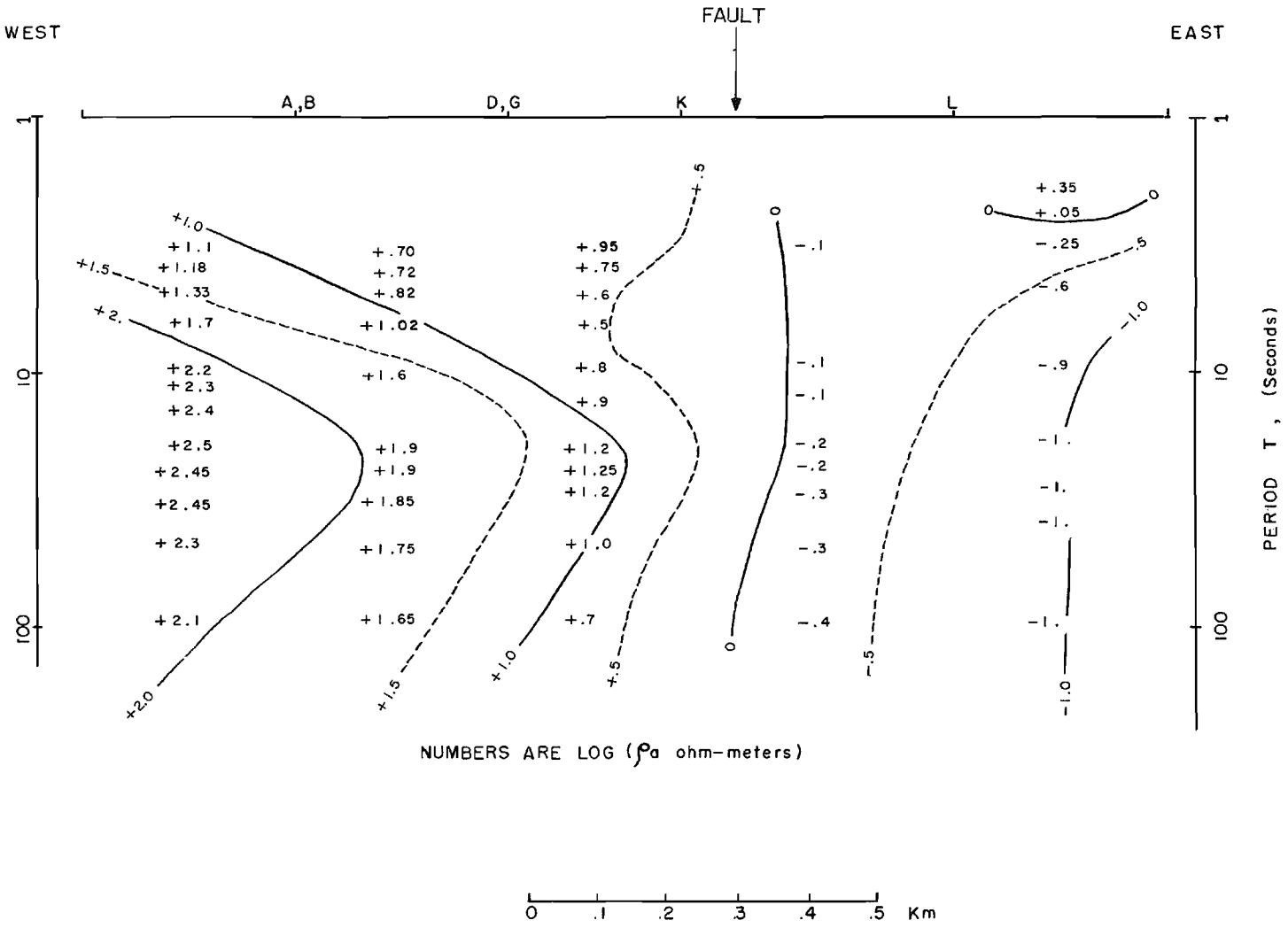


Figure 13. Apparent resistivity — southwestern United States — showing presence of fault.

testing the data to ensure both random polarization in H and insignificance of the off-diagonal terms in the impedance tensor. This leads us to the conclusion that all new magnetotelluric equipment should be capable of implementing the tensor approach in some form. The reasons for these statements are illustrated by the examples in Figures 14 and 15. The scalar (Cagniard) apparent resistivities (Figure 14) are smooth and very nearly equal over many decades. However a tensor analysis shows that, in fact, resistivity depends strongly on direction (Figure 15), that there is a difference (between maximum and minimum directions) of a factor of at least 3. The direction of the principal axis rotates through about 40 degrees over the frequency band employed. The only clues that the scalar resistivities might be misleading were the relatively low coherence observed between perpendicular E and H components, and the high coherency between the vertical magnetic component (H_z) and H_x over part of the band. The low E-H coherency will not be apparent if H happens to be linearly polarized within the horizontal plane. It should be emphasized that a scalar apparent resistivity can err on the high side by orders of magnitude.

Developments in interpretation

Interpretation is done by reference to models, where suitable models are available.

The recent extension by Madden of his two-dimensional computer modelling techniques to the plane EM field case enables us to calculate accurately the changes in *all* components associated with an arbitrary two-dimensional model, for both H parallel and H perpendicular to strike. Hence we now have the means to compute quantitative AFMAG and telluric models. In computing these models we find a number of interesting features. For example, in the case of a contact buried beneath a thin conductive overburden, the overshoot (in the $E\perp$ case) is rapidly reduced in size and, as overburden thickens, the overshoot disappears. At the same time, the vertical magnetic component associated with $E\parallel$ also diminishes quickly. Both effects are observed in practice. Likewise, a conductive substratum is very effective in reducing and smoothing the effects of a contact as seen at the surface. The models permit us to compute the change in amplitude and phase of the $H\perp$ component itself. Although it

Contents

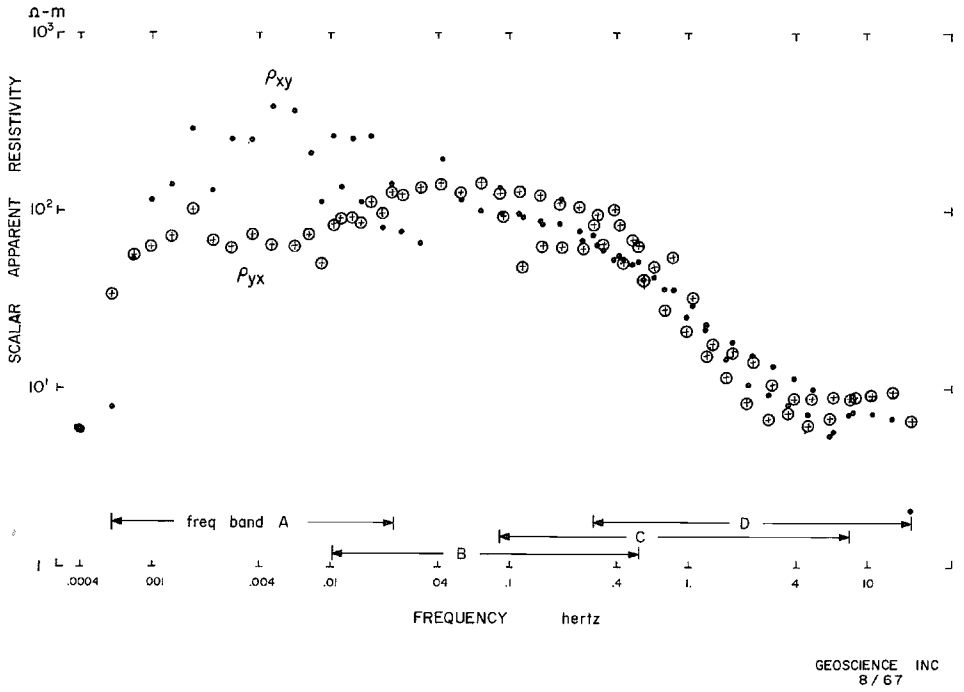


Figure 14. Scalar (Cagniard) apparent resistivity versus frequency, site 2-4.

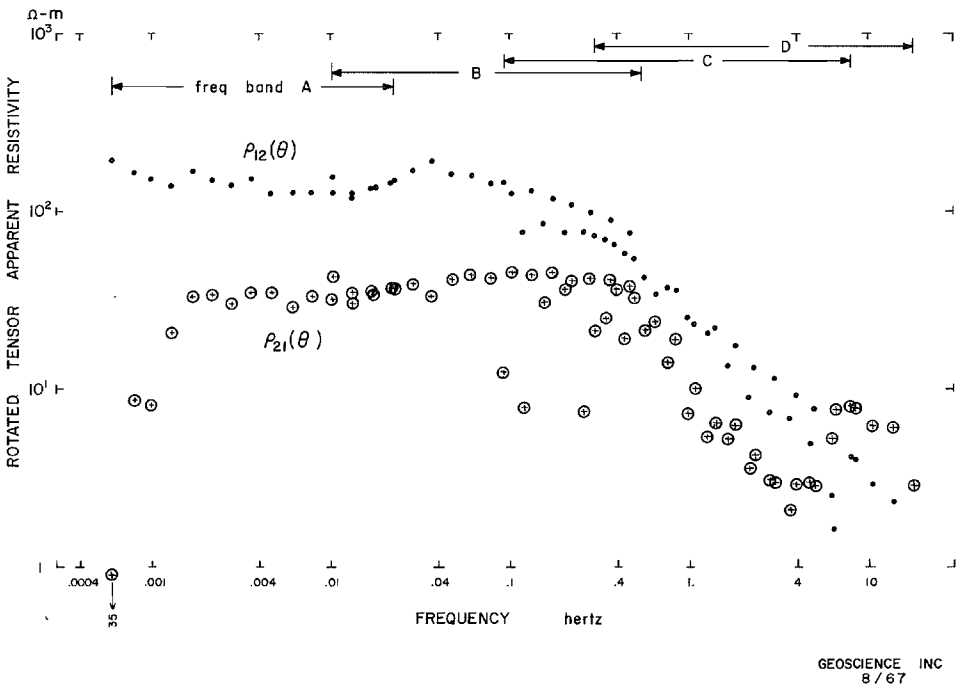


Figure 15. Rotated tensor apparent resistivity, site 2-4.

is often relatively small, measurement of this change could be used as the basis of an exploration technique.

Figures 16 and 17 (based on Swift, 1967) show two such examples. Note that the ratio of vertical to horizontal magnetic field components is the tangent of the AFMAG dip angle. In the first example, a buried vertical dyke, maximum dip is about 6 degrees. The magnetotelluric resistivity change is about 50 percent in this frequency range. Both the 5 degree dip angle and the 50% apparent resistivity change would be small, but usually detectable, anomalies at the present stage of development of these two techniques. The second example, a buried flat-lying body, shows a maximum dip angle of about 8 degrees, and the apparent resistivity over the target is one third of that away from the target at 3000 hertz. Both changes are detectable, although they would not be considered large anomalies.

It should be noted that, in the other apparent resistivity component, involving currents flowing across targets and magnetic fields along them, the bodies cannot be detected.

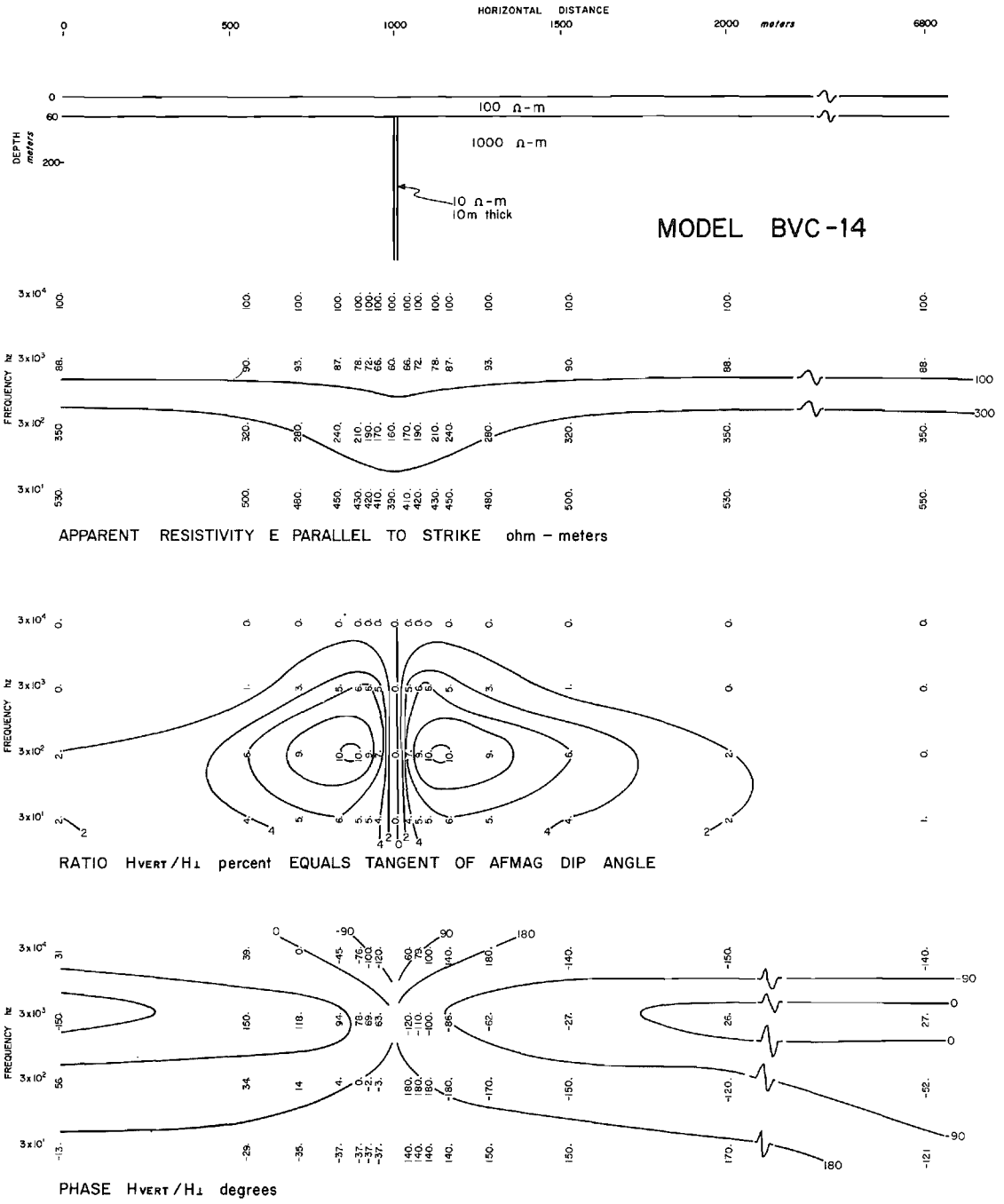


Figure 16. Two-dimensional magnetotelluric model, case BVC-14.

However, if the bodies were resistive rather than conductive the reverse situation would hold: apparent resistivities would be larger for currents flowing across strike.

It is also instructive to compare model results of this kind with induced polarization results on the same models. It quickly becomes apparent that AFMAG and magnetotellurics are sometimes superior to IP-resistivity, whereas the reverse is true in other models.

Despite the many things which we have learned from the models already computed we are still learning a great deal about their behavior. It should also be emphasized that they require nontrivial computation time on the largest commercial computers now available (IBM 360/75). Depending on their complexity, the models we have computed have taken between 2 minutes and 20 minutes each.

References

Bleil, D. (Ed.), 1964. *Natural electromagnetic phenomena below 30 KC/S.* New York, Plenum Press.

Cagniard, L., 1953. Basic theory of the magnetotelluric method. *Geophysics.* 18, no. 3: 605-635.

d'Erceville, I., and G. Kunetz, 1962. The effect of a fault on the earth's natural electromagnetic field. *Geophysics.* 27: 651-665.

Goldstein, N.E., and S.H. Ward, 1966. The separation of remanent from induced magnetism *in situ. Geophysics.* 31: 779-796.

Contents

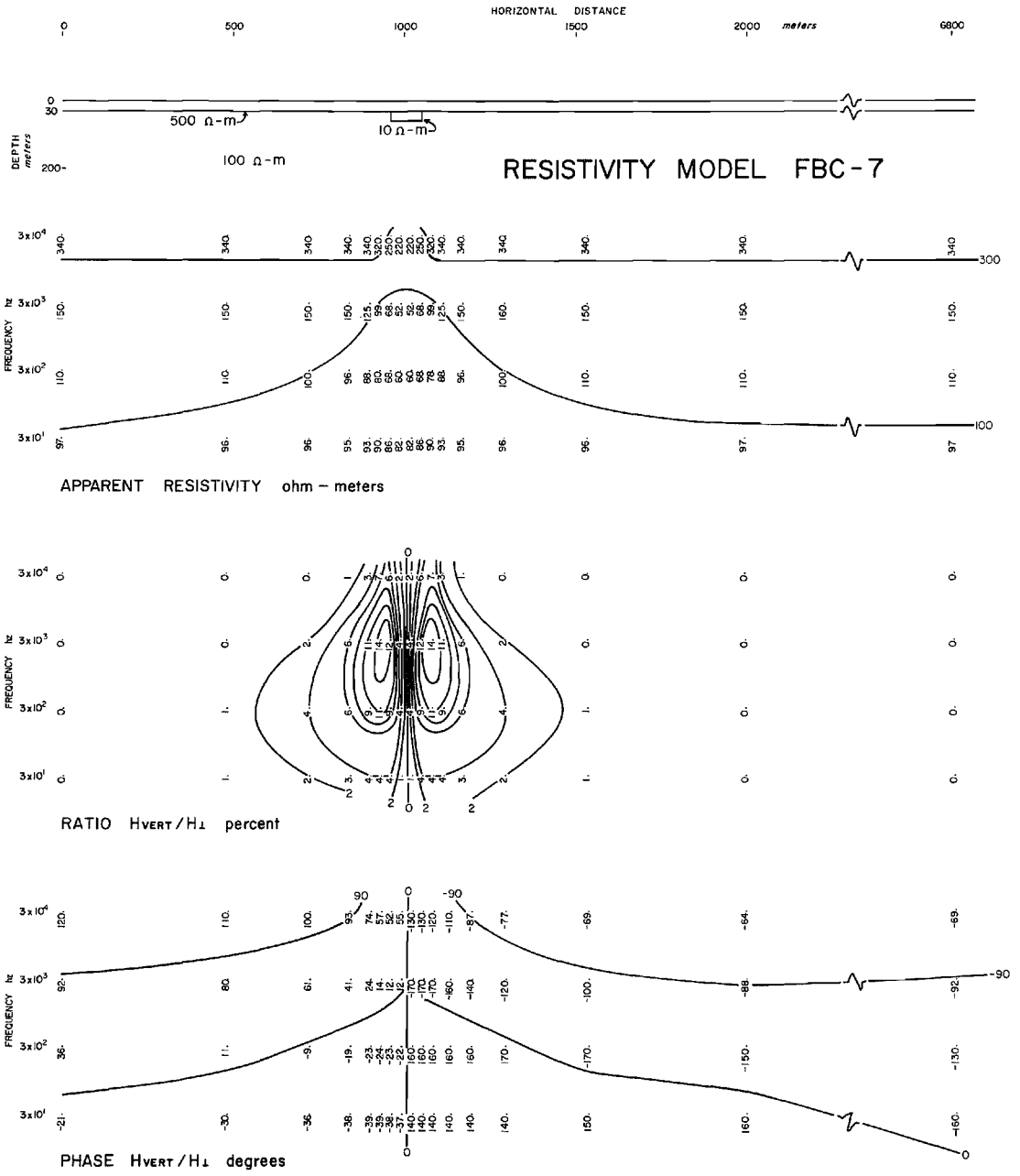


Figure 17. Two-dimensional magnetotelluric model, case FBC-7.

Madden, T.R., 1965. Personal communication.

Madden, T.R., and P. Nelson, 1964. A defense of Cagniard's magnetotelluric method. MIT, Cambridge, Massachusetts, Project NR-371-401.

Plouff, D., 1966. Magnetotelluric soundings in the southwestern United States. *Geophysics.* 31: 1145-1152.

Price, A.T., 1962. The theory of magnetotelluric methods when the source field is considered. *J.G.R.* 67: 1907-1918.

Rankin, D., 1962. The magnetotelluric effect on a dike. *Geophysics.* 27: 666-676.

Swift, C.M. Jr., 1967. A magnetotelluric investigation of an electrical conductivity anomaly in the southwestern United States. Ph.D. thesis, Geophysics Laboratory, MIT, August 1967.

Vladimirov, N.P., 1960. The possibility of the utilization of the alternating electromagnetic field of the earth for geological investigation. *Izv. Akad. Nauk, SSR 1, Ser. Geofiz.* 139-141.

Vladimirov, N.P., and V.A. An, 1961. A method of processing magnetotelluric oscillograms. *Izv. Geophysics Ser.:* 1649-1654.

Vladimirov, N.P., and S.M. Krylov, 1964. Characteristics of microvariations of the natural electromagnetic fields. *Izv. Geophysics Ser.:* 872-882.

Vozoff, K., H. Hasegawa, and R.M. Ellis, 1963. Results and limitations of magnetotelluric surveys in simple geologic situations. *Geophysics.* 28: 778-792.

Vozoff, K., R.M. Ellis, and M.D. Burke, 1964. Telluric currents and their use in petroleum exploration. *Bull AAPG.* 48: 1890-1901.

Vozoff, K., and C.M. Swift, Jr. Magnetotelluric measurements in the North German Basin. *Geophysical Prospecting.* In press.

Vozoff, K., and R.M. Ellis, 1966. Magnetotelluric measurements in southern Alberta. *Geophysics.* 31: 1153-1157.

Wait, J.R., 1954. On the relation between telluric currents and the earth's magnetic field. *Geophysics.* 19: 281-285.

Watt, A.D., F.S. Matthews, and E.L. Maxwell, 1963. Some electrical characteristics of the earth's crust. *Proceedings of IEEE.:* 897-910.

Yungul, S., 1966. Telluric sounding – a magnetotelluric method without magnetic measurements. *Geophysics.* 31: 185-191.

The induced polarization method

Harold O. Seigel

Scintrex Ltd.
Downsview, Ontario, Canada

Abstract. The induced polarization method is based on the electrochemical phenomenon of overvoltage, that is on the establishment and detection of double layers of electrical charge at the interface between ionic and electronic conducting material when an electrical current is caused to pass across the interface. In practice, two different field techniques (transient and frequency variation) have been employed to execute surveys with this method. These techniques yield essentially equivalent information. Instrumentation and field procedures using both techniques have evolved considerably over the past two decades. Much theoretical information for quantitative interpretation has been accumulated.

All naturally occurring sulphides of metallic lustre, some oxides and graphite, give perceptible induced polarization response when present in sufficient volume, even when such materials occur in low concentrations and in the form of discrete noninterconnected particles. Induced polarization is the only method presently available which has general application to the direct detection of 'porphyry type' and bedded copper deposits as well as bedded lead-zinc deposits in carbonate rocks. A number of case histories are documented where standard geoelectrical and other geophysical methods fail to yield an indication of sulphide mineralization detectable by the induced polarization method.

Each rock and soil type exhibits appreciable induced polarization response, usually confined to a relatively low amplitude range, which is characteristic of the specific rock or soil. Certain clays and platey minerals including serpentine, sericite and chlorite, sometimes give rise to abnormally high responses. These effects are attributed largely to so-called 'membrane' polarizations. Despite a moderate amount of laboratory and field investigation, it is still not feasible in general to differentiate between induced polarization responses due to overvoltage and nonmetallic sources, nor to differentiate between possible sources within each group. Because of other variables, it is likewise difficult to equate a specific induced polarization response to a unique percentage of metallic content.

Résumé. La méthode de polarisation provoquée est fondée sur la phénomène électrochimique de surtension, c'est-à-dire sur l'établissement et la détection de doubles couches de charges électriques à l'interface séparant des matériaux conducteurs d'ions et d'électrons, quand on provoque le passage d'un courant électrique à travers l'interface. En pratique, deux techniques différentes (transitoire et variation de fréquence) ont été utilisées pour effectuer des levés par cette méthode. Ces techniques donnent des renseignements essentiellement équivalents. Les instruments et les façons de procéder sur le terrain à l'aide de ces deux techniques ont évolué considérablement au cours des vingt dernières années. Un grand nombre de renseignements théoriques ont été accumulés pour l'interprétation quantitative.

Tous les sulfures à éclat métallique qui se présentent dans la nature, quelques oxydes et le graphite donnent des réponses perceptibles à la polarisation provoquée lorsque leur volume est suffisant, même si ces matériaux se trouvent à faible concentration et sous la forme de particules distinctes et non reliées entre elles. La polarisation provoquée est la seule méthode actuellement disponible qui s'applique de façon générale à la détection directe de gîtes du 'type porphyrique' et de cuivre stratifié de même que les gîtes stratifiés de plomb et de zinc dans des roches carbonatées. Il y a un certain nombre de cas précis où les méthodes géoélectriques classiques et les autres méthodes géophysiques n'ont pu déceler la présence de minéraux sulfurés qui peuvent être détectés par la méthode de polarisation provoquée.

Chaque roche et chaque type de sol donne une réponse appréciable à la polarisation provoquée; cette réponse est habituellement limitée à une gamme relativement restreinte d'amplitudes qui est caractéristique de la roche ou du sol particulier. Certaines argiles et certains minéraux feuilletés comprennant la serpentine, la séricite et la chlorite donnent parfois des réponses anormalement élevées. Ces phénomènes sont attribués en grande partie aux polarisations dites 'de membrane'. Malgré des études assez approfondies en laboratoire et sur le terrain, il n'est généralement pas possible de faire la distinction entre les réponses à la polarisation provoquée imputables à la surtension et aux sources non métalliques, ni de distinguer les sources possibles dans chaque groupe. A cause des autres variables, il est également difficile d'établir l'équivalence entre une réponse précise à la polarisation provoquée et un pourcentage unique du contenu métallique.

The induced polarization (commonly known as IP) method is the newest of our mining geophysical tools, having come into active use only in late 1948. Its roots extend somewhat farther back, however. Schlumberger (1920) reports having noted a relatively lengthy decay of the residual voltages in the vicinity of a sulphide body after the interruption of the primary DC current. Unfortunately, measurements in nonmineralized areas gave rise to rather similar residual polarization potentials, so he apparently abandoned his efforts.

In the late 1930s in the U.S.S.R. (Dakhnov, 1941) IP measurements were being made in petroleum well logging in an attempt to obtain information relating to the fluid permeability of the formations traversed by the well. Dakhnov mentions the possible application of the method to the exploration for sulphide mineralization, although apparently no such use was being made thereof at that time. Unfortunately Dakhnov's volume did not come to the attention of abstracters in North America until the spring of 1950.

Active development of the IP method as applied to mineral exploration in North America commenced with the writer's theoretical study in 1947 of the phenomenon of overvoltage and his report (Seigel, 1948) on its possible application to geophysical prospecting. Laboratory and subsequent field investigation, sponsored by Newmont Mining Corporation in 1948 eventually led to the development of a working field technique and the recognition of polarization effects in all rocks (Seigel, 1949).

Contemporaneously and independently D.A. Bleil (1953) indicated the possibility of utilizing IP in prospecting for magnetite and sulphide mineralization but apparently did not recognize the presence of nonmetallic polarization effects in rocks.

Until 1950 all IP measurements were of the 'time-domain' type. In 1950, as the result of some laboratory measurements, L.S. Collett and the writer suggested the method of measuring IP effects using sinusoidal current forms of different frequencies. J.R. Wait expanded greatly on the possibilities of this

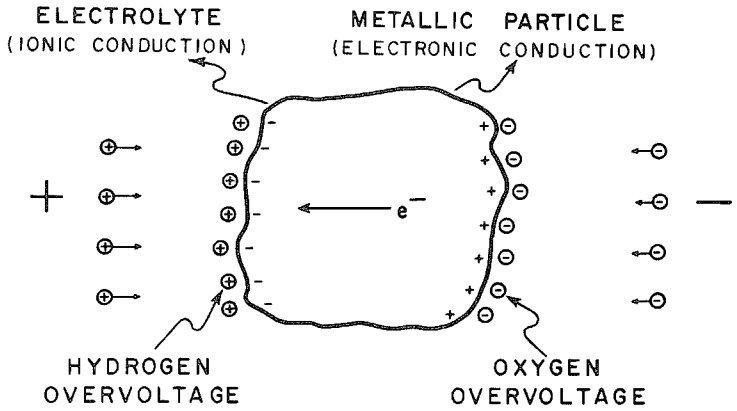


Figure 1a. Overvoltage on metallic particle in electrolyte.

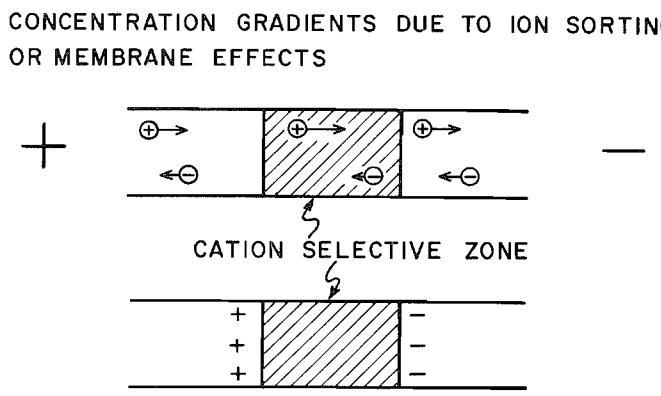


Figure 1b. Nonmetallic induced polarization agent.

approach and successful field tests were carried out in that year. The work of the Newmont group is summarized in a monograph (Wait, 1959).

Since 1950 several groups have been active in the development of the IP method by means of theoretical laboratory model and field studies. Prominent among these groups has been that at the Massachusetts Institute of Technology (Hallof, 1957; Madden, 1957; Marshall and Madden, 1959).

Induced polarization phenomena

Within the literal meaning of the term, polarization is a separation of charge to form an effective dipolar distribution within a medium. Induced polarization is therefore a separation of charge which is due to an applied electric field. It may also include phenomena which cause voltage distributions similar to those due to true polarization effects. For practical purposes, only polarization effects with time constants of buildup and decay longer than a few milliseconds are of importance. This usually excludes such phenomena as dielectric polarization and others which are encompassed by the normal electromagnetic equations.

In order to measure IP effects in a volume of rock one passes current through the volume by means of two contact points or electrodes and measures existing voltages across two other contact points. Theoretically, any time varying current form can be used, but in practice only two such forms are employed. In the first technique a steady current is passed for a period of from one second to several tens of seconds and then abruptly interrupted. The polarization voltages built up during the passage of the current will decay slowly after the interception of the current and will be visible for at least several seconds after the interception. This is termed the 'time-domain', 'transient', 'pulse', or 'DCIP' method by various workers. The writer will henceforth use the term time-domain to designate this technique.

The 'AC' or 'frequency-domain' method entails the passage of sine wave current forms of two or more low, but well separated, frequencies, e.g., 0.1 and 2.5 cps, or 0.5 cps and 10 cps. Since polarization effects take an appreciable time to build up, it can be seen that they will be larger at the lower frequency than at the higher, so that apparent resistivities or transfer impedances between the current and measuring circuits will be larger at the lower frequency. The change of measured resistivities with frequency is therefore an indication of polarization effects.

Further discussion of the precise quantities measured in the time- and frequency-domain methods will be resumed after a presentation of some of the polarization phenomena involved.

Overvoltage. When a metal electrode is immersed in a solution of ions of a certain concentration and valence, a potential difference is established between the metal and the solution sides of the interface. This difference in potential is an explicit function of the ion concentration and valence, etc. When an external voltage is applied across the interface a current is caused to flow and the potential drop across the interface changes from its initial value. If the electrode is a cathode it becomes more negative with respect to the solution, whereas if it is an anode, it becomes more positive with respect to the solution. The change in interface voltage is called the 'overvoltage' or 'polarization potential' of the electrode. If the electrode is a cathode, we speak of 'hydrogen overvoltage' and, if an anode, of 'oxygen overvoltage'.

These overvoltages are due to an accumulation of ions on the electrolyte side of the interface, waiting to be discharged. The charge of these ions will be balanced by an equal opposite charge due to electrons or protons on the electrode side of the interface. For small current densities the overvoltage is proportional to the current density, i.e., is a linear phenomenon. The variation of overvoltage with several other factors is presented in the writer's doctoral thesis (Seigel, 1949). The time constant of buildup and decay is around several tenths of seconds.

Overvoltage is therefore established whenever current is caused to flow across an interface between ionic and electronic conduction. In normal rocks the current which flows under the action of an impressed emf does so by virtue of ionic conduction in the electrolyte in the capillaries of the rock. There are, however, certain rock-forming minerals which have a measure of electronic conduction, and these include almost all the metallic sulphides (except sphalerite), graphite, some coals, some oxides such as magnetite, and pyrolusite, native metals and some arsenides and other minerals with a metallic lustre. When these are present in a rock subjected to an impressed emf, current will be caused to flow across capillary/mineral interfaces and hydrogen and oxygen overvoltages will be established. Figure 1a is a simplified representation of what happens to an electronic conducting particle in an electrolyte under the influence of current flow.

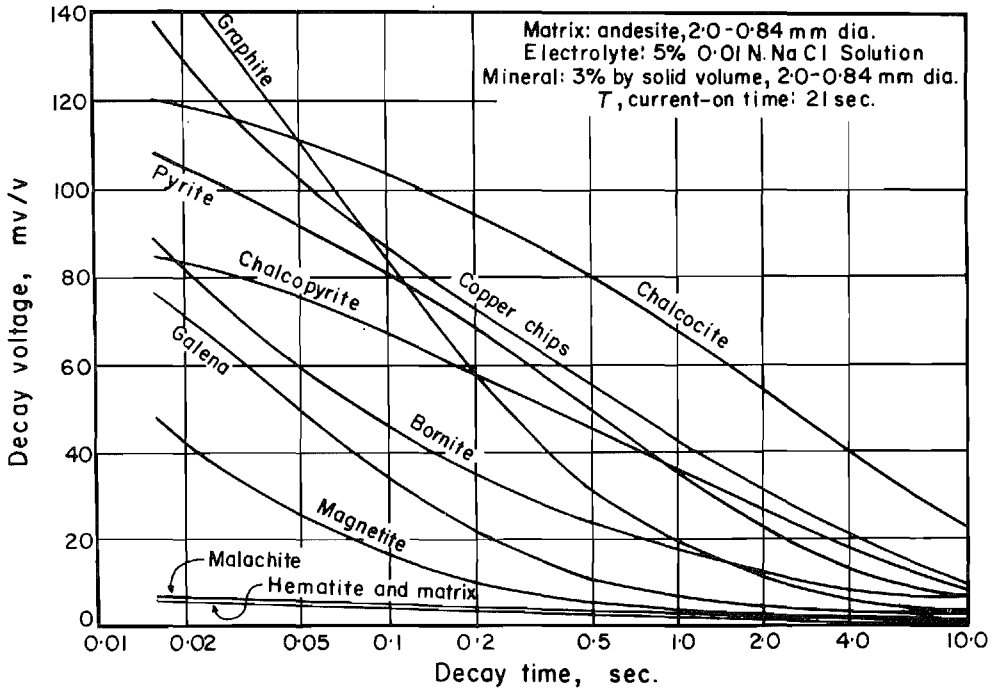


Figure 2. Decay curves for metallic and nonmetallic minerals (after Wait, 1959).

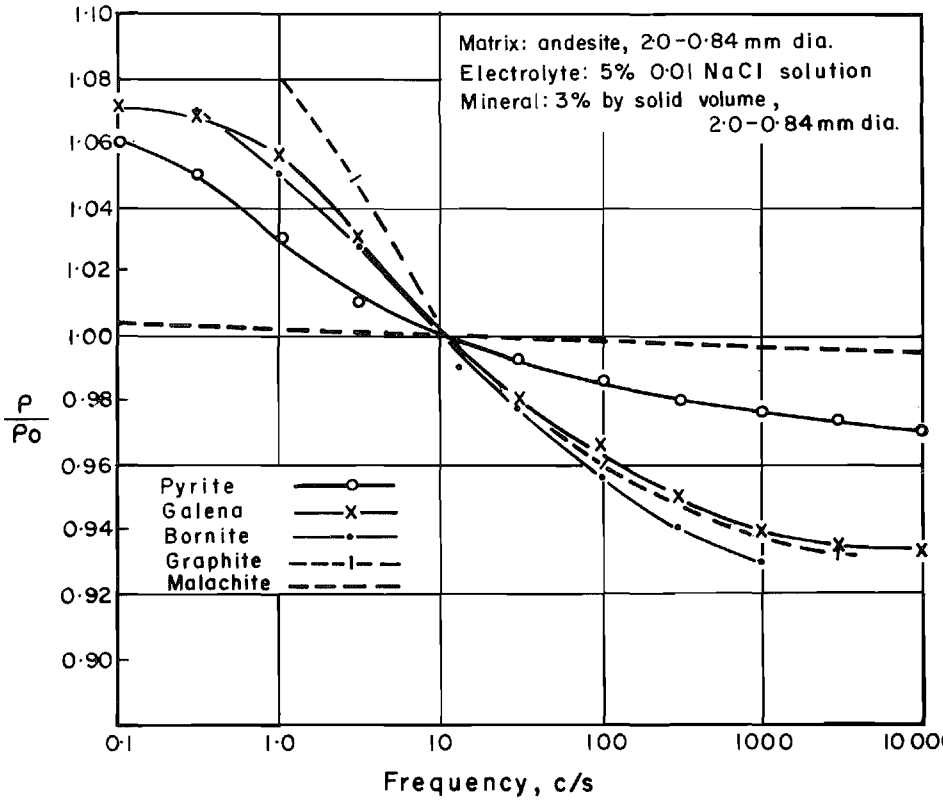


Figure 3. Resistivity-frequency characteristics of metallic and nonmetallic minerals (after Wait, 1959).

Nonmetallic polarization agents. Despite attempts by various workers to investigate the source of nonmetallic IP in rocks, an adequate explanation of all observed effects is still lacking. A number of possible contributory agents have been established. Vacquier (Vacquier, *et al.*, 1957) has carefully examined strong polarization effects due to certain types of clay minerals. These effects he believed to be related to electrodialysis of the clay particles. This is only one type of phenomenon which can cause 'ion-sorting' or 'membrane effects'. For example, Figure 1b shows a cation-selective membrane zone in which the mobility of the cation is increased relative to that of the anion, causing ionic concentration gradients and therefore polarization effects (see also Marshall and Madden, 1959). Much work remains to be done to determine the various agencies, other than clay particles, which can cause such membrane effects.

Contents

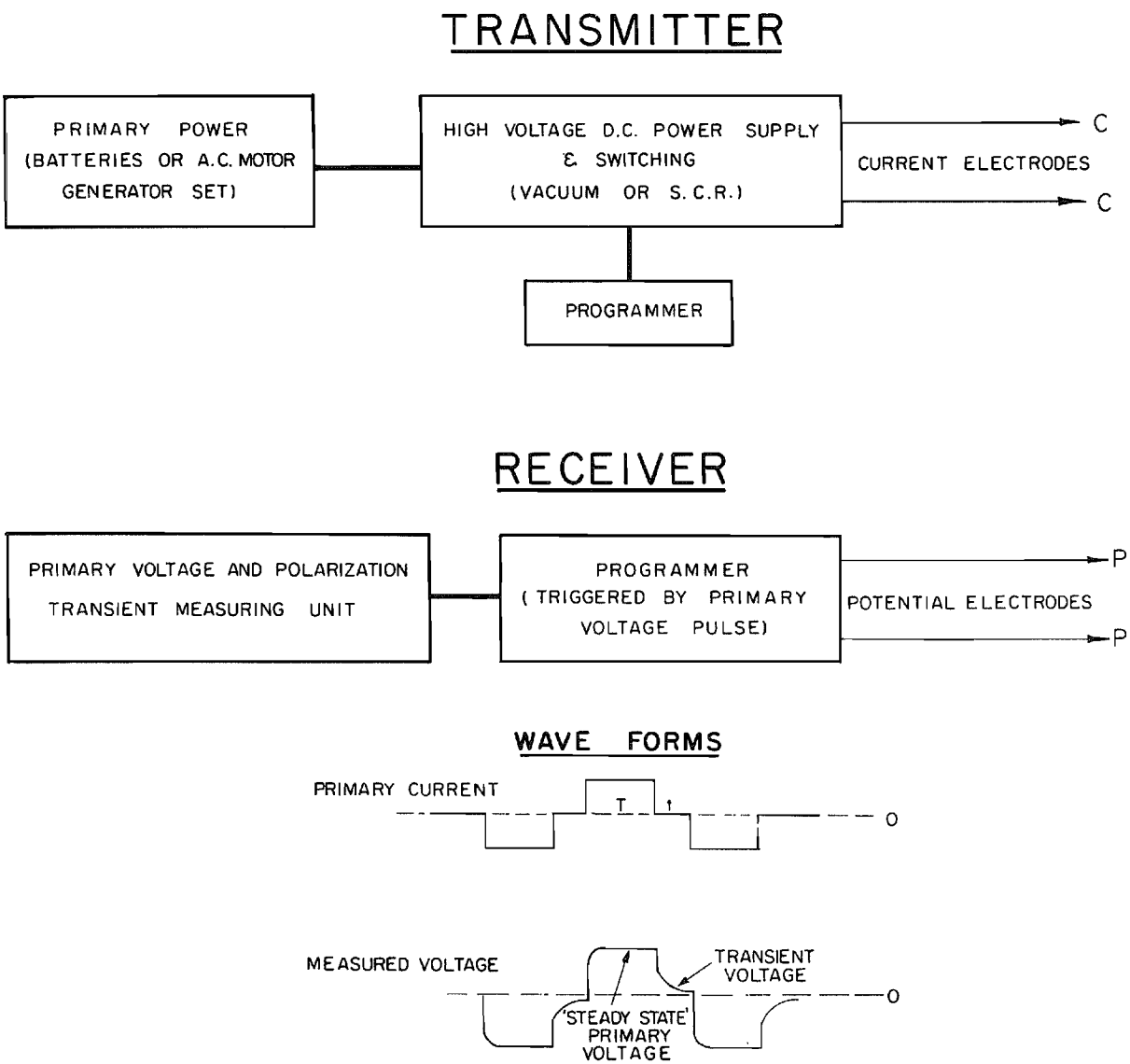


Figure 4. Time-domain, apparatus block diagram and wave forms.

A second group of phenomena, originally postulated by Dakhnov and the writer independently, includes electrokinetic effects. These combine electro-osmosis in the capillaries on the 'current on' time, the storage of energy in the compression of air bubbles and in hydrostatic heads, and the release of energy in return fluid motion when the current is intercepted. This, in turn, produces voltage gradients through the 'streaming potential' phenomenon. These voltage gradients will have the same external appearance as true polarization effects due to separation of charge. Generally speaking, electrokinetic effects seem less important than membrane effects in the over-all polarization picture.

Quantities measured. *Time-domain method* – Figure 2 shows the typical transient IP voltage decay forms for various rock-forming materials in a laboratory testing apparatus. A primary current time of around 21 seconds was employed on these tests. It will be noted that the voltages are plotted against the logarithm of the decay time and are approximate linear functions of the log t for reasonable lengths of time (t). The amplitude of the transient voltages has been normalized with respect to the steady state voltage existing immediately before the interception of the primary current.

To indicate the magnitude of the IP effects one may measure one or more characteristics of the transient decay curve and relate it back to the amplitude of the measured primary steady state voltage prior to the interception of the primary current. It may be shown that the ratio Vs/Vp, i.e., peak polarization voltage to the primary voltage just before interception is a physical property of the medium, which has been called M the 'chargeability' of the medium. Since it has been demonstrated that most IP decay voltages are similar in form but differ in amplitude (for the same charging time) one can take the average of several transient voltages at different times, or indeed use the time integral of the transient voltages as a diagnostic criterion. The advantage of averaging or integrating lies in the suppression of earth noises and of interline coupling effects.



Figure 5. Typical time-domain IP receiver (courtesy Scintrex Limited).

If the time integral is used the units of M will be in millivolt seconds/volt or milliseconds. If one or more transient voltage values are measured and normalized, M will be dimensionless.

For homogeneous, isotropic material, the value of M is independent of the shape or size of the volume tested and of the location of the electrodes on it. It is a true physical property. For a given medium it is dependent on the current charging time and on the precise parameter of the decay curve measured. There are also subsidiary variations with temperature and electrolyte content, etc.

Frequency variation method – Figure 3 shows typical curves of the variation of normalized resistivities with frequency for various sulphide, graphite and nonmetallic rock minerals in artificial mixtures. Both the fact of the variation of apparent resistivity with frequency and the presence of phase angle lags may be used to indicate the presence of IP effects, although generally only the first is so employed.

Since the IP phenomena may be shown to be linear, within the usual range of voltages and currents, there is a direct relationship between the transient curve form and the variation of apparent resistivity with frequency. To arrive at a dimensionless parameter equivalent to the chargeability, one would have to normalize the variation of the apparent resistivity, by dividing by the resistivity at one particular frequency. The factor used is called the 'percent frequency effect' or PFE and is defined as $((R1 - R2)/R1) \times 100$ where $R1$ and $R2$ are the apparent resistivities at the lower and higher frequencies used (Marshall and Madden, 1959).

A second parameter is sometimes employed which is really a mixture of physical properties. It is called the metal factor (MF) and is proportional to PFE/$R2$ or to M/R. As such, it serves to emphasize IP effects which occur in obviously conductive environments, i.e., concentrated sulphide deposits or sulphides and graphite in shear zones. Since it is not a dimensionless factor nor a true single physical property, it is subject to variation related to the changes of shape and resistivity of the medium under investigation, rather than simply to variations in polarization characteristics. In the writer's opinion, the metal factor has some merit in emphasizing IP anomalies due to concentrated metallic bodies, but should not be used as a primary indicator of abnormal IP conditions.

Field techniques

Figure 4 shows a block diagram of apparatus commonly used in field operations with the time-domain method and the primary current and resultant voltage wave forms. The transient voltage amplitudes are considerably exaggerated to be visible. Power sources up to 30 KVA, 5000 volts and 10 amperes have been employed where a considerable depth of detection is desired in low resistivity areas. The current-on time T, ranges from 1 second to as much as 30 seconds, and the current-off time may be as much as 10 seconds. It is not strictly necessary to employ a cyclic current wave form, but considerable advantages in signal-to-noise ratio are achieved thereby.

Most of the measuring units now employed are remote-triggering, i.e., they are internally programmed, triggered by the primary voltage pulse and do not require a cable interconnection to the cycle timer on the power control unit. Figure 5 shows a typical time-domain remote-triggered measuring unit. This particular measuring unit has several interesting features. For one, there is a memory device which provides an automatic self potential adjustment at the tail end of each cycle. For another, it has the ability to integrate the area either below the transient curve (standard M measurement) or above the transient curve (denoted as the L measurement) over a specific time interval. The

Contents

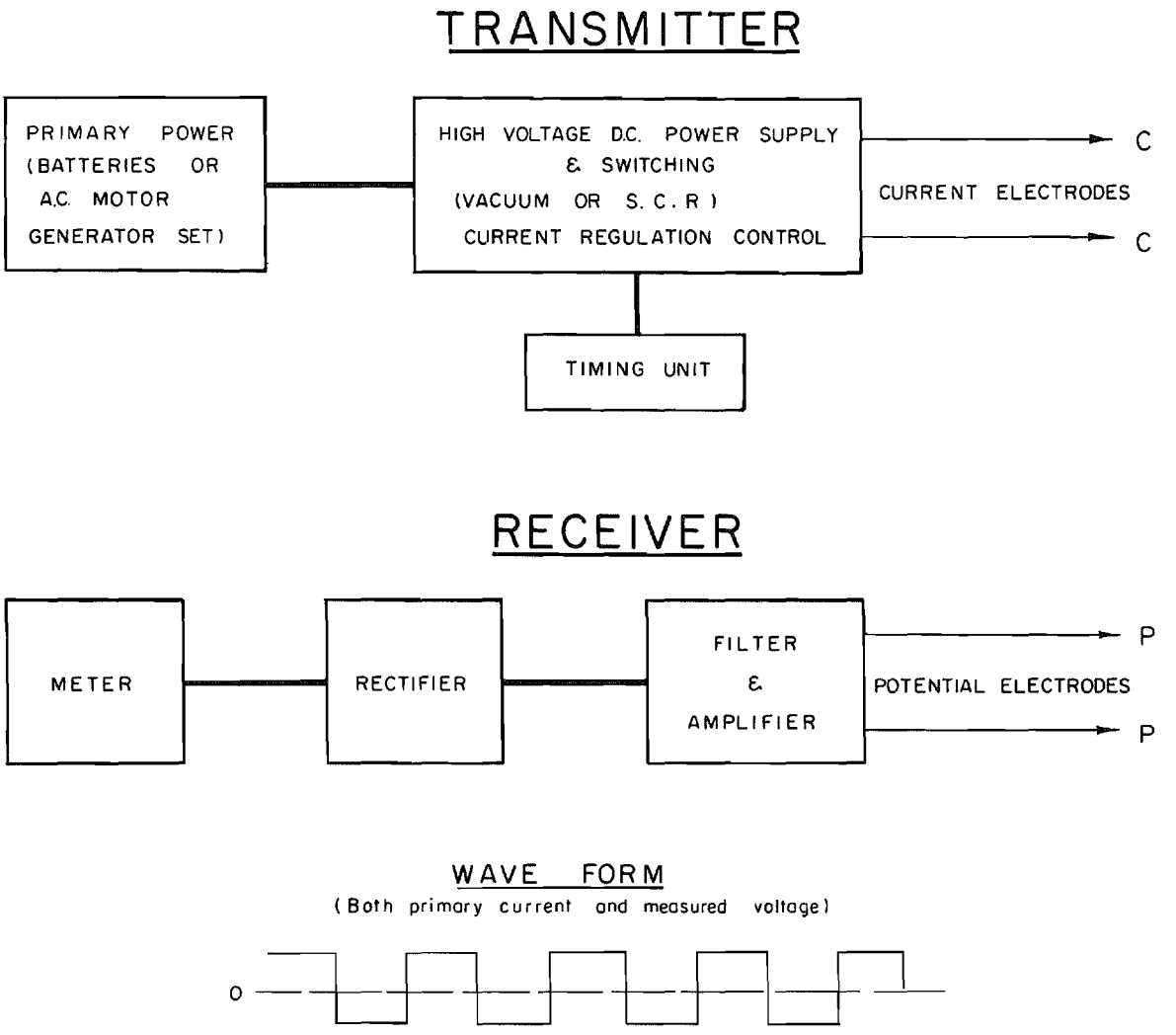


Figure 6. Frequency-domain, apparatus block diagram and wave forms.

ratio of these quantities gives a direct measure of the decay curve form, which may be of diagnostic value. In areas of low electric earth noise useful measurements may be made with primary voltages as low as 1 millivolt.

Figure 6 shows a block diagram of a typical frequency-domain field apparatus and voltage wave form. Since the primary current and earth voltages are usually measured by separate devices and their ratio employed to obtain the apparent earth resistivity and its variation with frequency, it is common practice to adjust the current to a standard value and maintain it there to the required accuracy. The primary wave form is usually a commutated DC. Commonly, up to 6 frequencies are available in the range of 0.05 to 10 cps. Figure 7 shows a typical modern frequency-domain measuring unit. This unit has a high degree of power line frequency (50 to 60 cps) rejection. It measures both the primary voltage and the change of primary voltage with change in operating frequency, the latter to an accuracy of about ± 0.3% when the former exceeds 100 microvolts. It has the added feature of a phase-lock voltmeter which can be used under low signal-to-noise conditions.

Array	Domain Employed	Advantages	Disadvantages
Wenner	Time	For local vertical profiling.	Poor depth penetration. Requires four linemen.
Three electrode (or pole-dipole)	Time and frequency	Three linemen. Universal coupling. Good depth penetration.	Susceptible to surface masking effects.
Dipole-dipole	Frequency	Good resolution. Universal coupling.	Complex curve forms. Low order signals.
Gradient	Time	Minimum masking. Two linemen only. Excellent depth penetration. Excellent resolution. Can use multiple receiver for speed.	Low order signals. Relatively insensitive to flatly dipping bodies or thin, steeply dipping dipping bodies parallel to the current flow.

Common field electrode arrays are shown in Figure 8. The electrodes marked *C* are current electrodes and those marked *P* are potential or measuring electrodes. Each of the electrode arrays has its own advantages and disadvantages in respect of depth of penetration, labour requirements for moving, susceptibility to earth noise, electromagnetic earth transients and interline coupling. The table summarizes the features of these arrays.

For each array (except the gradient array) the basic electrode spacing *a* is selected to give adequate penetration down to the desired depth of exploration. For the pole-dipole and double dipole it is customary to obtain several profiles, for integral values of *n* from 1 to as much as 6. For the symmetric arrays (Wenner and dipole-dipole) the measured values are plotted against the midpoint of the array. When using the three electrode array (time-domain) the station position is taken to be the midpoint of the moving current and the nearest potential electrode. When using the pole-dipole (frequency-domain) the station position is taken as the midpoint between the moving current electrode and the *midpoint* of the two potential electrodes. With the gradient array it is the midpoint of the two potential electrodes. For the three electrode array and pole-dipole these station locations are not unique and represent conventions only.

IP data may be plotted in profile form or contoured, although it should be noted that somewhat different results will be obtained with different line orientations so that contouring is not strictly justified. Profile interpretation is superior, particularly for shallow, confined bodies, because multiple peaked curves may arise from such bodies using certain electrode arrays; and the plotted peaks may give an erroneous impression of the location of the polarizable body.

To obtain the variation of physical properties with depth, expanding arrays may be used with any of the electrode systems, keeping the spread centre fixed and simply changing the relative spacing *a*. This is of particular value where it is known, or expected, that vertical variations of physical properties will be much greater than lateral variations. As the spacing is increased the influence of the deeper regions becomes more significant and the resultant resistivity and IP curves may often be interpreted to give the depth to discontinuities in physical properties and the physical properties themselves.

Common practice in presenting frequency-domain results is to plot the measured data below the line at a depth equal to the distance of the station position (as defined above) from the midpoint of the potential dipole. When this is done for a variety of values of *n* a pseudo-two-dimensional section results which shows, albeit in a markedly distorted fashion, the variation of physical properties with depth.

Interpretation methods

A mathematical representation of IP effects has been developed by the writer (Seigel, 1959), which relates the observed IP response of a heterogeneous medium to the distribution of resistivities and IP characteristics. To a first approximation it is equally applicable to any IP parameter measured in the time-and frequency-domains.

From this theory, one may predict the anomalous response to be expected from a specific body with a given chargeability and resistivity contrast. For example, Figure 9 shows the form factor *F* plotted for the three electrode array for various values of α, for

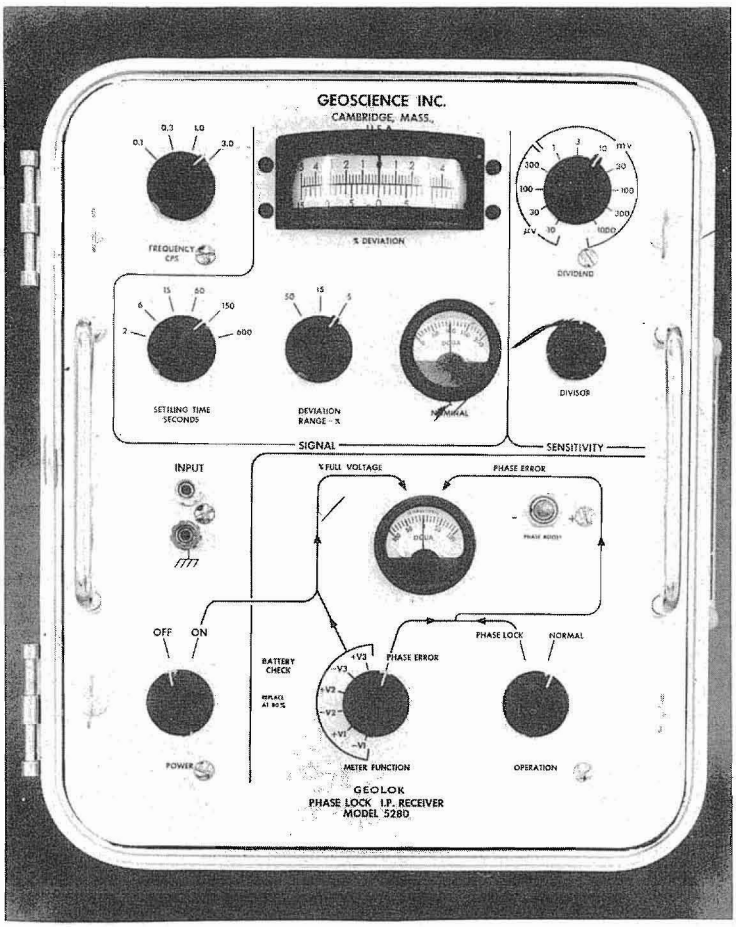


Figure 7. Typical frequency-domain receiver (courtesy Geoscience Inc.).

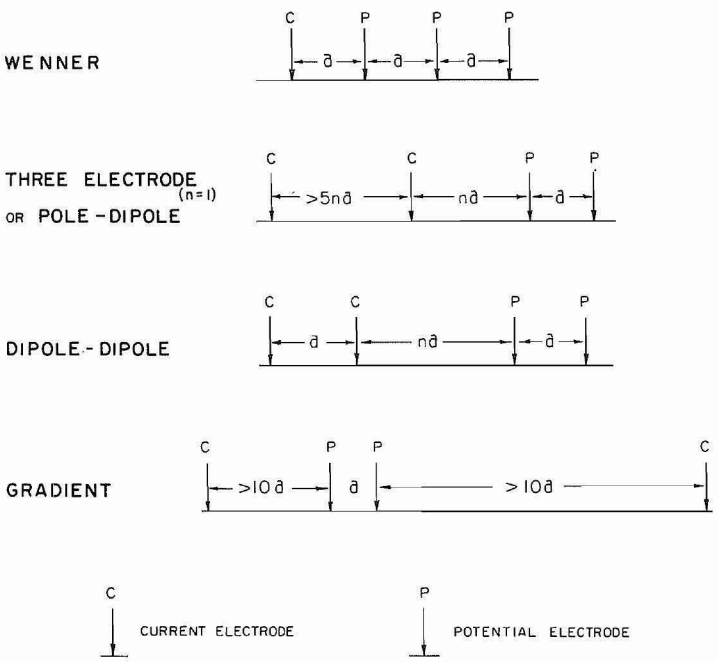


Figure 8. Common field electrode arrays.

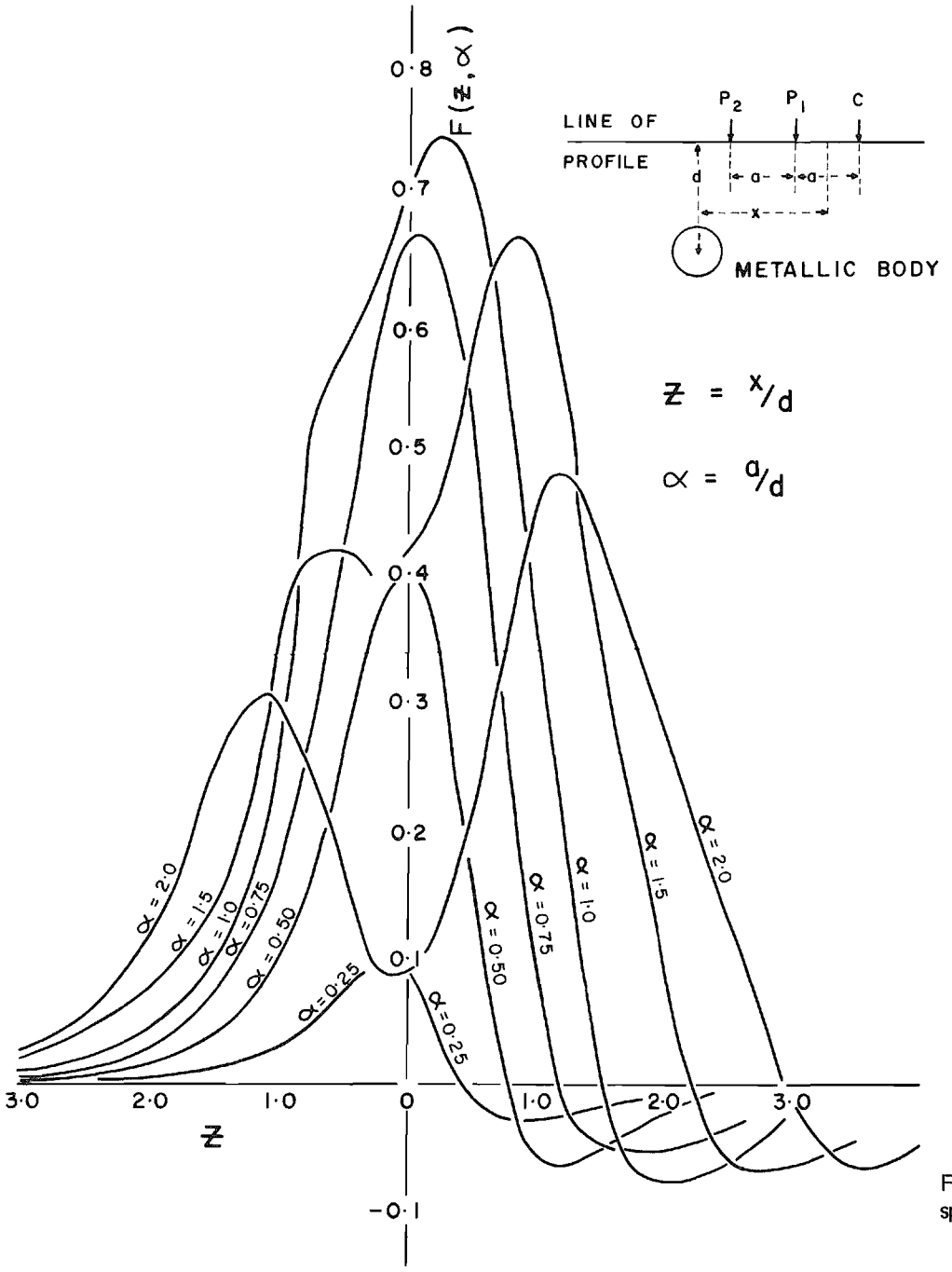


Figure 9. Theoretical response of a sphere, three electrode array.

a sphere, where α is the ratio of the electrode spacing to the depth to the centre of the sphere. The sphere response is proportional to F times the chargeability contrast, times its volume and times a resistivity ratio factor.

Curves of this sort permit one to interpret anomalies due to localized bodies. It will be seen that for each array there is an optimum spacing for a body at a particular depth, and therefore there is some meaning to the term 'depth of penetration'.

When the dimensions of the polarizable medium are large in comparison with its depth below surface, as is often the case, particularly in investigation of porphyry copper type deposits, a two-layer approximation is adequate. Theoretical curves based on this approximation (Figure 10) may be used to interpret the results of expanding Wenner or three electrode array depth determinations.

For more complex geometries mathematical solutions in closed form are often lacking. For such cases one may resort to model studies (e.g., Figure 11 for a buried dike) or to computer-calculated solutions.

Use of method

The most productive use of the IP method to date has been in the exploration for deposits of metallically conducting minerals, where the amounts and degree of interconnection of these

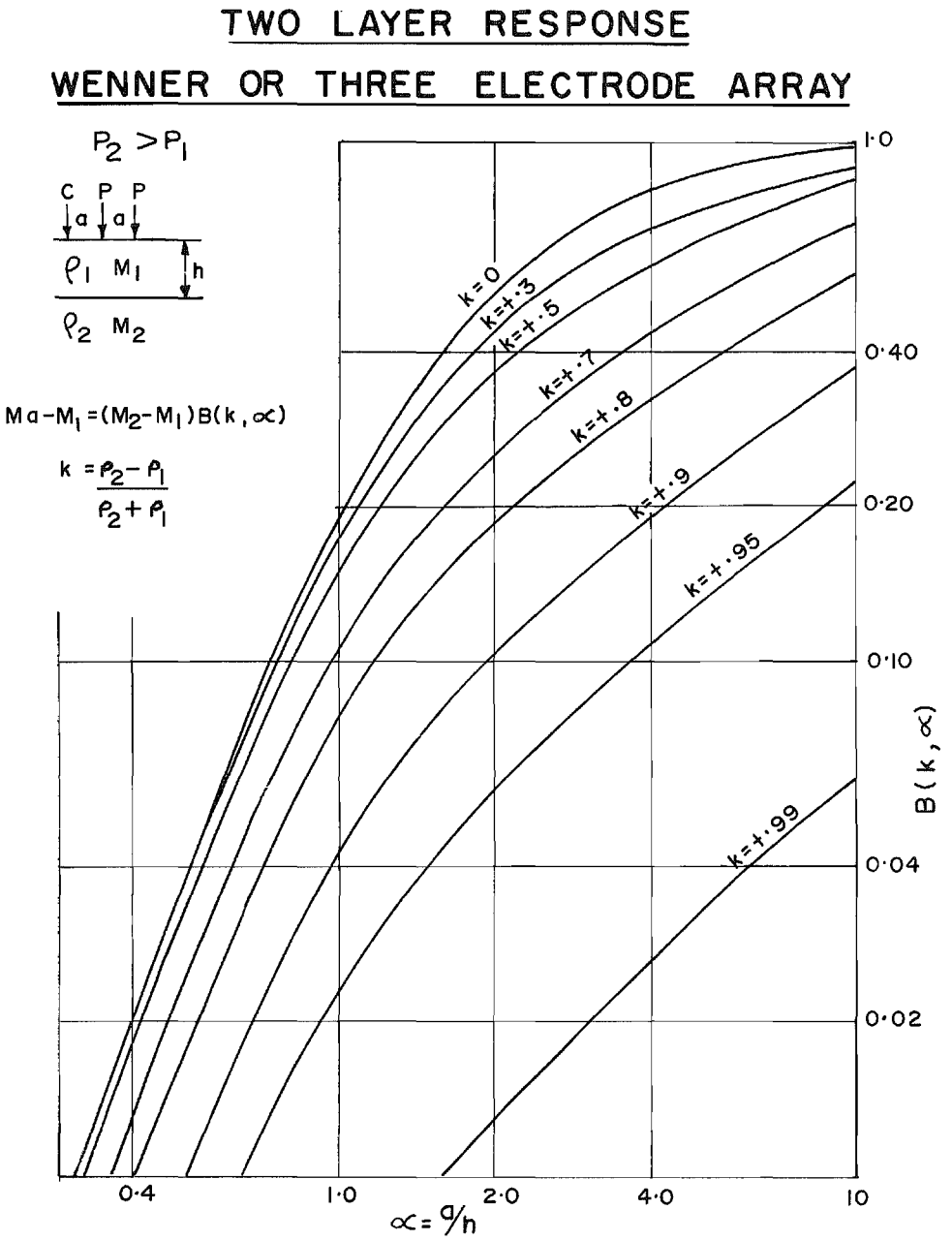


Figure 10. Theoretical two-layer response, Wenner or three electrode array.

minerals are too low to give rise to an electromagnetically detectable body. Where electromagnetic detection is feasible it is usually far more rapid and economical to apply electromagnetic induction methods to the problem. The IP method is the only geophysical tool available which is capable of detecting as little as 1% by volume of metallic conducting sulphides. It is best used, therefore, where there is a high ratio of economic minerals to total sulphide mineralization. Included in the proper IP range are such types of deposits as disseminated copper ores, in porphyry or bedded forms; lead-zinc deposits, particularly of the bedded type in carbonate rocks; gold and other deposits which have an association with disseminated metallic conductors. For many of these mineral occurrences the IP method is unique in providing detection.

Figure 12 shows time-domain discovery traverses over a typical newly discovered porphyry copper deposit in British Columbia. The lateral limits of the mineralization can be readily determined from the geophysical data, as well as depth to the upper surface of the mineralization.

Figure 13 shows a discovery traverse over a major bedded body of lead-zinc-marcasite mineralization in carbonate rocks in the Pine Point area, Northwest Territories, Canada. For comparison, both gravity and Turam electromagnetic profiles on the same section are shown. It is interesting to note that, despite an appreciable resistivity depression over the mineralization there is no significant Turam response. The conductivity of the ore is, in fact, no higher than that of the surficial deposits in the general area, so that electromagnetic and resistivity methods yield, in

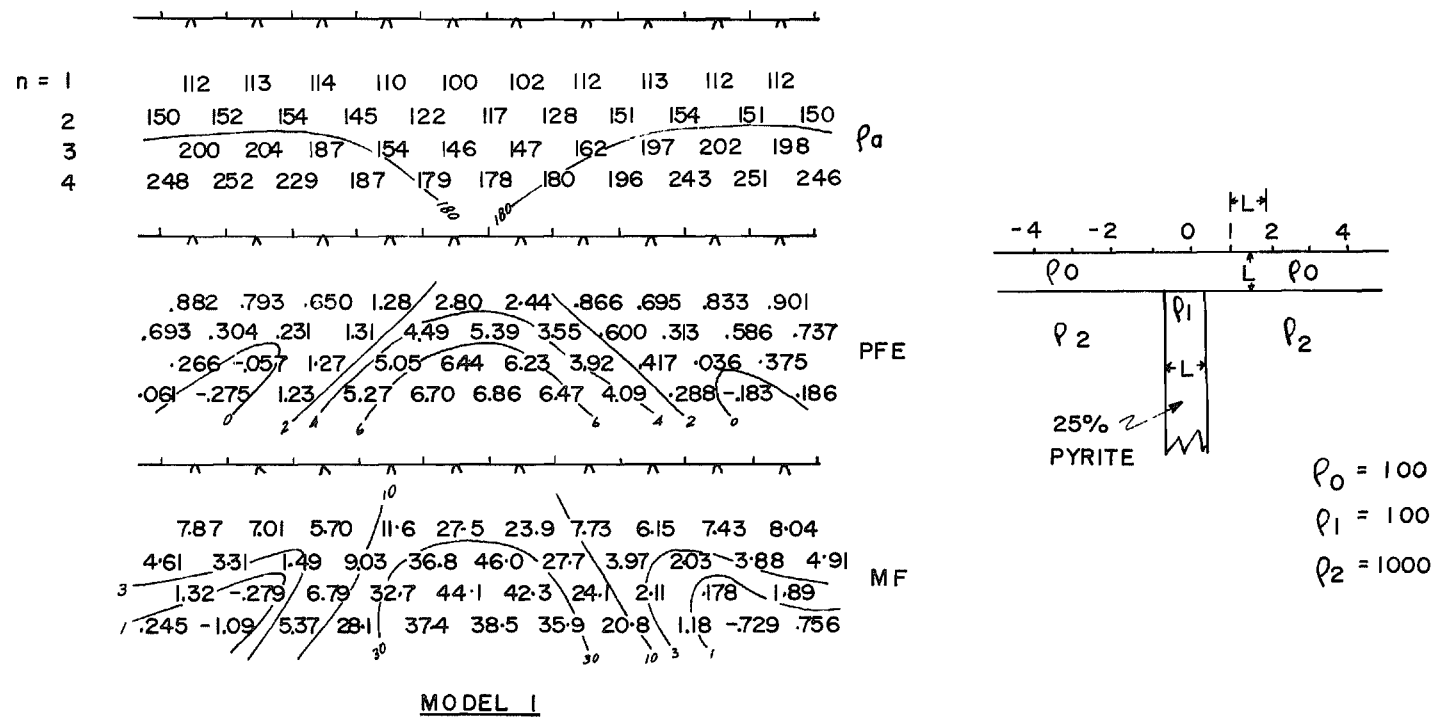
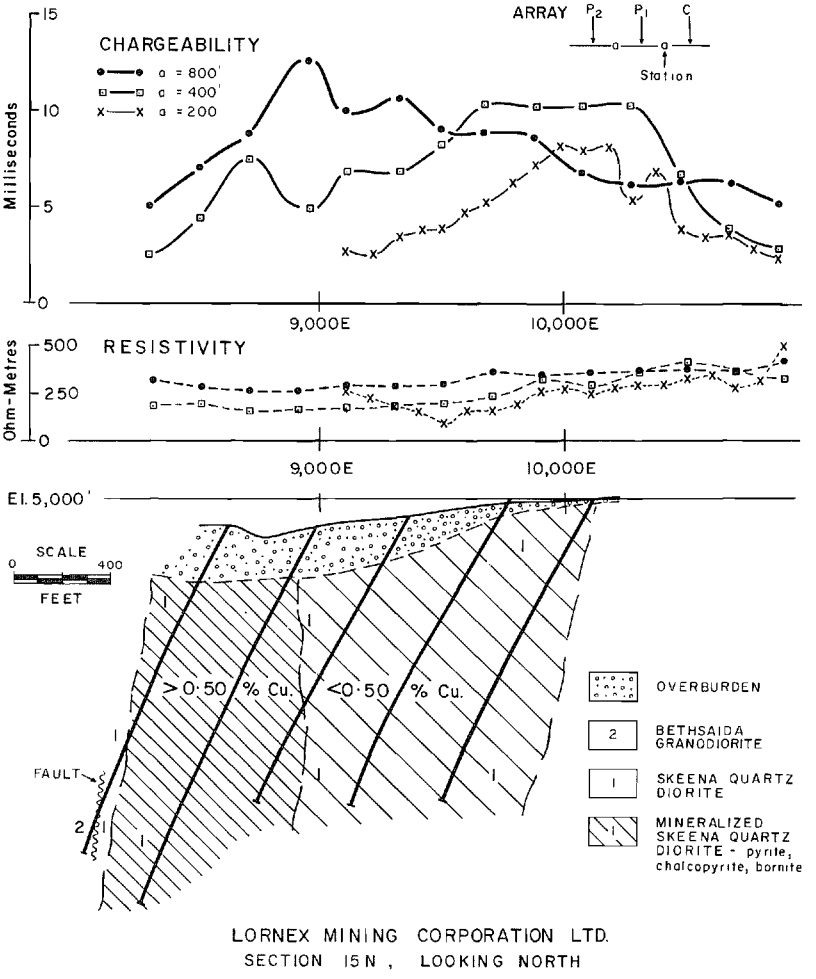


Figure 11. Model dike response, dipole-dipole array (courtesy K. Vozoff).

Figure 12. Geophysical and drilling results, Lornex porphyry copper orebody, British Columbia, Canada.



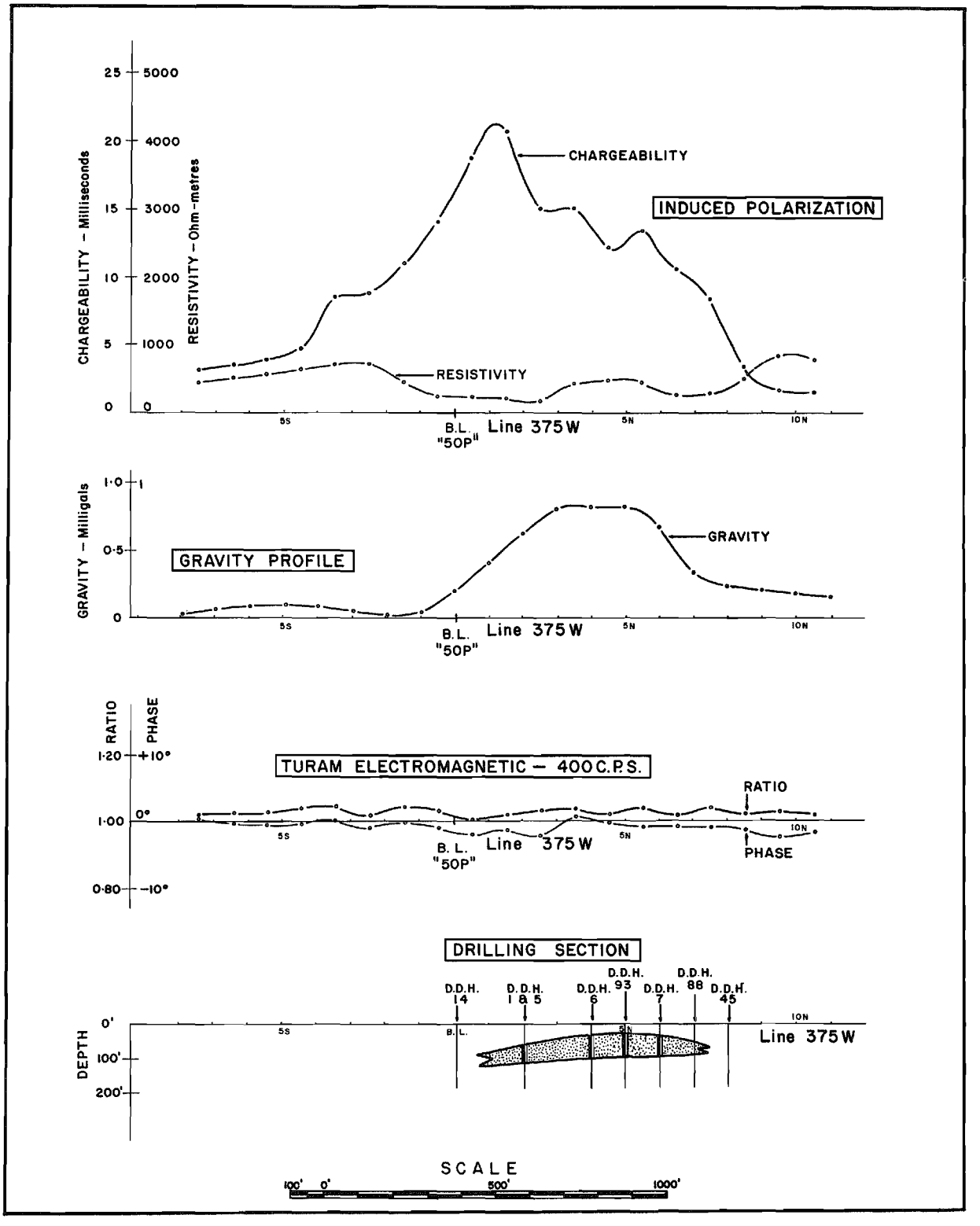


Figure 13. Geophysical and drilling results, Pyramid No. 1 lead-zinc orebody, Pine Point area, N.W.T., Canada.

Contents

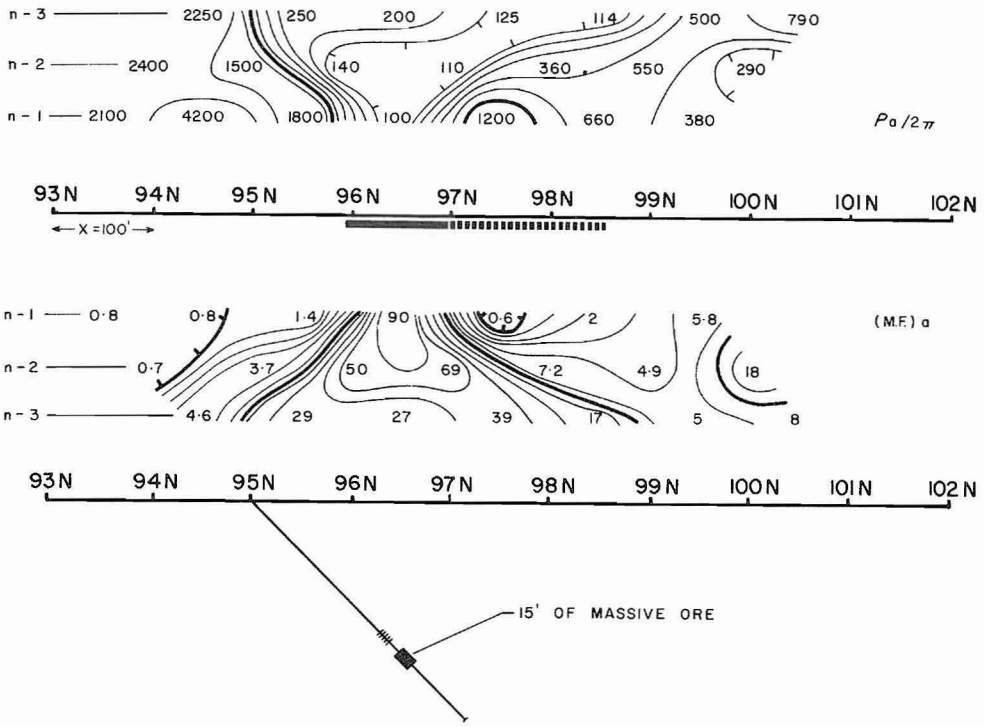
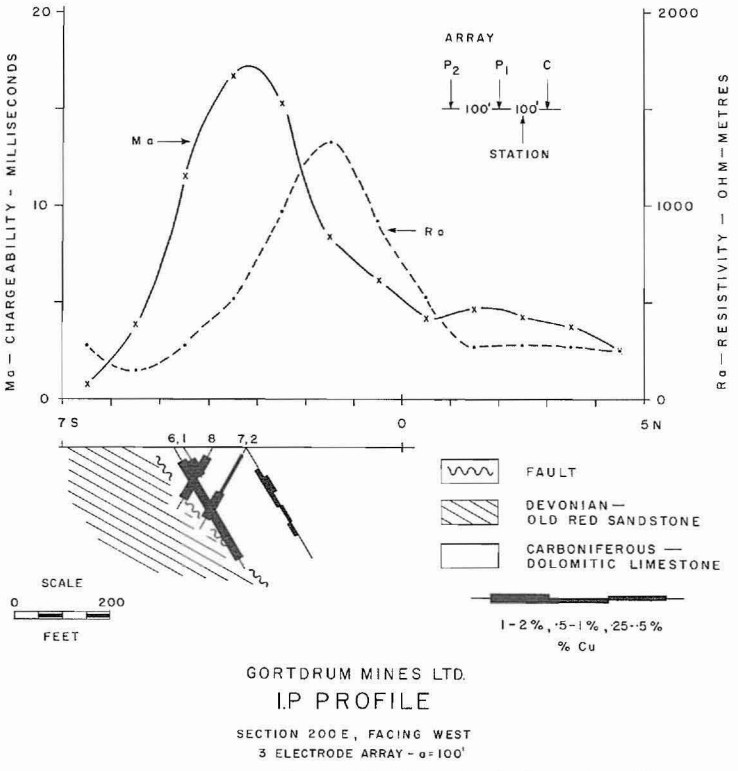


Figure 14. Geophysical and drilling results lead-zinc-copper orebody, Heath Steele Mine, New Brunswick, Canada (courtesy P. Hallof).



GORTDRUM MINES LTD.
I.P PROFILE
SECTION 200E, FACING WEST
3 ELECTRODE ARRAY - a = 100'

Figure 15. Geophysical and drilling results, copper-silver orebody, Gortdrum Mines, Ireland.

themselves, no useful information. The gravity method, although yielding a positive response in this instance, does not provide a good reconnaissance tool in this area because of karst topography and other sources of changes in specific gravity.

One occasionally encounters a deposit of the 'massive sulphide' type which is normally thought of as an electromagnetic type of target because of its high conducting sulphide content, but which, obviously because of the lack of large-scale continuity of the conducting sulphides, does not respond to the electromagnetic techniques. Figure 14 shows an intersection of ore-grade material of this type, in New Brunswick, Canada, where electromagnetic methods had yielded negative results.

In many types of ore deposits the bulk of the IP response is due to the accessory noneconomic sulphides, usually pyrite and pyrrhotite, and the ore minerals themselves are in the minority. A true test of the sensitivity of the IP method is an example of a low-grade disseminated deposit with no such accessory minerals. Figure 15 illustrates such a case, with an IP discovery section over the Gortdrum copper-silver deposit in Ireland. The ore minerals consist of chalcocite, bornite and chalcopyrite in a dolomitic limestone, and the average ore grade is only 1.2% Cu and 0.75 oz Ag per ton, indicating less than 2% average by volume of metallic conducting minerals.

Whereas the bulk of IP measurements in mineral exploration has, naturally, been made on surface, the technology of drill hole exploration has been well developed, particularly by the Newmont group (see Wagg and Seigel, 1963). The time-domain is more suitable for drill hole applications since it permits a relatively close coupling of the current and potential lines in a small diameter bore hole. The three electrode array has been extensively employed for logging purposes, with a variety of electrode spacings to give varying ranges of detection away from the hole. In this fashion the variation of electrical properties with distance from the hole may be determined. A second, 'directional

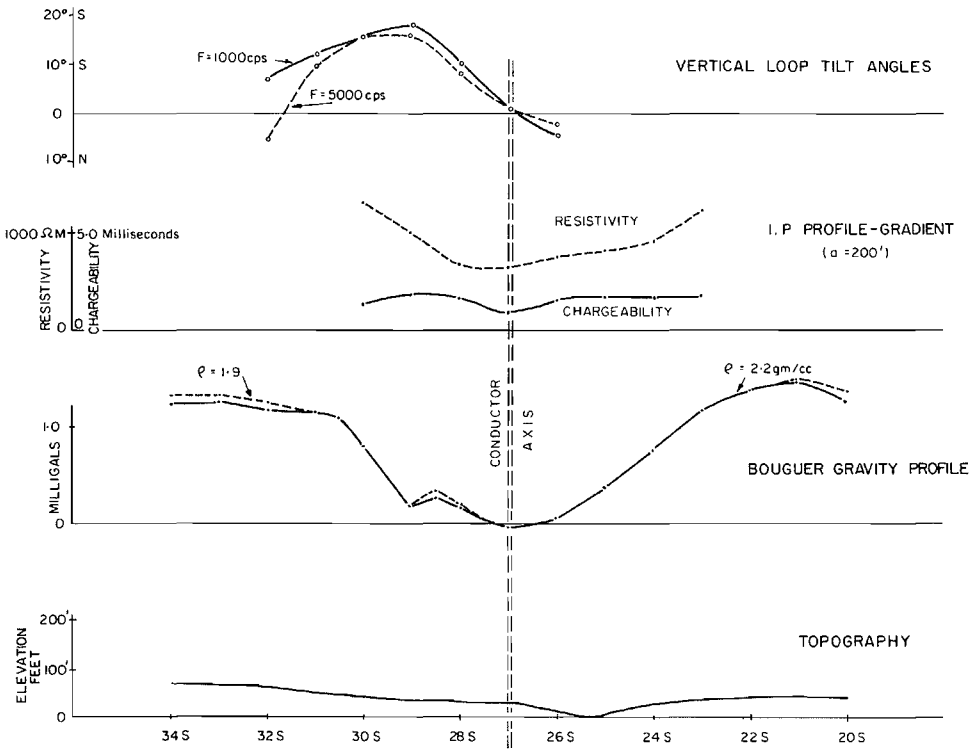


Figure 16. Geophysical recognition of overburden trough, Northwest Quebec, Canada.

log', then gives information on the direction of any anomalous material indicated by the detection log.

Whereas the IP method is usually employed as a primary exploration tool it may play an auxiliary role as well, such as to distinguish between metallic and ionic conducting sources of other types of electrical anomalies, e.g., electromagnetic. Figure 16 shows a typical conducting zone revealed by a ground electromagnetic survey which was later proven, by drilling, to be due to overburden conduction in a bedrock trough. The IP response is in the low-normal range. The gravity profile, also shown, corroborates the presence of the bedrock depression.

Attempts have been made by a number of workers to employ the I.P. method in the field of groundwater exploration (e.g., Vacquier, 1957) but with no consistent success. There are variations of chargeability from one type of nonconsolidated sediment to another, but these fall, in general, within a relatively small range, so that their degree of variation with water saturation is a second order effect. More investigation remains to be done in this area before a definitive conclusion can be reached.

Limitations of the method

The IP method has a number of recognized limitations, some of a fundamental nature and others of a temporary nature reflecting the current state of the art. On a unit coverage basis the method is relatively expensive to apply, costing between $200 and $500 per line mile surveyed, in most instances. This cost has, however, been progressively reduced by advances in instrumentation resulting in decreased weight, increased sensitivity and rejection of earth noise effects. Some degree of improvement is yet to be expected in this area.

The same geometric limitations apply as with the resistivity method employing the comparable array. As a rule, a body of up to 10% disseminated metallic conductors cannot be detected at a distance from its nearest point much exceeding its mean diameter. This detectability may be somewhat improved by the use of secondary criteria, but such improvement is likely to be only marginal.

Since overvoltage is essentially a surface phenomenon the IP response from a given volume percentage of metallic conductors generally increases as the individual particle size is decreased. From the usual simple IP measurements, therefore, one cannot reliably predict the percentage by volume of such conductors in a deposit as there may be a variation of particle size throughout the deposit. Still less can one differentiate between metallic conductors (e.g., chalcopyrite, galena, pentlandite) of economic interest and those of noneconomic interest (e.g., pyrite, pyrrhotite and graphite). In addition, we cannot even reliably differentiate between metallic and nonmetallic sources of IP responses. The latter may include certain types of clay and, in consolidated rocks, such platey alteration minerals as serpentine, talc and sericite. Figure 17 shows a section across each of two anomalous IP areas in the Pine Point area in Canada. Section *A* is a discovery traverse across an orebody containing one half million tons of 11.4% combined Pb and Zn and coming within 40 feet of the ground surface. Section *B* is a traverse across what proved, by drilling, to be a karst sink hole, filled in with a variety of unconsolidated material including boulders and clay. In such cases the gravimeter has sometimes proven to be of value in resolving the two types of occurrence but there is the very real possibility of the coincidence of a sink hole and a lead-zinc deposit, which would give rise to an uncertain resulting gravity response.

Contents

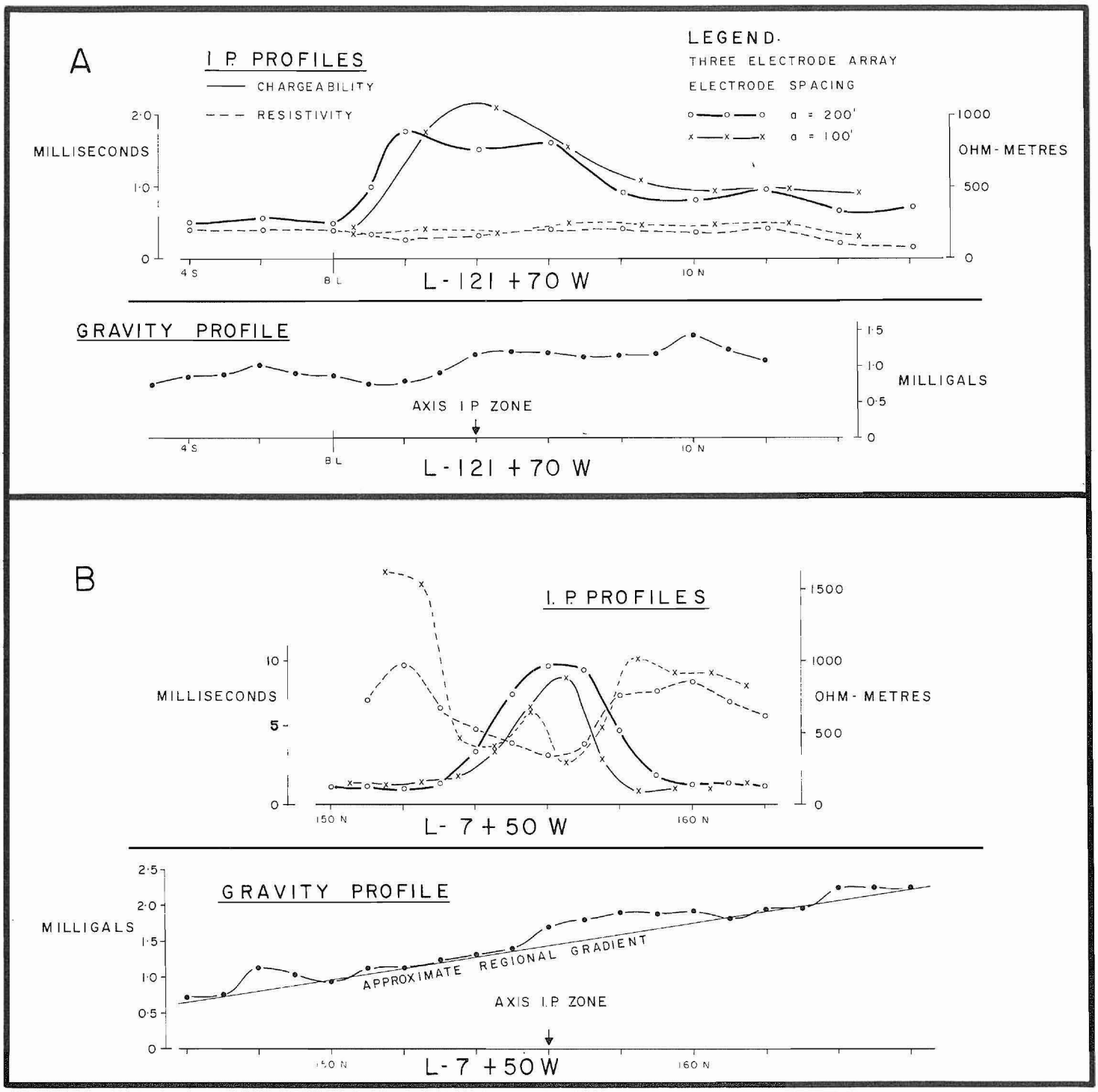


Figure 17. Possible ambiguity of induced polarization results, Pine Point area, N.W.T., Canada.

Any normal transient (time-domain) polarization decay and equivalently any curve of variation of apparent resistivity with frequency may be simulated by means of a mixture of metallic conductors of a suitable particle size distribution. It is, however, possible in an area of common geology, that the various possible sources of IP responses may have significantly different characteristic curves in each of these two domains. A more thorough analysis of these curves at significant points is, therefore, of value. Modern receivers in both domains (Figures 5 and 7) have the ability to give curve form information as well as a single quantity related to an IP amplitude. Komarov (1967) documents such an example over a copper-nickel deposit in the U.S.S.R. where,

effectively, the sulphide responses have a longer time constant than the normal nonmetallic polarization.

Another source influencing IP measurements is the electromagnetic response of the earth. For a given electrode array the electromagnetic effect is dependent upon the frequency times the conductivity and the square of the spacing (Sunde, 1949). In the frequency-domain this source becomes troublesome (communication from P.G. Hallof) when

1. The electrode spacing is 500 feet or over and $n = 3$ or greater,
2. The highest frequency employed is 2.5 cps or greater, and
3. The average earth resistivity is lower than about 25 ohm metres.

Electromagnetic effects are present in the time-domain measurements as well, of course, but are usually of far lesser amplitude for the same array and earth conductivity, particularly when the total cycle is 4 seconds or longer and when the polarization transients are integrated. This is accounted for by the fact that such measurements are closely related to the effective earth voltage phase shift at the total cycle frequency. This frequency is therefore less than 0.25 cps.

Comparison of methods

There is a continuing rivalry between protagonists of the time-domain and frequency-domain measurements. All that is clear is that neither method is superior in all respects to the other. The same phenomenon is being measured in different ways often with different arrays and the results are presented in different formats (pseudosections in the frequency-domain versus profiles or contour plans in the time-domain). The 'metal factor', which is a mixture of physical properties, is commonly presented with frequency-domain measurements only. These differences are largely superficial and are based on separate historical developments and subjective preferences.

There is a direct mathematical transformation between IP measurements in the two domains. Theoretically, at least, the same information can be obtained in either domain. Practically, however, there are certain differences. The time-domain measurements are absolute, i.e., are measured in the absence of the steady state voltage and are disturbed only by earth noises as a background. Such measurements can usually be made to an accuracy of better than 10%, even in unmineralized rocks. The limit of useful sensitivity is usually imposed only by the uniformity of the background IP response. In the frequency-domain the IP response is measured as a difference in transfer impedances. This difference can be measured with an accuracy of only 0.3% with extremely stable equipment (e.g., that of Figure 7). Since the nonmetallic background PFE over the interval of 0.1 to 2.5 cps is usually less than 1%, then the probable error of this measurement is of the order of at least 30%. It is seen that it is feasible to obtain greater sensitivity of measurement in the time-domain. This increased sensitivity is of value in areas of low 'geologic' and electrical noise. By geologic noise is meant the range of variation of IP parameters within the normal rock types of the area.

The frequency-domain equipment requires somewhat less primary power than the time-domain equipment because the former measurement is an AC one with the ability to use tuned filters and amplifiers as well as such devices as phase-lock voltmeters. This advantage is not so marked as it once was, as current time-domain equipment, with its self adjusting earth-voltage balance and ability to sum any desired number of integrations, provides a high degree of noise rejection. Under truly random noise conditions the summation of n integrations provides the usual $1/n$ reduction in statistical noise and is a powerful nonsubjective means of noise suppression.

Reference has already been made to the relative effects of the electromagnetic response of the earth in both methods. Similar remarks apply to capacitative and inductive coupling effects between current and potential cables, although such effects can be largely avoided in any event by careful positioning of the cables, except possibly in drill hole surveying. So far, only in the time-domain may useful drill hole measurements be made with both current and potential electrodes lying side by side in a small diameter bore hole.

Despite these slight effective differences both methods of IP exploration have amply demonstrated their value through important mineral discoveries in many parts of the world. The role of IP in mineral exploration is well acknowledged and rapidly expanding.

Acknowledgments

The writer wishes to thank the various sources of case histories and illustrations cited in the text and in particular Dr. Keeva Vozoff and Dr. Philip Hallof for valuable contributions.

References

Bleil, D.F., 1953. Induced polarization, a method of geophysical prospecting. *Geophysics,* 18: 636-661.

Dakhnov, B.N., 1941. *Electrical Well Logging, Interpretation of Electric Logs.* Moscow, Chapter IV.

Hallof, P.G., 1957. On the interpretation of resistivity and induced polarization results. Doctoral thesis, M.I.T. Department of Geology and Geophysics.

Komarov, B.A., 1967. Induced polarization method. Lecture read at Interregional Seminar of UNO on New Methods for Mineral Exploration with Emphasis on Geophysical Techniques. Moscow, U.S.S.R. July 1967, p. 40.

Madden, T.R., *et al.,* 1957. Background effects in the induced polarization method of geophysical exploration. *A.E.C. Report,* R.M.E. 3150.

Marshall, D.J., and T.R. Madden, 1959. Induced polarization, a study of its causes. *Geophysics.* 34: 790-816.

Schlumberger, C., 1920. *Étude sur la Prospection Électrique du Sous Sol.* Paris, Gauthier-Villars et Cie. Chapter 8 (Revised 1930).

Seigel, H.O., 1948. Theoretical treatment of selected topics in electromagnetic prospecting. – National Research Council of Canada, unpublished, pp. 34-53.

1949. Theoretical and experimental investigations into the application of the phenomenon of overvoltage to geophysical prospecting. Unpublished doctoral dissertation, University of Toronto.

1959. Mathematical formulation and type curves for induced polarization. *Geophysics.* 24: 547-563.

Sunde, E.G., 1949. *Earth Conduction Effects in Transmission Systems.* N.W., Van Nostrand Co. (Monograph).

Vacquier, V., *et al.,* 1957. Prospecting for groundwater by induced electrical polarization. *Geophysics.* 22: 660-687.

Wagg, D.M., and H.O. Seigel, 1963. Induced polarization in drill holes. *Can. Min. J.,* April.

Wait, J.R. (Editor), 1959. *Overvoltage Research and Geophysical Applications.* London, Pergamon Press.

The importance of induced polarization method for the exploration of ore deposits

V.A. Komarov

Union Inst. of Expl. Techniques
Leningrad, U.S.S.R.

Abstract. Interest in the induced polarization method has been rising steadily since 1951. It appears that this technique may be successfully employed for the detection and discovery of a rather large variety of minerals. A number of field examples are used to demonstrate the facility with which the experimental data may be interpreted during the course of the operation.

Résumé. La polarisation provoquée est actuellement une des meilleures méthodes de prospection pour la recherche d'une grande variété de minerais. Les mesures sur le terrain ne présentent aucune difficulté. Les résultats peuvent être facilement interprétés au cours des mesures comme le montrent les exemples ci-joints.

The induced polarization of rocks and ores has been investigated since the 1930s but it was only after World War II that this method found practical application in the search for ore minerals.

The growing interest in induced polarization may be judged by the increasing number of published papers. Prior to 1951 only six papers dealing with this subject were published. From 1951 to 1955 nine papers and from 1956 to 1960 some 38 papers were published, whereas from 1961 to 1965 the number exceeded a hundred. From year to year not only has the general quantity of papers published on induced polarization been increasing but also the quantity dealing with this method in the search for ore minerals. Ninety percent of the total number of papers on induced polarization have been published in the last five years.

The geological problems which may be solved by the induced polarization method are determined above all by the high sensitivity of the method to the dissemination of electronic-conducting minerals in rocks. Among the electronic-conducting minerals are argentite, arsenopyrite, bornite, wurtzite, galena, graphite and coal (amorphous carbon), ilmenite, covellite, magnetite, marcasite, nicolite, pentlandite, pyrite, titano-magnetite, chalcocite, chalcopyrite, native metals and other minerals.

The polarizability of rocks which do not contain electronic-conducting minerals generally does not exceed 2%, as is shown by a great number of laboratory and field investigations. The presence of a small dissemination of electronic-conducting minerals in rocks results in a higher polarizability. Numerical values of polarizability have been obtained from measurements made 0.5 second after a 3-minute charging. The polarizability of ore-bearing rocks quite often amounts to more than ten per cent, which is much higher than the upper limit of the polarizability of 'barren rocks'.

The quantitative relation between polarization and the ore content of minerals may be estimated from the results of laboratory investigations on samples of disseminated ores. Figure 1 shows data concerning the relation of the polarizability and the volume content of sulphides (pyrite and chalcopyrite) for massive samples of chalcopyrite ores from a Caucasian deposit.

The content of sulphides (pyrite and chalcopyrite) was determined by chemical analysis of the samples (for sulphur, iron, copper). The measurement of the polarizability and the chemical analysis were carried out on different samples within the same borehole interval. Therefore these investigations show statistically the most probable relationship of polarizability and sulphide concentration in rocks.

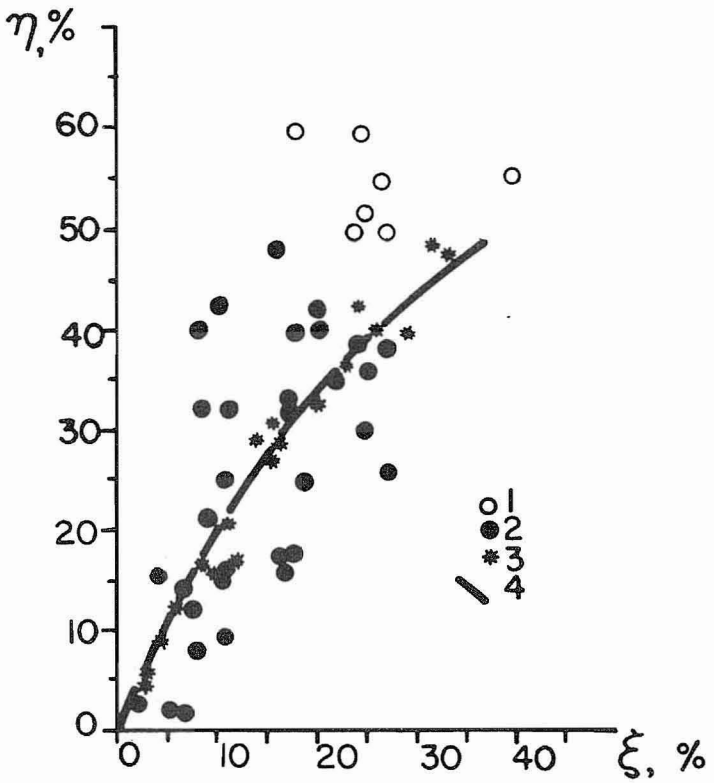


Figure 1. Relationship of polarizability of ore samples and the sulphide content. 1. Breccia ores. 2. Disseminated ores. 3. Mixture of quartz-sands and sulphide particles. 4. Theoretical graphs for $\beta = 2{,}6$.

In Figure 1 a distinct trend towards the increase of the polarizability with the increase of sulphide concentration is obvious.

Samples prepared of a mixture of quartz sand and sulphide particles display a similar behaviour in polarizability.

Table I. Commercial types of deposits.

Types of Deposits	Ore Minerals	Regions with IP Applications
Iron		
Sedimentary marine and lake deposits	Limonite, rarely siderite and iron chlorite	–
Metamorphic (ferruginous quarzite) deposits	*Magnetite,* hematite and martite	–
Skarn deposits	*Magnetite,* some amount of sulphides	West Siberia Caucasus
Magmatic (titanomagnetite) deposits	*Magnetite, ilmenite*	–
Hydrothermal deposits	Siderite, limonite	–
Weathering crust deposits	Limonite	–
Manganese		
Sedimentary marine and lake deposits	*Oxides,* hydroxides and *manganese carbonates*	–
Weathering crust deposits	Hydroxides of manganese	–
Hydrothermal deposits	Rhodochrosite, rhodonite, a small amount of *sulphides*	–
Metamorphic deposits	*Oxides, manganese silicates*	–
Chrome		
Hysteromagmatic deposits	Chrome-spinellides, chromic chlorites; a small amount of *magnetite, ilmenite* and *copper-nickel sulphides*	Caucasus
Early magmatic deposits		
BASE METALS		
Aluminum		
Sedimentary geosyncline marine deposits	Bauxites	–
Sedimentary platform, old lake and old river deposits	Bauxites	–
Weathering crust deposits	Bauxites	–
Copper		
Hydrothermal sheet deposits of disseminated ores (copper sandstones)	*Bornite, chalcopyrite, chalcocite*	Central Kazakhstan
Hydrothermal streaky impregnated deposits (porphyry-copper deposits)	In original ores: *chalcopyrite, pyrite;* sometimes *molybdenite*	Uzbekistan, Caucasus, Kazakhstan
Hydrothermal pyrite deposits	*Pyrite, chalcopyrite,* sphalerite	The Urals, Altai, Kazakhstan, Caucasus
Hydrothermal lode deposits	*Chalcopyrite, chalcocite, pyrite*	Caucasus
Copper-nickel magmatite liquation deposits	*Pyrrhotite, chalcopyrite, pentlandite*	The Kola Peninsula, Norilsk
Lead and Zinc (polymetals)		
Hydrothermal metasomatic deposits in tuff-effusive rocks	*Galena,* sphalerite, *pyrite, chalcopyrite,* sometimes arsenopyrite, bismuthine, *grey copper ores,* tellurium minerals	Altai, Kazakhstan
Hydrothermal metasomatic deposits in carbonate rocks:		
skarn deposits	*Sulphides of lead,* zinc, *iron,* sometimes *arsenic,* bismuth and others	Middle Asia, Kazakhstan, Far East, Caucasus
skarnless deposits	*Sulphides of lead,* zinc, *iron* and others	Middle Asia, Kazakhstan, Far East, Caucasus
Hydrothermal sheet bodies of disseminated ores in carbonate rocks	*Pyrite, galena,* sphalerite, sometimes *chalcopyrite*	South Kazakhstan, Middle Asia
Hydrothermal lode deposits	*Galena,* sphalerite, *pyrite* and others	Caucasus
Nickel		
Nickel and copper magmatic deposits	*Pyrrhotite, chalcopyrite, pentlandite*	The Kola Peninsula, Norilsk, Voronezh
Weathering crust deposits	Silicates of nickel	The South Urals
Hydrothermal lode deposits	*Sulphides* and *sulphoarsenites* of *nickel* and *cobalt* in association with *sulphides* of arsenic, *copper,* bismuth and others	–
Antimony		
Hydrothermal sheet deposits	Antimonite, sometimes pyrite, arsenopyrite, galena and others	–
Hydrothermal lode deposits	Antimonite, sometimes *pyrite, arsenopyrite, galena* and others	Middle Asia
RARE METALS		
Tin		
Placer deposits	Cassiterite	–
Hydrothermal deposits with cassiterite and sulphides	Cassiterite, *teallite, stannite, arsenopyrite, pyrrhotite*	Far East
Hydrothermal quartz-cassiterite deposits	Cassiterite, sometimes *arsenopyrite, molybdenite* and others	
Pegmatite deposits	Cassiterite	
Tungsten		
Skarn scheelite deposits	Scheelite, wolframite, *pyrrhotite,* sphalerite, *chalcopyrite, pyrite* and others	Kazakhstan
Scheelite deposits of stockworks	Scheelite, wolframite, *pyrite* and others	Kazakhstan
Hydrothermal lode deposits	Wolframite, scheelite, cassiterite, *molybdenite, arsenopyrite,* pyrrhotite and others	Kazakhstan, Altai
Placer deposits	Wolframite, cassiterite	–

Contents

Table I. Commercial types of deposits. (Concl.)

Types of Deposits	Ore Minerals	Regions with I P Applications	Types of Deposits	Ore Minerals	Regions with IP Applications
Molybdenum			**PRECIOUS METALS**		
			Gold		
Hydrothermal streaky impregnated deposits	*Molybdenite, pyrite,* chalcopyrite	Kazakhstan	Hydrothermal gold-quartz veins	*Gold, arsenopyrite, pyrite, pyrrhotite, chalcopyrite,* etc.	–
Skarn deposits	*Molybdenite,* scheelite, sulphides of iron and another	Caucasus, Kazakhstan	Hydrothermal gold-pyrite deposits	Auriferous sulphides	Urals, Altai, Kazakhstan, Middle Asia,
Hydrothermal lode deposits	*Molybdenite,* wolframite, cassiterite, *arsenopyrite* and another	Altai, Kazakhstan	Hydrothermal metasomatic zones of altered rocks containing gold	Gold, sulphides	Altai
			Placers	*Gold*	–
Cobalt			Metamorphosed auriferous conglomerates	*Gold, pyrite, magnetite*	–
Cobalt is extracted out of copper-nickel and polymetallic ores and other ores	*Pentlandite, pyrite, cobalt glance, arsenopyrite, glaucodite, magnetite, chalcopyrite,* and others	South Siberia, Middle Asia	Hydrothermal auriargenti, ferrous and telluric deposits	*Pyrite, chalcopyrite,* galena, sphalerite, etc.	–
			Platinum		
			Magmatic copper-nickel deposits containing platinum	*Sperrylite, platinum, pyrrhotite, pentlandite, chalcopyrite*	–
Mercury					
Hydrothermal sheet deposits	Cinnabar, *pyrite,* sometimes *metacinnabarite* and *mercury*	Middle Asia	Magmatic chromespinelid deposits containing platinum	Polyxene, *platinum,* chromite, titanomagnetite	–
Hydrothermal vein deposits	Cinnabar, *pyrite, marcasite*	–	Placers	Platinum, chromite, occasionally titanomagnetite	–
Hydrothermal lens-shaped deposits	Cinnabar, sulphides of iron and others	Carpathian Mountains			

Using some simplifying assumptions discussed in an earlier paper (Komarov, *et al.*, 1966) the dependence of the degree of polarizability of rocks η due to sulphides on the concentration of sulphide can be determined from Equation 1:

$$\eta = \frac{\beta \xi}{1 + \beta \xi} \qquad 1a$$

where β depends on the composition and structure of the dissemination, as well as on the times of charging and discharging corresponding to the moment of induced polarization measurement, and ξ is the volumetric concentration of the electronic-conducting minerals. In the experiments the effect of surface polarization rather than volume polarization was measured.

Using the experimental data shown in Figure 1 for each of the 33 samples of disseminated ore (seven samples of brecciated ore are not taken into account) the value of β was calculated from the equation

$$\beta = \frac{\eta}{(1-\eta)\,\xi} \qquad 1b$$

It was found that for eighteen samples, that is 58 per cent of cases, the value of β was from 1 to 3, that being its most probable variation limits. The average value of β for all the samples was equal to 2.6. The numerical values of η correspond to measurements made 0.5 second after the 3-minute discharge. In Figure 1 a calculated curve corresponding to this average value is represented.

Similar investigations were made on samples taken from different deposits. The average value of β proved to be 2.5 for the Urals chalcopyrite deposit and from 1.45 to 4.5 for some Tadjic polymetallic deposits.

In accordance with the data cited, marked IP anomalies caused by sulphide dissemination amounting to several per cent of total rock volume may be expected under favourable conditions.

Table I shows in what degree the electronic-conducting minerals are characteristic for various ores. The principal types of commercial deposits are listed. The table is composed according to the classification of ore deposits made by academician V.I. Smirnov (1957). In the list of ore minerals the electronic-conducting minerals are italicized.

At copper, polymetallic, nickel and rare-metal deposits as well as gold and other deposits, the electronic-conducting minerals are either the minerals sought for or accessory minerals. The application of the induced polarization method at such deposits gives satisfactory results.

In prospecting for base metals the IP method has become a leading one in the geophysical complex. This method makes possible the discovery of ore deposits buried at a depth of 100 to 200 metres and the discovery of orebodies unrevealed by other methods. Case histories of such discoveries are described in a collection of papers (Komarov, 1964) and in articles published in the bulletin *Razvedka nedr* (Volkov and Sirotakina, 1963; Gar'kovez and Khvalovsky, 1963; Markushin, 1964; Mustafabeily, *et al.*, 1966; Shapovalov, 1961).

In the case of deposits of rare and precious metals geophysical methods are mainly used in conjunction with geological mapping.

Direct detection of such ores by geophysical methods is a difficult task because of the low concentration of ore minerals. But where the desired minerals are associated with pyrite, pyrrhotite and arsenopyrite and when the volume concentration of the latter amounts to at least a few per cent, the IP method can be a good means of revealing mineralized zones including those covered by alluvium or barren host rocks. Good induced polarization results were reported at the rare-metal deposits of Kazakhstan (Morozov, 1965) and the gold deposits of Altai and Middle Asia (Zerman and Ovechkin, 1966; Bogdanov, *et al.*, 1967).

In iron-ore deposits the IP method has not yet found wide application because magnetite deposits are successfully revealed by a magnetic method and limonites are not electronic conductors. Nevertheless in some cases the IP method can be a helpful additional tool in magnetic surveys for estimating the depth and delineating magnetite deposits which occur among basic and ultrabasic rocks having a high magnetic susceptibility. The application of the IP method for this purpose in the Caucasus proved to be successful (Khessin and Novikova, 1966).

Chromite is not characterized by high polarizability, but in some cases the orebodies contain significant amounts of magnetite and the IP method becomes a convenient tool for the search of deposits, especially in regions of complicated and rough topography where the interpretation of gravity results is rendered difficult.

The application of the IP method in prospecting and exploration for manganese (pyrolusite) deposits also looks promising but experience in this field is still scanty.

In addition to ore deposits, the IP method can be used in prospecting for graphite, coal and other deposits containing electronic-conducting minerals.

Since the IP method responds even to a poor impregnation of ore minerals it is quite natural to use it for the location and delineation of wide zones of disseminated sulphide mineralization amounting to the size of ore fields.

In this case relatively small-scale surveys are being made, notably 1:100,000, 1:50,000 and 1:25,000, for the location and delineation of extensive zones of mineralization (ore districts and large ore zones) and in the search for ore deposits. 1:10,000 and 1:5,000 surveys are carried out for a detailed study of mineralized zones to reveal localities of high concentration of electronic-conducting minerals as well as for location and delineation of orebodies.

In recent years great significance and general recognition have been won by borehole IP measurements, which provide an effective means in the search for deepseated deposits, hidden under thick overburden and inaccessible to direct detection from the earth's surface.

The economic effectiveness of the IP method is mainly determined by its high reliability in detecting electronic-conducting minerals. With very rare exceptions, extremely deepseated and comparatively small sulphide deposits are reliably located by the IP method. In some areas of the Altai and Urals experimental work over known deposits has shown all of them to be marked by IP anomalies. Under the same conditions resistivity anomalies have been detected only over half of the deposits, and anomalies of the natural electric field, only over two thirds of the deposits.

The probability of missing a deposit in an areal IP survey is very small. Consequently, only areas marked by IP anomalies may be chosen as promising for sulphide mineralization, thus defining the priority in further exploration. As a rule it is not advisable to drill exploratory boreholes outside the IP anomalies. An example of how the IP method can reduce the areas which have previously been considered as promising can be illustrated by examples of the surveys carried out in the Urals and Altai. Here anomalous IP zones on the average occupy one tenth of the total area that had been recommended on a geological basis.

It should be noted that not every IP anomaly is associated with commercial orebodies. More frequent are zones of poor sulphide mineralization, and in some areas even graphitic rocks. According to the statistical data obtained by an expedition working in the South Urals, of the drilled IP anomalies, only one fourth proved to be associated with commercial ores. If one considers the fact that only one third of the IP anomalies discovered in the area of 500 sq km had been recommended for drilling it means that commercial ores were found in one out of the twelve anomalies. Still the value of the discovered orebodies covered the cost of the geophysical work hundreds of times.

The present state of theoretical development of the IP method is much the same as that of electrical prospecting methods, including methods long in use, such as the resistivity method and the self-potential method.

The apparatus designed and constructed for putting the IP method into practice and the field work procedures and methods of interpretation of data are fairly simple and can be used by personnel with ordinary technical training.

The geological effectiveness of the IP method as well as of other methods is determined by the quantity and quality of information derived from field measurements. Unfortunately the possibilities offered by the IP method are not utilized to their full advantage. The estimation of IP anomalies is sometimes exclusively based on the values of the apparent polarizability, wher t is advisable to interpret IP anomalies in terms of size, shape, depth and polarizability of the body causing the anomaly.

The quantitative interpretation of IP data may be easily made in the course of field work without the complicated laboratory processing of measurement data.

Quantitative information about the body greatly facilitates the evaluation of its geological significance and ultimately increases the effectiveness of geological exploration.

The most suitable for exploration is a gradient array with large spacing between the current electrodes, and measurements made along a profile, both between the electrodes and beyond them, as long as the ΔU_{IP} values are large enough to be reliably measured. Detailed exploration of the anomalies obtained and estimation of the depth of orebodies producing them can be performed with the same array but with a different position of the current electrodes. If the anomaly is first observed in the midsection between the current electrodes, repeat measurements are made with one of the current electrodes located in the centre of the revealed anomaly. With a stationary position of current electrodes, measurements are made over an area ranging from 0.1 to 2 sq km, depending on the current electrode spacing. The districts surveyed by the IP method usually have an area of tens of square kilometres and to explore them successively the current electrodes are moved from place to place.

Contents

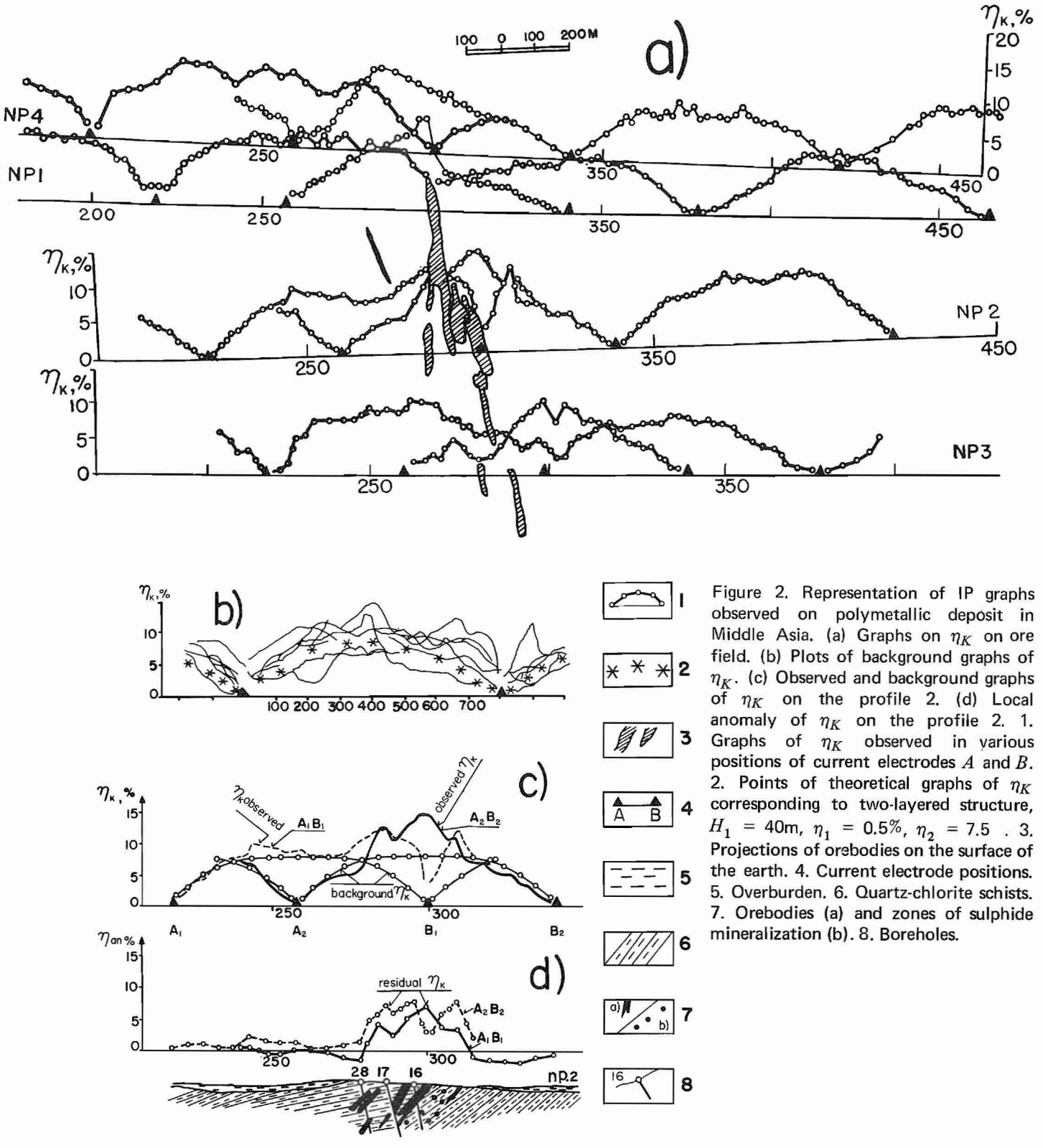


Figure 2. Representation of IP graphs observed on polymetallic deposit in Middle Asia. (a) Graphs on η_K on ore field. (b) Plots of background graphs of η_K. (c) Observed and background graphs of η_K on the profile 2. (d) Local anomaly of η_K on the profile 2. 1. Graphs of η_K observed in various positions of current electrodes A and B. 2. Points of theoretical graphs of η_K corresponding to two-layered structure, H_1 = 40m, η_1 = 0.5%, η_2 = 7.5 . 3. Projections of orebodies on the surface of the earth. 4. Current electrode positions. 5. Overburden. 6. Quartz-chlorite schists. 7. Orebodies (a) and zones of sulphide mineralization (b). 8. Boreholes.

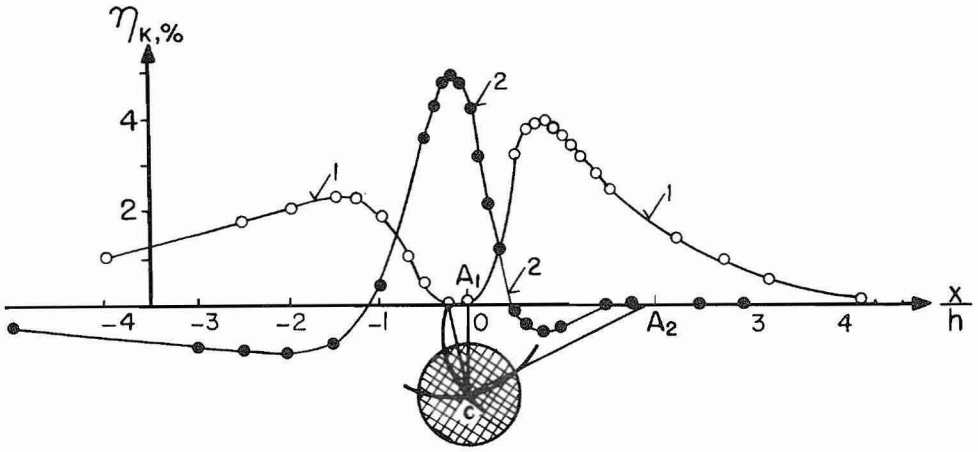


Figure 3. Theoretical curves of η_K anomalies for different configurations of the current electrode with respect to a spherical body. 1. Curve corresponding to position A_1. 2. Curve corresponding to position A_2 (the second current electrode is at 'infinity') $\eta_{excess} = 60\%$.

As a result, a considerable number of curves of the apparent polarizability is obtained for each area corresponding to different positions of current electrodes. Similarities in the curves are due to geological features in the district which can be approximated by a horizontally layered geological section, whereas the strongly marked deviations in the shape of some curves of apparent polarizability from the average curve may be considered an indication of a local anomaly in IP caused by a body of relatively smaller size but very strong polarizability.

Curves of the apparent polarizability obtained within an extensive zone of pyritized rocks are shown in Figure 2. A feature common to both curves is the decrease of apparent polarizability in the vicinity of the current electrodes, which is explained by a decrease of the polarization of rocks at the surface of the earth. This occurs because the polarizability of the overburden 20 to 40 metres thick is less than that of the bedrock and also because the sulphide content of rocks is smaller than at great depth, because of decomposition and weathering. The two-layer η_{ap} curve corresponding to a vertical distribution of polarizability reflects the general geological structure of the district and may be used for the evaluation of the thickness and the polarizability of the upper and lower layers of rocks. The polarizability of the bedrock usually increases as the site of ore formation is being reached and this may serve as a prospecting indication. On the other hand the difference between each observed curve and the above mentioned two-layer curve is a local IP anomaly. The form of η_{ap} curves will depend largely on the position of the current electrode with respect to the centre of the body.

Having curves for several positions of current electrodes, it is possible to evaluate the principal parameters of buried bodies.

According to our theoretical computations, in case of a single current electrode (the second electrode is assumed to be at 'infinity') the distance from the electrode to the anomaly produced by an isometric spherical body is approximately equal to the distance from the electrode to the centre of the body. In particular, if the current electrode is located over the body, the anomaly can be detected in any direction from the electrode at a distance equal to the depth of the centre of the body (Figure 3).

The centre of a body having an isometric shape in a uniform earth may be located by the intersection of the arcs of the circles drawn from two positions of the current electrode (the second current electrode is assumed to be located far away from the body) with a radius equal to the distance from the electrodes to its associated η_{ap} maxima (Figure 4). In case of elongated bodies the arcs intersect beneath the centre of the body if it is horizontal or gently dipping and above the centre of the body if it is steeply dipping. The effect of a highly conductive alluvium overlying the body always results in greater depths than the real ones.

Estimation of depth of horizontal dike-shaped bodies may be performed with the help of vertical sounding reference curves. Reference curves for apparent resistivity may be used as well as those for apparent polarizability. The method of using reference curves for apparent resistivity in the interpretation of the apparent polarizability curves is described by Yaroslavzev (1965).

It is difficult to prepare reference curves for bodies having a complicated shape. In this case it is convenient to apply a method based on the analysis of the extremal η_{ap} values and the position of bends on the η_{ap} curves. Experience with field measurements shows that the depth of the upper boundary of the body is approximately equal to the AO* spacing which produced a bend (changing of the curvature sign) on the η_{ap} curve (Figure 4). This method is used for the interpretation of the curves of ordinary four-electrode sounding and for η_{ap} curves obtained from measurements with a gradient array conducted near the current electrode, located above the body surveyed.

For estimating the horizontal dimensions of 'local' bodies it is convenient to use simple geometries corresponding to the position of the body in the middle of AB line. Along the profile passing over the body, the projection of the body onto the profile is marked by flexure points. But if the body width is greater than its depth, it may be considered equal to the width of the IP anomaly. Such an interpretation of η_{ap} curves is correct only for the profiles passing over the body and across its boundaries to be delineated. If the profile runs outside the body but near its boundaries, the anomaly is present though of course it attenuates with distance from the body.

To determine the dip of the body located in the central portion of the AB line it is advisable to use a method based on the fact that the η_{ap} curve is asymmetrical over the inclined body: a deeper valley and a steep rise in the η_{ap} curve are observed on the side of the bottom wall of the body, and the η_{ap} maximum is displaced from the top 'face' of the body in the direction of its

*AO is the distance between the current electrode and the centre of the receiving line.

Contents

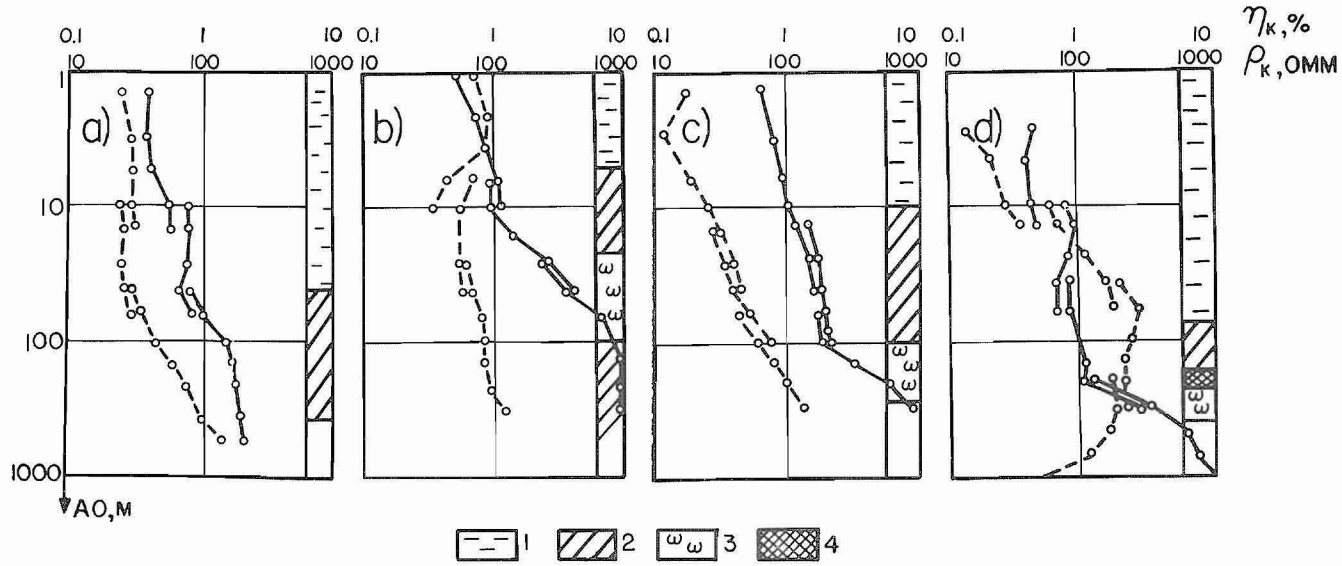
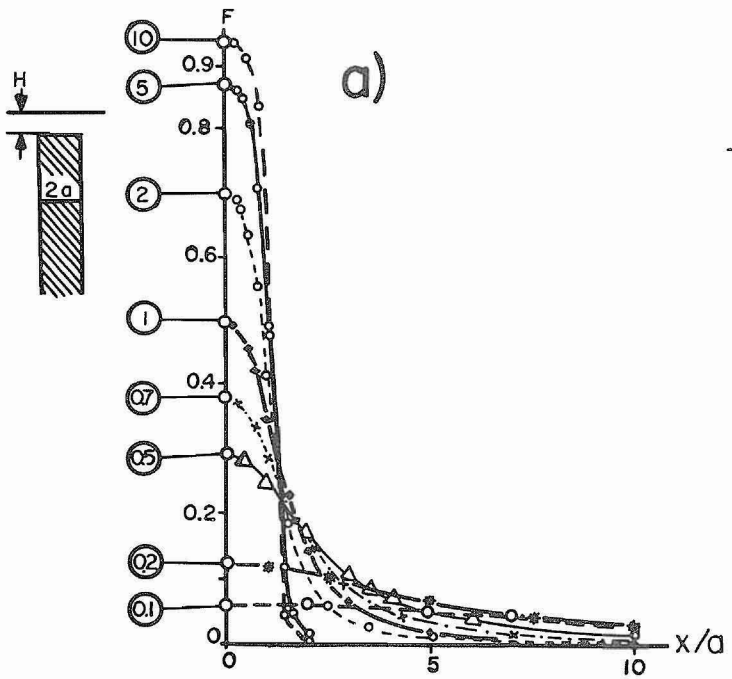
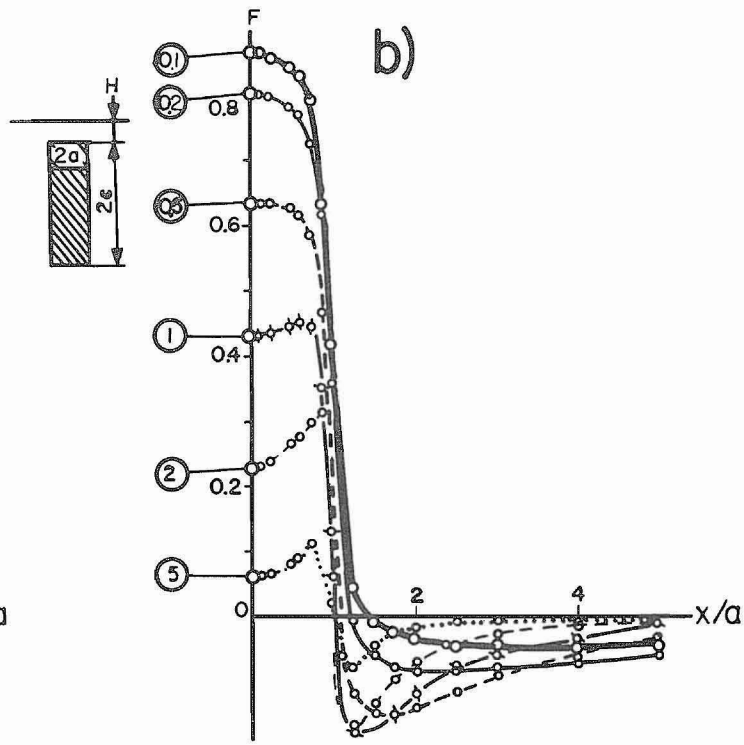


Figure 4. η_K curves (solid line) and ρ_K curves (dotted line) of vertical sounding in a barren area in the Altai (a), over impregnated copper pyrite ores in the trans-Caucasus (b) and in the Urals (c) and over copper-nickel ores in Norilsk (d). 1. Overburden. 2. Barren rocks. 3. Impregnated sulphide ores. 4. Veinlet-impregnated sulphide ores.

Figure 5. Theoretical graphs of anomaly η_K over vertical bed unlimited in the strike direction. (a) Unlimited strike of the orebody in the dipping direction, having various depths of the upper border-line of the orebody (H); numbers in circles indicate ratio of the horizontal half-thickness of the layer to its depth. (b) Constant depth of upper borderline of the orebody ($H = 0.1a$) and various strikes of orebody toward its dip; numbers in circles indicate value of $\frac{a}{H \times 2c}$, the ratio of horizontal half-thickness to the lower borderline of the orebody.





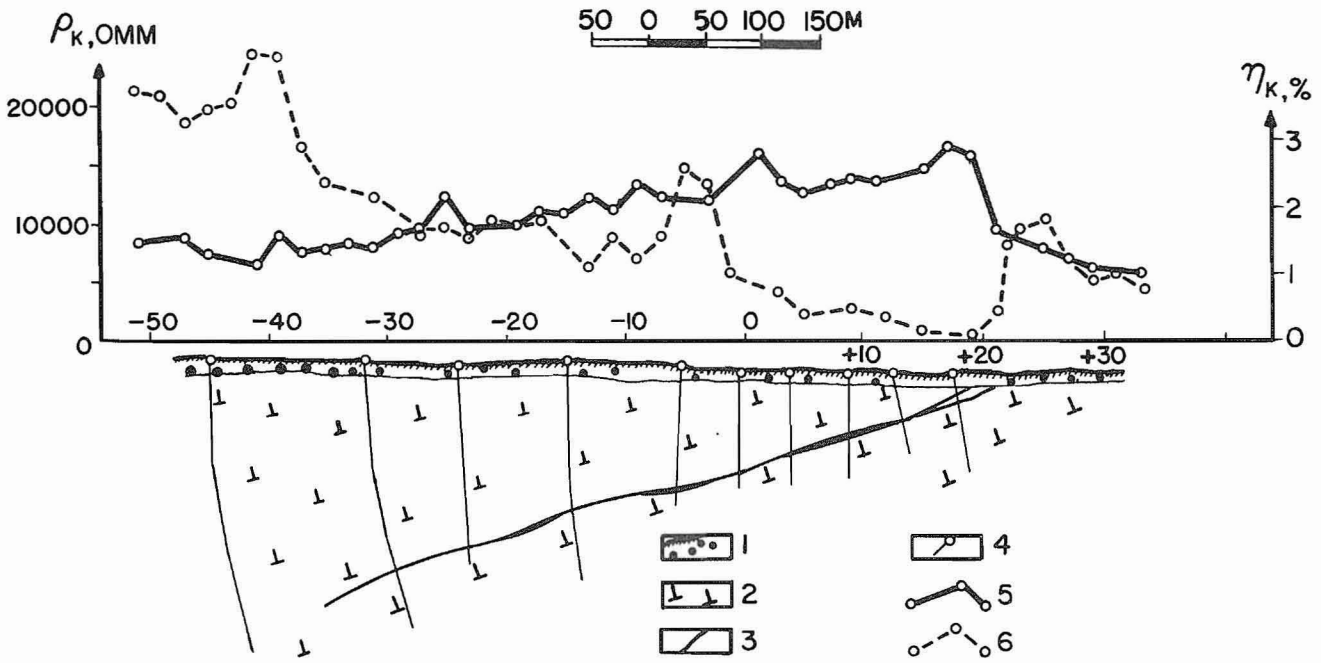
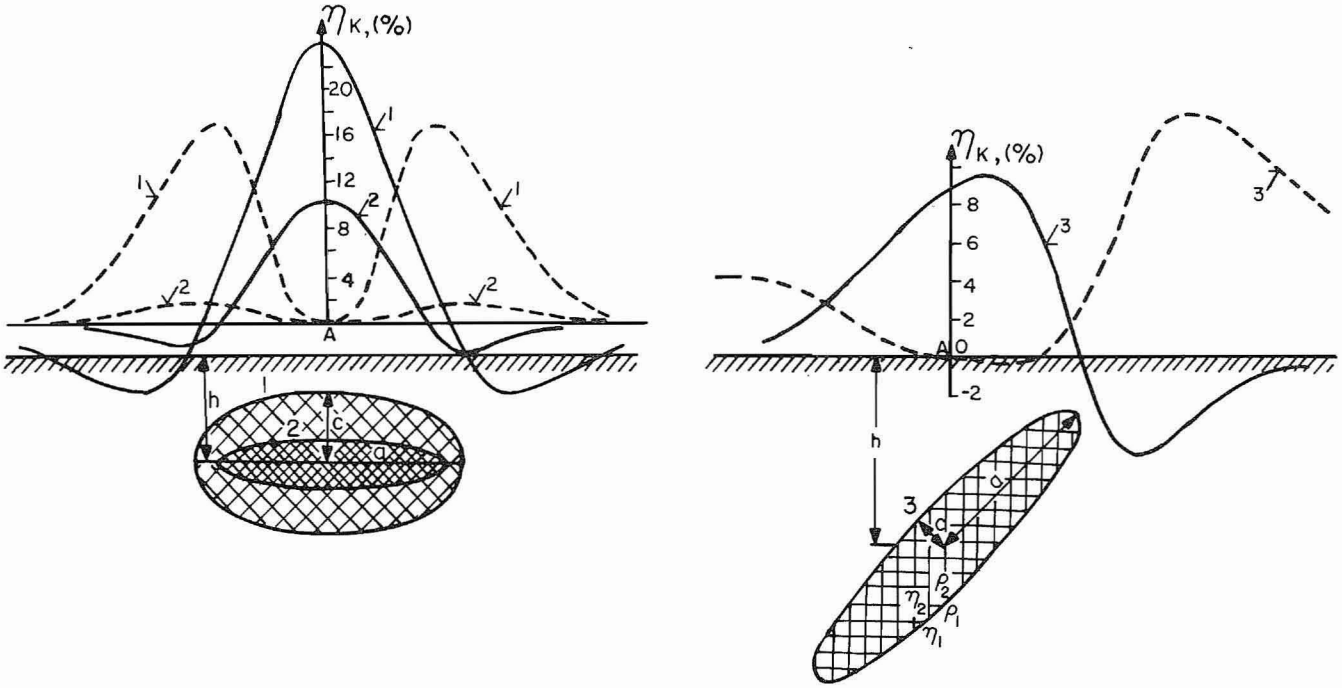


Figure 6. η_K and ρ_K curves along the profiles over a copper-nickel deposit. 1. Glacial deposits. 2. Granites, migmatites, amphibolites. 3. Sulphide ores. 4. Boreholes. 5. η_K curve from measurements with inverse-polarity charging equal to 10 seconds. 6. ρ_K curve.

Figure 7. Theoretical curves of η_K anomalies over ellipsoidal bodies located between current electrodes (solid lines) and under one current electrode (dotted line) $\eta_{excess} = 40\%$. 1. Horizontal ellipsoid, $a/c = 5$, $h = 4.5\ c$. 2. Horizontal ellipsoid, $a/c = 2$, $h = 1.5\ c$. 3. Inclined ellipsoid, $a/c = 5$, $h = 5\ c$.



Contents

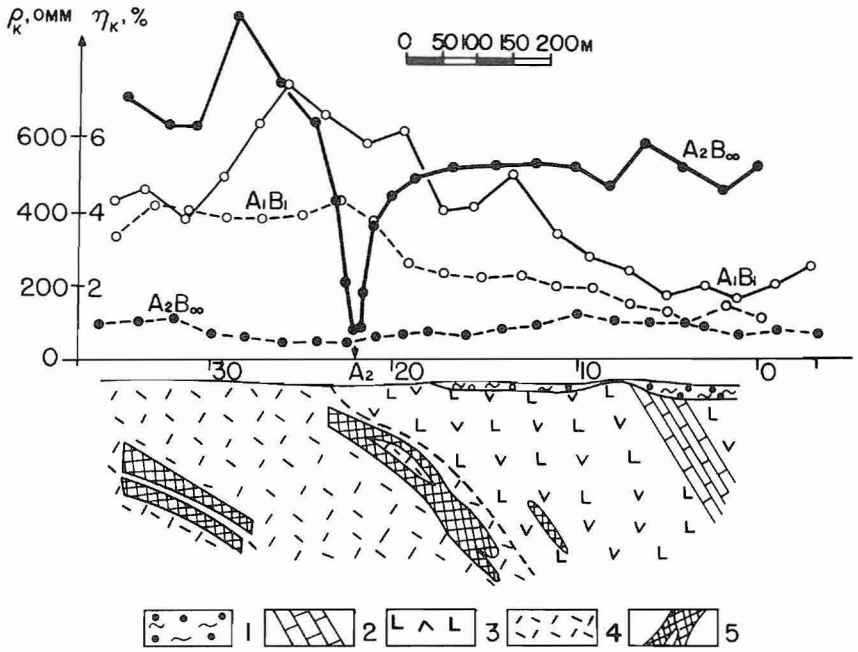


Figure 8. Field curves of η_K (solid line) and ρ_K (dotted line) along a profile over a copper-pyrite deposit for a different arrangement of the current electrodes. A_1 at point +50, B_1 at point −10. 1. Overburden. 2. Limestones. 3. Effusive rocks and tuffs of medium and basic compositions. 4. Orebearing pyritized albitophyres and their tuffs. 5. Copper-pyrite ores.

dip (Figures 3 and 4). Still more reliable is a technique obtaining the dip of the body from curves obtained with the current electrode located above the body. In this case a greater η_{ap} maximum is found at the side of the bottom wall of the body, and a smaller maximum at the side over the back of the body, the second one being more gentle and slowly fading out (Figures 6 and 7). The ratio of the magnitudes of the maxima may serve as some measure of the body's inclination. The nearer the dip of the orebody to 45°, the greater will be the ratio.

To estimate the polarizability of the body, the shape and depth of which are assumed to be known, one can use the equation

$$\eta_{excess} = \eta_{an} \left(\frac{h}{a}\right)^n \qquad 2$$

which shows a relation of the excess polarizability of the body η_{excess} with the depth of its centre h, the radius a, and shape factor n, if it is assumed that the enclosing earth is uniform, the body has the same resistivity and is located in the middle of the line connecting the current electrodes. The shape factor index in Equation 2 depends upon the shape of the body: for a two-layer earth n=0, for a horizontal layer n=1, for a horizontal circular cylinder n=2, for a sphere n=3.

The anomalous apparent polarizability, η_{an}, in Equation 2 corresponds to a spacing $AB \gg h$ for a two-layer earth, cylinder and sphere. Over a horizontal layer the η_{an} maximum is observed with an AB spacing which is equal to the depth of the centre of the layer if the layer is thick and which exceeds the depth to the centre of the layer if the layer is thin.

The estimation of the polarizability of a steeply dipping dike-shaped body can be made by means of the equation

$$\eta_{excess} \approx \eta_{an} \frac{\pi}{\alpha} = \eta_{an} \frac{180^\circ}{\alpha} \qquad 3$$

where α is the angle between the rays drawn from the point of measurement above the centre of the dike to its top. If the resistivity of the dike is lower than that of the enclosing earth, the value of the excess polarizability of the dike computed from Equation 3 will be an underestimate.

Knowing the excess polarizability of the body and assuming for convenience that the enclosing rocks do not contain electronic-conducting minerals, one can estimate the volumetric concentration of electronic conducting minerals in the body from the equation

$$\xi = \frac{\eta_{excess}}{2.6\ (1-\eta_{excess})} \qquad 4$$

which corresponds to Equation 1b, if β=2.6*.

If the dimensions and concentration of electronic-conducting minerals in the body have been determined, it is obviously not difficult to compute the total content of minerals. In cases where the total content of electronic-conducting minerals may be related to the content of the metal sought, an approximate estimation of the reserves of this metal in the discovered body can be made. For example, in one area with a great number of copper deposits it was found that the content of pyrite and chalcopyrite in the bodies on the average amounted to the ratio 2:1. That means that out of 300,000 cubic metres of electronic-conducting minerals computed in the body, the body contains some 100,000 cubic metres of chalcopyrite, i.e., some 150,000 tons of copper, which was in good agreement with the geological survey data.

To complete the survey of methods for determination of ore parameters causing IP anomalies we must consider an example of the sequence of interpretation (Figure 9). At first the η_{ap} anomaly was at the centre of the AB line; then one current electrode was placed at the centre of the revealed anomaly.

*The value of β depends on the times of charging and discharging and hence on the regime of the polarizing current used in the equipment.

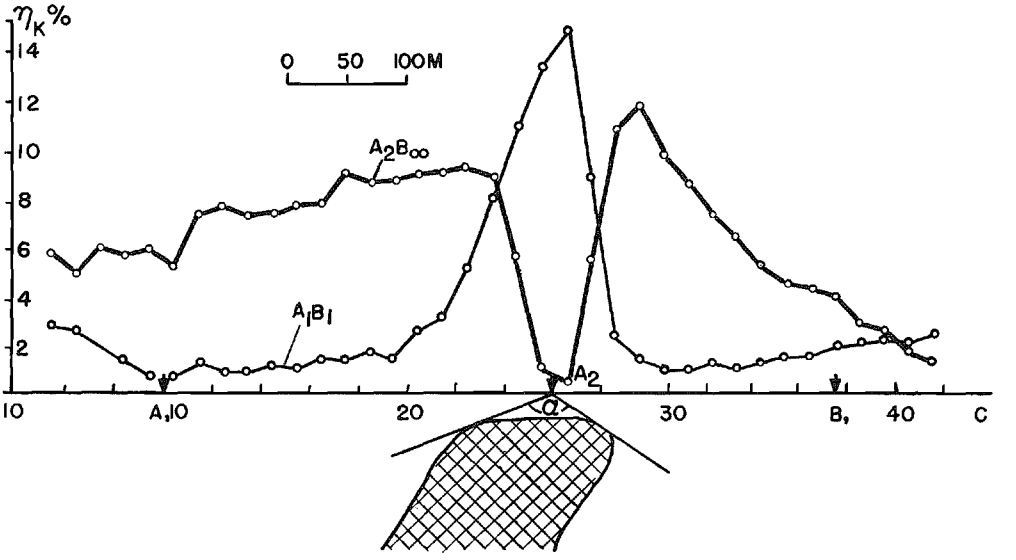


Figure 9. Field graphs of the η_K for two positions of current electrodes in relation to the source of IP anomaly. The orebody corresponding to the anomaly is indicated by striation.

From the asymmetrical shape of the first curve and the absence of sharply marked minima on the sides of the η_{ap} maximum, it is possible to establish that the body dips to the south (to the left in the plane of the drawing) and has a considerable depth. Judging by the width of the maximum, the projection of the 'head' of the body on the profile line is between observation points 23 and 28.

The maxima η_{ap} on both sides of the second curve are somewhat different in shape and intensity. The right hand η_{ap} maximum is more intense and disappears more rapidly than the left hand side maximum. This indicates that the body dips to the left and has considerable depth; in other words, the conclusion drawn from the first curve is corroborated. The bend in the left branch of the second curve takes place when $A_2O \approx 15\ m$ (equals approximately 15). Consequently the depth of the upper boundary of the body under observation point 26 is 15 metres.

Thus it has been established that the body has the shape of a dike dipping to the south, its horizontal thickness is about 100 metres and its depth 15 metres. This body is illustrated in Figure 9. The angle between the rays drawn from the point of the observed maximum on the first curve to the top of the dike constitutes 120° or 0.7 π. As the maximum is equal to 15% while the η background is 20%, the anomalous apparent polarizability is 13%.

Using Equation 3 we obtain η_{excess}=18%. Then from Equation 4 we estimate the concentration of electronic-conducting minerals in the body, which averages 8.5%. From the foregoing it follows that the body represents a weakly mineralized zone. The ultimate solution of the practical value of the revealed zone must take into account the geological surrounding and the results of other exploration methods.

The relation of IP to other methods is beyond the limits of this article. But it is necessary to note that the electronic-conducting minerals are equally well revealed by IP, but the differentiation of the mineral and chemical composition of rocks by the IP method still remains difficult.

It is considered rational to use IP in conjunction with geochemical prospecting methods for most districts.

References

Bogdanov, A.Sh., B.D. Borzov, G.G. Zhuravlev, and I.M. Zhigorlovsky, 1967. An application of electrical methods for prospecting in West Kolba. *Razvedka i Okhrana Nedr,* 1967, No. 8.

Gar'kovez, V.G., and A.G. Khvalovsky, 1963. New data on geophysical research of buried orebodies in the Almalyk region. *Razvedka i Okhrana Nedr,* 1963, No. 10.

Khessin, B.E., and O.V. Novikova, 1966. On some peculiarities of geophysical exploration used for searching gently dipping magnetite deposits. *Razvedka i Okhrana Nedr,* 1966, No. 12.

Komarov, V.A., 1957. On the nature of electrical fields of I.P. and the possibilities of their application for the search of ore deposits. *Vestnik* of Leningrad University, geological and geographical series, 1957, No. 6.

Komarov, V.A. (Ed.), 1964. Application of I.P. method for searching for ore deposits. *Sbornik statei,* Ed. 'Nedra', Moscow.

Komarov, V.A., A. Pishparevan, M.V. Semenov, and L.S. Khloponina, 1966. *The theoretical basis of I.P. data interpretation.* Ed. 'Nedra', Leningrad.

Komarov, V.A., and Yu.S. Ryss, 1959. Some results of the application of I.P. methods on polymetallic deposits of Rudniy Altai. *Razvedka i Okhrana Nedr,* 1959, No. 2.

Markushin, Ya.V., 1964. Effectivity of I.P. method in South Altai. *Razvedka i Okhrana Nedr,* 1964, No. 6.

Morozov, M.D. (Ed.), 1965. Geophysical prospecting in Kazakhstan. Sbornik statei, Ed. 'Kazakhstan', Alma-Ata.

Mustafabeily, M.A., B.E. Khassin, S.A. Muradkhanov, and V.V. Alekseev, 1964. Prospecting of copper-polymetallic deposits on the south slope of the Caucasus by geophysical methods. *Razvedka i Okhrana Nedr,* 1964, No. 9.

Revyakin, P.S., Yu,K. Anoshin, and V.D. Borzov, 1966. Application of geophysical methods for the search for polymetallic deposits in Rudniy Altai. *Razvedka i Okhrana Nedr,* 1966, No. 3.

Shapovalov, O.M., 1961. Application of I.P. method. *Razvedka i Okhrana Nedr,* 1961, No. 12.

Shkorbatov, S.S., 1963. Effectivity of I.P. in searching for copper-nickel deposits in the Kola Peninsula. *Razvedka i Okhrana Nedr,* 1963, No. 2.

Smirnov, V.I., 1957. *Geological basis in prospecting for ore deposits.* Ed. Moscow University.

Volkov, I.D., and T.N. Sirotkina, 1963. Application of geophysical methods for prospecting of ores in the Norilsk region. *Razvedka i Okhrana Nedr,* 1963, No. 2.

Yaroslavzev, A.M., 1965. Interpretation of I.P. vertical electrical soundings. *Razvedka i Okhrana Nedr,* 1965, No. 11.

Zerman, I.M., and V.V. Ovechkin, 1966. Effectivity of integral application of geologic-geophysical methods in searching for auriferous deposits in West Karamazar. *Soviet Geology,* 1966, No. 8.

Seismic methods in mining and groundwater exploration

George D. Hobson

Geological Survey of Canada
Ottawa, Canada

Abstract. Seismic methods have been applied to the solution of geological problems for many years while more recently these techniques have gained favour as a tool in the search for minerals and water. To date, the method has not been exploited extensively as an exploration device, except perhaps in Sweden. However many of the oil prospecting seismic techniques and equipment can be used with minor adaptation to the peculiar and particular problems associated with mineral and groundwater environments.

Compact portable seismographs are now available, most of which are used principally in the refraction mode while there are a few that can record reflected events. Most of these portable seismographs can be used with a hammer struck against a steel plate on the ground as a source of energy thus precluding the use of costly drill holes and explosives. Various types of repetitive sources of energy used in oil prospecting could also be used in mineral prospecting.

The various portable seismographs and their special adaptabilities or features, repetitive sources for land and marine seismic programs and some field techniques are presented for comparison and discussion. Some applications of shallow seismic techniques are set forth with a few typical field results from projects designed and conducted towards the search for minerals and water.

Résumé. Les méthodes séismiques ont été appliquées à la solution de problèmes d'ordre géologique depuis de nombreuses années, bien que récemment ces techniques aient gagné le faveur des spécialistes comme instrument de recherche des minéraux et de l'eau. Jusqu'ici, ces méthodes n'ont pas été utilisées à fond comme moyen d'exploration, sauf peut-être en Suède. Toutefois, une grande partie des techniques et de l'outillage propre à la prospection séismique du pétrole peut être utilisée avec des adaptations mineures aux problèmes spéciaux et propres aux milieux des minéraux et des eaux souterraines.

De petits séismographes de faible encombrement sont maintenant disponibles; la plupart sont utilisés pour l'enregistrement des ondes réfractées, bien que quelques séismographes puissent enregistrer les ondes réfléchies. La plupart de ces séismographes portatifs peuvent être utilisés à l'aide d'un marteau heurtant une plaque d'acier posée sur le sol servant de source d'énergie, éliminant ainsi l'usage de forages coûteux et d'explosifs. Divers types de sources d'énergie permettant la répétition des ondes et utilisées dans la prospection pétrolière pourraient aussi servir à la prospection minière.

L'auteur étudie et compare les divers séismographes portatifs, leurs caractéristiques et possibilités spéciales, les sources d'ondes répétées pour les programmes séismiques terrestres et marins de même que quelque techniques pratiques. Il mentionne ainsi que des résultats typiques obtenus à la suite de travaux conçus et exécutés pour la recherche de minéraux et d'eau.

"[The mining geophysicist] is not attracted to mining so much by an anticipation of great financial gains as by downright fascination and love for his subject.... He loves it because there is nothing simple, nothing monotonous about his geology; most every problem is different and a challenge to the imagination...." Dr. C.A. Heiland wrote these words in 1948 and they are as true today as when he wrote them. The petroleum geophysicist has long been set up on a higher pedestal than the mining geophysicist; this writer began his professional career as a petroleum geophysicist but the fascination and challenge presented by mining and groundwater geophysics has won him over to the latter fields. The mining geophysicist has a formidable array of factors lined up against him since geophysics has been used only to a limited degree in the solution of mining and groundwater problems. One cannot place the blame for this entirely upon the mining industry nor upon the geophysicist. On the one hand the mineral industry may once have lacked an understanding of the discipline and the problems of the geophysicists and also lacked the interest and initiative to use the tool. On the other hand the geophysicist has frequently been careless towards mining problems often backed up by a gross lack of geological training and imagination. The geophysicist in the past has been guilty of oversimplification of the problem and overselling his talents. In general the geophysicist has applied text book approaches to the solution of mining and groundwater problems with a fantastic lack of imagination. He has oversold his product and when the interpretation did not find a mine he merely shrugged his shoulders and moved on to another client. Fortunately for everyone concerned this attitude is changing – and changing very quickly.

The interpretation of geophysical data collected during surveys for minerals and groundwater is more difficult than that of data collected in the search for oil. This is due to the greater variety of rocks encountered and the greater complexity of structure. Mining geophysicists today are no less efficient than petroleum geophysicists. And the scope of geophysics in mining and groundwater problems is just as great as it is in the exploration for petroleum. It must be admitted, however, that the search for oil by geophysicists receives greater emphasis than the search for minerals.

There is one fundamental difference between prospecting for petroleum and for minerals and groundwater that both the geophysicist and geologist must appreciate. Petroleum is mainly restricted to sedimentary rocks that have undergone little metamorphism and the reservoir rocks are porous and permeable with a confining rock that is impermeable. Petroleum also normally occurs in structures wherein the largest dimensions are in the horizontal plane presenting a fairly large target for both geophysical methods and drilling. These petroleum structures are ordinarily much less complex than most ore-bearing structures. Most ore deposits in contrast have large vertical dimensions with relatively small horizontal extent. They present a small target and

methods of locating them must be precise. Petroleum reservoirs occur in a limited variety of rocks whereas ores occur in almost every common rock type. Rock structures, therefore, play a very important role in the localization of both petroleum and epigenetic mineral deposits. The difference is that whereas petroleum is generally localized in large-dimension elevated structures, almost every kind of known structure has at some place localized or helped to localize epigenetic minerals. Most epigenetic deposits have been localized by structure but to determine the exact structure responsible is often difficult or impossible. Therefore it is only realistic to admit the difficulties involved in solving the complexity of occurrence of many orebodies in rock structures. The application of geophysics to finding ore deposits would be much more successful if the deposition of those minerals were controlled by some simple structural relationship. Because of the complicated relations which do exist between structure and ore deposition, detailed geophysical surveys and detailed geological mapping must be undertaken complementary one to another.

The success of geophysics as a tool to prospect for ore deposits and groundwater may not rest so much with the geophysicist and his knowledge of geophysics per se but in his knowledge or lack thereof of geology. In the fields of mining and groundwater geophysics more intensive geological studies than we have been accustomed to make in the past would seem to be necessary as a proper basis for geophysical work. In these two fields the geologist and the geophysicist are always confronted with the one question, is the ore or water really confined only to one rock type? It cannot be overemphasized that the key to effective interpretation of geophysical data is a sound geological background. It is the writer's opinion that the qualifications for a geophysicist in the mining and groundwater fields are higher, or should be higher than in the exploration for petroleum reserves. He must have training and experience in physics, economic geology, mining techniques and problems, petrology, mineralogy, plus a high degree of imagination in matters geological. He must have an ability to evaluate the genetic evolution of a mineral deposit from the geophysical point of view. Men with such qualifications should be chosen to plan, direct and interpret the geophysical surveys undertaken in the exploration for ore and groundwater deposits. These men are not of the old classical school of geophysics but of the emerging breed of geophysicists who combine physical techniques with a broad geological background.

The burden of the long-range and fundamental studies of the Earth's crust and the application of various physical techniques to the measurement of anomalies within the crust must rest on the more substantial mining companies and on the various government agencies. As one of the government agencies it devolves upon the Geological Survey of Canada as part of its function to carry out experiments of a nature and scale which cannot be undertaken by most private concerns or universities but experiments which will contribute materially to the ultimate knowledge and specific usefulness of mining and groundwater geophysics.

Geophysical instruments that investigate the magnetic, electrical or gravitational characteristics of a prospective area have been used as exploration tools for many years to prospect for minerals. The seismic method has been applied only infrequently as a prospecting tool in the search for orebodies or to the solution of structural problems. It is a tool that has tremendous potential to assist the prospector and geologist to locate structures favourable to mineralization and to assist in answering structural problems. A little imagination and a good geological background are required to develop the novel approach to the solution of most mineral and groundwater problems. While bedrock depressions have been outlined by the seismic method on numerous occasions in the search for groundwater supplies and heavy mineral deposits, similar methods can be utilized to define structural problems associated with ore deposition.

It is not the intention of this paper to present seismic theory but rather to discuss instrumentation and techniques currently available for seismic refraction and reflection prospecting for minerals and groundwater. New and novel techniques have been developed and tried, some with reasonable success and others with mixed success. At this point it may be well to discuss the innovations in instrumentation available to the petroleum industry that may be adopted to the problems under discussion in this paper.

Today the geophysical industry is in the midst of revolutionary advances in its technology to meet the ever increasing complexities and demands of discovering new reserves be they petroleum, water or hard mineral. There have been recent major breakthroughs in highly sophisticated instrumentation for seismic data acquisition and processing as well as breakthroughs in interpretative techniques. Early emphasis has been placed upon proper analog instrumentation and procedures for data acquisition and presentation in the field and on interpretative talent as the controlling factors in the success of a seismic program. The advent of analog magnetic-tape data-recording and data-processing capabilities introduced the present trend in which the processing and analysis of data have replaced the former emphasis upon acquisition of those data. The present move to digital techniques is the latest in a long series of advances. Digital instrumentation provides higher resolution of the subsurface than has been possible with previous tools and methods. The recovery of very small signals which often lie below the noise level can most effectively be accomplished through digital methods and utilized by processing through a digital computer.

For mining and groundwater prospecting conventional oil-prospecting instrumentation is generally considered to be too costly and cumbersome to be practical in the field. However, there are problems in the mining field such as the exploration of sedimentary basins within the shield areas, in which conventional seismic instrumentation will definitely be required. Some projects will require field digital-recording instruments with the companion digital computer and an office playback system. This paper however will concentrate on the truly portable equipment and not the so-called portable conventional equipment where several bodies are required to move the instrumentation. Twelve and twenty-four trace instruments with all the refinements developed by the oil exploration industry can be very useful for shallow problems and these will be discussed throughout the paper but not in the detail with which the recently developed interval timers and truly portable refraction instruments will be discussed. Portability is the key word in instrumentation for mineral and groundwater prospecting.

Mining and groundwater problems can be solved cheaply, quickly and reliably without drilling except for occasional checks and standards. As has been mentioned above the conventional

oilfield prospecting equipment with its high cost, its nonportable bulk and weight and the necessity of explosives for energy, cannot be precluded from the solution of mining problems. However, let us now proceed with the discussion of equipment that has taken advantage of recent phenomenal advances in electronics with printed circuit boards and plug-in modules, highly portable and compact packages, instruments specifically designed for the solution of shallow problems. Repetitive sources for use on land and water will be discussed as they pertain to mineral and groundwater problems.

Shallow refraction methods and equipment

Principles of refraction theory. It is not the intention of this paper to present basic seismic theory since that is more than adequately covered by such authorities as Dobrin (1960), Heiland (1940), Jakosky (1942) and Nettleton (1940). For the purpose of this discourse, the refraction technique of seismic prospecting will be directed towards the solution of such problems as the determination of subsurface elevations of various strata within the overburden, the topography of the bedrock surface, stratification and structure within the bedrock, the elevation and extent of the water-table, and the location and physical extent of sand and gravel or mineral deposits.

The principle of seismic refraction is based on the fact that elastic waves travel at particular and, in some cases, well defined velocities through different materials. In general, the more dense the material the faster the wave travels through the medium. These velocities vary from as low as 400 ft/sec in light and dry top soil to 21,000 ft/sec in granites or 22,600 ft/sec in limestone or 24,500 ft/sec in ultrabasic rocks. All seismic waves travel through the various media following the laws of physical optics; Snell's Law, Fermat's Principle and Huygens' Principle are the fundamentals upon which refraction theory is based. In short, the receiving instrument detects and measures the time interval between the initiation of the elastic wave and its subsequent arrival at a detector.

The refraction method of seismic surveying demands that two requirements must be met in the subsurface horizons before depth to the various interfaces can be calculated accurately. These are as follows:

1. The velocity must increase with depth. If it does not, the seismic wave can never be refracted at the critical angle along the interface between two transmitting media and thus be returned to the detector. If a velocity inversion occurs, the seismic wave is refracted downwards until an increase in velocity is encountered at some lower interface thus refracting the seismic wave back to the detector on surface.

2. The various layers through which the refracted wave travels horizontally must have a thickness which permits transmission of the refracted wave. This thickness is a function of the depth of burial and of the velocity contrast between adjacent strata. If a layer is less than a minimum thickness, the refracted wave will not be transmitted horizontally through that layer but will traverse the layer until some lower horizon will permit transmission of the refracted wave horizontally.

The interpretation of shallow refraction data is seldom simple and straightforward. One of the greatest problems to a simplified interpretation is that of a velocity inversion with depth. In general this situation is unsolvable since the seismic wave is refracted downward rather than horizontally through the various strata leading one to a computation of depth which is always too great. Velocity inversions can be detected generally through an examination of drill-hole logs and particularly through the up-hole shooting method and plotting of wave-front diagrams. A perched water-table is a special situation of the velocity inversion since it often masks the layer beneath it. This is a special situation which presents problems to the interpretation of most refraction data but one for which the examiner may be looking if the problem is associated with groundwater prospecting. Perched water-tables are usually of short horizontal extent and can usually be recognized by typical velocities.

In many cases there is a considerable range of bedrock velocity over short horizontal distances; this is generally attributable to a change in geology. Once again a background knowledge of the project geology is essential to the interpretation of the geophysical data. A horizontal change in bedrock velocity may be due to dip on the bedrock surface or to an actual change in bedrock lithology.

Refraction techniques also tend to smooth out local highs and lows on the bedrock surface unless reversed profiles with close control are surveyed. If close control is obtained with reversed profiles, relatively minute changes in bedrock topography can be detected. Another interpretative problem is that of the blind zone within the surficial or bedrock material. A blind zone is thick enough to transmit seismic waves horizontally but is usually masked or unrecorded as a second arrival due to a considerable contrast in velocity between the blind zone and underlying formations. The velocity segments representing these blind zones must be introduced on all time-distance plots when their presence is known.

Theoretically it is possible to make an interpretation of all horizons that transmit refracted energy in the subsurface down to any depth of penetration using only one distance between the source of energy and the spread of detectors if this distance is great enough. In practice, however, there is an optimum shooting distance for any given refracting horizon.

Field procedure. Figure 1 shows a typical field layout for refraction surveying using a hammer seismograph. This figure indicates that data are acquired in one direction only and it is appreciated of course that reversed profiles should be utilized wherever necessary. In many types of surveys profiles in one direction are adequate while in others the reversed profiles are necessary for an intelligent interpretation of the data. The reversed profile can be attained readily when using twelve or twenty-four channel equipment by merely placing a source of energy at the two ends of the spread of detectors. Single channel instrumentation can yield a reversed profile readily by placing a geophone at both ends of the reversed profile and switching to the appropriate geophone as the energy source proceeds along the line of profile between the two detectors.

Basic methods of interpretation. The basic formulae set out by Dobrin, Heiland, Jakosky and Nettleton for the determination of thickness of various refraction strata involve velocities and either critical distance or intercept times. These formulae can become very involved and tedious when many refracting layers are encountered. The field and interpretation techniques set out by Pakiser and Black (1957), Hagedoorn (1959), and Hawkins (1961) are perhaps the most popular and easily used methods for

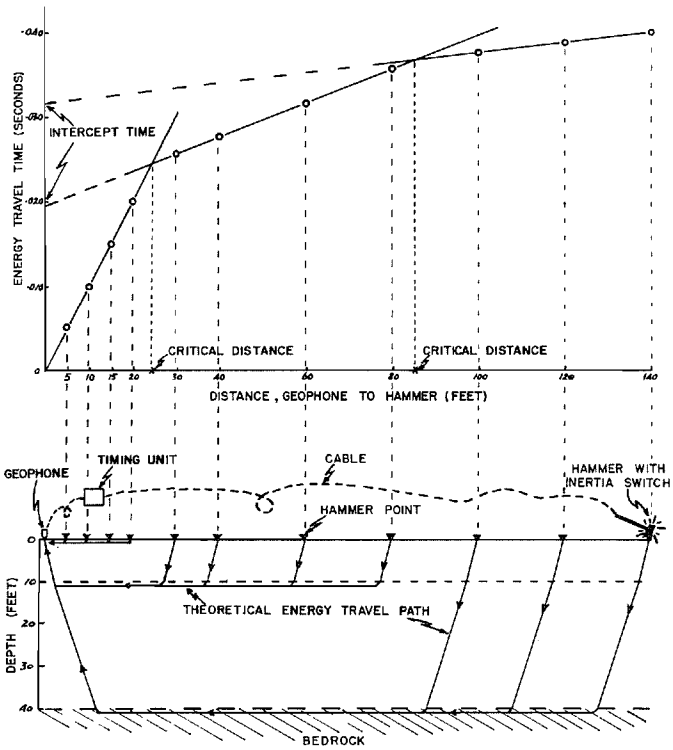


Figure 1. Typical field layout for hammer seismograph.

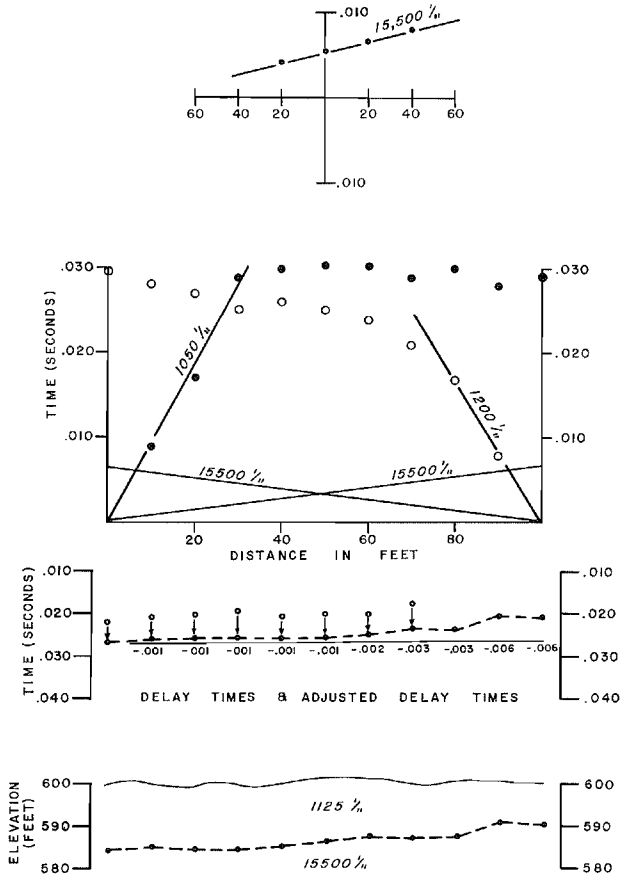
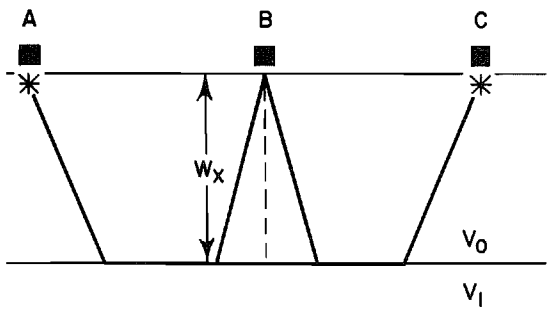


Figure 2. A refraction seismic method to determine thickness of weathered layer.

Figure 3. A typical shallow refraction seismic field plot and computation procedure for a reversed profile.



■ GEOPHONE

✳ SHOTS

THEN $W_X = \left(\frac{\overrightarrow{AB} + \overrightarrow{CB} - \frac{\overrightarrow{AC} + \overrightarrow{CA}}{2}}{2} \right) V_0$

WHERE W_X = WEATHERING DEPTH

AB = TIME INTERVAL FROM A TO B

CB = TIME INTERVAL FROM C TO B

AC = TIME INTERVAL FROM A TO C

CA = TIME INTERVAL FROM C TO A

V_0 = VELOCITY IN NEAR SURFACE LAYER

shallow refraction problems. The methods of Hagedoorn and Hawkins are basically very similar and are both based upon an early concept known as time-depth. This concept differs slightly from the delay-time concept of Pakiser and Black. All three methods can be used in multilayered overburdens. Another method of determining the thickness of the surficial weathered layer, also based on this early concept, is shown in Figure 2 with a particular application to twelve or twenty-four channel instrumentation. Energy sources are located at the ends of the spreads and time intervals to the central point are utilized.

The Geological Survey of Canada has used extensively a method very similar to that of Pakiser and Black with one minor innovation. Figure 3 shows a typical field plot and computation procedure for a simple refraction problem. With this method it is possible to determine the true velocity of bedrock and to determine the thickness of overburden under every geophone. This method is a delay-time analysis wherein delay-time is similar to that defined by Nettleton (1940). This method has been quite successful particularly in the determination of drift thickness overlying bedrock. Drift thicknesses, drift velocities and overburden and bedrock velocities can be determined fairly accurately and if control on reversed profiles is close, an accurate profile of the bedrock surface can be presented.

Shallow-refraction equipment. Portability is the key word in shallow-refraction prospecting equipment. The conventional 12

Contents

and 24 channel instrumentation will not be discussed in this paper; the emphasis will be upon the lightweight portable equipment that can be carried and operated by two men in the field using either explosives or a sledge hammer as a source of energy. In reconnaissance surveys where discrete observations at widely separated locations are adequate a great deal of the field time is spent in moving and setting up the equipment. Portability then becomes a definite advantage and necessity and can reduce greatly the transportation and mobilization costs of seismic surveys in remote areas. This paper will mainly discuss the equipment manufactured and used in North America, giving recognition of course to the fact that such companies as ABEM of Stockholm, Sweden, do have a portable refraction seismograph in production and in operation in the field.

Gough (1952) developed the original hammer seismograph utilizing one channel of information and a cathode ray tube display. This instrument was quickly followed by a very similar instrument developed in 1955 by Manfredini (1958). In North America the first two portable seismographs to be used extensively were the Model MD-1 developed in 1957 by Mooney and Kaasa (1958) and the Model FS-2 developed in 1961 by Hunting Survey Corporation.

MD-3. The Model MD-3 automatic engineering seismograph marketed by Soiltest, Inc. is the successor to the Model MD-1 originally manufactured by Geophysical Specialties that was used so widely in the early days of the shallow-refraction seismograph. The new model is lighter and smaller. Travel time appears on a digital readout dial immediately after the hammer blow is struck. It remains clearly visible until the next blow causes a new reading to register. There is an automatic reset option available for the instrument whereby the readout resets with each hammer blow to thereby speed up field procedures. The power supply consists of five rechargeable Nicad D batteries. The manufacturer claims that the instrument is designed to measure depths of 50 to 75 feet using an 8-pound sledge hammer as a source of energy. Explosives can be used to provide a more powerful energy source being detonated by an external blaster available for the instrument. This model is shown in Figure 4 and the various specifications for the instrument are set out in Table I.

FS-3. This model, the successor to the popular FS-2 model, became available in June 1965. It is manufactured by Huntec Limited. The readout for this instrument is a moving stylus burning signals into electrosensitive paper; the recorded signals are zero crossings of the positive pulse. Power supply consists of

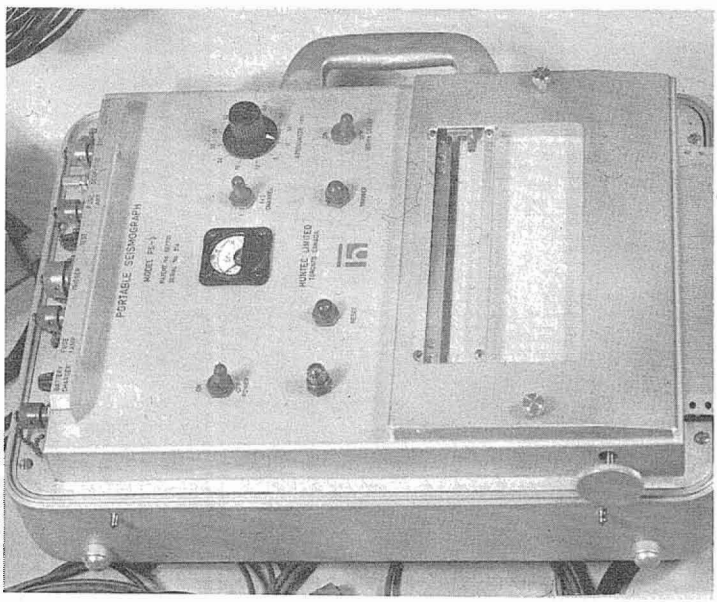
Table I. Shallow seismic instruments.

Manufacturer	Model	Travel Time Accuracy	Frequency Response	Readout Device	Recorder Range	Energy Source	Weight Without Source	Power Supply	Special Features
			(cps)		(ms)		(lb)		
Huntec Limited	FS-3	± 1%	12-200	electrosensitive paper	3-340	hammer or explosive	27.5	16-D Nicad or dry	Records all arrivals refracted, reflected shear
Soiltest, Inc.	MD-3	± 0.1 ms	5-500	direct digital	99.9 and multiples thereof	hammer or explosive	28	5-D Nicad	Automatic reset option
	R-150	± 0.25 ms	5-100	CRT and dial	250	hammer or explosive	30	6 volt Nicad or dry cell	Wave form display on CRT
	R-117B	± 0.05 ms		neon bulbs on direct digital	399	hammer or explosive	12	dry cell	
Tellurometer Inc.	VIATEC VH3-II			direct digital	999.9	hammer or explosive	8	4-6 volt mercury cells	Automatic reset
Electro-Tech., Mandrel	ER-75-A		15-125	Polaroid film	360	hammer or explosive	24	1-22½ 1-90 v Nicad	12 channels
Geo Space	GT-2	± 0.5 ms		Polaroid film	400	hammer or explosive	39	1-90 v 16-D dry cell or Exide Power Pak	12 channels
SIE Dresser	RS-4		5-125	dry-write photographic paper	unlimited	hammer or explosive	39	12 volt Nicad	12 or 24 channels, variable paper speed, unlimited record length
Craelius Terratest (ABEM)	TRIO 68	± 0.1%	10-300	wet or dry-write photographic paper	selected	hammer or explosive	45	24-D Nicad	Variable paper speed, unlimited record length



Figure 4. MD-3 automatic engineering seismograph (courtesy Soiltest, Inc.).

Figure 5. FS-3 portable facsimile seismograph (courtesy Huntec Limited).



sixteen D batteries either dry cell or rechargeable Nicad. The DC drive motor is digitally controlled. Five different transistorized circuit boards comprise the circuitry. A set of standard dry cell batteries lasts about four days' operating assuming about 20 locations per day. The instrument can be operated in noisy areas of traffic or high wind level. Two geophones can be used since the instrument provides a coincidence circuit to allow the operator to record only those events which arrive simultaneously at both geophones. A special feature of this instrument is that all events are recorded; this includes, of course, noise as well as the second and later cycles of refracted compressional and shear waves and reflections. It is generally possible to distinguish the various types of waves recorded. The manufacturer has introduced a technique for measuring shear wave velocities as well as longitudinal wave velocities to enable the operator to determine the moduli of elasticity of the soils and bedrock as a function of depth. The manufacturer claims penetration depth to 200 feet with a hammer although depths in excess of 300 feet with hammer source have been attained with a source-to-detector distance of approximately 1000 feet. A recent modification is a reflection gate involving changes on the correlator circuit board; this gate opening is adjustable by the operator to pass coincident signals from both geophones when operating in the reflection mode. The FS-3 then, is the only portable hammer seismograph designed to record refracted and reflected events and all phases of those events. The instrument is depicted in Figure 5 and the specifications are included in Table I.

R-150. The model R-150 Terra Scout refraction seismograph is manufactured by Soiltest, Inc. This instrument has a cathode ray tube similar to a television tube on which the operator can see the controlled seismic wave and any disturbing waves displayed. This 5-inch cathode ray tube has horizontal and vertical centring, intensity and focus controls. The cathode ray tube displays the actual wave form created by the hammer impact. The hammer man must thump several times with his specially designed hammer impactor to permit the instrument operator to adjust the calibrated dial so that travel time may be read directly. Three separate circuit configurations are contained within plug-in type modules. Power supply is either 6-volt dry cell or Nicad rechargeable batteries. The manufacturer claims that results to 50 or 100 feet depth are common with hammer or explosives as a source of energy. It is claimed also that the shape of the shock wave displayed can be used as a basis for the identification of materials penetrated. The model R-150 is depicted in Figure 6 and the specifications are included in Table I.

R-117-B. The model R-117-B supersedes the R-117-A seismic timer manufactured presently by Soiltest, Inc. and formerly manufactured and distributed by Dyna Metric Inc. The readout on this instrument is display lights on a direct digital readout. The power supply is one dry cell battery. No information is available as to depth of penetration of this instrument although one might assume that depths of 50 to 100 feet are attainable. The model R-117-B is shown in Figure 7 while the specifications are included in Table I.

Soiltest has also developed a model R-217 Micro-seismic Timer designed for using seismic wave velocities in engineering projects. It does not appear to have a very great range of penetration but seems to be designed more specifically as a detailing tool.

Contents

Viatec. The Viatec model VH-3 Mark II instrument is distributed in Canada and the United States by Tellurometer Inc. Four decade counters present a direct digital readout with an oscillator and gate circuitry. Four mercury cells provide the power for the circuitry. This instrument is designed for penetration to depths of 50 feet with hammer source and 80 feet or more with explosives. One feature of this instrument is that no resetting is required since a hammer blow automatically resets the previous reading on the meters and indicates the new reading. This instrument is shown in Figure 8 while the specifications are included in Table I.

ER-75-A. The model ER-75-A Porta-Seis refraction system is manufactured by Electro-Technical Labs, a division of Mandrel Industries, Inc. This unit is available in 3 or 12 traces, the latter being the more popular. Twelve transistorized refraction amplifiers pass the signal from the detectors to twelve galvanometers. An internal light source projects a light beam onto the mirror of each galvanometer from which it is reflected to a series of mirrors to Polaroid film. When a signal voltage from a seismic wave is supplied to the galvanometer, the galvanometer mirror deflects the light beam proportionately and reflects it to a rotating mirror which provides a sweep of the galvanometer traces along the record. The rotating mirror is provided motive force by a pendulum arrangement. The power supply for the system is comprised of two rechargeable Nicad batteries. Explosives are the common source of energy for this instrument although a kit is available as an accessory to use a hammer as an energy source. There is a built-in capacitor discharge-type blaster in the instrument. The instrument is shown in Figure 9 and the specifications are included in Table I.

GT-2. The model GT-2 portable refraction system is manufactured by Geo Space Corporation and supersedes the model GT-1 interval timer by Electrodynamic Instrument Corporation. It may



Figure 6. R-150 Terra Scout refraction seismograph (courtesy Soiltest, Inc.).

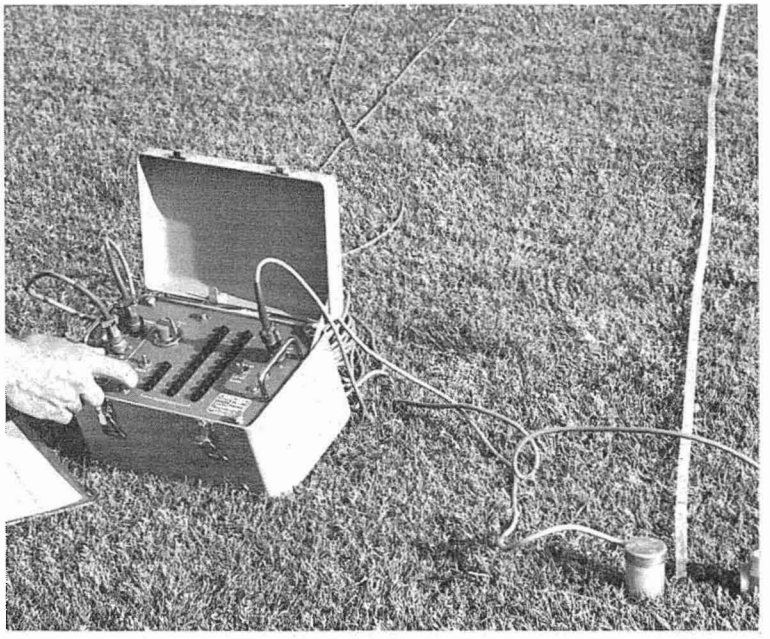
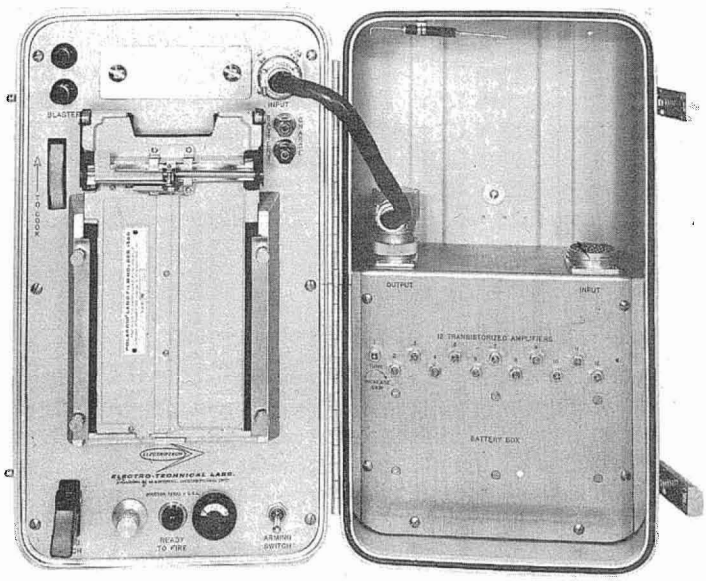


Figure 7. R-117 seismic timer (courtesy Soiltest, Inc.).



Figure 8. Viatec seismic hammer VH3 Mk II (courtesy Tellumoter Inc.).

Figure 9. ER-75-12 Porta-Seis refraction system (courtesy Electro-Technical Labs division of Mandrel Industries, Inc.).



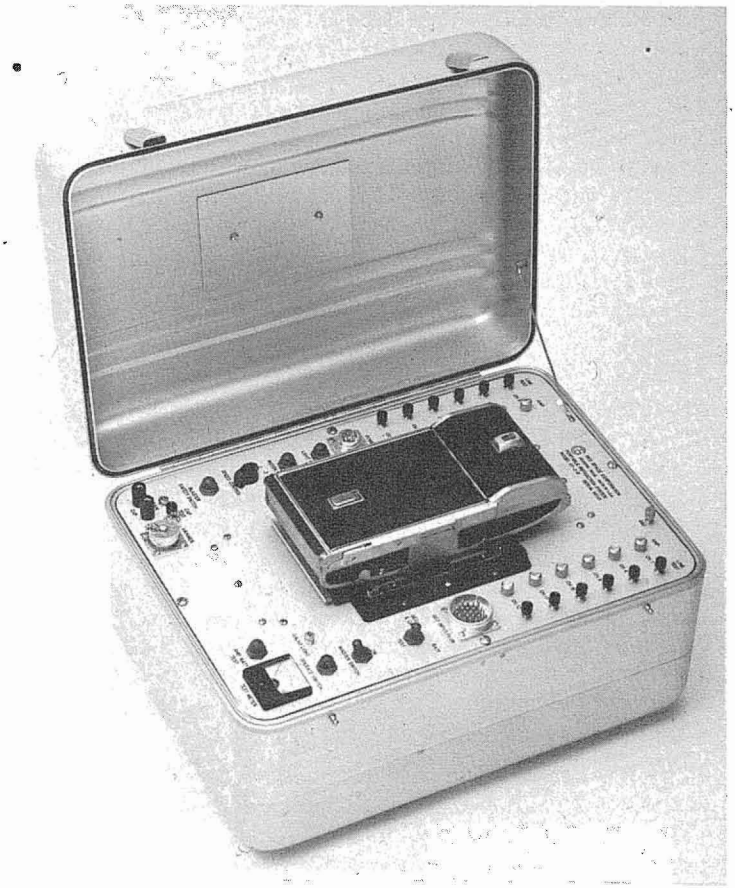


Figure 10. GT-2 portable refraction system (courtesy Geo Space Corporation).

Figure 11. RS-4 recording system (courtesy Dresser SIE, Inc.).



be obtained in either 3 or 14 traces which include timing and time-break traces. Transistorized refraction amplifiers carry the signal from detector to galvanometers for recording on Polaroid film. Once again it is a moving optics and stationary film system. Power supply is either dry-cells or an external rechargeable 'Exide portable power pak'. A self-contained capacitor discharge-type blaster is included in the instrument. A hammer may be used as an alternate source of energy. This instrument was originally designed as an interval-timer for up-hole shooting in the determination of near-surface velocities for petroleum prospecting but has applications as a shallow-refraction seismograph. The instrument is shown in Figure 10 with specifications included in Table I.

RS-4. The model RS-4 recording system is a portable seismograph manufactured by Southwestern Industrial Electronics, a division of Dresser Industries. Models are available with 2 to 12 traces plus a time-break and the read-out is a continuous roll of dry-write photographic paper with the seismic data recorded by means of galvanometers. Power is provided by Nicad batteries with built-in recharging circuitry. Variable recording speeds are available by merely changing gears. A built-in capacitor discharge-type blaster is incorporated in the instrument. A special feature of this instrument is its capability to run records to any desired length at several different speeds. This instrument is depicted in Figure 11 while the specifications are included in Table I.

TRIO 68. Craelius Terratest, previously ABEM, of Stockholm, Sweden have developed a new portable refraction seismic system TRIO 68. It is available in 15 or 25 channel models including timing and time-break traces. Read-out is through galvanometers onto conventional photographic paper or ultraviolet sensitive dry-write paper. Record length may be controlled between 10 and 50 cm by a selection switch or continuous flow. Three different recording speeds are standard while other speeds are available to order. Power supply is 30 volts of rechargeable Nicad batteries in a separate tray clipped to the recorder base. Explosives or a hammer may be used as an energy source. This instrument is shown in Figure 12 with the specifications included in Table I.

Nomograms. Most of the instrument manufacturers have developed nomograms which are generally included in the operating manuals for their instruments. These nomograms are a quick method of making depth determinations but frequently lack the accuracy of the calculations using conventional formulae. Meidav (1960), Knox (1958) and Lyons (1952) have published nomograms or similar aids to the computor while Huntec Limited has developed a nomogram for use with multilayer situations. Geo Space, Electro-Tech and Tellurometer instruments are accompanied by nomograms in the operator's manual. In general the approximations that are assumed in the design of these nomograms are to within a few percentage points if certain assumptions which are not too rigid or unlikely are made. The author still is inclined to use calculating procedures other than nomograms but must admit that such aids do have their place and can be of considerable assistance to men in the field.

General comments. All of the instruments discussed above require two men to operate although frequently one man can obtain data if speed of acquisition is sacrificed. It must be pointed out that in some areas a crew of three men is preferable.

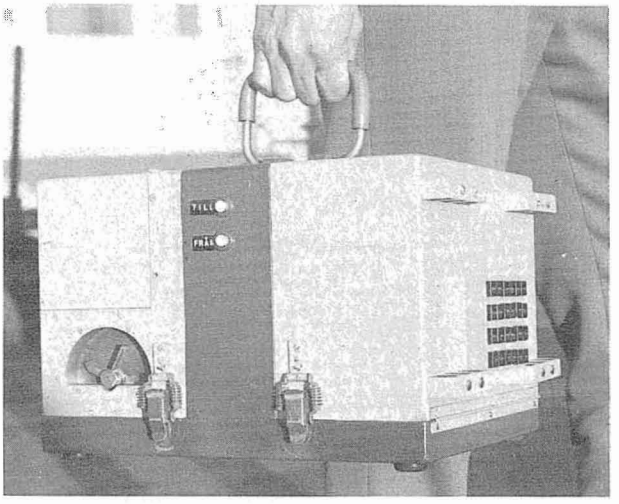


Figure 12. TRIO68 portable seismic refraction unit (courtesy Craelius Terratest, formerly ABEM).

This paper would not be complete without some mention of the various shapes of the plates that are struck by the sledge hammer. In all cases the plate and the hammer should be matched in weight and several experiments have been conducted to determine the optimum shape of these plates. The plate may be in the form of a hemisphere or a flat sheet of steel. A pipe struck horizontally may be used to generate shear waves. In general, a steel plate 8 inches square and 1 inch thick is a satisfactory anvil.

Field telephones or radios might be used where line-of-sight contact between instrument and hammer men is not possible. The former can be included in the cable used to transmit the hammer signal while the latter device obviously eliminates the need for cables. A high-frequency radio pulse transmission and reception system with range to 1000 feet can easily be developed. Soiltest, Inc. has developed such a device, which appears to be the first one on the market although other agencies have used such techniques in the past. Once again portability is the keynote in all such seismic surveys; any piece of equipment that can be eliminated from the field procedure tends to a more efficient and versatile survey.

Shallow reflection methods and equipment

Principles of reflection theory. Reflection seismic theory is also founded upon the basic laws of physical optics. Refraction and reflection techniques differ in two principle ways: (1) in the reflection mode the seismic energy meets and rebounds or reflects from an acoustical boundary whereas in the refraction mode the energy crosses the acoustical boundary and travels within the lower medium to be refracted back to surface from some point within that lower medium, and (2) the distance between energy source and detectors in the refraction mode is very much greater than the depth to which the energy penetrates whereas in the reflection mode the distance between source and detectors is very much less than the depth to which the energy penetrates and is reflected. Vertical velocities through strata may be determined by reflection techniques whereas horizontal velocities are obtained by refraction techniques. In both types of seismic surveying the velocity of the seismic wave within the various strata depends on both the density and the elastic moduli of the material.

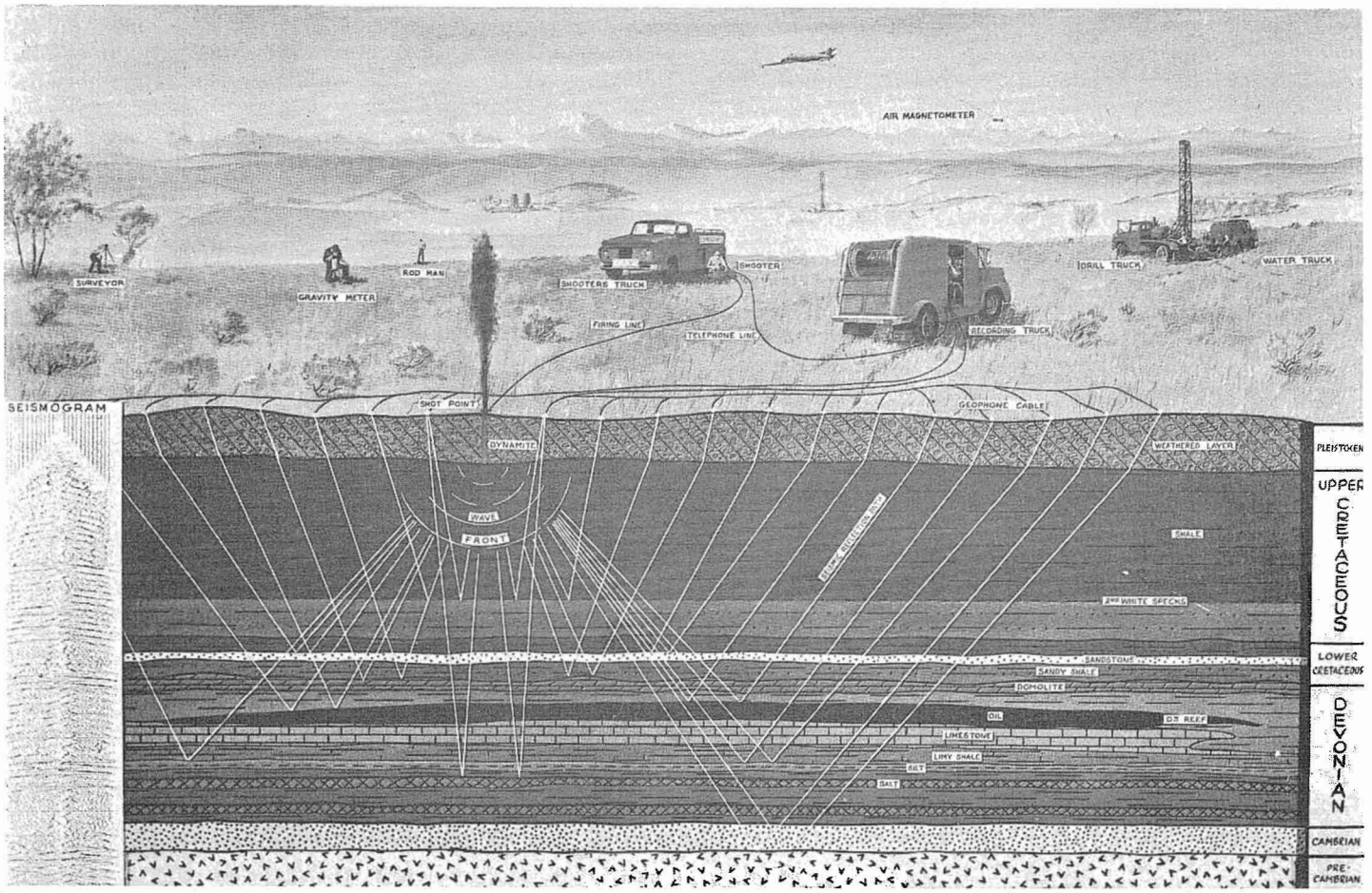


Figure 13. Generalized field layout for reflection seismograph (courtesy Seismic Service Supply (1958) Ltd.).

Field procedure. A generalized picture of a conventional reflection seismic crew in the field is depicted in Figure 13. With this equipment the continuous profiling technique is generally employed to obtain continuous subsurface coverage. If, however, a portable lightweight seismograph is used by a two-man crew to investigate the various strata to shallow depth, a technique may be employed whereby reflections are recorded at spot locations as opposed to continuous profiling. Continuous profiling with short spreads is recommended for 12 and 24 trace instruments whereas the spot location technique is recommended for the single channel equipment. These spot locations may be as close as twenty feet apart which in effect does give the operator a continuous subsurface profile.

The technique known variously as 'common depth point', 'horizontal stacking', or 'roll-along' has been developed to great efficiency particularly in the exploration for petroleum reserves. This same technique can be used for seismic exploration in the Proterozoic basins of the Precambrian shield wherein deep strata may be investigated to solve structural problems. The same technique should be adaptable to shallow reflection problems although the author is not aware of its application. This technique is almost as important as the development of the reflection seismograph itself. Mayne (1962, 1967), and Marr and Zagst (1967) are recommended authorities in the common depth point technique. In brief, the detector spreads and shot points are arranged so that the channels representing common depth points are recorded with appreciably different horizontal distances between the shot points and detector stations. The channels which have a common reflection point are combined, or stacked, after appropriate corrections for angularity and travel time to datum have been applied. Reflections which follow the assumed travel path are greatly enhanced and other events are reduced. In general, multiple reflections are discriminated against. This common depth point stacking technique has been employed very recently in a program near Elliot Lake, Ontario, within a Proterozoic basin in the Canadian Shield; the data are under consideration and interpretation at the present time. This technique has definite applications to deeper exploration programs but is probably not necessary for shallow exploration.

Vertical velocity to various strata and interval velocities within these strata must be determined so that accurate determinations of depth to the various horizons may be computed. These velocities are determined in general by means of the expanding reflection profile or the 'passing through' technique. These techniques have been described by Dix (1955), Green (1938), and Gardner (1946).

Reflection equipment. Pakiser and Warrick (1956) were among the first authors to report upon an evaluation of shallow-reflection seismic techniques. They pointed up that the water-table was a good reflector and also that multiple reflections presented many problems to any shallow interpretation. They used instruments with highly damped galvanometers and a fast AGC action and they used explosives in shot holes at depths of approximately 30 feet. Poulter (1950) made an early attempt to obtain an increased efficiency in the conversion of the energy of an explosion into useful seismic energy by detonating patterns of explosive charges supported on stakes above ground. Similar techniques with the charges detonated on the surface of the ground may be very useful in shallow prospecting.

Four of the instruments described above as refraction seismographs may be used in reflection seismic programs with limitations. The models ER-75-A of Figure 9 and GT-2 of Figure 10 are both instruments that record seismic data on Polaroid film through a system of lamps and galvanometers. Without heavy damping on these galvanometers the author estimates that reflections from horizons shallower than 300 feet in depth would be unobtainable. A similar situation holds for the model RS-4 seismograph of Figure 11 in which the seismic data are recorded through galvanometers to a dry-write photographic paper. These three instruments should be able to record shallow reflections if the galvanometers are damped adequately. There is no system of filters in these instruments.

The portable seismograph which seems to have the most promise at the present time for very shallow reflection surveying is the model FS-3 by Huntec Limited. Huntec has devised an effective wavelength filtering technique which eliminates almost all events other than seismic reflections on the FS-3 records. Reflections have a much longer apparent wavelength than surface waves or refractions. Thus a suitable array of geophones may completely cancel events other than reflections. This procedure extends the depth range of the instrument and enables the instrument to be used in the reflection mode when frozen ground or some other velocity inversion situation is encountered close to the surface. Special circuitry in the FS-3 seismograph has been developed to sense the time lag of positive zero crossings of the signal at two separate geophones and to record only those arrivals whose phase shift is smaller than an arbitrarily set amount (Meidav, 1967). A new correlator circuit board has been designed which contains a variable gate to discriminate against the input signals from two geophones if the phase shift of the positive signal in any one of them, relative to the other, is greater than an arbitrary time value ranging between 0.5 and 5.0 ms manually set by the operator. The variable gate correlator can then be used for receiving seismic waves which are characterized by an essentially vertical ray path. In short, if the time difference between the arrival of two seismic waves at the two detectors is less than the correlator gate setting, the stylus will imprint data on the electrosensitive paper.

The model FS-3 seismograph, particularly with the newly developed correlator board, can be used for reflection surveying. In this mode of operation both the hammer and the complete seismograph are moved together along the reflection profile, determinations being made generally at intervals of 25, 50 or 100 feet. To reduce the effect of the direct arrival, the geophones are usually placed on the same side of the hammer source and approximately one half wavelength apart. This is generally about 15 to 20 feet. Reflections from depths as shallow as 65 feet have been observed from ice-covered lakes and from 75 feet on land where a homogeneous clay overlies granite bedrock. Reflections have also been observed from depths as great as 900 feet near Winnipeg, Manitoba, where a thin overburden overlies the Ordovician Tyndall limestone overlying the Precambrian shield. The principal limitation of this method is the difficulty in identifying the reflections particularly where there is more than one reflecting horizon and where there are multiple wave paths.

Conventional analog or digital instrumentation may be necessary for the exploration of deep basins in the Precambrian shield areas or for the delineation of aquifers by special studies of amplitude and frequency. These instruments are bulky to transport and costly to purchase but as pointed out above may be quite necessary for the deeper prospecting of mineral deposits.

Zietz and Pakiser (1957) have described the application of a crystal sonar transducer to the problem of obtaining shallow reflections. The transducer was placed directly on the ground but somewhat indefinite results were obtained from the experiments. This technique apparently has appreciable potential as an exploratory tool although it has probably been superseded by the repetitive-type land source which has attained prominence of late.

General comments. Some general comments on reflection and refraction surveying may be timely. The reflection technique of seismic surveying has certain advantages over the refraction technique. These are as follows:

1. Greater subsurface detail may be obtained by the reflection technique.
2. There is no concern about the presence of blind zones or hidden layers in the subsurface strata.
3. A much shorter spread-length, that is distance between energy source and detectors, is required for reflection surveying to obtain data from the same acoustic boundary than in refraction surveying.
4. Reflection surveying does not depend on an increase in velocity with depth, as in refraction surveying.
5. Horizontal, vertical and interval velocities may be observed by carrying out an expanded reflection profile. Reflections can be observed from depth as well as energy refracted from subsequently deeper horizons as the detector to energy source distance is increased.
6. There is more energy reflected than is refracted at any interface thus reducing the amount of energy that must be introduced into the ground at the source.

It must also be appreciated that it is frequently difficult to separate reflections from other events and recognize them as such. It is also worthy of comment at this time that favourable velocity contrasts and continuous reflecting horizons are probably less likely to occur in mining areas than in oil-producing areas. The same situation definitely exists in the search for aquifers.

Continuous profiling marine seismic methods and equipment

The study and exploitation of the ocean, the ocean floor, the surrounding continental shelves and inland bodies of fresh water is a new area of interest and as such necessitates a continuing updating of scientific and instrumental techniques. The techniques and technology which are used with success today will be

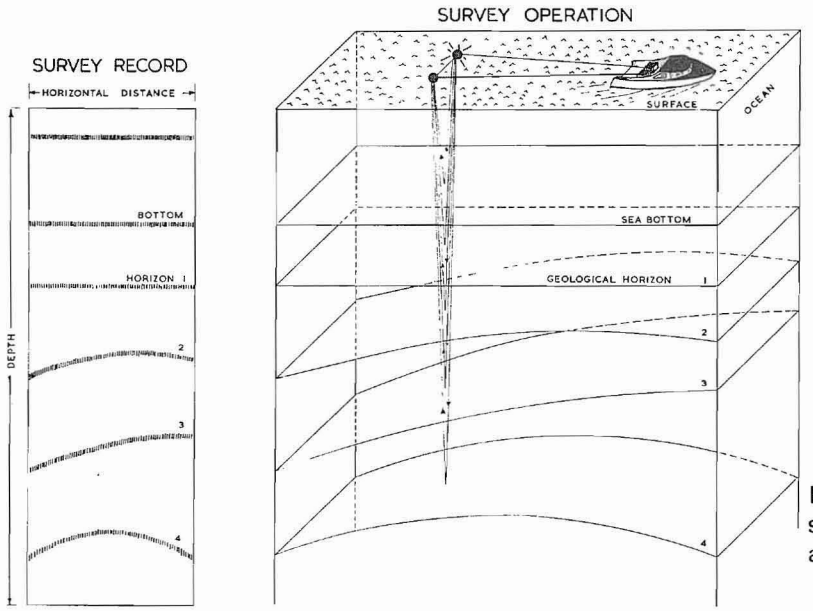


Figure 14. General principles of sparker seismic reflection method, after Maries and Beckmann.

outdated and replaced within a relatively short period of time. This is all very evident when one reviews the equipment that has been developed within the past ten years for the exploration of sub-bottom features in water-covered areas.

The general principles of the sparker seismic reflection method are shown in Figure 14 after Maries and Beckmann (1961). Similar principles apply to any continuous profiling marine seismic method regardless of the source of energy. The energy source and the hydrophone array may be trailed some distance behind the boat, as much as 200 feet, or both may be suspended over the bow of the boat. The method is actually very simple and at a speed of 6 or 8 knots a great deal of seismic data can be accumulated in a working day.

Energy reflected from the bottom of the water and from the strata beneath the water changes character with variations in the composition of the bottom sediments. Mud is a poor reflector and will absorb 80% or more of the signal. As the particle size of the bottom material increases the reflectivity increases and less signal is absorbed. There are several other factors that affect signal strength; some of these are biological scattering, receiver noise level, water noise, thermal noise, propeller cavitation, drive shaft vibration, engine noise and cavitation due to towing the hydrophones through the water. A bottom comprised of unconsolidated sediments high in organic content may absorb most of the signal introduced from the water surface. And one cannot dogmatically say that an inboard motor is quieter than an outboard motor on any given boat. There are many factors which must be considered and all of them must be considered to be impedimenta to the acquisition of interpretable data during any marine seismic survey.

Velocities within the unconsolidated bottom materials and the upper strata of bedrock can be determined using the repetitive sources in the marine environment. Either wide-angle reflection techniques or refraction techniques can be used to acquire data for such velocity determinations. The wide-angle reflection technique requires a steadily increasing separation between energy source and hydrophone while recording so that the angle between the incident and the reflected wave path increases progressively. Several successive approximations of velocity are required. This method is similar to the expanding reflection profile on land. Horizontal velocities are best obtained using the refraction technique. The recording boat is maintained at a specific location while the hydrophone is streamed to the full length of available cable. While the energy source repeatedly injects energy into the subsurface, the hydrophone cable is pulled into the vessel. Both refracted waves and water arrivals are recorded. The water arrival will be a straight line obliquely across the record while refracted rays will be recorded as earlier arrivals. With decreasing separation between hydrophone and energy source the lines of refracted arrivals approach the line of direct arrivals eventually meeting at the points where the refracted and direct waves have the same travel time. This latter point is then a critical distance. As in conventional refraction surveying, distance and time are known and velocities within the bottom sediments and bedrock can be determined.

Huntec Limited has developed a method to obtain velocity data by the analysis of any clear diffraction patterns present on their hydrosonde records. Diffraction patterns are due to any sharp irregularity protruding into a medium of a much different acoustic impedance. Normally these diffractions are caused by such phenomena as faulting where a hard layer lies opposite a less competent one, by sudden changes of dip or by other sharp irregularities. Two assumptions are made in the Huntec method; these are that the ray paths are straight lines and that the line of survey traverses the diffractor directly overhead.

Continuous profiling marine seismic equipment. It has been an extremely difficult task to accumulate data and specifications on the great number of continuous profiling marine seismic equipment available on the market to date. The author is well aware that there may be omissions in this discussion because certain pieces of equipment did not come to his attention. The data and specifications have been taken from brochures at hand at the time of writing. He intends the following presentation to be as complete as possible at the time of writing, realizing that as these words are written new devices are being developed.

In all cases, a sound-source transducer, pulled by a ship, emits repetitive acoustic (sound) pulses in the water. Each separate release of energy at surface is reflected by the various discrete sub-bottom acoustic layers and detected by an acoustic receiving system also towed by the vessel. The incoming reflected signals are processed electronically and transmitted to a shipboard graphic recorder where they are displayed in the form of tone shades on the chart of a facsimile recorder. The result is an acoustic cross-sectional profile displaying the layers in their corresponding relationships, depth and geographic positions. The seismic records display discrete geologic features in their continuity. Near-surface sediments, bedrock and other competent horizons are delineated simultaneously. As greater penetration is required, a source must be used which generates a pulse containing more energy in the low-frequency range.

Repetitive sources for continuous profiling in the marine environment may be broken down into several categories; these sources will be discussed on the basis of the physical principle upon which the energy source was designed.

Electric Spark

Sparker. Beckmann, *et al.* (1959) and Maries and Beckmann (1961) are among the first to describe electric spark discharge equipment and its use as a surveying tool. The Sparker was the forerunner of many other pieces of equipment based and designed upon the same principles.

Arcer. This instrument is a high powered sparking device developed by the Rayflex Division of Alpine Geophysical Associates Incorporated. Normal output of the source is 20,000 joules with accommodation for additional units up to 80,000 joules practical limit when the capacitor banks are discharged through one or more arcs. Seismic data are recorded on dry electrosensitive paper through a 19-inch helix recorder. In 1966 the equipment was modified to permit the recording of data on a standard 24-trace Techno tape transport. Timing control of the system comes from a precision power supply controlled by a tuning fork; this power supply also drives the recorder. Shor, *et al.* (1963) have described some deep-sea tests using this equipment.

A continuous stratification profile system by Alpine Geophysical Associates has a maximum 12,000 volt output across two condenser banks. Hydrophone arrays up to 1000 feet in length are used to detect signals. The frequency spectrum of the spark source used by Alpine is from 78 to 10,000 cycles per second. Depths of penetration to 5 kilometres are claimed for one project in the Gulf of Mexico.

Woods Hole instrument. This instrument was one of the pioneers in the repetitive-spark continuous-profiling field. Caulfield, *et al.* (1965) describe some of the recent modifications to that system. The new system has an electrical spark-sound source with a maximum stored energy of 100,000 joules. A streamlined and uniformly buoyant line-hydrophone array with a band-pass of 20 to 1000 cycles per second diminishes tow noise. An optimum signal-to-noise ratio is obtained by using a matched-filter detector that measures the correlation between the reflected signal and the wave form incident on the sea floor in the same frequency range as the reflection. Sub-bottom reflections of 0.8 second (one-way time) in continental shelf areas have been obtained at ship speeds of 11 knots and from 1.8 seconds beneath the ocean floor in the deep sea at 6 knots.

SUBOT (Sub Bottom) and SSP (Seismic Section Profiler). Both of these instruments have been developed by the Geotech Division of Teledyne Industries. Both systems utilize an AC generator to charge a bank of condensers discharging through electrodes into the water; the energy is detected by submerged arrays of crystal detectors and processed through to a facsimile recorder and tape transport. The SUBOT instrument is applicable to high-resolution continuous profiles with penetration depths to 2500 and 3000 feet. Penetration depths of 10,000 to 15,000 feet are claimed for the SSP system. This latter instrument discharges 120,000 joules of energy from the condensers.

EG & G systems. Edgerton, Germeshausen and Grier have several spark-source instruments available. The usual spark-sound source from EG & G consists of three electrodes in an arrangement called a sparkarray. The 1000 watt second per pulse sparkarray will penetrate to 200 metres in water depth of 200 metres while the 7000 watt second per pulse source will penetrate to 1500 metres in water depth of 1000 metres. The company now has a 21,000 joule sparkarray which has achieved penetration to 7000 feet beneath the North Sea. This company has also developed a 9 electrode sparkarray sound source for system energy levels to 27,000 watt seconds, a system which is available upon special order. A high-resolution system is now available for contract surveys only; this system has very high resolution and relatively low penetration.

Hydrosonde Mark 2-A. This is a sub-bottom profiling system developed by Huntec Limited, which can be used with various energy sources. A high-voltage supply charges a 2-microfarad capacitor to about 13,000 volts to store approximately 165 joules of energy. The capacitor is discharged by a hydrogen-thyratron triggered from the receiver timing logic at rates of 4, 8 or 16 times per second. The circuitry of the hydrosonde has been designed for use with magnetostrictive hydrophones but can also be obtained with circuitry suitable for use with other types of pressure-sensitive detectors. Digital techniques have been utilized in the recorder-drum drive and timing pulse and the timing pulse programming circuitry. Any three-channel tape recorder with frequency response to 30,000 cycles per second can be attached to the receiver. Wide-band hydrophone signals and recorder logic signals are both recorded; the hydrophone signals then can be played back through the filtering system for reproduction on the facsimile recorder. The digital servo action keeps the facsimile recorder slaved to the prerecorded logic signals on the tape recorder thus cancelling distortion. Self-adjusting filter systems have been developed for this instrument and will be discussed later in the paper. Miller (1965) has discussed the hydrosonde as a marine seismic profiling device. The hydrosonde instrument is shown in Figure 15.

WASSP. WASSP (Wire Arc Seismic Section Profiler) is a recent spark source developed by Geotech, a Teledyne Company. A fine wire, 0.010 to 0.015 inch thick, is continuously carried off a spool and down a tube by a flow of water. The wire becomes one side of the circuit of a 14,000 to 17,000 volt source as a current up to 30,000 amps passes through the wire to the other side of the towed fish array. Approximately 4 inches of wire are

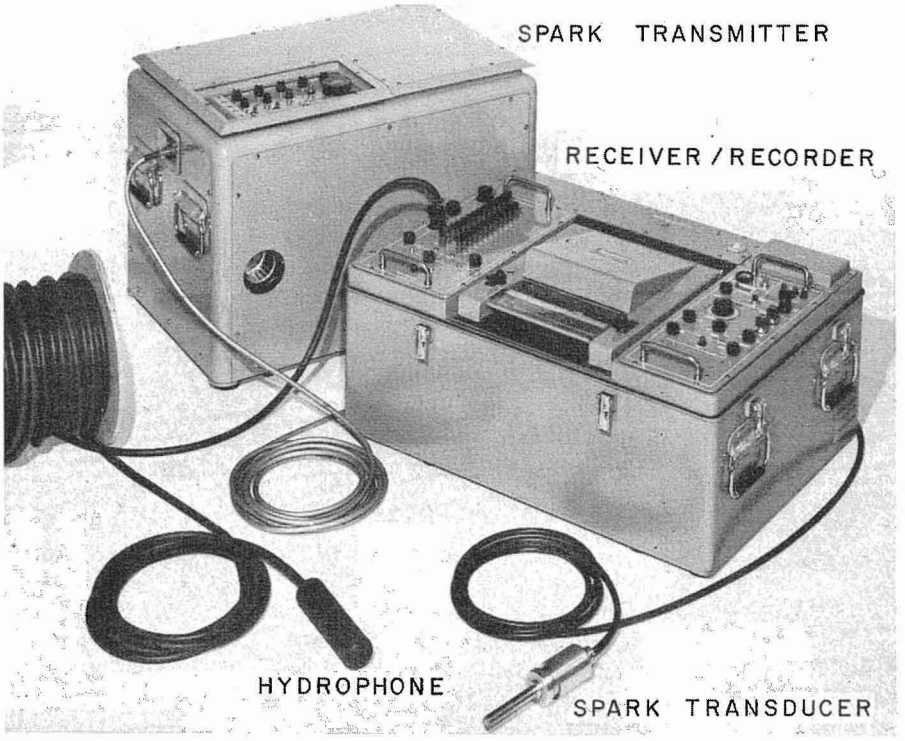


Figure 15. Hydrosonde Mark 2A (courtesy Huntec Limited).

used with each discharge to develop 40,000 joules of energy. Four WASSP sources may be used in synchronization and are claimed to be effective in salt or fresh water or even in air. The device may be towed at a speed of 10 knots. No penetration data are available at time of writing.

Gas sources

Gas exploder. The original gas exploder was developed at Lamont Geological Observatory with commercial rights assigned to Alpine Geophysical Associates Inc. It was a multiple source with three explosion chambers fired simultaneously, the energy being detected by a hydrophone array. In 1960 penetration to 4000 feet was claimed with the device while in 1966 that penetration was quoted as 2 seconds one-way travel time. All data can now be recorded on a 24-trace Techno tape transport.

GASSP. This gas source seismic profiler was developed by Shell Development Company and licensed to the Geotech Division of Teledyne Industries. Through synchronized control valves, metered amounts of acetylene and oxygen are combined in a combustion chamber and ignited by the discharge of a controlled-time firing spark plug. The detonated gas transmits energy to the water through expandable neoprene tubes which can be used in multiples connected in series to afford a long-line acoustic source. Reflected energy is recorded on a facsimile recorder and a tape transport. Tapes can be digitized and computer processed to improve signal recoverability.

SUE. The Seismic Underwater Explorer was originally developed by Mobil Oil Company and is now a trade name for Geophysical Services Inc. This device uses a mixture of propane, oxygen and compressed air with a detonation rate of once every 3 seconds. In 1966 penetration to 8000 feet was claimed. The same instrument has now matured to digiSUE.

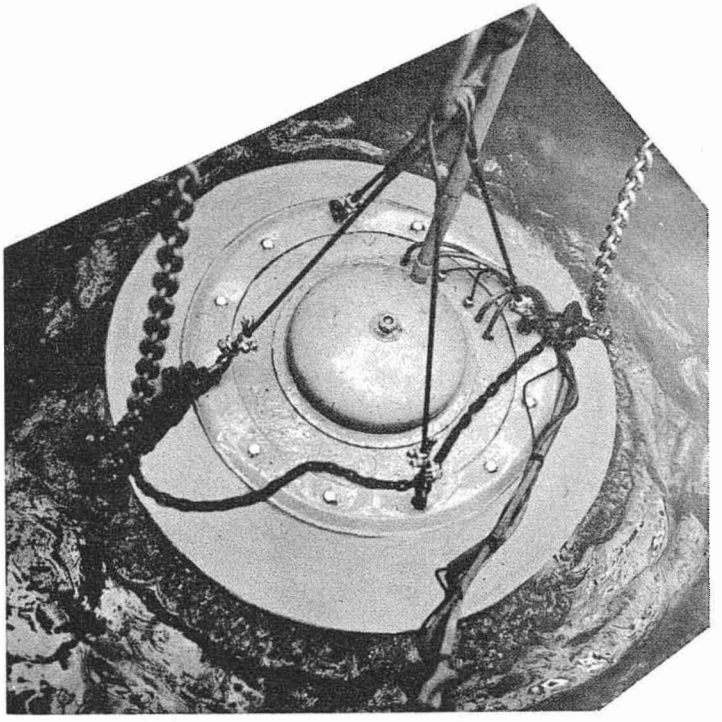


Figure 16. Marine Dinoseis (trademark, Sinclair Research Incorporated) gas exploder (courtesy Geo Space).

Dinoseis. The Dinoseis system was developed by Sinclair Research Incorporated and is a trade name of that corporation. It has been licensed to several seismic contracting companies. The Dinoseis seismic source is an extensible explosion chamber in

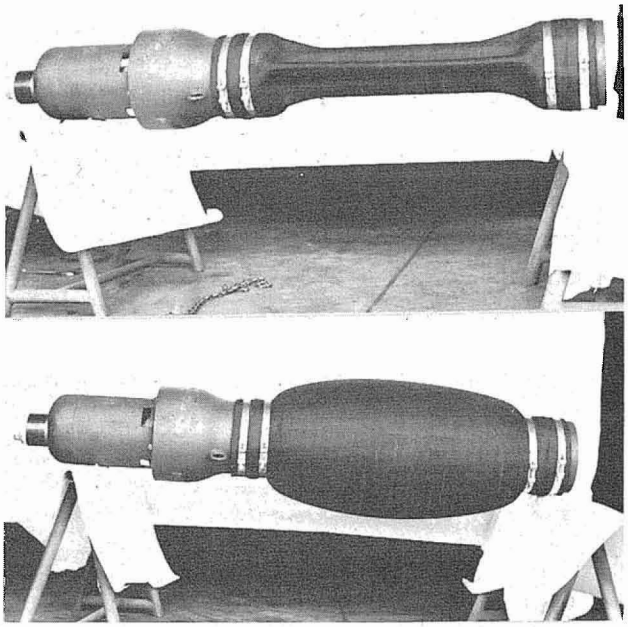
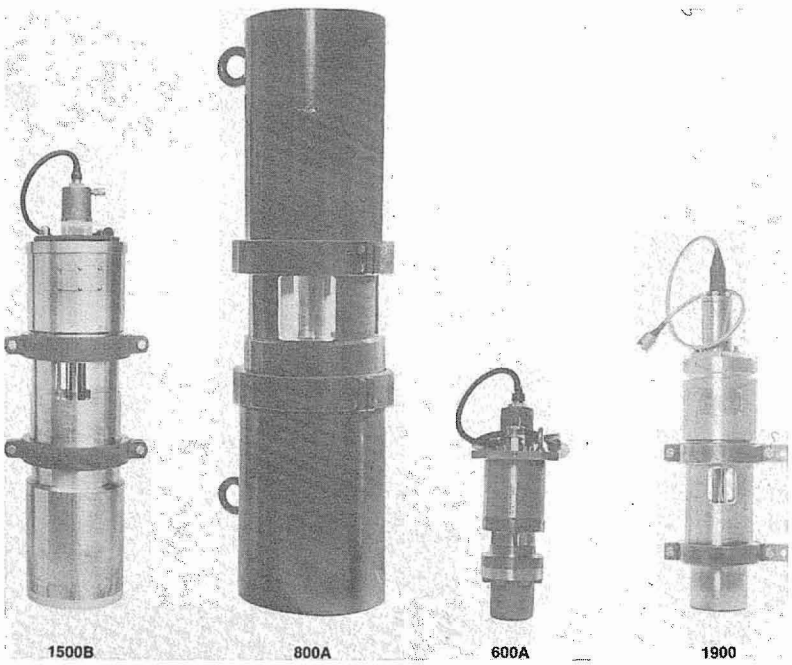


Figure 17. Aquapulse chamber in expanded and collapsed states (courtesy Western Geophysical Division of Litton Industries).

Figure 18. Par sound source by Bolt Associates, Inc.



which a mixture of propane and oxygen is ignited to generate approximately 100,000 foot pounds of seismic energy. This is a completely contained explosion and a steel diaphragm in the bottom of the gun transfers the impulse to the water. The device can be towed in water depths varying from several inches to several hundred feet at a speed of approximately 5 knots. The frequency spectrum is from 10 to 100 cycles per second. The device functions very well in shallow water where the top of the gun may even be exposed above the water at times. The electronic firing system controls filling, arming and firing of the device in synchronism with the magnetic tape recording system. A marine Dinoseis unit is shown in Figure 16.

Aquapulse. This system has been recently designed and developed by Esso Production Research Company and licensed to Western Geophysical Division of Litton Industries. A flexible sleeve is impulsively expanded by the ignition of a mixture of propane and oxygen in a chamber within the device. Expansion of the sleeve produces a sharp acoustic impulse in the surrounding water. Energy is concentrated in the seismic band and produces virtually no 'bubble pulse'. Four sources can be used simultaneously in a rectangular array as normal operating procedure. The depth of the sources within the water is controlled by a towing harness and is monitored by depth gauges. No penetration depths are available for this recent development. Figure 17 shows the chamber in expanded and collapsed states.

Compressed air sources

PAR pneumatic sound source. The PAR sound source developed by Bolt Associates Incorporated, Figure 18, is claimed to have several times the penetrating capability and higher resolution than spark discharge, gas exploders or electromagnetic impulse type sources. It has definite advantages over the gas-exploding sources. An air compressor is required on board the vessel instead of a supply of bottled gas or liquid oxygen, a feature which from the safety point of view is definitely more attractive. High-pressure air is explosively released into the water with 80–90 per cent of the energy in the 5 to 80 HZ spectrum. Chamber volumes are available from 1 to 2000 cubic inches with operating pressures from 200 to 2000 pounds per square inch. All units are fired electrically. The smallest units may be fired as often as 4 times each second while the minimum firing time for the larger units is 6 seconds. The Huntec hydrosonde Mark 2-A instrument has been used with this pneumatic source with extremely impressive results. Ewing and Zaunere (1964) reported on a similar pneumatic sound source.

GSI Digital-Air Gun. Geophysical Service Inc. has developed a new Digital-Air Gun equipment and technique. Several different sized air guns or units are used at one time to broaden the spectrum of the recorded data since each unit alone yields a narrow frequency band. The units vary in length from a few inches to a couple of feet. A minimum of 2 to 3 feet of water is required for satisfactory operation. Data quality is controlled by varying the amount of energy input for each record and by varying the number of records stacked. Penetration has been attained to 20,000 feet.

Implosion source

Hydro-Sein. A nonexplosive energy source, Hydro-Sein, has been very recently developed by Marine Geophysical Services Corp. It is an adaptation of the General Dynamic high-velocity actuator as an acoustical source for water exploration. It utilizes a high-pressure air-driven piston as a power source. About 350,000 pounds of compressed air pressure force the piston, piston rod and one metal plate to move about 12 inches in less than 40 ms. This creates a massive cavitation between the two plates of the system. An implosion results as water rushes into the void. Since no explosion or combustion is involved, there is no gaseous residue to create a secondary pulse or 'bubble effect'. Each of the piston arrangements weighs about 8000 pounds, two being used in synchronization during a survey. Impulses are repeatable at intervals of 10 seconds or less. It can operate in shallow or deep water. Reflections from over 4 seconds in depth have been observed.

Explosive Source

Flexotir. The only repetitive type source using explosives is Flexotir developed by Compagnie Générale de Géophysique. The explosive charge is detonated in the centre of a steel sphere specially adapted to the weight of the charge and the average depth of the explosion. The normal sphere is about 2 feet in diameter and is perforated with many small holes. The end result is to cancel any bubble effect and to allow deep shooting (40 feet). This depth permits small charges to be used. Firing rate is claimed to be as much as one every 18 seconds. The device can be used with single trace or 24 trace streamers of hydrophones. The company claims that good records have been procured with data from 3 seconds two-way travel time.

Electrohydraulic sources

Vibroseis. Vibroseis was developed originally by the Continental Oil Company and the first full-scale application of the system to marine exploration was carried out by that company during the summer and fall of 1965. The unit was originally designed as a repetitive source for land operations. Several marine seismic contractors have been licensed to use the system now. The principle of the Vibroseis system is to search the record for the precisely known unique transmitted signal by cross-correlation techniques. The system is shown in operational mode in Figure 19. It is a proven nonexplosive repetitive source that may be used in multiple units, two over each side of a ship excited in synchronization. As with other repetitive sources the amplifiers in



Figure 19. Marine Vibroseis (trademark, Continental Oil Company) (courtesy Ray Geophysical Mandrel).

this system are much simpler than those in conventional instruments in that they have no low-cut filtering, no AGC and no suppression. The record cycle is started at the beginning of the sweep transmission with an energy input sweep every 13 seconds. Horizontally travelling signals are poor with the vibroseis method because of recording during the vibration of the 7 second sweep. These horizontal arrivals are minimized by offset distance, geophone patterns and vibrator patterns. Because of this the Vibroseis record does not normally show strong 'first breaks'. The signal which is used to introduce a band of frequencies consecutively into the transmitting medium is a simple sweep, typically from 15 to 90 cycles per second and of about 7 seconds duration. Nowhere does any part of the signal repeat itself. The vibration units are slaved to the master control signal transmitted from the recording unit; this assures that all units are operating in phase with one another permitting several to be used at the same time. It has been claimed that penetration has been achieved to 20,000 feet or more with this system.

Dyna-Pulse. This system was developed by Globe Exploration Company Inc. and is a means of transforming electrical energy into mechanical energy without the usual conventional intermediate links. Electrical energy is stored in capacitors at high voltage and is discharged between a pair of electrodes under the surface of a liquid medium causing a channel or bubble of hot, highly ionized gaseous plasma. This bubble of plasma tends to expand but the high incompressibility of the surrounding liquid medium resists expansion resulting in an extremely high plasma pressure. The pressure at the plasma-liquid interface begins to be relieved by an intense pressure wave and outward motion of the liquid medium resulting in a shock wave. The system may be used with the usual analog or digital recording equipment. Four units may be used in synchronization to optimize the enhancement of the useful seismic signals recorded. The system has been used to obtain analog records of good resolution at depths to 30,000 feet.

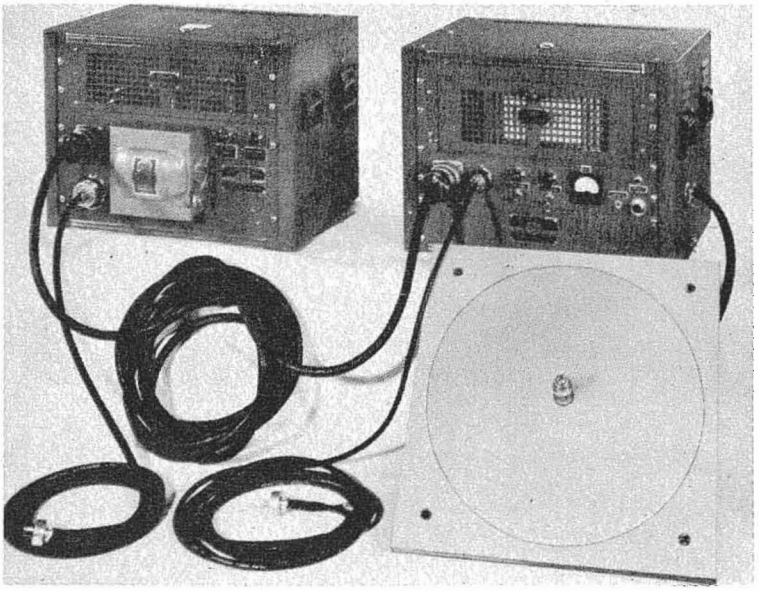


Figure 20. Surface sonar boomer EG & G model 230 with power supply and capacitor bank (courtesy EG & G International Inc.).

Electromagnetic sources

EG & G Boomer. The boomer sonar source has been developed by EG & G International Inc. and was originally described by Edgerton and Hayward (1964). The boomer has a lower frequency spectrum than spark sources. The boomer sound source is a transducer which is essentially a flat encapsulated copper coil sandwiched between spring-loaded aluminum plates. The plates are repelled from the coil with explosive force when stored electrical energy from the capacitor banks is discharged through the coil. The sudden movement of the plates against the water produces a repeatable and spherical pressure pulse which has significant output components in the range of 30 to 1000 cycles per second. The hardware of the system is shown in Figure 20. It is possible to obtain models of this system with electrical input energy to the transducer of 14,000 watt seconds. Reflection penetration of 2000 to 3000 feet have been obtained in water depths of 18,000 feet using the 5000 watt second system.

EG & G also has a high-resolution boomer seismic profiling system with a ten-element linear array hydrophone eel. The key element in this new high-resolution technique is a method whereby the cavitations in the water of the boomer transducer have been virtually eliminated. The result is that the sound source emits clear, discrete acoustic pulses without the undesired noise generation and record interference normally introduced by transducer cavitation. In the past this cavitation 'noise' picked up by the profiler's receiving system, tended to mask or hide the first

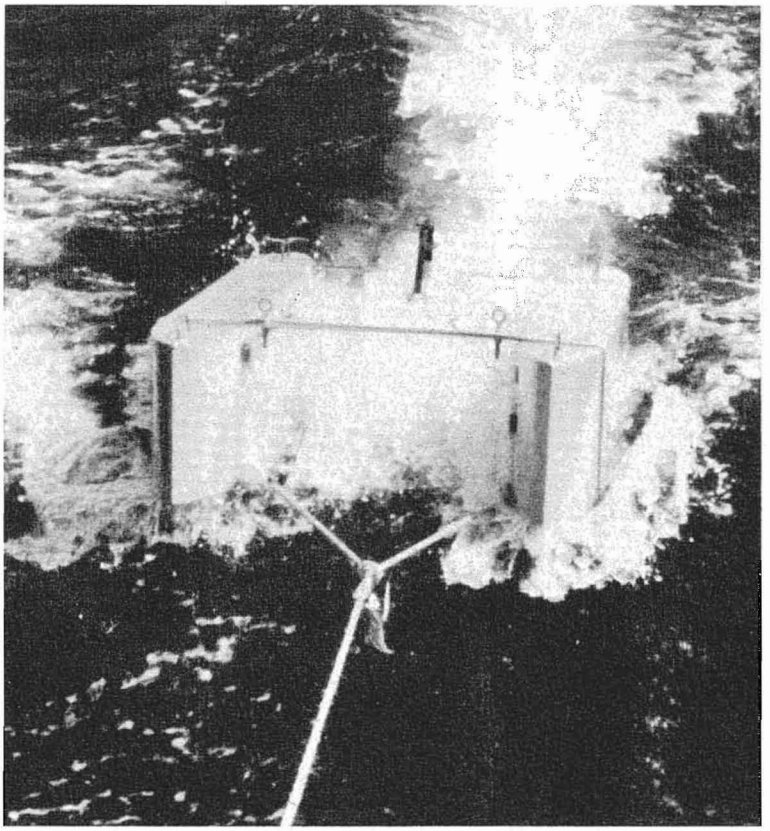


Figure 21. High-resolution boomer transducer on catamaran (courtesy EG & G International Inc.).

15 to 30 feet of the sub-bottom profile on the record. Characteristically, the details of the sub-bottom's near-surface sediment layers were lost when deep penetration seismic profiling was conducted. Previously two systems were required, one for deep penetration and another for resolution of near-surface sediment layers. This new system is claimed to give the complete picture. Recent tests with this system against the conventional EG & G boomer system have been highly satisfactory. This equipment is good for very shallow definitions and depth to 250 to 400 feet. The high-resolution boomer is shown in tow mounted on a catamaran in Figure 21. A typical record recorded through this equipment is shown in Figure 22, obtained during a survey in Lake Ontario for the Geological Survey of Canada.

Transit sonar, echo sounders. In these systems the acoustic pulses are directed from near-surface in either a vertical pattern or in a slant pattern. The pulses impinge on any objects lying on the bottom and their reflections are deflected and recorded.

King (1967) has made very good use of a conventional echo sounder, Kelvin Hughes model 26 B Navigation Echo Sounder, to delineate sedimentary boundaries and identify those sediments. This instrument emits a signal with a dominant frequency component of 14.25 kc/s and a pulse length of less than 1 ms. Echogram classification is based upon the shape of the surface of the bottom, and the relative degree of compaction of the bottom sediments, as interpreted from the depth to which sound penetrates the bottom. The relative degree of compaction is to a large extent a function of the clay content. At least 40 metres penetration through soft uncompacted bottom sediments has been achieved. The echo sounder must be properly tuned since the use of excessive gain increases penetration but results in a loss in resolution. King has found it possible off the Nova Scotia coast to distinguish and delineate sand and gravel facies, sand facies, silt facies, clay facies and glacial till.

EG & G has developed a side-scanning sonar system which has had considerable success in delineating the extent of sand deposits and other geological formations. The transducer in the towed fish emits simultaneous, fan-shaped acoustic beams from both sides perpendicular to the direction of travel. The beams have a frequency of 260 kHz and are approximately 1 degree wide in the horizontal plane and broad enough in the vertical plane to cover the bottom from directly below the towing vessel out to the full system range. Normal towing speed is 3 to 6 knots.

Haslett and Honnor (1966) describe the simultaneous use of sideways-looking sonar, a strata recorder and echo sounder and suggest that all three should be used simultaneously from the one vessel.

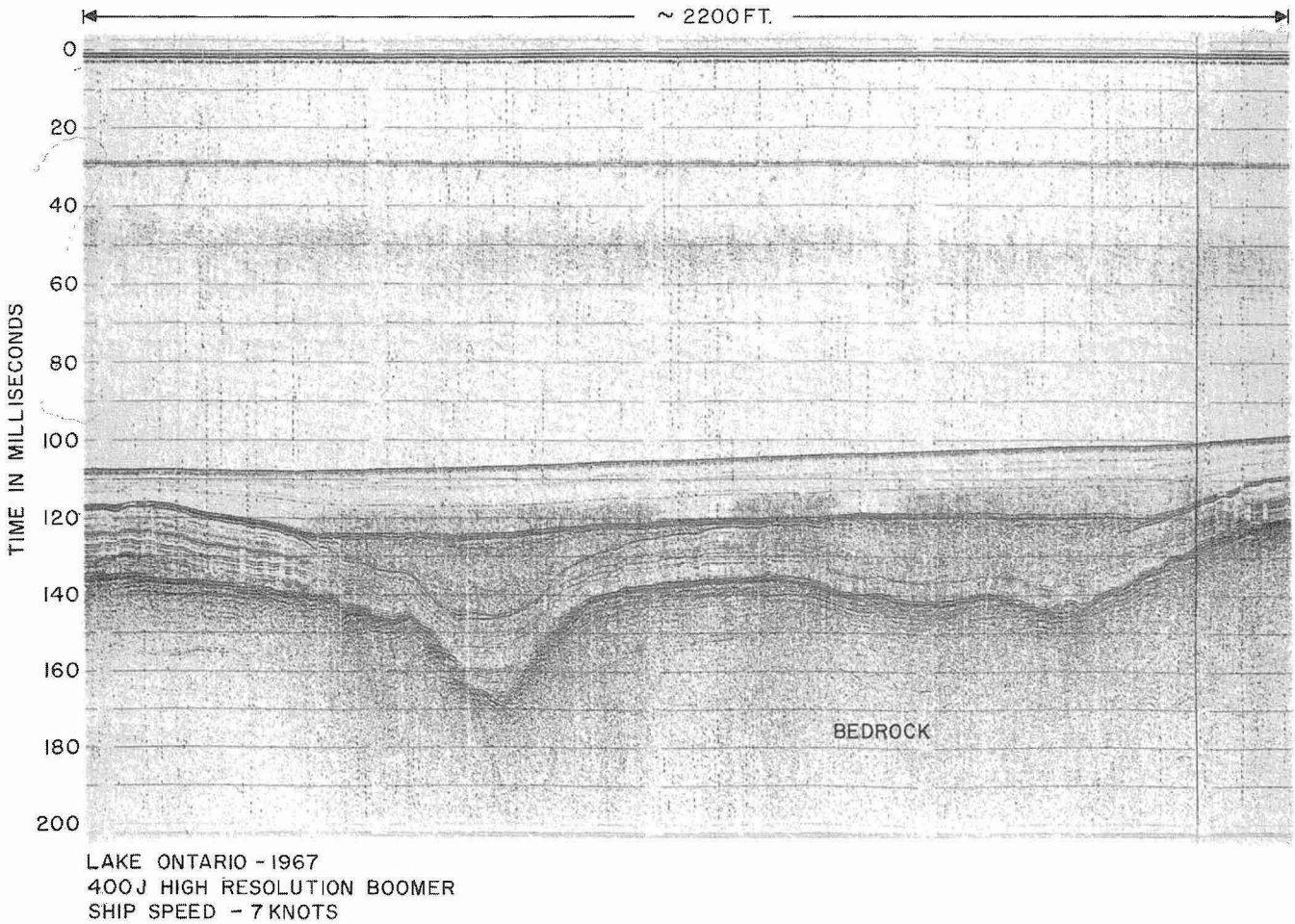


Figure 22. Typical high-resolution Boomer record from Lake Ontario.

Contents

An Ocean Bottom Scanning Sonar (OBSS) has been developed by Western Geophysical Division of Litton Industries. An array of transducers along each side of the OBSS fish radiates an intense narrow (1/2°) beam of high-frequency acoustic waves (150 to 160 kc/s). Reflections from the bottom and sub-bottom are recorded as a line of varying intensity. Two scales are available to cover 2460 feet or 416 feet of ocean bottom. The former scale may be useful in mapping larger geological features while the latter scale being somewhat limited in scope, may be useful in finding ocean-bottom mineral deposits. The manufacturers of the equipment require 30 feet of water for operation and claim that gravel and sand deposits can be readily distinguished. The OBSS is shown in Figure 23.

Self-adjusting filters. Hutchins (1965), and Meyerhoff (1966) have described a linear filtering network composed of a set of band-pass sections with variable parameters which are automatically adjusted to optimum settings for use in marine seismic equipment. Since the spectral content of signals arriving at later times following the initiation of a pulse is different from early arrivals, the filter can only be optimum over a small interval. The automatic setting operation of the parameters occurs over a time interval which can be controlled by the operator. Strobe marks are positioned over a certain time interval to bracket the part of the record of main interest. The self-adjusting action which sets the parameters of the filter to their optimum value only operates during a short time interval at the predetermined time following a transmission. The filter operates in real time. It is expected that the self-adjusting filter system will reduce the effect of multiple reflections and reduce other noncorrelated noise. A receiving filter will always be matched to the medium and to the transmitted signal making it possible to automatically provide a matched filter for the transmitted signal having a pulse shape that is subject to continuous adjustment. By this means, an operator can match the transmitted signal to the medium as well, to bring out the class of geological detail with which the survey is particularly concerned.

Airborne techniques. Barringer Research Limited has exploited and modified an acoustic echo sounder developed and patented by Mr. Courtland B. Converse which can be used from a fixed-wing aircraft. It has been operated in a sonar system configuration as a means of profiling the water-sediment interface. A probe with a transducer on the end of a flexible line attached to a winch in the aircraft is the basis of the system. This system is in the research and experimental stages but does appear to have potential as a shallow prospecting tool.

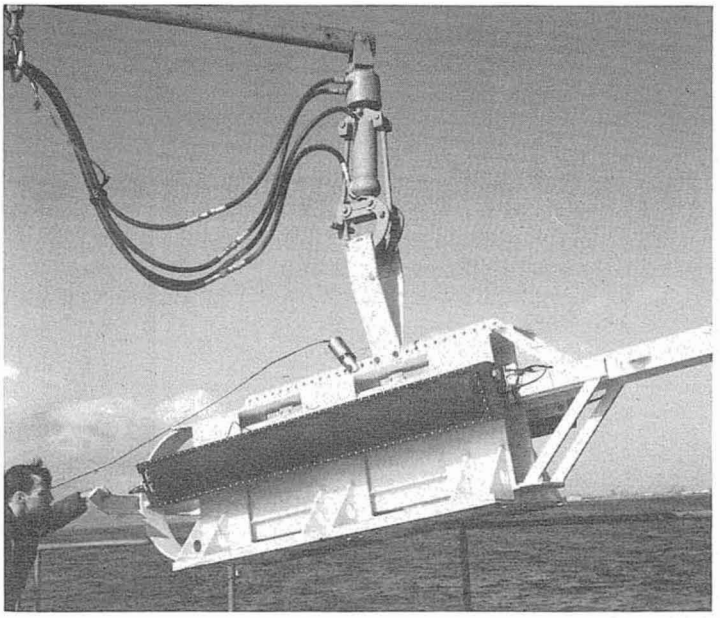


Figure 23. An Ocean Bottom Scanning Sonar (OBSS) (courtesy Western Geophysical Division of Litton Industries).

Repetitive land sources — a summary

A summary of repetitive land sources is included in this paper since such sources could be used in mineral prospecting. However, their weight, bulkiness and high cost do not lend their application to fast economical prospecting for minerals or ground water in the shallower horizons. However since seismic techniques can be used to explore for minerals at great depths, the systems will be described briefly.

These surface sources minimize surface damage and disturbance and allow seismic surveys to be conducted in industrial and urban areas where shot holes and dynamite are not permitted. Also these sources have extensive use in areas where it is next to impossible to drill a shot hole, whether because of near-surface conditions or inaccessibility. Johnson (1967) has provided the most recent survey of surface sources of seismic energy.

The history of repetitive-type seismic sources is traced back to Hubert (1925), and McCollum at about the same time. These men reported on perhaps the earliest experimental studies of the generation of seismic waves by dropping weights. In recent years magnetic recording techniques have provided efficient means to procure seismic records routinely from weight drops along continuous traverses. Domenico (1958) describes some experiments in the field in the generation of seismic waves by dropping of weights. In the early days masses of 3 tons or more were

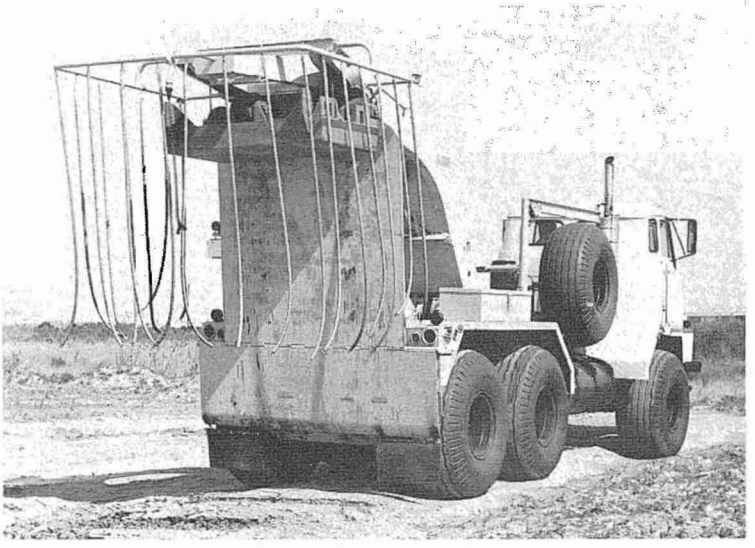


Figure 24. Geograph Thumper (trademark Mandrel Industries) (courtesy Ray Geophysical Mandrel).

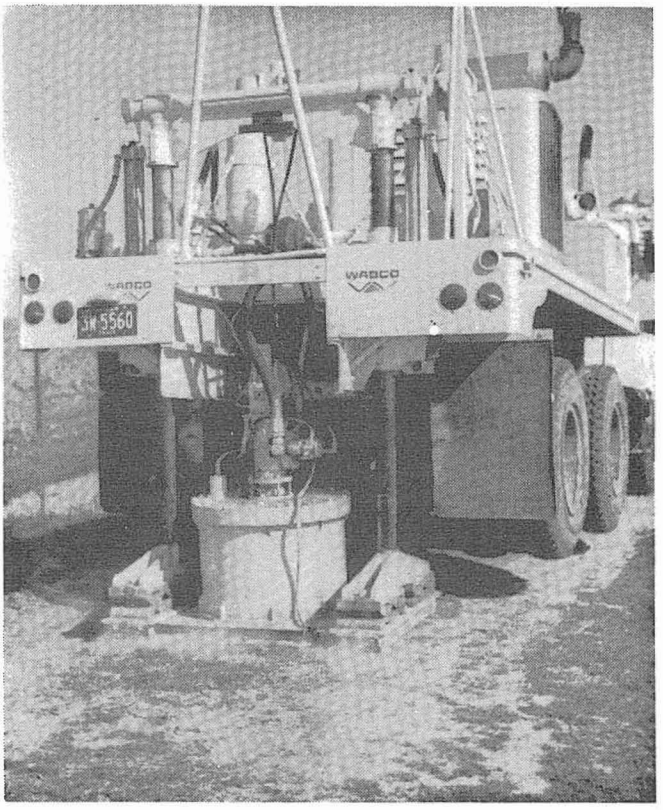


Figure 25. Vibroseis system (trademark Continental Oil Company) (courtesy Ray Geophysical Mandrel).

dropped from heights of about 10 feet. Experiments have even been conducted dropping concrete balls from a helicopter; this experiment was called off when the observers lost sight of the weights after release from the helicopter. The Geograph Thumper was first used by McCollum in 1952 with magnetic tape recorders; a recent model is shown in Figure 24. The advent of magnetic tape recorders at this time helped make possible the stacking or integration of a series of pulses.

Neitzel (1958) reported on some field experiments using a dropped weight source and concluded that the efficiency of the weight dropped was approximately 100 times the efficiency of a dynamite shot. This observation was based upon the amplitudes of reflected arrivals but was somewhat inconsistent as reported by Neitzel.

About 1952 Continental Oil Company developed the Vibroseis system, a device using a vibrator and controlled-frequency wave trains. The first models used a mechanical vibrator while the later models utilize a servohydraulic system. A land Vibroseis system is shown in Figure 25. The system has been licensed to several seismic contractors and is used widely throughout the world. The vibrating system is pressed down against the earth surface to put energy into the ground over a 7 second interval. Recording is carried out simultaneously with this sweep over a selectable vibratory frequency range and for about 6 seconds thereafter. The reflected energy is then stacked into a single pulse through a computer correlating the recorded record with the reference sweep. A radio signal from the field recording unit is used to control the vibrator to ensure that the input signal being introduced into the earth is an exact duplication of the master synchronizing signal as well as insuring precise in-phase matching of the vibrators operating simultaneously. As many as four vibratory sources may be mounted on trucks and used simul-



Figure 26. Dyna-Pulse (courtesy Globe Exploration Company Inc.).

Contents



Figure 27. Dinoseis mounted on a LeTourneau (trademark Sinclair Oil Company) (courtesy Sinclair Oil Company).

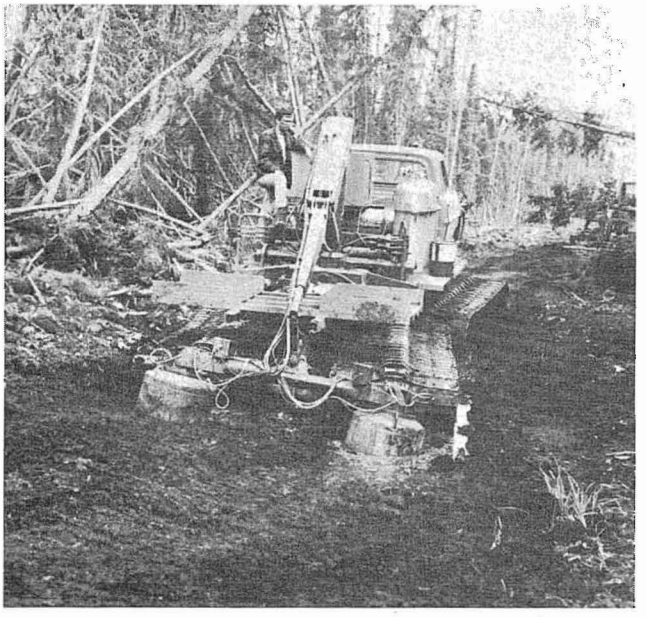


Figure 28. Dinoseis in muskeg operation (trademark Sinclair Oil Company) (courtesy Sinclair Oil Company).

taneously. As mentioned above, Vibroseis records do not normally show strong 'first breaks' but neither would conventional records shot with the same source and spread geometry that is used with the Vibroseis system. The present-day systems are hydraulically operated transducers, the electromagnetic transducers having historical interest only to the petroleum industry. However, these electromagnetic transducers may be of use to a system for shallow work such as prospecting for groundwater or shallow deposit minerals.

Rogacord is a vibratory system developed by General Atomics Corporation and Rogers Explorations Inc. This system uses a linear array of ten or twelve small hydraulic vibrators secured to the ground with expansion packers in shallow drill holes. This system has not been used widely.

Since 1960 a new type of surface source has been developed in which the surface of the earth is impacted at a high terminal velocity. The frequency spectrum so produced is approximately that produced by explosives. Imperial Industries developed a system known as ISD (Impact Seismic Device). This system consists of a 750-pound hammer driven by a heavy coil spring to impact with a coupler plate on the ground. United Geophysical Company has also developed a similar device in which compressed air is used to drive a free piston inside a cylinder against an anvil on the ground. The kinetic energy of this latter system is about 70,000 ft lb.

Seiscor, a division of Seismograph Service Corporation, offers both servohydraulic and electromagnetic vibratory systems for contract which are similar to Vibroseis. The electromagnetic system is described as having only about 37% of the output of the hydraulic system.

In 1965 Alpine Geophysical Associates introduced to seismic prospecting a high-energy seismic shock actuator known as Terrapak which was an adaptation of the high-velocity actuator developed by General Dynamics Corporation. The shock of energy is imparted to the earth's surface by means of a pneumatic-hydraulic actuator. The actuator is powered by a self-contained supply of compressed air acting on a piston integral with a massive impact hammer. When the hammer is triggered, the actuator uses the stored energy as air compressed to 2000 pounds per square inch to impact the hammer mass upon the earth's surface. The force considerably exceeds 100,000 ft lb of energy. The nominal workable output of 85,000 ft lb may be expressed in joules as 115,260. The velocity of the mass striking the ground can be varied by changing the mass of the hammer or by changing the air pressure.

A more recent system is Dyna-Pulse. The operation of this system has been described above wherein energy is released rapidly in a liquid medium and directed to a work space coupled with the earth. The resulting electrohydraulic effect produces a shock wave within the liquid. The signal is reproducible at 12-second intervals. The normal capacitor bank of 60,000 joules provides the discharge of electrical energy. Figure 26 shows the Dyna-Pulse system mounted on a truck.

In 1962 Sinclair Oil Company developed Dinoseis, Figures 27 and 28. This contained gas-exploder source is mounted on a converted LeTourneau or Euclid bucket or on a tracked or wheeled vehicle. The explosion is a mixture of propane and oxygen and is contained within an expandable cylinder rather than the explosive gases contacting the earth directly. Multiple units can be fired in unison with less than 1 ms time lag. The bottom plate of the chamber is free to move with respect to the mass above. The bottom plate weighs about 500 pounds and responds quickly to the explosive shock transferring approximately 100,000 ft lb of energy to the earth. Once again this source reduces surface damage and eliminates the need of shot holes and explosives.

One new explosive source has been developed recently by Imperial Chemical Industries Limited. This explosive is known as Geoflex. Two strands of linear explosive Geoflex (similar to Primacord) are buried simultaneously to a depth of about 18 inches by a two-bottom plough attached to a farm tractor. It has been put to good use in desert areas. The company claims that its advantage over other surface sources is the elimination of the need for stacking records. The author does not know whether the material is fired in patterns or how long a piece of the material is fired at one time. Presumably the material is used for reflection prospecting.

Approximate equipment costs

Some of the highly portable refraction seismographs utilizing a hammer as a source of energy can be purchased for under $3000 Canadian funds. The Huntec model FS-3 sells for about $4000. The smaller portable instruments that require cables and twelve geophones cost about $7000. A complete set of digital instruments starts at a minimum basic price of $120,000 plus truck and playback facilities. For the smaller instruments, $1000 is sufficient to provide a complete set of spare parts in case of breakdown in the field. In addition to these costs one must supply a source, be it a sledge hammer and steel plate or explosives or a repetitive source mounted on a truck or boat. These are representative of the cost of some of the instruments described above and complete information must of necessity be obtained from the manufacturer.

Limitations of the seismic method

Seismic techniques harbour a number of dangers, ignorance of which may lead to disappointing results. These limitations should be kept in mind and properly evaluated for every project undertaken. A geophysicist should never undertake a project or sell his services without advising his fellow scientists or his client of the limitations of the method. The seismic method is not the panacea to all geological problems but it does give a view into the third dimension which can assist the geologist or prospector.

There are problems associated with the incompetent materials comprising the very loose soil immediately below the ground surface. Longitudinal seismic waves in the uppermost layers frequently travel with a velocity which is less than that of the air wave. Mooney and Kaasa (1962) have discussed air waves and the problems presented to an interpretation by these arrivals. The velocity of seismic waves in the near-surface layers may be as low as 300 feet per second while the velocity of the air wave is approximately 1100 feet per second. Depth calculations then can be highly erroneous and misleading if the air wave only is recorded. In all cases an attempt must be made to record the velocity of the seismic energy through the surficial materials and not the velocity of the air wave which is rather easily recorded.

Seismic layers do not necessarily conform to geologic strata. A clay layer may overlie weathered shale bedrock or compacted till overlie weathered limestone bedrock. In such cases the velocity interface detected will not be the top of the bedrock but an acoustic boundary beneath the weathered layer and some several feet below the bedrock surface. Once again it is pointed up that seismic results must be correlated with drilling logs and geologists must be consulted before an interpretation can be made.

The blind zone is a layer which has a velocity lower than that of the layer above. Such a layer is not detectable by seismic refraction energy because it is refracted downwards and never at a critical angle on the interface between the two media. Refracted energy never returns from the upper surface of a lower-velocity medium. Ignorance of the existence of such a layer leads to a computation of depth which is much too great to the next higher velocity layer. Hawkins and Maggs (1961) have devised nomograms applicable to the blind zone problem. Once again drill holes are required to correlate seismic interpretation with geological strata.

Hidden layers also can be a problem to seismic interpretation. The seismic refraction technique is based upon the fact that deeper layers have increasingly higher velocities and also increasingly greater thickness. In a three-layer case, if the thickness of the second layer is small compared to the total thickness and if V_3 is very much greater than V_2 then the refracted wave into the third layer, travelling at higher velocity, may overtake the first arrivals from the second layer and arrive before them at the geophone site. Soske (1959) discusses this problem. Within the instruments that utilize galvanometers the arrival of energy from this hidden layer may be masked out by the trailing effects of the arrivals of first energy on the galvanometers. In most hammer seismographs the second layer is not detected at all. However, the facsimile recording method of the Huntec model FS-3 does permit the recording of a hidden layer. The presence of this second layer is often detectable by a definite lineup of second arrivals with an obviously different slope to those of the first or third arrivals. This has been the experience of the Geological Survey of Canada in some recent work near Welland, Ontario, where the blind zone was most obvious on the facsimile records of the FS-3 recorder (Figure 29). To ignore the hidden layer leads to serious errors in depth computations to underlying layers. Existence of the problem should be suspected by the geophysicist when either a second layer which has been positively identified along the traverse thins out and vanishes from the record, or drilling or geological information confirms the presence of such a layer and the computed thickness of seismically detected strata is continually less than the thickness known from geologic or drilling information. In many cases the hidden layer is still present but is too thin to refract and transmit energy, or velocity conditions are such as to hide it. It is a situation that cannot be ignored for a proper interpretation.

The advantages of the reflection technique over refraction shooting have been set out earlier in this paper. However it must be pointed out at this point that reflection techniques are not prejudiced by velocity inversions in the subsurface and that the energy requirements are much less than for refraction profiles.

Contents

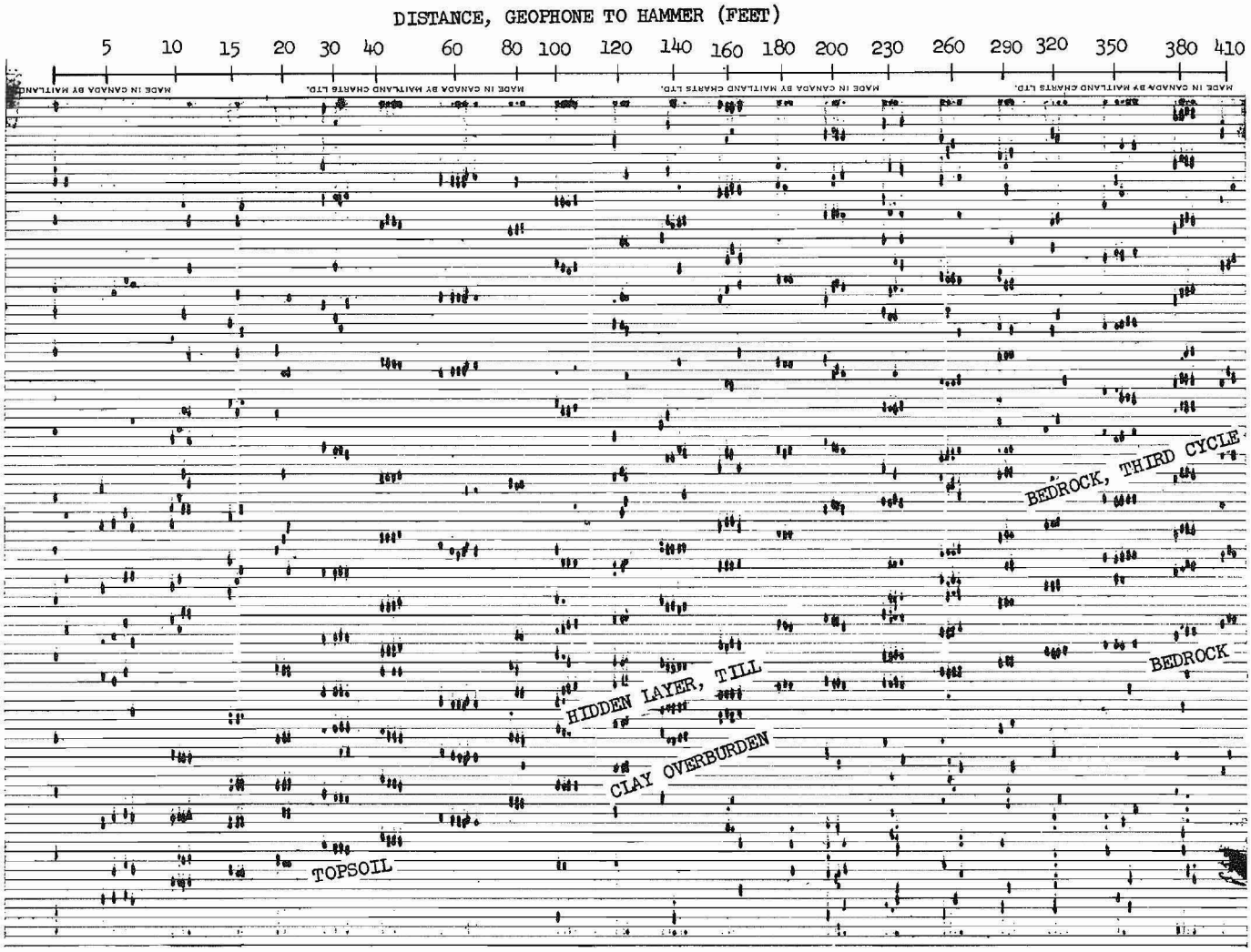


Figure 29. Typical FS-3 seismograph record showing hidden layer.

Reflection profiling in permafrosted areas is not affected by the permafrost whereas refraction techniques can be nullified completely. The permafrost presents to the seismologist a high-velocity surface layer which is not generally amenable to refraction techniques.

Coverage or field progress

One complete refraction profile using portable hammer seismic equipment can be completed in about 20 minutes. Difficult terrain or exceptionally long profiles may require as much as 1 hour. It is quite possible in a normal working day to complete fifteen or twenty locations. As many as 43 locations per day have been completed over 50 feet of overburden in the Moncton, New Brunswick, area (Hobson and Carr, 1968). The Red River floodway around the city of Winnipeg, Manitoba, required 40 working days for a two-man hammer crew to complete the 33 miles of coverage with seismic control every 600 feet. This figure includes interpretation, surveying, etc. (Hobson, *et al.*, 1964).

Some surveys require reversed refraction profiles while others can be satisfied with single-ended profiles. The reversed refraction profile yields continuous subsurface sections of layers of distinct and increasing velocity. It is possible as described under 'Refraction Methods' to compute the depth under every hammer station if a hammer is used as a source with a single-channel instrument. Similar computations can be made under every geophone if a multiple trace instrument is used.

Reflection seismic surveys using single-channel equipment can be conducted at a rate of 15 to 20 locations per working hour. If spacing between observations is 100 feet, then 120 to 160 stations may be completed in a day, which is 12,000 or 16,000 feet of coverage. If the separation is decreased to 50 feet or 20 feet, then the coverage per day is proportionally decreased. If the operations are conducted in the bush or muskeg-covered areas it may be possible to complete only ten locations per hour or eighty per day or approximately 8000 feet of coverage. If twelve-trace equipment is used in conjunction with explosives or hammer, be the instruments conventional or Polaroid, approximately one half hour is required for each spread.

It must be pointed out that these figures for the average coverage attained in a day depend on surface conditions and the ability of the personnel.

Accuracies and errors.

Shallow-refraction seismic methods yield results that are generally considered to be accurate to ± 10%. This accuracy may be as much as 20% or even more in error but many times it is around 1% or 2%. The accuracy is determined of course by having drill-hole control for bedrock and for overburden correlation with seismic velocity.

There are many factors which will contribute errors to the interpretation of seismic data. The interpreter must be continually aware of the accuracy of his velocities. It has been pointed out that air waves can be recorded over almost every profile but give erroneous calculations. Velocity inversions have a serious effect upon refraction computations. Vertical and interval velocities must be determined for accurate interpretation of reflection data. In the marine environment navigational errors can contribute significantly to a poor interpretation of the seismic data. A weathered or fractured bedrock surface will transmit energy very poorly and this layer may be missed completely in the interpretation. In the final analysis the experience of the interpreter is the major factor. Materials with a high velocity may be described as sandstones or shales whereas upon drilling they may be found to be a consolidated till. If reversed profiles are not surveyed, the dip of the subsurface strata may be sufficient to present erroneous velocities to the seismograph. High velocities may be caused by the profile being shot up-dip and conversely low velocities may be due to surveying down-dip.

The distance by which the detectors and energy source are separated is not pertinent to the accuracy of the survey. Refraction profiles have been extended as far as 1000 feet at Amherst, New Brunswick, using a hammer source while on Manitoulin Island, Ontario, a similar source could not be observed beyond 180 feet from the detector. The extent of a refraction profile is determined by the depth of penetration required and by the energy content of the source. Reflection-profiling is concerned mainly with the energy available from the source.

Possible applications

There are many possible applications of the seismic method to mining and groundwater exploration and only a few of them will be presented. It is difficult to organize these applications into any categories of instrumentation or geological situation so that the following list has the appearance of being somewhat random in nature. The seismic method could be applied in the following situations:

- Overburden thickness for diamond-drill hole locations can be determined.

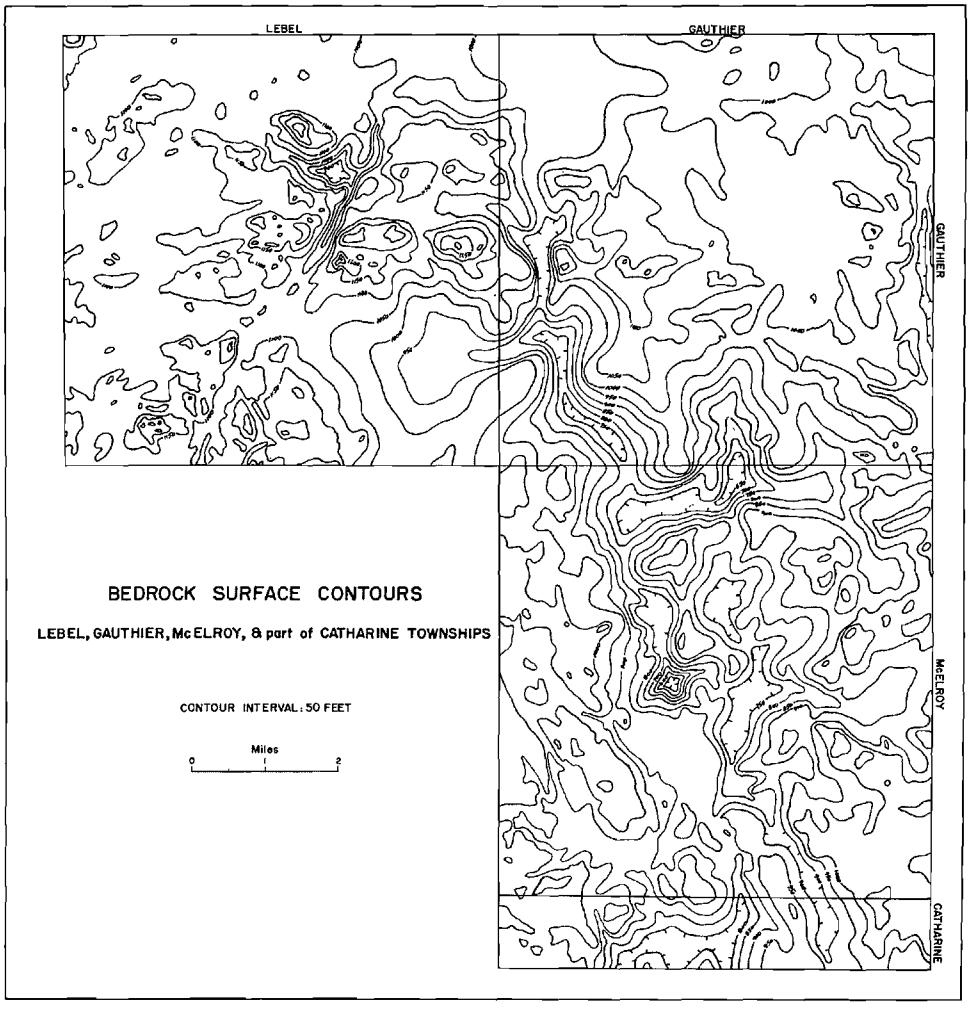


Figure 30. Bedrock channel system, Kirkland Lake area, Ontario.

Contents

- Shallow structural features can be mapped, such as faults which may disappear under overburden or under the waters of a lake. Shear zones and contact zones may be delineated by the method.
- The strike and dip of geological formations may be determined.
- Nonmetallic mineral deposits such as gypsum, limestone and cement may be delineated using refraction methods.

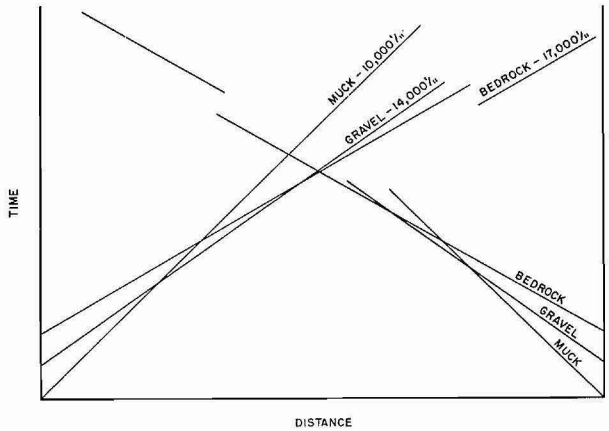
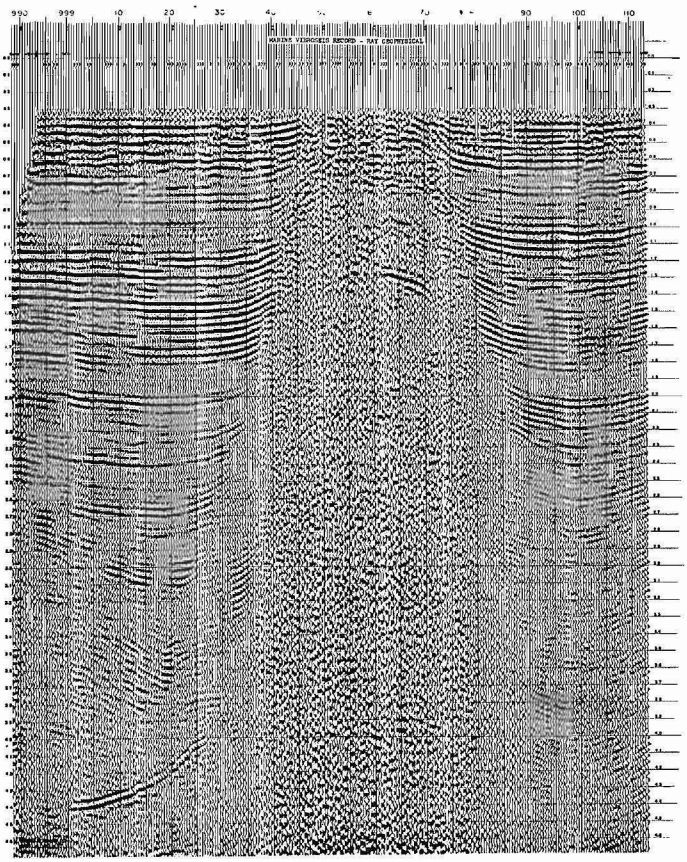


Figure 31. Seismic velocities in a permafrost area, Klondike, Yukon Territories.

Figure 32. Marine vibroseis record over a salt dome, Gulf of Mexico (courtesy Ray Geophysical Mandrel).



- Orebodies, particularly if near to surface, may be delimited if the orebody transmits seismic waves at a velocity appreciably higher or lower than does the surrounding country rock. Elliot (1967) has described such an application using refraction fan shooting.
- Placer deposits may be located in the overburden materials above bedrock by outlining preglacial depressions in the bedrock topography. Such projects have been undertaken in the Yukon (Hobson, 1966), Beauce County and Kirkland Lake (Hobson and Grant, 1964; Hobson and Lee, 1967). A typical bedrock channel system, in which placer deposits may have accumulated is shown in Figure 30.
- The vertical extent of potash deposits in Saskatchewan have been determined by the unique upside-down application of seismic methods by Genzwill (1966).
- Coal deposits have been outlined as well as slumping in the section by Krey (1963) on shore while Maries and Beckmann (1961) have conducted a similar program in the marine environment.
- The technique has been used in the permafrosted areas of the Yukon to outline areas of differential thawing, the knowledge of which has been invaluable to the placer gold mining companies in their thawing operations prior to dredging (Hobson, 1966). Figure 31 shows data from a permafrosted area.
- Overburden thickness in conjunction with anticipated open-pit mining operations can be determined readily by this method.
- The extent of gravel deposits both on shore and off shore particularly in the latter environment are readily identifiable.
- Faults can be readily identified in the marine environment using the repetitive source of energy.
- Igneous intrusions can be delineated both on shore and off shore.
- Salt domes and similar intrusions can be delimited. A marine Vibroseis record over a salt dome is shown in Figure 32.
- Tin deposits have been located and delimited in Thailand (Paterson, 1965).
- The elastic modulae of soils and bedrock *in situ* can be determined with seismic techniques; this may be useful in the locating of a shaft for mines (Hobson and Hunter, 1969).
- Acidic and basic rocks display a particular range of velocities. Some work has been done in the Kirkland Lake, Ontario, area in which the acidic and the basic rocks exhibit a definite range of velocities with an overlap in these velocities. The velocity in basic rocks has been measured in the Muskox intrusion (Hobson and Findlay, 1966).
- Bedrock lithology can be determined on the basis of seismic velocities (Tremblay and Hobson, 1962). An example of such differentiation is shown in Figure 33.
- Interfaces within the Precambrian shield can be detected and perhaps identified to assist the geologist in the solution of structural problems.
- Proterozoic sedimentary basins within the Precambrian shield can be outlined. Such a survey has been carried out using common depth point reflection techniques at Elliot Lake, Ontario, and using refraction profiles over the Athabasca sandstones in northern Saskatchewan.
- Shallow structure can be outlined as at Cobalt, Ontario. Some geologists believe that the silver deposition was controlled by structure in that camp. It is possible in that area by

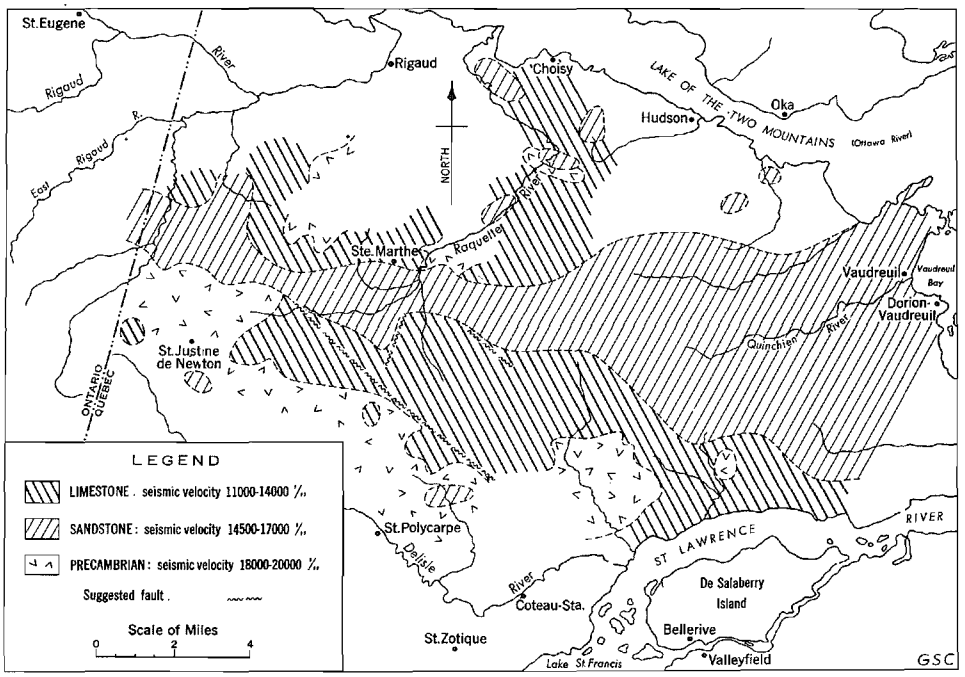


Figure 33. Bedrock lithology differentiated on the basis of seismic velocities, Vaudreuil area, Quebec.

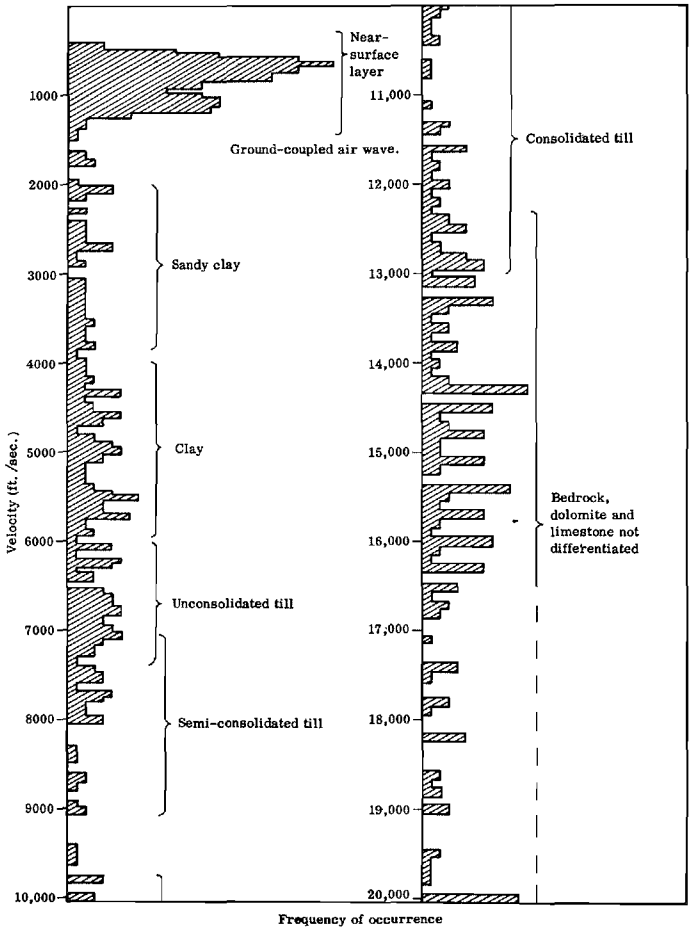


Figure 34. Histogram of velocity vs. occurrence with velocity correlated to Pleistocene materials, Red River Floodway, Winnipeg, Manitoba.

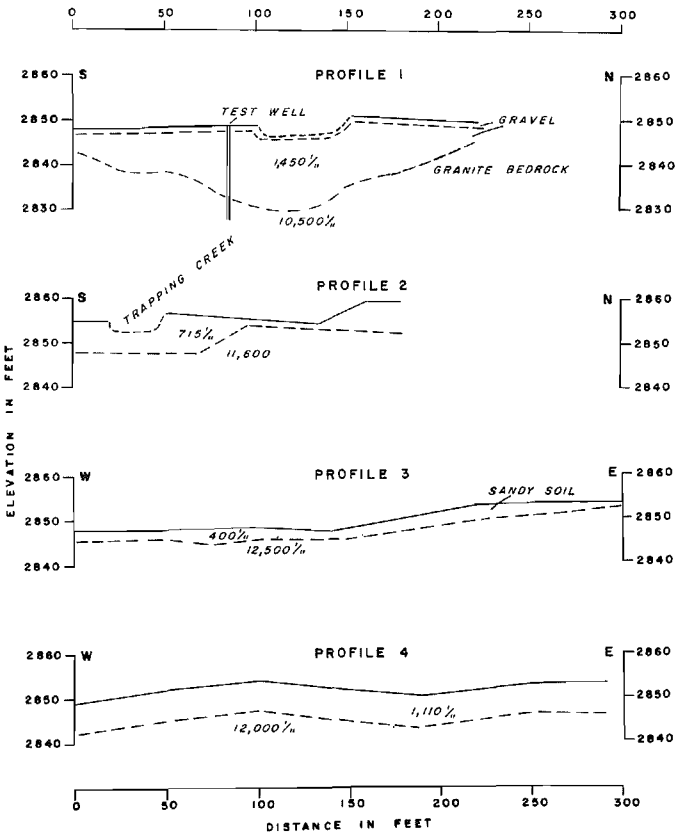


Figure 35. Results of a hammer seismic survey within a limited drainage basin, Trapping Creek, British Columbia.

Contents

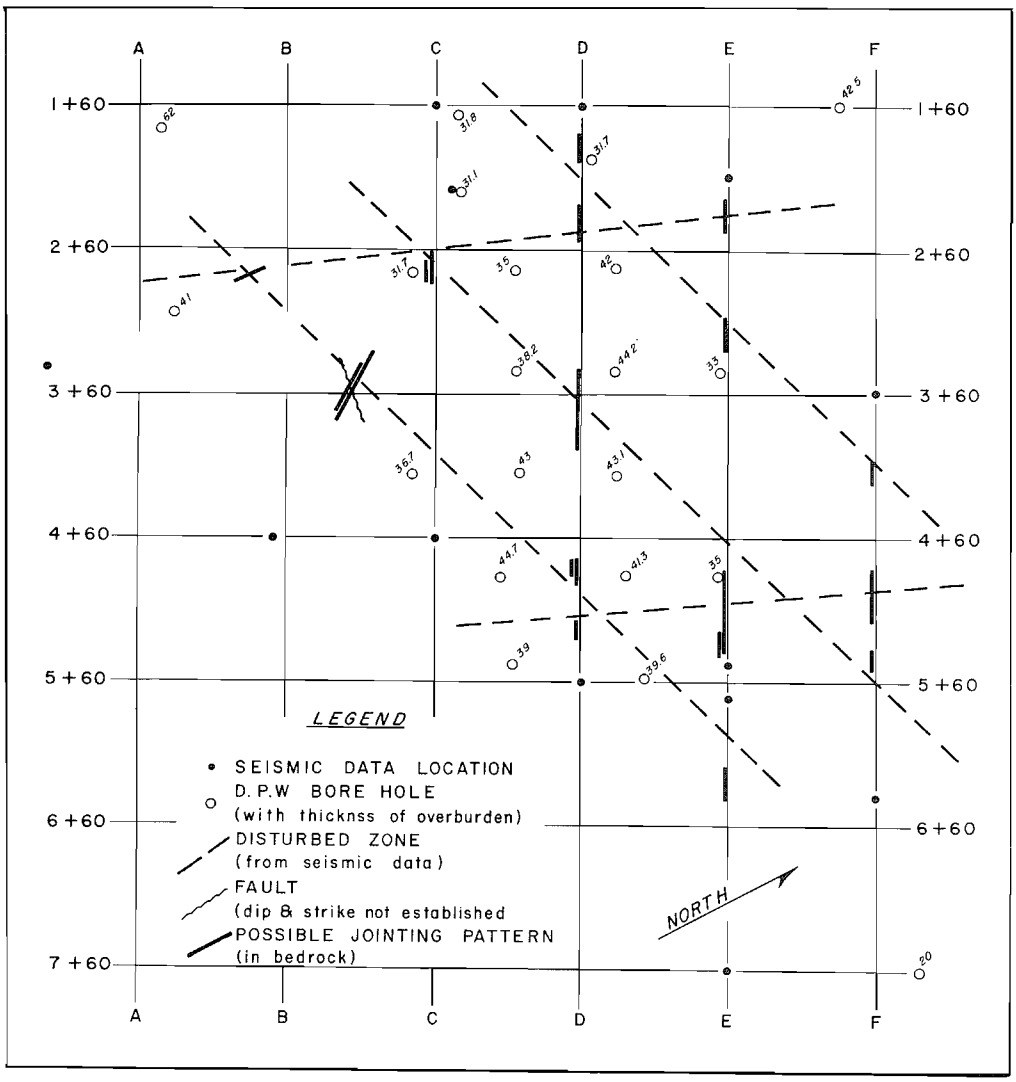


Figure 36. Fault and block pattern outlined in limestone bedrock suitable as an aquifer.

shallow-reflection techniques to define the interface between the Cobalt conglomerate and Keewatin rocks or the Nipissing diabase but the interface between the Keewatin and Nipissing diabase is not detectable.

- A continuous reflection line across the boundary between two geological provinces may cast some light on geological structure, which may define major mineralized belts within the shield.
- The seismic method has been used in a new biogeochemical-prospecting technique to determine the thickness of the overburden and the type of pleistocene material overlying a known mineral deposit (Hobson, 1967).

Similar applications are suggested to the solution of groundwater problems. Several geophysicists have published on the application of seismic methods to groundwater problems, for example Lennox and Carlson (1967), Warrick and Winslow (1960). Geophysical techniques can be used in groundwater exploration for the detection of groundwater itself, for the detection of potential aquifers and for the detection of geological situations favourable for the occurrence of aquifers. Buried preglacial valleys commonly contain deposits of permeable sand and gravels of sufficient thickness and extent to constitute important aquifers. A detailed knowledge of the configuration of buried valleys is often useful to interpret the glacial history of a region. However success in delineating aquifers depends greatly on advanced knowledge of velocity conditions in the surficial materials and in the uppermost bedrock layers. Without this knowledge it is difficult to understand and deal with the interpretative problems presented by a lack of velocity contrasts in drift and bedrock materials present in many regions.

Some of the possible applications of the seismic method to groundwater exploration are as follows:

- Pleistocene materials may be differentiated upon the basis of seismic velocities. Sand, gravel, clay and till can be differentiated by correlating materials with seismic velocities, as is shown in Figure 34.
- Drainage basins in the sedimentary or Precambrian areas can be defined. The reservoir and recharge characteristics of the basin can be set out more definitely by the hydrogeologist if he is aware of the type of Pleistocene materials within the basin and the bedrock topography. The results of an investigation of a small drainage basin are shown in Figure 35.

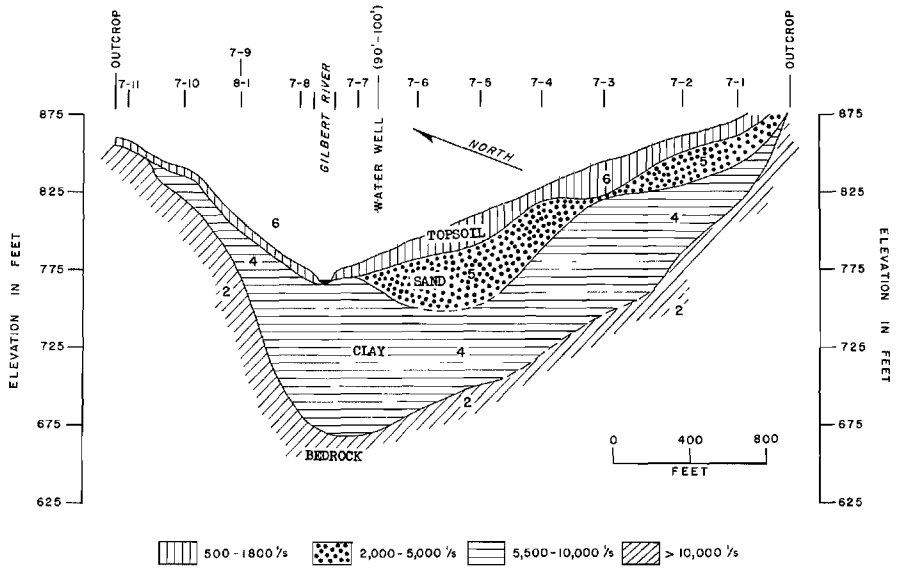


Figure 37. Bedrock depression infilled with clay and a sand aquifer, Beauce County, Quebec.

- Glaciers can be investigated by the reflection technique as part of the water inventory of the country.
- The water-table and areal extent of some aquifers can be determined by seismic methods. This is of importance in drainage basin studies and on construction sites.
- Shear waves may be used to determine the depth of the water-table. Meidav (1965, 1967), Paterson and Meidav (1965), and Whitcomb (1966) have conducted experiments which are directly applicable to this type of study. At a certain depth over a refraction seismic profile the longitudinal-wave velocity may increase but there will be no change in the shear-wave velocity. Paterson and Meidav have concluded that the water-table can be established at that depth.
- A combination of the longitudinal- and shear-wave velocities determined by refraction techniques can also be useful in the classification of materials.
- Aquifers truncated by channels may be delimited. This may be important on the sea coast of a country where an aquifer may be truncated so that there may be infiltration of salt water. This would limit the amount of fresh water that may be withdrawn under normal recharging. Similarly, dredging operations could expose an aquifer to salt water intrusion and so contaminate a fresh water source on shore.
- Fractured granite or limestone may present enough porosity for an aquifer. Fractured granites generally have a seismic velocity less than unfractured granite but greater than glacial till. Seismic methods should be able to determine the thickness of the fractured material and its extent. A fault and block pattern in limestone bedrock is shown in Figure 36; fracture porosity frequently provides accommodation for a good aquifer.
- Water-bearing channels filled with sand or gravel or glacial till may be located. A bedrock channel infilled with clay and a sand aquifer is shown in Figure 37.
- Pervious strata in bedrock may be determined. This may be the delimiting of the weathered surface of the bedrock which is frequently an aquifer.
- Cemented aquifers and impervious strata can be outlined by the seismic method.
- Perched water-tables can be outlined as to extent only. The blind zone beneath the perched water-table presents problems to interpretation of data recorded from underlying strata.
- The amplitude and frequency characteristics of identifiable refraction and reflection events have been studied and the application of seismic methods to delineating aquifers in the prairie regions of western Canada. Uphole wave front surveys indicate a lack of velocity contrasts between overburden and bedrock; in fact bedrock velocity is less than the overburden velocity. There are changes in the character of reflections from horizons within the bedrock as a survey proceeds over a gravel-filled bedrock depression. The seismic tool is not an exploratory tool in this environment but may be used to delineate an aquifer after it has been found (Burke, 1969).

There are no doubt many, many more applications of the seismic method that could be added to these short lists for mining and groundwater exploration. However these suggestions may serve to plant a seed in the mind of some investigator with a problem.

Acknowledgments

I would like to sincerely thank the oil companies, seismic contractors and instrument manufacturers who have supplied photos and brochures of instruments and energy sources. It is a distinct pleasure to acknowledge their cooperation.

References

Beckmann, W.C., A.C. Roberts, and B. Luskin, 1959. Sub-bottom depth recorder. *Geophysics.* 24 (4): 749-760.

Burke, K.B.S., 1969. A seismic study of the surficial deposits in the Stenen area, Saskatchewan. *Geol. Surv. Canada*, Paper 68-60.

Caulfield, D.D., H. Hoskins and R.T. Novak, 1965. Improvements in the continuous seismic profiler. *Geophysics.* 30 (1): 133-138.

Dix, C.H., 1955. Seismic velocities from surface measurements. *Geophysics.* 20 (1): 68-86.

Dobrin, M.B., 1960. *Introduction to geophysical prospecting.* New York, McGraw-Hill Book Co.

Domenico, S.N., 1958. Generation of seismic waves by weight drops. *Geophysics.* 23 (4): 665-683.

Edgerton, H.E., and G.G. Hayward, 1964. The "Boomer" sonar source for seismic profiling. *J. Geophys. Res.* 69 (14): 3033-3042.

Elliot, C.L., 1967. Some applications of seismic refraction techniques in mining exploration. In *Seismic Refraction Prospecting.* Soc. Expl. Geoph. Ed. A.W. Musgrave: 522-538.

Ewing, J., and R. Zaunere, 1964. Seismic profiling with a pneumatic sound source. *J. Geophys. Res.* 69 (22): 4913-4915.

Gardner, L.W., 1946. Vertical velocities from reflection shooting. *Geophysics.* 12 (2): 221-228.

Genzwill, D.J., 1966. An underground application of seismic refraction in a Saskatchewan potash mine. Preprint M-11, presented to 36th annual S.E.G. meeting, Houston, Nov. 1966.

Gough, D.I., 1952. A new instrument for seismic exploration at very short ranges. *Geophysics.* 17 (2): 311-333.

Green, C.H., 1938. Velocity determinations by means of reflection profiles. *Geophysics.* 3 (4): 295-305.

Hagedoorn, J.G., 1959. The plus-minus method of interpreting seismic refraction sections. *Geophys. Prosp.* 7 (2): 158-182.

Haslett, R.W.G., and D. Honnor, 1966. Simultaneous use of sideways-looking sonar, strata recorder and echo sounder. Reprinted from *Proc. IERE Conference on Electronic Engineering in Oceanography,* Southampton, Sept. 1966, Paper no. 7.

Hawkins, L.V., 1961. The reciprocal method of routine seismic refraction investigations. *Geophysics.* 26 (6): 806-819.

Hawkins, L.V., and D. Maggs, 1961. Nomograms for determining maximum errors and limiting conditions in seismic refraction survey with a blind-zone problem. *Geophys. Prosp.* 9 (4): 526-532.

Heiland, C.A., 1940. *Geophysical exploration.* Englewood Cliffs, N.J., Prentice-Hall Inc.

Heiland, C.A., 1948. How can geophysics be of better service to the mining industry. *Geophysics.* 13 (4): 535-539.

Hobson, G.D., 1966. A shallow seismic experiment in permafrost, Klondike area, Yukon Territory. In *Report of Activities.* Geol. Surv. Canada, Paper 66-2: 10-14.

Hobson, G.D., 1967. Shallow seismic investigations used to determine depth of surficial material. In *Progress report on biogeochemical research at the Geological Survey of Canada 1963-1966.* Geol. Surv. Canada, Paper 67-23, part I: 82-83, by J.A.C. Fortescue and E.H.W. Hornbrook.

Hobson, George D., and P.A. Carr, 1968. Hammer seismic survey, Moncton Map-area, New Brunswick. *Geol. Surv. Canada,* Paper 65-43.

Hobson, George D., and D.C. Findlay, 1966. Down-hole geophysical studies on the Muskox intrusion, Coppermine River area, District of Mackenzie. *Geol. Surv. Canada,* Paper 66-44.

Hobson, G.D., and A.C. Grant, 1964. Tracing buried river valleys in the Kirkland Lake area of Ontario with a hammer seismograph. *Can. Min. J.* April: 79-83.

Hobson, George D., and J.A. Hunter, 1969. In situ determination of elastic constants in overburden using a hammer seismograph. *Geoexploration,* in press.

Hobson, G.D., and H.A. Lee, 1967. Thickness of drift, Lebel, Gauthier, Boston and McElroy Townships, Ontario. *Geol. Surv. Canada,* Map 11-1967.

Hobson, G.D., J.S. Scott, and R.O. van Everdingen, 1964. Geotechnical investigations Red River Floodway, Winnipeg, Manitoba. *Geol. Surv. Canada,* paper 64-18.

Hubert, F., 1925. Earth tremors by falling weights. *Zeit. Geophysik.* 1: 197.

Hutchins, R.W., 1965. A self-adjusting filter for seismic signals; presented at *Can. Electronics Conf.,* Oct. 5.

Jakosky, J.J., 1940. *Exploration geophysics.* Los Angeles, Trija Publishing Co.

Johnson, J.F., 1967. Surface sources of seismic energy. Panel discussion No. 6, *7th World Petroleum Congress,* Mexico City, April.

King, L.H., 1967. Use of a conventional echo-sounder and textural analyses in delineating sedimentary facies: Scotian Shelf. *Can. J. Earth Sci.* 4 (4): 691-708.

Knox, W.A., 1958. A slide rule for near-surface refraction problems. *Geophysics.* 23 (1): 154-163.

Krey, T.C., 1963. Channel waves as a tool of applied geophysics in coal mining. *Geophysics.* 28 (5): part I, 701-714.

Lennox, D.H., and V. Carlson, 1967. Geophysical exploration for buried valleys in an area north of Two Hills, Alberta. *Geophysics.* 32 (2): 331-362.

Lyons, P.L., 1952. Nomogram for simple two-layer seismic refraction problem. *Geophysics.* 17 (4): 962-963.

Manfredini, A., 1958. Apparacchiatura sismica per problemi di ingeneria civile. *Bolletino del Servizio Geologica d'Italia.* 78: 495-502.

Maries, A.C., and W.C. Beckmann, 1961. A new geophysical method for the exploration of undersea coalfields. *Inst. Min. Eng.* no. 4, paper 3847: 262-276.

Marr, J.D., and E.F. Zagst, 1967. Exploration horizons from new seismic concepts of CDP and digital processing. *Geophysics.* 32 (2): 207-224.

Mayne, W.H., 1962. Common reflection point horizontal data stacking techniques. *Geophysics.* 27 (6) part II: 927-938.

Mayne, W.H., 1967. Practical considerations in the use of common reflection point techniques. *Geophysics.* 32 (2): 225-229.

Meidav, T., 1960. Nomograms to speed up seismic refraction computations. *Geophysics.* 25 (5): 1035-1053.

Meidav, T., 1965. *Dynamic testing of soil with the seismic method.* Toronto, Huntec Limited, private circulation.

Meidav, T., 1967. *Reflection seismics in engineering geophysics.* Toronto, Huntec Limited, private circulation.

Meidav, T., 1967. Shear wave velocity determination in shallow seismic studies. *Geophysics.* 32 (6): 1041-1046.

Meyerhoff, H.J., 1966. A self-adjusting filter for shallow seismic exploration. *Geophysics.* 31 (2): 340-345.

Millar, R.A., 1965. Hydrosonde – a marine seismic profiler. *Elect. & Comm.* 23-25, 43.

Mooney, H.M., and R.A. Kaasa, 1958. New refraction seismograph. *Rev. of Scient. Inst.* 29: 290-294.

Mooney, H.M., and R.A. Kaasa, 1962. Air waves in engineering seismology *Geophys. Prosp.* 10 (1): 84-92.

Neitzel, E.B., 1958. Seismic reflection records obtained by dropping a weight. *Geophysics.* 23 (1): 58-80.

Nettleton, L.L., 1940. *Geophysical prospecting for oil.* New York, McGraw-Hill.

Pakiser, L.C., and R.A. Black, 1957. Exploring for ancient channels with the refraction seismograph. *Geophysics.* 22 (1): 32-47.

Pakiser, L.C., and R.E. Warrick, 1956. A preliminary evaluation of the shallow reflection seismograph. *Geophysics.* 21 (2): 388-405.

Paterson, N.R., 1965. Recent developments in geophysical instrumentation. *Western Miner.* 30: 34-36.

Paterson, N.R., 1967. Underwater mining – new realms for exploration. *Mining in Canada,* April.

Paterson, N.R., and T. Meidav, 1965. Geophysical methods in highway engineering. Presented at *48th Annual Conv., Can. Good Roads Assoc.,* Saskatoon, Sask., Sept.

Poulter, T.C., 1950. The Poulter seismic method of geophysical exploration. *Geophysics.* 15 (2): 181-207.

Shor, G.G. Jr., D.G. Moore, and W.B. Huckaby, 1963. Deep-sea tests of a new nonexplosive reflection profiler. *J. Geophys. Res.* 68 (5): 1567-1571.

Soske, J.L., 1959. The blind zone problem in engineering geophysics. *Geophysics.* 24 (2): 359-365.

Tremblay, J.J.L., and G.D. Hobson, 1962. Vaudreuil map-area, Quebec, Part II, The Seismic method applied to a bedrock channel problem. *Geol. Surv. Canada,* paper 61-20.

Warrick, R.E., and J.D. Winslow, 1960. Application of seismic methods to a groundwater problem in northeastern Ohio. *Geophysics.* 25 (2): 505-519.

Whitcomb, J.H., 1966. Shear-wave detection in near-surface seismic refraction studies. *Geophysics.* 31 (5): 981-983.

Zeitz, I., and L.C. Pakiser, 1957. Note on an application of sonar to the shallow reflection problem. *Geophysics.* 22 (2): 345-347.

Radioactive methods in mineral exploration

R.S. Foote

Texas Instruments Inc.
Dallas, Texas, U.S.A.

Abstract. Terrestrial gamma radiation has been measured on the surface and airborne near the surface by integral and spectral techniques. Current measurements utilize the spectral composition of gamma radiation to differentiate between the radiation from the decay of natural uranium, thorium and potassium, and to remove the undesired contributions from cosmic radiation and fission fallout. Airborne measurement of the uranium daughter product Bi^{214}, the thorium daughter product Tl^{208}, and K^{40} normalized to constant surface elevation provide intensity and radiation balance profiles and isoradiation maps indicating the trend of soil types, and allow lesser anomalous radiation to be identified.

Various sizes of NaI(Tl) detectors have been used up to a composite of 11 1/2 × 4 inches for surface and airborne measurements. These data have been measured as 400-channel spectra with readout of record sequence number, surface altitude and time on to high-speed magnetic tape. The use of magnetic tape has allowed computer data reduction programs to be developed which minimize the time and expense of analysis of high-volume spectral data. Computer-controlled plotting of isoradiation maps and of composite radiation profiles provides radiation maps comparable with geologic data. Examples of data reduction of mineralization in a phosphate-enriched region are given. Correlation of gamma-radiation types with certain minerals will be shown.

Résumé. Le rayonnement gamma terrestre a été mesuré au sol et à bord d'avions à faible altitude à l'aide de techniques intégrales et spectrales. Les mesures récentes utilisant la composition spectrale du rayonnement gamma pour le différencier du rayonnement provenant de la désintégration de l'uranium, du thorium et du potassium naturels et pour éliminer tous les effets indésirables du rayonnement cosmique et des retombées radioactives. Les mesures aériennes du rayonnement du produit de filiation Bi^{214} de l'uranium, du produit de filiation Tl^{208} du thorium et du K^{40} normalisées à une hauteur constante fournissent des profiles d'intensité et d'équilibre du rayonnement et des cartes d'isorayonnement qui permettent d'identifier les divers genres de sol et de reconnaître les rayonnements anormaux de moindre importance.

Des détecteurs NaI(Tl) de diverses dimensions ont été utilisés, y compris un appareil composite de 11 1/2 pouces de diamètre sur 4 pouces d'épaisseur, pour mesurer au sol et à bord d'avion. Les données ont été mesurées comme spectre à 400 voies avec énoncé du numéro de séquence, de la hauteur de la surface et du temps, sur ruban magnétique à grande vitesse. L'emploi d'un ruban magnétique permet de mettre au point des programmes de réduction des données qui réduisent le temps et le coût de l'analyse d'un fort volume de données spectrales. Le tracé de cartes d'isorayonnement et de profiles de rayonnement composé à l'aide d'ordinateur donne des cartes de rayonnement semblables aux cartes portant des données géologiques. L'auteur donne des exemples de la réduction des données provenant de minéralisations d'une région riche en phosphate. La corrélation qui existe entre les divers rayonnements gamma et certains minéraux sera indiquée.

Association of radioactivity with minerals, either directly or indirectly, has long been recognized. Natural radioactivity is associated with the radioactive decay of the uranium and thorium series and from potassium-40. These radioactive elements exist in some balance in all natural materials. Natural abundance of these radioactive elements is correlated to the geological age and formation types. Many nonradioactive minerals are correlated chemically with those that are radioactive, and can be measured according to this association. Anomalous abundances of these radioactive elements indicate abnormal concentrations that can lead to ore-grade mineralization either on the surface, in the near surface or at depth. Described briefly are current and past radiation measurement techniques used. Discussed in more detail are methods that will more accurately measure and identify lower levels of radioactive and nonradioactive elements.

Present methods — surface and airborne

In the past the majority of all surface radioactivity measurements have been made in the search for uranium through the use of portable total gamma-ray counting geiger counters and scintillation detectors. The use of these counters led to many discoveries in the search for uranium where anomalous surface outcropping existed. The scintillation counter measures all gamma radiation in the energy range from about 50 keV, as controlled by the mechanical structure enclosing the scintillation detector, to high-energy cosmic events with an event-detection efficiency of about 100 percent. Comparable measurements using

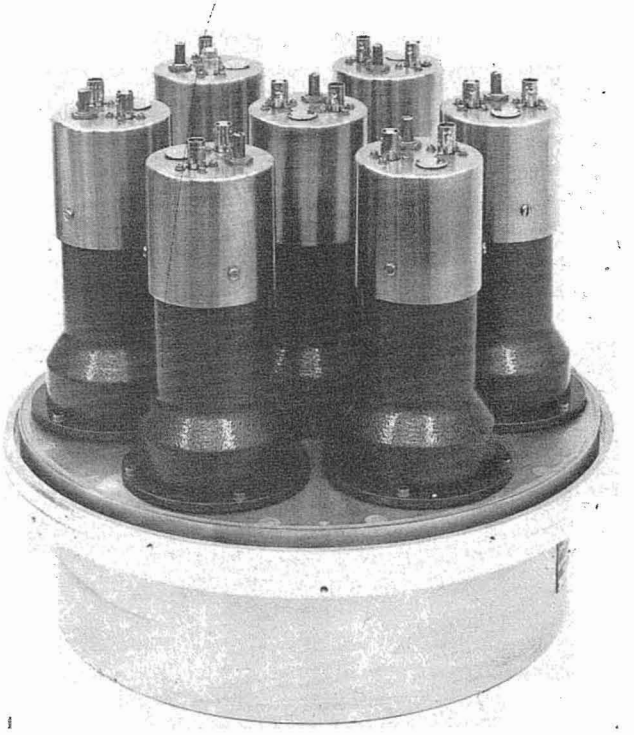


Figure 1. NaI(Tl) detector, 11 1/2 by 4 inches.

Contents



Figure 2. Thermally insulated NaI(Tl) detector.

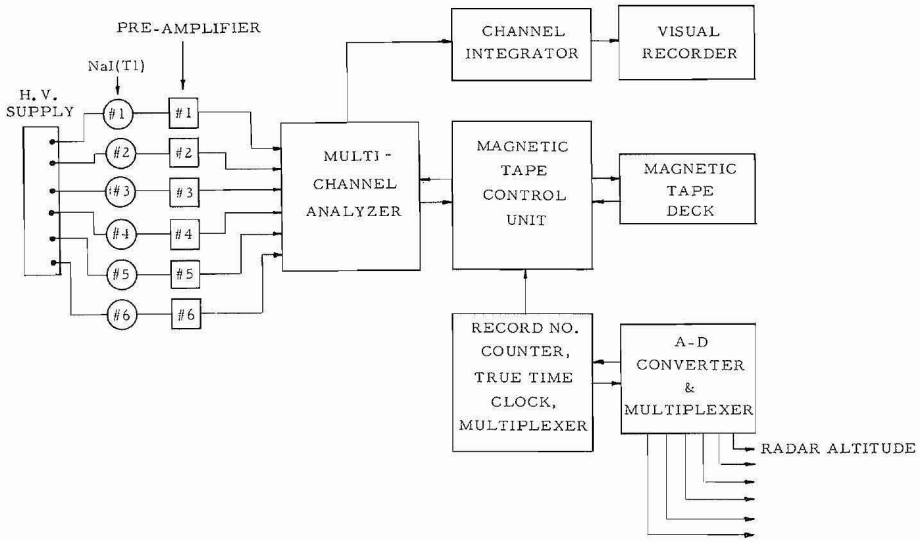


Figure 3. Electronic block diagram.

Geiger tubes give about 1 percent measurement efficiency for gamma-ray measurement, but allows measurement of the higher-energy beta radiation. Both counters are applied to logging of radiation as a function of depth in subsurface drill holes.

The total event counting scintillation detector of gamma radiation has been applied to airborne measurements where the detector volume and surface area have been increased to provide statistically valid data as a function of desired ground resolution and aircraft speed. None of these techniques has provided for separation of data originating from the decay of the uranium and thorium series and from potassium-40. Separation of gamma radiation created from the decay of the thorium-232 series by measurement of Tl^{208}, of the uranium-238 series by measurement of Bi^{214}, and of potassium by measurement of K^{40} is possible through spectral data acquisition and subsequent analysis. Application of the gamma-ray spectral techniques to airborne reconnaissance provides for rapid data acquisition and analysis to indicate trends and anomalous concentrations of the natural radionuclides. The ability of systems to measure surface gamma radiation is a function of the number and size of available NaI(Tl) detectors and the aircraft speed. The system to be discussed uses up to six 11 1/2 by 4 inch detectors to provide a statistically valid counting rate.

Airborne detection equipment

The large NaI(Tl) detector is shown in Figure 1. The seven photomultipliers are required to provide equal pulse output for equal gamma-ray energy loss anywhere within the detector. This detector is thermally shielded to prevent rapid temperature changes from cracking the crystal detector, and is indicated in Figure 2. The electronic block diagram for the system which records the energy lost to the NaI(Tl) for each measured incoming gamma or cosmic ray is shown in Figure 3. This energy of each gamma ray given up within the NaI(Tl) detector provides a proportional light pulse and subsequent electrical pulse which is sorted by the multichannel pulse analyzer to provide spectra showing the total counts/channel as a function of channel number. Spectral data reduction provides the information on Bi^{214}, Tl^{208} and K^{40} content. All data are recorded by fast start-stop magnetic tape equipment with each spectral record following recording of the particular record number, true time, radar surface altitude and doppler navigation. Also recorded for immediate visual observation are specific energy regions associated mainly with Tl^{208}, Bi^{214}, K^{40}, total count, radar altitude and initiation of each record.

Data processing

Airborne gamma-ray spectra should be gathered at intervals sufficiently spaced to allow resolution of anomalous

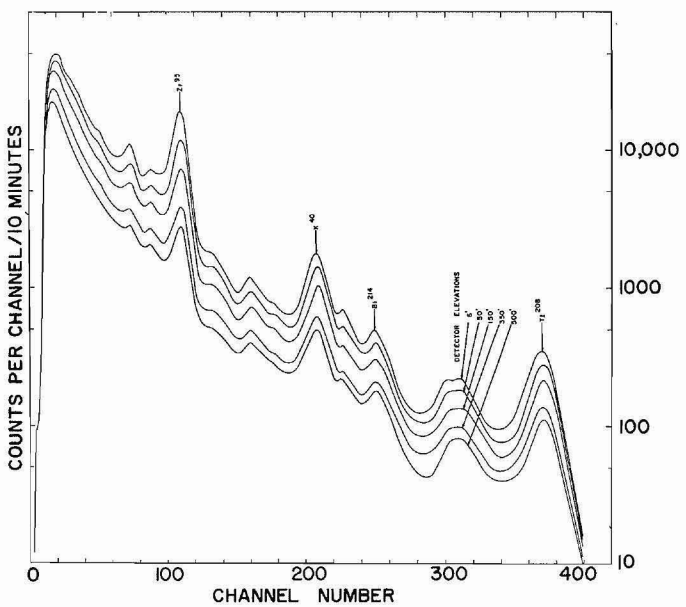


Figure 4. Surface gamma-ray spectra as a function of altitude.

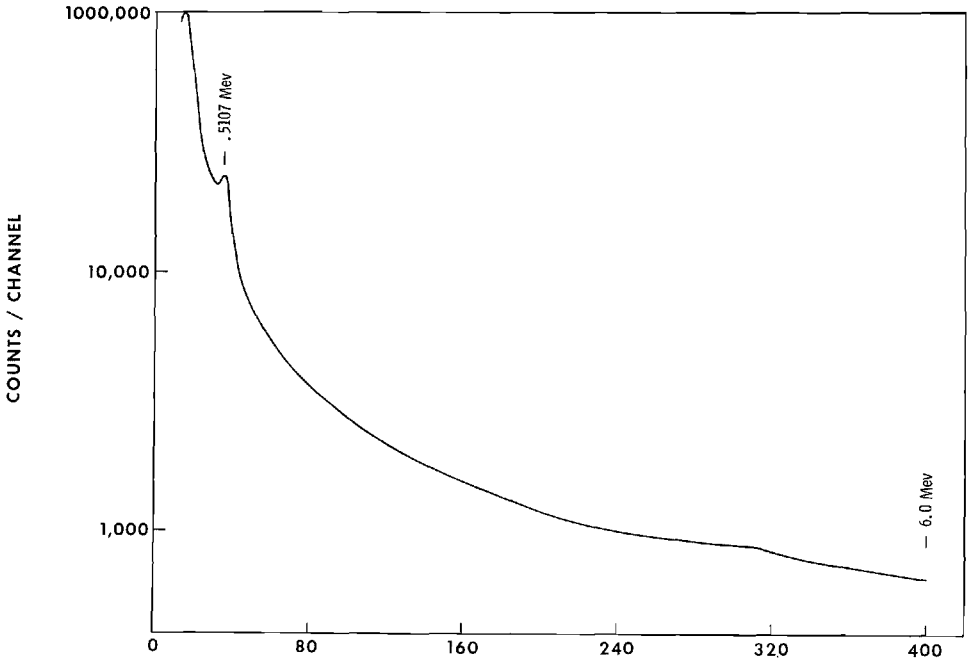


Figure 5. Cosmic radiation spectrum.

radioactivity. Experience has shown 400-foot surface elevation to be the most practical flight altitude. The manner in which radiation is attenuated as a function of altitude is shown in Figure 4 (Bowman, *et al.*, 1966).

The energy shape of the cosmic-created spectrum has been determined to be nearly constant in the altitude range from sea level to 20,000 feet as shown in Figure 5. Variation with altitude is shown in Figure 6. Knowledge of the cosmic contribution, which constitutes about 10 percent of the average surface background gamma-ray spectrum at sea level, is necessary to perform accurate data reduction.

Field calibrations for the thorium-232 daughter product scheme is presented in Figure 7. Figure 8 shows the gamma-ray spectrum of the uranium-238 daughter product scheme measured over the Haystack mine near Grants, New Mexico. Figure 9 shows

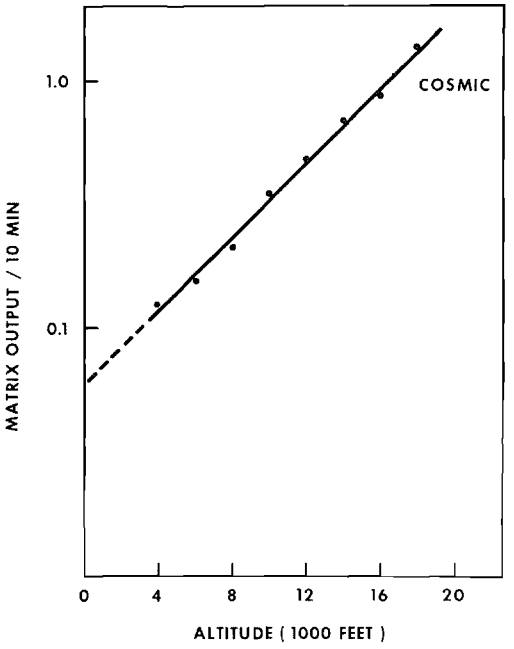


Figure 6. Cosmic radiation intensity as a function of altitude.

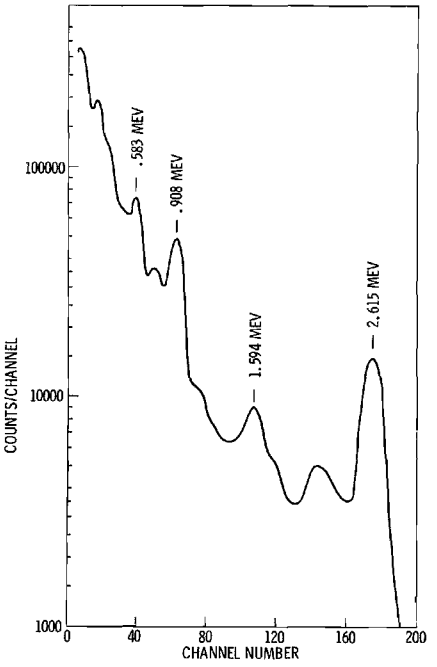


Figure 7. Thorium-232 daughter product gamma-ray spectrum.

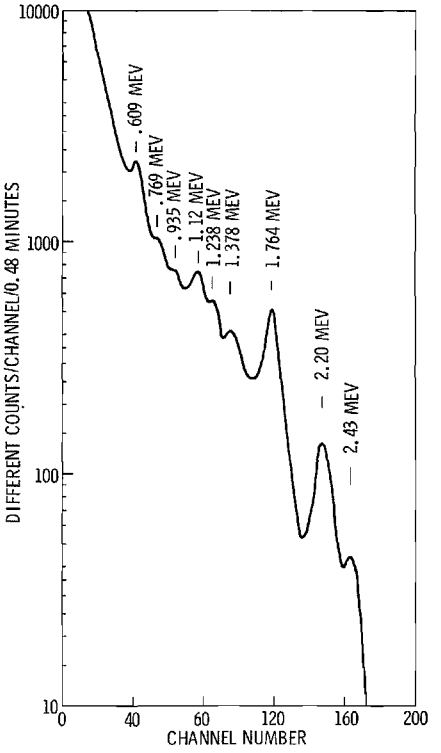


Figure 8. Uranium-238 daughter product gamma-ray spectrum.

Contents

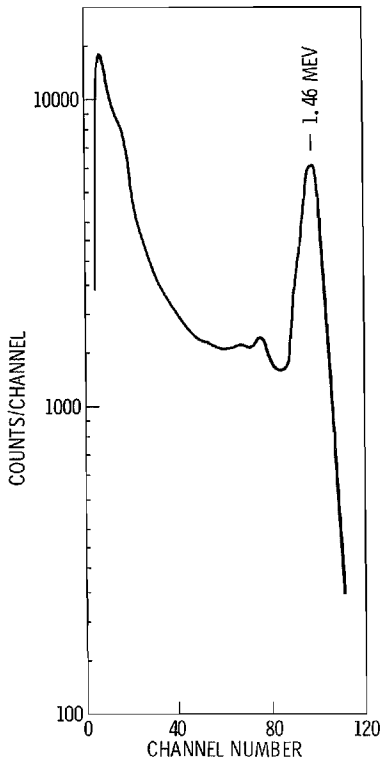


Figure 9. Potassium-40 gamma-ray spectrum.

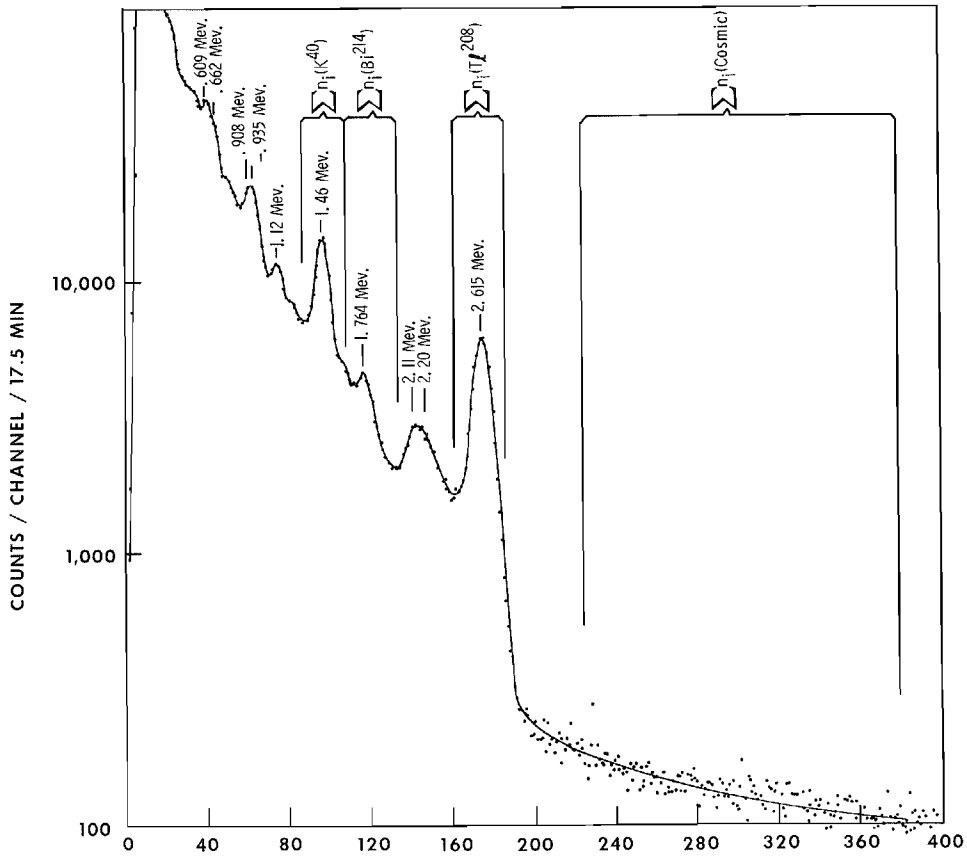


Figure 10. Airborne gamma-ray spectrum gathered at 400 feet.

the potassium-40 spectral standard. The presence of fresh fission debris will interfere with data reduction only if the La^{140} (12.8-day half life) spectral standard is not included in the data reduction (Foote, 1965). The summation of 17.5 minutes of field data gathered at a surface elevation of 400 feet is shown in Figure 10. The energy intervals used for the matrix data reduction are shown. The near-surface atmosphere contains radon and its subsequent daughter products.

A measurement of the fraction of Bi^{214} resulting from the air volume surrounding the aircraft at 400 feet compared to that resulting from surface emission has been made during daylight hours with average wind flow, where low-temperature inversion layers have been removed, ranges from 10 to 40 percent. Since the atmosphere radon-created Bi^{214} cannot be differentiated, an average atmospheric concentration of 15 percent has been used.

High-volume data reduction involves spectral energy calibration, correction to a constant surface altitude of 400 feet, calculation of the amounts of Bi^{214}, Tl^{208} and K^{40} contributing to the spectra, and of the balance of radiation, Bi^{214}/K^{40}, Tl^{208}/K^{40}, and Bi^{214}/Tl^{208}. Use of the balance of radiation minimizes effects caused by geological formation changes, surface moisture contents and noncorrected altitude changes.

Examples of data analysis

Examples of these results for data gathered over a phosphate-enriched area in central Florida are shown. Data are presented as computer-plotted stacked flightline profiles (Figure 11) and as isoradiation contour maps for the six variables and for total count (Figures 12 – 18). Trends in radiation intensities and changes in balance can be seen.

Surfacing of the phosphate-enriched Ocala limestone is mapped by the surface uranium daughter product intensity and by the balance of the Bi^{214} to the normally constant potassium-40 and correlates to geological maps which indicate penetration of the Ocala limestone through the Hawthrone formation.

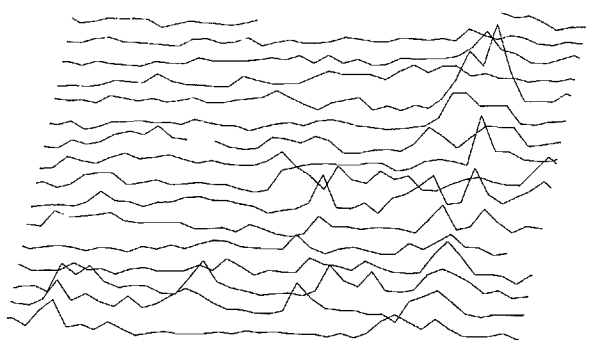


Figure 11. Florida phosphate Bi^{214} flightline radiation profiles.

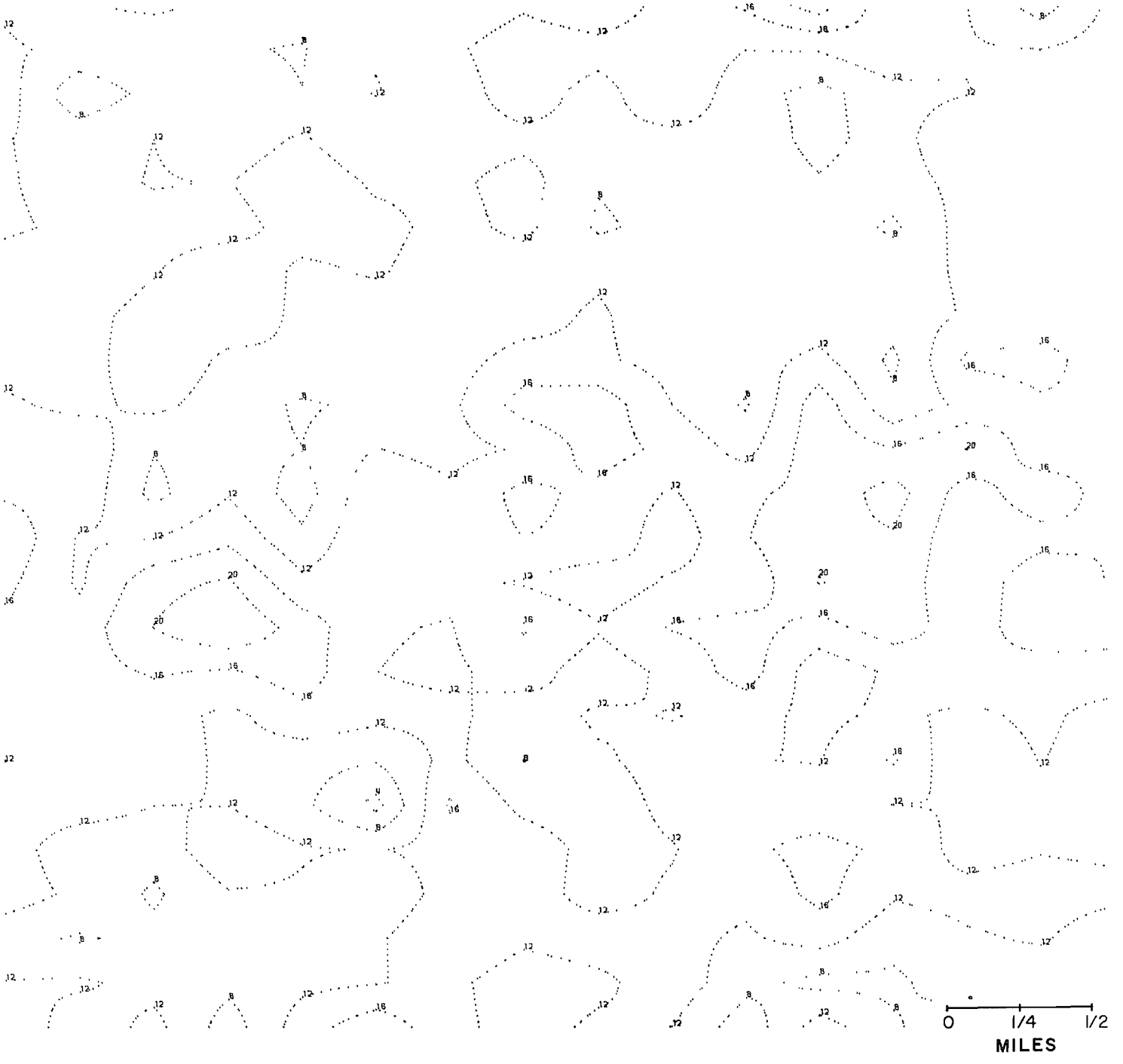


Figure 12. Tl^{208} isoradiation contour map — Florida phosphates.

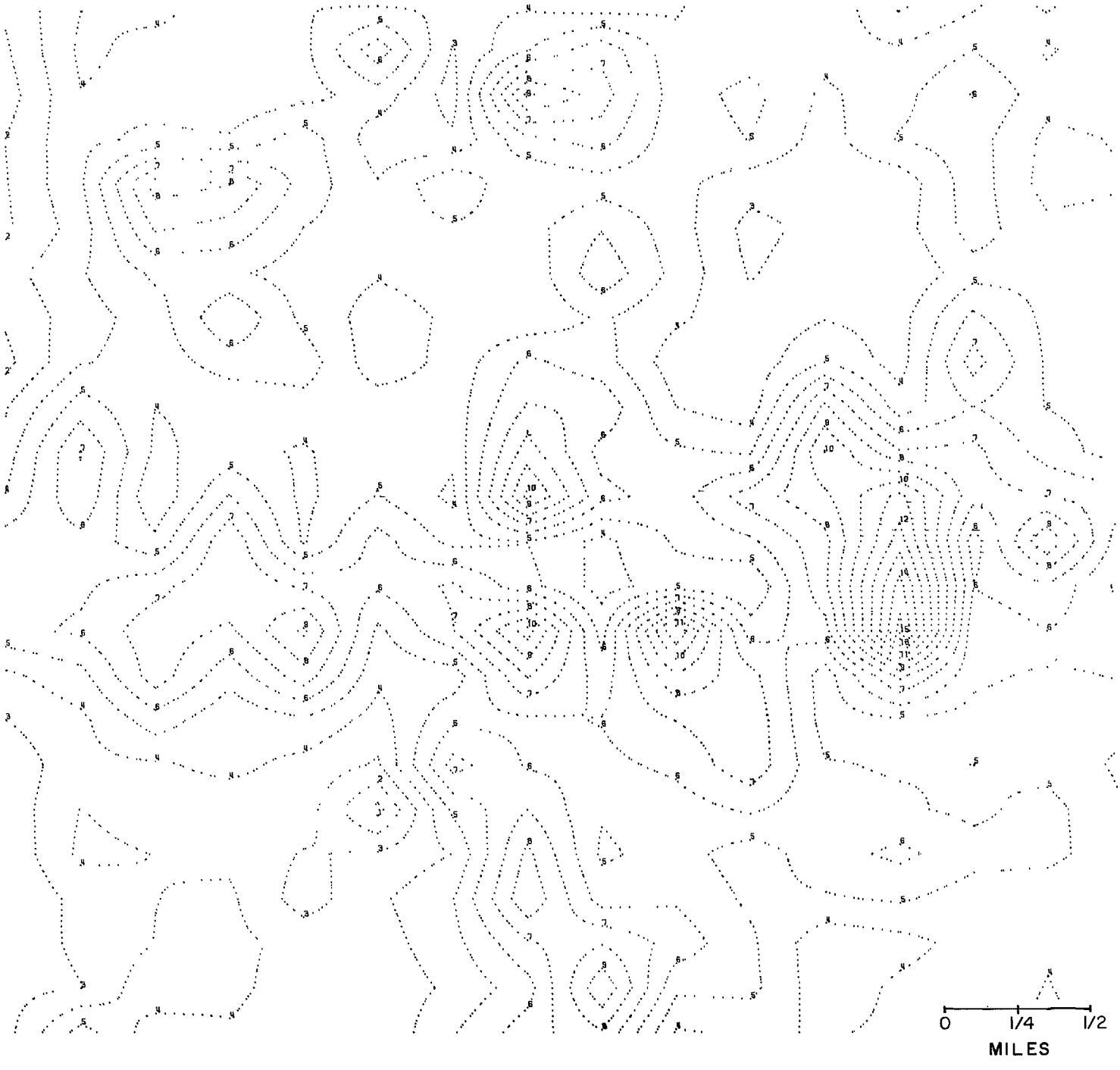


Figure 13. Bi^{214} isoradiation contour map — Florida phosphates.

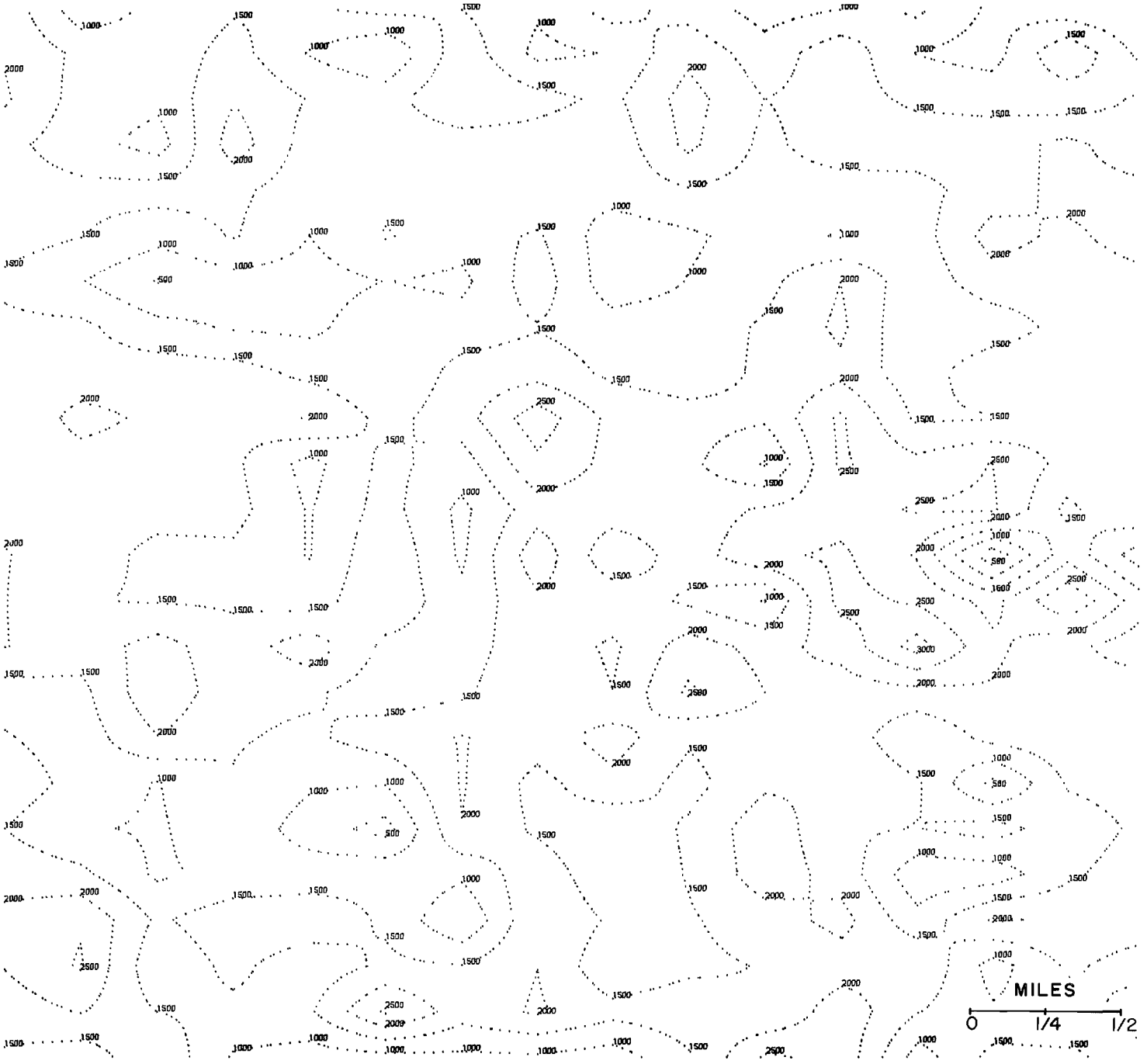


Figure 14. K^{40} isoradiation contour map — Florida phosphates.

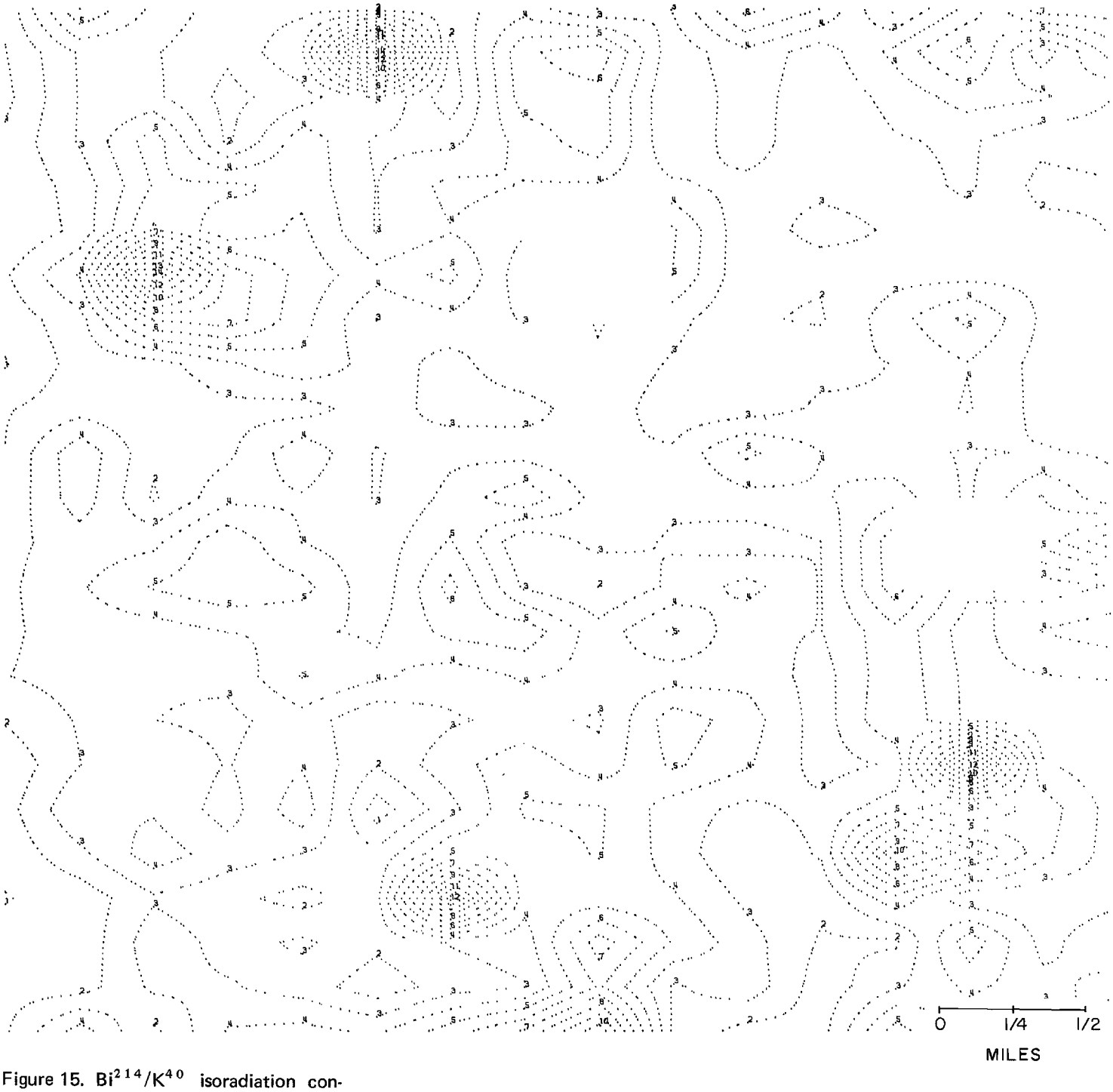


Figure 15. Bi^{214}/K^{40} isoradiation contour map – Florida phosphates.

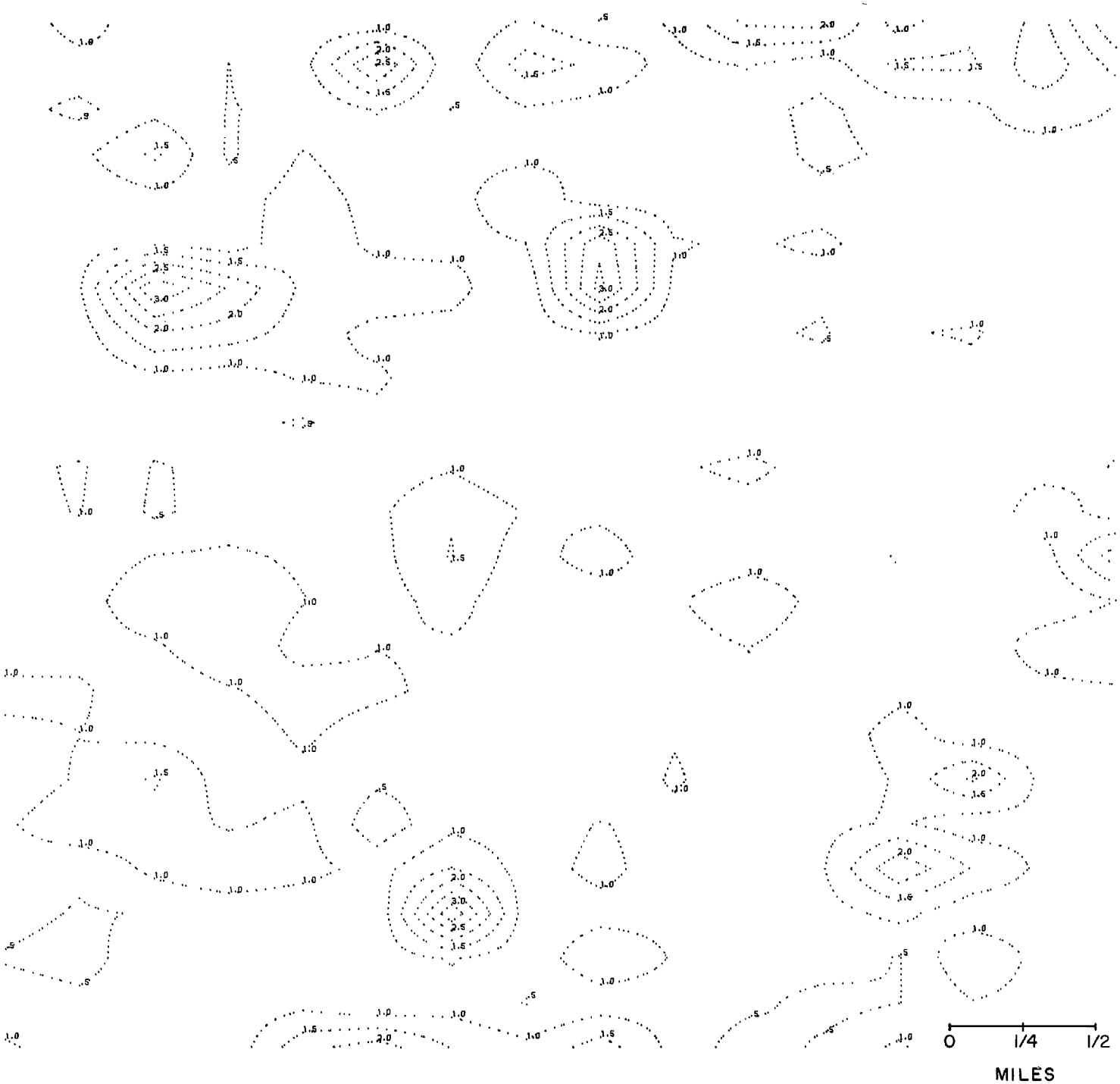


Figure 16. Tl^{208}/K^{40} isoradiation contour map — Florida phosphates.

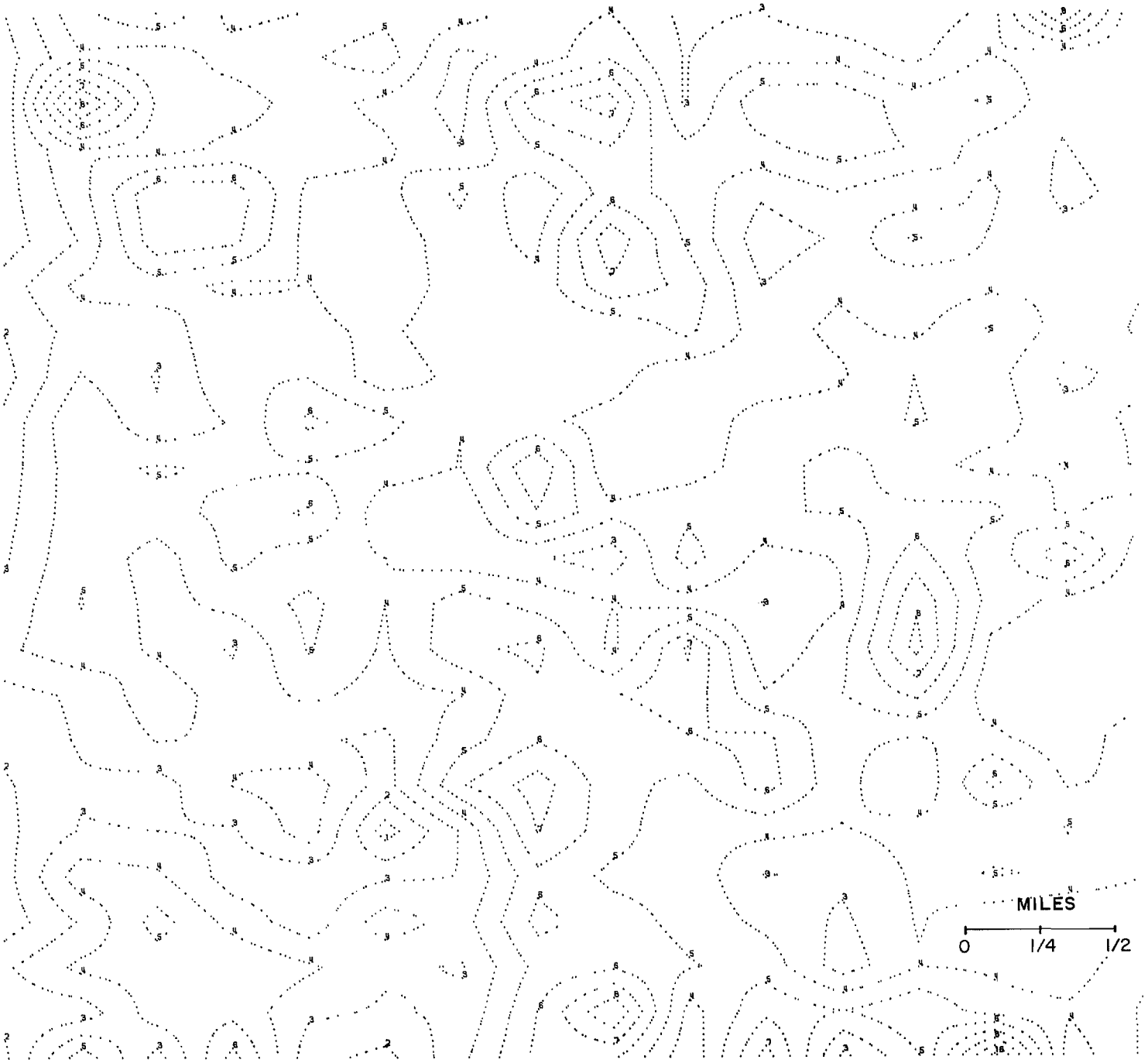


Figure 17. Bi^{214}/Tl^{208} isoradiation contour map — Florida phosphates.

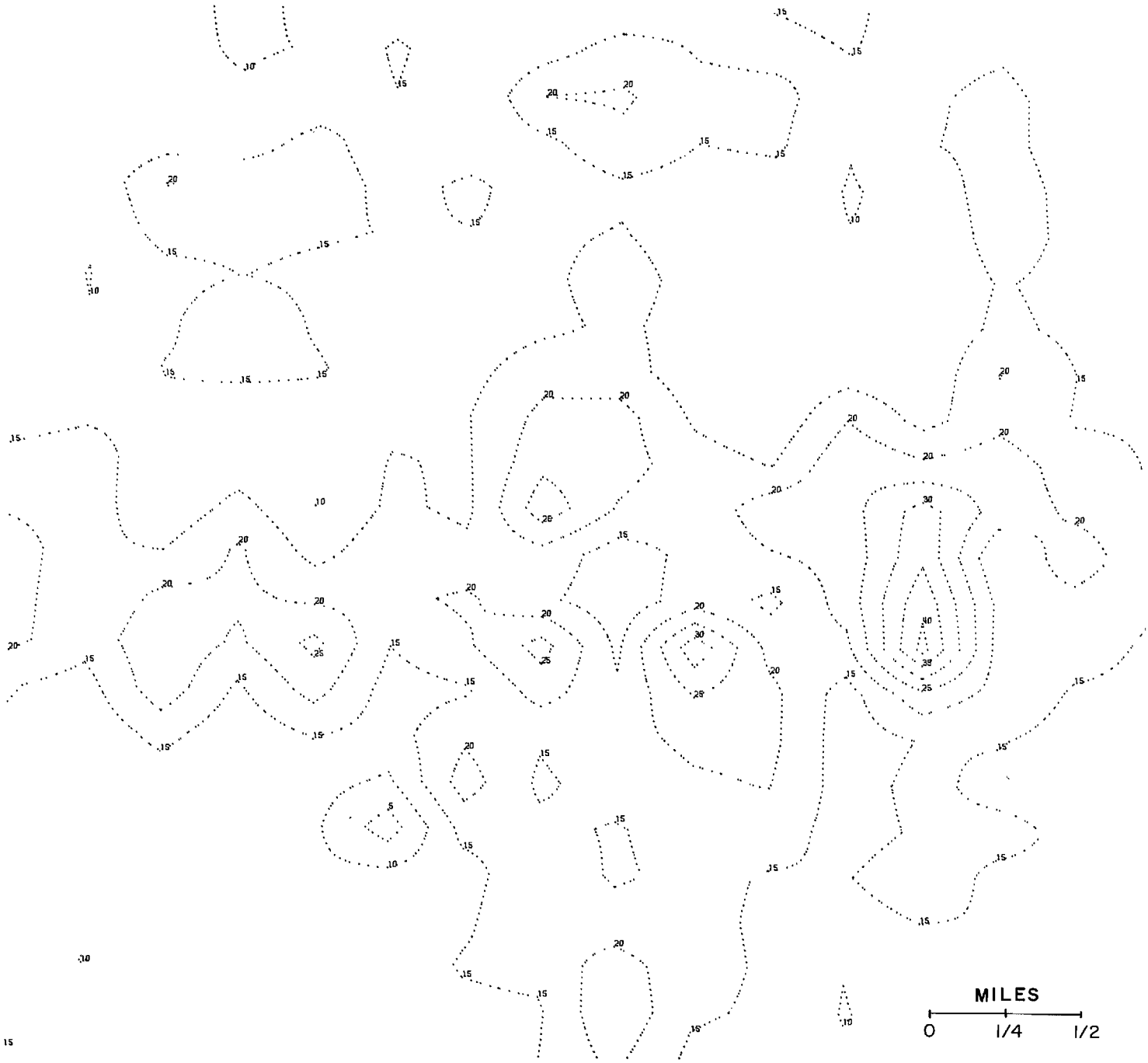


Figure 18. Total count isoradiation contour map — Florida phosphates.

Contents

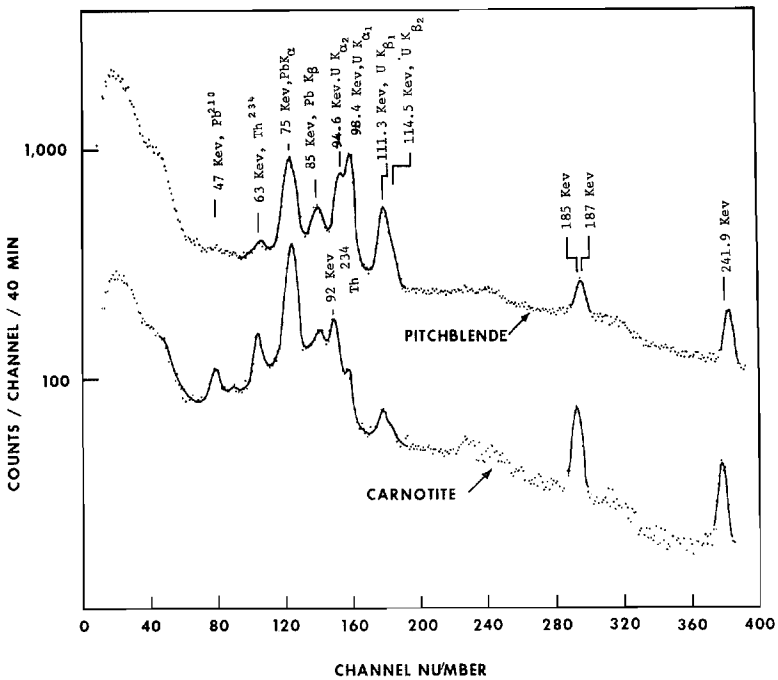


Figure 19. Gamma-ray energy spectral measurement of ~3% U_3O_8 carnotite sample and ~20% U_3O_8 pitchblende by 1.25 cc Ge(Li) detector.

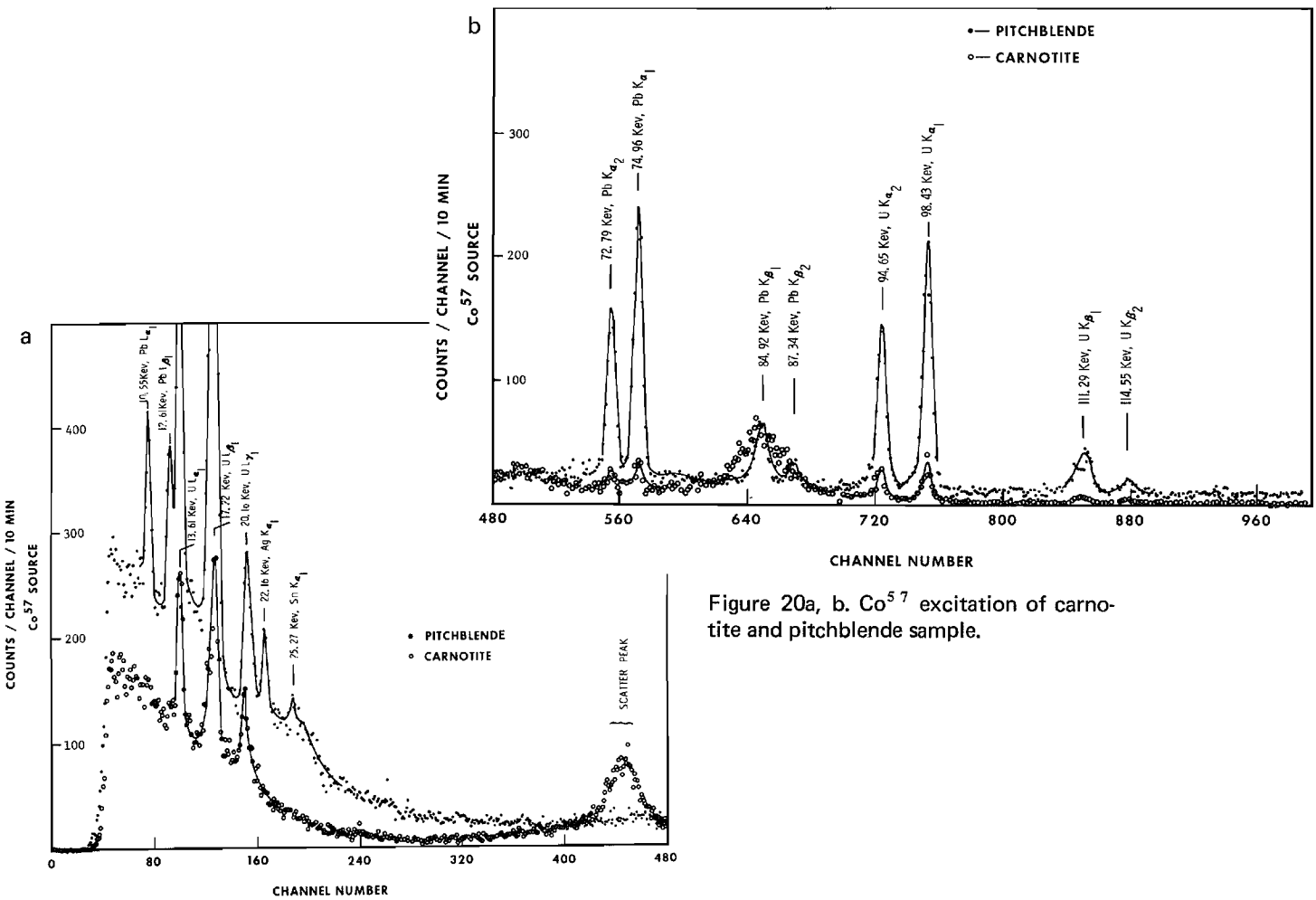


Figure 20a, b. Co^{57} excitation of carnotite and pitchblende sample.

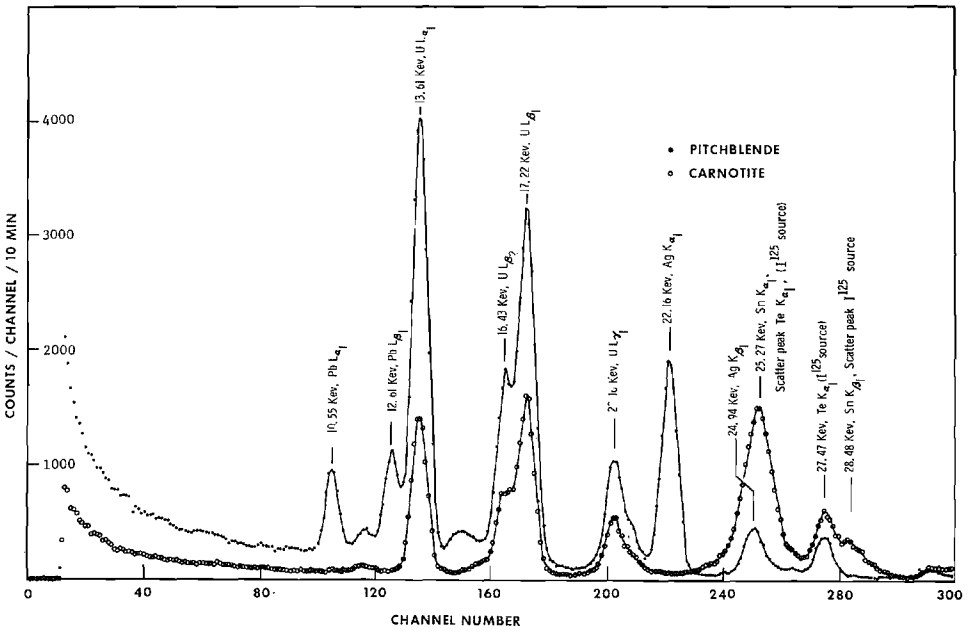


Figure 21. I^{125} excitation of carnotite and pitchblende sample.

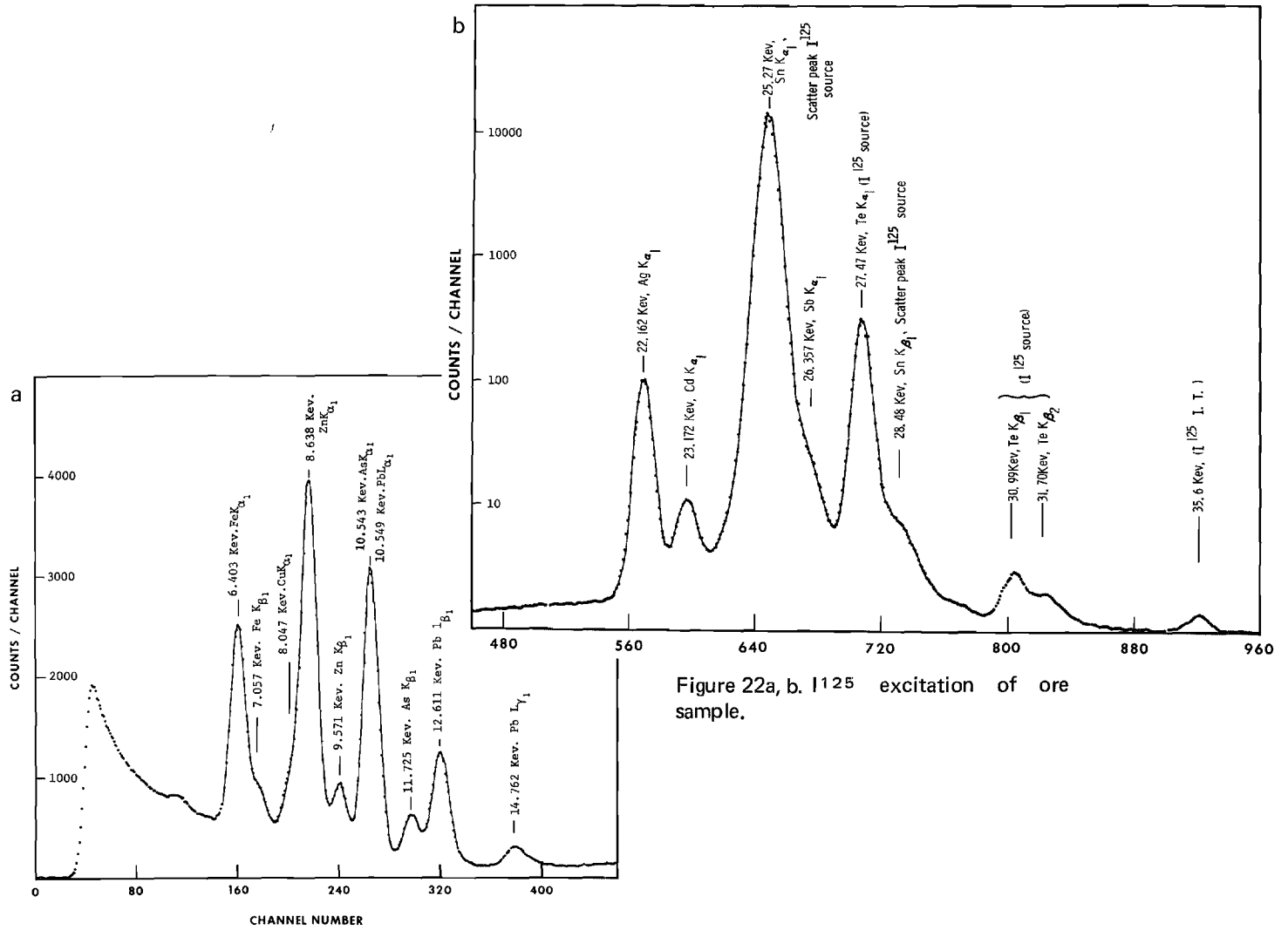


Figure 22a, b. I^{125} excitation of ore sample.

Mineral detection using high-resolution gamma spectroscopy and X-ray fluorescence

Recent advances in the use of large Ge(Li) semiconductor detectors have provided detectors with sufficient probability for stopping higher-energy gamma radiation with energy resolutions better than 4.0 keV FWHM (Jones and Carpenter, 1967). Liquid nitrogen must be supplied periodically to keep the detector cool. Detector sizes range to 50 cc of Ge(Li). Uranium ore can be analyzed in the field for equilibrium condition and for percent U_3O_8. The presence of thorium-232 daughter products and potassium-40 are readily identifiable. Figure 19 shows the low-energy spectrum of a pitchblende and carnotite uranium sample.

The use of X-ray fluorescence offers great promise for field identification of unknown mineral samples (Purvis and Foote, 1964; Senftle and Turner, 1967). Here excitation of the *K* and *L* electron shell of the various atoms leads to the emission of the energy lines according to the particular atom. The use of liquid nitrogen cooled Si(Li) detectors with resolutions as low as 350 to 500 eV are available. This excellent resolution provides the ability for separation of otherwise superimposed X-ray fluorescence lines and allows identification to lower concentrations. Subjecting the same pitchblende and carnotite samples to Co^{57} and I^{125} excitation sources gives the data of Figures 20a and b and 21. Several other elements are identified.

A mineral sample analyzed by X-ray fluorescence gives the data shown in Figures 22a and b. Elements in atomic number from uranium to chlorine can be measured ranging in concentrations to less than 50 ppm depending on the concentrations of other elements, system resolution, and upon the energy and intensity of the excitation source.

References

Bowman, H.R., E.K. Hyde, S.G. Thompson, and R.C. Jared, 1966. *Science.* 151:152,

Foote, R.S., 1965. Measurement of radioactive fallout by field total absorption gamma-ray spectroscopy. Report No. 5, USAEC contract AT (40-1)-3147.

Jones, W.B., and R.A. Carpenter. Presented to *Second International Symposium on Nucleonics in Aerospace.* July 1967.

Purvis, A.E. and R.S. Foote, 1964. Atmospheric attenuation of gamma radiation. In *Natural Radiation Environment,* J.A.S. Adams and W.M. Lowden, Eds., p. 747-756.

Senftle, F.E., and A.B. Turner, 1967. Presented to *Second Symposium on Low-Energy X and Gamma Sources and Applications.* April.

Geophysical applications of systems modern computer

G.F. West and L. Martin

University of Toronto
Toronto, Canada

F.S. Grant

Computer Application & Systems Engineering
Toronto, Canada

Abstract. Mining and groundwater geophysicists are making limited use of computers at the present time, but a rapid expansion is to be expected as soon as plotting devices, improved data input systems, and small fieldworthy computers become more widely available. Present applications utilize mainly the ability of the computer to evaluate numerically the massive algebraic expressions for such things as the theoretical anomalies produced by idealized geological structures. To some extent the ability of the computer to operate plotting devices is being employed to draw graphs and contour plans of data that the computer has produced. Progress has also been made in computing theoretical anomalies directly by numerical methods rather than by evaluating mathematical solutions. This is a particularly promising development for resistivity and IP calculations where ordinary mathematical solutions are limited to very simple shapes.

Numerous demonstrations have been given of the reduction and plotting of field data by computer, but few companies seem yet to be doing their routine work by machine. Time-series analysis and least-squares optimum filtering methods which are so widely used in seismic prospecting have not yet found great application in mining and groundwater geophysics. An exception is in the processing of aeromagnetic data (continuation, etc.). Digital data acquisition systems are now being operated in conjunction with small computers by oceanographers and marine geophysicists to produce maps of reduced data during and immediately after completion of the surveys. Such techniques may well be practical in airborne geophysics. Besides the advantage of fast and accurate data reduction they offer the possibility of applying complicated corrections, correlations and filtering processes to the data for little added cost. Basic data can also be filed in a manner that will permit reprocessing according to a different prescription if the initial choice proves to be less than optimum.

Résumé. Les géophysiciens des mines et des eaux souterraines se servent peu des ordinateurs dans leurs travaux, mais il faut s'attendre à une expansion rapide de l'usage de ces machines quand les appareils de rapport, les systèmes améliorés d'introduction des données et les petits ordinateurs appropriés aux travaux sur le terrain deviendront plus faciles à obtenir. Les applications présentes utilisent surtout la capacité de l'ordinateur à évaluer numériquement l'expression algébrique massive pour des quantités comme les anomalies théoriques produites par des structures géologiques idéalisées. Jusqu'à un certain point, la capacité de l'ordinateur à faire fonctionner des mécanismes de rapport est utilisée pour tracer des graphiques et des plans de courbes de niveau à partir des données que l'ordinateur a produites. Des progrès ont également été réalisés dans le calcul des anomalies théoriques directement par des méthodes numériques plutôt que par l'évaluation de solutions mathématiques. Ceci constitue un perfectionnement particulièrement prometteur pour les calculs de la résistivité et de la polarisation provoquée alors que les solutions mathématiques ordinaires sont limitées aux formes très simples.

On a donné de nombreuses démonstrations de réduction et de rapport par ordinateur, des renseignements recueillis sur le terrain, mais peu de sociétés semblent jusqu'à maintenant exécuter leurs travaux ordinaires à l'aide des machines. L'analyse des séries chronologiques et les méthodes de filtrage optimal par les moindres carrés qui sont si souvent employées dans la prospection séismique n'ont pas encore trouvé de grandes applications dans la géophysique des mines et des eaux souterraines. Il y a une exception dans le cas du traitement électronique des données aéromagnétiques.

Les systèmes d'acquisition des données numériques sont maintenant utilisés conjointement avec de petits ordinateurs par les océanographes et les géophysiciens de la mer pour produire des cartes à partir des données réduites durant et immédiatement après la parachèvement des levés. De telles techniques peuvent fort bien servir en géophysique aéroportée. En plus des avantages d'une réduction rapide et précise des données, elles offrent la possibilité de leur appliquer des corrections compliquées, des corrélations et des procédés de filtrage en échange d'une légère augmentation du coût. Les données fondamentales peuvent également être versées aux dossiers d'une façon qui permettra de les utiliser de nouveau pour des exigences différentes si le choix initial s'avère moins que parfait.

The applications of modern computers in mining and groundwater geophysics are so many and so extremely diverse that presenting a review paper on the subject is difficult. It is certainly impossible to make an exhaustive survey of such a subject. The following remarks are therefore confined to a discussion of generalities and trends, and are followed with a few examples with which the authors have had some personal experience. It is hoped that these will illustrate and give substance to the generalities.

It should first be remarked that mining and groundwater geophysicists are not generally making great use of computers. Their use of these devices certainly does not compare in the slightest degree with that of the petroleum geophysicists. There are various reasons for this, but possibly the most important is that organizations in the mining and groundwater field are usually small, certainly unable to afford their own computer, and are often unspecialized so that any appreciable capital investment in programming, etc., that is only applicable to a single type of work is uneconomic. This may ultimately have very serious repercussions, as the regular use of computers has a certain 'spin-off' value in addition to the accomplishment of the immediate task. It is possible that many of the important improvements in geophysical technique that will be made in the next decade will be intertwined so closely with computer technology that a person

Contents

unfamiliar with computer programming, and particularly with the organization of work methods and technique that goes with it, will be very hard pressed to keep up with new developments, much less contribute to them.

Trends in computer hardware

The most obvious development taking place at present is the installation of much larger, much faster, and more expensive computers at more and more places throughout the world. The economics are such that the supercomputer should be able to make available more computing capacity to more users through a large number of input terminals (many located at considerable distance from the main device) than can a number of intermediate size machines. Numerous multiterminal computers now exist, and they are certainly a technical success. (Two companies offer services based in Toronto.) It would seem that the practical utility of such machines is now more limited by the program software which controls their operation than by the electronics.

Parallel to the development of better computing facilities is the development of improved input-output devices. As far as the mining and groundwater geophysicist is concerned the problems of output are now minimal. There are few applications where data are wanted in a form other than graphs, sections, maps, or the typewritten page; and all these forms are readily available. Improvements will certainly be made, but no major breakthroughs are necessary.

Progress has also been made on input devices, but it is not at the moment so useful to the mining and groundwater geophysicist. For many computer users, the bottleneck of getting all their data into a machine-readable form such as punched cards, has been overcome with digital electronic measuring devices connected either directly to the computer or to a computer-compatible digital magnetic tape recorder. This is the development that triggered the recent instrumental revolution in seismic prospecting. However, the problem is still acute in mining and groundwater geophysics. Digital recording equipment is still not man-portable and it would seem that a device that will replace the instrument operator's notebook, yielding field notes in machine- and man-readable form, is what is badly needed.

A third field in which great progress has been made and in which even more can be expected in the near future, is in the development of small, cheap, fieldworthy computers. Several such computers have been on the market for some time, and now a new generation of integrated circuit devices is becoming available. These devices can read data from a typewriter, punched tape, digital measuring devices, or magnetic tape, and they can output on the typewriter or on a graph-map plotter. Marine geophysicists are already using such small computers at sea to compile, reduce, and plot geophysical observations and navigational data. It is to be expected that the use of such computers will become common in airborne geophysics, operating either in the aircraft or at the field base, and that they may also be used routinely, at first in the office, and ultimately at field headquarters, to work up ground survey results. The utility of these small computers will not be found so much in their ability to work up data more cheaply and more quickly than is possible at present, but in their ability to handle many additional data processing and interpretation tasks for very little increase in cost. These are jobs that are conceptually possible now but are only carried out in special circumstances. Some examples are upward or downward continuation of aeromagnetic surveys, routine correction of aero EM data for flight height, calculation of Bouguer gravity maps for several values of Bouguer density so as to minimize correlation with topography – and even more important, the carrying out of procedures for correlating several types of measurements to eliminate unwanted effects (for example the processing of multifrequency EM measurements to reduce overburden response).

Trends in computer software

In North America at least, scientific computing is almost invariably programmed in FORTRAN. While this is supposed to be a universal language, it is not entirely so. The versions of FORTRAN used on different computers are sufficiently different (especially FORTRAN II and IV) that programs require minor, and occasionally major, changes to enable them to run on different machines. However, an experienced FORTRAN programmer suffers few problems in changing from one machine to another. It is our opinion that the publication and exchange of computing algorithms will be of more permanent value than the preservation of programs themselves. Exchange of programs is likely to be of some use to mining and groundwater geophysicists, but most users will likely have to write their own programs, although they may not have to develop the computing method. Smaller companies may purchase programming services from specialist firms. Larger companies may have programmers on their own staff.

The more important software developments are at the machine language level. In many cases, the usefulness of hardware

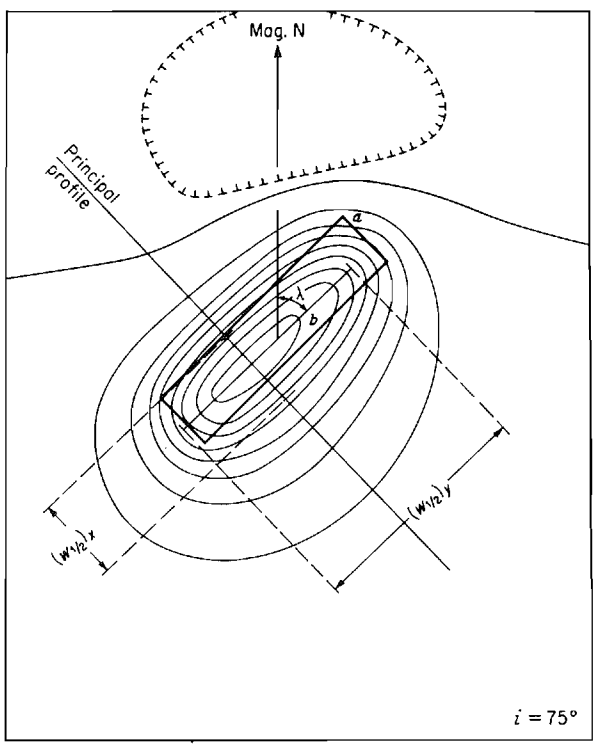


Figure 1. Total field aeromagnetic anomaly over a vertically sided prism.

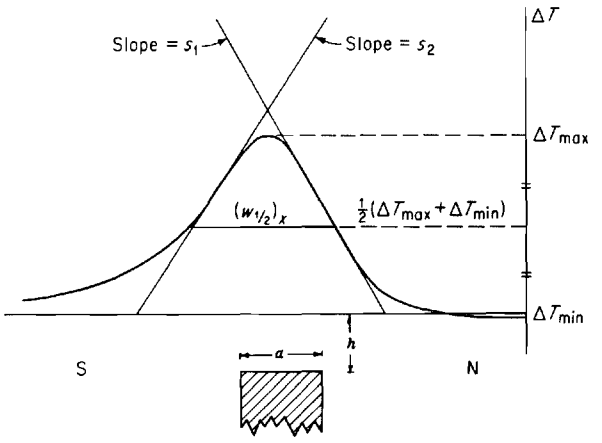


Figure 2. Principal aeromagnetic profile over a prism, showing the characteristic measures of the anomaly.

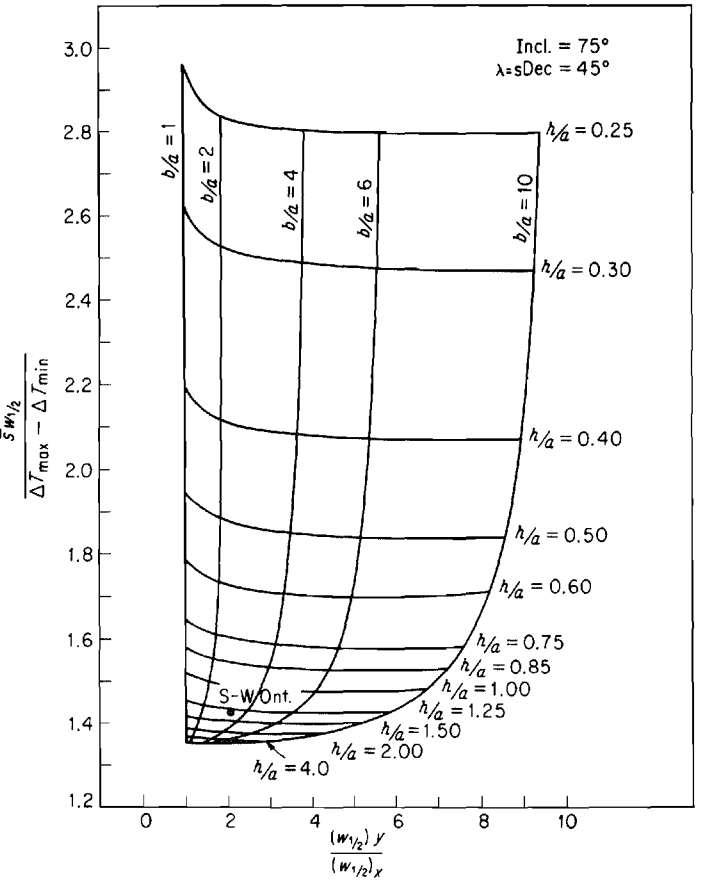


Figure 3. Characteristic curves for the prism model, for the case $\lambda = 45°$, inclination = 75°. The ratios b/a and h/a are found from the measured characteristics.

such as plotters, small computers, digital tape recording systems, etc., depends critically on the software that is available with the device. Frequently the software is of as much, or sometimes even of more importance than the hardware in a purchase decision. It is tempting for a prospective user of a device to feel that he can program the basic routines for it himself, and this is true.

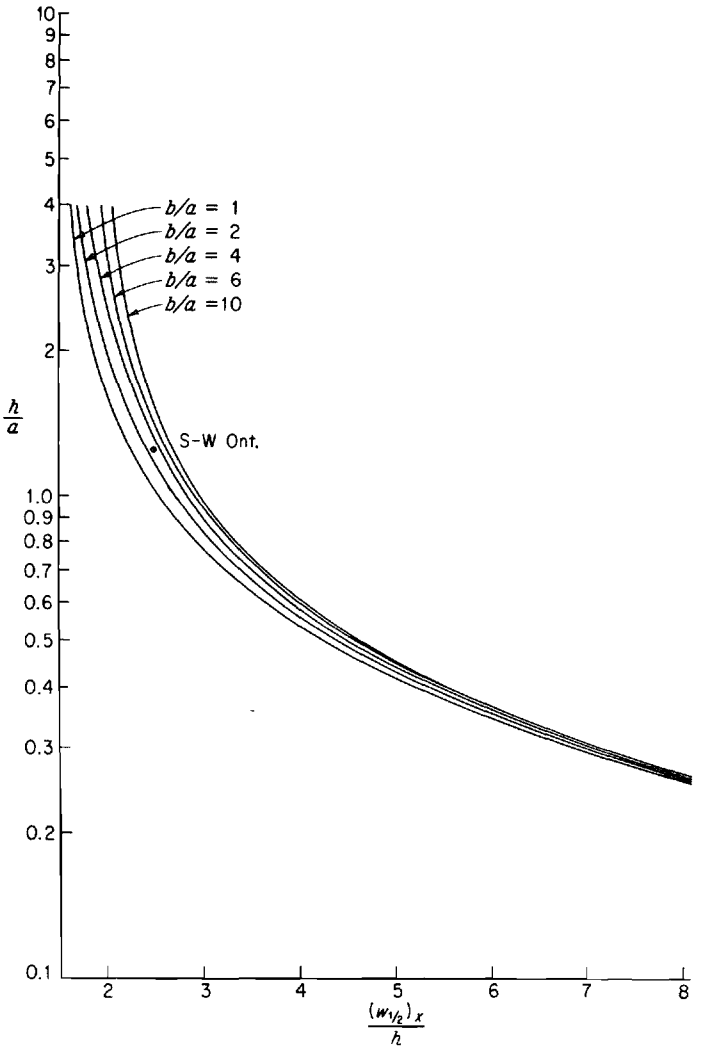


Figure 4. Supplementary curves for the prism model for the case $\lambda = 45°$, inclination = 75°. The values of h, b and a are found from the ratios b/a, h/a and the measured characteristics.

However, many hours of highly skilled labour are required and this must be taken into account in any cost appraisal.

Examples of computer use

To give some idea of the various applications of computers in mining and groundwater geophysics, we shall describe several examples with which we have had some experience: the first is in developing methods of quantitative interpretation of total field magnetic anomalies. The computer used was the IBM 7094 at the University of Toronto. A large, fast machine was needed to handle the massive quantities of arithmetic economically. Interpretation methods such as this could not possibly be produced without the help of a large computer unless they were restricted to a very few elementary models such as single poles or dipoles. A large machine makes it possible to calculate directly all of the characteristic features of magnetic anomalies over bodies such as prisms, plates and the like – features such as the maximum slopes, widths, amplitudes, and so on – which geophysicists generally like to use in making their interpretations. When

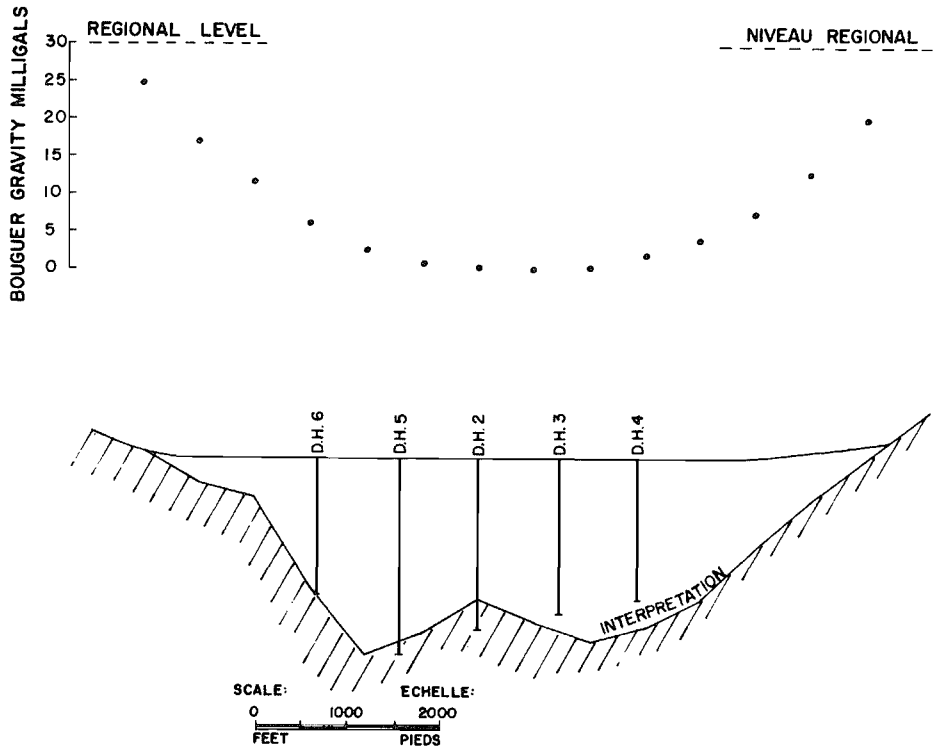


Figure 5. A gravity profile across the Salmon Glacier to which a two-dimensional polygonal model has been fitted by automatic iteration. The drill holes show at what depth the bottom was actually found.

selected combinations of these features are assembled in pairs and plotted against one another, we obtain sets of characteristic curves which make life very much easier for the geophysicist wishing to do quantitative interpretations. Let us look at one example. The favourite model of many geophysicists for making interpretations of airborne magnetic data is the vertical sided rectangular prism. Having developed the formula for the total-field anomaly at a height h above the prism assuming that it has a uniform magnetic susceptibility, it is a fairly straightforward matter to program the machine to calculate directly from it the anomaly itself and quantities such as those illustrated in Figures 1 and 2, namely, the half-widths of the anomaly pattern in the strike direction and in the direction perpendicular to the strike; the maximum horizontal gradients of the profile that is normal to the strike, and the total amplitude of the anomaly. With these quantities we are then able to construct Figures 3 and 4, which are characteristic curves for the prism model at a magnetic inclination of 70°. The first gives us values for the ratios b/a (the length-to-width ratio of the prism in plan) and h/a (the ratio of flight height to prism width) directly from the anomaly; and the second converts these values into actual values for h, b, a. One may judge how efficient of the interpreter's time are techniques such as this when one compares them with the older curve-matching methods. The computer is not required for each interpretation, only for preparation of the characteristic curves. However, if a computer is available the interpreter is wise to calculate the anomaly of the interpreted body and compare it with the field data as a final check.

There are occasions, especially in doing gravity work, when the computer can be allowed to play a more direct hand in doing the actual interpretations, with a great saving of time and effort on the part of the geophysicist. These occasions arise in general whenever there is a distinct well isolated anomaly to which one wishes to fit a particular model. All that it is usually necessary to do is to give the computer a set of trial estimates for the dimensions for the model, and by some self-regulated cycling process it will refine these estimates to almost any desired degree. As a simple case in point, consider the gravity profile shown in Figure 5. This was taken from a survey done on a glacier for the purpose of mapping the ice thickness. Since the glacier is very long, the model chosen to represent it may be assumed to be two-dimensional. We allow it to be a prism with a polygonal cross section and a horizontal upper surface. The number of sides is limited only by the number of stations at which data are available. The machine can be instructed to form a trial cross section from the Bouguer gravity values, and then to use the discrepancies between these data and the calculated values to adjust the depths of the vertices. After several repetitions of this process, the discrepancies can as a rule be reduced to the level of observational error or to any other preassigned level. One of the difficulties with this particular problem was that the base level for the Bouguer gravity anomaly was uncertain. Notwithstanding this, the computer solved the problem, including the setting of the base level, for four different density contrasts in less than 1 minute. Compare this performance against the use of a graticule, or integration chart.

The same approach can be extended to problems in three dimensions, as well as to magnetics. The difficulty with using automatic procedures in magnetic interpretations, however, is that one is rarely certain of the direction of the magnetization in the body causing the anomaly; and if a serious error is made in this assumption the iterative processes tend to become oscillatory and may lead nowhere.

There is still another role for the computer in the field of interpretation which we have not mentioned yet. This is in the production of type curves and other numerical aids to interpretation in those areas where theoretical solutions cannot be obtained in any closed, algebraic form. Here the role of the machine is

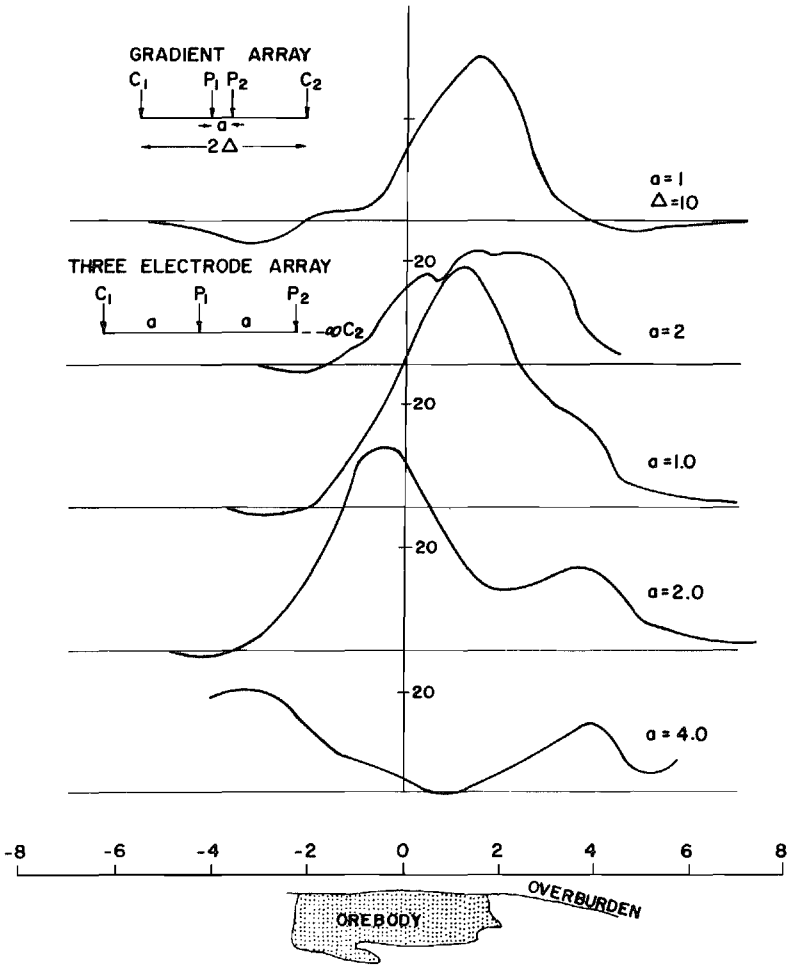


Figure 6. IP profiles observed at Pine Point and the cross section of the mineralized zone.

vital. No longer is it a question merely of increasing the speed and economy of the calculations, but of getting answers which cannot be obtained by any other means. The outstanding example in mining geophysics is to be found in the methods of resistivity and induced polarization. A variety of numerical techniques are available. The first which comes to mind is direct numerical solution of Laplace's equation, which works well in two dimensions but is not yet really feasible in three dimensions. In another approach the resistivity and the IP response of a theoretical body such as a spheroid or an ellipsoid imbedded in a half space is shown to be the solution of an inhomogeneous integral equation. The integral equation can be solved numerically on the computer, and type curves constructed for various electrode configurations.

One example may be sufficient for illustration. Figure 6 shows a set of field observations taken in the Pine Point area using a 3-electrode expander array. In Figure 7 is plotted a set of type curves for a flat-lying triaxial ellipsoid in a half space. These curves provide us with the closest over-all similarity to the field data that we could find among the profiles that have so far been calculated. The correspondence may not be all that one might hope for, but it is good enough to hazard an interpretation; and in this case the interpretation turned out rather well. The real point is, however, that without these type curves, in the production of which the computer was an indispensable agent, it would not have been possible to make any sort of quantitative interpretation at all.

A different application of the computer is to be found in the processing of field data. Some field methods, such as IP and gravity surveys require a lot of time-consuming routine work to present the data in a standard interpretable form. While it may be necessary for the operator to calculate and plot his data in the field, it is usually necessary to recalculate it in the office to check for errors and to replot it in a form that is standardized and neat enough to be presented to a client. An example of how IP survey data might be treated is as follows:

The field measurements are recorded on forms that facilitate transcription onto punched cards. Additional information on the geometry of the picket lines and the electrode configuration is added to the card deck and the data is input to the computer. The apparent resistivities and chargeability (or resistivity and metal factor, as the case may be) are then computed and the results treated for graphical output on a peripheral or off-line plotter.

Examples of IP graphical output are shown in Figures 8 and 9. These have been done on a Calcomp plotter using a very economical contouring program. Their elegance could easily be enhanced with a little increase in computer time and also by use of a different type of plotter. The point to note, however, is that

Contents

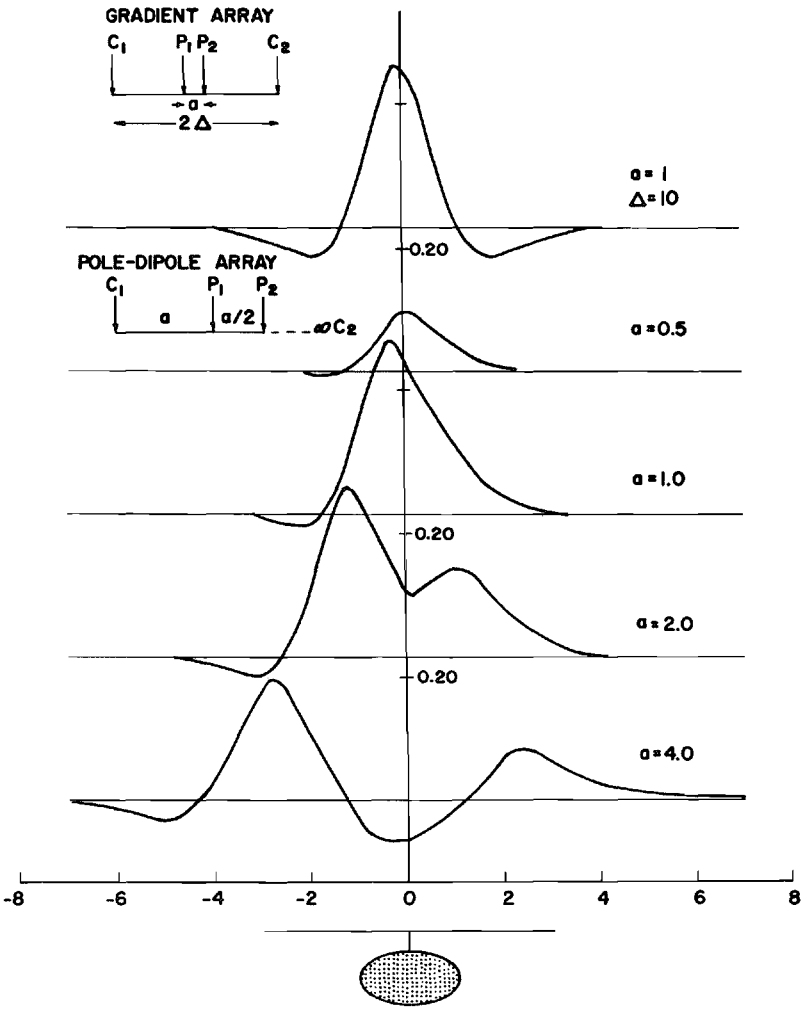
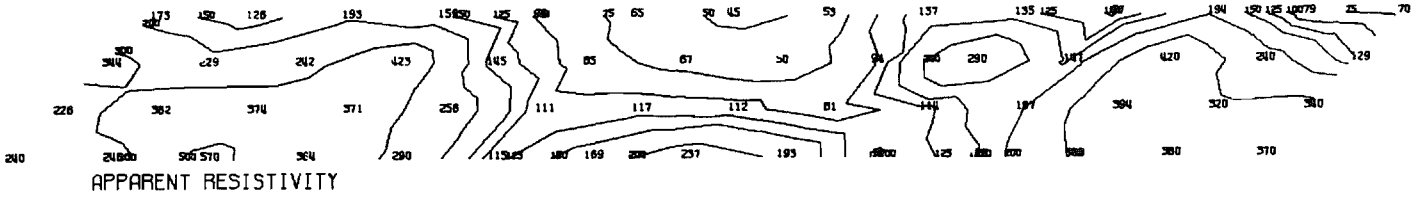


Figure 7. Theoretical IP profiles, for electrode configurations similar to those used at Pine Point, over a horizontal triaxial ellipsoid. The curves are calculated by numerical solution of an integral equation.



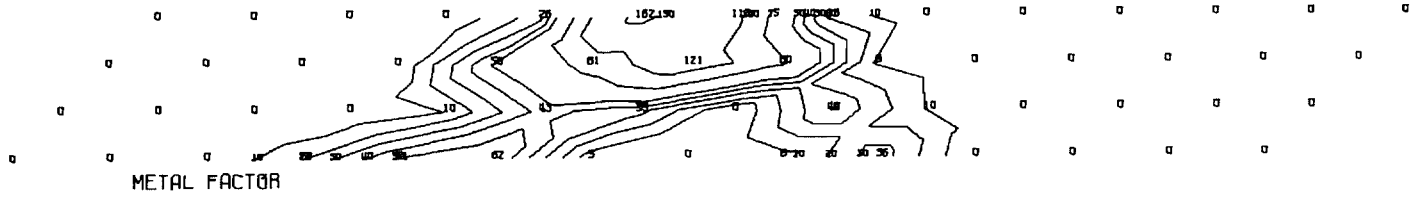


Figure 8. Apparent resistivity and metal factor sections plotted by computer from the field data.

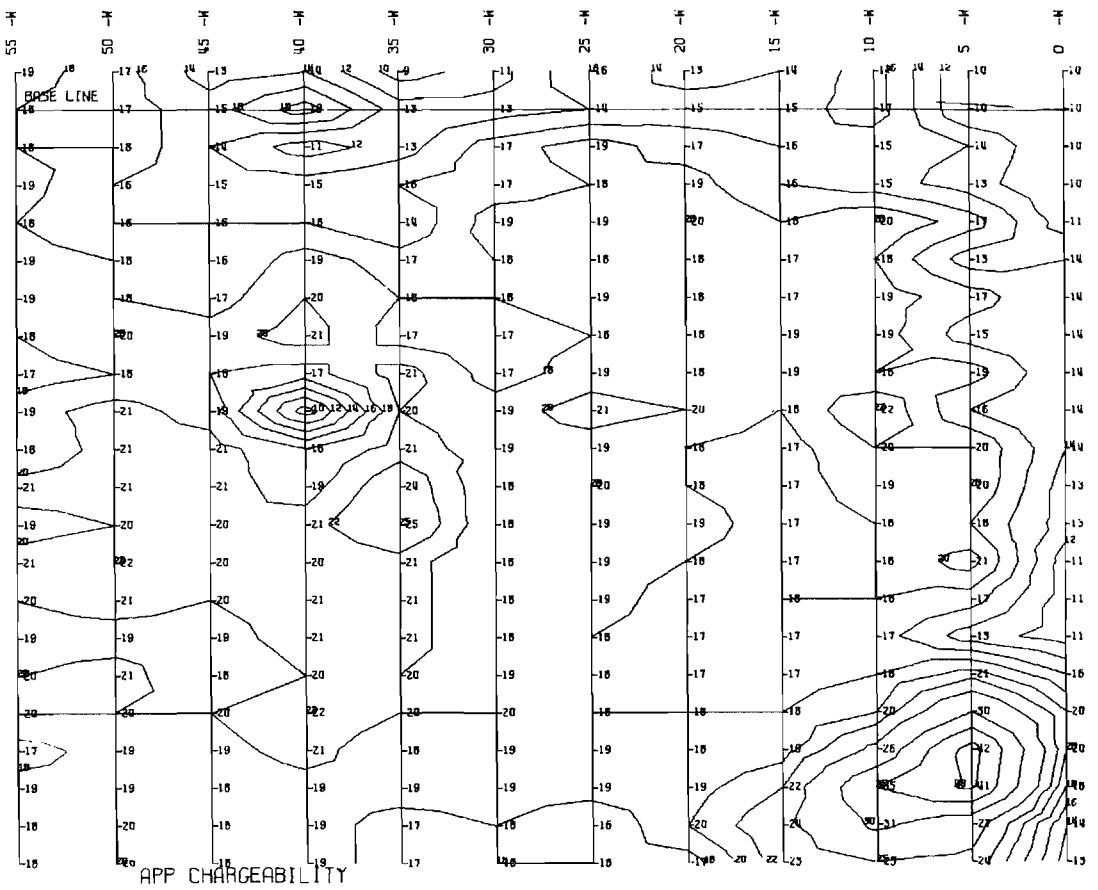


Figure 9. Chargeability map plotted by computer from the field data.

the field data can be handled very quickly, accurately and economically by computer.

Another growing use for large computers with graphical output devices is in the processing of aeromagnetic data. Heretofore, regional studies have been pretty much restricted to the visual recognition of major patterns, trends or changes in 'character', without any quantitative techniques being applied. It is a process that in the industry is often referred to as 'eyeball' interpretation. Now this approach continues to have great value, but there is a growing awareness that more quantitative evaluation methods are also needed. At the present time, efforts appear to be directed toward three goals, viz: (1) determining depths to the sources of magnetic disturbances from the general 'roughness' of the contour maps, through the use of power spectra; (2) determining major trend directions and regional anomaly patterns by removing extraneous 'noise' from the data; and (3) processing data (e.g., reducing to the pole, finding derivatives, continuing upward or downward) to extract information relating to specific geological questions, such as whether remanently magnetized bodies are present, where there are faults and other structural controls, and so on.

All of these undertakings require a great amount of processing of the data. Mostly they employ techniques that either involve, or are closely related to, Fourier analysis which, if it is to be done effectively on two-dimensional data, requires a machine of high speed and storage capacity. These techniques also demand a means of displaying the processed information quickly and cheaply; for otherwise they would impose an enormous burden upon the drafting departments of the institutions which use them, and lead to intolerable delays in the assessment of the results. The geophysicist may thus manipulate his data in almost any way he chooses, and within a few minutes he may view the contoured result. Aeromagnetics has thus achieved the fullest use of computing machinery of any mining geophysical method – as befits the very rapid acquisitions of data by this method.

We shall take a brief look at two examples. The first is from an aeromagnetic survey flown across a section of the Grenville province of the Canadian Shield in Quebec Province. The map is shown in Figure 10. In this case the map was digitized and passed through a low-pass filter, with the result of the smoothing shown in Figure 11. The gross dimensions of the anomalous bodies can be much better estimated from the smoothed map than from the original data. The other example is taken from a survey flown in the region of Alberta, where the prime object was to determine basement depth. Here the map (Figure 12) was digitized and a 'power' spectrum was plotted (Figure 13). This graph enables us to estimate the depth to the top of the sources directly, without having to depend on finding well isolated anomalies for analytical interpretation. Having got this depth, we may then continue the data downward toward the level of the sources, as shown in Figure 14. This process brings the magnetic anomalies much more sharply into focus, and reveals certain features which

Contents



Figure 10. A tracing of the main contours from the GSC aeromagnetic map of Lac Matonipi.

cannot be clearly seen in the original map, such as evidence for strike slip faulting.

Figures 11, 12 and 14 are also interesting examples of computer contouring. Figures 12 and 14 were done on a Calcomp incremental plotter using a high-quality contouring program. The contouring is generally excellent but some roughness of the lines remains, particularly in areas of low relief. Figure 11 shows an example of using an analogue plotter in its slewing mode. Contouring of this quality is probably considerably better than can be done manually, equalling manual work in smoothness and surpassing it in accuracy and objectiveness.

The foregoing examples are all state-of-the art applications of computers. As a final topic we may say something about how a small computer might possibly be used in an aircraft as an integral part of a geophysical surveying system.

First, and least interesting from a geophysical point of view, is the problem of precise navigation. Continuous strip photography has served us well, but it has drawbacks that are well known. Electronic navigating systems, of which there are a great variety, are going to be used more and more. One of their chief disadvantages is that the basic devices are mainly useful for finding out where the aircraft went, not where at any instant it is, in meaningful map coordinates. Integrated with a computer, one or a combination of several electronic navigation devices can plot the aircraft's track continuously and indicate to the pilot the deviation from the flight plan. Geophysical measurements can then be logged directly in terms of position coordinates and exceptional anomalies noted during flight can be reflown at closer line spacing or at different elevations. With the computer available, several different kinds of navigational devices can be integrated, greatly enhancing the practicality of electronic navigation. Commercial Doppler systems already contain a computer in them.

Turning to the computer's application in the geophysical apparatus, we shall discuss how it might be employed in a futuristic air EM system of the 'flying laboratory' rather than reconnaissance type. Present systems are undesirably limited in their depth penetration by noise of various kinds. The different noise sources can be classified as follows:

1. Basic system thermal agitation noise;
2. Electromagnetic interference: natural, aircraft generated, cultural;
3. Relative motion of receiver and transmitter coils;
4. EM response of the aircraft, varying due to motion of coils relative to aircraft, or changes in configuration of the aircraft (aeleron, elevator, rudder motions, etc.; and
5. EM response from uninteresting conductors.

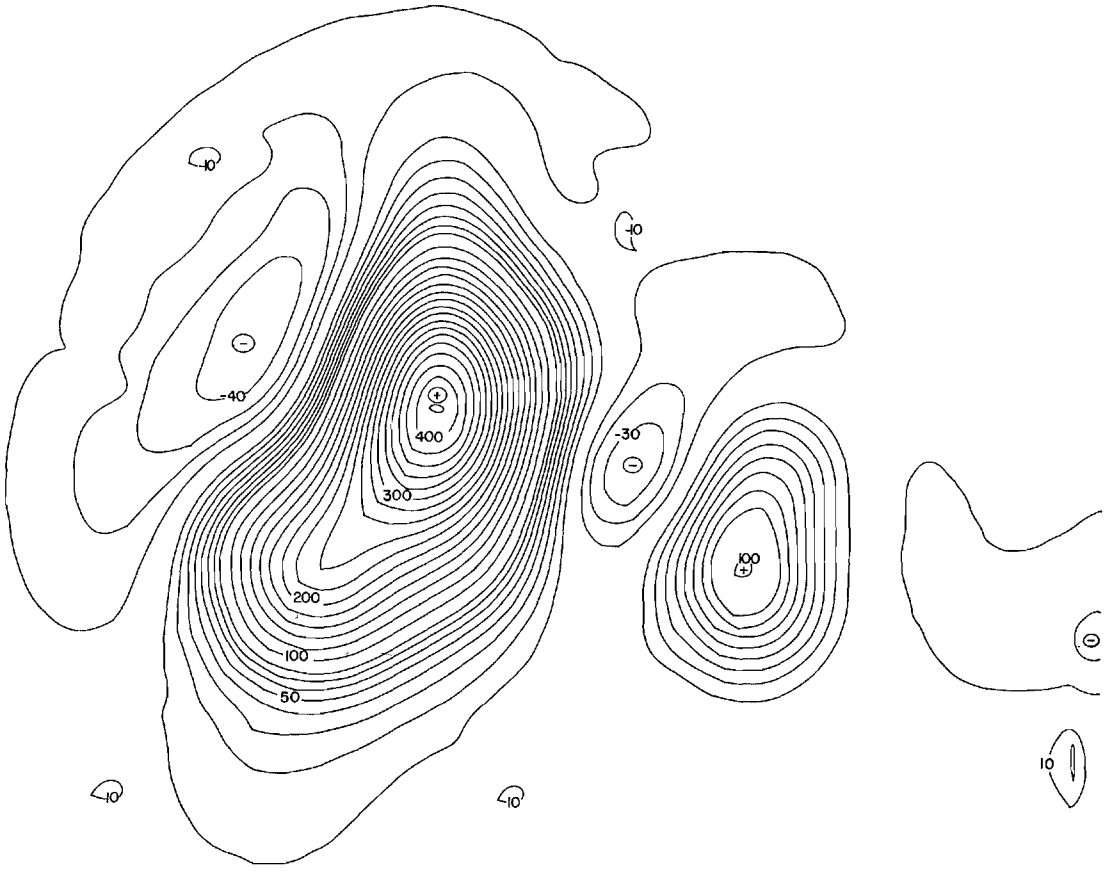


Figure 11. A high-quality, computer contouring of the smoothed Matonipi anomaly.

Future large systems need not be limited by noise of type 1 or 2 since if no other cure is possible the transmitter power can always be raised to a point where they are not too important. Noise of types 3, 4 and especially 5 is our problem and the computer can help in reducing them.

Noise of types 3 and 4 is well understood but often very difficult to eliminate in present systems. However, if changes in the relative positions of the receiver and transmitter coils can be accurately sensed, along with changes in position of the coil system and the aircraft and changes in configuration of the aircraft itself, there is no reason why accurate corrections cannot be applied to the EM measurements. Some 25 sensors might be required for this task, but none of the required measurements are beyond present strain, displacement and orientation-measuring technique. A small computer can sample and store the output of twenty-five devices every few tenths of a second without substantially reducing the time available for computing. Provided the correction equations can be kept in a simple form, say by expansion in power series, the computer should have no trouble keeping up with the correction calculations, while also plotting the corrected outputs on a graphic recorder. For safety the basic data could be stored on a digital magnetic tape, thus allowing recomputation with improved, more complicated, correction formulae at a later date, if this seemed advisable. It is my feeling that a system such as this might reduce the type 3 and 4 noise levels by a factor of 10 to 100. It will certainly be simpler than introducing active analogue control systems to stabilize each of the noise-generating factors, a possibility now being contemplated by instrument builders.

Assuming success in drastically reducing noise types 1 to 4, we find ourselves left with no improvement in type 5, the noise which already predominates in many of our best EM systems. At this point the ingenuity of the geophysicist, rather than of the instrumentation engineer, must be called upon. The solution will not be so easily found, for while we know and understand fairly well the physics of our apparatus we certainly do not have an adequate knowledge of the electrical properties of all the possible types of terrain we wish to prospect. Since it is not possible to describe in clear and quantitative physical terms what sort of conductors should, ideally, produce a response from our system and what should not, it is obviously more difficult to design a system to discriminate between them.

However, the difficulty is perhaps overstated. Experience with present-generation EM systems has shown vividly that different systems respond differently to conductors of different types. Also, it is clear that no simple present-day system can differentiate between wanted and unwanted conductors in all cases. Therefore it seems that our futuristic instrument must be a multiple sensor EM system. The different components must be chosen so that the comparative response of each system to

Contents

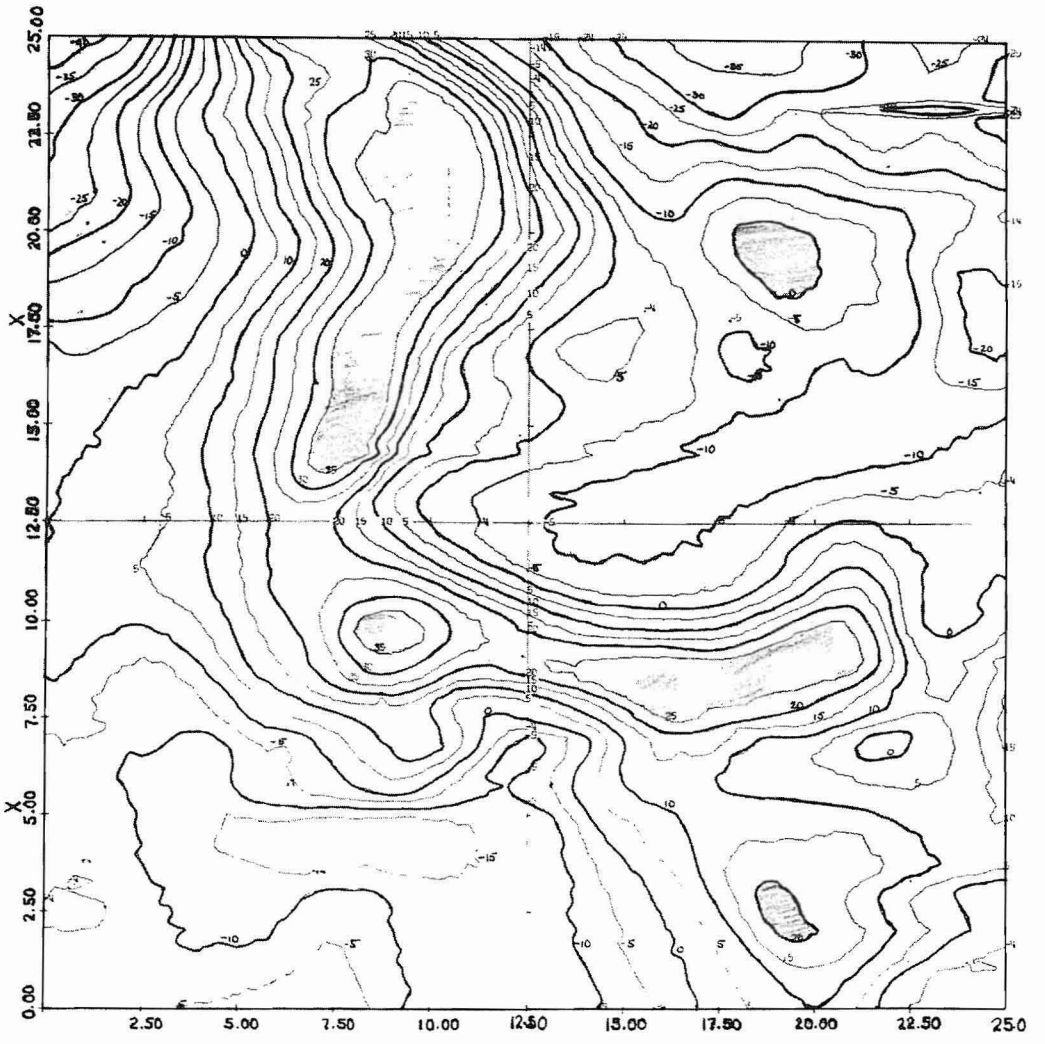


Figure 12. A Calcomp contouring of digitized data taken from the GSC Wabiscaw aeromagnetic map (Alberta).

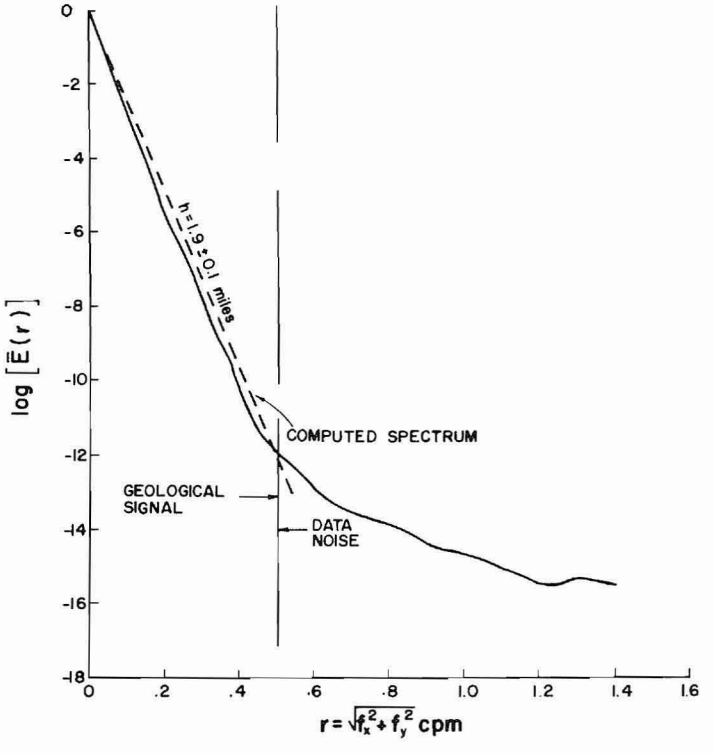


Figure 13. The circularly averaged power spectrum of the Wabiscaw map.

different types of conductors is markedly different for each system. For instance one system might give larger response for horizontal than vertical conductors, another the opposite; one might respond equally to large poor conductors and small highly conducting, concentrated ones; another only to small, good conductors. The task of the computer then will be to correlate the outputs of the different sensors and produce from them a small number of outputs which are each most sensitive to conductors of a specific type.

Along with the selection of the different EM sensors the computer correlation program will have a tremendous influence on the results. Indeed one can foresee several competitive companies all employing the same hardware but using it differently, each with its own program incorporating its own interpretation experience. Different routines undoubtedly would be required in different geological environments.

As envisaged, the design of the correlation routine might be partially based on the results of model experiments. However these would have more influence on the initial selection of

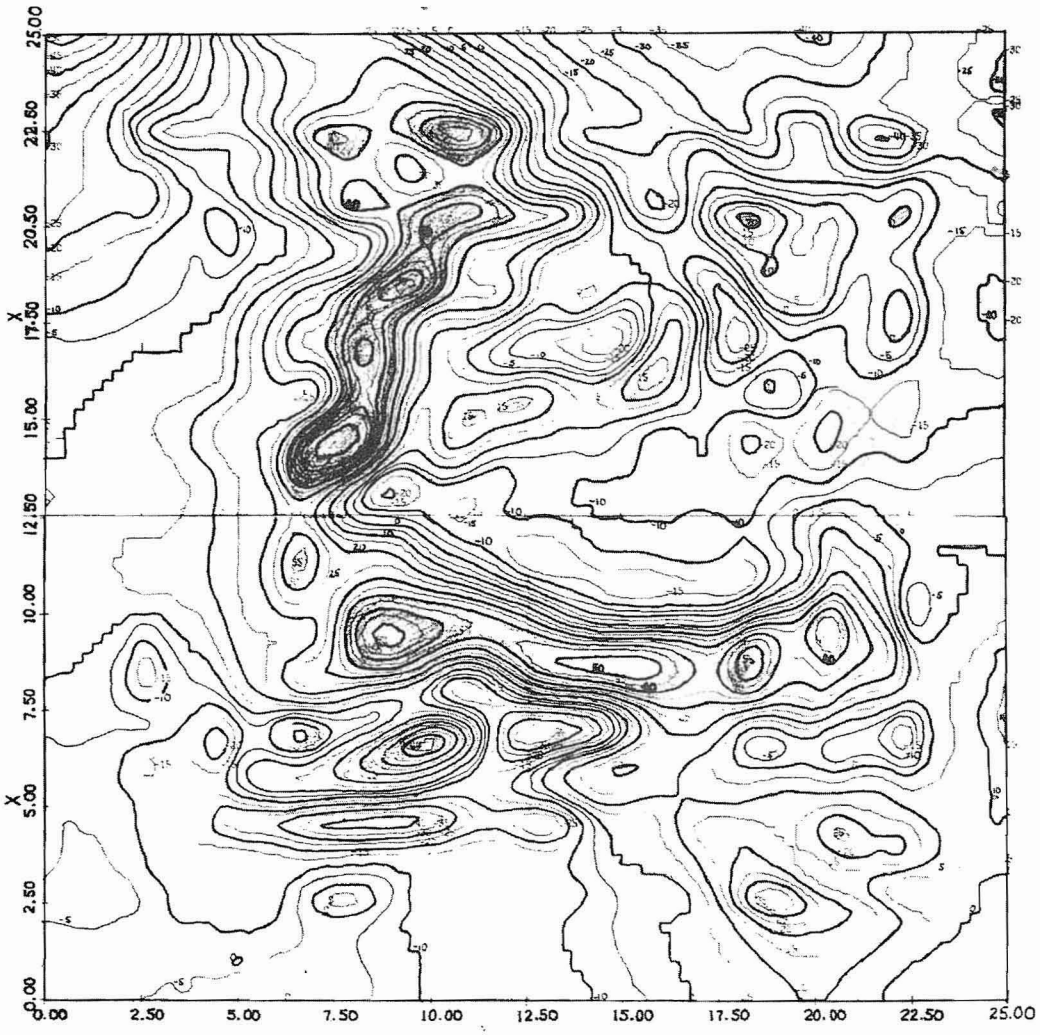


Figure 14. A downward continuation of the Wabiscaw map, plotted by Calcomp.

sensors than on the programming. If the correlation routine could be set up in the framework of multichannel, least-squares optimum filtering then the essential information required, besides the EM sensor signals, is a series of auto- and cross-correlation functions. These are statistical measures of the average kind of sensor outputs obtained in the geological region being surveyed and of the typical kinds of responses given by wanted bodies. These would be acquired by actual flight experience, just as a present-day interpreter gets the feel of his data after working with a lot of it. It would therefore be very desirable to tape record the basic data of a survey while plotting the preliminary processed output in the aircraft, so that experience in ground-checking the conductors could be used to select a more efficient filtering routine. The survey data could then be reprocessed one or more times during the ground-checking period to increase the efficiency of identifying interesting anomalies.

Acknowledgments

We wish to thank Mr. Allan Spector, graduate student in the Geophysics Laboratory, University of Toronto, for supplying us with the examples of aeromagnetic data processing (Figures 11 to 14).

Regional reconnaissance techniques applied to exploration

A.R. Barringer

Barringer Research
Rexdale, Ont., Canada

Abstract. There is a major requirement for environmental geophysical and geochemical techniques which enable large areas to be scanned at low cost per unit area in order to select regions of major ore potential. Approaches to solving this problem are discussed and the use of a multiparameter airborne system is proposed for the detection of target areas based on geophysical and geochemical expressions of favourable geological conditions. A new airborne system called "Radiophase" is described which employs VLF radio fields transmitted by government stations. Brief mention is made of other new airborne geophysical and geochemical techniques under development.

Résumé. Il existe un besoin général de techniques d'exploration géophysique et géochimique à l'échelle régionale permettant l'étude de vastes régions à un coût peu élevé afin de découvrir des minéralisations intéressantes. L'auteur traite de différentes façons d'aborder ce problème et propose l'emploi d'un système aéroporté à paramètres multiples pour la détection des régions cibles, fondé sur les expressions géophysiques et géochimiques des conditions géologiques favorables. Il décrit un nouveau système aéroporté appelé "Radiophase" qui emploie des ondes radioélectriques à très basse fréquence (VLF) émises par des postes de l'état. Il mentionne également d'autres systèmes géophysiques et géochimiques aéroportés en voie d'élaboration.

A principal target in the development of new geophysical techniques is to provide improvements in exploration efficiency and depth of penetration. One of the main problems that exist today is the high cost of discovery. Very large numbers of anomalies are drilled at great expense which do not lead to orebodies, but instead to barren sulphides, graphitic bands, or other natural conditions which can provide misleading or ambiguous results. We know from experience that orebodies tend to occur in certain specific areas and that when faced with large tracts of country to explore, our chances of success obviously would be much higher if we could initially define with a reasonable degree of certainty the areas of good ore potential. Thus, there appear to be two requirements to be met in the development of new exploration technology. First, we want improved methods of selecting target areas; and secondly, we would like to be able to detect orebodies down to the full economic mining depths in already proven mining camps as well as new exploration regions.

Obviously it would be desirable if we could develop methods of discriminating against barren sulphides and directly detecting commercial ore by means of instruments. At the present time, however, there appears to be no promising approach to achieving this end and the most practical avenue for research seems to be the development of methods which can assist the geologist in identifying the environmental associations or orebodies.

It would be a great advantage if methods could be developed for covering very large areas, amounting to hundreds of thousands of square miles, with techniques which, at a cost of only a few dollars per square mile, could reliably identify highly promising target areas within these broad regions. The higher-cost methods of detailed airborne exploration, ground geophysics and geochemistry, could then be focussed on these high-priority areas. At the present time it is extremely costly to cover large geographical and geological units with detailed airborne geophysical surveys, and inevitably broad-scale coverage leads to expensive and often disappointing ground follow-up programs in areas which prove to be devoid of economic mineralization.

If we examine the existing geological information on the world's major mining camps in an attempt to look for common denominators which might be detected geophysically, there are certain features that stand out. There is a clearcut association of large orebodies with what might be called primary crustal structures. Thus, in a study of North American deposits in which production and reserves gross more than one billion dollars worth of ore, it has been found that thirty out of thirty four of these deposits are reported as being associated with major structures (Billingsley and Locke, 1935; 1941; Goodwin, 1965; James, *et al.*, 1961; King, 1966; Kornick and MacLaren, 1966; Latulippe, 1956; Leech, 1966; Mardirosian, 1966; Mayo, 1958; Ohle, 1959; Park, 1964; Roddick and Green, 1961; Savage, 1964; Stevenson, 1962; Stockwell, 1957; Titley and Hicks, 1966; Turneaure, 1955; Wilson, 1967; Wisser, 1959). The recognition of these deep structures has been based upon conventional geological mapping and the percentage is probably even higher since it appears that many major deep structures go by unrecognized on geological maps, a fact which can be established by comparison of existing maps with airphoto mosaics, high-altitude satellite photographs and regional aeromagnetic compilations. Thus, it appears that recognition of major crustal fracturing is of great importance in exploration.

It will be noted, however, that the association between orebodies and major crustal structures is often fairly loose and mineral occurrences may occur as much as ten miles away from these structures. Supplementing this loose primary structural association, there is often strong local control of ore deposition by structure, and descriptions and case histories abound in the literature (CIM, 1948; Goodwin, 1965; Roddick and Green, 1961; Savage, 1964; Stockwell, 1957; Titley and Hicks, 1966; Wisser, 1960). These structures may be termed secondary structures to differentiate them from the deep crustal features, and represent a further target for recognition by geophysical techniques. Another well known association of orebodies is the presence of certain favourable rock types. In the Canadian Shield, for example, there is a growing recognition of the relationship

between ores and volcanic suites of rocks. Both acid and basic volcanics almost invariably occur in the proximity of mineral deposits in the Canadian Shield (Goodwin, 1965; Wilson, 1967). This characteristic association has a geophysical expression which is amenable to recognition by airborne geophysical methods.

This abbreviated discussion on the environmental characteristics of orebodies provides some background for a general consideration of geophysical and geochemical techniques applied to the area selection problem. Thus with regard to the recognition of deep crustal structures, it has become apparent in recent years that regional aeromagnetic coverage is extremely effective in identifying such structures. The gradually expanding aeromagnetic coverage of Canada has been developing a remarkable picture of the Shield and it has been shown by Kornick and MacLaren (1966) that many magnetic lineaments can be traced for hundreds of miles. Statistical studies of trends on aeromagnetic maps by Affleck (1963) have shown that recurrent trend patterns remarkably complement the directions of faulting and lineation which have been recognized by structural geologists. Frequency histograms of the distances between magnetic trends also suggests an order in the crustal features of portions of the continent which is possibly related to the much more clearly defined magnetic patterns occurring beneath the oceans (Badgley, 1965; Raaf and Mason, 1961; Vine and Wilson, 1965; Vine, 1966). Much of the broad-scale structural fabric that appears on regional compilations of detailed aeromagnetic maps seems likely to be revealed by flying traverses at relatively widely spaced intervals. Thus, in work carried out by the U.S. Geological Survey (Zeitz, *et al.*, 1966) flights flown at five-mile intervals at heights of up to 15,000 feet, disclosed magnetic lineaments of hundreds of miles in length. The writer has experimented with optical filtering on the magnetic coverage of the Canadian Shield and has established that virtually all of the magnetic lineaments of 100 miles in length or greater could have been revealed by flight patterns spacing of five miles. It is contended that features of this length are likely to have depth extensions which extend all the way down to the Curie Point and to the bottom of the upper crust, since this distance is only a fraction of the lineament length.

If it is accepted that major crustal features are of considerable economic importance because of their frequent relationship with major mining camps then the fact that these can be traced very rapidly and at relatively low cost by wide-spaced traversing is significant. One might conclude that there would be an important advantage in carrying out a large national survey program by making a preliminary reconnaissance of an entire country by wide traversing prior to carrying out detailed work. This would give exploration geologists and geophysicists valuable basic information at an early date. Furthermore, the information that could be extracted from wide traversing extends well beyond that of defining lineament patterns. The recognition of magnetic provinces of the type which have been described by Affleck (1963) is feasible on a broad scale from wide traverse interval magnetic data. These magnetic provinces are differentiated as crustal units of distinct magnetic character and pattern with regard to magnetic intensity, distribution of lineaments and spatial frequency content. There is also scope for the use of three component magnetics of the type used by Serson (1967) as a further aid to defining magnetic provinces. These can be flown on a wide traverse survey using a multiple fluxgate magnetometer mounted on a stabilized platform or a proton magnetometer with field coil attachments, digital recording and a high quality vertical reference.

The definition and plotting of magnetic provinces can be supplemented by reconnaissance geochemical surveys aimed at identifying geochemical provinces. The effectiveness of regional geochemistry has been demonstrated in recent surveys by Taylor, Nichol and Webb (1967). Correlation of favourable trace element assemblages with major crustal features appears in theory to be of great significance for exploration purposes and geochemical techniques have a potential comparable in importance in both reconnaissance and detailed exploration with geophysical methods.

Reference has so far been made solely to the use of magnetics for defining major lineaments and magnetic provinces, but it appears that the use of complementary techniques operated simultaneously with the magnetometer could greatly enhance the value of aeromagnetic reconnaissance surveys. It would be attractive to use multiple systems such as infrared scanning, side look radar and multiband photography, but these involve high capital costs. In addition both operational and data costs are multiplied. Viewing exploration surveys in terms of cost effectiveness, it is desirable to use modern light twin-engine aircraft which can be purchased relatively cheaply and operated at a low cost. The choice of instruments which can be used in conjunction with the magnetometer will depend to some extent upon the circumstances. In general, there is poor compatibility between geophysical survey and aerial photography requirements, since photography unlike geophysics generally calls for high-altitude flying and minimum cloud coverage. Photographic coverage is therefore usually carried out in separate surveys. Regional geophysical reconnaissance requires complementary instruments to the magnetometer which will assist in identifying deep-seated structures that reach the surface or near surface and which also help to characterize rock types by different physical properties, such as conductivity.

Research is under way at the present time on the use of VLF radio signals for conductivity mapping. A new system known as the Radiophase technique has been developed and is described below. This equipment is very light and forms an excellent complement to the airborne magnetometer since it can be flown in the same aircraft and is capable of giving good signal-to-noise ratios under all conditions suitable for aeromagnetic surveying. A related technique known as Teltran which employs the electric and magnetic components of natural sferic fields at 390 and 10,000 Hertz is also under development for the detection of deep conductive structures.

Further equipment which is compatible with the other two systems and which can provide valuable supplementary geological information is the gamma-ray spectrometer. There is a complementary relationship between the magnetite content and potassium content in rocks, with basic types tending to have high susceptibility and low potassium content whilst acidic rocks occupy the reverse position. The classification of rock types by the ratio of magnetic response to potassium count should prove of assistance in identifying complexes of acid and basic rocks and the degree of differentiation within intrusive bodies. Filtering techniques can be used in the case of magnetics to help in

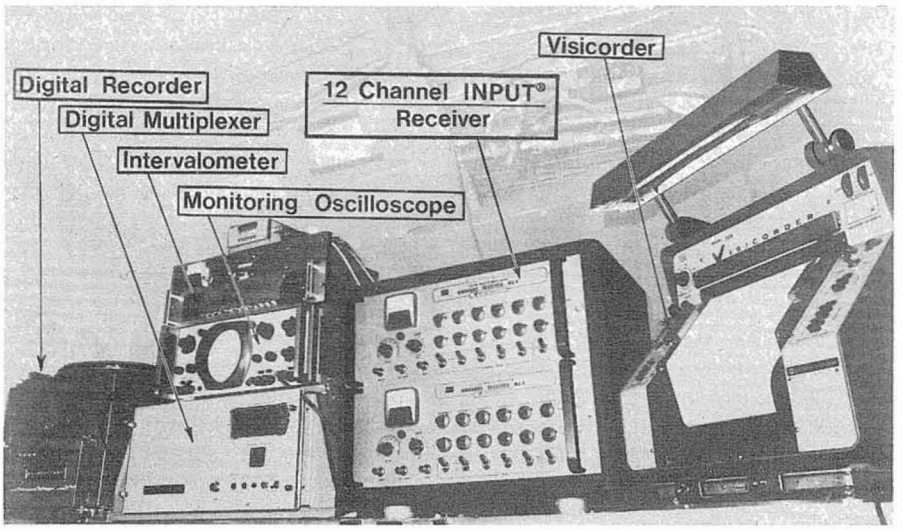


Figure 1. Annotated drawing of the digital Input® system in an aircraft installation.

identifying the susceptibility of near-surface rocks for correlation with the gamma-ray spectrometer outputs. Confirmation of the potential of gamma ray surveys for geological mapping has been shown in surveys by the USGS and others (Boltneva, *et al.*, 1964; Moxham, *et al.*, 1965; Popenoe, 1962; Williams and Lorenz, 1957).

The analysis of data resulting from regional coverage with multiparameter geophysical instrumentation is designed to lead to the definition of major tectonic features and crustal blocks and ultimately to the selection of target areas. Interpretation calls for the utilization of all of the available ground information, existing geological mapping, listing of known mineral deposits, etc. It has also been shown that regional geochemical reconnaissance for the identification of geochemical and metallogenetic provinces is capable of providing an invaluable addition for the interpretation of regional geophysical reconnaissance surveys.

The technique of following up with a second phase of more detailed traversing can utilize the same instrumentation as in the first phase, but with the different objective of defining secondary geological structures and providing more detailed information on the distribution of rock types. The systems (magnetometer, Radiophase, and gamma-ray spectrometer) outlined are capable of providing a wealth of geological information when flown on a traverse interval, for example, of one mile. During this phase of exploration, it is possible to look for favourable associations of rock types in conjunction with structures which may branch off from the deep crustal structures defined in the first phase. It is also feasible to eliminate areas which are clearly devoid of a geological environment favourable to mineralization. Because of the use of wide-traversing intervals of typically one mile and the relatively low aircraft costs, this phase can cost as little as $10 to $20 per square mile, which is a fraction of that required for detailed airborne survey. The favourable and high-priority target areas can be selected at this stage of survey for detailed airborne coverage. Once again, this phase calls for the integration of all of the existing ground information plus the use of geochemical and other ground truth techniques for confirming some interpretations and supplementing the data with information on the distribution of trace elements within the areas.

The third airborne phase utilizes deep penetration airborne electromagnetic techniques in conjunction with the instruments described below. This stage is more costly since traverse intervals of typically five lines per mile are required and in addition the electromagnetic survey equipment calls for heavier and more costly aircraft. Costs are likely to be in the vicinity of $100 per square mile, but, as a result of the preparatory phases, the coverage is now focussed on high-priority areas where, from the geophysical, geochemical and geological point of view, the chances of finding ore are considered to be far above average. For this reason special emphasis should be given at this stage to the quality of coverage with no effort being spared to achieve optimum survey results with regard to penetration and interpretation of results.

The benefits of applying airborne geophysical techniques to the recognition of conductive anomalies which sit in favourable structural zones has not been heavily stressed in the past. The use of plane-wave systems which use signals transmitted from a distant source, such as VLF radio signals, can achieve far higher sensitivity to shear zones, contacts and conductive horizons than conventional EM. This feature, which until recently has tended to be regarded as a disadvantage, is a distinct advantage when used as a geological tool in a fashion complementary to active airborne electromagnetic systems, since it enables patterns of folding and faulting to be traced out in the vicinity of potential orebodies.

Three airborne phases of exploration have been discussed. These may be carried out concurrently with various types of ground geochemistry and followed up by ground geophysics such as EM, gravity and induced polarization. Ground methods naturally play a key role in defining drilling targets and there is much scope for new developments in the area of improving the penetration and resolution of existing equipment. In particular the deep penetration techniques that show promise for the future include magnetotelluric systems and ground electromagnetic pulse transient systems. Low-frequency natural fields have the advantage of penetrating to great depth and the analysis of these fields by variants of magnetotelluric method enable structures and buried conductive sulphide bodies to be detected at depths of 1000 feet or greater. Considerable improvement is also feasible with electromagnetic systems employing locally generated fields. The ground-operated pulse method, for example, has been used extensively by Russian geophysicists and offers the advantage of having multifrequency components, which enables sophisticated

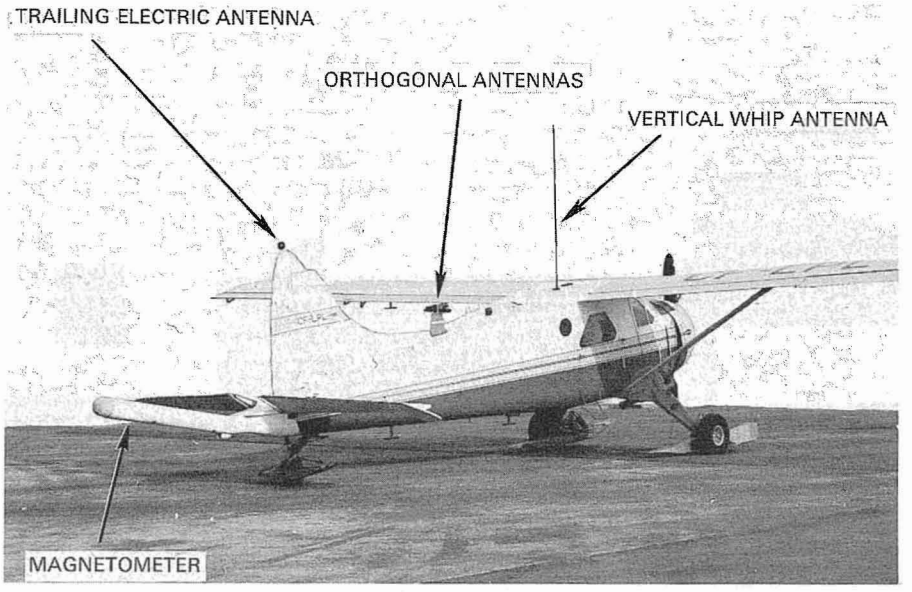


Figure 2. Radiophase system showing the orthogonal loop antennas mounted on the aircraft along with the vertical whip antenna.

analyses to be carried out as a means of determining numerous geometrical and conductivity parameters.

In the field of geochemistry, statistical methods of analysis of geochemical data and new chemical techniques are improving resolution and depth penetration. For example, differential extractions of mercury from soils shows promise of differentiating mercury arising from nearby base metal deposits as compared with mercury that has travelled considerable distances.

Data processing and magnetic recording

In the field of data interpretation, the arrival of low-cost microcircuitry on the commercial market has given birth to a whole new generation of low-cost small digital computers which can be readily adapted to many geophysical data problems. In particular, the use of digital filtering techniques, such as those developed by Bhattacharyya and Raychaudhuri (1967) will find increasing application for airborne geophysical data.

The problems of data interpretation and data handling become significant when a number of geophysical instruments are used simultaneously. The use of magnetic recording techniques becomes essential if large volumes of airborne data are to be handled efficiently. Experiments are being carried out on the use of both digital and FM magnetic recording techniques. Some of this work has been carried out on behalf of the Canadian Geological Survey under the direction of L.S. Collett. Digital magnetic equipment in use is shown in Figure 1. Difficulty has been encountered in using digital recording equipment, and with regard to ruggedness and reliability it is not as good as FM recording methods. In the writer's experience to date, FM methods have been preferred for data gathering with subsequent digitization of the tapes being used during data handling.

The great advantage of using magnetic recording techniques for gathering data is that maps can be prepared very rapidly by the computer. Computer programs for contouring have improved to the point where they are fully acceptable. Furthermore data manipulation such as filtering is now feasible on a scale which was previously impracticable. It is predicted that this will have a major impact on airborne geophysics in the near future. Some geophysical data problems lend themselves to processing by optical filtering methods including two dimensional fourier analysis (Pincus and Debrin, 1966) and it is expected that there will be attempts to combine digital and optical techniques to utilize the special advantages of both. Imaging methods such as aerial photography, side-look radar and infrared scanning are particularly suitable for optical processing including methods of pattern enhancement and statistical analysis of structure. Processing the large volumes of data which will be produced by orbiting satellites is an obvious future application for these techniques.

Discussion of some specific airborne systems follows, representing some current developments fitting into the regional reconnaissance approach that has been outlined.

Radiophase system

This system is based on the measurement of the phase and amplitude relationships between the electric and magnetic field components of signals transmitted from radio stations. The preferred frequency range lies in the VLF region where the U.S. Navy and other government organizations propagate signals from high-power stations which travel over distances of thousands of miles. These stations have frequencies which typically lie in the vicinity of 20 kilohertz and operate at powers up to 2 million watts. Skin depths at these frequencies vary between about 50 and 500 feet in overburden in the 10 to 1000 ohm meter resistivity range, whilst skin depths in bedrock of high resistivity can be in excess of 1000 feet. This has been verified in underground tests in mines and drillholes (Paal, 1965). It is therefore apparent that VLF signals have considerable potential for electromagnetic mapping of surface and subsurface resistivity.

The principal feature of the Radiophase system is the use of a vertical whip electric antenna as a phase reference. It can be shown from the work carried out on radio propagation by Norton (1937), and others (Howe, 1940; Wait, 1962) that over a homogeneous flat earth, the vertical electric component of the

Contents

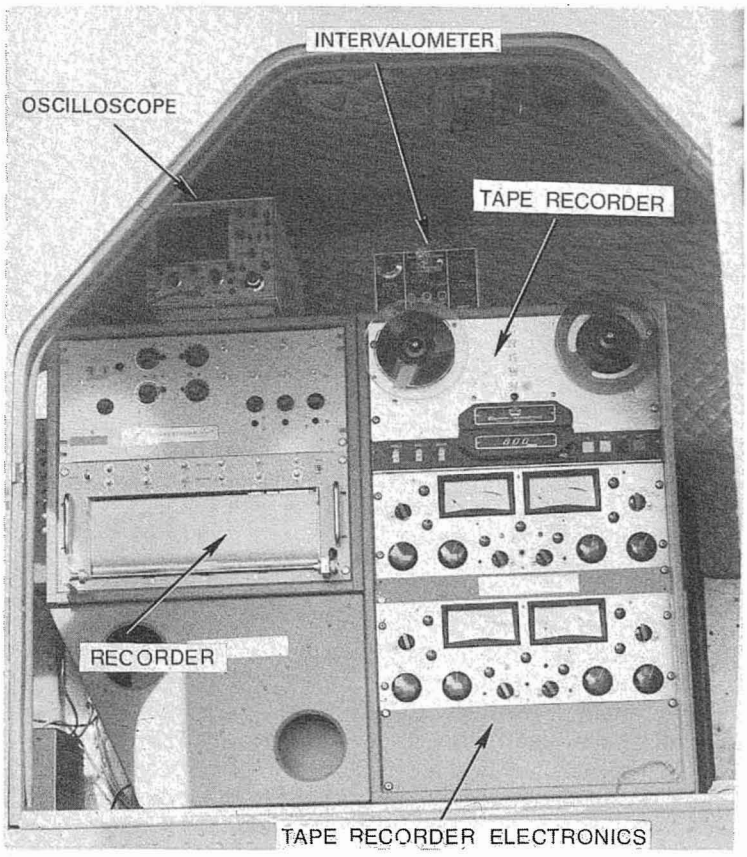


Figure 3. Aircraft Radiophase installation.

propagated electromagnetic field is in phase with the horizontal magnetic component. This relationship holds only in the far field at distances greater than 5 wavelengths from the transmitter and at these distances the surface or groundwave generally predominates over the spacewave when close to the ground. Thus, in a low-flying aircraft there will be no component of the horizontal magnetic field in phase quadrature with the vertical electric field providing that the underlying terrain has homogeneous conductivity down to the skin depth of penetration of the radio wave. However, in the presence of a dipping conductive sheet, eddy currents are induced in this sheet which generate secondary electromagnetic fields. When this dipping conductive plane is traversed by the system, its near field radiation is found to be largely in the magnetic field. Pronounced phase and amplitude changes are noted in the magnetic antenna while the electric antenna maintains relative phase stability. It is therefore possible to measure a quadrature component in the magnetic antenna using the vertical electric antenna as a phase reference. This method gives anomalies which peak directly over the top of the outcrop of the conductive sheet. Both in-phase and out-of-phase measurements can be made on two orthogonal magnetic field antennas but for simplicity, measurements are at present restricted to quadrature components only. The ratio of the two quadrature outputs of the magnetic antennas enables the azimuth direction of the secondary field to be determined. This direction is perpendicular to the strike direction of the conductive sheet at the position where the anomaly peaks, a fact which allows the strike of the dipping sheet to be readily determined in a single traverse. It is also possible to use a third vertical axis magnetic field antenna to provide information on dip.

In experimental surveys carried out with the Radiophase system, contoured maps have been prepared of the total horizontal intensity of the component of the magnetic field in phase quadrature to the vertical electric field. Orthogonal loop antennas are mounted on the aircraft along with the vertical whip antenna as shown in Figure 2. The outputs of the quadrature components of the loop antennas are recorded on paper chart recorders or magnetic tape (Figure 3) and are digitized during the data processing. A computer is used to determine the square root of the sum of the squares and thereby provide horizontal intensity measurements. Flight path recovery is carried out by standard procedures and the fiducial points on the flight lines are digitized in X and Y co-ordinates. The computer is then used to produce maps of horizontal intensity and strike-angle of the field.

An example of the horizontal intensity map is shown in Figure 4a. This is an area 10 miles north of Noranda in Quebec. The transmitter used in this survey is located to the east-southeast of the area. In the northern half of the map the Radiophase contours are seen to flank the magnetic high and to correlate with the trend of the magnetics (Figure 4b), the geology and the photolineaments (Figure 4c). In the southern half of the map the conductivity pattern crosscuts both the geology and the magnetic trend, while correlating with the E-W lineament pattern. It appears that the crosscutting shearing in this direction is conductive and is connected with the known mineralization. The relationship between the conductivity and magnetic contouring appears to be of particular interest since conductivity assumes special significance in terms of mineralization when it is associated with magnetic patterns indicative of geology favourable for mineralization.

The response to ground conductivity of the Radiophase system is related to the transmitter direction, and when a conductive feature is perpendicular to the direction of field propagation, it will not be detected. For this reason it would be an obvious advantage to fly surveys whilst simultaneously recording two stations. Similarly both the in-phase and out-of-phase components of magnetic field should be recorded to facilitate interpretation. These features are being added to a more comprehensive system under construction.

Teltran system

A system which has been called Teltran (an abbreviation of telluric transients) is under development as an outgrowth of the AFMAG system developed by McLaughlin, Cartier, Ward and others. It uses low-frequency natural electromagnetic fields generated by lightning discharges and differs from the AFMAG system in that the airborne receiver records three components of field instead of two and the recordings are normalized against a base station which synchronously records three field components on magnetic tape. This enables the results to be processed in the computer according to the direction of propagation of the natural electromagnetic fields and facilitates the preparation of maps of the residual secondary field showing strike, dip and intensity. Preliminary airborne surveys have indicated the feasibility of making airborne magnetic recordings along with synchronized base station recordings and it is believed that this approach will ultimately prove very important in tracing deep structure and

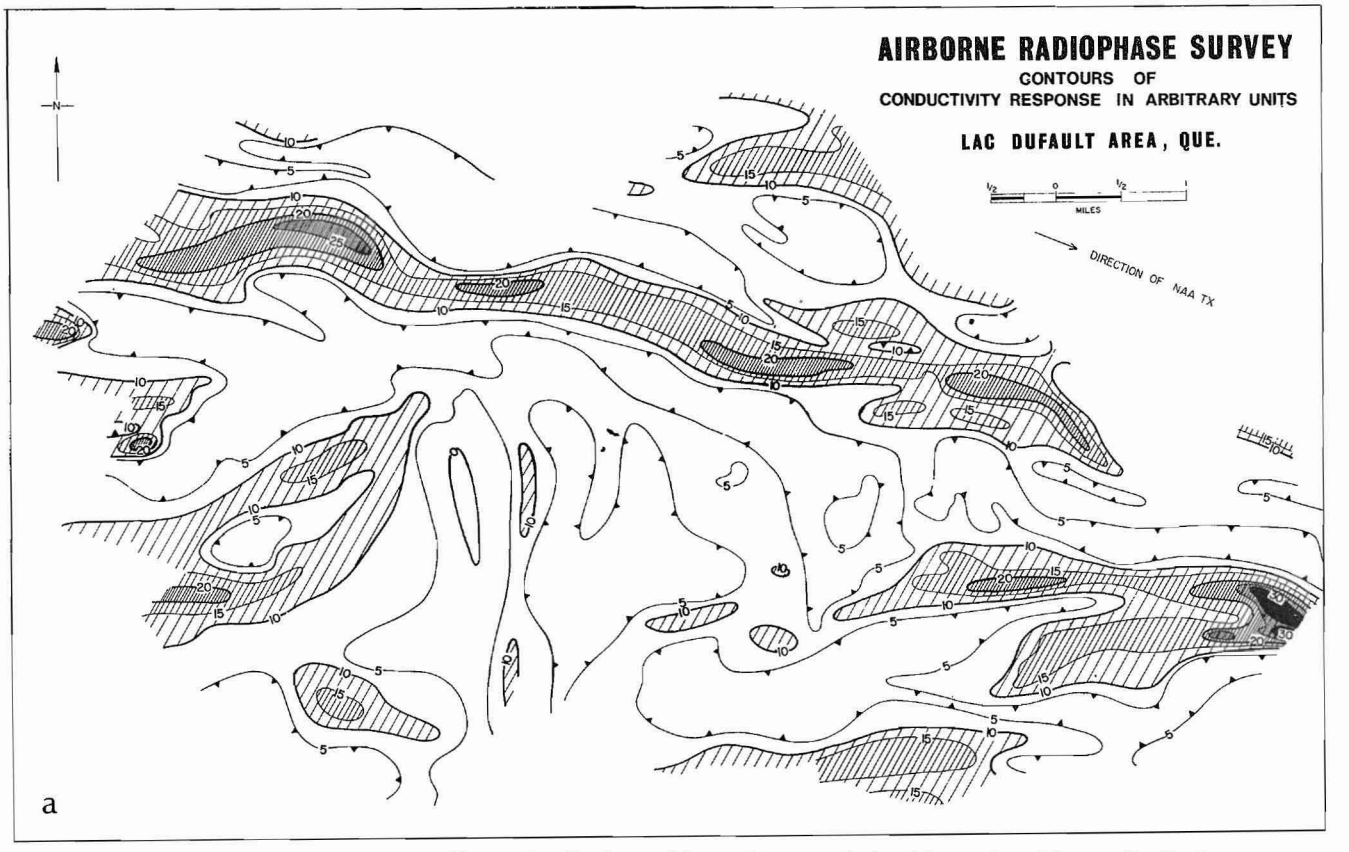
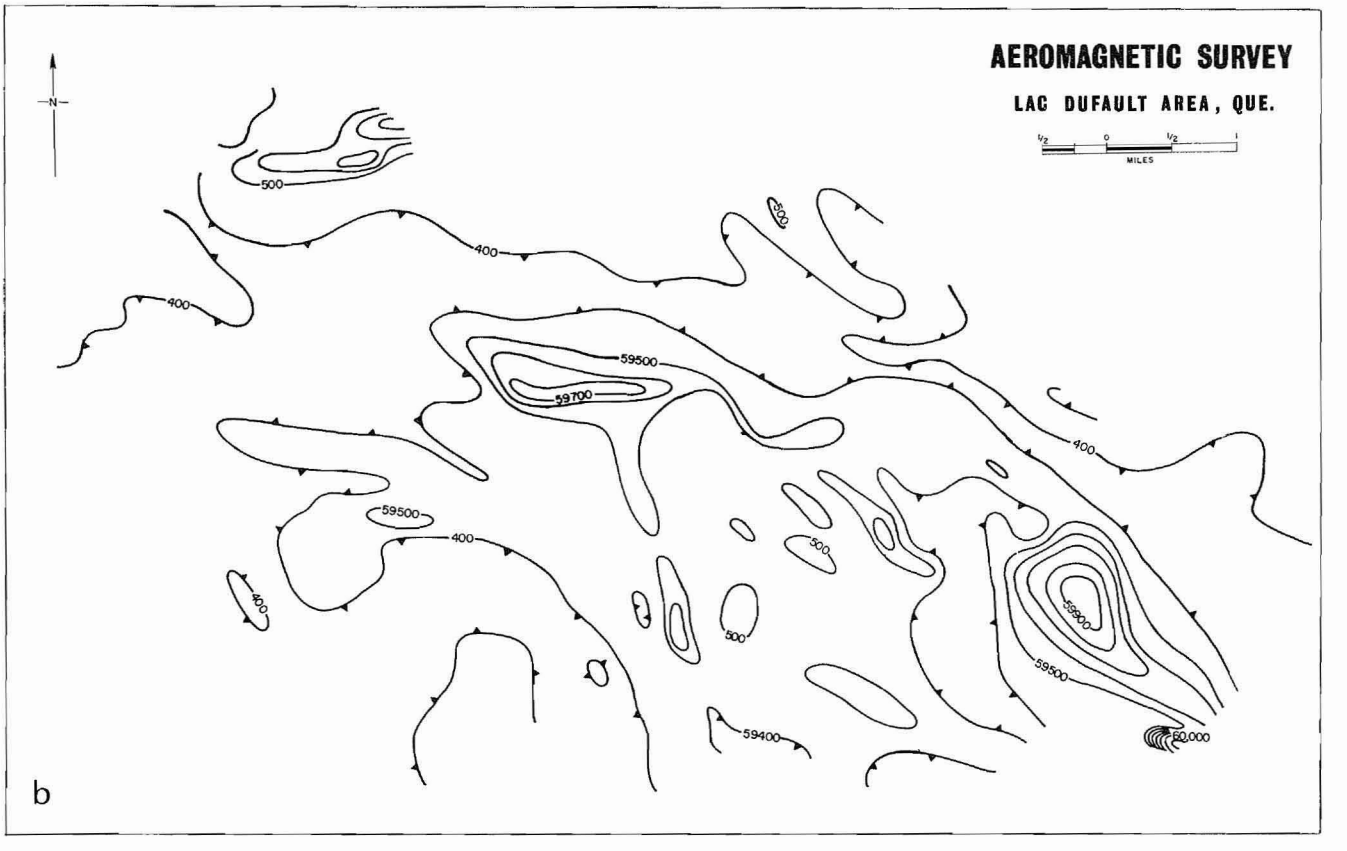


Figure 4a. Horizontal intensity map derived from the airborne Radiophase survey.
Figure 4b. This map illustrates the magnetics of the same area as in 4a.



Contents

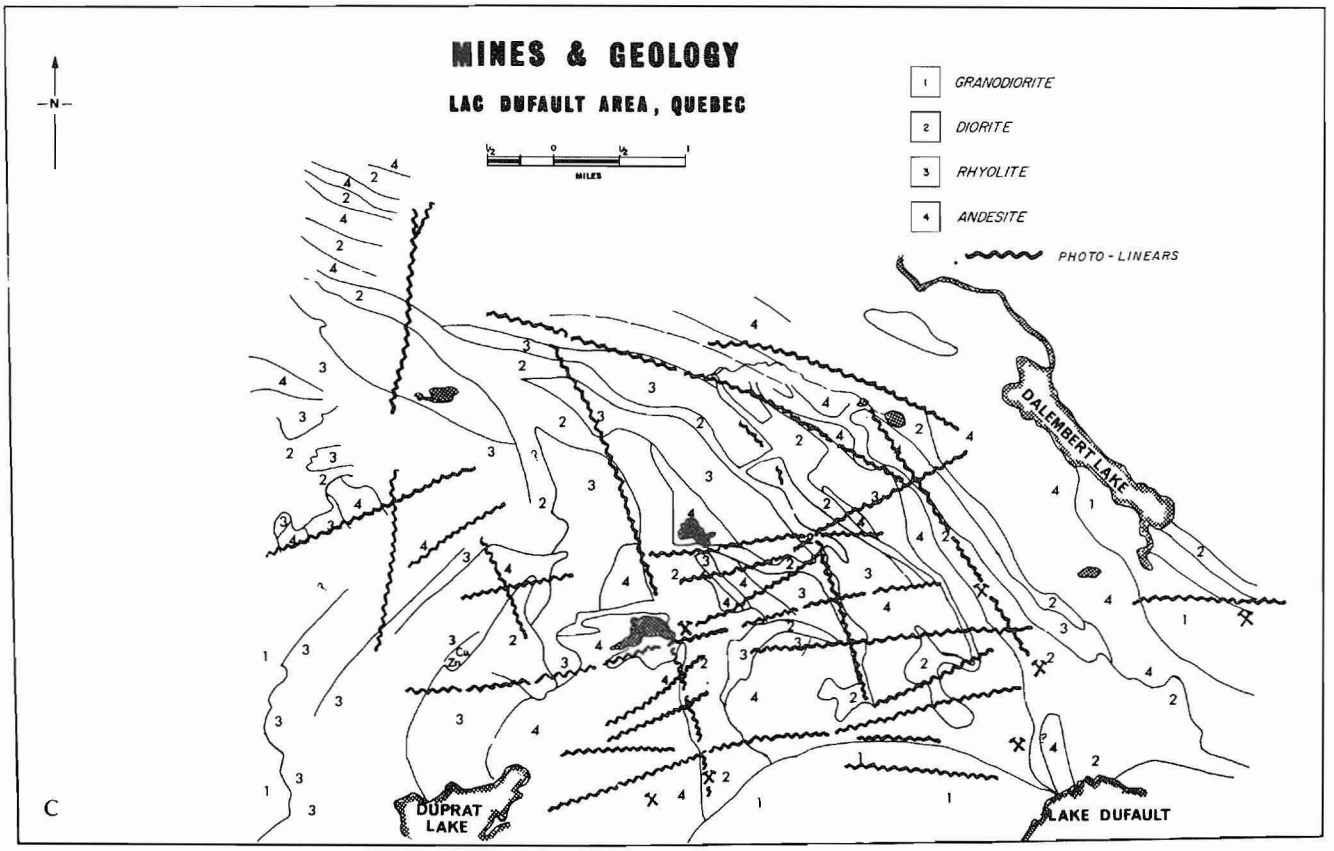


Figure 4c. This map illustrates the geology and the photolineaments of the same area as in 4a and 4b.

identifying the presence of conductive sulphide bodies down to depths of perhaps 1000 feet.

The advantages of measuring three components of field and using the computer in data processing are manifold. Many of the ambiguities of interpretation which arise when the direction of the primary field is unknown are eliminated, and much fuller use can be made of the broad information content of the signals.

Airborne geochemistry

Experimental work is being carried out by the writer and his colleagues in the development of instruments for detecting trace quantities of vapours. Particular interest has been centred on mercury vapour, iodine and sulphur dioxide. Mercury instrumentation has been developed which can detect 10^{-10} grams of mercury and is subject to minimal interference from organic vapours. This equipment has to date been used chiefly for the analyses of soil samples, and a ubiquitous relationship has been noted between base metal mineralization and mercury. Most base metal deposits, and indeed many precious metal occurrences, are associated with mercury anomalies in overlying soils. With regard to mercury in air, a vapour sampling unit has been constructed for use in a truck, but this work was carried out under nongeological sponsorship and the equipment in question has not been tested as a geological tool. However, airborne instrumentation is under construction with a view to evaluating its application in defining mercury geochemical provinces from the air and locating mercury vapour anomalies over orebodies (Barringer, 1964; Barringer, *et al.*, 1968; Barringer and Schock, 1966).

An airborne sulphur dioxide and iodine monitor has been constructed under the sponsorship of the National Aeronautics and Space Administration and it is hoped to place a version of this instrument into orbit during the 1970s. The airborne prototype (Figure 5) has been used principally for air pollution measurements to date, but some preliminary studies in Yellowstone Park have indicated its application to fumarole detection and to geothermal exploration. The instrument is capable of sensing 10 parts per billion of both sulphur dioxide and iodine over a 100-metre pathlength. There is a possibility that both sulphur dioxide and iodine anomalies may be associated with some oxidizing ore deposits. Iodine minerals are known to occur in association with some ore deposits such as Broken Hill in New South Wales and Chuciquimata in Chile, while sulphur dioxide can be expected to arise from oxidizing ore. Iodine is also of interest because of its association with oilfield brines, and since it is a relatively volatile element, it can be expected to get into the atmosphere in anomalous quantities whenever anomalous conditions of iodine concentration occur on the surface. The whole field of airborne geochemical dispersions remains largely unexplored at the present time and presents a difficult technological challenge in developing the extremely sensitive analytical techniques required. Nevertheless, it is an area of promise, particularly when considered in conjunction with complementary techniques of the type that have been outlined in this paper.

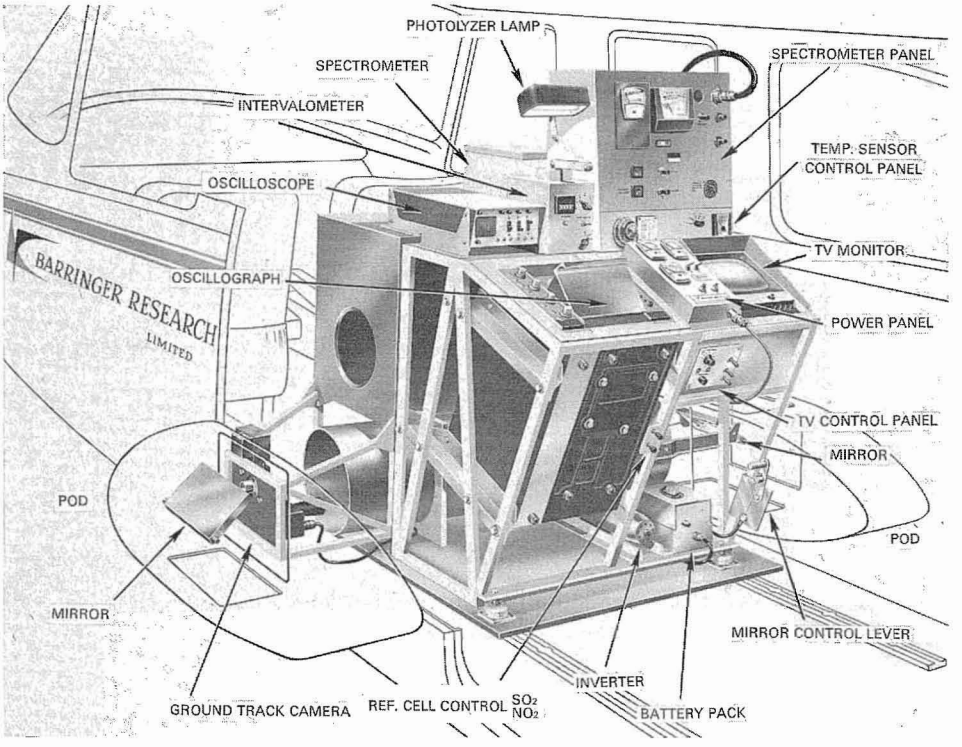


Figure 5. Annotated drawing of a remote sensing airborne spectrometer installation.

Conclusions

It is expected that new and future developments will have particular significance in two areas, as follows: (1) the development of new environmental geophysical methods and interpretive techniques as an aid to geological mapping and specifically channelled towards improved methods of selecting areas for more detailed prospecting; and (2) the development of improved deep penetration methods for use in known mining camp areas or regions selected as particularly favourable as a result of operations of the type outlined above.

The use of multiparameter airborne geophysical techniques in reconnaissance will inevitably dictate the use of magnetic recording methods in the aircraft. The substitution of automatic map-making techniques for the present-day laborious hand methods will be of immense value to the exploration community in providing data rapidly. Furthermore improvements in interpretation and the cross-correlation of very large quantities of data made possible with the computer will provide for major advances in exploration techniques.

References

Affleck, J., 1963. Magnetic anomaly trend and spacing pattern. *Geophysics.* 28(3): 379-395.

Badgley, Peter C., 1965. *Structural and Tectonic Principles.* New York, Harper and Row, p. 501, figs. 11-35.

Barringer, A.R., 1964. Developments towards the remote sensing of vapors as an airborne and space exploration tool. Third Symp. Remote Sensing of Environment, Univ. Michigan, Ann Arbor, Mich.

Barringer, A.R., B.C. Newbury, and A.J. Moffat, 1968. Surveillance of pollution from airborne and space platforms. Fifth Symp. Remote Sensing of Environment, Univ. Michigan, Ann Arbor, Mich.

Barringer, A.R., and J.P. Schock, 1966. Progress in the remote sensing of vapors for air pollution, geologic and oceanographic applications. Fourth Symp. Remote Sensing of Environment, Univ. Michigan, Ann Arbor, Mich.

Bhattacharyya, B.K., and B. Raychaudhuri, 1967. Aeromagnetic interpretation of a section of the Appalachian belt in Canada. *Can. J. Earth Sci.* 4(6): 1015-1037.

Billingsley, P., and A. Locke, 1935. Tectonic position of ore districts in the Rocky Mountain region. *AIME Trans.* 115: 59-68.

Billingsley, P., and A. Locke, 1941. Structure of ore districts in the Continental framework. *AIME Trans.* 144: 9-64.

Boltneva, L.I., V.N. Vasilenko, and A.V. Dmitriev., V.A. Ionov, R.M. Kogan, Z.V. Kuznetsova, I.M. Nazarov, I.V. Yagodovskii, 1964. An Experiment for Studying the Radioactivity of Granitoid Intrusions by Airborne Gamma Spectrometry. *Izv. Geophys. Ser.* 1964 (6): 858-871. Translated by C.M. Wade.

Canadian Institute of Mining and Metallurgy, 1948. *Structural Geology of Canadian Ore Deposits,* Jubilee volume.

Goodwin, A.M., 1965. Mineralized volcanic complexes in the Porcupine – Kirkland Lake – Noranda region. *Econ. Geol.* 60: 955-971.

Howe, G.W.O., 1940. Wireless Waves at the Earth's Surface. *Wireless Engineer,* 17(204): 385-387.

James, A., W. Smith, and J. Welsh, 1961. Geology of the Bingham mining district and northern Oquirrh Mountains. *Utah Geol. Soc.* Guidebook 16, pp. 49-69.

King, P.E., 1966. Tectonic History and Mineral Deposits of the Western Cordillera. *CIM. Symp. Vol.* pp. 1-25.

Kornick, L.J., and A.S. MacLaren, 1966. Aeromagnetic study of the Churchill Superior boundary in northern Manitoba. *Can. J. Earth Sci.* 3: 547-557.

Latulippe, M., 1956. Noranda-Senneterre mining belt. *Quebec Dept. Mines* Map 1127.

Leech, G.B., 1966. The Rocky Mountain trench. In *GSC* Paper 66-14, The world rift system, p. 312.

Mardirosian, G.A., 1966. Mining Districts and Mineral Deposits of Utah (map) Salt Lake City, Utah.

Mayo, E.B., 1958. Lineament tectonics and some ore districts of the Southwest. *AIME Trans.* 211: 1169-1175.

Moxham, R.M., R.S. Foote, and C.M. Bunker, 1965. Gamma-ray spectrometer studies of hydro-thermally altered rocks. *Econ. Geol.* 60(4): 653-671.

Norton, K.A., 1937. The propagation of radio waves over the surface of the earth and in the upper atmosphere. *Proc. IRE.* 25(9): 1367-1387.

Ohle, E.L., 1959. Some considerations in determining the origin of ore deposits of the Mississippi Valley type. *Econ. Geol.* 54: 769-789.

Paal, G., 1965. Ore prospecting based on VLF radio signals. *Geoexploration.* 3(3): 139-147.

Park, C.F., 1964. Is geologic field work obsolete? *Econ. Geol.* 59: 527-537.

Pincus, H.J., and M.B. Debrin, 1966. Geological applications of optical data processing. *J. Geophys. Res.* 71(20): 4861-4870.

Popenoe, P., 1962. Aeroradioactivity survey and areal geology of parts of east-central New York and west-central New England (ARMS-I). *U.S. Geological Survey and Division of Biology and Medicine,* USAEC, Aug. p. 39.

Raaf, A.D., and R.G. Mason, 1961. Magnetic survey off the west coast of North America, 40° N latitude to 52° N latitude. *Geol. Soc. Amer.* Bull. 72: 1267-1270.

Roddick, J.A., and L.H. Green, 1961. Tay River. *Geol. Surv. Can.* Map 13-1961.

Savage, W.S., 1964. Mineral resources and mining properties in the Kirkland Lake – Larder Lake area. *Ont. Dept. Mines Mineral Res.* Circ. 3: 108.

Serson, P., 1967. Magnetism in Canadian upper mantle resort, 1967. *Geol. Surv. Can.* Paper 67-41: 85-116.

Stevenson, J.S. (ed), 1962. *The Tectonics of the Canadian Shield.* Univ. Toronto Press, p. 180.

Stockwell, C.H. (ed), 1957. Geology and economic minerals of Canada. *Geol. Surv. Can.* Ec. Geol. Ser. No. 1, 4th edition, p. 517.

Taylor, D., I. Nichol, and J.S. Webb, 1967. Enrichment of base metals in the Triassic sandstones of south Derbyshire. *Inst. Mining & Metallurgy Trans.* 76: B214, B215.

Titley, S.R., and C.L. Hicks, (ed), 1966. *Geology of the Porphyry Copper Deposits, Southwestern North America.* Univ. Arizona Press, p. 287.

Turneaure, F.S., 1955. Metallogenetic provinces and epochs. *Econ. Geol.* 50th Anniv. Vol., pp. 38-98.

Vine, F.J., J.T. Wilson, 1965. Magnetic anomalies over a young oceanic ridge off Vancouver Island. *Science.* 150: 485-489.

Vine, F.J., 1966. Spreading of the ocean floor: new evidence. *Science.* 154: 1405-1414.

Wait, J.R., 1962. Introduction to the theory of VLF propagation. *Proc. IRE.* 50(7): 1624.

Williams, W.J., and P.J. Lorenz, 1957. Detecting subsurface faults by radioactive measurements. *World Oil,* Exploration Progress Section 144(5): 126-129.

Wilson, H.D.B., 1967. Volcanism and ore deposits in the Canadian Archaean. *Geol. Assoc. Can. Proc.* 11-32.

Wisser, E.H., 1959. Cordilleran ore districts in relation to regional structure. *CIM* Bull. 52: 34.

Wisser, E.H., 1960. Relation of ore deposition to doming in the North American Cordillera. *Geol. Soc. Am.* Memoir 77, p. 117.

Zeitz, I., E.R. King, W. Geddes, and E.G. Lidiak, 1966. Crustal study of a continental strip from the Atlantic Ocean to the Rocky Mountains. *Geol. Soc. Am.* Bull. 77: 1427-1447.